A Hybrid Analytical and Machine Learning Workflow for Completion Design Optimization in Unconventional Reservoirs

by

Tamer Moussa

A thesis submitted in partial fulfillment of the requirements for the degree of

Doctor of Philosophy

in
Petroleum Engineering

Department of Civil and Environmental Engineering

University of Alberta

Abstract

Hydraulic fracturing combined with horizontal drilling is the key to unlocking tight reservoirs. However, understanding the relationship between reservoir characteristics, completion design and well productivity remains challenging. In the past decade, over 40,000 multi-fractured horizontal wells (MFHWs) have been completed in the Western Canadian Sedimentary Basin (WCSB). Despite completion intensity surging by nearly 100%, hydrocarbon productivity only rose by 20%. Why doesn't hydrocarbon production growth align with the increase in completion intensity? Is the efficiency gap attributed to formation characteristics, injection fluid properties, or the fracturing strategy?

The main objective here is to develop a comprehensive analytical and machine learning (ML) workflow to evaluate and predict the recovery performance of MFHWs as a function of reservoir characteristics and completion design, and to optimize the completion design based on reservoir characteristics to maximize the productivity of MFHWs.

While there have been advancements in the ML-based modelling approaches to predict well performance in tight reservoirs, there are limited studies focus on the comprehensive development of these resources considering both the reservoir characteristics and completion design. Therefore, this study seeks to address two main questions: i) how can the optimal sweet spots for MFHWs be efficiently identified? And ii) how can the completion design be optimized based on the reservoir quality and geomechanical properties? By addressing these questions, this thesis aims to provide a more holistic and effective approach for optimizing well performance in tight reservoirs.

To achieve this objective, several new approaches are proposed to build this workflow. Initially, an iterative method is proposed to estimate dynamic fracture volume, porosity, and compressibility based on downhole pressure. Following this, a characteristic fracture closure rate is derived to describe the rate at which the effective fracture volume decreases during flowback. Subsequently, a water-oil-ratio model (WORM) is introduced to explain the observed log-linear relationship between WOR and load recovery as an analogy to the log-linear relationship between the water/oil relative-permeability ratio and water saturation. The coefficients from WORM are then coupled with key petrophysical properties using a neural network to predict WOR as a function of load recovery, forecast ultimate load recovery, and estimate effective fracture volume. Another data-driven model is proposed to predict oil production as a function of load recovery during the matrix-dominated flow regime. A support vector machine model is also developed to predict permeability from well log data, which facilitates the creation of high-resolution 3D maps of different petrophysical properties across the Montney formation, utilizing data from over 14,000 oil and gas wells. Similarly, sonic log data are utilized to estimate formation fracability, which is then interpolated using 3D kriging across the Montney formation. These developed petrophysical properties are incorporated to derive a Reservoir Quality Index (RQI), serving as a unified measure of reservoir quality based on petrophysical properties. Then, a series of ML-based proxy models are designed, trained, and proposed to correlate the oil and gas productivities of more than 10,000 oil and gas MFHWs with reservoir characteristics and completion design, alongside their mathematical representation for broader applicability. Finally, a supplementary study is proposed to explore the geothermal potential of suspended oil and gas MFHWs completed in WCSB. The aim is to identify the most suitable candidates for repurposing, especially considering the substantial investment initially made to complete these wells.

Abstract

The key results from this work show that the functional dependence of well productivity on completion-design varies depending on reservoir quality. In low-quality reservoirs, the effect of completion-design on productivity is less pronounced and the productivity follows reservoir quality. However, in high-quality reservoirs, the effect of completion-design becomes more significant, and the productivity can be reduced due to inefficient completion-design. Moreover, the productivity can be maximized by less intense completion-design in low-quality reservoirs. However, in high-quality reservoirs, intense completion significantly improves the productivity. Additionally, the application of a completion design to achieve a similar effective fracture volume on child wells does not necessarily lead to similar oil productivity compared to parent wells. It also depends on the quality of the reservoir at which the parent/child wells are completed. Finally, completion design parameters generally exhibit a greater influence compared to formation characteristics on both effective fracture volume and well productivity.

Preface

All parts of Chapters 2-8 have been published, with the exception of Chapter 7, which is currently being prepared for submission to a peer-reviewed journal. I was responsible for the data preparation, problem formulation, feature engineering, model development, writing and editing these papers. My co-authors were responsible for providing useful comments and discussions, reviewing the manuscript drafts.

The necessary approvals to include the journal papers as chapters in this thesis are provided in sequential order in the **Copyright Permissions** section. The reference style from the Society of Petroleum Engineers[1] was used in this work.

[1] Society of Petroleum Engineers (SPE) Style Guide (2023 Edition). https://www.spe.org/en/authors/resources/ (las accessed 2023-10-16)

Dedication

This is for my amazing parents, my rock-solid and supportive wife, and my incredible kids. You've all been my cheerleaders, believing in me every step of the way. And to everyone who's been a part of my journey, this one's for you. Your support has meant the world to me.

Thank you.

Acknowledgements

I would like to thank my supervisor, Dr. Hassan Dehghanpour, whose guidance, support, and encouragement have been invaluable throughout my PhD journey. His passion for scientific inquiry and engineering challenges has been a constant source of inspiration. His critical comments have significantly contributed to my professional growth.

I extend my honest thanks to my supervisory committee members, Dr. Irene Cheng and Dr. Japan Trivedi, as well as Dr. Alireza Nouri, Dr. Clayton Deutsch, and Dr. Shahab Mohaghegh for their invaluable insights that have enriched this work. I am also grateful to Robert Hawks, Darby Witt, and Melanie Popp for their technical support.

I am grateful to Natural Sciences and Engineering Research Council of Canada (NSERC) and Alberta Innovates for supporting this study. I would also like to acknowledge geoLOGIC systems Ltd. for providing access to the geoSCOUT platform, which allowed us to use specific public Montney formation data to examine the application of our developed models in this study.

I would like to appreciate my colleagues Mohammad Yousefi, Sabbir Hossain, Lin Yuan, Amin Alinejad, Saman Mohammadi and Yanze Zhang for their insightful discussions. I would also like to acknowledge the administrative staff members of the Civil and Environmental Engineering Department - Arlene Figley, Jomana Haymour, and Trina Cattral - for their unwavering assistance and support.

Table of Contents

List of Tables

List of Figures

Chapter 1.
General Introduction

1.1 Overview

This section briefly outlines the key terminologies and field practices referenced in the subsequent chapters, helping to position this work in the proper perspective.

1.1.1 Unconventional Reservoirs

Unconventional reservoirs are typically characterized as sedimentary formations that necessitate stimulation for the economical extraction of hydrocarbons, primarily due to the rock's low permeability or the fluid's high viscosity [11]. In the context of this research, the term "unconventional" is used to denote the tightness of the rock matrix, characterized by low porosity and permeability. More specifically, unconventional reservoirs in this research cover tight and shale oil/gas reservoirs. Tight reservoirs are non-source rocks like sandstones and carbonates that have low permeability but are capable of producing hydrocarbons [12]. On the other hand, shale reservoirs are fine-grained, organic-rich formations that could produce hydrocarbons.

Fig. 1.1 – Unconventional basins in North America [1]. The three studied basins in this research are highlighted

Fig. 1.1 demonsrates the distribution of major unconventional basins across North America. A significant portion of these resources are situated in the central and southern regions of the United States, as well as Western Canada. This research primarily focuses on the Western Canadian Sedimentary Basin (WCSB), with supplementary discussions on the Eagle Ford and Niobrara basins. These specific basins are prominently highlighted on the map.

The permeability spectrum of various conventional and unconventional reservoirs is illustrated in **Fig. 1.2**. The defining characteristic of unconventional reservoirs is their ultra-low permeability, typically less than 100 μD, as noted by [13]. This makes the development of these unconventional reservoirs a significant challenge. However, the combination of hydraulic fracturing and horizontal drilling has emerged as a pivotal strategy for unlocking the potential of these unconventional reservoirs.

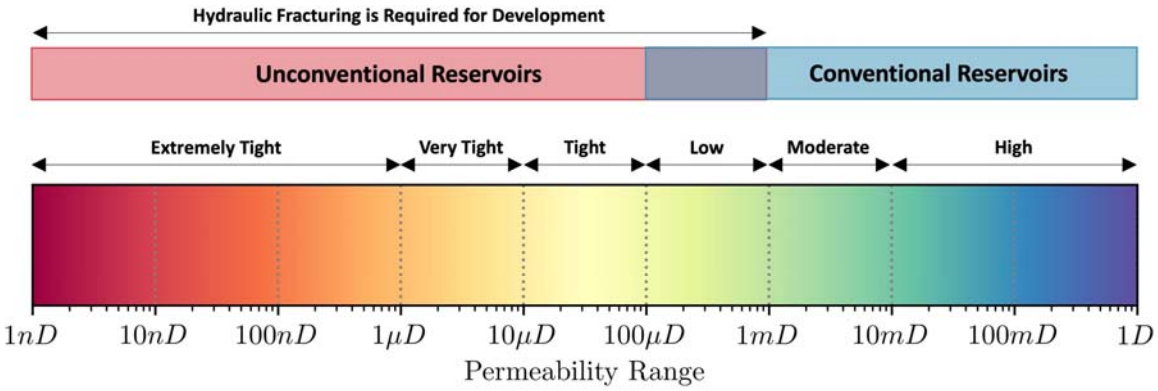

Fig. 1.2 – Permeability ranges of different reservoir types

1.1.2 Horizontal Well Technology and Multiwell Pad Drilling

Fig. 1.3 provides a comprehensive overview of the primary operational activities involved in the development of unconventional reservoirs. The process commences with the drilling of a horizontal well, followed by the initiation of the hydraulic fracturing operation, which involves the application of multi-stage hydraulic fracturing. Subsequent to this, there may or may not be a shut-in period before the fracturing fluid is returned to the surface in a procedure known as flowback. In certain wells, the shut-in period could be extended up to several months to facilitate the preparation of flowback and production equipment at the wellhead.

Horizontal wells play a key role in improving hydrocarbon production from unconventional reservoirs. In comparison to vertical drilling, horizontal drilling augments the contact area between the reservoir and the wellbore, thereby boosting well productivity. The process of drilling a horizontal well commences with a vertical hole drilled to a predetermined depth, known as the kickoff point. Subsequently, the well is drilled at an increasing angle until it reaches the target formation, followed

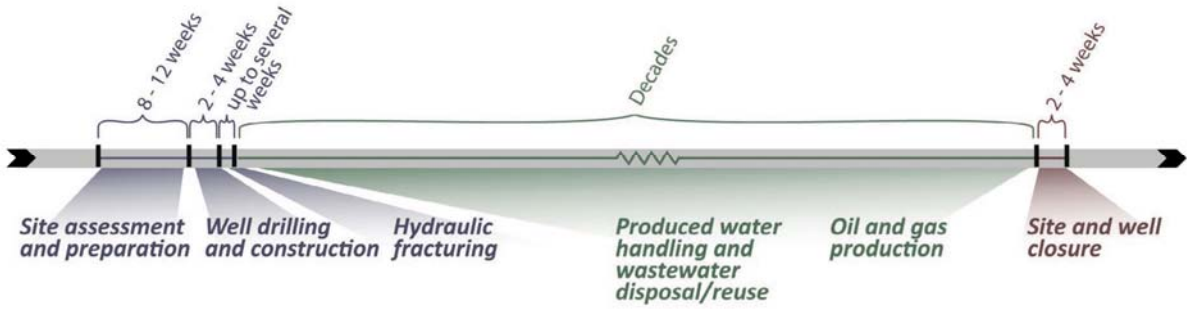

Fig. 1.3 – General timeline of activities at multi-fractured horizontal wells, modified from [4].

by the drilling of a horizontal section to the designed lateral length. Horizontal drilling is particularly crucial for the development of unconventional reservoirs with thin pay zones and natural fractures [14].

Recently, oil and gas operators have been inclined towards drilling multiple wells from a single pad to develop unconventional reservoirs efficiently while minimizing costs and mitigating environmental impacts. Recent data shows that over 58% of the wells drilled in unconventional reservoirs in the United States have been drilled on multiwell pads [15]. Multiwell pad drilling not only maximizes reservoir penetration with minimal surface disturbance but also curtails costs associated with drilling, fracturing, and production operations, thereby reducing environmental impacts.

1.1.3 Multi-stage Hydraulic Fracturing

Even with the integration of horizontal well technology and multi-well pad drilling, many unconventional reservoirs still do not produce hydrocarbons at economic flow rates. To attain higher production rates, horizontal wells necessitate hydraulic fracturing at multiple stages. This not only increases the contact area between the wellbore and the reservoir but also establishes additional pathways for hydrocarbon flow, as shown in **Fig. 1.4**. Furthermore, hydraulic fractures facilitate a connection between the well and existing natural fractures.

The fracturing process typically begins from the stages at the toe and progresses towards the stages at the heel. Each fracturing stage primarily includes two crucial steps:

i. A section of the wellbore is perforated to create openings that connect the wellbore and formation. These perforation holes permit the entry of fracturing fluid and proppants into the formation, and subsequently allow hydrocarbons to flow into the wellbore.
ii. Fracturing fluids carrying proppants and additives are pumped down the wellbore under high pressure to create or reopen in-situ fractures. A frac plug is commonly utilized to isolate

previous stages before fracturing the subsequent stage. Post-fracturing treatment, these frac plugs are drilled out prior to flowback.

1.1.4 Hydraulic Fracturing Design

1.1.4.1 Fracturing and Stimulation Fluids Design

he primary roles of fracturing and stimulation fluids are to propagate fractures and transport proppants into the formation. Typically, the fracturing fluid is a slurry composed of water and chemical additives. In addition, gels, foams, and compressed gases such as nitrogen, carbon dioxide, and air can also be injected. The conventional fracturing fluid used for unconventional wells is predominantly composed of water (about 90%) and a small fraction of chemical additives (up to 1%).

1.1.4.2 Proppant Design

The primary function of proppants is to prevent the induced fractures from closing post-fracturing. Proppants typically range in size from 8 to 140 mesh (106 μm to 2.36 mm). Silica sand is the most frequently used proppant. Other types of proppant materials include resin-coated sand and ceramic proppants. Resin materials are applied to sands to smooth the surface and create a more uniform

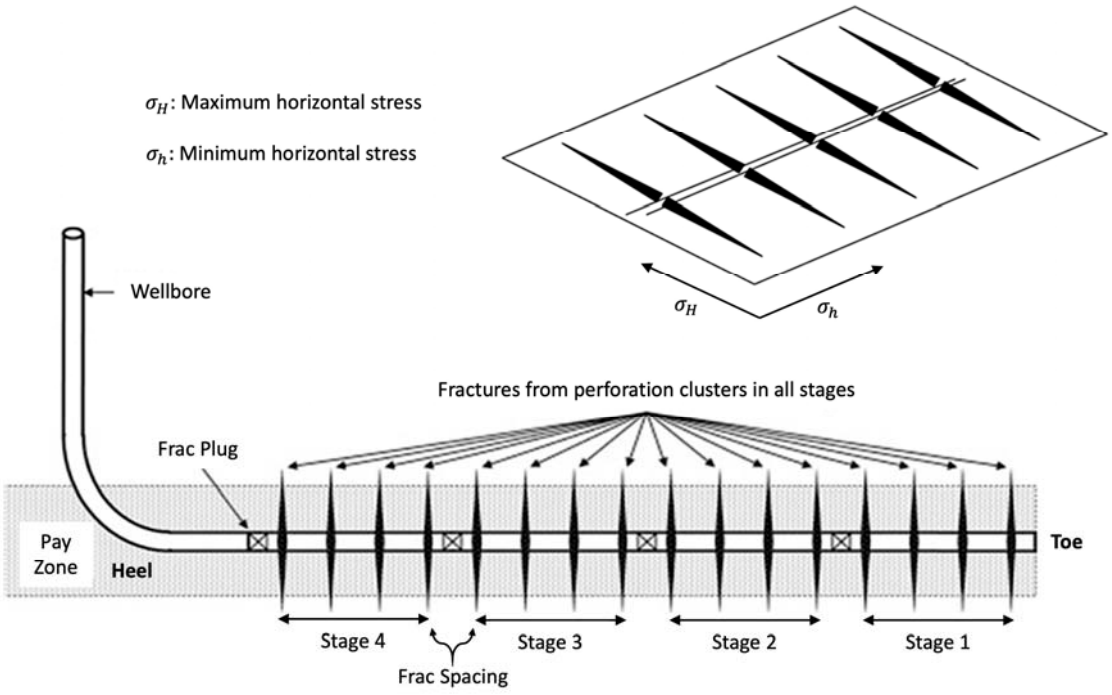

Fig. 1.4 – Schematic of the key concepts of multi-fractured horizontal wells, modified from [3].

shape. Resin-coated sand also possesses higher strength, enabling it to resist fracture closure. Ceramic proppants are considered the most effective due to their uniform shape and relatively high strength.

1.1.4.3 Stages and Clusters Design

Horizontal wells in unconventional reservoirs are typically fractured in multiple stages, sometimes exceeding 50 stages. The average spacing between stages varies from less than 100 to 200 meters, and each stage is perforated with anywhere from 1 to more than 5 clusters. The completed length of these wells can range from 1000 to over 2500 meters. Recent studies have highlighted the significant role that cluster spacing plays in the effectiveness of the hydraulic fracturing process [16, 17], emphasizing the need for optimization to ensure efficient treatment.

1.1.5 Flowback

Following hydraulic fracturing, there is typically a soaking (or shut-in) period before the well is opened for flowback operations. The duration of this soaking mainly depends on the understanding of water leak-off rates into the reservoir matrix and the time required to prepare surface facilities for production. Subsequently, wells undergo a flowback period to prepare them for hydrocarbon production. Flowback is essentially a cleanup process aimed at recovering as much of the injected fluid as possible from the well, thereby preparing it for optimal, long-term hydrocarbon production. This process, usually of short duration, may involve some proppant production. The flow of these recovered proppants through tubing can potentially damage control devices such as valves, chokes, and probes. While optimal well management during flowback impacts long-term well performance, best practices are dependent on geology, fracturing fluid, and completion. In unconventional reservoirs, generally less than 30% of fracturing fluid is recovered to the surface during flowback [18, 19]. However, the flowback water tends to have a relatively high concentration of salts after coming into contact with underlying shale and tight rocks. The salinity of flowback water can reach up to 80 kppm [19]. This flowback water is typically disposed to prevent contamination of freshwater resources at the surface.

1.1.5.1 Flowback Data Analysis

In the past, flowback data were often overlooked following fracturing treatment. However, it has been recognized that flowback data offer the earliest opportunity for fracture characterization, thereby aiding in the evaluation of fracturing treatment and production forecasting. The salinity data derived from flowback water have been utilized to characterize fracture complexity in shale reservoirs [20]. Furthermore, flowback tracer data have been employed to assess the effectiveness of completion and fracturing, as well as to identify interwell connectivity of the fracture network [21].

Thanks to recent advancements in probe technology, the frequency and quality of flowback data have seen significant improvements. High-frequency rate and pressure data collected during flowback have been interpreted using analytical techniques to estimate parameters such as fracture half-length, fracture permeability, fracture conductivity, and effective fracture pore-volume. Numerical simulation has been applied to flowback rate and pressure data to qualitatively characterize fractures in unconventional reservoirs. Several studies have simulated the flowback process of shale gas wells to investigate how fracture parameters impact flowback rate and pressure [17, 22]. However, quantitatively characterizing fractures through numerical simulation of the flowback process remains a challenge. This is due to the requirement of numerous uncertain inputs for numerical simulation, leading to considerable non-uniqueness of fracture parameter estimates.

1.1.6 Flowback Data Recognition and Digitization

Flowback data is typically found in the format of pressure-test reports. In public databases, these reports are often categorized alongside other types of pressure tests, such as pressure-gradient tests, absolute open flow (AOF) tests, and DFIT tests. Our study aims to extract flowback data from over 10,000 multi-fractured horizontal wells (MFHWs) in the Montney formation. To achieve this, we initially identified 800 reports containing flowback data within the pressure-test reports.

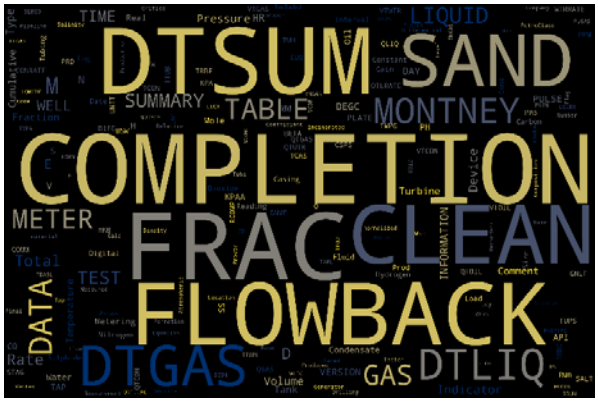

Fig. 1.5 - Flowback keywords' frequency map

Following this, we digitized these PDF reports to extract keywords and their frequency, as shown in the **Fig. 1.5**. We then constructed a dataset using the frequency of these keywords as input features and the presence of flowback data as the output. This dataset was fed into a neural network, enabling us to classify whether a pressure-test report contains flowback data based on the frequency of specific keywords. Finally, we processed all the flagged flowback reports to extract the data into a tabulated format.

1.1.7 Artificial Neural Network Modelling

Recently, Artificial Neural Networks (ANN) have emerged as one of the most effective techniques for classifying and recognizing complex systems and patterns that even exceed human cognitive capabilities. The concept of ANN was inspired by the biological neurons in the human brain[23].

Neurons serve as the primary processing elements in the ANN technique. An ANN model comprises three fundamental components: network architecture, training algorithm, and transfer function [24].

The ANN model typically consists of at least three layers: input, hidden, and output. Weights are used to connect each layer with the others, and the adjustment of these weights governs the performance of the ANN model [25]. The training of the ANN, which is the first step in modeling with ANN, employs a backpropagation of errors. Data processing occurs from the input layer to hidden layer(s), and then to the output layer. A comparison is then made between estimated and actual data in the output layer. The individual weights between each connection and the biases of each layer are updated based on the difference between estimated and actual data. The training process continues for all data sets until a predefined improvement is achieved, and the error is reduced to a certain predefined limit [26], or until the maximum number of iterations is met.

In addition to these fundamental components, hyperparameter optimization plays a crucial role in enhancing the performance of an ANN model. Hyperparameters include learning rate, number of hidden layers, number of neurons in each layer, etc., which are not learned during training but are set prior to it. Techniques such as grid search or random search can be used to find optimal hyperparameters.

Furthermore, cross-validation is an important technique used in machine learning, including ANN, to assess how well a model will generalize to an independent data set. It involves partitioning a sample of data into complementary subsets, performing the analysis on one subset (training set), and validating the analysis on the other subset (validation set). This helps prevent overfitting and provides an unbiased estimate of model generalization on unseen data.

1.2 Research Motivation

There is a significant demand for natural gas production in the western Canadian sedimentary basin (WCSB). Canada Energy Regulator (CER) has recently approved several liquid natural gas (LNG) plans that require boosting natural gas production [27]. In addition, a $1.3 billion investment was announced in June 2021 for the first phase of a hydrogen project in Edmonton [28] to support Canada's position as one of the top 10 hydrogen producers in the world [29]. However, natural gas is still the main methane source for hydrogen production. Therefore, the industry is expecting a boom in natural gas production in WCSB especially from the unconventional resources developed by using horizontal drilling and multi-stage hydraulic fracturing.

In the last decade, more than 40,000 multi-fractured horizontal oil and gas wells were completed in WCSB. These wells allowed Canada to play an important role in the global energy security and become the 3rd largest exporter of oil in the world [30]. **Fig. 1.6a** shows that from 2010 to 2020, there is a 20% increase in the hydrocarbon productivity of the multi-fractured horizontal wells (MFHWs). However, the completion intensity has been increased by almost 100% during the same period. Here the hydrocarbon productivity is represented by the average monthly barrel of oil equivalent[2] (BOE) per well, and the completion intensity combines five completion-design parameters; total injected water volume, number of stages, completed length, amount of proppant placed and fracture spacing. It is also observed that more than 56 billion gallons of water – sourced from rivers, lakes and water wells – was used to fracture these wells with more than 30 billion gallons of water unrecovered. This

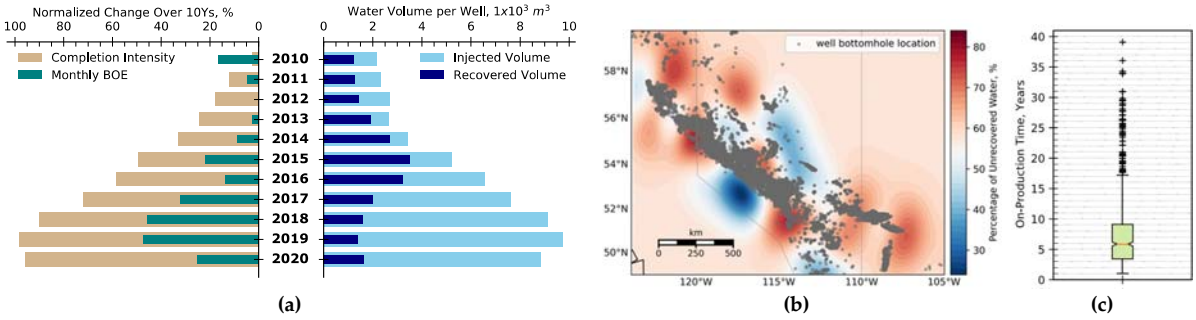

Fig. 1.6 – Normalized change in the hydrocarbon productivity and completion intensity of the MFHWs completed in WCSB from 2010 to 2020. **(b)** contour map demonstrating the distribution of unrecovered fracture water in WCSB. **(c)** MFHW's lifetime

unrecovered water volume is equivalent to more than the annual water consumption of the city of Edmonton for almost 5 years [31]. Moreover, in the last 5 years, the percentage of recovered water has been decreased while increasing the volume of water injection per each well as shown in the figure. **Fig. 1.6b** demonstrates the high variation in the efficiency of fracturing-water recovery performance of the MFHWs completed in WCSB with an average 46%.

These observations raise two main questions that motivate this research:

1. Why the increase trend in hydrocarbon production from MFHWs does NOT follow the increase trend in the completion intensity?
2. Is the current completion-design approach efficient enough to make use of each gallon of fresh water injected?

Another concern related to the MFHWs is that despite spending tens of millions of dollars for drilling and completing a multi-well pad, hydrocarbon production rate rapidly declines below the economic

[2] Barrel of oil equivalent (BOE) = 6,000 ft3

rate after few years and the operators have to shut in and suspend/abandon those wells. **Fig. 1.6c** demonstrates the short lifetime of MFHWs completed in WCSB. On average, MFHWs are suspended after less than 6 years of completion. 75% of the MFHWs are suspended less than 10 years after completion. Canada has more than 65,000 suspended oil and gas wells completed in WCSB with reported bottomhole temperature. Among these wells, there are more than 3,000 suspended MFHWs. Can these wells be retrofitted to generate geothermal power? This question motivates us to investigate the potential of producing geothermal energy from the suspended oil and gas wells completed in WCSB.

1.3 Research Objectives

The main objective of this research is to develop a comprehensive analytical and machine learning workflow to i) evaluate and predict the recovery performance of MFHWs as a function of reservoir characteristics and completion design; and ii) optimize the completion design based on reservoir characteristics to maximize the productivity of MFHWs. Therefore, this thesis seeks to address two main questions: i) how can the optimal sweet spots for MFHWs be efficiently identified? And ii) how can the completion design be optimized based on the reservoir quality and geomechanical properties? By addressing these questions, this thesis aims to link well productivity to the completion design, reservoir characteristics and geomechanical properties and to provide a more holistic and effective approach for optimizing well performance in tight reservoirs while improving the efficiency of fracturing water to get the most out of each gallon of water injected. This leads to practical guidelines for optimizing future fracturing operations and minimizing environmental footprints for the wells to be completed in WCSB. Another complementary goal of this research is to investigate the potential of producing geothermal energy from the suspended wells completed in WCSB.

The proposed research will address five technical objectives:

1. Develop a hybrid analytical and ML -based proxy models to link early-time flowback recovery to long-term well productivity in terms of ultimate load recovery and cumulative oil predictions.
2. Develop a reservoir quality index, serving as a unified measure of reservoir quality based on petrophysical properties.
3. Develop data-driven proxy model for predicting well productivity as function of completion design, reservoir characteristics and geomechanical properties.
4. Propose a workflow for evaluating geothermal energy production from suspended wells and identifying the best candidate wells for repurposing.

1.4 Organization of Thesis

Beside the introductory chapter, which provides a comprehensive overview and outlines the motivation and objectives of this research, and the concluding chapter, which presents key findings from this study and offers recommendations for future research, this research is structured into seven chapters. All of these chapters have been published, with the exception of Chapter 7, which is currently being prepared for submission to a peer-reviewed journal. While each chapter represents a distinct unit of study complete with its own nomenclature, they are designed to be read sequentially to maintain a coherent narrative throughout the research.

Chapter 2 analyzes the single-phase flowback data of 22 oil and gas MFHWs completed in the Eagle Ford basin to evaluate changes in effective fracture volume and its correlation with completion-design parameters. This chapter introduces a novel iterative approach to estimate dynamic fracture volume, porosity, and compressibility as functions of downhole pressure during flowback. It also presents a new parameter to characterize the rate of fracture closure, providing insights into the rate at which the effective fracture volume diminishes during flowback.

Chapter 3 presents a supervised fuzzy clustering algorithm to rank reservoir quality and completion intensity of 1,784 oil and gas MFHWs completed in the Western Canadian Sedimentary Basin (WCSB). This chapter addresses the question of which parameters control well productivity in unconventional reservoirs: reservoir quality or completion intensity.

Chapter 4 explores the nature of multi-phase flow regime in the stimulated volume by analyzing flowback and post-flowback data of six black-oil MFHWs completed in the Eagle Ford basin. It investigates whether oil flow is coupled with water flow or if they are stratified under natural drawdown conditions. It also examines the effect of oil breakthrough from matrix into fracture on the water flow regime.

Chapter 5 introduces A water-oil-ratio model (WORM) that uses a combined analytical and data-driven approach to explain the observed log-linear relationship between WOR and load recovery, analogous to the log-linear relationship between the water/oil relative-permeability ratio and water saturation. It also proposes a cumulative oil production model (COPM) which is a data-driven model to predict oil production as a function of load recovery during the matrix-dominated flow regime.

Chapter 6 demonstrates the application of WORM as an early-time diagnostic tool to evaluate the completion efficiency of 19 oil MFHWs completed in Niobrara and Codell formations that are classified into parent and child groups, comparing their productivity performance in terms of load

and oil recovery. This chapter also investigates potential well interference between child and parent wells.

Chapter 7 presents high-resolution 3D maps of different petrophysical properties across the Montney formation utilizing more than 14,000 oil and gas wells. It proposes a ML-based model to predict permeability from well log data and a workflow to estimate formation fracability from sonic log data. This chapter introduces a Reservoir Quality Index, serving as a unified measure of reservoir quality based on petrophysical properties. It also introduces new methodologies to evaluate the efficiency of fracture stage positioning and the effective distances between MFHWs, considering both 3D spatial and directional distances. It further proposes a series of ANN-based proxy models to correlate well productivity of more than 10,000 Montney MFHWs with reservoir characteristics and completion design.

Chapter 8 proposes a supplementary study to explore the geothermal potential of suspended oil and gas MFHWs completed in WCSB. This chapter aims to identify the most suitable candidates for repurposing, especially considering the substantial investment initially made to complete these wells.

Chapter 9 provides a brief summary of the principal conclusions derived from this research, while also addressing the limitations encountered and offering recommendations for future investigations.

Following Chapter 9, a comprehensive collection of all references cited throughout the chapters is presented. Subsequently, all appendices from each chapter are combined and displayed, providing supplementary information relevant to this research.

Chapter 2.
The Use of Flowback Data for Estimating Dynamic Fracture Volume and Its Correlation to Completion-Design Parameters: Eagle Ford Cases

2.1 Introduction

Hydraulic fracturing (HF) process involves injecting a mixture of water, sand and chemical additives under high pressure into tight reservoirs to create fractures and reactivate existing fractures. After HF, part of the injected fracturing fluid is produced back to the surface through a process called flowback. Although flowback is a short-time process, it carries important well and reservoir information.

Recent studies analyzed flowback data (rate and pressure) to characterize fracture network in unconventional reservoirs. Ilk, Currie [32] qualitatively interpreted flowback data by constructing diagnostic plots to investigate wellbore unloading and fracture clean-up trends. Abbasi, Dehghanpour [33] developed a single-phase flowing material balance model (linear relationship between rate-normalized pressure and material balance time) to estimate effective fracture volume (V_{ef}) using water flowback data. Ezulike and Dehghanpour [34] developed a flowback analysis model which accounts for transient 2-phase flow in fractures. Alkouh, McKetta [35] estimated V_{ef} of shale-gas wells by developing a tank model based on observations from simulation studies. They observed that gas drive is the most significant production mechanism from fractures when water saturation is below 70%. However, their proposed model is not applicable to single-phase water flowback since it neglects water expansion and fracture-closure mechanisms. Fu, Dehghanpour [36] and Ezulike, Dehghanpour [9] analyzed single-phase water flowback data of oil and gas wells completed in the Woodford Formation. They estimated V_{ef} and concluded that fracture closure is the primary drive mechanism during single-phase water production. Zhang and Emami-Meybodi [37] presented a workflow utilizing flowback and long-term production data to evaluate HF closure and changes in fracture properties. Zhang and Emami-Meybodi [38] proposed two multiphase flowback models for gas and

water phases under boundary dominated flow condition by considering gas influx from matrix into the fractures. They also utilized water-phase and gas-phase flowback data to quantitively estimate hydraulic fracture half-length, fracture permeability and fracture closure during flowback.

Optimizing HF operations requires understanding the relationships between HF efficiency and its design parameters. Dahi-Taleghani and Olson [39] presented a HF propagation model based on an extended finite-element method to optimize treatment parameters under complex fracture-propagation conditions. Kazakov and Miskimins [40] used a multivariate analysis method to study the effects of slickwater fracturing parameters on well productivity. They developed correlations between 1) total injected water volume (TIV) and water recovery, and 2) injected proppant volume with TIV and net pay. Bazan, Brinzer [41] outlined the key parameters necessary to design HF operations in unconventional reservoirs, including number of fracture stages, stage length and number of clusters. Fu, Dehghanpour [36] investigated the correlations between fracture volume and several CDPs using Pearson correlation coefficient. They concluded that TIV and average cluster spacing are the most significant design parameters for creating larger fracture volume. Zhou, Wang [42] applied data analytics method to understand the relationship between gas production and flowback water of shale gas wells completed in wet and dry gas regions of northwestern West Virginia. The results indicated that the relationship between produced gas and flowback water in wet-gas and dry-gas regions are positive and negative, respectively. Lin, Guo [43] applied back-propagation neural network to correlate petrophysical properties and CDPs with flowback ratio (load recovery) and first-month cumulative production, then correlate these two parameters with stimulated reservoir volume (SRV) in shale gas reservoirs. The results showed no specific correlation between SRV with flowback ratio or first-month cumulative production.

The previous studies focused on developing robust correlations among V_{ef}, CDPs and well productivity. The next challenge is understanding the effects of CDPs on the rate of fracture closure, controlling the surface area available for matrix depletion. Therefore, this paper introduces a new characteristic parameter to represent fracture closure rate (FCR) that describes how fast V_{ef} shrinks during flowback. This enables us to understand the relative effects of CDPs on fracture closure profile. In addition, we introduce an iterative approach to capture and consider the change in fracture porosity (ϕ_f) and compressibility (C_f) during flowback. We also use multiple linear regression (MLR) approach to account for possible interdependency among CDPs and to develop data-driven correlations between CDPs with V_{ef_i} and FCR. Such correlations are useful for evaluating well performance and optimizing future fracturing operations.

2.2 Methodology

This study uses flowback, post-flowback, and CDP data of 16 gas wells and 6 oil wells completed in the Eagle Ford formation. Flowback data include hourly water rate and bottom-hole pressure recorded after hydraulic fracturing while post-flowback data include daily pressure and rate recorded after the increase of hydrocarbon-water ratio and installation of production tubing. The target CDPs include number of stages, stage length, total injected water volume (TIV), total injected proppant mass (M_{prop}), average treatment rate (q_i) in barrel per minute, total vertical depth (TVD), shut-in time (t_{sh}), and choke-size. Our methodology consists of the following steps: 1) estimate V_{ef_i} using HD model; 2) develop an iterative approach to capture the change in ϕ_f and estimate V_{loss} during flowback; 3) develop dimensionless type curves for determining FCR; and 4) develop correlations to model V_{ef_i} and FCR as functions of CDPs by using MLR, and evaluate the relative effect of each CDP on V_{ef_i} and FCR.

2.2.1 Flowback Water-Rate Decline Analysis

During flowback, the decline in water rate could be modeled by both the hyperbolic and harmonic decline models with similar fitting accuracy as shown in **Fig. 2.1a** and **b**. This implies that, utilizing only the short-term flowback data, both decline models give similar fitting results. Mohaghegh [44] showed that, generally, for the early 3 months, various decline-curve analysis (DCA) models would fit well with early production data of shale-gas wells. **Fig. 2.1** shows that 1) exponential decline model doesn't match flowback data; and 2) statistically, both hyperbolic and harmonic decline models could be used to forecast the ultimate water production. Although hyperbolic decline model has higher

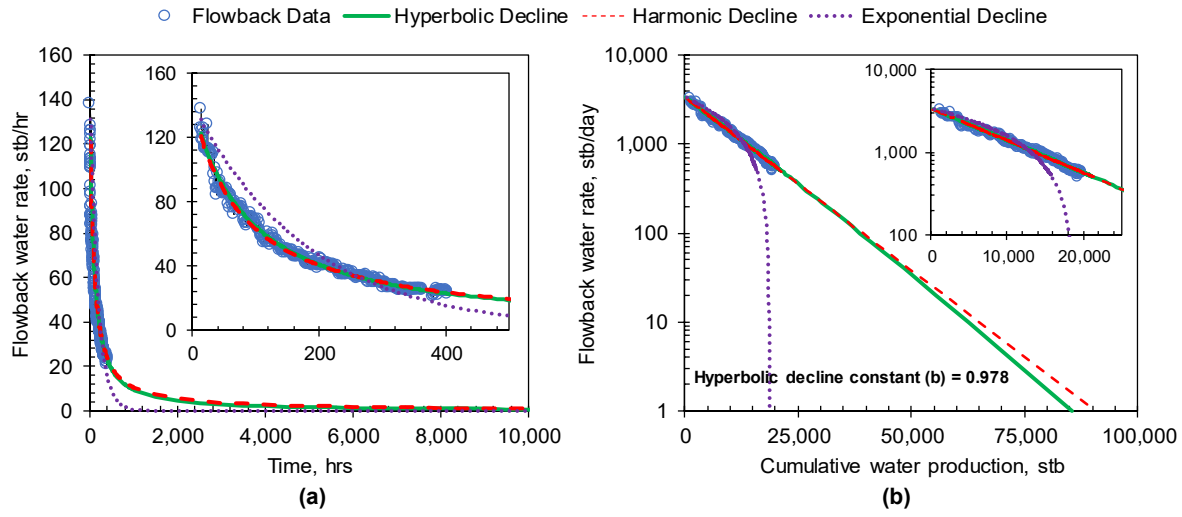

Fig. 2.1 – Comparison between hyperbolic, harmonic and exponential decline models on fitting flowback water rate. The hyperbolic decline constant (*b*) giving the best match is 0.978.

degree of freedom compared to HD model, the hyperbolic decline constant (*b*) that gives the best match is 0.978 (very close to harmonic in which b = 1). Therefore, the HD model is used in this study to predict the ultimate water recovery for statistical reasons; In HD model, there are fewer fitting parameters to be tuned compared to hyperbolic model to match flowback data and forecast ultimate water recovery. This overcomes the dilemma of non-uniqueness associated with matching production data while tuning more than one control parameter. In addition, the objective of this step is to, qualitatively, rank the studied wells depending on the created effective fracture volume, rather than a quantitative analysis. Fu, Dehghanpour [10] observed that flowback water rate of shale gas wells, completed in Eagle Ford and Montney formations, generally exhibits HD trend after hydrocarbon breakthrough from matrix into fractures. They concluded that a HD model can be used to estimate an ultimate water production (UW_P). Thy argued that UW_P may approximate V_{ef_i} assuming that effective fractures are initially saturated completely with fracturing water and that formation water is immobile. The HD model [45] relates water rate to cumulative volume of produced water by

$$q_w = q_{w_i}.\exp\left(\frac{-d_i}{q_{w_i}}W_p\right) \tag{2.1}$$

taking the logarithm of both sides and rearranging Eq. results in

$$\log\left(q_w\right) = \log\left(q_{w_i}\right) - \left(\frac{d_i}{q_{w_i}}\right)W_p \tag{2.2}$$

where;

q_w : instantaneous water rate, stb/day

q_{w_i} : initial water rate as flowback starts, stb/day

d_i : initial decline rate, 1/day

W_p : cumulative water production, stb

The y-axis intercept and line slope in the semi-log plot of q_w versus W_p in Eq. (2.1) are $\log\left(q_{w_i}\right)$ and $\left(-d_i/q_{w_i}\right)$, respectively. W_p at a predefined critical water flow rate (q_{w_c}) is referred to as UW_P. Here, q_{w_c} is assumed to be 1 stb/day and UW_P can approximate V_{ef_i} as will be explained in the following section.

2.2.2 Estimating Initial Effective Fracture Volume and Its Reduction with Time

During hydraulic fracturing and early hours of flowback, the average fracture pressures (p_f) is significantly higher than matrix pore pressure (p_m), referred to as pressure-supercharge conditions

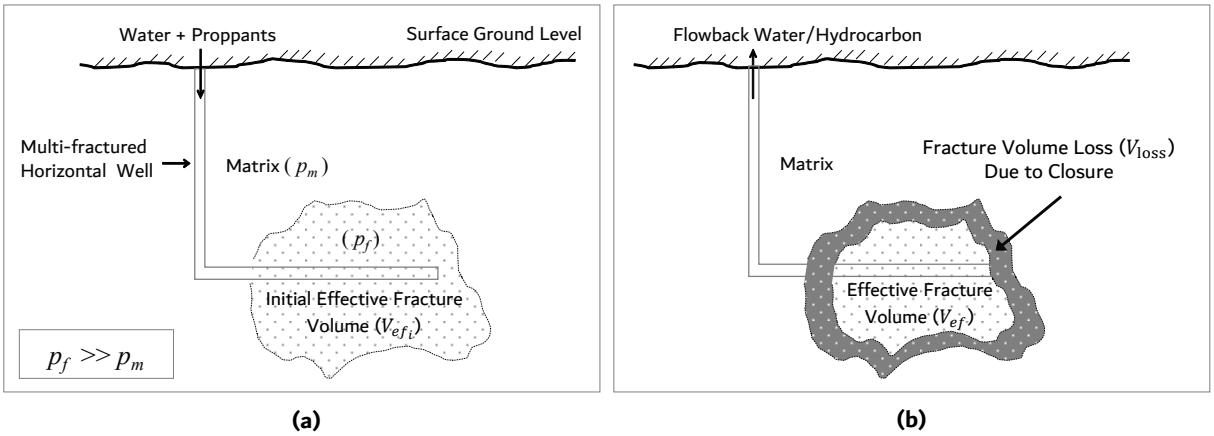

Fig. 2.2 – Schematic of **(a)** hydraulic fracturing process demonstrating the pressure-supercharge effect before flowback starts, and **(b)** fracture volume loss during flowback modified from [9]. p_m and p_f are the average pressures in the matrix and effective fractures, respectively.

as illustrated in **Fig. 2.2a**. Under these conditions, UWP estimated by the HD model can approximate V_{ef_i} assuming that 1) fluid influx from matrix to fractures is negligible; 2) fractures are completely filled with water initially; and 3) water production is mainly from fractures. During flowback, p_f decreases and V_{ef} consequently shrinks due to fracture closure as shown in **Fig. 2.2b**. Here, we propose an iterative approach to estimate V_{ef} during flowback as a function of downhole pressure (p_{wf}).

2.2.2.1 Fracture Compressibility Estimation

Fracture compressibility (C_f) is a key parameter in estimating fracture volume loss. Aguilera [8] introduced a graphical method to estimate C_f from **Fig. 2.3** using net stress on fracture (p_n) and mineralization ratio (η). p_n is the difference between in-situ minimum principal stress (σ_{min}) and p_f . Assuming insignificant difference between p_f and p_{wf} (compared to σ_{min}), due to high fracture conductivity at early flowback, p_n can be estimated as $p_n = \sigma_{min} - p_{wf}$. Since σ_{min} is often unknown, $p_{closure}$ can be used as a proxy to σ_{min} such that p_n becomes

$$p_n = p_{closure} - p_{wf} \tag{2.3}$$

Here, $p_{closure}$ is equivalent to minimum in-situ stress, defined as fluid pressure required to initiate the opening of a fracture (the fracture is open when fracture pressure is greater than $p_{closure}$ and vice versa) [46]. $p_{closure}$ can be estimated by analyzing diagnostic fracturing injection test (DFIT) data [47]. Since DFIT data are not available for all wells, Fu, Dehghanpour [36] introduced an approach to estimate $p_{closure}$ using fracture gradient (G_f) and instantaneous shut-in pressure (ISIP). G_f is calculated at each fracturing stage by dividing ISIP by TVD. Then, closure pressure gradient ($G_{closure}$) is calculated by averaging G_f from all stages:

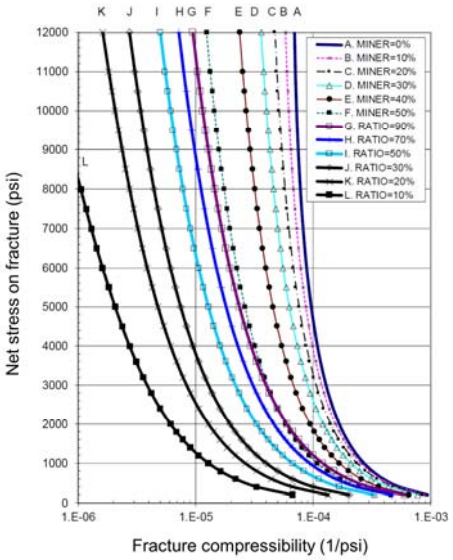

Fig. 2.3 – Chart for estimating fracture compressibility by using mineralization ratio and net stress on fracture. Miner in curves A to F represents mineralization ratio, estimated as 1- fracture porosity. The ratio in curves G to L equals to fracture porosity divided by the total secondary porosity including fractures, vugs and caverns [modified from: [8]]

$$G_{\text{closure}} = \frac{\alpha}{n}\sum_{i=1}^{n} G_{\text{f}_i} \tag{2.4}$$

Here, n is the total number of stages and α is the coefficient relating G_f to G_{closure} which can be obtained from nearby wells with available DFIT data. Finally, p_{closure} is calculated by

$$p_{\text{closure}} = G_{\text{closure}} \times \text{TVD} \tag{2.5}$$

The mineralization ratio (η) is the percentage of minerals in the fractures which can serve as a proxy for total proppant volume in fractures Williams-Kovacs 2017. Here, η can be estimated as

$$\eta = \left(1 - \phi_{\text{f}}\right) \times 100 \tag{2.6}$$

where ϕ_{f} is fracture porosity, which is an unknown parameter that significantly affects C_f. Fu, Dehghanpour [36] assumed that ϕ_{f} is constant during flowback, but the proposed methodology relaxes the assumption by introducing an iterative approach to estimate ϕ_{f} as a function of pressure. Then, we conduct a comparative analysis to show the effects of considering variable ϕ_{f} on estimated V_{loss}.

2.2.2.2 An Iterative Approach to Estimate Fracture Porosity and Volume

Fig. 2.4 illustrates a flowchart of the iterative method for estimating ϕ_{f} and V_{ef}. The pseudo-code algorithm is presented in **Appendix A** the summary of the method is given as follows:

1. Initialize V_{ef} with V_{ef_i} estimated from the HD model, and estimate total proppant volume in fractures as

$$V_{\text{prop}} = 0.178 \frac{M_{\text{prop}}}{\rho_{\text{prop}}} \tag{2.7}$$

where M_{prop} is mass of total injected proppant, ρ_{prop} is proppant density and 0.178 is a unit conversion constant. Then, estimate ϕ_f as

$$\phi_f = \frac{V_{ef}}{V_{ef} + V_{\text{prop}}} \tag{2.8}$$

2. Use estimated p_n and η from Eqs. (2.3) and (2.6), respectively, to estimate C_{f} from **Fig. 2.3**. C_{f} is related to V_{ef} by $C_{\text{f}} = \left(1/V_{\text{ef}_{\text{i}}}\right) \cdot \left(dV_{\text{ef}}/dp_{\text{f}}\right)$. Then, we can estimate V_{loss} by assuming insignificant difference between dp_{f} and dp_{wf}:

$$V_{\text{loss}} = \frac{dV_{\text{ef}}}{V_{\text{ef}_{\text{i}}}} = C_{\text{f}} dp_{\text{wf}} \tag{2.9}$$

3. Update V_{ef} by $V_{\text{ef}} = \left(1 - V_{\text{loss}}\right) V_{\text{ef}_{\text{i}}}$, then update M_{prop} if proppant production ($M_{\text{prop}_{\text{prod}}}$) is significant by $M_{\text{prop}}^{\text{new}} = M_{\text{prop}} - M_{\text{prop}_{\text{prod}}}$.

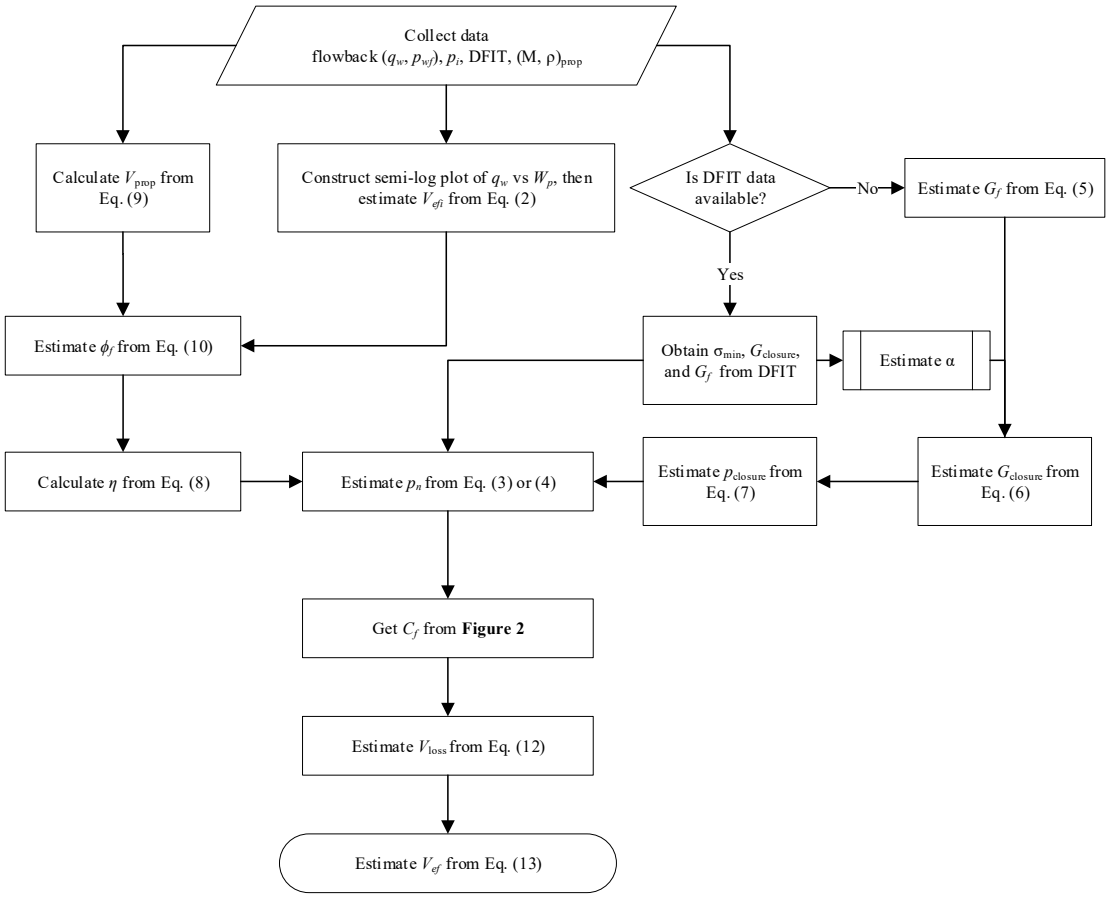

Fig. 2.4 – Flowchart for estimating dynamic fracture volume while capturing and considering dynamic fracture porosity and compressibility, and produced proppant during flowback

4. Finally, V_{prop} and ϕ_f are updated by Eqs. (2.7) and (2.8), respectively, then steps 2 to 4 are repeated until reaching the end of flowback.

2.2.3 Multivariate Data Analysis

Here, we follow these steps to correlate V_{ef_i} and FCR with CDPs: 1) eliminate CDPs with low coefficient of variation (CV); 2) find the correlation coefficients (CCs) among CDPs using correlation matrix. CC is a value between 0 to 1, where 0 means no correlation while 1 means perfect correlation as defined in **Appendix A**. In order to have a stable correlation, the CC between CDPs shall not exceed 0.7 [48]; 3) model V_{ef_i} and FCR as function of CDPs using MLR with a stepwise forward selection algorithm modified from Mundry and L Nunn [49] and Hocking [50].

The prediction accuracy of MLR is mainly controlled by the difference between the number of observations (n) and number of variables (p). In this study, n is the number of wells and p is the number of CDPs. To enhance the MLR's prediction accuracy, the ratio n/p should be very large [51]. The first step in data preparation is to minimize the number of CDPs in the correlation without losing their impacts on V_{ef_i} and FCR. Therefore, we introduce gross perforated interval (GPI) to combine the number of stages and stage length. GPI is given by multiplying number of stages by stage length. So, the new set of CDPs is M_{prop}, TIV, t_{sh}, GPI, q_i, TVD and choke-size. To enhance MLR's performance, we investigate the variation of each CDP using CV which is a measure of relative standard deviation in a data set. **Fig. 2.5** shows that choke size has the lowest CV among the CDPs. This is due to the low choke size variation during flowback of the 22 wells. Hence, choke-size cannot be considered as input

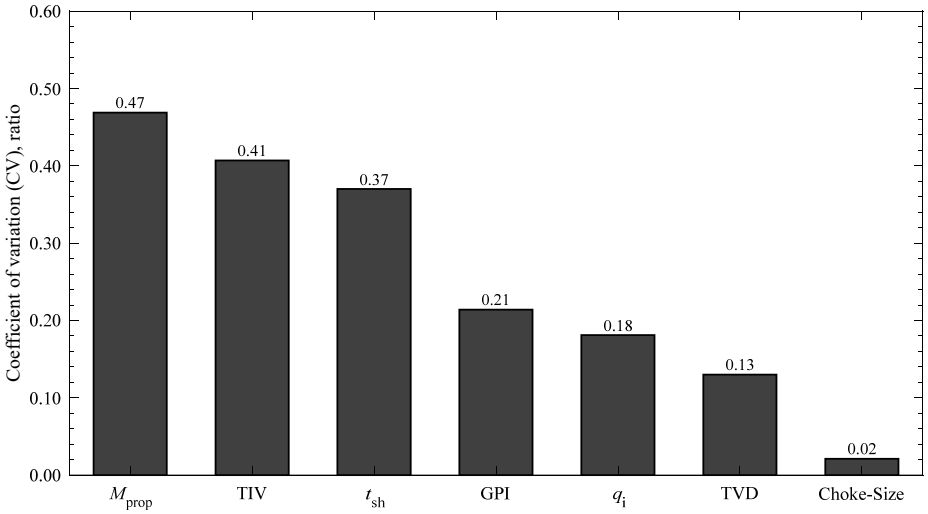

Fig. 2.5 – Coefficient of variation (CV) for each of the CDPs. Total proppant mass (M_{prop}) and choke size have the highest and lowest variations, respectively.

parameter in this study as it could not be taken as a representative sample. The updated set of CDPs becomes M_{prop}, TIV, t_{sh}, GPI, q_i and TVD.

2.2.3.1 Correlation Matrix

Multicollinearity between input variables is core statistical problem in MLR which results in unstable solutions [48]. It occurs when variables are highly correlated (linearly dependent) that can be represented by CC. To have a stable correlation, CC among input variables should not exceed 0.7 [48]. The CCs among the target CDPs, presented in **Fig. 2.6a,** suggest strong bivariate correlations between GPI and TIV, GPI and M_{prop}, and TIV and M_{prop}. Since none of these parameters is redundant, one possible solution to reduce multicollinearity is parameter reformulation. Therefore, we combine M_{prop} and TIV to form a new parameter called proppant concentration as $C_p = M_{prop}/\text{TIV}$. Similarly, we combine TIV and GPI to form a new parameter called total injected water volume per foot as $\text{TIV}_F = \text{TIV}/\text{GPI}$. **Fig. 2.6b** shows that after parameter reformulation, all bivariate correlations fall below the threshold value of 0.7. The final set of CDPs is C_p, TIV_F, t_{sh}, GPI, q_i and TVD.

2.2.3.2 Multiple Linear Regression

MLR is one of the common regression methods for correlating independent features with target(s). We use MLR to obtain correlations between CDPs as features, and V_{ef_i} and FCR as targets, expressed as

$$f(\mathbf{x}) = \sum_{j=0}^{d} w_j x_j \tag{2.10}$$

where $\mathbf{w} = (w_0, w_1, w_2, \ldots, w_d)$ is a set of unknown weights, $\mathbf{x} = (x_0 = 1, x_1, x_2, \ldots, x_d)$ is a set of known features (CDPs), $f(\mathbf{x})$ is a set of known targets (V_{ef_i} and FCR), and d is the problem

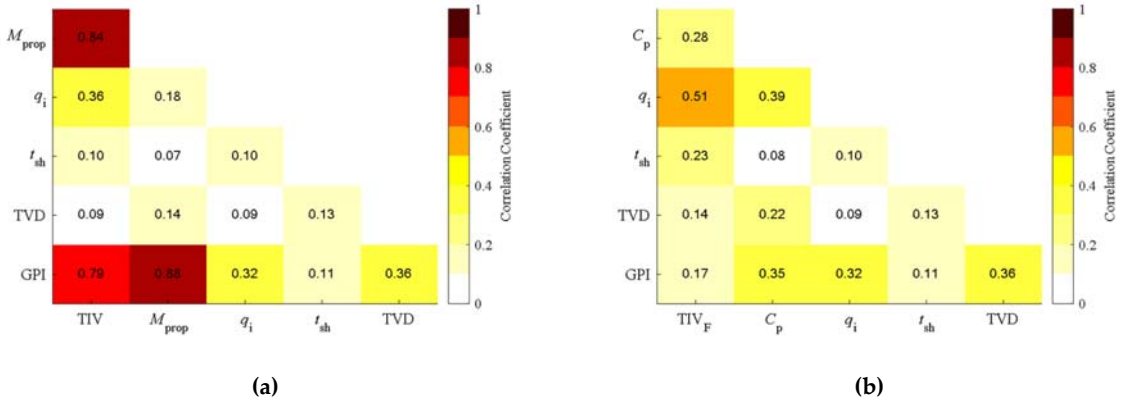

(a) **(b)**

Fig. 2.6 – Correlation matrices showing correlation coefficients (CC) among completion-design parameters, **(a)** before parameters' reformulation, and **(b)** after parameters' reformulation.

dimension (number of CDPs). Finding the best coefficients (maximum likelihood), $\mathbf{w}_{ML}$, is the goal of this MLR problem. The closed form solution of $\mathbf{w}_{ML}$ derived in **Appendix A** can be expressed as

$$\mathbf{w}_{ML} = \mathbf{X}\left(\mathbf{X}^{T}\mathbf{X}\right)^{-1}\mathbf{X}^{T}y \tag{2.11}$$

Here, the predicted target can be expressed as

$$\hat{y} = \mathbf{X}\,\mathbf{w}_{ML} \tag{2.12}$$

where,

$\mathbf{X} = \{\mathbf{x}_i\}_{i=1}^{n}$: matrix of input data sets

$\mathbf{x}_i = \{x_j\}_{j=1}^{d}$: vector of CDPs (inputs)

n : number of wells.

d : number of CDPs

y : real target vector (V_{ef_i} and FCR)

$\hat{y}$: predicted target vector.

We solve Eq. (2.12) using stepwise forward selection to understand the relative contribution of each CDP to the outputs of MLR correlations (V_{ef_i} and FCR). This involves the following steps:

1. Solve Eq. (2.12) while considering each of the CDPs individually to predict V_{ef_i} and FCR.
2. Select the CDP which gives the highest R^2 estimated from individual correlations.
3. Test the effect of incrementally adding each remaining CDP by recalculating R^2.
4. Add the CDP whose inclusion gives the highest R^2.

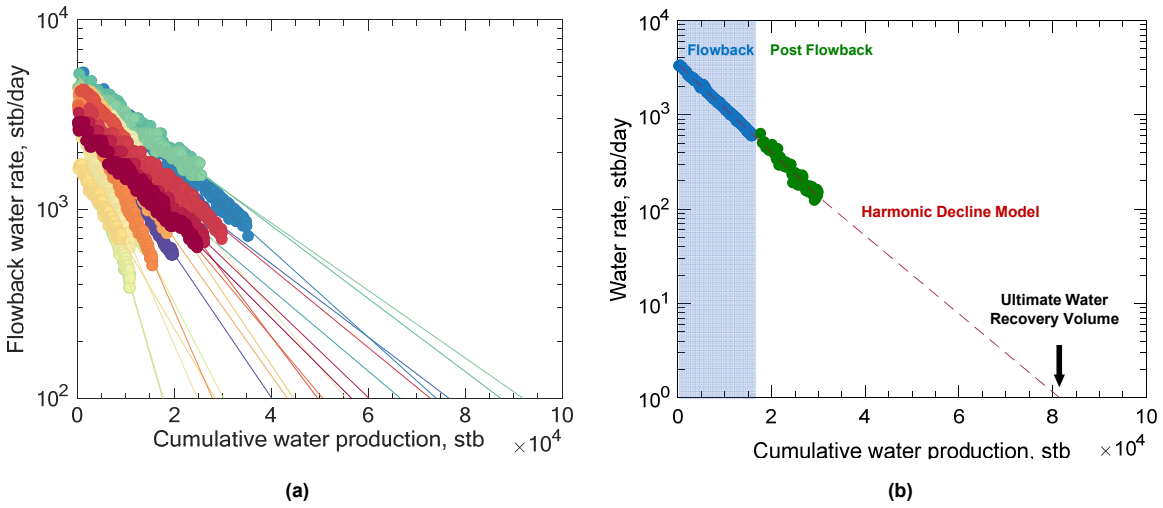

Fig. 2.7 – Semi-log plot of **(a)** flowback water rate versus cumulative water production volume for the 22 wells completed in the Eagle Ford generally shows a straight-line trend, and **(b)** water rate during flowback and post-flowback versus cumulative water production volume. The dashed line, representing harmonic decline model resulted by fitting the flowback data, reasonably fits the post-flowback data

5. Repeat steps 1 to 4 until no further addition of CDP(s) improves the correlation to a statistically significant extent.

2.3 Results and Discussions

2.3.1 Estimating Initial Effective Fracture Volume using HD Model

2.3.1.1 Estimating Ultimate Water Recovery

Fig. 2.7a shows a semi-log plot of flowback water rate versus cumulative water production from the 22 wells completed in Eagle Ford Formation. All wells show straight-line trend representing harmonic decline. The slopes and y-axis intercepts are used in Eq. (2.2) to estimate $W_p\left(\text{at } q_{w_c} = 1 \text{ stb/day}\right)$. **Fig. 2.7b** shows a semi-log plot of water rate versus cumulative water production during flowback and post-flowback periods. It demonstrates that the HD model for flowback data can reasonably predict post-flowback water production rate and ultimate water recovery that is assumed to approximate V_{ef_i} in this study.

2.3.1.2 Uncertainty in Estimated Ultimate Water Recovery

We calculate the average absolute percentage error (AAPE), which measures the fitting error between the measured post-flowback data and the predicted values using the HD model. AAPE is defined in **Appendix A**. **Fig. 2.8** shows the histogram of fitting errors between measured and predicted water production rate using the HD model during post-flowback of the 22 wells. It shows that the HD model can predict the post-flowback water rate with an estimated average error of 8%. The histogram is right-skewed which represents good fitness of the HD model as the majority of the fitting errors are

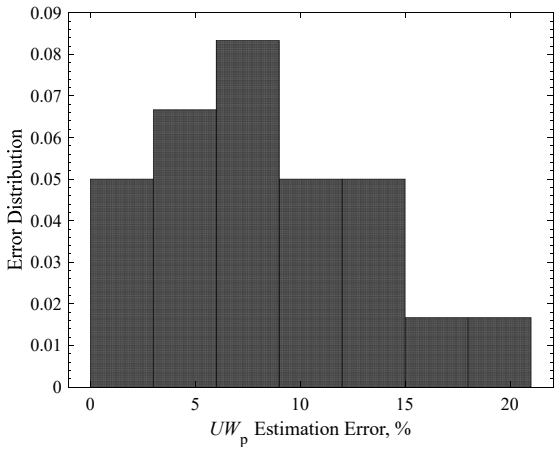

Fig. 2.8 – Histogram of fitting error between measured and predicted post-flowback water rate by the harmonic-decline model of the 22 Eagle Ford wells. The minimum, average and maximum error is 2, 8 and 20%, respectively.

stacked toward zero. Assuming that ultimate water recovery approximates V_{ef_i}, the prediction error of V_{ef_i} follows the same error distribution.

2.3.2 Estimating the Loss in Effective Fracture Volume

During flowback, V_{ef} and C_f decrease as bottom-hole pressure decreases. **Fig. 2.10** shows the change in bottom-hole pressure, ϕ_f, C_f, and V_{loss}. **Fig. 2.10b** and **7c** demonstrate that the decline profiles of ϕ_f and C_f are similar to the profile of bottom hole pressure drop during flowback (**Fig. 2.10a**). This highlights the significance of chock-size management during flowback and its effect on fracture volume loss. **Fig. 2.9** shows the profiles of fracture volume loss during flowback time for 16 studied wells (6 wells are excluded from this analysis due to high uncertainty in their bottom hole pressure data). The figure demonstrates that the maximum percentage of fracture volume loss by the end of flowback varies from 5 to 25% of V_{ef_i}. **Fig. 2.11** shows the effects of considering the reduction in ϕ_f during flowback on estimated V_{loss}. The figure displays $\Delta\phi_f$, Δp_{wf} and ΔV_{loss} for each well; where, $\Delta\phi_f$ and Δp_{wf} are the difference beween initial and final ϕ_f and p_{wf} during flowback, respectively. ΔV_{loss} is the difference between estimated V_{loss} considering dynamic ϕ_f and the estimated value when considering constant ϕ_f (average ϕ_f during flowback). The figure shows that ΔV_{loss} varies between 0.2 to 7.3%. For wells 5 and 6, the estimated V_{loss} does not significantly change when considering dynamic ϕ_f compared with the case with constant ϕ_f. However, Wells 7, 8, 11 and 14 show considerable change in V_{loss} between the two cases. The figure also shows that the variations in ΔV_{loss} are corelated to the variations in $\Delta\phi_f$ and Δp_{wf}. This suggests that when $\Delta\phi_f$ and/or Δp_{wf} is large, it is crucial to consider the reduction in ϕ_f for estimating V_{loss} during flowback. This could be further explained by the dependence of C_f on p_n and mineralization ratio (1 - ϕ_f), as illustrated in **Fig. 2.3**. Therefore, a significant change in ϕ_f and/or p_{wf} during flowback leads to a significant change in C_f and hence the estimated V_{loss}.

2.3.2.1 Uncertainty in Estimated Fracture Volume Loss

Fig. 2.12a shows a crossplot between estimated V_{loss} and measured W_P during flowback for the wells in this study. It shows a good positive correlation between estimated V_{loss} and measured W_P which indicates that more fracture closure will cause more water production during flowback process. The figure demonstrates that, generally, the estimated V_{loss} is slightly less than W_P for all wells. This insignificant difference is due to hydrocarbon expansion, specially, at late flowback time when there is a sufficient hydrocarbon influx from the matrix into the fracture. This could be depicted by **Fig. 2.12b** as it shows that at late flowback time, the difference between CDI and HDI decreases which indicates that with time the hydrocarbon expansion dominates the fracture closure.

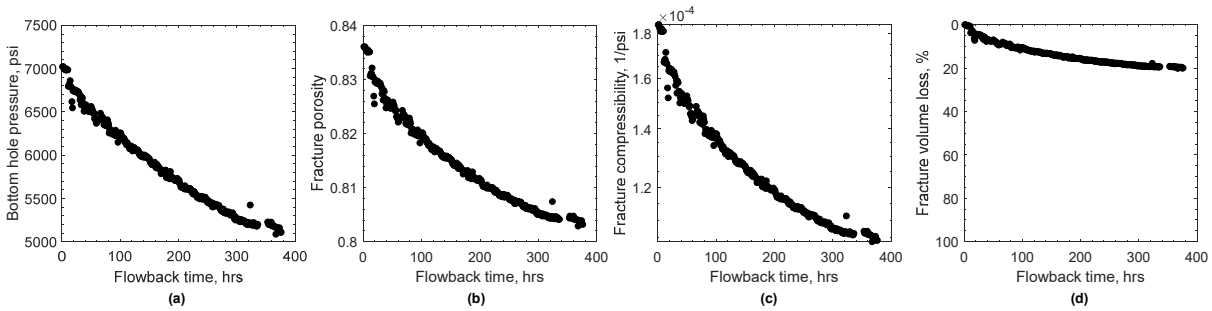

Fig. 2.9 – Decline in **(a)** bottom hole pressure, **(b)** fracture porosity, **(c)** fracture compressibility, and **(d)** percentage fracture volume loss during flowback

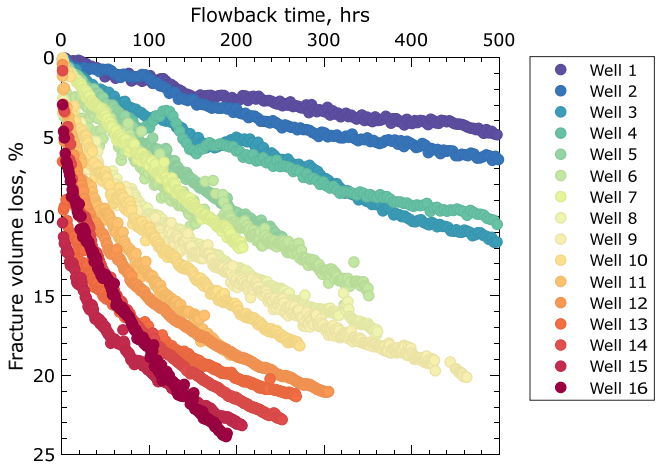

Fig. 2.10 – Percentage fracture volume loss profiles during flowback time. The maximum percentage of fracture volume loss varies from 5 to 25% by the end of flowback for the studied wells.

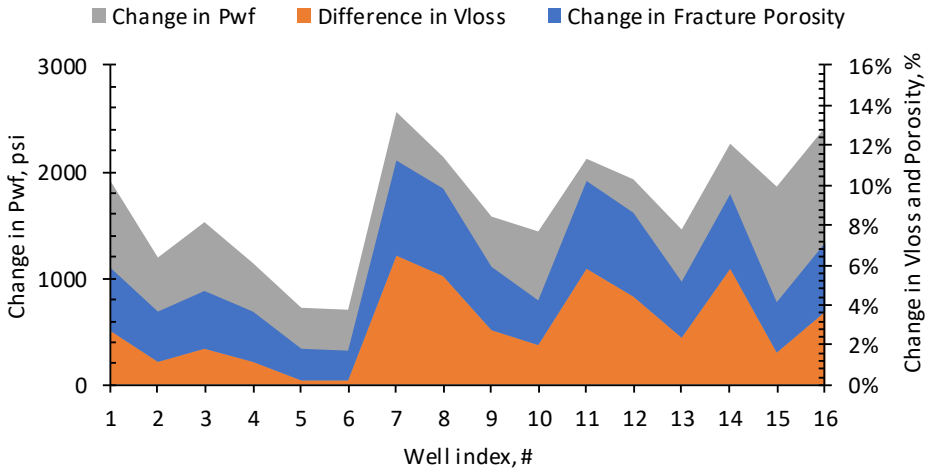

Fig. 2.11 – Effects of the reduction in fracture porosity during flowback on the estimated fracture volume loss (V_{loss}) for the 16 wells. Orange area represents ΔV_{loss} when considering variable fracture porosity compared with the case when fracture porosity is assumed constant during flowback time. Blue and gray areas represent $\Delta\phi_{\text{f}}$ and Δp_{wf}, respectively, during flowback.

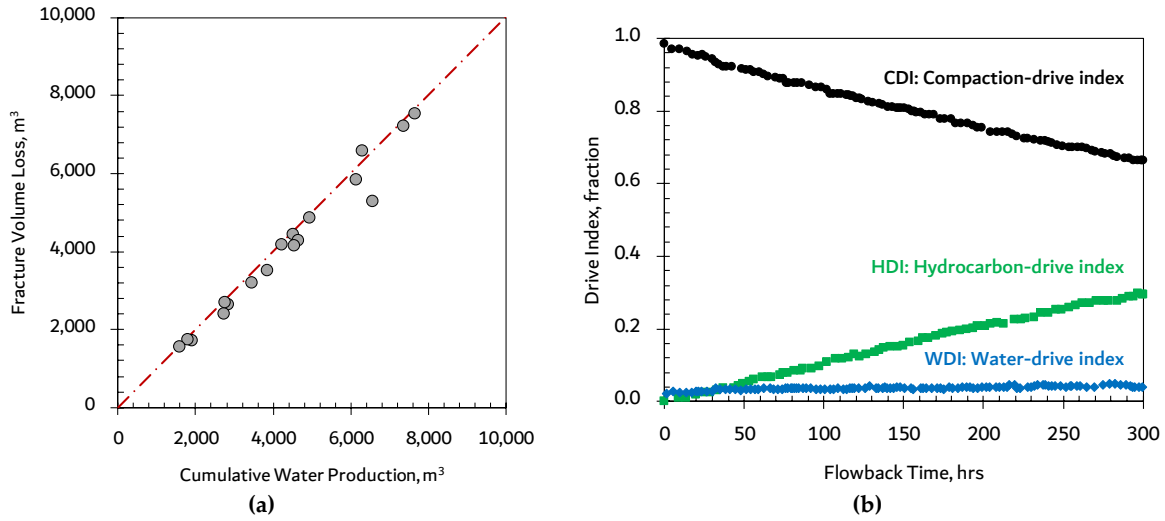

Fig. 2.12 – (a) Estimated fracture volume loss (V_{loss}) versus cumulative water production (W_P,) measured during flowback for the studied wells. **(b)** Driving mechanisms during flowback time. CDI is the dominating driving mechanism due to fracture closure during flowback period, modified from [10]

2.3.2.2 Characteristic Fracture Closure Rate (FCR)

Here, we introduce a new parameter called characteristic fracture closure rate (FCR) to represent how fast the effective fractures close. Since the wells have different flowback durations, we normalize the fracture volume loss as $V_{loss_n} = \left(V_{loss} - V_{loss_{min}}\right) / \left(V_{loss_{max}} - V_{loss_{min}}\right)$ and flowback time as $t_{fb_n} = \left(t_{fb} - t_{fb_i}\right) / \left(t_{fb_{max}} - t_{fb_i}\right)$. **Fig. 2.14a** shows that V_{loss_n} versus t_{fb_n} can be described by a power-law model:

$$V_{loss_n} = \left(t_{fb_n}\right)^{1-FCR} \tag{2.13}$$

where,

t_{fb} : flowback time, hrs

t_{fb_i} : initial flowback time, hrs

t_{fb_f} : final flowback time on record, hrs

$V_{loss_{min}}$, $V_{loss_{max}}$: minimum and maximum V_{loss} estimated during flowback, %

This approach is applied on the target 16 wells and the results are shown in **Fig. 2.14b**. The average, minimum and maximum values of R^2 among the 16 wells profiles are 0.962, 0.873, and 0.995, respectively, which denotes good fitness of the proposed power-law model. The curvature of the type curves is controlled by FCR. Higher FCR represents faster fracture closure. This is further revealed by **Fig. 2.13** comparing V_{loss} and V_{loss_n} profiles for 4 wells. The figure shows that wells with higher FCR values have higher fracture volume loss at a fixed flowback time (200 hours).

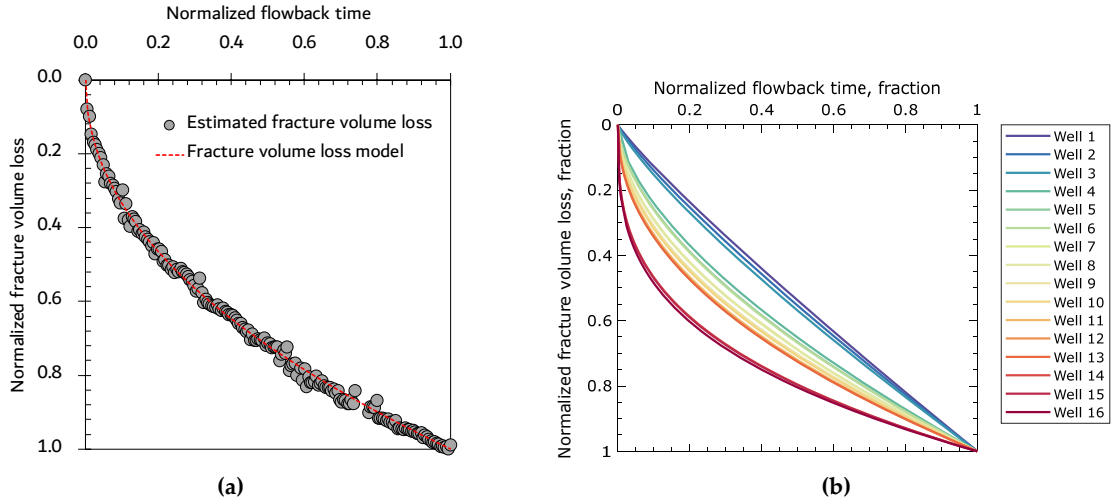

Fig. 2.14 – Normalized fracture volume loss versus normalized flowback time for **(a)** for a candidate well, the dashed line represents the fitting model expressed by Eq. (2.13). **(b)** for the 16 Eagle Ford wells, well 1 has the lowest FCR while well 16 has the highest FCR value.

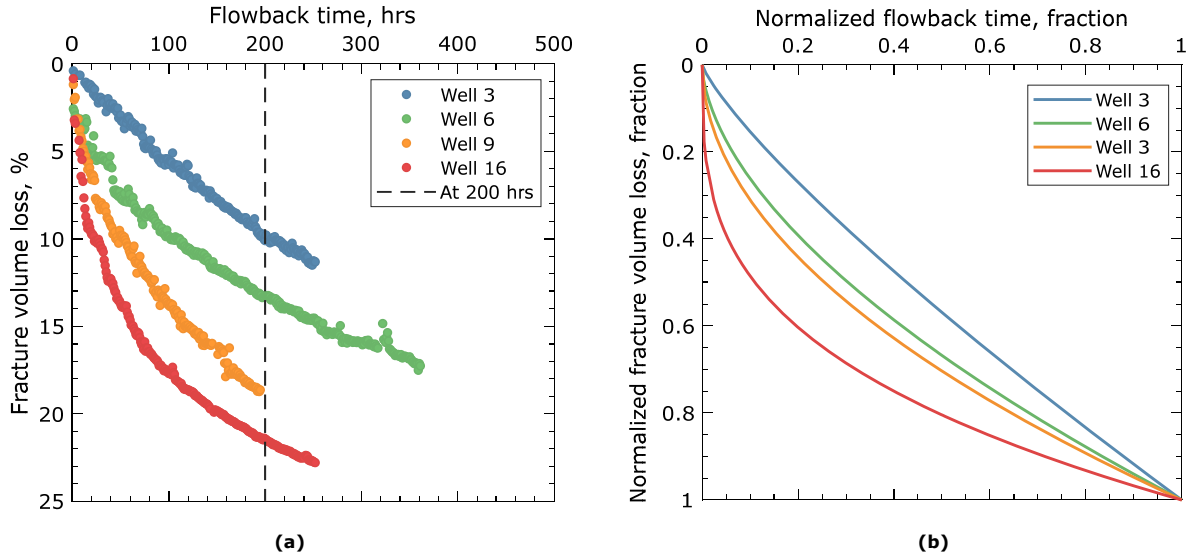

Fig. 2.13 – **(a)** Estimated fracture volume loss during flowback of 4 Eagle Ford wells. **(b)** Normalized fracture volume loss profiles of the same wells. FCR values of wells 3, 6, 9 and 16 are 0.186, 0.417, 0.503 and 0.686, respectively. The wells with higher FCR show more fracture volume loss after 200 hrs.

2.3.3 Data-Driven Correlations Using Multiple Linear Regression

2.3.3.1 Initial Effective Fracture Volume and Completion-Design Parameters

To correlate V_{ef_i} to CDPs, we solve Eq. (2.12) using stepwise forward selection approach as mentioned in the **Multiple Linear Regression** section. First, we applied linear regression between V_{ef_i} and each CDP separately. The first row in **Fig. 2.15** shows the estimated R^2 between each CDP and V_{ef_i}. GPI has

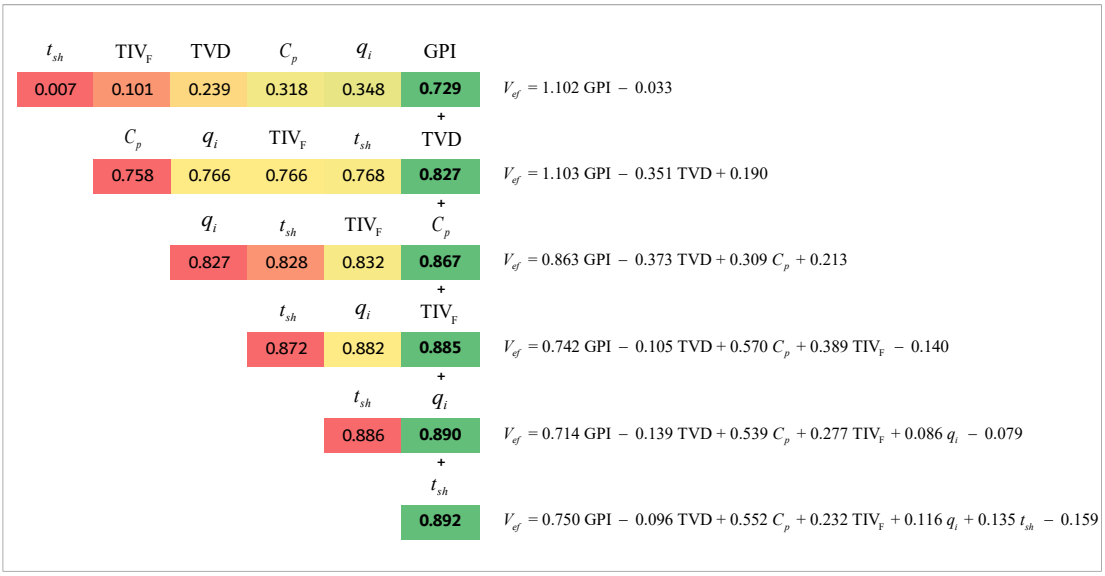

Fig. 2.15 – Workflow of stepwise multiple linear regression (MLR) with forward selection.

the highest correlation with V_{ef_i}. Then, we incrementally added each of the remaining parameters (q_i, C_P, TVD, TIV$_F$ and t_{sh}) to the previous correlation and re-estimated R^2. The results show that TVD has the second highest correlation with V_{ef_i}. This incremental process is repeated to consider all CDPs one-by-one.

The final correlation between V_{ef_i} and CDPs is given by

$$V_{ef_{in}} = 0.750\ GPI_n - 0.096\ TVD_n + 0.552\ C_{p_n} + 0.232\ TIV_{F_n} + 0.116\ q_{i_n} + 0.135\ t_{sh_n} - 0.159 \quad (2.14)$$

The independent parameters in Eq. (2.14) are normalized CDPs defined as $x_n = (x - x_{min})/(x_{max} - x_{min})$, where x, x_n, x_{min}, and x_{max} represent real parameter, normalized parameter, minimum and maximum values, respectively. The values of x_{min} and x_{max} are listed in **Table 2.1**. The normalization step is necessary before applying MLR for 1) having a common scale for all design parameters without distorting differences in the ranges of values, and 2) having consistent units on both sides of Eq. (13). Therefore, the real value of V_{ef_i} is given by

$$V_{ef_i} = V_{ef_{in}} \left(V_{ef_{i_{max}}} - V_{ef_{i_{min}}} \right) + V_{ef_{i_{min}}} \quad (2.15)$$

where $V_{ef_{i_{min}}}$ and $V_{ef_{i_{max}}}$ are the minimum and maximum values of initial effective fracture volume estimated by the HD model, as listed in **Table 2.1**.

Fig. 2.16a shows the V_{ef_i} values predicted by MLR [Eq. (2.12)] versus the values estimated from the HD model for the 22 wells. The results show a good match with R^2 of 0.91 and AAPE of 11%. More than 80% of the V_{ef_i} values are accurately predicted using the MLR correlation that is good considering the limited data points (22 wells) available.

Table 2.1 – Minimum and maximum values of CDPs, V_{ef_i} and FCR

Parameter	Minimum value (x_{min})	Maximum value (x_{max})
C_P, lb/bbl	33.13	82.96
GPI, ft	4,074	10,176
q_i, bpm	66.70	90.66
TVD, ft	9,436	11,015
t_{sh}, days	1	77
TIV_F, bbl/ft	22.65	63.74
V_{ef_i} , m^3	7,121	36,171
FCR, fraction	0.106	0.686

Fig. 2.16b shows the sensitivity of V_{ef_i} to CDPs. GPI has the highest positive effect on V_{ef_i} ; increasing GPI by 10% increases V_{ef_i} by 8.82%. GPI can be increased by increasing number of stages or the stage length depending on operational constrains. q_i has the second highest positive effect on V_{ef_i} . Increasing q_i by 10% increases V_{ef_i} by 1.24%. This suggests that assuming constant injection pressure, increasing q_i during fracturing operation slightly increases the created V_{ef_i} . TVD has negative effect on V_{ef_i} which can be explained by the higher values of in-situ stresses in deeper wells [52]. Increasing TIV_F or C_P by 10% increases V_{ef_i} by less than 1%. t_{sh} has positive-but-insignificant effect on V_{ef_i} , suggesting that soaking time after fracturing has insignificant effect on the created initial effective fracture volume.

2.3.3.2 Correlation Between Characteristic Fracture Closure Rate and Completion-Design Parameters

After calculating FCR for each well, solving Eq. (2.12) using the stepwise forward selection approach, gives the following correlation between FCR and CDPs:

$$FCR_n = -0.675\, C_{P_n} + 0.073\, TVD_n - 0.367\, TIV_{F_n} - 0.051\, GPI_n - 0.405\, q_{i_n} - 0.660\, t_{sh_n} + 1.490 \quad (2.16)$$

The absolute value of FCR is given by

$$FCR = FCR_n \left(FCR_{max} - FCR_{min}\right) + FCR_{min} \quad (2.17)$$

Table 2.1 lists the values of FCR_{min} and FCR_{max}. As mentioned before, only 16 wells are considered in this case due to uncertainties in bottom-hole pressure data of the other 6 wells. **Fig. 2.16c** compares the values of FCR predicted by MLR [Eq. (2.16)] and Eq. (2.13). The prediction accuracy is 80%, which is a reasonable considering the limited number data points (16 wells). The good match is confirmed by an AAPE of 12% and R^2 of 0.88.

Fig. 2.16d shows sensitivity of FCR to CDPs. C_P has the most significant effect on FCR. Increasing C_P by 10% reduces FCR by 10.53%, suggesting that increasing C_P decelerates fracture closure. t_{sh} has the second highest effect on FCR. Increasing t_{sh} by 10% reduces FCR by 1.78%. Increasing q_i or GPI decreases FCR by less than 1%. Increasing TVD increases FCR by 0.58%. This means in deeper wells

(higher TVD), the effective fractures are exposed to faster closure rate. TIV_F has insignificant effect on FCR.

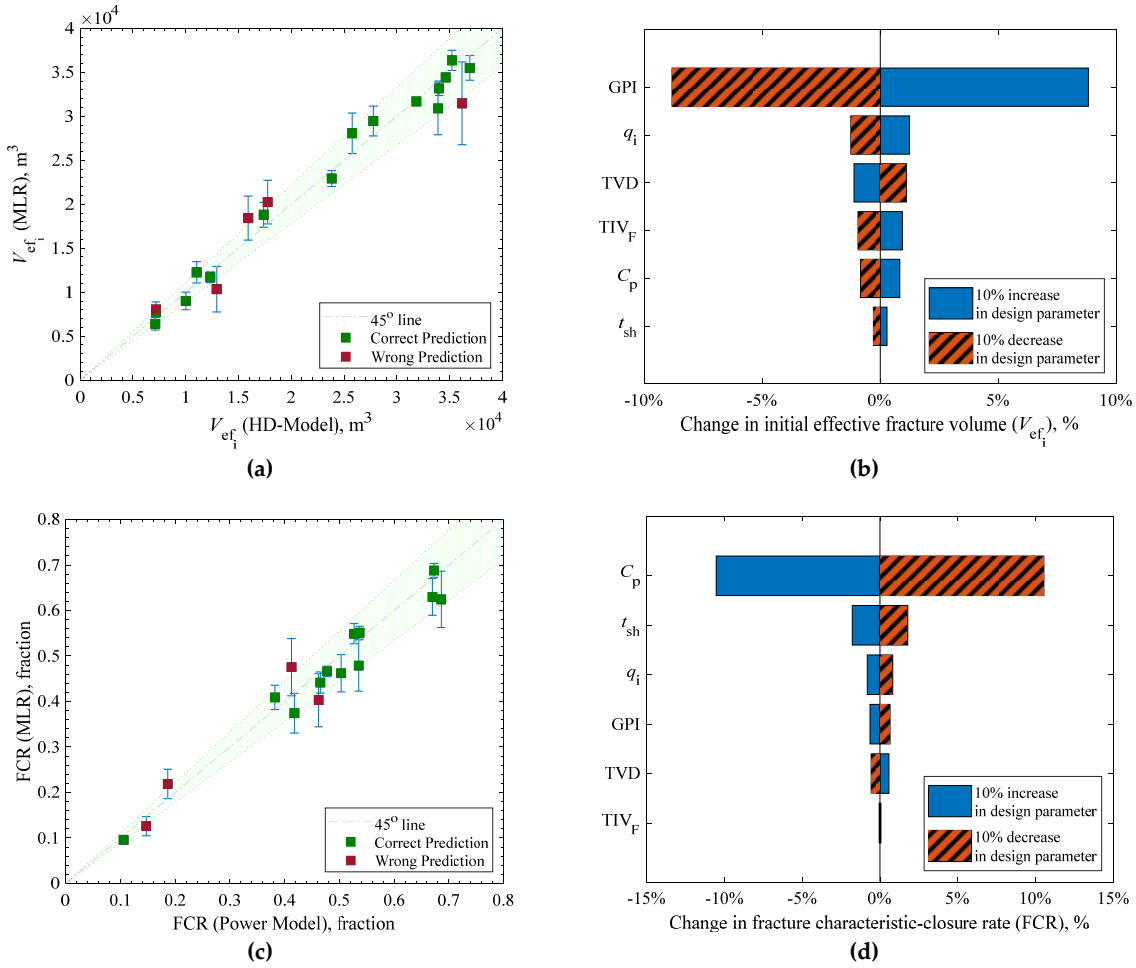

Fig. 2.16 – (a) Crossplot of initial effective fracture volume estimated using the HD model and MLR. **(b)** Sensitivity of initial effective fracture volume (V_{ef_i}) to completion design parameters. **(c)** Crossplot of estimated values of FCR using Eq. (2.13) and predicted values using MLR. **(d)** Sensitivity of characteristic fracture closure rate (FCR) to completion design parameters.

2.4 Summary

This paper proposes; 1) an iterative approach to estimate effective fracture volume as a function of pressure and time. The proposed approach showed that capturing dynamic fracture porosity is crucial when estimating fracture volume loss during flowback; 2) a dimensionless type curve to describe how fast effective fracture volume reduces during flowback. The reduction in fracture volume can be modelled by a power-function of characteristic fracture closure rate (FCR) as $t^{1\text{-FCR}}$; 3) two empirical correlations using multiple linear regression (MLR) to correlate completion-design parameters with initial effective fracture (V_{ef_i}) volume and FCR. The results suggest that the gross perforated interval

has the most significant positive effect on V_{ef_i}, and that proppant concentration is a key parameter that controls FCR and dimishes fracture closure during flowback.

2.5 Nomenclature

AAPE : average absolute percentage error
CC : correlation coefficient
FCR : fracture characteristic-closure rate, ratio
DFIT : diagnostic fracturing injection test
GPI : gross perforated interval, ft
HD : harmonic decline
ISIP : instantons shut-in pressure, psi
MLR : multiple linear regression
TIV : total injected water volume, stb
TIV_F : total injected water volume per foot, stb/ft
TVD : total vertical depth, ft
t_{sh} : shut-in time, days
C_f : fracture compressibility, 1/psi
d_i : initial decline rate, 1/day
M_{prop} : total injected proppant mass, lb
p_n : net stress on fracture, psi
p_{wf} : bottom hole pressure, psi
$p_{closure}$: closure pressure, psi
q_i : pumping rate, bpm
q_w : water production rate, stb/day
q_{w_i} : initial water production rate, stb/day
t_{fb} : flowback time, hrs
t_{fb_n} : normalized flowback time, ratio
V_{ef} : effective fracture volume, stb
V_{ef_i} : initial effective fracture volume, stb
V_{loss} : effective fracture volume loss, ratio
V_{loss_n} : normalized fracture volume loss, ratio
V_{prop} : proppant volume, bbl
W_p : cumulative water production, stb
ϕ_f : fracture porosity, ratio
η : mineralization ratio, %
σ_{min} : in-situ minimum principal stress, psi
ρ_{prop} : proppant density, lb/ft^3

Chapter 3.
Reservoir Quality Versus Completion Intensity: An Application of Supervised Fuzzy Clustering on Western Canadian Well Data

3.1 Introduction

Tight oil and gas reservoirs have been rapidly developed in North America due to the advances in horizontal well drilling technology combined with multi-stage hydraulic fracturing. Recently, large amounts of data have been gathered as more wells have been drilled and fractured [53]. The accumulated data of reservoir characteristics and well-completion design can be analyzed to evaluate their relative impacts on hydrocarbon productivity of the wells. Such evaluations are essential for optimizing future drilling and completion operations. This is made more critical by the recent downturn in oil prices which introduces a big challenge to the oil and gas industry to effectively develop tight reservoirs. Recently, field-data mining has been the most growing tool in the oil and gas industry [54].

Olaoye and Zakhour [55] introduced a workflow based on multivariate statistics on 1,114 wells completed in the Midland and Delaware basins of West Texas to optimize completion design and enhance wells' productivity. The critical completion-design parameters considered in this study are lateral length and proppant loading. The results show that, generally, increasing proppant loading improves well performance by a nonlinear relationship.

Mohaghegh [56] developed a workflow for data-driven analytics to evaluate the parameters controlling production of 800 wells in different shale plays in Texas. The results show that Frac-Hit has the dominant effect on wells' productivity, followed by cross-linked gel concentration and proppant loading, choke setting, formation characteristics and finally completion-design.

Moussa, Dehghanpour [57] quantitively analyzed the effect of completion-design parameters on dynamic fracture volume for 22 oil and gas wells completed in the Eagle Ford formation. The results

show that gross perforated interval has the most significant effect on the initial effective fracture volume and that proppant concentration has the highest effect on fracture closure rate. However, in this study the effect of reservoir characteristics was not considered.

Al-Alwani, Britt [58] analyzed completion design of 80,000 wells completed in different unconventional resources in the United States in terms of the amounts of injected water and proppant, and lateral well length between 2011 and 2018. The results show a significant increasing trend in the volume of water and proppant consumed over the explored period. Another study done on 2,000 wells completed in the Marcellus shale found that the long-term cumulative hydrocarbon production is increased by increasing the volumes of pumped water and proppant per foot up to a threshold value, after which it shows a negative trend [59]. Therefore, there is one critical question: Is it really necessary to inject such high volumes of water and proppant to improve wells' productivity? In this study, we analyze the effects of completion design as a function of reservoir characteristics. We try to answer the following key questions: Does intensive completion design assist in improving hydrocarbon productivity of wells completed in low-quality reservoirs? Can completion-design negatively affect the formation productivity in high-quality reservoirs?

In this paper, we first introduce the difference between fuzzy- and crisp-set theories, and the application of fuzzy-set theory to classify each of the studied reservoir characteristics and completion-design parameters. Next, we develop SFC algorithm in which we use fuzzy rules to correlate these parameters to reservoir quality and completion intensity for each well. Subsequently, we investigate the relative impacts of reservoir quality and completion intensity on wells' productivity. Finally, we discuss the results from SFC analyses and present the conclusions.

3.2 Methodology

To understand the relative impacts of reservoir quality and completion-design parameters on wells' productivity, we collected the related data for 1,784 multi-fractured horizontal oil and gas wells completed in different tight formations in the Western Canadian Basin. The reservoir characteristics are represented by average formation porosity (ϕ_{avg}), initial reservoir pressure (p_i), hydrocarbon saturation (S_{hc}) and net pay thickness (h_{net}). The completion-design is represented by number of fracture stages (N_s), average injected water volume per stage ($q_{i,s}$) and proppant concentration (C_p) in the injection fluid. The well's productivity is represented by first year cumulative barrel of oil equivalent (BOE) because both oil and gas wells are included in this study.

Fig. 3.1 shows the variation of reservoir characteristics among the studied wells and it demonstrates that the contour maps do not overlap. The part of a reservoir with high ϕ_{avg} (**Fig. 3.1a**) does not

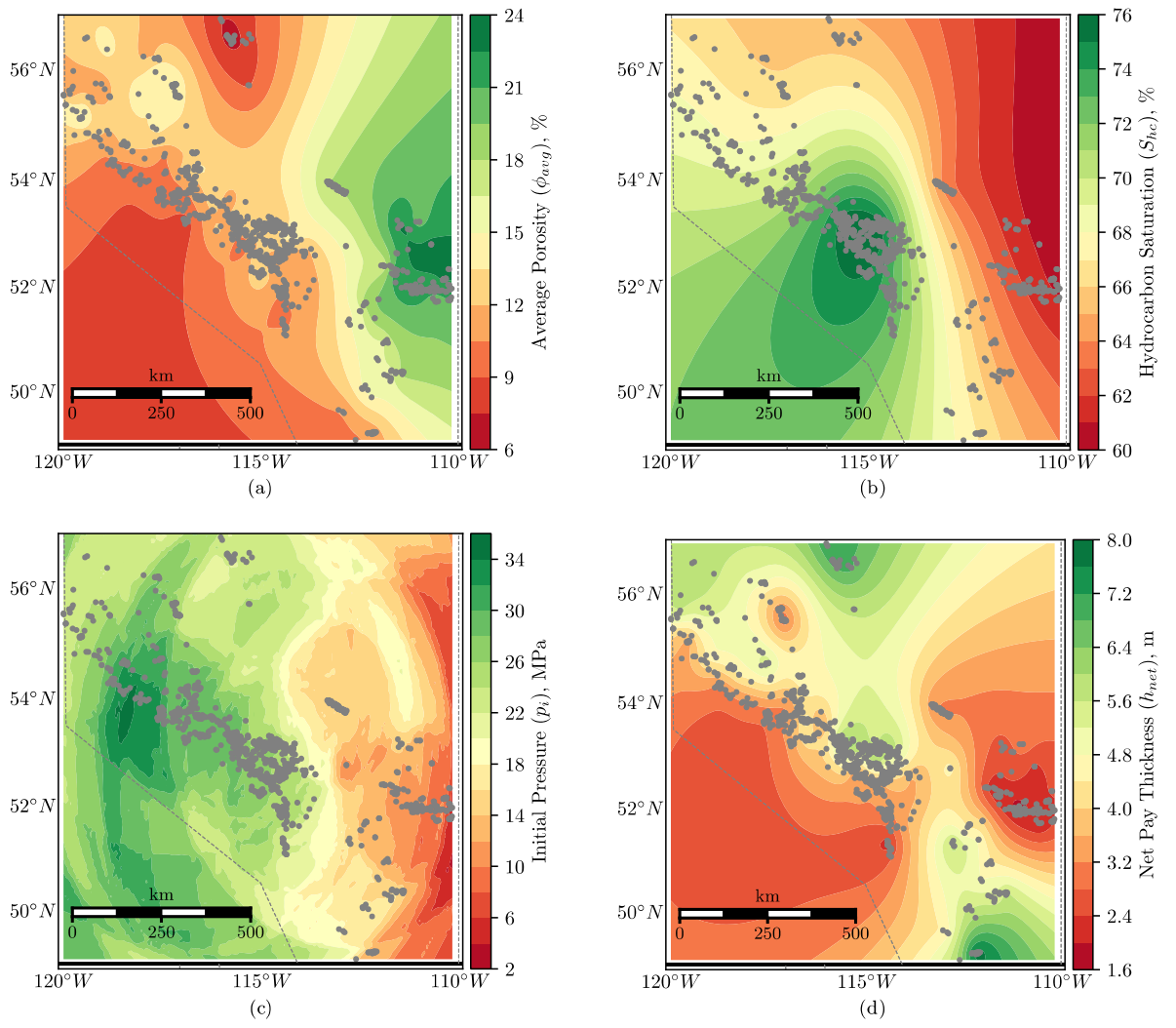

hydrocarbon saturation, **(c)** initial reservoir pressure and **(d)** net pay thickness

necessarily have high S_{hc}, p_i and h_{net} (**Fig. 3.1b**, **c** and **d**, respectively). This conveys the importance of applying multivariate analysis in this study, compared to single-variable analysis, to combine these characteristics in one term as reservoir quality, and to investigate its correlation with BOE.

In this study, we develop a supervised fuzzy clustering (SFC) algorithm as a multivariate analysis tool to 1) classify reservoir quality and completion intensity for each well; and 2) correlate them with wells' productivity in terms of BOE. Reservoir quality refers to the quality of the part of the formation where each well is completed. Good reservoir quality refers to relatively higher p_i, S_{hc}, ϕ_{avg} and h_{net}, while poor reservoir quality refers to the opposite. Completion intensity represents how intense the completion-design is by considering the combined effects of N_s, $q_{i,s}$ and C_p. Higher completion

intensity refers to more stages, higher proppant concentration and larger volume of injected water per stage.

3.2.1 Fuzzy Set Theory

In this study, fuzzy classification method is used instead of other pure statistical classification methods (such as k-means) for a physics-based data analysis. In crisp sets, in pure statistical classification techniques, a value either belongs to a specific cluster or not [60]. For example, assume that poor-quality reservoirs can be defined as those with $S_{hc} \leq 60\%$ and that good-quality reservoirs are those with $S_{hc} \geq 60\%$. Therefore, if S_{hc} of a reservoir is 59.9%, it will be classified as a poor-quality reservoir and if S_{hc} = 60.1% it will be classified as a good-quality reservoir. However, from the petroleum engineering prospective, 0.1% difference in S_{hc} does not change the reservoir quality.

In fuzzy classification, we have $M_A(x) = m$, meaning that the membership of value x in fuzzy set A is m, where m is between 0 to 1. **Fig. 3.2** shows hydrocarbon saturation profiles using three membership functions (Low, Medium and High) as an application of fuzzy set theory. The figure demonstrates that if S_{hc}=58%, it is not considered 100% a low-, medium- or high-saturation. Instead, it has 12% membership in the fuzzy set Medium ($M_{Medium}(58) = 0.12$) and 88% membership in the fuzzy set Low ($M_{Low}(58) = 0.88$). In fuzzy set theory, every value is a member in each set but with different membership-degree. In this study, fuzzy-set profiles are generated for **a)** reservoir characteristics: p_i, ϕ_{avg} S_{hc} and h_{net}; **b)** completion-design parameters: N_s, $q_{i,s}$ and C_p; and **c)** reservoir quality and completion intensity.

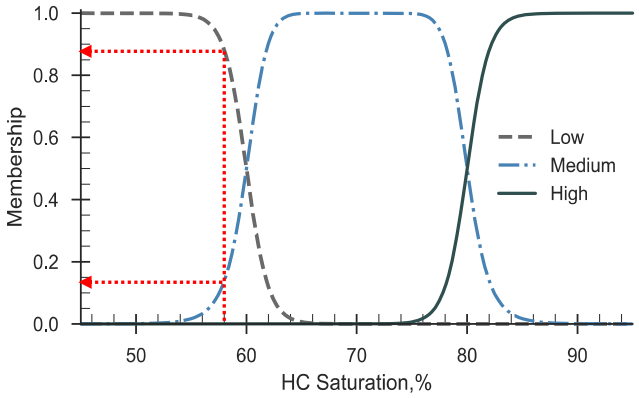

Fig. 3.2 – Hydrocarbon saturation profiles as membership functions of low, medium and high in the fuzzy theory. Hydrocarbon saturation of 58% is considered to have 12% membership in fuzzy set Medium and 88% membership in fuzzy set Low

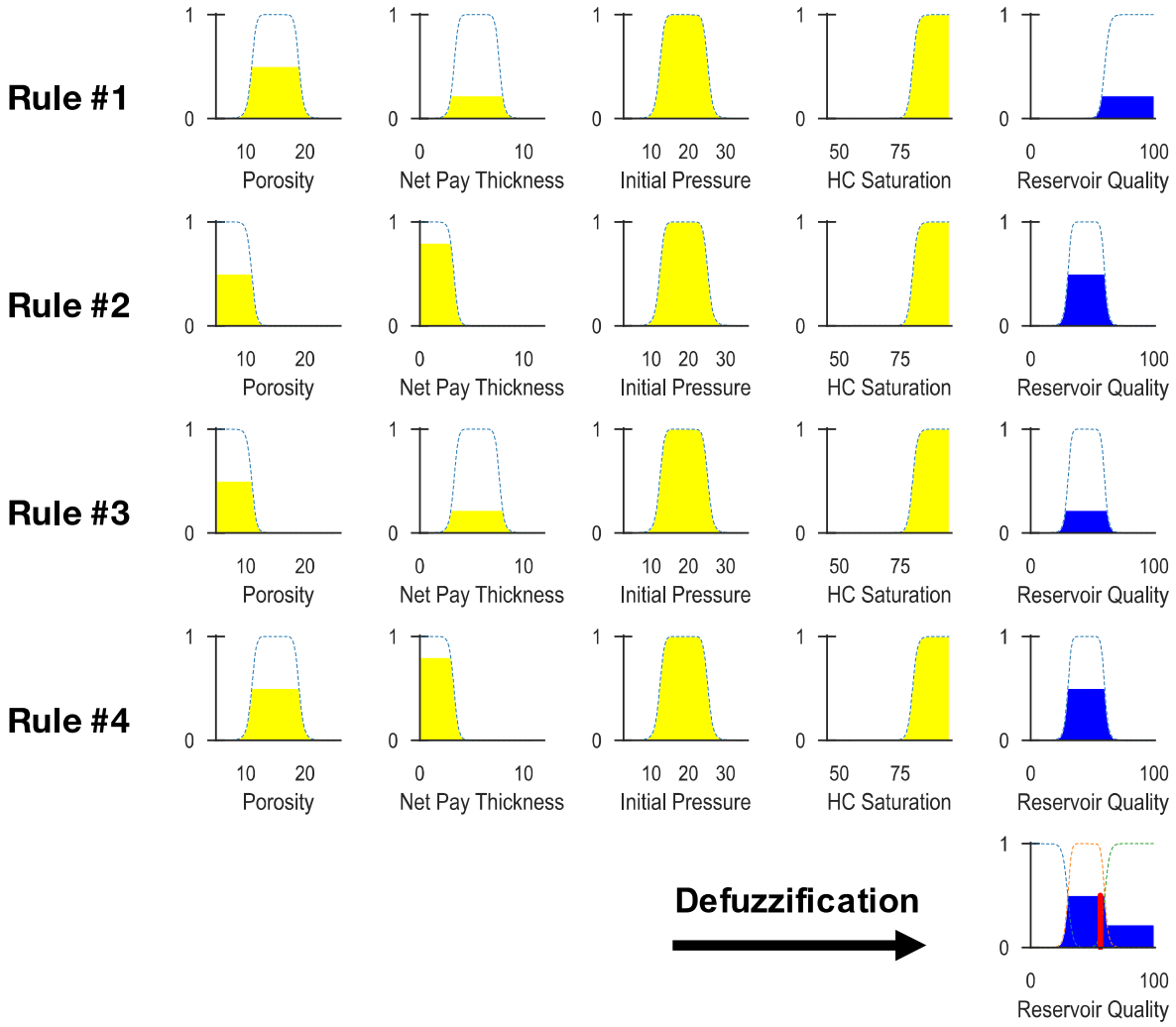

Fig. 3.3 – Example of fired fuzzy rules based on input reservoir characteristics [ϕ_{avg}, h_{net}, p_i, S_{hc}] = [11%, 3m, 20Mpa, 90%] to estimate reservoir quality.

3.2.2 Approximate Reasoning

We use approximate reasoning (fuzzy rules) to connect the fuzzy-sets of reservoir characteristics to reservoir quality, and those of completion-design parameters to completion intensity. In fuzzy rules, linguistic variables (low, high, poor, good, etc.) and operators (and, or) are used for connecting fuzzy sets. The correlation between inputs and output is achieved through SFC algorithm in three steps:

I. Activation of input membership function: **Fig. 3.3** shows an example of the four activated (fired) rules when the input is a well completed in a part of a reservoir with [ϕ_{avg}, h_{net}, p_i, S_{hc}] = [11%, 3m, 20Mpa, 90%]. As per the defined fuzzy sets, ϕ_{avg} of 11% is considered between low and medium fuzzy sets. Therefore, their two membership functions are activated, and the

same for h_{net} as shown in the figure. p_i of 20Mpa and S_{hc} of 90% are considered medium and high, respectively. Therefore, only the medium and high membership functions are activated for p_i and S_{hc}, respectively.

II. Activation of output membership function: This is done by fuzzy rules. Rule #1 shown in **Fig. 3.3** states that "IF ϕ_{avg} is Medium AND h_{net} is Medium AND p_i is Medium AND S_{hc} is High THEN Reservoir Quality is Good". In this case, the membership function of Good for reservoir quality is activated as shown in right-top corner of the figure. As the operator AND is used, the minimum value of the input membership functions is assigned to the output membership function. In Rule #3, ϕ_{avg} becomes Low, while other characteristics are the same, therefore, the reservoir quality is considered Average instead of Good.

III. Defuzzification: After applying all the fuzzy rules to connect p_i, ϕ_{avg}, S_{hc} and h_{net} to reservoir quality for each rule, we combine the output fuzzy sets together. Then, we defuzzify the final set as shown in the right-bottom corner of the figure to obtain one value representing the reservoir quality. There are several defuzzification methods but the most common one is the centroid method [61].

The main challenge for applying fuzzy clustering approach is the curse of dimensionality [62] which means that the number of fuzzy rules increases significantly with increasing the number of variables and/or membership functions. The number of fuzzy rules is estimated as $\prod_i^n m_i$, where n is the number of input variables and m is the number of membership functions of each variable. In the case of reservoir quality classification, there are four input variables (p_i, ϕ_{avg}, S_{hc} and h_{net}) and each parameter has three membership functions (Low, Medium and High). Therefore, the total number of fuzzy rules is 81. Similarly, for the completion intensity, the number of fuzzy rules is 27 as there are three input variables (N_s, $q_{i,s}$ and C_p) and each variable has three membership functions. In this study, we generate the fuzzy rules by first digitalizing linguistic variables to create digital rules, then convert the rules back to linguistic format as valid inputs for the SFC algorithm.

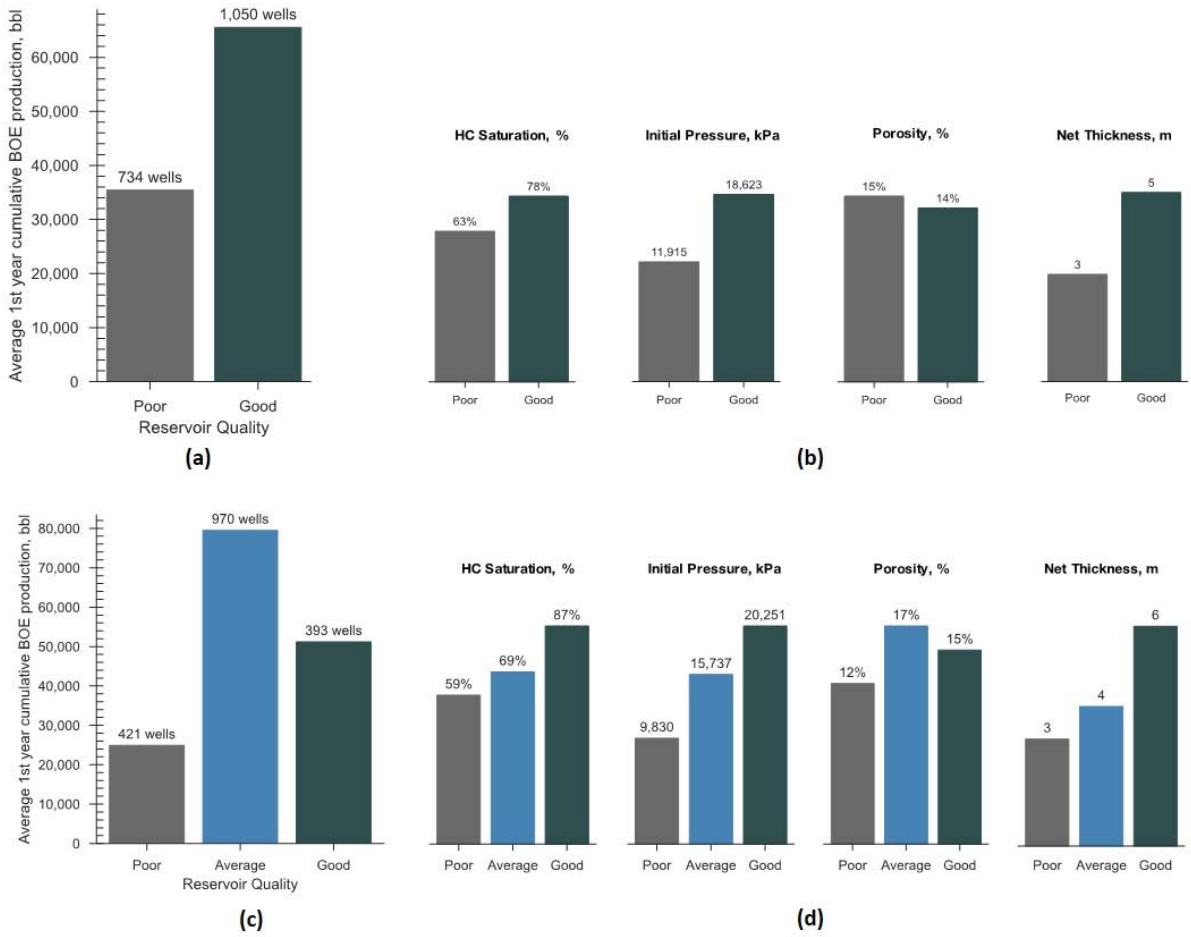

Fig. 3.4 –Classification results of 1,784 oil and gas wells in terms of **(a)** two clusters of poor and good quality reservoirs versus $Q_{BOE,1}$ and **(b)** associated average reservoir properties in each cluster. **(c)** Three clusters of poor, average and good quality reservoirs versus $Q_{BOE,1}$ and **(d)** associated average reservoir properties in each cluster

3.3 Results and Discussion

3.3.1 Does Productivity Follow Reservoir Quality?

For a comprehensive analysis, we classify the studied 1,784 wells into two categories of poor and good in terms of reservoir quality. **Fig. 3.4** shows the results of this analysis based on the reservoir characteristics. **Fig. 3.4**a demonstrates that wells completed in good-quality reservoirs (GQR) have higher productivity, in terms of average first year cumulative BOE production of each well ($Q_{BOE,1}$), compared to wells completed in poor-quality reservoirs (PQR). Almost 40% of the studied wells are completed in PQR and around 60% of the wells are completed in GQR. **Fig. 3.4b** shows that GQR has average S_{hc}, p_i, ϕ_{avg} and h_{net} of 78%, 18,623 kPa, 14% and 5m, respectively. Therefore, GQR

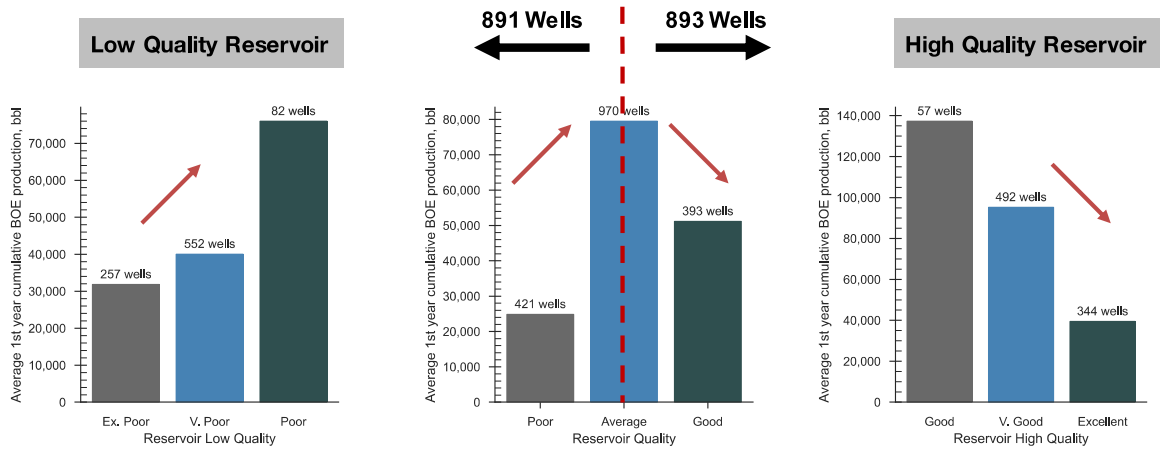

Fig. 3.5 –Increasing the classification granularity from three clusters (poor, average and good) to six clusters. Low quality reservoir consists of Extremely poor-, very poor- and poor-quality reservoir. High quality reservoir consists of good, very good and excellent quality reservoir

represents thicker reservoirs with higher hydrocarbon saturation and initial reservoir pressure, validating the results of SFC.

Fig. 3.4c shows the classification results when the granularity increases from two clusters to three clusters of poor, average and good in terms of reservoir quality. The figure shows that more than 50% of the wells are completed in average-quality reservoirs (AQR) and that these wells show more productivity than the wells completed in GQR. In this case, the productivity does not follow reservoir quality. $Q_{BOE,1}$ of each of the 970 wells completed in AQR is almost 80,000 bbl compared to 50,000 bbl for each of the 393 wells completed in GQR. Yet, GQR still represents better reservoir characteristics in terms of higher S_{hc}, p_i, and h_{net} compared to AQR as shown in **Fig. 3.4d**.

To understand why the productivity does not strictly follow reservoir quality, we increase the classification granularity of the 1,784 wells from three clusters to six clusters as shown in **Fig. 3.5**. The figure shows that almost 50% of the wells are completed in extremely poor-, very poor- and poor-quality reservoirs and we combine these three clusters as low-quality reservoirs (LQR). The other 50% of the wells are completed in high-quality reservoirs (HQR), representing good-, very good-, and excellent-quality reservoirs. In LQR, the productivity follows reservoir quality. Therefore, wells completed in poor-quality parts of the reservoir have more BOE productivity than wells completed in very poor and extremely poor parts, respectively. However, in HQR, wells productivity shows negative correlation with reservoir quality. Wells completed in excellent parts of the reservoirs show less BOE productivity than wells completed in

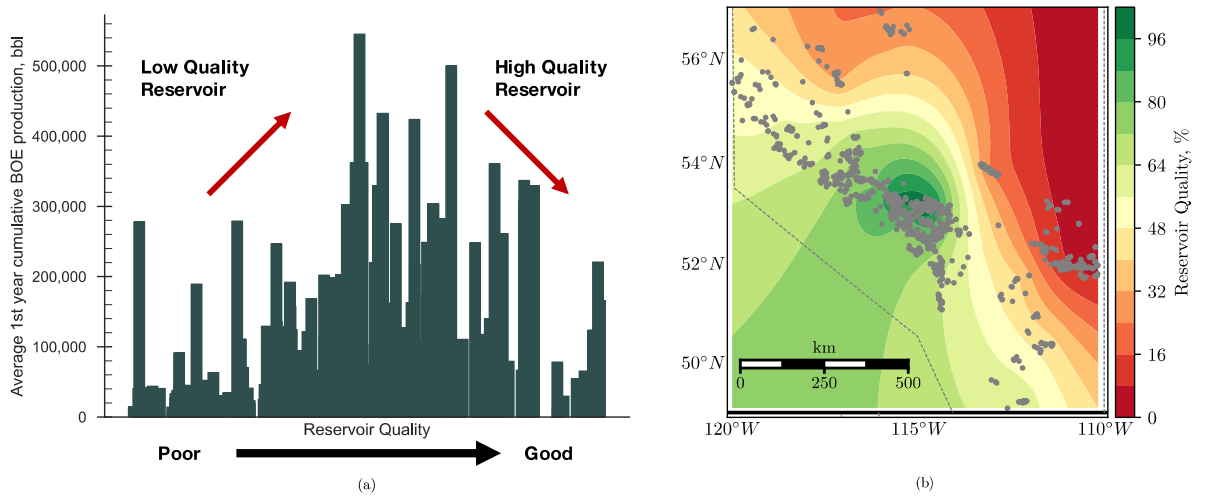

Fig. 3.6 –(a) Increasing the reservoir quality classification granularity to 100 clusters between poor and good reservoir quality versus average first-year cumulative BOE production. **(b)** contour map of the estimated reservoir quality of 1,561 wells completed in Alberta.

very good and good parts of the reservoirs. To verify this trend, we increase the classification granularity to 100 clusters from poor- to good-quality reservoirs as shown in **Fig. 3.6a**. This higher-resolution classification confirms our previous observation that in LQR, productivity follows reservoir quality, while it does not show the same trend in HQR. Therefore, unlike the common concept that the quality of conventional reservoirs is the key parameter controlling well's productivity, in tight reservoirs this concept is not always valid [63]. This is an interesting observation, particularly as the standard practice in the oil and gas industry is to complete as many wells as possible in good parts of the reservoir. This is demonstrated in **Fig. 3.6b**, where the majority of wells completed in Alberta are in good-quality parts of the reservoirs. However, this standard practice, alone, does not guarantee higher productivity for the wells completed in HQR compared to the wells with more efficient completion-design completed in AQR. Therefore, it is important to understand the effect of completion-design parameters on productivity of the wells completed in HQR.

3.3.2 Effect of Completion Design on Wells' Productivity

3.3.2.1 Completion Design in High-Quality Reservoirs

Fig. 3.7 demonstrates the average value of C_p, N_s and $q_{i,s}$ for each reservoir-quality cluster in HQR (893 wells). The wells in excellent-quality reservoirs are completed with less $q_{i,s}$ and C_p than the wells in GQR. Therefore, this might be the reason for relatively low productivity of excellent-quality reservoirs compared with that of GQR. However, N_s does not follow this trend. Therefore, single-variable analysis cannot explain the negative correlation between wells' productivity and reservoir

quality in HQR. In the next section, multivariate analysis is applied using SFC to clarify the effect of completion-design parameters on wells productivity.

3.3.2.2 Completion Intensity Controls Wells' Productivity

In order to understand the combined effects of C_p, N_s and $q_{i,s}$ on wells' productivity, we apply SFC to classify the 1,784 wells based on completion intensity. Higher completion intensity represents more stages, larger volume of water injection per stage and higher proppant concentration. **Fig. 3.8a** shows classification of the studied wells into three clusters of low, moderate and high completion intensity versus $Q_{BOE,1}$. The figure indicates positive correlation between completion intensity and wells'

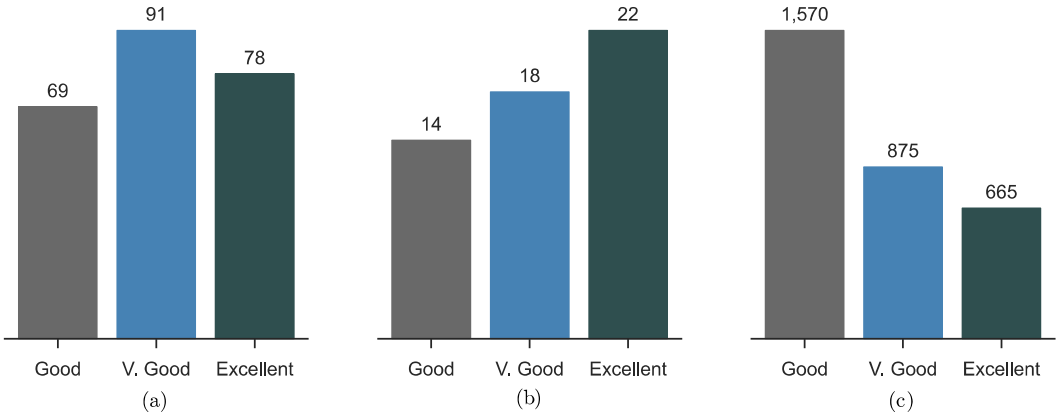

Fig. 3.7 –(a) Average completion-design parameters of each cluster of reservoir quality. **(a)** proppant concentration, lb/bbl. **(b)** number of stages. **(c)** injected water volume per stage, bbl

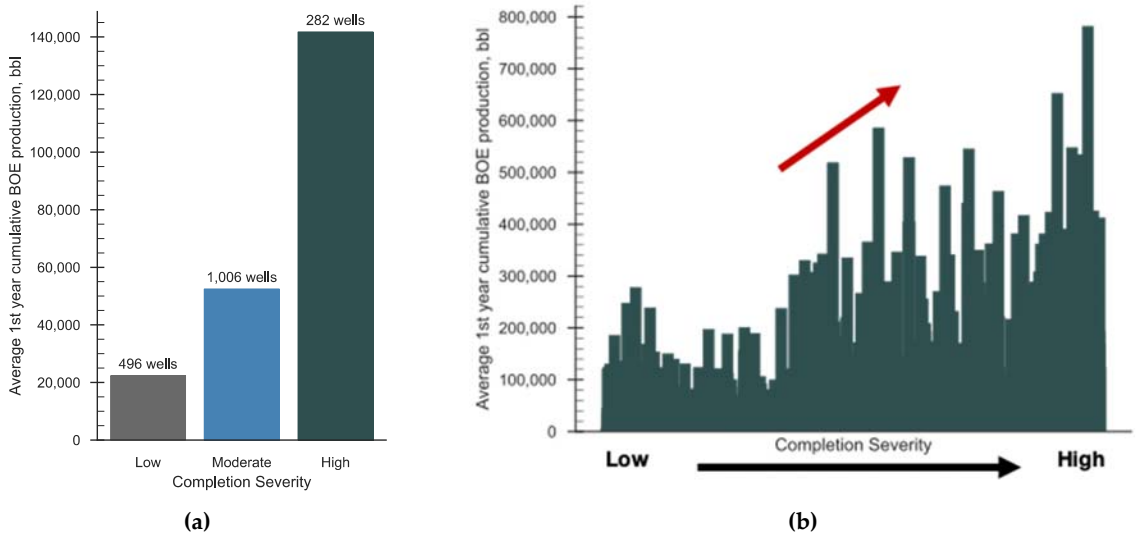

Fig. 3.8 – Classifying completion intensity versus average first-year cumulative BOE production into **(a)** three clusters of low, moderate and high, and **(b)** 100 high-resolution clusters from low to high

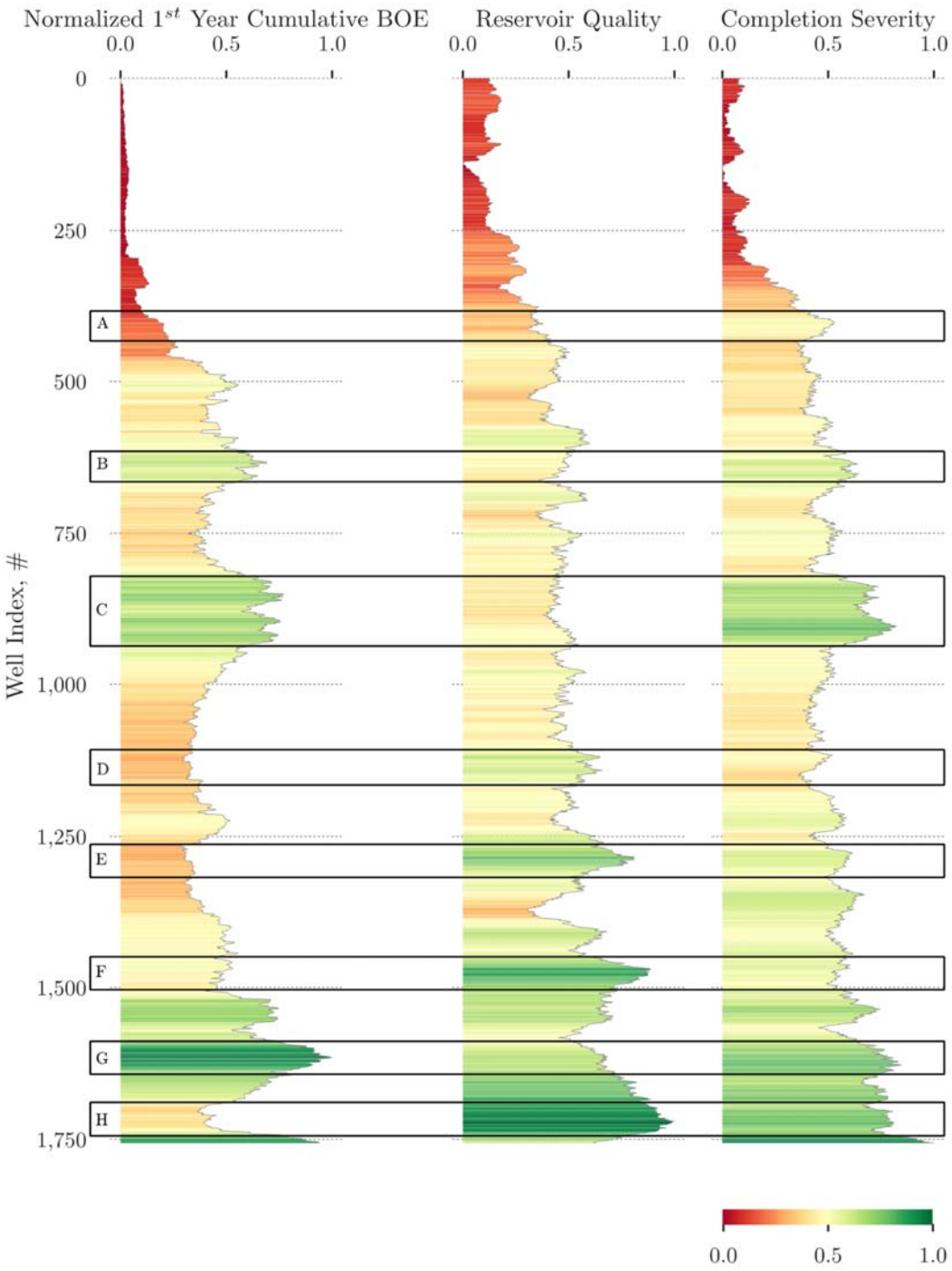

Fig. 3.9 – Normalized first year cumulative BOE, reservoir quality and completion intensity versus well index of the 1,784 studied wells with different regions highlighted; A – H.

productivity regardless of reservoir quality. Wells completed intensively with more stages, larger water volume injection per stage and more proppant concentration, generally, produce more BOE

than wells with less completion intensity. This outcome still holds when the classification granularity increases to one hundred clusters, as shown in **Fig. 3.8b**.

Fig. 3.9 shows normalized first-year cumulative BOE, reservoir quality and completion intensity estimated for all the studied wells calculated using $x_n = (x - x_{min})/(x_{max} - x_{min})$. Here, x_n is the normalized value of x based on minimum and maximum values, x_{min} and x_{max}, respectively. Therefore, a value of zero for normalized first year cumulative BOE, reservoir quality or completions intensity refers to the lowest productivity, quality or intensity among the studied wells, respectively, while a value of one refers to the highest. There are several observations from this figure:

a) In low-quality reservoirs, the effect of completion design on well productivity is not significant as shown in Region A in the figure. Although the completion intensity is medium, the wells' productivity is low due to low reservoir quality. This observation emphasizes that in low-quality reservoirs, well productivity follows reservoir quality.
b) In medium- to high-quality reservoirs, the effect of completion design becomes more significant. Regions B and C show more than average well productivity and more than average completion intensity, although reservoir quality is below the average. Region G shows high well productivity, intense completion, and average reservoir quality. On the other hand, Regions D, E and F show less than average well productivity, less intense completion, and good reservoir quality.
c) In high-quality reservoirs, the well productivity could be limited as a result of non-intense completion design as shown in Region H. Although the wells of these regions are completed in the highest-quality parts of the reservoirs, the wells' productivity is below average. It should be mentioned that in this region, the completion intensity is above average, but it is not as intense as that in Region G which shows more productivity despite its average reservoir quality.

3.4 Summary

We classified 1,784 oil and gas wells completed in different formations in the Western Canadian Basin Sedimentary using a supervised fuzzy clustering approach, and arrived at the following conclusions: a) Almost 50% of the studied wells are completed in poor-to-average (low quality) parts of the reservoirs and the other 50% are completed in average-to-good (high-quality) parts of the reservoirs;

b) In low-quality reservoirs, the effect of completion-design on productivity is less pronounced and the productivity follows reservoir quality; c) In high-quality reservoirs, the effect of completion-design becomes more significant and the productivity can be reduced due to inefficient completion-design; and d) The productivity can be maximized by less intense completion-design in low-quality reservoirs. However, in high-quality reservoirs, intense completion significantly improves the productivity.

This case study shows how the functional dependence of well productivity on completion-design varies depending on reservoir quality. Outcomes of this study can assist oil and gas operators to optimize completion-design parameters as a function of reservoir quality to maximize the economic return.

3.5 Nomenclature

ϕ_{avg} : v E" ,•;"spb ,X •<Db, s^b ,brD<>5aP s

K @A§5fs s: v E" ,•;"spD,r<s>"•,s`zX z•<DE"s@A§s^ ,biz`<Db, s

v K « s susv E" ,•;"sK z•<D<>s« "r" ,EbD,s

@A§s sus@•,,"<rsbpsA D<s§jzDE•<",<s

C_p s susv E" ,•;"s^ ,b^^•,<s`b, `",<,•<Db, 5s<a|aa<s

ŧ K « s sus+ bbisK z•<D<>s« "r" ,EbD,s

h_{net} s susw "<s^•>s<yD`L, "rr5sX s

\ K « ss sus\ D;ysK z•<D<>s« "r" ,EbD,s

N_s s susw zX a" ,sbpsp,•`<z ,"sr<•;"rs

¡ K « s sus¡ bb ,sK z•<D<>s« "r" ,EbD,s

$p_{i\,s}$ sus&,D<D•<s,"r" ,EbD,s^ ,"rrz ,"5s7 ^•s

$q_{i,s}$ s susv E" ,•;"sD,¢"`<"is/•<" ,sEb<zX "|r<•;"5saa<rs

WS } s susWz^" ,EDr"isS zYY>s} <zr<" ,D,;s

$S_{hc\,s}$ sus\ >i ,b`•,ab,sr•<z ,•<Db, 5sP s

Chapter 4.
Coupled Versus Stratified Flow of Water and Hydrocarbon During Flowback And Post-flowback Processes

4.1 Introduction

Multi-fractured horizontal well (MFHW) is a proven technology to produce oil and gas from tight formations. Hydraulic fractures increase wells' productivity by increasing the surface area in contact with formation and providing highly-conductive paths to the wellbore. The use of diagnostic plots to identify water and hydrocarbon flow regimes is an important step to evaluate and optimize the performance of MFHW.

Song, Economides [64] analyzed field data from several shale gas formations. They observed that the typical flow regimes during production include fracture storage, linear flow normal to transverse fractures and pseudo-steady state. Compound linear flow and infinite-acting regimes have been added for completeness, but typically an economic rate limit is reached before these flow regimes can be observed. Recent studies reported pseudo-steady state (PSS) behavior of water flow at early production time in the presence of hydrocarbon influx from matrix into fractures. This PSS behavior of water is indicated by a unit-slope in the RNP diagnostic plots. Alkouh, McKetta [35] introduced a field case of MFHW completed in the Barnett Formation. Early production data showed PSS of water in the presence of gas flow in fractures (two-phase flow). Similar observations were reported by Jia, Cheng [65]. Hossain, Ezulike [66] analyzed post-flowback production data of six shale-oil wells completed in the Eagleford Formation and showed that at early flowback period, wells did not show PSS behavior. However, during post-flowback period, the authors observed prolonged unit-slope signature on water RNP plots. Clarkson, Yuan [67] analyzed early production data of MFHW completed in a Canadian tight oil reservoir and reported PSS behavior of water before and after oil breakthrough into fractures. Zhang and Emami-Meybodi [68] showed that two-phase boundary-dominated flow in fractures is the most dominant regime for water flow during the early production period.

Semi-log plots of WOR versus cumulative oil production has been utilized as a simple technique to predict oil recovery in reservoirs undergoing waterfloods. Bush and Helander [69] studied 86 successful waterfloods in Oklahoma and observed the hyperbolic decline trend in oil production rate (q_o) as WOR increases during water flooding. Ambastha and Wong [70] conducted a detailed investigation of production decline data from 78 oil pools under waterflooding in the Western Canadian Sedimentary Basin. They showed that q_o generally follows a hyperbolic decline trend when the reservoir is under waterflood condition. Yang [71] proposed a production-decline analysis method to forecast waterflood performance from historical production data. This method is derived on the basis of the Buckley Leverett's 1D displacement theory, assuming a semi-log relationship between the ratio of oil and water permeabilities and water saturation. The author presented field cases that showed that his method could be utilized to predict ultimate oil recovery.

In this paper, we 1) investigate the relationship between water and oil production from six fractured horizontal wells before and after installing jet pumps showing that the general observation of PSS water flow indicates water production from the stimulated part of the reservoir, which is acting like a pseudo-closed tank, in the presence of simultaneous hydrocarbon production; 2) extend the diagnostic analysis of water and oil flow regimes and presenting a novel observation, from field production data, that both oil and water can flow independently with different flow regimes at early production time; and 3) extend the concept of WOR decline from waterflood systems to forecast recovery performance of MFHWs completed in tight formations.

4.2 Methodology

This paper hypothesizes that 1) oil and water can flow independently with different drive mechanisms at early production time, and 2) semi-log plot of WOR versus cumulative water production can be used as a relatively more robust diagnostic tool to evaluate well performance. We analyze early production data of six multi-fractured horizontal black-oil wells completed in Eagleford Formation to qualitatively test our hypotheses by analyzing various diagnostic plots in the following steps:

Table 4.1 – Summary of drilling and fracturing parameters of the six target wells

Well Name	Measured Depth, ft	True Vertical Depth, ft	Gross Perforated Interval, ft	Fracture Stages	Total Fluid, bbl	Total Proppant, 10^6 lbs	Soaking Days
Well-1	12,577	5,609	6,507	26	359,817	10.67	69
Well-2	12,533	5,564	6,443	25	362,690	10.68	69
Well-3	12,695	5,531	6,611	27	352,939	10.96	69
Well-4	12,411	6,715	6,481	26	386,322	10.23	55
Well-5	12,442	5,455	6,577	26	369,887	10.66	54
Well-6	12,502	5,427	6,526	26	368,851	10.39	54

1- Prepare field data by cleaning and validating surface data measurements and converting them to bottomhole conditions.
2- Analyze diagnostic plots of early production rates and pressure of the target wells. Key output of this step is estimating initial reservoir pressure utilizing the approach proposed by Jones, Pownall [72].
3- Construct diagnostic water and oil rate-normalized pressure (RNP) plots to identify water and oil flow regimes.
4- Quantify and compare the drive mechanisms of fracture closure, water expansion and hydrocarbon expansion during early production time to identify the dominant drive mechanisms during this period and the effect of hydrocarbon breakthrough.
5- Derive HD model of water production rate to estimate ultimate water recovery and analyze the effects of aggressive drawdown on water and oil recovery.
6- Examine the HD behavior of WOR data versus cumulative water production volume and how it could be utilized to compare load recovery performance of the target wells.
7- Analyze the effects of completion-design parameters on oil and water productivity.

4.2.1 Reservoir and Well Information

Fig. B.1a shows the location of the six multi-fractured horizontal black-oil wells completed in the oil window of the Eagleford Formation. **Fig. B.1b** shows the layout of Wells 1-3 and Wells 4-6 in Pads A and B, respectively. The lateral spacing between these wells varies from 732 to 764 ft. The wells were drilled with true vertical depth (TVD) varying from 5,426 to 6,715 ft as listed in **Table 4.1**. Well-4 is almost 1,200 ft deeper than the other wells. The wells were completed with 25 to 27 fracture stages, total injected water volume (TIV) of 360 to 386 x 10^3 bbl, and proppant mass of 10.23 to 10.96 x 10^6 lbs. The shut-in period, between the completion date and first production date, varies from 54 to 69 days.

4.2.2 Early Production Rate and Pressure Analysis

Fig. 4.1a shows semi-log plots of the early 3-months daily rates (water, oil and gas) and surface pressure (casing and tubing) data for Well 2. **Fig. B.2** shows the plots of the other wells. The sudden increase in tubing pressure after 1,500 – 1,800 hours of production is due to jet-pump installation. The choke-size is kept at 28/64" until jet-pump installation, then it is increased to 64/64". The casing pressure initially decreases then increases during early period of production before jet-pump

installation. The decrease in casing pressure indicates the wellbore and fracture storage, while the increase suggests wellbore unloading. After jet-pump installation, the surface casing pressure remains almost constant as the wells are produced through tubing.

4.2.2.1 Low Initial Reservoir Pressure

Wells 5 and 6 are the only wells that demonstrate early single-phase flowing period as shown in **Fig. B.2d** and **e**. During this period, the casing pressure declines until reaching a minimum value of 350 to 375 psi. Following the procedure proposed by Jones, Pownall [72], we approximate the initial reservoir pressure by the bottomhole pressure when the minimum casing pressure is reached. By considering the hydrostatic pressure, the estimated reservoir pressure gradient for wells 5 and 6 is in the range of $0.491 - 0.515$ psi/ft. that is relatively low compared with Eagleford wells [66], explaining their relatively low oil rates. In addition, this relatively low reservoir energy could explain the significant decrease in water production before jet-pump installation which suggests consistent pressure depletion in fractures without sufficient pressure support from matrix.

4.2.2.2 Single- and Multi-Phase Flow

Fig. B.2d and **e** demonstrate 4 days of single-phase water flow for wells 5 and 6. However, the other wells show immediate multiphase production. Although the six wells are located in the same area of the reservoir and they also have similar completion designs, there are two possible reasons for the immediate multiphase production: 1) Relatively-longer shut-in periods for wells 1, 2 and 3 as listed in **Table 4.1** compared to wells 5 and 6. Therefore, during long shut-in time, fracture pressure might be dropped below reservoir pressure allowing oil influx into fractures. 2) For well 4, the immediate multiphase production is possibly due to a relatively higher initial reservoir pressure compared to the other wells as it is almost 1,200 ft deeper than the other wells as listed in **Table 4.1**. Therefore, the fracture pressure may drop below reservoir pressure during shut-in period, leading to immediate multiphase production.

4.3 Results and Discussion

4.3.1 Behavior of Oil Production Rate

Fig. 4.1a shows that, in general, q_o increases, stabilizes and then declines; in the early 500 hours, the q_o increases, then reaches to a plateau until the jet-pump installation when it increases sharply and then declines. The gas rate also shows similar variations. Therefore, the produced gas is expected to be sourced from the dissolved gas in produced oil. However, the figure shows that water production rate (q_w) exhibits an independent decline trend before the jet-pump installation, then it is coupled with

oil production decline after the pump installation. This observation suggests that before the pump installation, oil and water production rates are controlled by two different drive mechanisms. However, after pump installation and aggressive drawdown, both oil and water are apparently produced under similar drive mechanisms.

The choke-size remains constant before installing the jet-pumps, and thus, it is not the reason of increasing oil production in the early 500 hours. According to Darcy's law, q_o is proportional to fracture permeability (k_f), oil relative permeability (k_{ro}) and pressure differential in fractures which could be approximated by the difference between average pressure in fracture ($p_{f,avg}$) and bottom hole pressure (p_{wf}):

$$q_o \propto k_{ro} k_f (p_{f,avg} - p_{wf}) \tag{4.1}$$

So, in general, the observed three trends of q_o could be explained as follows:

a) The early increase in q_o is due to consistent oil influx from the matrix into fractures, increasing oil saturation (S_o) and relative permeability.

b) The plateau of q_o can be possibly explained by the balance between increasing S_o and pressure depletion in fractures. In other words, the drawdown decreases with time since the fracture pressure decreases. In addition to the reduction in absolute fracture permeability due to fracture closure. However, the reduction in driving force is masked by the increase in average oil relative permeability in fractures.

c) The significant decline in oil production after the jet-pump installation suggests the dominance of pressure depletion mechanism over the increase in S_o in fractures. It also suggests that oil is drained from a limited effective stimulated reservoir volume as illustrated by Hossain, Ezulike [66].

4.3.2 Independent Flow Regimes for Water and Oil

In order to diagnose flow regimes of water and oil during early production period before jet-pump installation, we use plots of rate-normalized pressure for water and oil (RNPW and RNPO) versus time. RNPW and RNPO are defined as $(p_i - p_{wf})/q_w$ and $(p_i - p_{wf})/q_o$ for water and oil respectively. p_i is initial pressure in the stimulated region around wellbore (psi), p_{wf} is the flowing bottomhole pressure (psi), and q_w and q_o are the production flow rate (bbl/day) of water and oil at bottom hole conditions respectively.

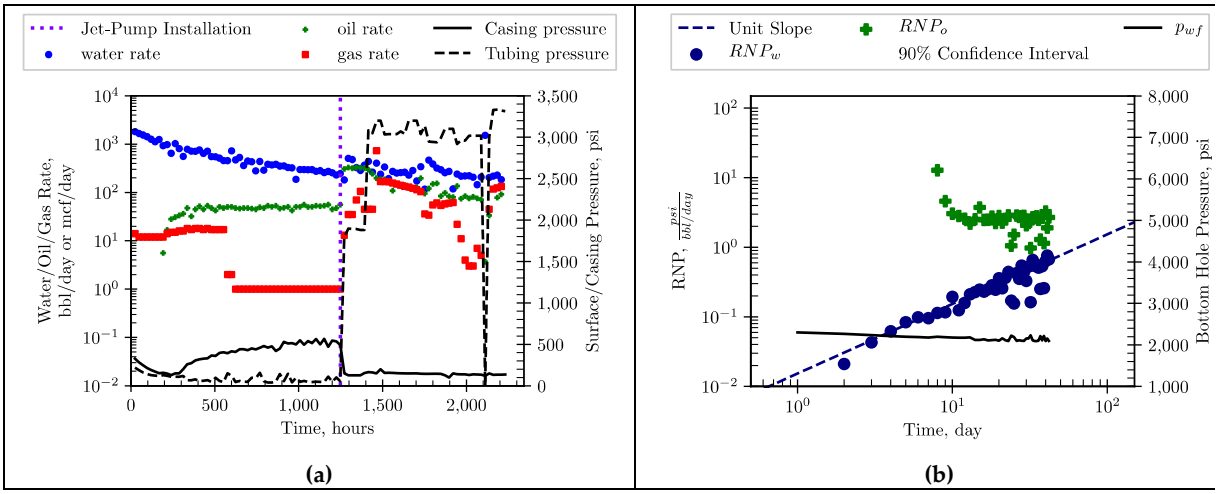

Fig. 4.1 –(a) Semi-log plot of water/oil/gas rates and tubing/casing pressure for Well 2. Sudden increase in rates and tubing pressure is due to jet-pump installation after 1,500 hours. **(b)** Log-Log plot of water/oil rate-normalized pressure (RNP) before jet-pump installation for Well 2.

Fig. 4.1b shows the diagnostic plots of RNPw and RNPo under bottomhole conditions for Well 2 before jet-pump installation. **Fig. B.3** shows the plots of the other wells. Generally, plots of RNPw for all the wells show a pronounced unit slope during early production time indicating PSS flow regime or boundary-dominated flow. This suggests depletion of water from a closed tank with no-flow outer boundaries. In other words, the stimulated region acts like a tank for water with no water influx from matrix. The stimulated region here represents induced fractures and the surrounding stimulated matrix.

The plots of RNPo of all the wells reveal a steady state flow of oil phase. The flat (zero-slope) period suggests that there is oil influx from matrix into fractures and that it is equivalent to the produced oil. So, the pressure depletion in the fracture system is compensated by the increase in oil relative permeability due to the increase of S_o in fractures as oil expands due to reduction in average fracture pressure.

The early negative slope (noticeable in Wells 1, 2, 4 and 6) suggests the domination of oil relative permeability effect over pressure depletion in fractures. So, although these wells show continuous decrease in p_{wf} which means an increase in $\Delta p = (p_i - p_{wf})$, RNPo decreases with time. This could be explained by the increase of q_o during this time, which suggests a significant increase in oil relative permeability due to substantial increase of S_o in fractures that overcomes the effect of pressure depletion on q_o. RNPo of Well 4 does not exhibit a clear zero-slope due to the instability/noise in the estimated p_{wf} as shown in **Fig. B.3c**.

4.3.3 Quantification of Drive Mechanisms

As mentioned earlier, Wells 5 and 6 show single-phase water flow at early time before oil breakthrough. However, **Fig. B.3d** and **e** demonstrate PSS flow of water (unit slope) before and after oil breakthrough for Wells 5 and 6, respectively. This may brace the concept of independency between water and oil flow regimes. So, in this section, we quantify the drive mechanisms to understand the reason of insignificant effect of oil breakthrough on the PSS flow of water.

The possible drive mechanisms during this stage include fracture closure and expansion of hydrocarbon and water. As illustrated by Ezulike, Dehghanpour [9], these drive mechanisms could be quantified by compaction-drive index (CDI), hydrocarbon-drive index (HDI) and water-drive index (WDI):

$$CDI = \frac{c_f}{c_t} \tag{4.2}$$

$$HDI = \frac{S_o c_o + S_g c_g}{c_t} \tag{4.3}$$

$$WDI = \frac{S_w c_w}{c_t} \tag{4.4}$$

$$CDI + HDI + WDI = 1 \tag{4.5}$$

1. Plot the unit-slope data of PSS duration of water on Cartesian plot and estimate the slope (m).

2. Estimate effective fracture volume and fracture compressibility profiles as functions of bottom hole pressure as demonstrated by Moussa, Dehghanpour [57].

3. Estimate total compressibility (c_t) where $c_t = \frac{1}{mV_{ef}}$ as explained by Ezulike, Dehghanpour [9].

4. Estimate average water saturation in fracture from Eq. (4.7)

5. Estimate CDI, WDI and HDI from Eqs. (4.2), (4.4) and (4.5) respectively.

Fig. 4.2 – Flow diagram of estimating compaction, water and hydrocarbon drive indices.

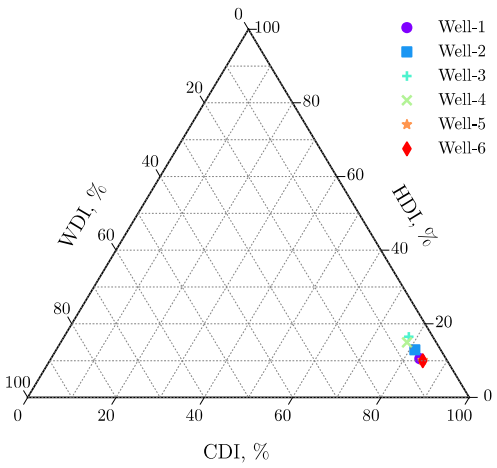

Fig. 4.3 – Ternary diagram of average compaction-, hydrocarbon- and water-drive indices (CDI, HDI and WDI, respectively) for the six target wells during early production period before installing jet-pump.

In this paper, we complement the approach proposed by Ezulike, Dehghanpour [9] to estimate the three drive indices by considering dynamic effective fracture volume [57]. **Fig. 4.2** demonstrates the procedure to estimate CDI, HDI and WDI profiles as functions of bottom hole pressure. **Fig. B.4** shows the profiles of CDI, HDI and WDI during this stage. Due to the relatively low bottom hole pressure, which is lower than the closure pressure, fracture closure comes into effect from the beginning of production. The figure demonstrates that fracture closure is the dominant drive mechanism during early production. It also shows that with time 1) CDI decreases due to the decrease in fracture pressure and hence the fracture compressibility, 2) HDI increases due to the increase in hydrocarbon saturation in fractures, and 3) WDI decreases due to the combined effects of decreasing water saturation and pressure in the fractures. The change in the driving indices is not significant due to the slight decrease (10%) in bottom hole pressure during this period. However, it obviously shows the dominance of fracture closure over hydrocarbon and water expansion during this period, as demonstrated by the ternary diagram presented in **Fig. 4.3** showing the average CDI, HDI and WDI of each well during this stage. The dominance of fracture closure could explain the insignificant effect of hydrocarbon breakthrough on PSS flow regime of water (unit-slope) observed before and after the breakthrough. **Fig. B.4d** and **e** show that after hydrocarbon breakthrough for Wells 5 and 6, fracture closure is still the dominant driving mechanism and that CDI accounts for 80 to 90% of the early water production before and after hydrocarbon breakthrough. Therefore, the water flow regime is not significantly affected by the hydrocarbon breakthrough in these two wells.

One may argue about the insignificant effect of wellbore storage in these wells. The reason for not detecting the wellbore storage effect is the large volume of water recovered in the first day (≈ 1,400

bbl) compared to the wellbore volume (≈ 380 bbl), suggesting that the wellbore storage comes to an end after the first day of production.

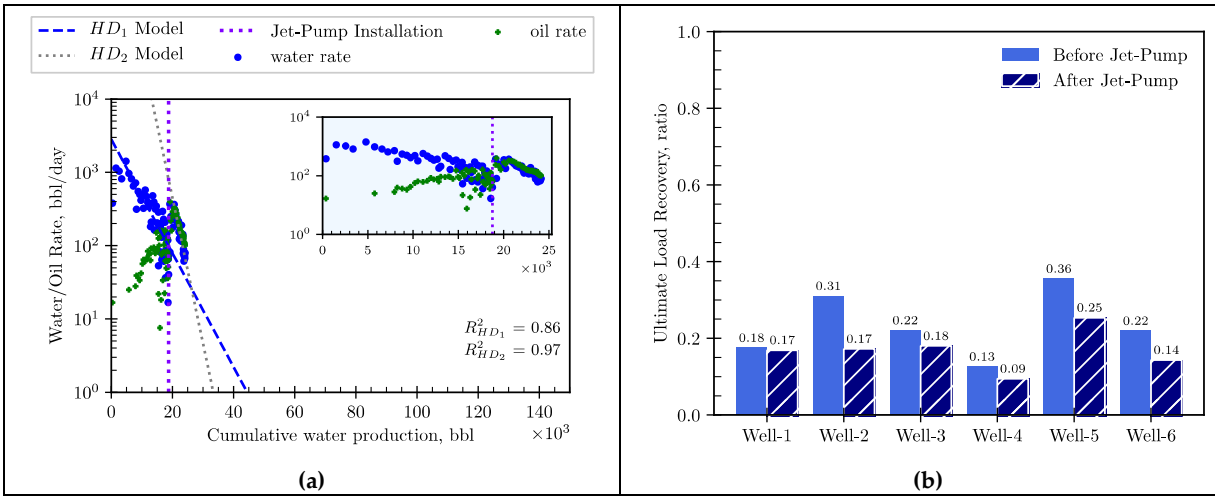

Fig. 4.4 –(a) Semi-log plot of water and oil rates versus cumulative water production volume for Well 2. Sudden increase in rates is due to jet-pump installation. The inset plot zooms the early water and oil rates. **(b)** Ultimate load recovery estimated based on the water-rate decline trend before and after jet-pump installation for the six target wells

4.3.4 Harmonic Decline Analysis Before and After Pump Installation

Fig. 4.5a shows the semi-log plots of water and oil rates versus cumulative water production volume for Well 4, and the plots of remaining wells are shown in **Fig. B.5**. The q_w can be fitted by the HD model with a relatively good match, represented by average coefficient of determination (R^2) of 0.83 and 0.82 before and after jet-pump installation, respectively. Generally, after installing the jet-pump, the water rate declines faster. The figure shows a slight increase in water-rate decline trend in Well-1 and a relatively small increase in Wells 3 and 4. Wells 2, 5 and 6 show relatively bigger increase in water-rate decline after pump installation. Consequently, and assuming that the HD trend continues and that it can be used to estimate ultimate water recovery [57], less fracturing water is expected to be recovered due to jet-pump installation. In other words, an aggressive production strategy may lead to more significant loss in load recovery with more fracturing water remaining unrecoverable as shown in **Fig. 4.5b**. The ULR estimated from the water-decline trend after pump installation is less than the value estimated before aggressive production. The figure also shows that the highest ULR (0.36) is for Well 5, while the lowest (0.13) is for Well 4. The relatively low ULR may also suggest that the early oil breakthrough increases S_o in fractures, reducing water relative permeability which allows bypassing of water by oil in fractures and consequently less ULR. Well 4 that shows the lowest ULR is 1,200 ft deeper than the other wells and has the highest average tubing pressure before pump-installation. The higher reservoir pressure suggests stronger oil influx from matrix into fractures

during early production period. However, early oil breakthrough results in bypassing of water in fractures and thus lower ULR.

4.3.5 Water Oil Ratio

Fig. B.6 shows the semi-log plots of WOR versus cumulative water production for the six wells. The results highlight two key observations: 1) a general straight-line behavior in WOR data suggesting a HD; and 2) the effect of operational changes such as jet-pump installation and choke-size adjustment have less pronounced effect on shifting HD trend compared to water rate-decline as demonstrated in **Fig. B.5**. The average R^2 between WOR data and the fitted HD model is 0.90 compared to 0.83 for the case of water-rate data.

Our interpretation for the first observation is that the plot of WOR versus cumulative water production can be used as a proxy to the change in the ratio between water and oil relative permeabilities with water saturation. So that 1) WOR is equivalent to the ratio between water and oil relative permeabilities according to Darcy's law, as WOR is mainly a function of mobility ratio, which depends on relative permeability assuming a relatively constant oil/water viscosity as expressed by

$$WOR = \frac{q_w}{q_o} \propto \frac{k_{rw}}{k_{ro}} \tag{4.6}$$

Therefore, WOR is not expected to be sensitive to the operational changes, especially choke-size change and it could be treated as a reservoir response. This also interprets our second observation; and 2) the change in water production could be considered proportional to the change in average water saturation in fractures. Ezulike and Dehghanpour [34] showed that assuming negligible mobile formation water, average water saturation (S_w) in fractures could be estimated as a function of

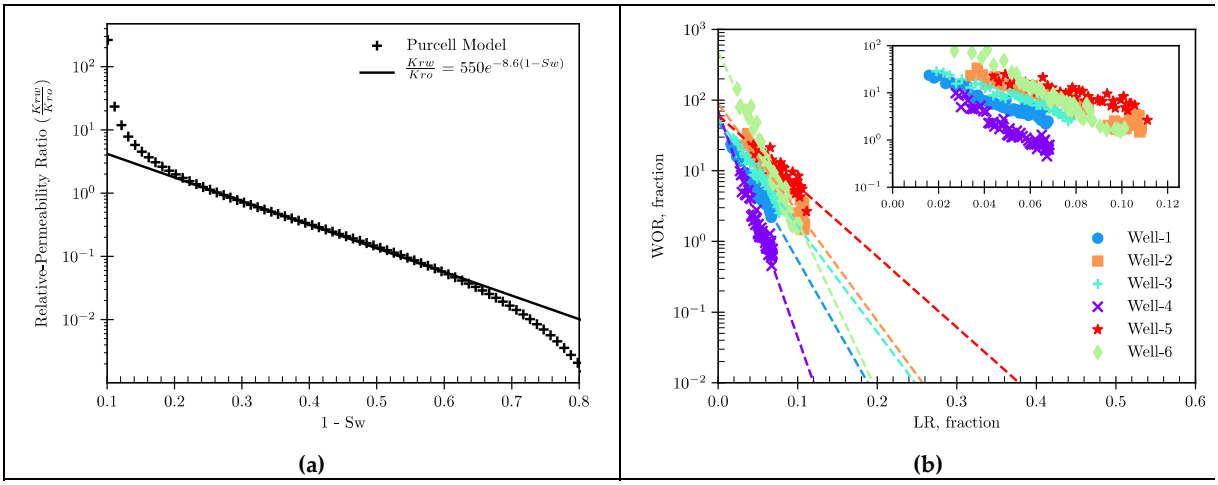

Fig. 4.5 – Semi-log plots of **(a)** water/oil relative permeability ratio estimated by Purcell model shows approximate linear section in the middle portion of water saturation range. **(b)** water-oil ratio versus load recovery generally shows straight-line decline behavior for the six target wells.

cumulative water production (Q_w), effective fracture volume (V_{ef}) and initial water saturation (S_{w_i}) in the fractures:

$$S_w = S_{w_i} - \frac{Q_w}{V_{ef}} \tag{4.7}$$

Fig. 4.5a shows $\frac{k_{rw}}{k_{ro}}$ calculated from Purcell [73]'s model:

$$\frac{k_{rw}}{k_{ro}} = \frac{(S_w^*)^{\frac{2}{\lambda}+1}}{1-(S_w^*)^{\frac{2}{\lambda}+1}} \tag{4.8}$$

Here, S_w^* is normalized water saturation and λ is the pore-size distribution index. An approximate semi-log linear segment can be observed in the intermediate range of water-saturation (0.35 – 0.80). This

section can be fitted by using the exponential model [74, 75] expressed by Eq. (4.9), where a and b are obtained by regression of the linear segment.

$$\frac{k_{rw}}{k_{ro}} = ae^{b(1-S_w)} \tag{4.9}$$

Similar to the observations of Yang [71], this result shows that exponential model can be used to approximate Purcell model for a wide range of water saturation. This explains the HD trend observed in the semi-log plots of WOR versus cumulative water production.

Fig. 4.5b compares the semi-log plots of WOR versus load recovery for the six wells, confirming the HD behavior. Wells 4 and 5 have the highest and lowest decline slopes. Assuming that WOR can be approximated by Eq. (4.9), the results suggest that a slight change in water saturation in fractures contributes to a significant change in k_{rw}/k_{ro} for Well 4 and less significant change for Well 5. This

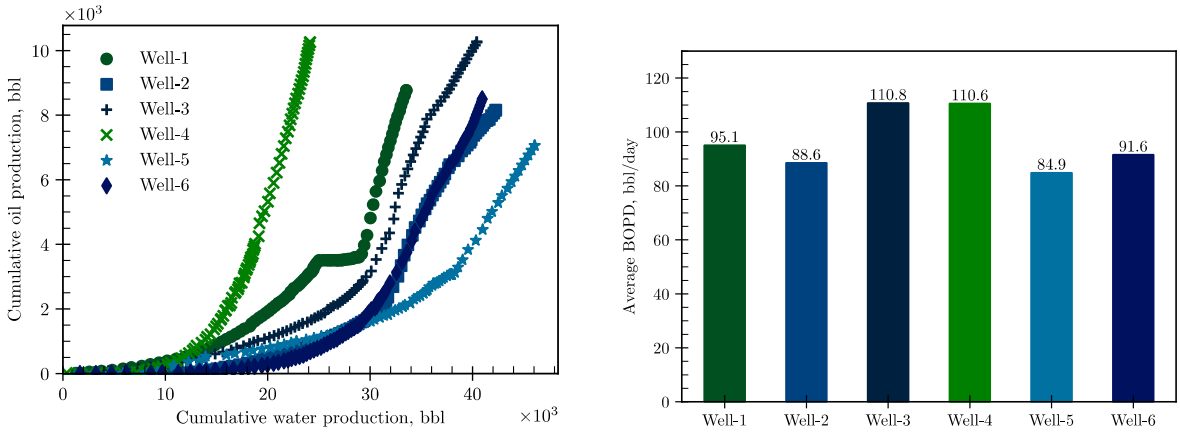

Fig. 4.6 – Comparison of early-production behaviour of the target wells in terms of **(a)** cumulative oil production versus cumulative water production and **(b)** average oil production rate in the early 3 months of production.

demonstrates that multiphase effect plays an important role in water and oil production of the target wells. **Fig. 4.5b** also shows that Well 4 has the lowest load recovery followed by Wells 1, 6, 3, 2, and 5, qualitatively similar to the trend observed in **Fig. 4.4b**. So, considering that WOR decline trend versus load recovery is less sensitive to operational changes compared to water rate-decline, it might be utilized as a more accurate tool to compare load recovery of different wells.

4.3.6 Completion-Design Effects on Wells' Productivity

Fig. 4.6a shows the cumulative oil production versus cumulative water production for the six candidate wells. There are two main observations: 1) the asymptotic behavior of the oil production suggests that a negligible amount of formation water is being produced. 2) the mobility ratio tends to favor oil production for Well 3 and 4, whereas it tends to favor the water production for Well 5. Generally, Well-4 shows the highest slope while Well 5 shows the lowest slope. This means that recovering the same volume of water leads to more oil production in Well 4 compared to Well 5. The figure also shows that Wells 3 and 4 produce the largest volume of oil during the first 3 months of production, while Well 5 produces the least oil volume during the same period. Similar behavior could be noticed in **Fig. 4.6b** which shows the average daily oil production (BOPD) for the early 3 months of production (excluding down times) for the six wells. Again, Wells 3 and 4 show the maximum BOPD while Well 5 shows the lowest rate.

To understand the possible reason(s) for the observed variations in oil and water productivity of the six wells, we estimated the correlation coefficient (CC) between completion-design parameters with the estimated BOPD and ultimate load recovery (ULR) as shown in **Fig. 4.7**. The completion-design parameters considered in this study are number of fracture stages, injected water volume per stage (IVPS), proppant concentration (PC) and total vertical depth (TVD). The figure shows that both BOPD

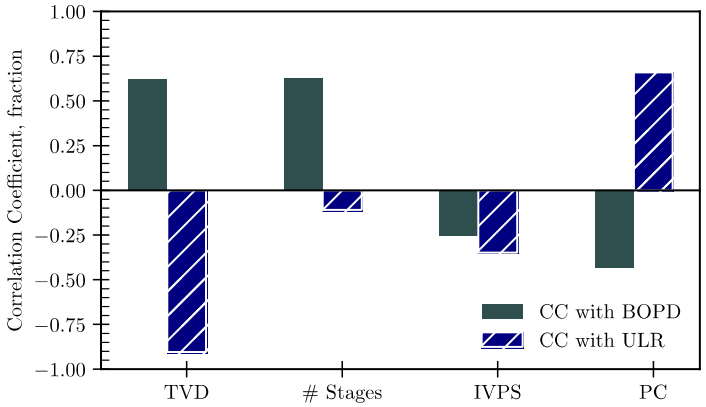

Fig. 4.7 – Correlation coefficient of completion-design parameters with average oil production rate (BOPD) and ultimate load recovery (ULR). TVD: true vertical depth, IVPS: injected water volume per stage, and PC: proppant concentration.

and ULR values are positively correlated to TVD and number of stages. So, deeper wells with more fracture stages produce more than shallower wells with less stages. Deeper wells are expected to have more reservoir energy (higher pressure), and increasing the number of stages leads to larger contact area between the wellbore and formation. However, both parameters have negative effects on ULR, suggesting more water leak-ff and trapping in deeper wells with higher number of fracture stages. IVPS has negative effects on both the early oil production and ULR. So, more water injection per stage leads to more unrecovered water and consequently less oil productivity due to the relative permeability effects. Although PC has a positive effect on ULR, it negatively affects the early oil productivity. Increasing PC enhances fracture conductivity and reduces the chance for fracture closure and leak-off, both leading to more water recovery. The negative correlation between PC and BOPD could be due to two reasons: 1) The reduction in fracture closure and water leak-off reduces the counter-current production of hydrocarbon from matrix during the shut-in period. 2) Increasing PC leads to less complex fracture network as more viscosifier agents are needed to enhance proppant carrying capacity of the fracturing fluid. Increasing the viscosity leads to simpler induced fracture network and consequently less interface for oil production. Although the negative correlation between PC and BOPD is less pronounced (-0.43), the results illustrated in **Fig. 4.6** support this observation. Wells 1, 3 and 4, which show the best early oil-productivity (i.e. highest BOPD and cumulative oil production), have the lowest PC values among the target wells, while Well 5, with lowest oil productivity, has the highest PC.

4.4 Summary

We analyzed multiphase production data of six multi-fractured horizontal black-oil wells completed in the Eagleford Formation. Below is a summary of the key results of this study:

1. During early production time, oil flows under steady-state conditions due to the oil influx from the matrix, but water flows under pseudo steady state conditions. After installing the jet pump and maximizing the choke size, oil-flow becomes coupled with water-flow, indicating similar production drive mechanisms due to the additional drawdown provided by the pump.
2. Oil breakthrough shows insignificant effect on water flow regime, as the dominant drive mechanism of water production is the fracture closure, and oil tends to flow independently through its own network.
3. Rate decline analysis demonstrates that water production rate follows harmonic decline trend and that aggressive production could lead to less ultimate load recovery.

4. Semi-log plot of water-oil ratio versus cumulative water production volume obeys a harmonic decline behavior that is less sensitive to operational changes compared with the water rate-decline plots, and it can be utilized to compare load recovery performance of different wells.
5. The comparative analyses suggest that increasing the injected water volume per stage leads to less load recovery due to water trapping and leak-off, and consequently, less oil productivity at early time as a result of the relative permeability effects. However, increasing proppant concentration leads to less fracture closure and fracture-network complexity that could lead to more load recovery but less oil productivity.

The results of this study are significant for: i) developing next-generation rate-transient models for characterizing wells completed in Eagleford and other similar unconventional formation; and ii) representative analysis of early production data to come up with best practices for future enhanced oil recovery operations.

Chapter 5.
A Hybrid Analytical and Data-Driven Approach for Improved Prediction of Recovery Performance in Tight Oil Reservoirs

5.1 Introduction

The evaluation and prediction of load and oil recovery performances of MFHWs in tight oil reservoirs is a complex challenge. This challenge arises in how to characterize two-phase (oil-water) flow performance using analytical solutions due to the heterogeneity of tight reservoirs, along with their complex geologic characteristics and the completion practices used [76]. Furthermore, the requirement of prolonged production observations after post-frac flowback for rate-transient analysis (RTA) to identify underlying driving mechanisms for evaluating and predicting MFHWs performance adds to the complexity [77]. Despite these difficulties, the evaluation and prediction of load and oil recovery performances of MFHWs in tight oil reservoirs remains a crucial aspect of reservoir management and evaluation.

In conventional reservoirs, a semi-log plot of WOR versus cumulative oil production (Q_o) is commonly used as a diagnostic tool to evaluate and predict waterflood performance [78]. This simple method is applicable for the analysis of late-time production behavior only when a straight line can approximate the WOR function. This log-linear relationship of WOR and cumulative oil production enables the extrapolation of the observed straight line to a threshold WOR value for determining the expected ultimate recovery. Several theoretical approaches have been proposed to establish a correlation between the WOR performance in waterflooding reservoirs and relative permeability ratio. Ershaghi and Omorigie [74] and Ershaghi and Abdassah [75] developed the X-Plot waterflood-analysis technique based on the semilog linear oil/water relative permeability ratio for intermediate water saturation (S_w) values. Utilizing this linearity feature and the Buckley-Leverett frontal displacement theory, a linear relationship between $\ln(1/f_w - 1) - 1/f_w$ and oil recovery factor was developed, where f_w is water fractional flow. This linear model can be calibrated on production data to predict

waterflood performance if the swept volume is known. Lijek [79] utilized the semi-log-linearity feature of the relative permeability ratio to develop a relationship between WOR and cumulative water injection for waterflood performance analysis. This was further extended by Yortsos, Choi [80] to derive a model that describes WOR as a function of displacement time, which is defined as the ratio of cumulative liquid production to the total swept volume of the formation. On the basis of the assumption of log-linear relationship between oil/water relative permeability ratio and S_w, and considering the Buckley-Leverett equation, Yang [71] developed an analytical solution that characterizes the oil fractional flow (f_0) as a function of the fraction of cumulative liquid production to the related formation volume (t_D), relative permeability ratio parameter (B) and the volumetric sweep efficiency (E_V). This diagnostic involves two linear plots which can be utilized for waterflood reservoir analysis; i) a log-log plot of $f_o(1-f_o)$ and t_D that has a slope of -1 and intercept of E_V/B; and ii) a Cartesian plot of $f_o(1-f_o)$ and $1/t_D$ that has a slope of E_V/B and an intercept value of zero. Both plots can be applied for the diagnostic analysis of waterflood reservoirs. Yang [71] showed field case studies to demonstrate the benefits of this diagnostic as a production-decline analysis tool in waterflood performance analysis.

Could similar diagnostics be extended to evaluate the recovery performance of MFHWs in tight oil reservoirs? To the best of our knowledge, no such studies have been published that specifically analyze the WOR performance of MFHWs in tight oil reservoirs and to predict their late-time load and oil recoveries. However, several studies have investigated the gas-oil-ratio (GOR) behavior of MFHWs completed in tight oil reservoirs and how it is different from conventional reservoirs. Chaudhary, Ehlig-Economides [81] demonstrated that the GOR and depletion performances of MFHWs in tight oil reservoirs are not uniquely dependent on reservoir properties but also the completion design applied. They proposed a sensitive analysis based on a numerical simulation study of the Eagle Ford formation to show how the recovery performance varies with both reservoir and completion parameters. Lei and Cheng [82] highlighted the differences in the depletion performance of MFHWs in tight oil reservoirs as compared to conventional reservoirs. They concluded that conventional depletion performance modelling techniques, such as material balance and decline curve analysis, are not generally recommended for tight oil reservoirs. The primary reason for this is the highly sensitive dependence of MFHWs depletion performance in tight reservoirs on completion design and the more heterogeneity and complex geology present in tight reservoirs compared to conventional reservoirs. Shahamat and Clarkson [83] supported this conclusion, showing that in tight reservoirs, complexities such as significant water production/injection, geomechanical effects, and multiwell-production effects may further restrict the use of flowing-material-balance analysis in tight reservoirs. Jones [84] analyzed the producing GOR behavior of MFHWs in tight oil reservoirs by using numerical simulations and field examples from the Anadarko Basin in central Oklahoma. The study

concluded that i) during boundary-dominated flow regime, GOR is more a function of Q_o than of calendar time; and ii) GOR can decline at later stages of production if late-linear transient flow develops. However, this analysis relied on numerical simulations and utilized a single-layer ideal planar-fracture model, which may not accurately represent real-field fractures with associated complex and heterogenous patterns. The production from a MFHW is the sum of many individual-stimulated volumes with varying characteristics, which can alter the GOR patterns described in this study.

On the other side, there are several studies showing the potential of utilizing the early time flowback data for well performance analysis and fracture characterization. Clarkson and Williams-Kovacs [85] presented two-phase flowback models for estimating key fracture parameters such as fracture permeability and total-fracture half-length for MFHWs completed in shale-gas reservoirs. The models were developed by analyzing two-phase (gas and water) flowback data and were based on the analogy of the flowback process to the simultaneous production of gas and water in coalbed methane reservoirs. However, the lack of fracture relative permeability and porosity data resulted in some challenges in achieving a unique match. Fu, Dehghanpour [36] and Moussa, Dehghanpour [57] attempted to determine the effective fracture volume by analyzing single-phase water flowback data of MFHWs in the Woodford and Eagleford Formations. They utilized harmonic decline curve analysis to relate water flowback and cumulative water production volume. Their method relied on the assumption that the harmonic decline in the water production rate would continue until all the fracturing water was produced. However, long-term production data has shown a deviation from this trend as ultimate load recovery approaches, resulting in an overestimation of the effective fracture volume. Recently, Zeinabady, Clarkson [86] integrated flowback analysis with diagnostic fracture injection tests to develop a diagnostic tool for identifying reservoir heterogeneities prior to main-stage hydraulic fracturing.

Despite the extensive use of reservoir simulation to study tight oil reservoirs, there remains a need for simpler, data-driven models to diagnose and predict the recovery performance of MFHWs. The conventional WOR forecasting theory, commonly used to analyze waterflood performance in conventional reservoirs, may be adaptable to tight oil reservoirs. This adaptation would allow petroleum engineers to forecast load and oil recoveries and diagnose production performance using historical field data.

In this paper, we show that the observed field 2-phase flowback and post-flowback data exhibit a log-linear relationship between WOR and load recovery (l_r). Load recovery refers to the amount of fracturing water produced back after hydraulic fracturing operations. We find that this relationship is similar to the log-linear relationship of water/oil relative-permeability ratio (k_{rw}/k_{ro}) and S_w reported

by Honarpour and Mahmood [7]. Based on this analogy, we propose a novel WOR model (WORM) that predicts WOR performance as function of l_r. The WORM model is analytical in nature and has been validated through comparison with reservoir simulation results and application to field cases. The model relates WOR to l_r rather than the calendar time directly. l_r implicitly incorporates the operational and completion aspects of fracturing water recovery. This aspect of the WORM model is of critical significance, since the WOR performance of multi-fractured horizontal oil wells depends on the oil and water saturations in fractures that rely on the volume of fracturing water injection and the fracture network complexity. Then, we use a neural network to link WORM's coefficients to matrix and fracture petrophysical properties. This enables us to history-match WORM on 2-phase flowback and post-flowback data allowing for the prediction of late-time WOR performance and ultimate load recovery (l_{r_u}). Furthermore, this comprehensive approach also facilitates the estimation of the initial effective fracture volume (V_{ef_i}). In addition, we propose a cumulative oil production model (COPM) that describes the observed log-linear relationship between Q_o and l_r during matrix-dominated flow regime. Both WORM and COPM are developed specifically for tight oil reservoirs that exhibit negligible water influx from matrix into fractures and are targeted at MFHWs that do not exhibit interference with other wells. To further demonstrate their field-applicability, these models have been successfully employed to evaluate the productivity of 19 MFHWs completed in the Niobrara and Codell formations.

5.2 Methodology

This paper presents a holistic workflow for predicting long-term well productivity and fracture characteristics from early-time 2-phase flowback data. The well productivity is represented by WOR and Q_o performances, as well as l_{r_u}. The fracture characteristics are represented by initial effective fracture volume (V_{ef_i}), average fracture porosity (ϕ_f) and initial water saturation in fracture (S_{wi_f}). This workflow is developed based on two novel models to forecast the WOR and Q_o performances as functions of l_r.

The first model, WORM, is a hybrid analytical and data-driven model that describes the log-linear relationship of WOR and l_r as an analogy to the log-linear relationship of water/oil relative-permeability ratio (k_{rw}/k_{ro}) and S_w proposed by Honarpour and Mahmood [7]. WORM has three control parameters, β_1, β_2 and β_3, that describe the early-, mid- and late-time WOR behavior with respect to l_r. Then, an artificial neural network (ANN) is constructed to link those parameters to the key petrophysical properties, namely, ϕ_f, fracture and matrix permeabilities (k_f and k_m, respectively), residual oil saturation (S_{or}) and irreducible water saturation (S_{wr}). The impact of fracture-face damage skin, represented by a transmissibility multiplier (T_m), is also considered in this

model. A positive skin indicating a flow restriction between matrix and fracture is represented by $T_m < 1$ while a negative skin indicating a stimulation is represented by $T_m > 1$.

The second model, COPM, is a data-driven model based on the log-linear relationship between Q_o and l_r observed during the matrix-dominated flow regime. This relationship is analogous to the logit function that is commonly used in data transformations in machine learning [87]. COPM is derived from both field and simulation flowback data during the matrix-dominated flow regime.

In the following subsections, the detailed methodology is proposed, **Fig. 5.1** summarizes the coupled approach for predicting well productivity and fracture characteristics from flowback recovery. This approach involves the following steps:

1. Process 2-phase flowback data obtained from multi-fractured horizontal oil wells and plot WOR versus l_r on a semi-log plot. This data typically includes measurements of water and oil production rates over time in 30 minutes intervals.
2. If the petrophysical data (ϕ_f, k_f, S_{wi_f}, k_m, S_{wr} and S_{or}) are available, apply WORM to history match the WOR profile versus l_r and determine the WORM fit parameters (β_1, β_2 and β_3). By adjusting the model's parameters (β_1, β_2, and β_3), we can obtain a fit that accurately represents the observed WOR behavior during the flowback process.
3. If the petrophysical data is not available, i) curve fit WORM to obtain β_1; ii) estimate S_{wi_f}; and iii) apply the proposed statistical approach to estimate β_2 and β_3.
4. Utilize the developed WORM model with the tuned β_1, β_2 and β_3 to forecast the WOR performance as a function of l_r.
5. Estimate l_{r_u} assuming a critical WOR of 0.01 stb/stb.

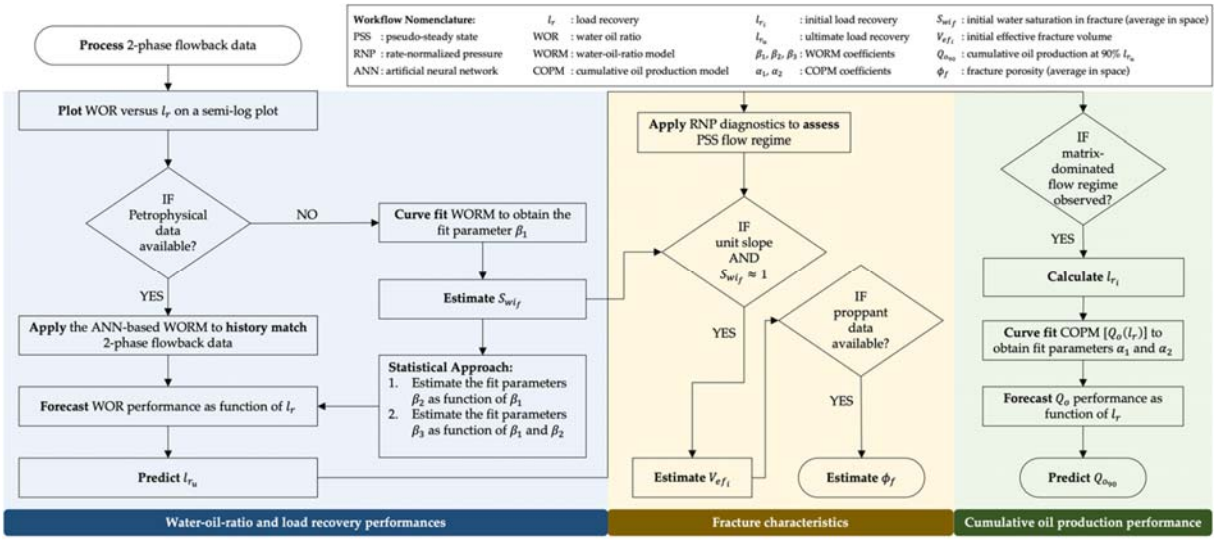

Fig. 5.1 – Flowchart for analyzing 2-phase flowback data to predict water-oil-ratio, load recovery and cumulative oil production performances, and fracture characteristics by utilizing WORM and COPM

6. Apply rate-normalized pressure (RNP) diagnostics to assess the pseudo-steady-state (PSS) flow regime of flowback water. If the RNP analysis concludes a closed-tank system for flowback water and $S_{wi_f} \approx 1$ (from Step 2), estimate V_{ef_i}, then use the proppant data [injected proppant mass (M_p) and density (ρ_p)] to estimate ϕ_f.
7. If the flowback data is long enough to observe the matrix-dominated flow regime, apply COPM to forecast Q_o performance as a function of l_r.

5.2.1 Development of the WOR model as an analogy to relative-permeability ratio

We first introduce a flowback WOR diagnostic analysis for oil wells in tight reservoirs in which we plot flowback and post-flowback WOR versus l_r on a semi-log plot as shown in **Fig. 5.2a**. We observe that during the early two-phase flowback period WOR drops significantly then it declines exponentially (following a straight-line trend) until it declines sharply at late-time production. To confirm this observation, we construct a 3D numerical simulation model that presumes a singular

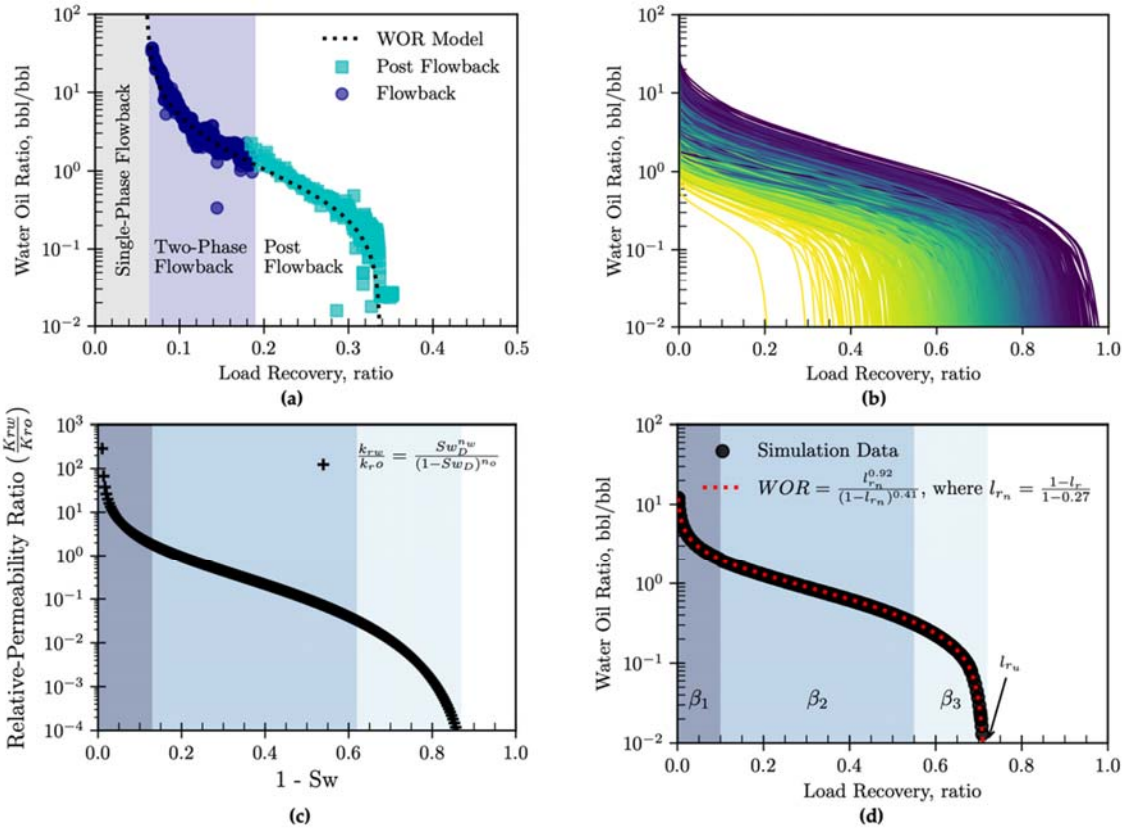

Fig. 5.2 – Developing water-oil ratio as an analogy to relative permeability ratio for oil wells in tight reservoirs. **(a)** Field WOR data versus load recovery. **(b)** Simulation WOR versus load recovery demonstrating intermediate straight-line trend. **(c)** Relative permeability ratio (k_{rw}/k_{ro}) versus oil saturation model by Honarpour and Mahmood [7]. **(d)** Simulation WOR versus load recovery fitted with the developed WOR model as function of normalized load recovery.

hydraulic fracture in an oil well completed in a tight formation, where the formation water is immobile, as demonstrated in **Appendix C**. Then, we apply a Monte Carlo sampling method developed by Hastings [88] to generate four thousand realizations considering different k_f, ϕ_f, S_{wi_f}, k_m, S_{or}, S_{wr} and T_m with ranges listed in **Appendix C.** The main objective of this numerical simulation is to evaluate our proposed analogy between the performance of WOR as a function of load recovery, and the performance of water/oil relative permeability as a function of hydrocarbon saturation introduced by Honarpour and Mahmood [7]. an increase in hydrocarbon saturation within the fracture/matrix typically results in a decrease in both the water/oil relative permeability ratio and the WOR. Here, we assume that these Monte Carlo simulation cases encompass an exhaustive spectrum of potential WOR profiles in relation to load recovery in tight oil reservoirs. This assertion is supported by the broad scope of initial WORs, varying from as low as 1 stb/stb to as high as 100 stb/stb, and ultimate load recovery ranging from 0.2 to 1. Considering no formation water influx from matrix into fracture, we do not anticipate l_{r_u} higher than 1. **Fig. 5.2b** shows that all the simulation cases demonstrate similar behavior to the field data. To study this WOR behavior during load recovery, we consider the power-law model expressing the relative-permeability ratio (k_{rw}/k_{ro}) as a function of S_w introduced by Honarpour and Mahmood [7], represented in **Fig. 5.2c** and defined as

$$\frac{k_{rw}}{k_{ro}} = \frac{(S_{wD})^{n_w}}{(1 - S_{wD})^{n_o}} \tag{5.1}$$

where n_w and n_o are Corey exponents for wetting and nonwetting phases, respectively. S_{wD} is normalized water saturation and defined as

$$S_{wD} = \frac{S_w - S_{wr}}{1 - S_{or} - S_{wr}} \tag{5.2}$$

where S_{wr} and S_{or} are residual water and oil saturations, respectively. From Darcy's law, surface WOR is mainly a function of mobility ratio and can be expressed as

$$WOR = \frac{q_w}{q_o} \propto \frac{k_{rw}}{k_{ro}} \frac{\mu_o}{\mu_w} \tag{5.3}$$

where q_w and q_o are water and oil surface-flowrates, respectively. μ_o and μ_w are oil and water viscosities, respectively. We use surface WOR derived from surface water and oil production rates during both flowback and post-flowback periods. Consequently, we don't incorporate the formation volume factor. Assuming constant μ_o and μ_w throughout a well's production life, Eq. (5.3) can be approximated as

$$WOR \propto \frac{k_{rw}}{k_{ro}} \tag{5.4}$$

Ezulike and Dehghanpour [34] showed that assuming negligible mobile formation water, space-average water saturation in fractures (S_{wf}) could be estimated as a function of cumulative water production (Q_w), V_{ef_i} and S_{wi_f} as

$$S_{wf} = S_{wi_f} - \frac{Q_w}{V_{ef_i}} \tag{5.5}$$

Assuming V_{ef_i} is positively proportional to the total injected water volume (TIV), l_r can be approximated as

$$l_r = \frac{Q_w}{TIV} \propto \frac{Q_w}{V_{ef_i}} \tag{5.6}$$

combining Eqs. (5.5) and (5.6), l_r can be expressed as

$$l_r \propto S_{wi_f} - S_{w_f} \tag{5.7}$$

assuming that the effective fracture volume is initially (at the instantaneous shut-in time after fracturing) filled with water (i.e., $S_{wi_f} \approx 1$), l_r can be expressed as

$$l_r \propto 1 - S_{w_f} \tag{5.8}$$

Eqs. (5.1) to (5.8) show that WOR and l_r are equivalent to k_{rw}/k_{ro} and $(1 - S_w)$, respectively. Therefore, WOR can be estimated as a function of l_r as

$$WOR = \frac{(l_{r_n})^{\beta_2}}{(1 - l_{r_n})^{\beta_1}} \tag{5.9}$$

where l_{r_n} is normalized load recovery, defined as:

$$l_{r_n} = \frac{1 - l_r - \beta_3}{1 - \beta_3} \quad where\ 0 \leq \beta_3 < 1 \tag{5.10}$$

Eqs. (5.9) and (5.10) are analogies to Eqs. (5.1) and (5.2), where β_1, β_2 and β_3 are tuning parameters that could be estimated by using curve-fitting techniques. β_1, β_2 and β_3 control the early-, mid- and late-time curvatures of the WOR profile, respectively. **Fig. 5.2d** shows that WORM demonstrates a good fit with the simulated WOR data at early-, mid- and late-time load recovery. We calculate the average absolute percentage error (AAPE), which measures the fitting error between the simulation WOR data of the 4,000 realizations shown in **Fig. 5.2b**, and the estimated values using WORM presented in Eq. (5.9). WORM can fit simulated WOR with an estimated AAPE of 3.5% as shown in **Fig. C.1** in **Appendix C**. The histogram exhibits a right-skewed distribution, indicative of the goodness-of-fit of the WORM model. This skewness signifies that the majority of the fitting errors gravitate towards zero, thereby underscoring the model's efficiency. Assuming a critical-minimum WOR of 0.01 stb/stb, we can estimate l_{r_u} as shown in **Fig. 5.2d** which can be used to approximate V_{ef_i} assuming that 1) fractures are completely filled with water initially; 2) formation water influx from matrix to fracture is negligible; and 3) water production is mainly from fractures. V_{ef_i} is estimated as

$$V_{ef_i} = l_{r_u} \times TIV \tag{5.11}$$

then, ϕ_f is estimated as

$$\phi_f = \frac{V_{ef}}{V_{ef} + V_p} \tag{5.12}$$

where V_p is the total proppant volume in fracture that can determined by

$$V_p = \frac{M_p}{\rho_p} \tag{5.13}$$

where M_p is mass of total injected proppant and ρ_p is proppant density.

5.2.2 Correlating the WOR model parameters to petrophysical properties using a neural network

Here, we link the WORM parameters β_1, β_2 and β_3 to formation and fracture properties. We develop a feedforward artificial neural network (ANN) with one hidden layer and five neurons as illustrated in **Fig. C.2** to predict β_1, β_2 and β_3 as functions of k_f, ϕ_f, S_{wi_f}, k_m, S_{or}, S_{wr} and T_m. The dataset to train and test the ANN is prepared utilizing 4,000 numerical simulation runs with different realizations of the above-mentioned formation and fracture properties. The comprehensive design of experiment (DoE), which elucidates our selection of the specific petrophysical properties, is presented the **Appendix C** for detailed reference. The resulting WOR profile versus l_r from each simulation run is fitted by the developed WORM so that each datapoint in the dataset includes k_f, ϕ_f, S_{wi_f}, k_m, S_{or}, S_{wr} and T_m as input variables, as well as the WORM parameters (β_1, β_2 and β_3) as target variables. The training and testing datasets have 3,000 (75%) and 1,000 (25%) datapoints, respectively. Then, we apply different transferring (activation) functions to map the input variables (k_f, ϕ_f, S_{wi_f}, k_m, S_{or}, S_{wr} and T_m) to a new representation in the hidden layer of the neural network with 5 neurons. Each neuron in the hidden layer (h_i) is indexed by $i \in \{1, \dots, 5\}$. Each h_i consists of a transformation of a linear-weighting of the input variables as: $h_i = f\left(\sum_{j=1}^{d} x_j w_{ij}\right) = f(\mathbf{x}\mathbf{w}_i)$, where f is a transferring function, d

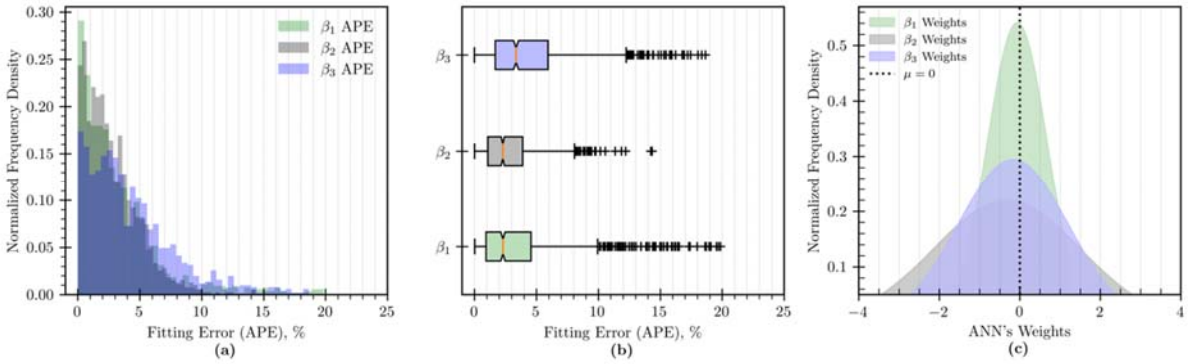

Fig. 5.3 – Goodness of Fit of WORM as **(a)** ANN fitting error (APE) distribution of β_1, β_2 and β_3; **(b)** APE box plots and **(c)** ANN's hidden layers weights distribution

is the dimension of the input layer (i.e., $d = 7$), $\mathbf{x}$ is a 7-dimensional input vector where $\mathbf{x} = \left[k_f, \phi_f, S_{wi_f}, k_m, S_{or}, S_{wr} \text{ and } T_m\right]$, $\mathbf{w}_k \in \mathbb{R}^d$ represents the weights in kth input layer utilized to generate the ith neuron in the hidden layer. In this study, we test different transferring (activation) functions; rectified linear unit (ReLU) where $f(z) = z^+ = \max(0, z)$; Sigmoid where $f(z) = 1/(1 + e^{-z})$; and Softplus where $f(z) = \log(1 + e^z)$. The Sigmoid transfer function shows the best fitting performance of the trained ANN on testing datasets for β_2 and β_3 with an AAPE of 2.74 and 4.28%, respectively. Softplus transfer function leads to a trained ANN model for β_1 with an AAPE of 3.34%. **Fig. 5.3** visualizes the fitting performance of the three developed ANN models predicting β_1, β_2 and β_3. More than 75% of the datapoints are predicted with an absolute percentage error (APE) of less than 6%. Both the histograms and box plots of Absolute Percentage Error (APE) exhibit right-skewness, signifying the robust performance and strong goodness-of-fit of the trained ANN models. This skewness towards zero effectively illustrates that the majority of the fitting errors are closely clustered around zero, indicating highly accurate model predictions. **Fig. 5.3c** shows that the hidden layer's weights in the ANN models follow gaussian distributions with a mean (μ) very close to zero; -0.06, -0.32 and -0.16 for β_1, β_2 and β_3, respectively, indicating a generalized ANN model with no sign of overfitting.

5.2.2.1 Deriving β_1, β_2 and β_3 empirical correlations from ANN (white-box models)

The extracted empirical correlation from the developed ANN shows that the β_1 could be estimated as

$$\beta_1 = 0.859\beta_{1_n} + 0.008 \tag{5.14}$$

where β_{1_n} is the normalized β_1 defined as

$$\beta_{1_n} = \sum_{i=1}^{N} w_{2_i} \log(1 + e^{y_i}) + b_2 \tag{5.15}$$

where b_2 is the bias in the output layer and estimated at -0.005, w_{2i} is a coefficient (weight) connecting the N neurons ($N = 5$) in the hidden layer to the output layer as shown in **Table 5.1**. y_i is the linear transformation of the input variables defined by

$$y_i = \sum_{j=1}^{M} w_{1_{i,j}} x_{n_j} + b_{1_i} \tag{5.16}$$

where b_{1_i} is the bias in each neuron (h_i) in the hidden layer, $w_{1_{i,j}}$ is the weight of the jth input variable in each neuron (h_i), M is the number of input variables ($M = 7$). The trained values of b_{1_i} and $w_{1_{i,j}}$ are listed in **Table 5.1**, x_{nj} is the jth normalized input variable (x_j), calculated by

$$x_{n_j} = \frac{x_j - x_{j_{\min}}}{x_{j_{\max}} - x_{j_{\min}}} \tag{5.17}$$

where $x_{j_{\min}}$ and $x_{j_{\max}}$ are the minimum and maximum values of the input variables considered in this study and listed in **Table 5.2**. The weights, biases, and coefficients formulated in the developed

Table 5.1 – Weights and biases in the trained ANN model of β_1. The values for β_2 and β_3 are listed in **Appendix B**

i	$w_{1_{i,1}}$	$w_{1_{i,2}}$	$w_{1_{i,3}}$	$w_{1_{i,4}}$	$w_{1_{i,5}}$	$w_{1_{i,6}}$	$w_{1_{i,7}}$	B_{1_i}	w_{2_i}
1	0.30	0.20	-0.94	0.06	-0.33	-0.97	0.81	0.35	0.51
2	0.12	-1.14	-0.09	-0.04	0.21	0.54	-0.70	0.02	-0.79
3	0.25	1.22	0.11	0.02	-0.18	0.12	-0.59	-0.06	-0.55
4	0.22	0.73	0.25	-0.02	0.03	0.76	0.54	-0.04	0.55
5	0.07	-1.28	-3.53	-0.05	-0.22	0.67	-0.11	-0.59	0.54

Table 5.2 – Range of input variables utilized to train the ANN models

j	x_j	$x_{j_{min}}$	$x_{j_{max}}$	unit
1	k_f	1,000	2,000	md
2	ϕ_f	0.50	1.00	fraction
3	k_m	1.00	10.00	µd
4	So_r	0.10	0.25	fraction
5	Sw_r	0.10	0.25	fraction
6	TM	0.50	1.50	ratio
7	Swi_f	0.50	1.00	fraction

correlations are specifically tailored to the range of input variables outlined in the table. It is crucial to note that if these input variables deviate from the specified training range, the predictive accuracy of the model might be compromised, as articulated by Livshin [89]. Similarly, the empirical correlations of β_2 and β_3 are derived in **Appendix C**.

5.2.3 WORM sensitivity to petrophysical properties

Here we analyze the sensitivity of WORM to k_f, ϕ_f, S_{wi_f}, k_m, S_{or}, S_{wr} and T_m to; i) understand the relative impacts of those petrophysical properties on the WOR and load recovery performances; and ii) derive an empirical correlation to estimate S_{wi_f} from the early 2-phase flowback data. **Fig. 5.4a**, **b** and **c** demonstrate the WORM parameters (β_1, β_2 and β_3) sensitivity to $\pm$5% and $\pm$10% uncertainties in k_f, ϕ_f, S_{wi_f}, k_m, S_{or}, S_{wr} and T_m. A comprehensive exploration into the effect of capillary pressure on the WOR performance is thoroughly illustrated in **Appendix C**. As mentioned earlier, β_1, β_2 and β_3 control the early-, mid- and late-time WOR performance, respectively. The figure demonstrates that the early-time WOR performance is mainly driven by the fracture properties; S_{wi_f} and ϕ_f. Then, the intermediate performance is mainly governed by the fracture properties; S_{wi_f}, ϕ_f and k_f as well as k_m. Finally, the late-time WOR performance and ultimate load recovery are governed equivalently by the fracture and formation properties. $\pm$10% uncertainy in k_f, ϕ_f, S_{wi_f}, k_m, S_{or}, S_{wr} or T_m leads to $\pm$4% to $\pm$8% changes in β_3 that control the late-time WOR performance and estimated l_{r_u}.

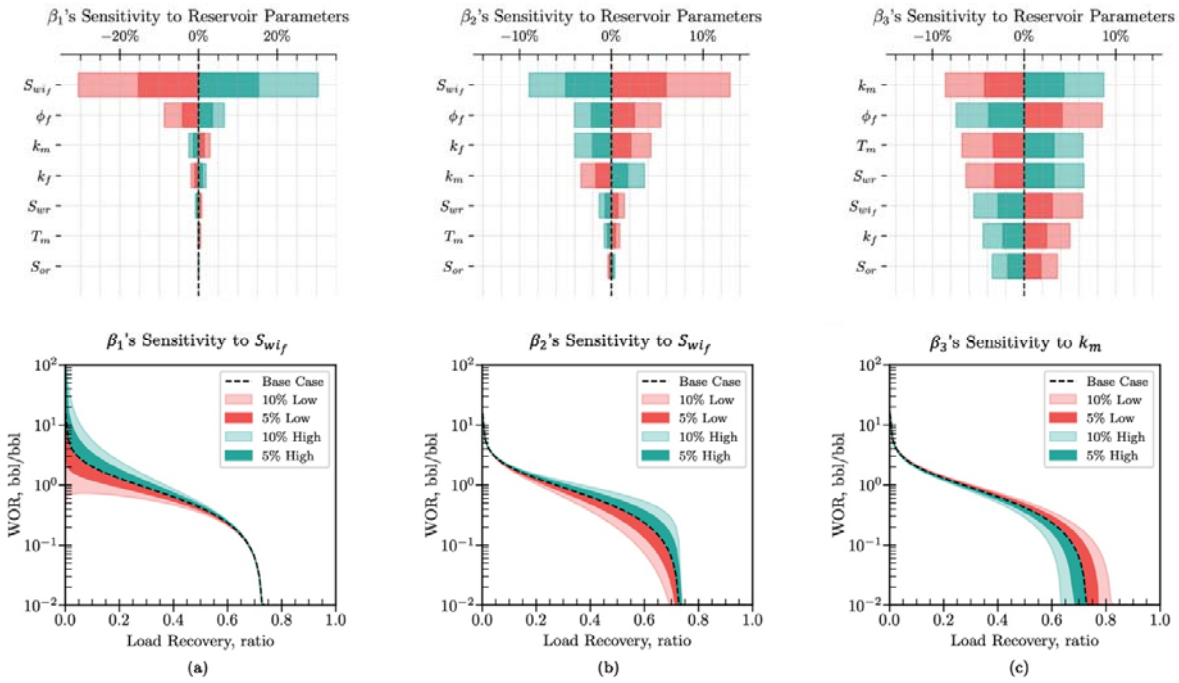

Fig. 5.4 – WORM parameters β_1, β_2 and β_3 sensitivity to petrophysical properties

The key observation here is that β_1, governing early-time WOR performance, is significantly sensitive to S_{wi_f}; $\pm 10\%$ change in S_{wi_f} leads $\pm 30\%$ proportional variation in β_1 as shown in **Fig. 5.4a**. This demonstrates the high WOR sensitivity to relative permeability ratio in fracture at early 2-phase flowback period. Therefore, we hypothesize that WORM could be employed to estimate S_{wi_f} utilizing the early-time flowback WOR data. First, we curve-fit WORM on early flowback WOR by tuning β_1. Second, we estimate β_{1_n} using Eq. (5.17). Then, Eq. (5.15) could be rearranged as a function of S_{wi_f}, defined as

$$f\left(S_{wi_{f_n}}\right) = \sum_{i=1}^{N} w_{2_i} \log\left(1 + e^{w_{1_{i,7}} S_{wi_{f_n}} + b_{1_i}} . e^{y_i^*}\right) + b_2 - \beta_{1_n} = 0 \tag{5.18}$$

where y_i^* could be estimated as

$$y_i^* = \sum_{j=1}^{M-1} w_{1_{i,j}} x_{n_j} \tag{5.19}$$

this equation is similar to Eq.(5.16), but it doesn't include the hidden layer bias b_{1_i}, the input variable S_{wi_f}, and its weights in the hidden layer. Then, S_{wi_f} could be estimated as

$$S_{wi_f} = S_{wi_{f_n}} \left(S_{wi_{f_{\max}}} - S_{wi_{f_{\min}}}\right) + S_{wi_{f_{\min}}} \tag{5.20}$$

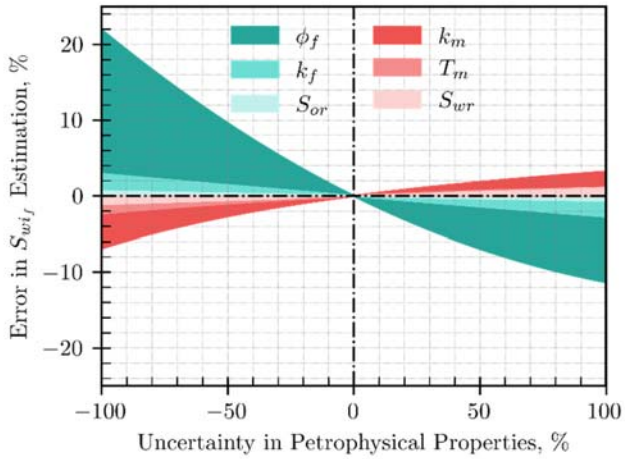

Fig. 5.5 – Uncertainty in the initial water saturation in fracture (S_{wi_f}) inversely estimated from the developed ANN model [Eq. (5.14) to (5.21)] considering the uncertainty in other petrophysical properties

where $S_{wi_{f_{\min}}}$ and $S_{wi_{f_{\max}}}$ are the minimum and maximum values of S_{wi_f} used to train WORM as listed in **Table 5.2**. We solve the nonlinear Eq. (5.18) utilizing the iterative Powell's method introduced by Powell [90] which combines Gauss-Newton algorithm with gradient descent to find the minimum of the non-linear least squares objective function. **Fig. 5.6** demonstrates the sensitivity of S_{wi_f} to the uncertainties in other petrophysical properties. ϕ_f and k_m have the most significant impact on estimating S_{wi_f}. Ignoring ϕ_f or k_m could lead to an error ranging from -7% to 22% in estimating S_{wi_f}. This is due to the multicollinearity between those input parameters when estimating WOR using Eq. (5.9). **Fig. 5.4a** demonstrates that ϕ_f and k_m have the second and third largest impacts on WOR behavior at early flowback period. Similar to S_{wi_f} , ϕ_f has a positive effect on WOR. In other words, the increase in either S_{wi_f} or ϕ_f leads to an increase in WOR. Therefore, if ϕ_f is missing in Eq. (5.9), the value of S_{wi_f} proportionally reformed to compensate the missing ϕ_f. Therefore, a missing ϕ_f could lead to 22% error in estimating S_{wi_f}. On the other side, k_m and S_{wi_f} have contradictory impacts on WOR. Unlike S_{wi_f}, increasing k_m leads to more oil influx from the matrix into fractures, assuming immobile formation water, and ultimately leads to a drop in WOR at early flowback period. Therefore, ignoring k_m could result up to -7% error in estimating S_{wi_f}. Ignoring, k_f, S_{o_r}, t_m, or S_{w_r} could result up to 2.8, 0.6, -2.3 and -1.1% error in estimating S_{wi_f}, respectively. After determining the value of S_{wi_f}, it can be employed in conjunction with other petrophysical properties to estimate the remaining WORM parameters β_2 and β_3 by using Eqs. (58) and (62), respectively. This approach is valid only if the petrophysical properties are available. If not, the statistical approach introduced in **Appendix C** is used alternatively. In the proposed statistical approach, β_1 is estimated by curve-fitting WORM on the early-time 2-phase flowback data. Then, β_2 is estimated as a function of β_1 by using Eq. (66). Finally, β_3 is estimated by Eq. (67) as a function of both β_1 and β_2.

5.2.4 Predicting cumulative oil production performance from flowback

In this section we develop COPM that describes Q_o performance as a function of l_r. We first construct three diagnostic plots of 1) Q_o versus Q_w; 2) Q_o and Q_w versus time; and 3) water and oil flowback rates versus time as shown in **Fig. 5.5**. Our observations indicate two distinct flow periods. So, we hypothesize that the first period is dominated by fracture and the second one is dominated by the matrix. The signature of the fracture- dominated flow regime is clear in the three diagnostic plots.

Fig. 5.5a shows that Q_o demonstrates a linear increase versus the Q_w on a semi-log plot during the fracture-dominated flow period. Then, in the matrix-dominated period, the trend is transformed to a power-law model which is developed in this paper. During the fracture-dominated flow period, fractures demonstrate a pressure-supercharge effect [91] as the bottomhole flowing pressure is higher than the initial reservoir pressure as shown in the figure. The traces of oil observed during this period is primarily sourced from the effective fracture volume, with little to no significant oil influx from the matrix. Therefore, Q_o follows a straight-line trend when plotted versus Q_w. Once the average fracture pressure drops below the initial reservoir pressure, the matrix-dominated flow period starts and a significant increase in the oil production rate is observed, suggesting oil influx from the matrix into the fracture. Therefore, we hypothesize that if the flowback period is long enough to capture the matrix-dominated flow period, the 2-phase flowback data could be utilized to predict the Q_o performance as a function of l_r.

To confirm the field observation and verify our hypothesis, we build a simulation data file to capture the fracture- and matrix-dominated flow periods as shown in **Fig. 5.8a**. During the fracture-dominated period, the fracture demonstrates a pressure-supercharge effect ($p_f > p_m$), which is generally observed at the beginning of flowback [91]. During this period, there is no oil influx from the matrix into the fracture and the produced oil traces are due to the initial average oil saturation in the effective fracture. This effect is simulated by constraining the lateral transmissibility between matrix and

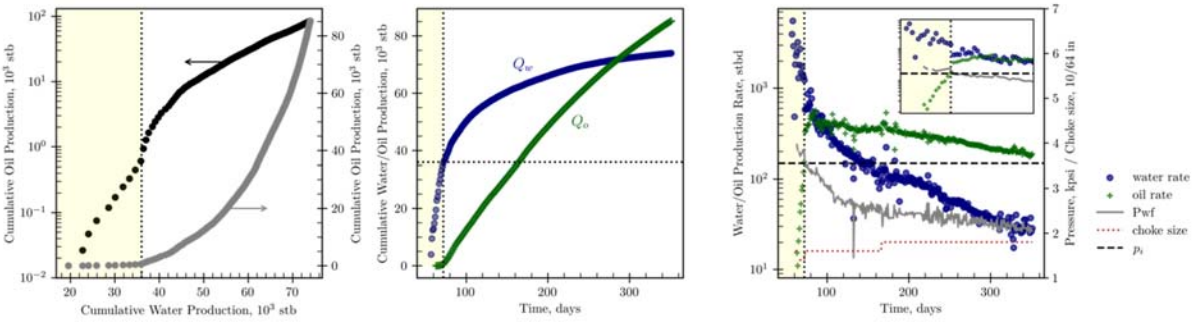

Fig. 5.6 – Diagnostic plots of cumulative oil production during flowback and post-flowback. **(a)** cumulative oil production versus cumulative water production. **(b)** cumulative water and oil production versus time. **(c)** production rates, bottomhole pressure and choke size versus time. The inset figure shows flowback rates and estimated initial reservoir pressure

fracture during early-time flowback until p_f approaches p_m. **Fig. C.4** shows the pressure distribution in fracture and matrix at the supercharge condition and at different timestamps until depletion. This figure suggests a PSS flow regime during the pressure-supercharge period in the fracture network. This PSS depletion continues until p_f approaches p_m, then the water blockage at the fracture interface is decreased, so that the fluid support from the matrix to the fractures is activated. This effect is simulated by increasing the transmissibility multiplier back to one to eliminate the water blockage effect. **Fig. 5.8a** and **b** show the similarity between the simulated and field Q_o profiles, respectively. In the fracture-dominated flow period, the oil production is mainly due to the initial average oil saturation in the effective fracture network with no influx from the matrix. Then, when p_f approaches p_m, oil starts to flow from the matrix into fracture and Q_o trend deviates from the straight-line behavior observed in the first period identifying an oil breakthrough. **Fig. 5.8b** demonstrates that during the fracture-dominated flow period, the first thousand barrel of oil is produced after producing 35 kstb of water, while during the matrix-dominated flow period, the first 10 kstb of oil is produced while producing 10 kstb of water. The simulated Q_o profile in **Fig. 5.8a** shows that when approaching l_{r_u}, Q_o is bended up due to the low S_{w_f} and the relative-permeability end-points effect. This log-linear relationship of Q_o and l_r is similar to the logit function that is commonly used in data transformations in machine learning [87], but on a semi-log scale, where Q_o increases significantly at the beginning of oil breakthrough, then it stabilizes until approaching l_{r_u} at which it surges up. According to Cramer [92], Logit function maps the probability values from (0,1) to real numbers in $(-\infty, +\infty)$. However, the domain of Q_o profile versus l_r, assuming immobile formation water, is (l_{r_i}, l_{r_u}), where l_{r_i} is the initial load recovery at the start of the matrix-dominated flow regime. l_{r_u} is the ultimate load recovery which

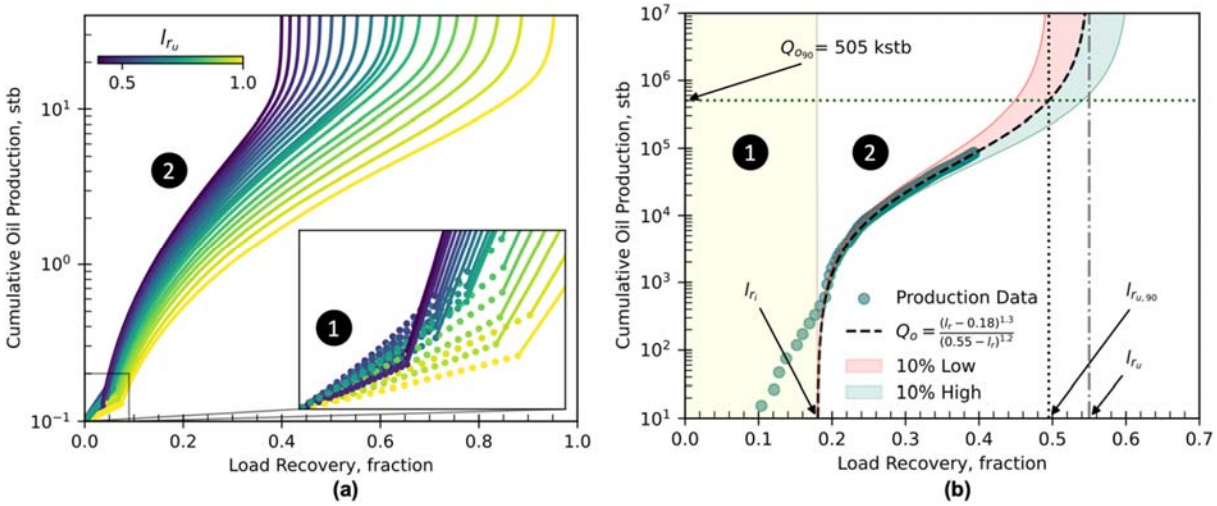

Fig. 5.7 – **(a)** Simulated cumulative oil production profile during the fractured- and matrix-dominated flow periods. **(b)** COPM and its fitting performance on field production data

could be estimated from the WORM developed earlier. Considering this analogy, Q_o can be defined as a function of l_r as

$$Q_o = \frac{\left(l_r - l_{r_i}\right)^{\alpha_1}}{\left(l_{r_u} - l_r\right)^{\alpha_2}}, \qquad l_{r_u} > l_r > l_{r_i} \tag{5.21}$$

where α_1 and α_2 are model tuning parameters. a_1 controls the early curvature of Q_o profile at l_{r_i}, while α_2 controls the late curvature of Q_o profile when approaching l_{r_u} as shown in **Fig. 5.7a** and **b**, respectively. The term curvature here represents the rate of change in oil production with respect to load recovery (RoC_o). **Fig. 5.7a** shows that RoC_o is negatively correlated to α_1. Increasing α_1 decreases RoC_o meaning that q_o increases smoothly (with respect to l_r) after oil breakthrough into the fracture. In contrast, decreasing α_1 results in a sharp increase in q_o after oil breakthrough. Similarly, RoC_o is negatively correlated to α_2. Increasing α_2 leads to a relatively smoother increase in RoC_o when approaching l_{r_u}, but it also may suggest a higher oil/water relative-permeability ratio ($\frac{kr_o}{kr_w}$) as it leads to a higher slope as shown in **Fig. 5.7b**. The intermediate period is mainly governed by both α_1 and α_2. Low values of α_1 and α_2 lead to a low slope suggesting low $\frac{kr_o}{kr_w}$, while large values of both α_1 and α_2 result in higher slope, suggesting high $\frac{kr_o}{kr_w}$. l_{r_i} and l_{r_u} control the span of the Q_o profile as shown in **Fig. 5.7c** and **d**, respectively. In the proposed methodology, i) l_{r_i} is measured from the flowback data, if the flowback period is long enough to capture the matrix-dominated flow regime. In the proposed case study, this regime is generally observed at $l_r \leq 0.2$. Otherwise, post-flowback data could be utilized to identify this value; ii) l_{r_u} is estimated from WORM; and iii) α_1 and α_2 are estimated by curve-fitting COPM on 2-phase flowback data after observing the matrix-dominated flow regime as demonstrated in **Fig. 5.8b**. Since $Q_o\left(l_r = l_{r_u}\right) \to \infty$, we choose to estimate the cumulative oil production at 90% of the ultimate load recovery (Qo_{90}) to assess and compare the oil productivity performance of the studied wells **Fig. 5.8b** shows the estimated Qo_{90} at 90% of l_{r_u} with the associated uncertainty resulted from both the fitting error of COPM and l_{r_u} estimation from WORM. The figure

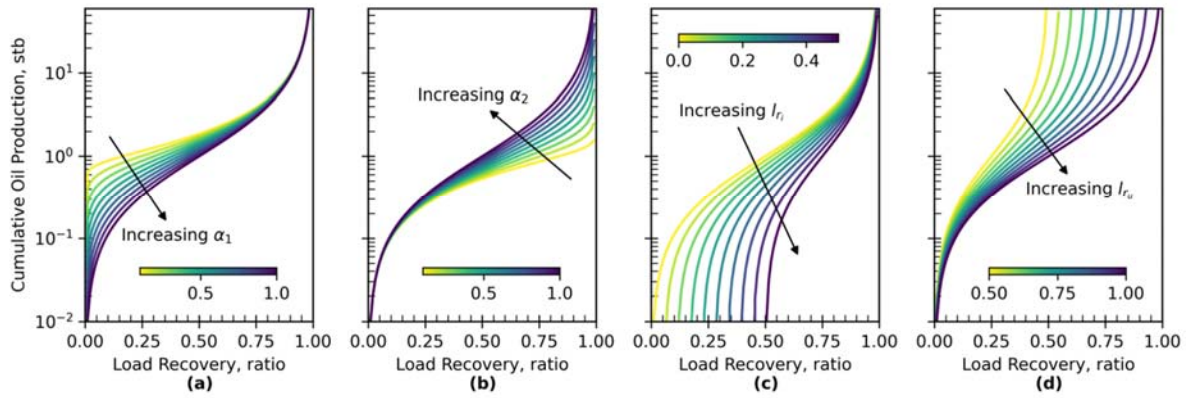

Fig. 5.8 – Sensitivity of Q_o model to parameters α_1, α_2, initial load recovery (l_{r_i}) and ultimate load recovery (l_{r_u})

demonstrates that the uncertainties in the estimated l_{r_u} from WORM superimpose the fitting error of COPM. In this case, l_{r_u} is estimated from WORM at 0.55 while l_{r_i} is measured at 0.18. the parameters α_1 and α_2 that generate the best-fit COPM are 1.3 and 1.2, respectively. Therefore, Eq. (5.21) becomes $Qo = (l_r - 0.18)^{1.3}/(0.55 - l_r)^{1.2}$, where $0.55 > l_r > 0.18$. At 90% of l_{r_u}, Qo_{90} is estimated at 505 kstb as illustrated in **Fig. 5.8b**.

5.3 Application of WORM and COPM

Here, we apply the proposed methodology to analyze the flowback and post-flowback data of a multi-well pad with 19 oil MFHWs completed in Niobrara and Codell formations with 3D trajectories shown in **Fig. 5.9**. The true vertical depth of those wells varies from 6,975 to 7,261 ft as demonstrated in the inset figure. There are 15 and 4 wells completed in Niobrara and Codell formations, respectively. Those wells are categorized according to their producing formation, which is reflected in their well names as illustrated in the inset schematic in **Fig. 5.9**. The main goal of this case study is to assess and compare the productivity performance of those wells by utilizing our proposed holistic workflow. **Error! Reference source not found.** provides further examples of WORM applications, showcasing an a dditional 24 oil MFHWs completed in Montney formation. It also shows how formation water mobility and well interference could impact on the WOR profile versus load recovery.

Here, we propose three performance indicators: l_{r_u}, V_{ef_i} and $Q_{o_{90}}$. Both l_{r_u} and V_{ef_i} require a prior investigation of formation-water influx from matrix into effective fractures to formulate the required assumptions for estimating those indicators. Therefore, we conduct the following analyses:

i) Analyze the flow regimes of water and oil during flowback and post-flowback periods by investigating the rate-normalized pressure profiles for water and oil (RNP_w and RNP_o, respectively) versus material-balance time (t_{mb}) for all the studied wells. t_{mb} is defined as the ratio of cumulative water production (Q_w) to water production rate (q_w). We chose to use this

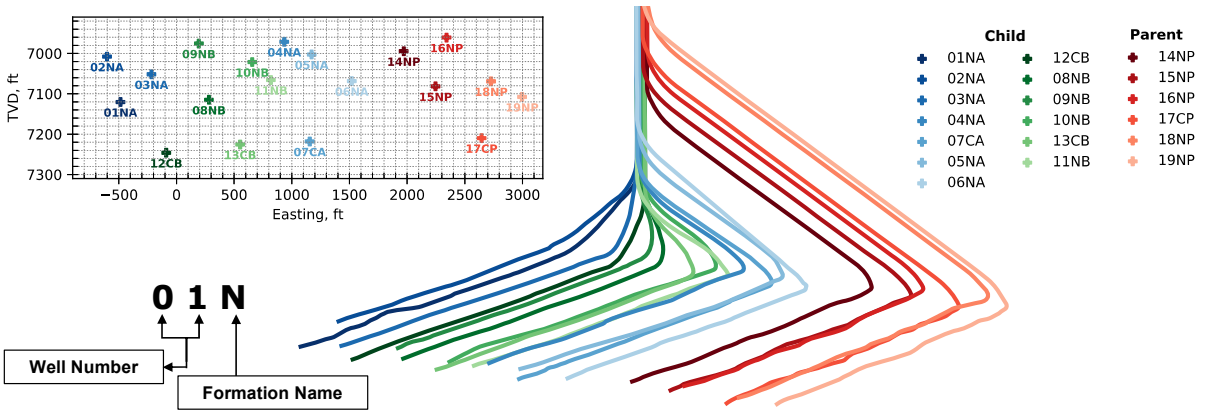

Fig. 5.9 – 3D trajectories of the studied wells. The inset figure shows wells toes' true vertical depth. The well naming procedure is illustrated in the bottom left of the figure.

unified water-rate-based t_{mb} for two reasons: firstly, to provide a consistent x-axis for both water and oil RNP plots; and secondly, because our primary focus in this paper is on analyzing RNP_w to investigate formation-water mobility. RNP_w and RNP_o are defined as $(p_i - p_{wf}/q_w)$ and $(p_i - p_{wf}/q_o)$, respectively. q_w and q_o are the production flowrate of water and oil at bottomhole conditions, respectively. p_{wf} is the flowing bottomhole pressure, and p_i is the initial average reservoir pressure in the stimulated region around wellbore.

ii) Apply the proposed WORM to predict l_{r_u} and estimate S_{wi_f} by utilizing Eq. (5.20). Then, we estimate V_{ef_i}, assuming a) that the effective fractures are initially filled with water; and b) negligible water influx from the matrix into the fractures. The first assumption is validated by the estimated S_{wi_f}, while the second assumption is validated in the previous step (RNP diagnostic analysis).

iii) Apply COPM to assess the oil productivity of the studied wells by predicting $Q_{o_{90}}$.

5.3.1 Rate-normalized-pressure diagnostic analysis

Fig. 5.10a shows the flowback and post-flowback RNP_w and RNP_o versus t_{mb} for well 01N. The figure demonstrates a pronounced unit slope for RNP_w during flowback and post-flowback periods, indicating a PSS flow regime. This suggests a close-tank system for water production with no-water-flow outer boundary. A similar behavior is observed for all the studied wells as presented in **Fig. C.5**. Therefore, the RNP diagnostic analysis indicates that there is no water influx from the matrix into fracture during flowback and post-flowback, fulfilling the first assumption associated to WORM. This argument is also confirmed by the S_w log data calculated along the lateral section and presented in **Fig. 5.10b**. S_w data is based on open-hole log data provided by the operator of the studied wells. These data were computed from resistivity logs and measured along the lateral section of the wellbore for

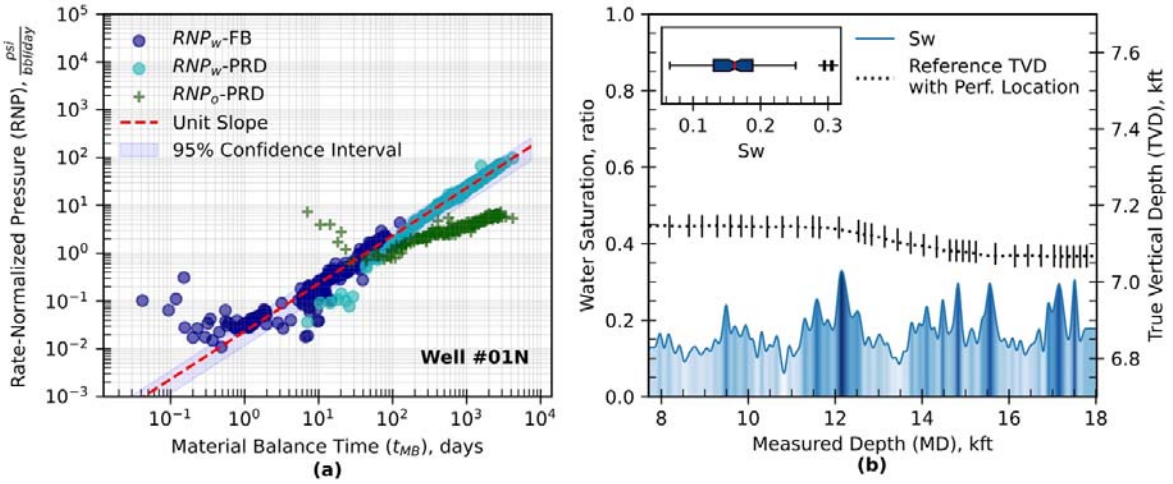

Fig. 5.10 – (a) RNP plots of flowback and post-flowback water and oil for Well 01N. **(b)** Water Saturation profile along the lateral section with the reference TVD and perf. Locations. The inset figure shows the boxplot of water saturation statistics

the given well. The figure shows $0.31 \geq S_w \geq 0.06$ along the wellbore in the lateral section with an average S_w estimated at 0.16. The inset boxplot shows that 75% of the measured S_w data is less than 0.18, demonstrating relatively low S_w around wellbore. In addition, the figure demonstrates that the operator avoids perforations in the intervals showing a relatively high S_w to avoid any potential of mobile formation water. These observations support the RNP diagnostics outcomes and support our assumption of no water influx from matrix into fracture. On the other side, the half-slope for RNP_o suggests a transient linear behavior. This may be attributed to factors such as: i) production from fractures that extend to reservoir boundaries [93]; ii) transient drainage of low-permeability matrix into adjacent fractures; and iii) the linear shape of the reservoir [94].

5.3.2 WORM application to estimate fracture characteristics and well performance

Here, we apply WORM to estimate S_{wi_f}, l_{r_u} and V_{ef_i}. **Fig. 5.11a** shows a semi-log plot of WOR versus l_r during flowback and post-flowback periods. First, WORM is tuned to fit the flowback data and to estimate S_{wi_f}. Second, WORM is further validated by post-flowback data to predict l_{r_u} as shown in the figure. β_1 resulted from fitting WORM on the early flowback data is estimated at 0.81. Then, we use Eq. (5.20) to estimate S_{wi_f} at 0.98, verifying that initially the fracture is filled with water. This is also supported by observing a single-phase-water flowback for 6 days before oil breakthrough as illustrated in **Fig. 5.10a**. In addition, the first traces of oil production are observed after producing more than 15 kstb of water. These observations support our second assumption of having the fracture filled with water at early flowback time. Therefore, WORM can be utilized to predict l_{r_u} and V_{ef_i}. Then, β_2 and β_3 are estimated by Eqs. (66) and (67) at 1.24 and 0.64, respectively. Therefore, the profile of WOR as a function of l_r can be described as $WOR = \left(l_{r_n}\right)^{1.24} / \left(1 - l_{r_n}\right)^{0.81}$ where $l_{r_n} = (1 - l_r - 0.64)/(1 - 0.64)$ as shown in **Fig. 5.11a**, predicting l_{r_u} at 0.36 ± 0.04 assuming a critical WOR of 0.001 stb/stb that represents the end of load recovery. The average l_{r_u} of all the studied wells is estimated at 0.44 as shown in **Fig. 5.11b**. This relatively low l_{r_u} endorses the argument of negligible formation water influx from the matrix into effective fractures as concluded from the RNP diagnostics. The figure also demonstrates the measured 3-, 7- and 9-month l_r for each well. Here are the main observations: i) generally, Codell wells show higher measured l_r and estimated l_{r_u} compared to the Niobrara wells. On average, Codell and Niobrara wells show l_{r_u} of 0.69 and 0.37, respectively; ii) wells with higher 3-, 7- and 9-month l_r show higher l_{r_u}; and iii) more than 50% of the predicted l_{r_u} is produced back within the first 3 months of production.

From l_{r_u}, we can estimate the ultimate water production volume by knowing the total injected water volume (TIV), then it can approximate V_{ef_i} with the assumptions listed and justified earlier. **Fig. 5.11c**

shows the estimated V_{ef_i} for each well. There are two main observations here: i) Generally, Codell wells show a larger V_{ef_i} compared to Niobrara wells. Although Codell wells are completed with 10% less TIV compared to Niobrara wells, Codell wells show more than 27% larger V_{ef_i} compared to the Niobrara wells. This might be due to the relatively higher fracability of the Codell formation wells as shown in **Fig. 5.11d**. The figure demonstrates the average fracability-index profile along the wellbore for Codell and Niobrara wells.

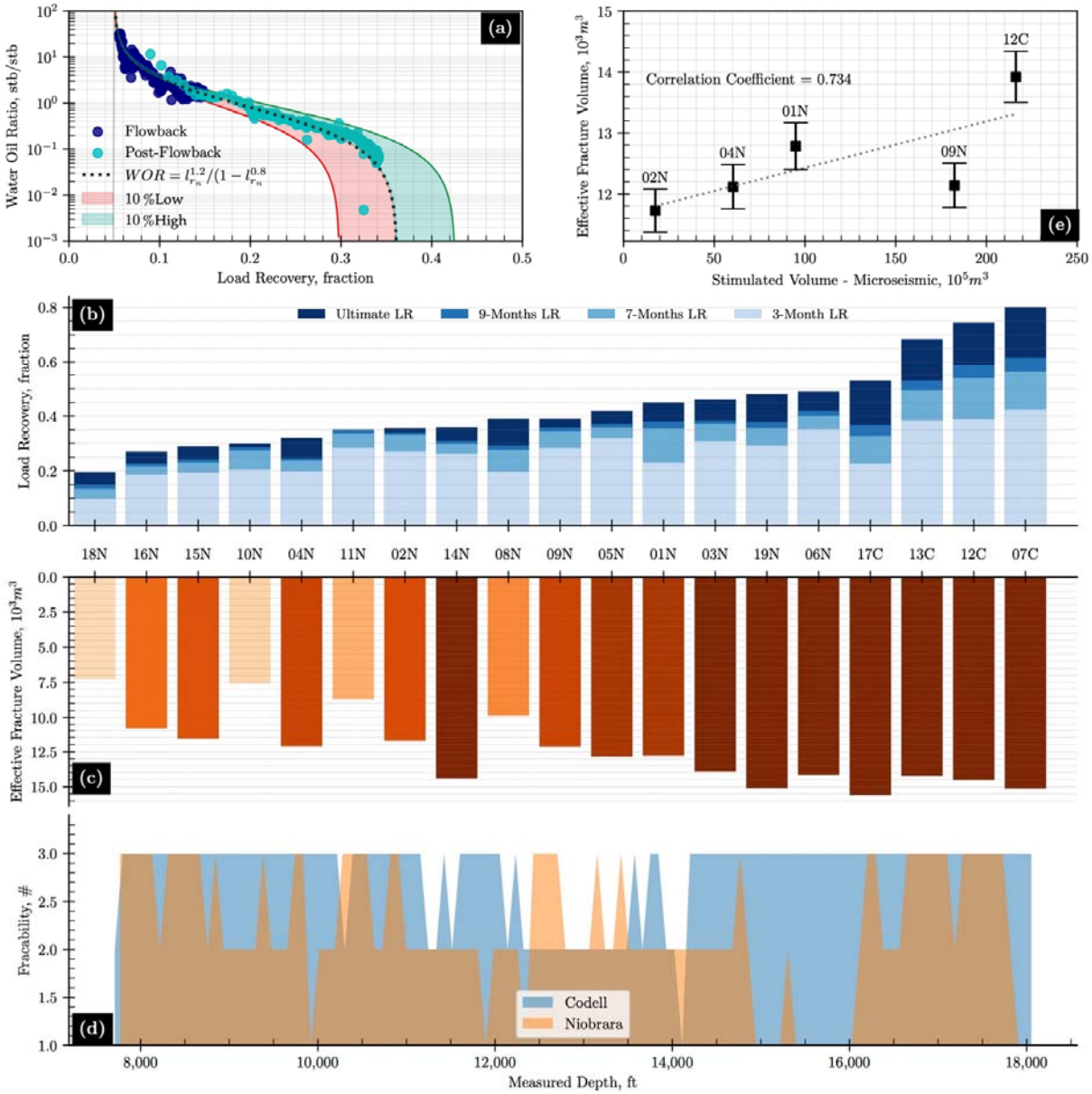

Fig. 5.11 – **(a)** Predicted WOR profile as a function of load recovery. **(b)** Ultimate and measured load recoveries at different production times. **(c)** Estimated effective fracture volume. **(d)** Average fracability index along wellbore for Niobrara and Codell wells. **(e)** Crossplot of the estimated effective fracture volume and the stimulated volume estimated from microseismic data

On average Codell show 26% more fracability compared to Niobrara which is almost the same difference in the average V_{ef_i} estimated for both groups of wells (clustered by the formation name); and ii) larger V_{ef_i} does not necessarily represent higher l_{r_u}. Well 14N shows +16% above-than-average V_{ef_i}, despite its -18% below-than-average l_{r_u}, shedding the light on the effect of completion design on both l_{r_u} and V_{ef_i}. This well was completed by 32% more TIV and 7% less proppant concentration compared to the other wells. Therefore, the larger TIV might lead to a relatively larger V_{ef_i}, but it also might result in more fracturing water losses and trapping which also could be emphasized by the relatively low proppant concentration, leading to a relatively low l_{r_u}.

Next, we compare the estimated V_{ef_i} from WORM to the volume estimated by microseismic events (V_{me}) for each well. **Fig. C.7** demonstrates the microseismic event dimensions grouped to each fracture stage in terms of length, width and height for wells 01N, 02N, 04N, 09N and 12C. The figure shows that the events count varies from less than 10 to 250 events per fracture stage. In this study, we use 70 events as a cut-off. Fracture stages with more than 70 counted microseismic events are utilized to estimate their volume giving their microseismic dimensions (length, width, and height). Then, we sum the estimated volumes of fracture stages for each well to estimate its V_{me}. **Fig. 5.11e** shows a crossplot between V_{ef_i} and V_{me} for the 5 wells. The figure demonstrates a positive correlation coefficient of 0.734 between V_{ef_i} and V_{me}. Therefore, wells with larger V_{me} generally demonstrate larger V_{ef_i}, except for Well 09N that showed almost triple V_{me} of Well 04N, but with similar V_{ef_i}. Further investigation is required to understand why this well shows such a dissimilar behavior and remains to be studied in future. Another observation is that Codell well 12C exhibits the largest V_{me} compared to the other Niobrara wells, supporting our previous observations of the relatively higher l_{r_u}. and V_{ef_i} of Codell compared to Niobrara wells.

5.3.3 Oil productivity performance

Here we assess and compare the oil productivity performance of the studied wells. **Fig. 5.12a** shows the measured 3-, 7- and 9-month Q_o as well as $Q_{o_{90}}$ estimated at 90% l_{r_u}. The wells are sorted by $Q_{o_{90}}$. The general statistics of $Q_{o_{90}}$ clustered by formation is displayed as boxplots in the inset figure. Here are the main observations: 1) Generally, the parent wells show better oil recovery performance compared to the child wells. Parent wells (14N, 15N, 16N, 17C, 18N and 19N) showed more than 53% higher $Q_{o_{90}}$ compared to the child wells. 2) Well 14N's $Q_{o_{90}}$ is estimated at 240 kstb, which is 75% higher than the average $Q_{o_{90}}$ of the studied wells. In addition, its 3-, 7- and 9-month measured Q_o are 37, 39 and 44% higher than the average 3-, 7- and 9-month Q_o of the studied wells, respectively, demonstrating its superior oil recovery performance. This well is among the three first Niobrara wells that was drilled and completed in this pad. Therefore, probably this well has the best sweet spot

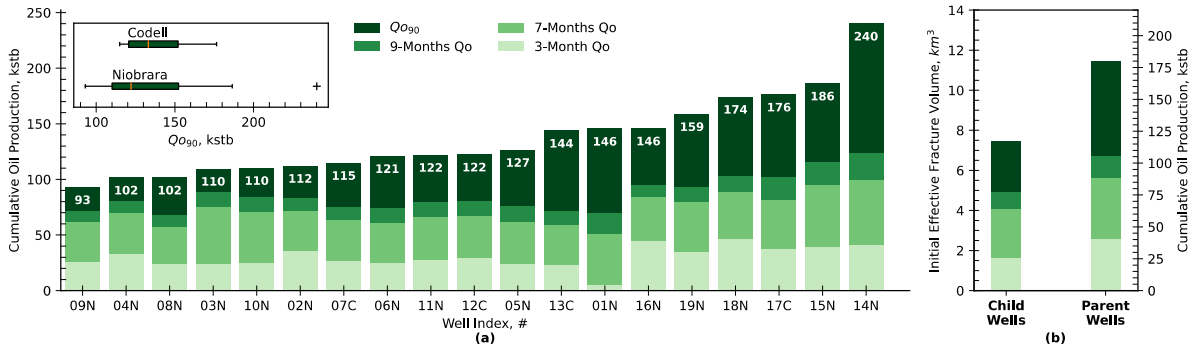

Fig. 5.12 – (a) Cumulative oil production predicted by Qo-Model at 90% load recovery (Qo_{90}) and the measured cumulative oil production at 3-, 7- and 9-month. The inset figure shows a boxplot statistic of Qo_{90} for Niobrara and Codell wells. **(b)** Comparing cumulative oil production and V_{ef_i} of parent and child wells.

among the other studied wells with the highest reservoir quality. Moreover, this well has the second largest V_{ef_i}, and thus a larger contact to a relatively higher quality reservoir, allowing this well to outperform the other studied wells in oil recovery. 3) On average, both Codell and Niobrara wells show similar oil recovery performance, despite the variation of load recovery performance, suggesting stratified flow regimes for water and oil in the effective fracture as proposed by Moussa, Fu [6]. Niobrara and Codell wells show an average $Q_{o_{90}}$ of 137 and 139 kstb. In both formations, 75% of the studied wells show $Q_{o_{90}}$ value of less than 152 kstb. 4) **Fig. 5.12b** compares oil productivity relative to the effective fracture volume for parent and child wells. On average, the parent wells show more than 50% higher $Q_{o_{90}}$ compared to the child wells, although both have similar average V_{ef_i}. In addition, parent wells demonstrate 61%, 37% and 36% higher 3-, 7- and 9-month Q_o compared to child wells, exhibiting a relatively better oil recovery performance.

Hypothetically, the parent wells are generally completed in a better sweet spot compared to the child wells. In addition, part of the child wells stimulated volume might have been already drained by the parent well. Therefore, applying a completion design to develop a similar effective fracture volume on child wells, does not necessarily lead to similar oil productivity compared to the parent wells. In other words, it is not just V_{ef_i} that designate the productivity performance, it also depends on the quality of the reservoir at which the parent/child wells are completed.

The successful application of WORM delivers a critical tool for predicting well performance and determining initial water saturation in the fracture, contributing to an improved understanding of fracturing efficiency. The insights on oil productivity between parent and child wells by utilizing COPM offer valuable implications for multi-well pad drilling strategies. Furthermore, the correlation between the initial effective fracture volume and microseismic events offers potential for developing a data-driven method of estimating fracture volume, which can be beneficial for better reservoir management and improved hydraulic fracturing designs.

5.4 Summary

In this study, we introduce two novel models to predict water-oil-ratio and cumulative oil production performances from early 2-phase flowback data as functions of load recovery in tight oil reservoirs. The first model, WORM, is a hybrid analytical and data-driven model describing the observed log-linear relationship of WOR and load recovery as an analogy to the log-linear relationship of water/oil relative permeability ratio and water saturation. The parameters of WORM are coupled with key petrophysical properties using a neural network, allowing us to analyze the impact of fracture and formation properties on the WOR performance on different stages of load recovery. Beside forecasting the WOR performance. WORM is also utilized to predict ultimate load recovery, initial effective fracture volume and initial water saturation in fracture. The second model, COPM, is a data-driven model describing the log-linear relationship of Q_o and load recovery during the matrix-dominated flow regime. It can be coupled with WORM to predict Q_o when approaching the ultimate load recovery. Both WORM and COPM are derived for tight oil reservoirs based on the assumptions of negligible water influx from matrix into fractures and that water production is mainly from fractures with no observed interference between different MFHWs. The application of WORM and COPM on 19 MFHWs completed in Niobrara and Codell formations showed that:

1) The effective fracture volume estimated using WORM is positively correlated with the estimated volume of microseismic events.
2) Generally, Codell wells exhibit better load recovery and larger effective fracture volume compared to Niobrara wells, despite the similar completion-design practices applied to both formations. This highlights the significance of selecting the completion-design as a function of reservoir characteristics and geomechanical properties.
3) Both Codell and Niobrara wells display similar oil recovery performance, despite the variation of load recovery performance, suggesting independent flow regimes for water and oil in the effective fractures. This conclusion is also supported by the negligible effect of the oil breakthrough on the water flow regime observed in RNP diagnostics.
4) The application of a completion design to achieve a similar effective fracture volume on child wells does not necessarily lead to similar oil productivity compared to parent wells. It also depends on the quality of the reservoir at which the parent/child wells are completed.

In conclusion, this study demonstrates the potential of WORM and COPM as early-time diagnostic tools for evaluating and predicting load and oil recoveries of MFHWs in tight oil reservoirs. However, the accuracy of these models is dependent on the availability of petrophysical properties and the assumption of negligible water influx from matrix into fractures. Future research could investigate the impact of mobile formation water on the WOR profile and the applicability of these models to other reservoir types or under different conditions.

5.5 Nomenclature

MFHW: multi-fractured horizontal well
WOR : water oil ratio
GOR : gas oil ratio
WORM: water oil ratio model
COPM : cumulative oil production model
PSS : pseudo steady state
APE : absolute percentage error
AAPE : average absolute percentage error
ANN : artificial neural network
ReLU : rectified linear unit function
RNP : rate normalized pressure
RNP_w : water-rate-normalized pressure
RNP_o : oil-rate-normalized pressure
t_{mb} : material-balanced time
Q_o : cumulative oil production
Q_w : cumulative water production
S_w : water saturation
f_w : water fractional flow
f_o : oil fractional flow
k_{rw} : water relative permeability
k_{ro} : oil relative permeability
l_r : load recovery
l_{r_i} : initial load recovery
l_{r_u} : ultimate load recovery
S_{wi_f} : initial water saturation in fracture
S_{wf} : average water saturation in fracture
V_{ef} : effective fracture volume
V_{ef_i} : initial effective fracture volume
V_p : total injected proppant volume
ϕ_f : fracture porosity
k_f : fracture permeability
k_m : matrix permeability
S_{or} : residual oil saturation
S_{wr} : irreducible water saturation
T_m : transmissibility multiplier
M_p : proppant mass
ρ_p : proppant density
n_w : Corey exponent for wetting phase
n_o : Corey exponent for nonwetting phase
S_{wD} : normalized water saturation
S_{wi} : initial water saturation
q_w : water flowrate
q_o : oil flowrate
μ_w : water viscosity
μ_o : oil viscosity
μ : gaussian distribution mean
$\beta_1, \beta_2, \beta_3$: WORM's control/tuning parameters
α_1, α_2 : COPM's control/tuning parameters
h_i : ANN's ith hidden layer
$\mathbf{w}_k$: weights in kth input layer
RoC_o : rate of change in oil production with respect to load recovery
p_i : initial reservoir pressure
p_{wf} : bottomhole flowing pressure

Chapter 6.
Linking Flowback Recovery to Completion Efficiency: Niobrara-DJ Basin Case Study

6.1 Introduction

Load recovery refers to the amount of fracturing water produced back after hydraulic fracturing operations. Unrecovered fracturing water either a) leaks off into the formation during fracturing treatment and the following shut-in period; or/and b) is trapped in the fractures. This unrecovered fracturing water inside the formation and fractures may also affect hydrocarbon recovery due to relative permeability effects. Therefore, maximizing load recovery is an important target to enhance hydrocarbon productivity of MFHWs. Several numerical and analytical techniques have been implemented to analyze the flowback process [91, 95-100]. Generally, these studies demonstrated that load recovery is affected by reservoir properties and completion-design parameters. One common issue in these studies is the assumption that fracture properties and dimensions are constant during well production. However, hydraulic fracture characteristics are also affected by geomechanical properties around the wellbore, leak-off rate, pumping schedule, operational parameters such as choke-size changes and shut-in periods, making modeling and prediction of load recovery very challenging with lots of uncertainties. Another challenge encountered in the previous studies is the requirement of determining fracturing-water saturation within and around the hydraulic fractures. Therefore, we present an application for water-oil-ratio (WOR) diagnostic analysis to model load recovery during flowback and predict ultimate load recovery by utilizing flowback and post-flowback data.

Another parameter that is used in this paper to assess the completion efficiency is the effective fracture volume (V_{ef}). However, direct measurement of V_{ef} is challenging. Alkouh, McKetta [35] utilized water-flowback and production data to estimate V_{ef} of shale-gas MFHWs by introducing a tank model based on simulation results. The main concern in this model is that it neglects fracture closure effect and water expansion mechanism which makes it not applicable to single-phase water flowback. Fu, Dehghanpour [36] and Moussa, Dehghanpour [57] analyzed single-phase water flowback data of oil

and gas wells completed in Woodford and Eagleford Formations to estimate V_{ef} using harmonic decline (HD) curve analysis of water flowback versus cumulative water production volume. They assume negligible water influx from matrix into fracture and that HD in water production rate continues until producing all the fracturing water. However, long-term production data generally shows late-time deviation from that pattern when approaching ultimate load recovery, leading to an overestimation of V_{ef}. Therefore, in this study, we estimate initial effective fracture volume by applying a WOR model that accounts for the relative permeability effects particularly when approaching saturation endpoints [6].

In the last decade, understanding the impact of completion-design parameters on the recovery performance of oil and gas MFHWs completed in unconventional resources has gained the attention of many researchers [101-108]. However, the parent-child fracture interference becomes the recent key factor in determining the completion-design parameters for infill wells [109-112]. In this paper, we show a field-case study in which the operator applied a less intense completion-designed strategy to child wells to mitigate their communication with the parent wells. Does it work? In case of avoiding parent-child fracture interreference, does parent-wells depletion affect the hydrocarbon recovery of child wells? Does larger effective fracture volume result in better oil recovery? If the same set of completion-design parameters are applied to parent and child wells, will the recovery performance be similar?

6.2 Methodology

In this study, we analyze flowback, post-flowback and completion-design data of a pad composed of 19 MFHWs completed in Niobrara and Codell formations with 3D trajectories displayed in **Fig. 6.1**. The true vertical depth (TVD) of these wells varies from 6,975 to 7,261 ft. From these wells, 15 are completed in Niobrara formation and the remaining are completed in Codell formation. The studied

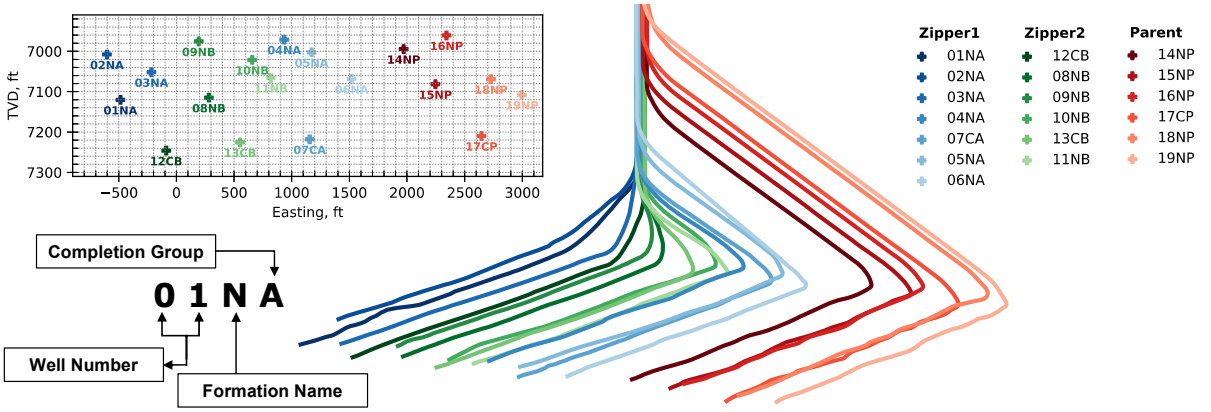

Fig. 6.1 – 3D- well trajectories. Inset figure shows well toe's true vertical depth. Inset schematic illustrates well naming

wells are categorized according to their producing formation and completion group as listed in **Table 6.1**. Parent wells were completed in 2018 with similar completion design. Then, in 2020, Zipper-1 wells were completed first with variable design parameters with the intention to mitigate their communication with the Parent wells. Therefore, in Zipper-1 wells, different completion strategies were tested. This includes applying different cluster spacing, cluster density, proppant and fracturing

Table 6.1 – Completion-design summary of the studied wells which are categorized into Parent, Zipper 1 and Zipper 2

Well ID[1]	Completion Group[2]	Proppant[3] lbs. / Ft	Cluster Spacing	Clusters / Stage	Cluster Density (Ft)	designed gal / Ft	Total Perfs	EHD[4] (inch)	Designed pump rate (bpm)
01NA	ZIPPER 1	500-750-1000	150-200-250	4,8,10	22,33	variable by stage	26,16,20	0.38,0.36,0.36	50,60,70
02NA	ZIPPER 1	500-750-1000	150-200-250	4,8,10	22,33	variable by stage	26,16,20	0.38,0.36,0.36	50,60,70
03NA	ZIPPER 1	500-750-1000	150-200-250	4,8,10	22,33	variable by stage	26,16,20	0.38,0.36,0.36	50,60,70
04NA	ZIPPER 1	500-750-1000	150-200-250	4,8,10	22,33	variable by stage	26,16,20	0.38,0.36,0.36	50,60,70
05NA	ZIPPER 1	500-750-1000	150-200-250	4,8,10	22,33	variable by stage	26,16,20	0.38,0.36,0.36	50,60,70
06NA	ZIPPER 1	500-750-1000	150-200-250	4,8,10	22,33	variable by stage	26,16,20	0.38,0.36,0.36	50,60,70
07CA	ZIPPER 1	500-750-1000	200-250-300	5,9,11	38,25	variable by stage	30,18,22	0.38,0.36,0.37	50,60,70
08NB	ZIPPER 2	750	350	14	23	708	14	0.36	50
09NB	ZIPPER 2	750	350	14	23	708	14	0.36	50
10NB	ZIPPER 2	750	350	14	23	708	14	0.36	50
11NB	ZIPPER 2	750	350	14	23	708	14	0.36	50
12CB	ZIPPER 2	750	350	14	23	708	14	0.36	50
13CB	ZIPPER 2	750	350	14	23	708	14	0.36	50
14NP	PARENT	1000	150	4	33	980	26	0.38	50
15NP	PARENT	1000	150	4	33	980	26	0.38	50
16NP	PARENT	1000	150	4	33	980	26	0.38	50
17CP	PARENT	1000	150	4	33	688	26	0.38	50
18NP	PARENT	1000	150	4	33	980	26	0.38	50
19NP	PARENT	1000	150	4	33	980	26	0.38	50

[1] **Formation Abbreviation:** N= Niobrara, C=Codell

[2] **Completion Groups:** A= Zipper 1, B= Zipper 2, P= Parent

[3] **Proppant Type Used:** 100 mesh & 20/40 for all wells

[4] **EHD**: Entrance Hole Diameter

fluid amounts, number of perforations, entrance hole diameter (EHD), number of clusters per stage and pumping rate as listed in **Table 6.1**. Then, Zipper-2 wells were completed with a relatively smaller number of perforations, cluster density, injected fluid and proppant per feet, but with larger cluster spacing and more cluster per each stage compared to the Parent wells. Well name reflects the completion group and producing formation of each well as illustrated in the inset schematic in **Fig. 6.1**. The first 2 digits in well name represent well number, the third letter denotes producing formation (N=Niobrara and C=Codell), and the fourth letter represents the completion group (A=Zipper 1, B=Zipper 2, P=Parent).

The main objective of this study is to investigate the effects of completion design on well productivity performance. Here, we propose three performance indicators: ultimate load recovery (ULR), initial effective fracture volume (V_{ef_i}), and ultimate cumulative oil production (UQo) assuming a critical oil rate of 1 stbd. For the first two indicators, former investigation of formation-water influx to effective fractures shall be done to formulate the required assumptions for estimating ULR and V_{ef_i}. In this paper, we utilize rate-normalized pressure (RNP) diagnostic plots to investigate the flow regimes during flowback and post-flowback periods for both the parent and child wells. RNP analysis requires estimating initial reservoir pressure (p_i). Therefore, the following methodology is approached in this paper:

1. Apply qualitative analysis of early-time flowback and post-flowback rate and pressure data of the studied wells to a) differentiate between single- and multi-phase flow periods; b) identify if wells show pressure supercharge behavior at early flowback period; and c) calculate average p_i by applying the approach proposed by Jones, Pownall [113] on early flowback data. This method is based on estimating p_{wf} and its flattening comportment when approaching hydrocarbon breakthrough while the well is flowing back its fracturing fluid.
2. Assess the calculated p_i against DFIT data available for five Zipper-1 wells out of which four wells are completed in Niobrara formation (02NA, 04NA, 05NA and 06NA) and one well (07CA) is completed in Codell formation.
3. Investigate the flow regimes of water and oil during flowback and post-flowback periods by plotting rate-normalized pressure for water (RNP_w) and oil (RNP_o) versus material-balance time (t_{MB}) for all the studied wells. RNP_w and RNP_o are defined as $(p_i - p_{wf})/q_w$ and $(p_i - p_{wf})/q_o$ for water and oil, respectively. q_w and q_o are the production flow rate of water and oil at bottomhole conditions, respectively. p_{wf} is the flowing bottomhole pressure, p_i is the

initial average reservoir pressure in the stimulated region around wellbore and is estimated/validated in the previous step. RNP-diagnostic analysis is also applied to investigate the communication between child and parent wells.

4. Apply WOR-diagnostic analysis [6] to predict ULR and estimate V_{ef_i} assuming that fracture is initially filled with water, and negligible formation water production. These assumptions are validated in steps 1 and 3, respectively.
5. Construct diagnostic plots of oil production rate (q_o) versus cumulative oil production (Q_o) on semi-log plots and apply hyperbolic decline analysis to estimate UQo of each of the studied wells assuming a minimum daily oil production rate of 1 stbd.
6. Analyze the effect of completion-design strategies applied to parent and child wells on their recovery performance in terms of a) 3-, 7- and 9-month measured LR; b) estimated ULR and V_{ef_i}; c) 3-, 7- and 9-month measured Qo; and d) predicted UQo.

6.3 Results and Discussion

6.3.1 Initial reservoir pressure estimation from flowback data

Fig. 6.2a shows the hourly flowback water, oil and gas rates and calculated p_{wf} during flowback process of Well 01NA. The figure demonstrates an initial single-phase water flowback for 6 days with a slight decrease in p_{wf}. The initial hydrocarbon traces are observed after flowing back more than 15 kstb of fracturing water (more than 25 times of the wellbore volume) which suggests an initial supercharge effect. The sudden increase in the estimated p_{wf} as hydrocarbon production starts might be due to gas influx into the wellbore and lighting the fluid column. Then, p_{wf} becomes flat for almost 3 days before declining while the oil production rate increases significantly. Therefore, the stabilized value of p_{wf} is approximated to be the estimated average reservoir pressure [113]. **Fig. C.11** shows the early flowback data for all the studied 19 wells and the estimated p_i. For the parent wells, the flowback period is not long enough to observe a continuous decline in p_{wf} after a flatten period. Therefore, the estimated p_i for those wells are not reliable. The p_i of the studied wells is estimated to be between 3,700 and 4,350 psi with an average p_i of 4,094 psi. Niobrara and Codell wells show an average p_i of 4,110 and 4,037 psi, respectively. This leads to a pore pressure gradient of 0.582 and 0.560 psi/ft for Niobrara and Codell wells, respectively. DFIT analysis gives a pore pressure of 3,880 psi for well 06NA which is 2% higher than the estimated p_i for this well as shown in **Fig. C.11**. Although the DFIT data

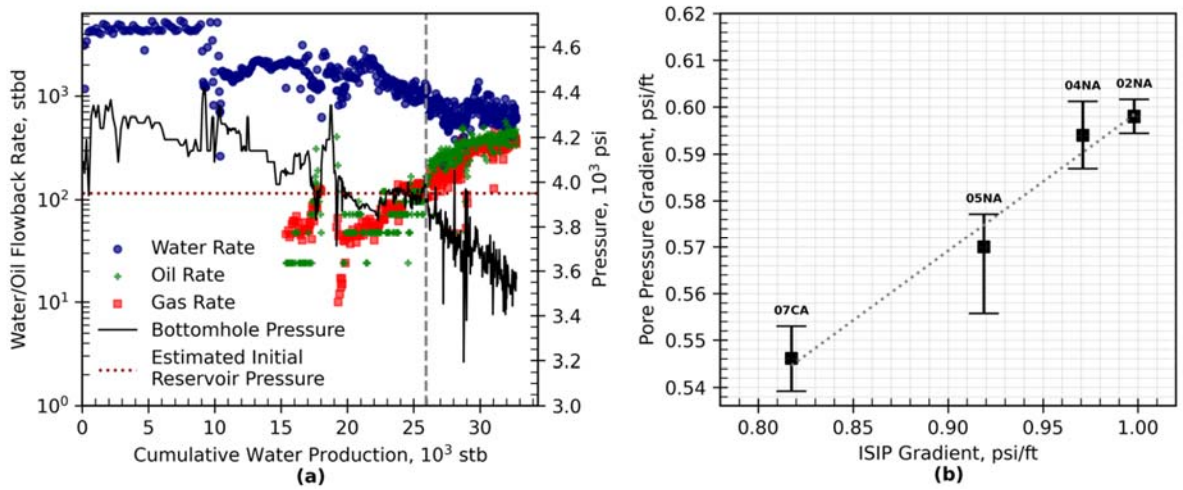

Fig. 6.2 – (a) Hourly flowback data for Well 01NA shows initial single-phase water production, then flattening bottomhole pressure (p_{wf}), then a decline in p_{wf} at the end of flowback period. **(b)** cross-plot between estimated pore pressure gradient and ISIP gradient from DFIT

is also available for wells 02NA, 04NA, 05NA, and 07CA, the pore pressure could not be estimated due to the poor falloff pressure data quality. However, the bottomhole instantaneous shut-in pressure (ISIP) for those wells are reported as 7,009, 6,783, 6,448 and 5,931 psi, respectively. **Fig. 6.2b** shows that the pore pressure gradient (estimated from flatten p_{wf} period) has a pronounced positive correlation with ISIP gradient resulted from DFIT. Wells with higher ISIP gradient show higher pore pressure gradient. The figure also shows that generally the pore pressure gradient is 35-40% less than ISIP gradient reported for those wells.

6.3.2 Rate-normalized-pressure diagnostic analysis

Fig. 6.3 shows flowback and post-flowback water and oil RNP versus material-balance time for a child-Zipper-1 well (01NA) and a parent well (17CP). RNP plots for the other wells are presented in **Fig. C.5**. RNP_w for all wells follow a pronounced unit slope during flowback and post-flowback periods indicating a boundary-dominated or a pseudo-steady-state (PSS) flow regime. This indicates a closed-tank system for water production with no-flow outer boundary. In other words, RNP_w plots indicate that there is no water influx from the matrix during flowback and post-flowback. Even for the parent wells with more than 2 years of production, the closed-tank system of water is not interrupted while completing the child wells (Zipper 1 and Zipper 2 wells). On the other side, RNP_o shows half-slope suggesting a transient linear behavior which might be as a result of a) producing from fractures that extend to reservoir boundaries [93]; b) transient drainage of low permeability matrix into adjacent fractures; and c) linear shape of reservoir [94]. It should be mentioned here that the parent wells were pre-loaded with water and shut-in during fracturing the child wells. After putting back the parent wells on production, RNP_w still follows a pronounced unit-slope, although

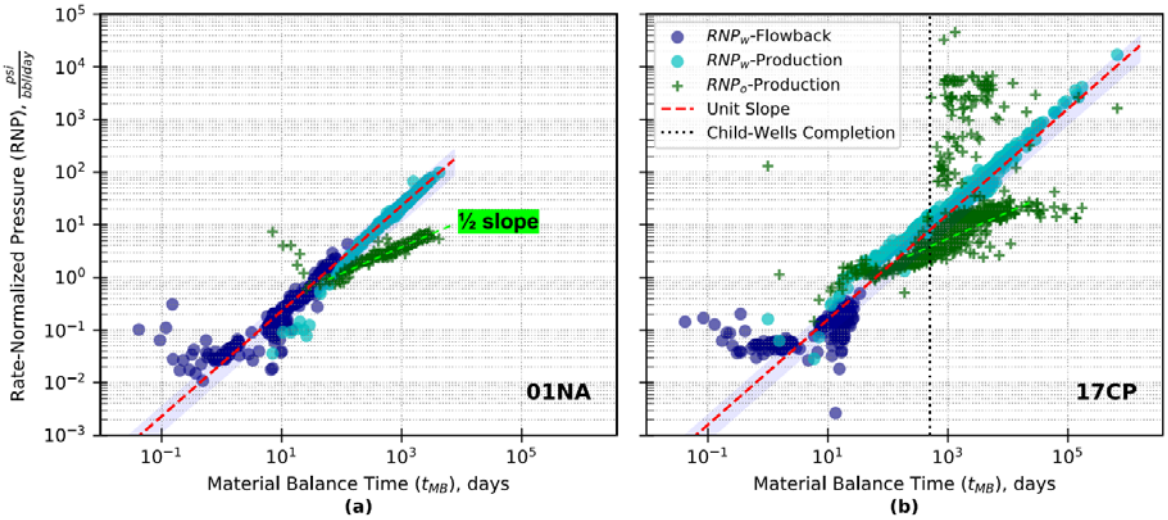

Fig. 6.3 – Rate-normalized pressure plots of flowback and production water and oil for **(a)** child-well 01NA and **(b)** P-well 17CP

RNP_o indicates a sharp decline in the oil production rate. This is mainly due to the water pre-loading process which increases the water saturation in the stimulated region around wellbore and hence reduces the oil relative permeability and consequently the oil production rate at this period. The pronounced unit-slope displayed by RNP_w of parent wells before and after completing the child wells and the fact that the decrease in oil rate is due to the pre-loading effect, indicate no significant interference between the stimulated volumes of child and parent wells. In addition, the obvious unit-slope of RNP_w for both the child and parent wells in Niobrara and Codell formation indicates insignificant formation water influx from the matrix into the stimulated region around the wellbore of the studied wells. This is an important conclusion as it solidifies our assumption when estimating the initial effective fracture volume of the studied wells.

6.3.3 Initial effective fracture volume estimation

Fig. 6.4a shows that WOR during flowback and post-flowback periods follows a logit trend when plotted on a semi-log plot versus load recovery [6]. A WOR model can fit the flowback data and further validated by post-flowback data to predict ULR. The figure shows ±10% uncertainty when applying WOR model on only the early-time flowback WOR to predict ULR. However, this uncertainty is significantly reduced when the post-flowback WOR becomes available and utilized to tune the model parameters. Therefore, assuming a critical WOR of 0.001 stb/stb that represents the end of load recovery, the ULR in this case is estimated to be around 34%. The average ULR of all the studied wells is estimated at 44% as shown in **Fig. 6.4b**. This relatively low ULR endorses the outcome of negligible formation water influx from the matrix into effective fracture concluded from RNP diagnostic plots presented in the previous section. In this figure, the wells in each completion group are sorted based

on their ULR. Measured 3-,7- and 9-month load recovery are also demonstrated for each well. There are five main observations from this figure: a) generally Codell wells show the highest measured LRs and estimated ULRs in each completion group; b) wells with higher LR at 3-, 7- and 9-month show higher ULR; c) if only Niobrara wells are considered, Zipper-1 wells show the highest average ULR, then Zipper-2 and Parent wells, respectively; d) more than 50% of the predicted ULR is produced back within the first 3 months of production; and e) on average, the child wells show 32% more load recovery compared to the parent wells.

The estimated ultimate water production volume can approximate the initial effective fracture volume (V_{ef_i}) assuming a) fractures are completely filled with water initially (supported by the initial single-phase water flowback); b) pressure-supercharge conditions at early days of flowback as illustrated in **Fig. 6.2a**; and c) water production is mainly from fractures. **Fig. 6.4c** shows the estimated V_{ef_i} sorted

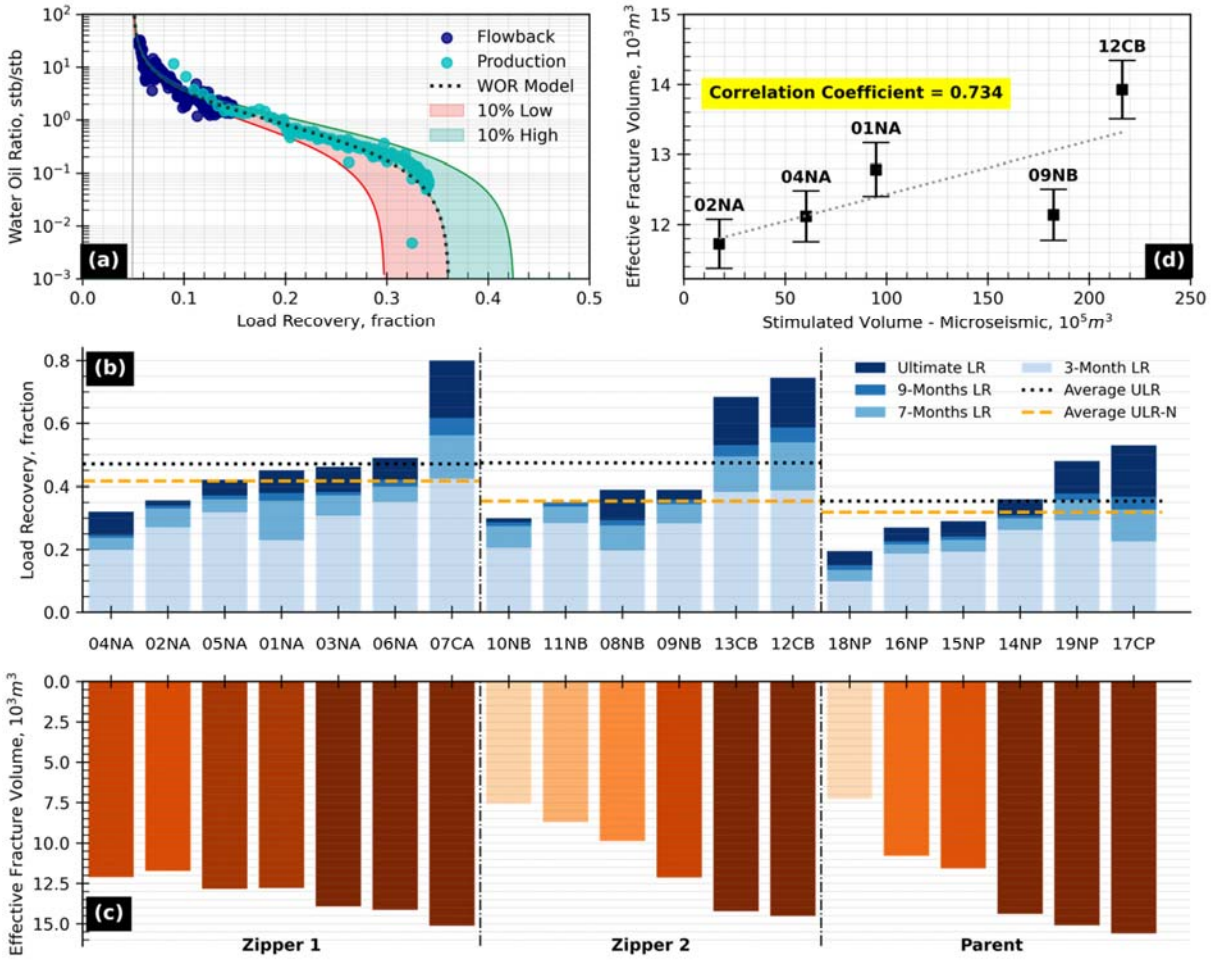

Fig. 6.4 – (a) Estimated ultimate load recovery using WOR model [6]. **(b)** Ultimate load recovery and measured ones for the studied wells at different production times. **(c)** Estimated Vef for the studied wells. **(d)** crossplot between estimated Vef from WOR and the stimulated volume from

for each completion group. It could be noticed that Codell wells show larger V_{ef_i} compared to Niobrara wells in each group. Zipper-1 wells show the largest average V_{ef_i} with the least variations. The effects of completion-design on V_{ef_i} will be discussed in the next section.

6.3.3.1 Comparing effective fracture volume against microseismic dimensions

Fig. C.7 demonstrates the microseismic event dimensions grouped to each fracture stage in terms of Length, Width and Height for wells 01NA, 02NA, 04NA, 09NB and 12CB. The figure shows that the events count varies from less than 10 to 250 events per fracture stage. In this study, we use 70 events as a cut-off. Fracture stages with more than 70 counted microseismic events are utilized to calculate their volume giving their microseismic dimensions (length, width, and height). Then, we sum those estimated fracture-stage volumes to estimate the microseismic-events volume (V_{ME}) for each well. **Fig. 6.4d** presents a crossplot of estimated V_{ef_i} versus V_{ME}. The figure demonstrates a positive correlation coefficient of 0.734 between V_{ef_i} and V_{ME} for the 5 wells. So, generally wells with V_{ME} demonstrate largerV_{ef_i}. In addition, this positive correlation allows us to utilize V_{ef_i} as a performance indicator in this study.

6.3.4 Completion-design effect on well productivity performance

The results presented in **Fig. 6.5a** suggest that Zipper-1 wells have the largest average V_{ef_i} then Parent and Zipper-2 wells, respectively. This difference even increases when only the Niobrara wells in each group are considered. As illustrated in **Table 6.1**, unlike Parent and Zipper-2 wells, the completion-design parameters for Zipper-1 wells vary per stage. Therefore, the polar chart in **Fig. 6.5b** illustrates the difference in completion design between Zipper-2 and Parent wells. For Zipper-2 wells, the

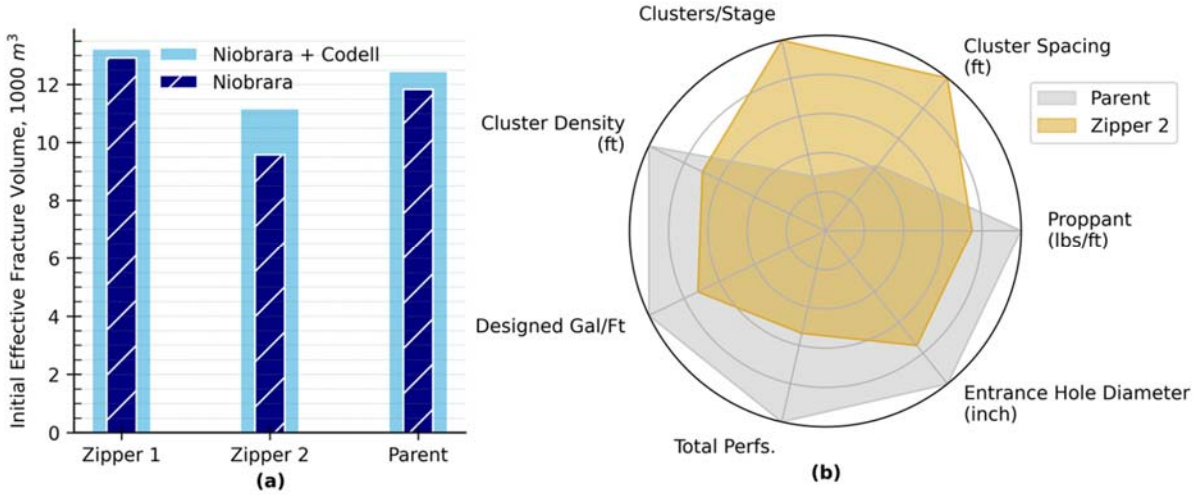

Fig. 6.5 – (a) Average initial effective fracture volume per well in each completion group. **(b)** average completion-design parameters of Parent and Zipper 2 wells

objective was to mitigate the interreference between the wells, compared with the parent wells, the operator decided to reduce the cluster density, injected fluid volume and proppant per feet, total number of perforations and the entrance hole diameter of each perforation for the child wells. On the other side, the operator increased the number of clusters per stage and cluster spacing as shown in **Fig. 6.5b**. The RNP diagnostic analysis discussed previously shows that this adapted completion design for Zipper-2 wells is successful in mitigating the inter-well communication with the Parent wells while fracturing the Zipper-2 wells. However, it led to a relatively smaller effective fracture volume compared to the Parent wells as shown in **Fig. 6.5a**. This difference is even emphasized in Niobrara wells.

6.3.4.1 Injected water volume and effective fracture volume

For a single-variable analysis, **Fig. 6.6** gives deeper insight on the relationship between V_{ef_i} and injected water volume per feet (IWV_f). Generally, more IWV_f results in larger V_{ef_i} regardless of the completion group of the target well. A Lower-level analysis also confirms this trend. However, V_{ef_i} for Zipper-2 wells becomes more sensitive to IWV_f as shown in the figure. Therefore, a larger V_{ef_i} could have been achieved if more IWV_f was applied to Zipper-2 wells. Zipper-2 wells were completed by IWV_f between 380 to 400 bbl/ft. Zipper-1 wells were completed by IWV_f more than 420 bbl/ft and yet did not cause significant communication with the Parent wells, although wells 04NA, 05NA and 06NA (with IWV_f of 442, 432 and 437 bbl/ft) in Zipper-1 are the laterally closest wells to the Parent wells as shown in **Fig. 6.1**.

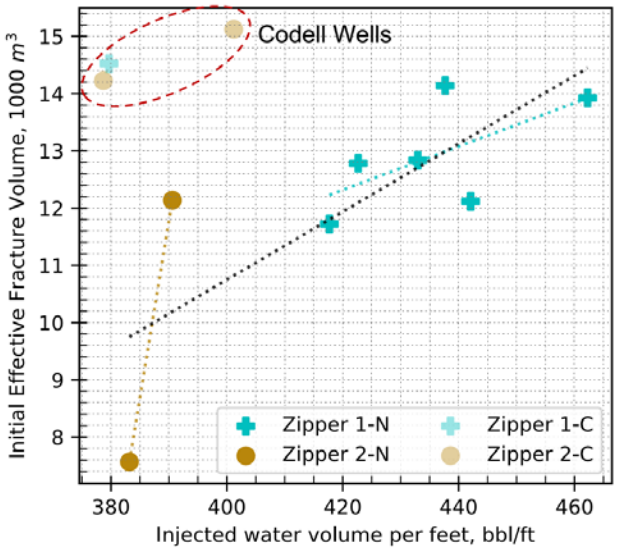

Fig. 6.6 – Crossplot between estimated initial effective fracture volume and injected water volume per perforated feet. Faded points represent Codell (C) wells. Dotted lines represent the linear regression/fit between each group's points while the black dotted line represents the linear regression between Niobrara wells

6.3.5 Oil productivity performance

The previous discussions showed that Zipper-1 wells performed the best in terms of ultimate load recovery and initial effective fracture volume. Zipper-2 wells showed more load recovery compared to the Parent wells, but with less effective fracture volume. Here we compare the oil productivity performance of the wells the three groups. **Fig. C.12** shows that the oil production rate of child and parent wells (with more than 2 years of daily production data) follows a hyperbolic decline trend when plotted versus cumulative oil production (Qo) on a semi-log plot. Therefore, in this paper, we use hyperbolic decline model to predict Qo when the oil production rate drops to a critical value of 1 stbd, and we define it as ultimate cumulative oil production (UQo). we use it as a performance indicator for oil productivity among the studied wells. In addition to the estimated UQo, **Fig. 6.7**displays the measured 3-, 7- and 9-month Qo. The wells in each group are sorted by UQo. There are several outcomes observed from this figure: a) Parent wells show higher measured 3-, 7- and 9-month Qo compared to the child wells; b) average UQo predicted for Parent wells is 50% more than what is predicted for the child wells; c) Child wells exhibit an average hyperbolic decline constant (b) of 0.01 which is very low (very close to exponential) compared to parent wells with average b of 0.31; and d) despite the intense completion-design strategy applied to Zipper-2 compared to Zipper-1 wells, both groups demonstrate similar oil recovery performance in terms of the measured 3-, 7- and 9-month Qo and UQo.

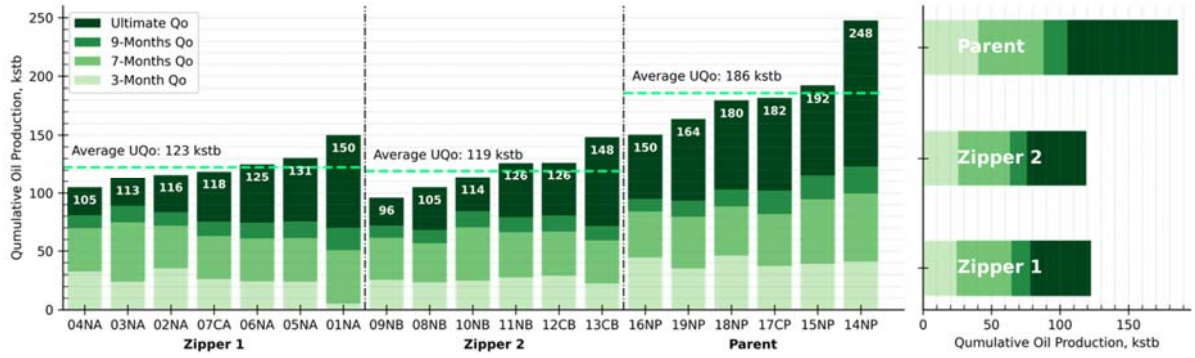

Fig. 6.7 – Ultimate cumulative oil production predicted by the hyperbolic decline model (considering critical oil production rate of 1 stbd) and the measured cumulative oil production at 3, 7 and 9 months

6.4 Summary

We analyzed the early production and completion data of 19 MFHWs completed in Niobrara and Codell formations that led to the following results:

1. Flowback data of the studied wells show an average 6-day period of single-phase water production. This period increased by 25% on average for Zipper-1 wells which were completed with a relatively more intense design strategy.

2. Estimated pore pressure gradient of 0.587 and 0.546 psi/ft from flowback pressure profiles for Niobrara and Codell wells, respectively, show an acceptable match with the DFIT results.
3. RNP diagnostics plots suggest a) negligible water flow between matrix and effective fractures during flowback and post-flowback periods; and b) that effective fracture networks for both the parent and child wells behave as closed tanks during flowback and post-flowback periods
4. Generally, Niobrara wells show less load recovery and effective fracture volume compared to Codell wells in each completion group.
5. Zipper-2 wells showed 35% smaller effective fracture volume and less capability to recovery fracturing water compared to Zipper-1 wells due to altering the design strategy by reducing injected water volume and proppant per feet, cluster density and total number of perforations while increasing cluster spacing and number of clusters per stage. However, both groups showed similar oil recovery performance. In other words, although Zipper-1 wells showed larger effective fracture volume compared to Zipper-2 wells, both groups showed similar oil recovery performance. This suggests that the completion intensity for child wells does not help much to recover more oil.
6. Although the child wells demonstrated better load recovery performance in terms of measured LR and 32% more predicted ULR, parent wells showed 38% and 50% more 9-month Qo and UQo, respectively. This is mainly affected by the quality of the formation where each group is completed.
7. For both the parent and child wells, more than 50% of the predicted ULR is produced back within the first three months of production.

Chapter 7.
Proxy Model Development for Completion Design Optimization as Function of Reservoir Quality

7.1 Introduction

Optimizing the completion design of multi-fractured horizontal wells (MFHWs) in tight reservoirs is a complex task. This complexity arises from factors such as: 1) identifying the optimal sweet spots for positioning a MFHW within a heterogeneous tight reservoir, while mitigating potential interference with existing parent wells; 2) defining the wellbore trajectory and direction to align with the minimum horizontal stress, and choosing between a flat, upward, or downward toe orientation, is critical to ensure efficient proppant transportation to the toe section while minimizing significant proppant settlement within the wellbore; 3) choosing between open- or cased-hole completion to balance between matrix-to-wellbore connectivity and potential formation damage; 4) selecting a fracturing fluid that minimizes the risk of skin or formation damage during fracturing while effectively carrying the proppant away from the wellbore; 5) determining the type and amount of proppant that maintains the developed fractures open without excessive packing that might reduce fracture conductivity; 6) deciding on a pumping design to efficiently propagate fractures without introducing water blockage within the reservoir; and 7) selecting the optimal completion design concerning the number of stages, stage lengths, fracture spacing, number of clusters within each stage, perforation density, and deciding whether to allow the well to soak post-fracturing or to directly flowback the fracturing fluid to the surface. Each of these factors requires careful consideration to achieve a well-balanced, effective fracturing design, demonstrating the multifaceted nature of optimizing MFHWs in tight reservoir scenarios.

Many operators have employed different techniques to analyze and optimize the completion design of MFHWs in tight formations, yielding different results. Usually, these methods address individual aspects of this complex process, consequently not leveraging all available data concurrently. Typically, an integrated workflow is employed using commercial software to optimize field development planning, leading to business decisions. The initial step in this workflow involves constructing a comprehensive 3D geological model for reservoir characterization, utilizing available core, well-log

and seismic data. Next, hydraulic fracture modeling is conducted using numerical simulators, integrating DFIT and microseismic data to estimate fracture geometries and conductivities. Then, analytical and numerical flow modeling, which utilize outputs from the geological and completion models, PVT analysis, and downhole/surface pressure and rate data to forecast the expected drainage for each well. These calibrated fracture and reservoir models serve as the foundation for optimization studies for well and fracture spacing. However, each model was developed independently. This independence posed challenges in seamlessly transitioning from one model to the next step of the workflow.

Generally, the success of tight reservoir development depends heavily on the effectiveness of the completion design. However, the reservoir characteristics shall be understood before optimizing well completion. Holderby, Dahl [114] showcases three wells completed in the Barnett Shale to demonstrate the benefit of improved reservoir understanding before optimizing completion design. It was observed that the average Estimated Ultimate Recovery (EUR) of the three wells improved by nearly 30% with a completion design optimized based on reservoir characteristics. In addition, Considering the geomechanical properties and specifically the presence of natural fractures while in completion design optimization might signigicanly enhance the hydrocarbon recovery from MFHWs [115] . This improvement is likely due to the reopening or interconnection of the existing natural-fracture system in a reservoir through a completions design. The design aims to generate a complex-fracture network, creating conductive flow paths that expose more surface area compared to planar fractures [116].

Jaripatke, Samandarli [117] presented a workflow for optimizing completion design in the Eagle Ford Shale, including thorough reservoir and economic analyses associated with each tested completion parameter. It was illustrated that different completion parameters significantly influence well performance and economics. The study concluded that optimum completion practices could vary with different reservoir characteristics.

Furui, Zhu [118] investigated how to determine well configurations based on formation properties, employing skin-factor models to evaluate different completion types for cased- and open-hole completions. A proposed workflow utilizes different skin factor models to identify optimal completions for horizontal wells. It highlights key parameters impacting completion performance including reservoir permeability, permeability anisotropy, fluid properties, formation damage effects, and geomechanical properties. They concluded that a cased and perforated well completion is preferable in formations with significant permeability damage.

In a seven-well study aimed at optimizing completion design and well spacings in the Wolfcamp Formation, a 3D geological and wellbore fracture-propagation model was initially developed then transitioned into a reservoir simulation model and calibrated with production history [119]. The results indicated that well spacings and respective completion designs significantly influenced fracture hits/well interference and drainage volume. The study concluded that tighter cluster spacing and higher fluid and proppant intensity in the southern Midland Basin's Wolfcamp Formation could enhance the initial production rate and ultimate recovery.

In the last decade, numerous studies have been conducted to optimize the performance of well production utilizing ML techniques. Wang and Chen [120] developed a machine learning based predictive model to assess the performance of MFHWs in the Montney formation, using 6-month cumulative production data as an output. They utilized 11 well completion parameters as input parameter to their model, including the number of stages, fracture spacing, and proppant per stage. By integrating cluster data mining techniques with neural network, they introduced a predictive model to optimize the well productivity. Similarly, Bowie [121] employed machine learning modelling to optimize the completion designs of MFHWs completed in the Duvernay Formation. Their model yielded solutions with the potential to enhance well production performance by over 50% by optimizing different completion design parameters, including the volume of fluid pumped and proppant concentration. However, these models are not coupled with reservoir properties or/and geomechanical properties so that they are not applicable for sweet spots identification.

Mohaghegh, Gaskari [122] incorporated reservoir characteristics such as porosity, Total Organic Content, and water saturation alongside completion-design parameters like proppant loading and injection rate in their data analytics and predictive ML modeling. Focusing on the 30-day cumulative production in Marcellus formation. They developed type curves for completion-design optimization. The analytical findings revealed that among the reservoir parameters, only net thickness exhibited a limited influence on the 30-day cumulative production in the Marcellus shale.

Tandon [123] explored the use of integrated ML-techniques for identifying sweet spots in unconventional reservoirs. Utilizing eight primary geomechanical parameters such as stiffness, geostress, and fracture toughness as predictors, predictive ML modeling was conducted based on the numerical results from 200 hydraulic fracturing simulations. The study focused on impacts of the geomechanical parameters on identifying the sweet spots.

Recently, a thorough methodology involving data analytics and predictive machine learning modelling was proposed, employing techniques like Random Forest (RF), Generalized Additive Model (GAM), and Deep Neural Network (DNN) [124]. The objective was to identify the sweet spots

in the Montney formation and optimize completion designs by leveraging reservoir and completion properties, aiming to enhance the MFHWs' productivity. The approach utilized over 30 reservoir and completion parameters as input features. For measuring productivity, 3- and 12-month cumulative production data were employed as target metrics. However, the model was trained on a relatively modest dataset of only 77 MFHWs in the Montney formation, which might hinder its generalizability across the formation. The validation tests displayed reasonable predictive accuracy with RF and GAM techniques, while the DNN model seemed to necessitate further refinement and hyperparameter optimization, potentially due to the limited number of data points available for training.

While there are many ML-based predictive modeling approaches to forecast well performance in tight reservoirs, there are limited studies focused on the comprehensive development of the Montney formation considering both reservoir characteristics and completion design. Specifically, this study seeks to answer two main questions: 1) How can sweet spots for MFHWs in the upper, middle and lower Montney formation be accurately identified? and 2) How can the completion design be optimized based on the reservoir quality and geomechanical properties? By addressing these questions, we aim to provide a more holistic and effective approach to optimizing well performance in the Montney formation.

In this study, data from over 14,000 oil and gas wells completed in the Montney formation are analyzed. Utilizing core analysis and well log data, a support vector machine (SVM) model is developed to predict formation permeability as function of porosity, bulk density, gamma ray (GR), and short and deep resistivities. Employing hierarchical clustering, the lithology of each sub-formation is categorized using key well log data. The application of 3D kriging interpolation aids in filling the missing data points, subsequently leading to the creation of high-resolution petrophysical maps for the upper, middle, and lower Montney formations. From these maps, a Reservoir Quality Index (RQI) map is derived, facilitating the identification of optimal sweet spots.

Following this, a methodology is introduced to estimate a formation's fracability, as represented by the brittleness index, from sonic log data. A novel metric termed Stage Positioning Efficiency (SPE) is also proposed. SPE serves as a valuable gauge for evaluating the effectiveness of fracture stage placements in alignment with the RQI along the wellbore. Additionally, a new term, effective distance to nearby wells, is proposed to estimate the minimum effective distance between a well and its surrounding wells based on both 3D spatial distance and directional difference.

Finally, all gathered petrophysical, geomechanical, and completion design data are coupled with historical production data. This incorporated data serves as the foundation for developing a neural

network-based proxy to predict well performance as function of both reservoir quality and completion design.

7.2 Methodology

7.2.1 Lithology-Based Sub-Clustering of Montney Formation

Here, we classify the Montney Formation into sub-clusters based on its varied lithologies. For identifying lithologies, we use ϕ, GR, ρ_b, and PE well log data, finding over 4,000 Montney wells with these four well log data sets available. A semi-supervised clustering method is employed for lithology identification. Initially, hierarchical clustering is applied, which is a method that groups similar data points together based on the given parameters, with a visual representation known as a dendrogram shown in **Fig. 7.1**a. This helps to understand our dataset better, assisting in choosing an appropriate number of clusters for the next step. The chosen approach is essential as we don't have prior knowledge regarding the number of lithology clusters expected for Montney based on the given input data of ϕ, GR, ρ_b, and PE. The dendrogram provides a preliminary insight into the likely number of clusters, which is then used as input for a more advanced supervised clustering algorithm known as Agglomerative clustering. Agglomerative clustering is a method where each data point starts as an individual cluster, and pairs of clusters are merged as one moves up the hierarchy, aiming for a final classification [125]. This is demonstrated in **Fig. 7.1**b, which identifies three distinct lithology clusters within Montney. Cluster 3 is noted to be the deepest and hosts the majority of Montney wells (75%), followed by Cluster 1 (20%) and then Cluster 2 (5%). In the discussion section, we explore why most Montney operators opt to complete their wells in Cluster 3, then Cluster 1. Lastly, **Fig. 7.1**c shows that

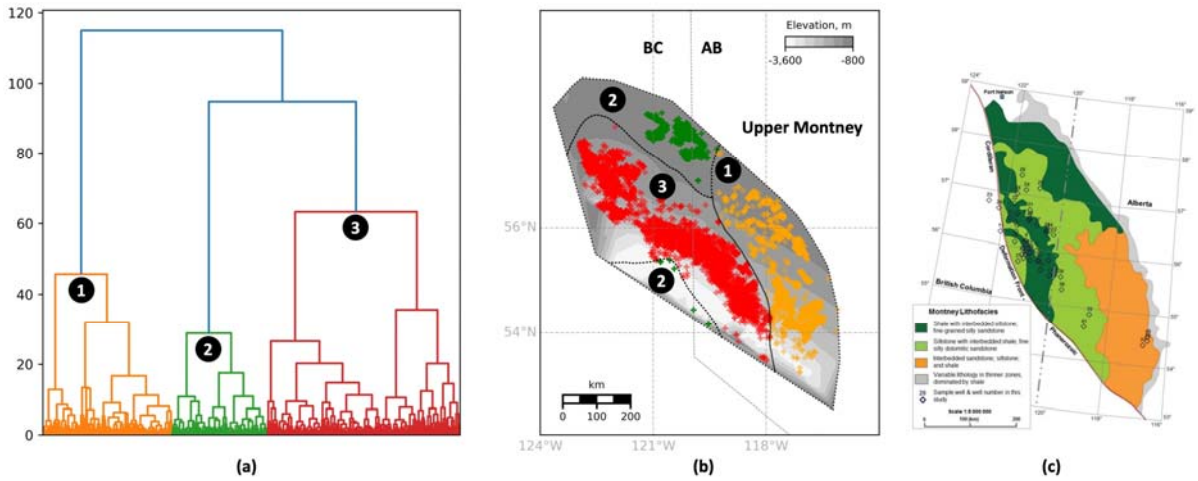

Fig. 7.1 – Hierarchical clustering approach for lithology identification in the Montney Formation, **(a)** dendrogram of the potential clusters, **(b)** clusters mapped on the Montney formation, **(c)**, Montney lithofacies [5]

our lithology-based clustering aligns well with the distribution of Montney lithofacies as presented by Edwards, Barclay [5].

7.2.2 3D Kriging Interpolation

For each identified cluster, we applied 3D kriging to interpolate the petrophysical properties in wells with incomplete well log data. The choice of 3D kriging was motivated by its geostatistical interpolation capability, utilizing longitude, latitude, and elevation as a three-dimensional framework to interpolate missing petrophysical properties based on the observed ones. A grid search was conducted to fine-tune the parameters and select the optimal model. This search explored a predefined parameter grid, encompassing three variogram models (linear, spherical, exponential) to capture the spatial correlation among data points, three distinct numbers of averaging bins for the semi-variogram (4, 6, 8), and a boolean flag weighting semi-variance at shorter lags, concluding in a comprehensive examination of 18 unique configurations.

Fig. 7.2 illustrates the application of 3D kriging to interpolate missing values of ϕ in Cluster 1 within the upper Montney formation. **Fig. 7.2**a shows the wells with available ϕ data alongside those with missing values. Subsequently, in **Fig. 7.2**b, 3D kriging is employed to interpolate porosity values to wells missing this data, by utilizing their respective longitude, latitude, and elevation coordinates. **Fig. 7.2**c presents a porosity contour map interpolated for Cluster 1. This methodology is extended to all other clusters, as well as to the middle and lower Montney formations, to generate high-resolution 3D maps of the studied petrophysical properties.

7.2.3 Permeability Estimation from Well Logs

In this section, we demonstrate the method of correlating well log data, specifically, ϕ, ρ_b, GR, shallow resistivity (R_s) and deep resistivity (R_d), with reservoir permeability (k) using a Support Vector

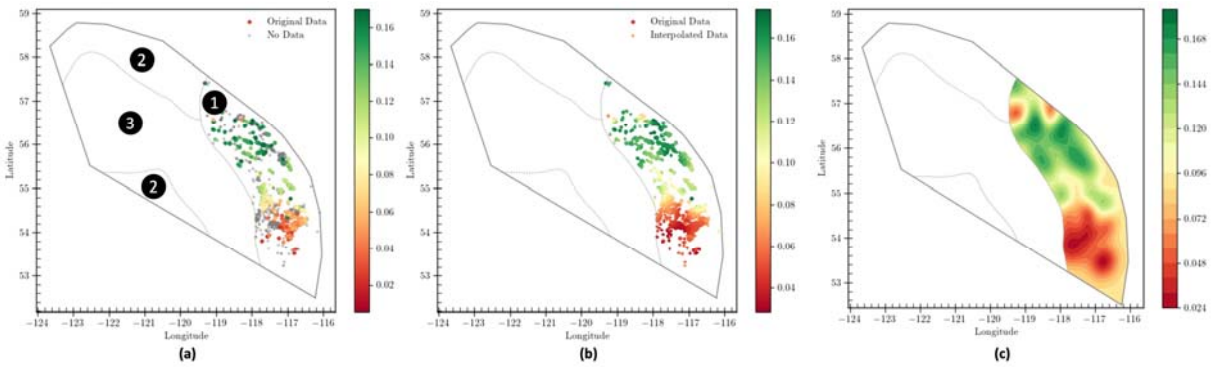

Fig. 7.2 – 3D kriging application to interpolate missing ϕ in Cluster 1 in the upper Montney Formation, **(a)** before interpolation, **(b)** after interpolation for the existing wells and **(c)** contour map of interpolated ϕ

Machine (SVM) modeling approach. The rationale behind selecting these particular input parameters stems from the general expectation that rocks with higher ϕ and lower ρ_b, which are relatively cleaner as suggested by GR, are likely to exhibit higher permeability. Additionally, the ratio between R_d to R_s can signify fluid/mud invasion, providing a direct indication of rock permeability [126]. Therefore, R_d and R_s are restructured into a new term ($r_R = \log R_d/R_s$), to better capture its relationship to k in our analysis.

7.2.3.1 Well-log Data Validation Utilizing Core Data

A critical step in this process is the validation of well log data against core data, given that the output in the SVM model is derived from core permeability. Therefore, a crossplot is constructed comparing bulk densities as estimated by well log versus core analysis, as shown in **Fig. 7.3**. For each core sample, both the ρ_b from core analysis and well log are available. The equality line in the crossplot is then shifted upward by 3% to account for rock compaction and reduced pore volume, a consequence of the difference in rock compressibility between downhole and laboratory conditions. This 3% correction is computed based on an average reservoir pressure of 3,000 psi and an average formation compressibility of 1×10^{-6} psi^{-1}, resulting in a 3% change in pore volume ($\Delta V_p = c_f V_p \Delta p$). This change in pore volume is considered approximately equivalent to the change in ρ_b from downhole to surface conditions. Additionally, a margin of +/-5% is established around this line to accommodate

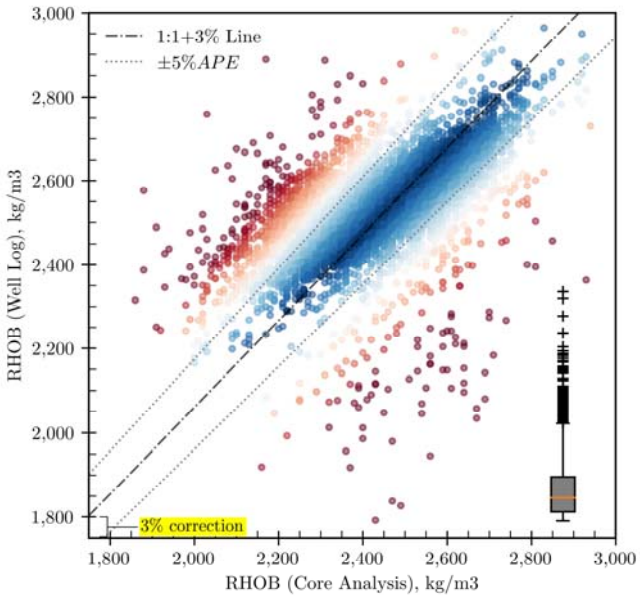

Fig. 7.3 – Crossplot of bulk densities estimated from well log versus core analysis

measurement accuracy, and data points within this region are flagged as valid. Through this validation step, a total of 1,022 Montney wells with 3,067 valid core samples are identified.

7.2.3.2 SVM model development for permeability prediction

In this study, we employ the Support Vector Machine (SVM) modelling to predict k utilizing ϕ, ρ_b, GR, R_s and R_d as input parameters. SVM operates by mapping the input data into a higher-dimensional space and optimizes a hyperplane to minimize the error between the predicted permeability $\hat{k}$ and k. The optimization of this hyperplane is governed by hyperparameters, namely the kernel type, regularization parameter (C), and ϵ. The kernel type was considered as a categorical parameter with four potential selections: Linear, Poly, RBF and Sigmoid. On the other hand, C and ϵ were treated as continuous parameters with ranges of (0.1, 100) and (0.01, 1) respectively. The selection of appropriate hyperparameters is crucial as it significantly influences the model's performance and its capability to generalize well on unseen data. To systematically and efficiently navigate through the hyperparameter space, we employed Bayesian Optimization. This probabilistic model-based optimization technique iteratively evaluates the performance of selected hyperparameters, learning from previous evaluations to identify the optimal set.

7.2.4 Brittleness Estimation from Sonic Log

Here, we illustrate the methodology of utilizing sonic log data to estimate the formation's fracability, as indicated by the brittleness index (B_i). First, we collect the sonic-log data available for Montney wells. Then, we extract both the compression and shear transient times (DT_{co} and DT_{sh}, respectively). Second, estimate compression velocity (V_c) and shear velocity (V_s) by simply inverse the wave transient time ($1/DT_{co}$ and $1/DT_{sh}$, respectively). Third, we use the correlation provided by E. Fjær [127] to estimate the dynamic Young's modulus (E_d) and Dynamic Poisson's ratio (v_d) as follows:

$$E_d = \frac{\rho V_s^2 (3V_c^2 - 4V_s^2)}{V_c^2 - V_s^2} \tag{7.1}$$

$$v_d = \frac{V_c^2 - 2V_s^2}{2(V_c^2 - V_s^2)} \tag{7.2}$$

Then, we use E_d and v_d to estimate the brittleness index according to the hypothesize proposed by Grieser and Bray [128] as they showed that ductile rocks, generally, exhibit a low Young modulus (E) and high Poisson's ratio (v), whereas brittle rocks, generally, exhibit a moderate to high E and low v. Next, we apply the fuzzy set theory introduced by Zadeh [129] to convert the crisp classification of brittleness resulted from the previous step to fuzzy classification as shown in **Fig. 7.4**. Finally, we apply this workflow to all Montney wells with available sonic log data, followed by employing 3D

kriging to interpolate the B_i for wells missing this log, thereby creating a comprehensive 3D map of B_i across the Montney formation.

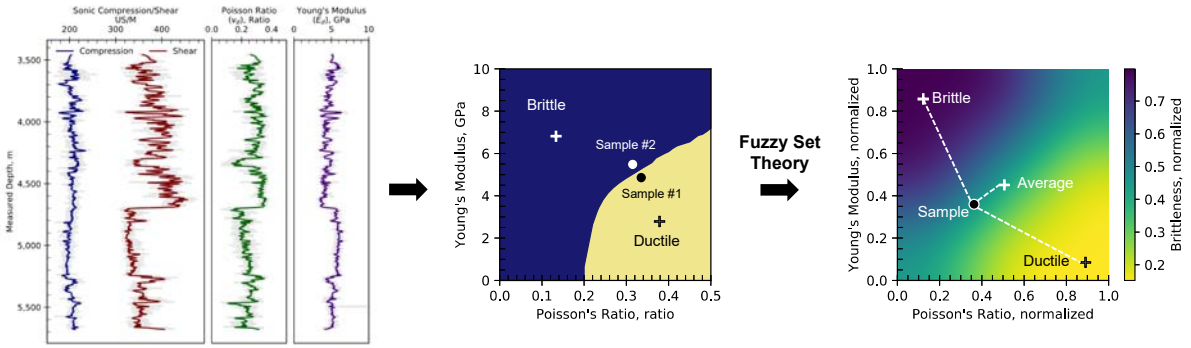

Fig. 7.4 – Workflow to estimate brittleness index from sonic-log data

7.2.5 Reservoir Quality Indexing using Fuzzy Logics

Here, we utilize the supervised fuzzy clustering (SFC) algorithm, detailed in **Chapter 3**, as a multivariate analysis tool to combine p_i, S_{HC}, ϕ, k, h_{net} and B_i and develop a reservoir quality index (RQI). RQI serves as a classifier of the reservoir quality for each studied well. The term reservoir quality refers to the quality of the part of the formation where each well is completed. A higher RQI refers to relatively higher p_i, S_{HC}, ϕ, k, h_{net} and B_i while a lower RQI refers to the opposite. The outcome of this step is an estimated RQI for each Montney well. Then, we create a 3D spatial representation of the RQI, generating a comprehensive map across the Montney formation.

7.2.5.1 Stage Positioning Efficiency Determination

In a practical extension of the RQI, we propose a characteristic term known as Stage Positioning Efficiency (SPE). SPE serves as an innovative metric for gauging the effectiveness of fracture stage placements in alignment with the RQI along the wellbore, while also incorporating a global normalization of RQI across the entire Montney formation. Initially, we assess the overlap of each fracture stage with intervals of high RQI. A greater overlap with high RQI intervals signifies a higher placement efficiency for a fracture stage. Following this, we compute the average placement efficiencies of all fracture stages within each well to derive its SPE, thereby indicating the degree of effectiveness in stage positioning relative to the reservoir quality.

Fig. 7.5 illustrates the estimation of SPE for two scenarios with differing distributions of fracture stages, although having an identical number of stages and the same minimum fracture spacing. This illustration highlights the significance of aligning the fracture stages as function of RQI. In scenarios where fracture stages are uniformly distributed along the completed length in the lateral section, the

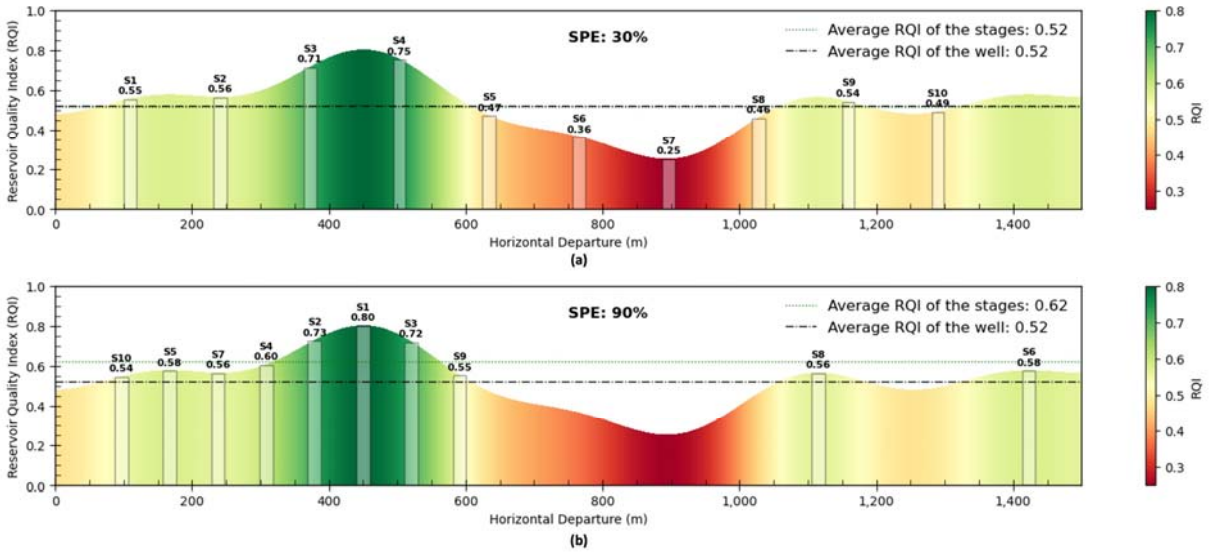

Fig. 7.5 – Stage positioning efficiency (SPE) in **(a)** evenly distributed fracture stages, and **(b)** fracture stages placed as function of RQI

SPE is found to be suboptimal (at only 30%). In such a scenario, it's observed that the average RQI of the stages aligns with the average RQI of the well. However, when RQI is factored into the positioning of the fracture stages, a substantial enhancement in SPE to 90% is achieved. This indicates that the average RQI of the fracture stages surpasses the average RQI of the well, showcasing the potential for optimized stage positioning.

7.2.6 Completion-Design Parameters Formulation

In the developed proxy, we categorize different completion parameters into six individual groups: 1) Completion Technology, 2) Completion Fluid, 3) Proppant Design, 4) Pumping Design, 5) Well Profile, and 6) Completion Design, as illustrated in **Fig. 7.6**. Under Completion Technology, we take into account the technological groupings such as Ball and Seat, Plug and Perf, Sliding Sleeve, etc.... We also evaluate whether it's an open or cased hole, the type of ball used (conventional, dissolvable, or combination), and similarly, the type of bridge plug utilized.

For Completion Fluid, considerations include the volume of fluid pumped per stage (V_{inj}), fluid type, energizer type (if any), the use of foam and its quality, and the utilization of acid for pre-flush, along with the quantity of acid injected. In Proppant Design, we consider the proppant concentration (C_{prop}) within the injected fluid and the type of proppant.

Under Pumping Design, the average injection pressure (p_{inj}) and rate (q_{inj}) are considered. For the Well Profile, we consider the formation (upper, middle, or lower Montney), the location of the well, its lateral length (L_l) and Total Vertical Depth (TVD), wellbore direction, and toe direction (up, down,

or flat). A new characteristic, the minimum effective distance to nearby wells (d_e), has been introduced to measure the effective distance among the studied wells, with the following section detailing how d_e is estimated.

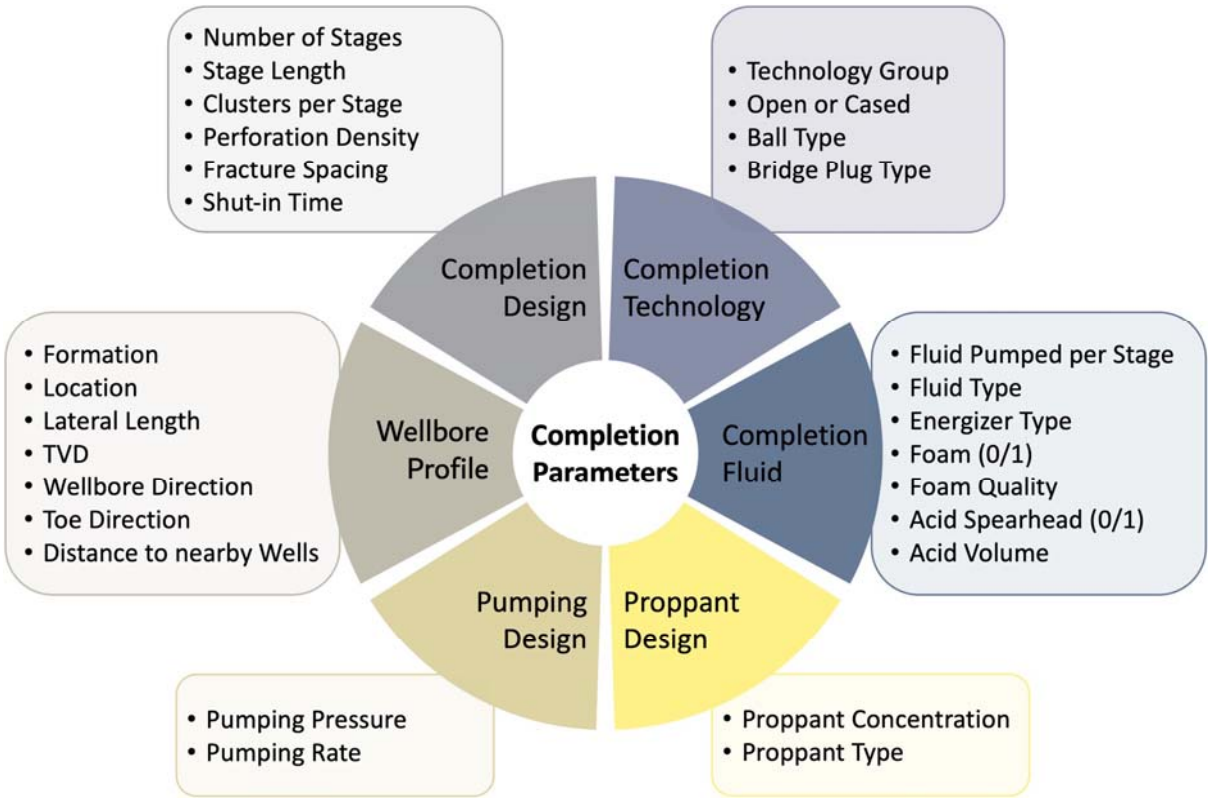

Fig. 7.6 – Completion-design parameters utilized to develop the ANN-based proxy

Finally, in Completion Design, we evaluate the number of stages (N_s), stage length (L_s), number of clusters/intervals per stage (C_s), perforation density (d_{perf}), average fracture spacing (d_s), and the soaking period or shut-in time (t_{sh}) from the end of fracturing until flowback.

7.2.6.1 Effective Distance to Nearby Wells

In this section, a new term as effective distance to nearby wells (d_e) is introduced. d_e estimates the minimum effective distance between a well and surrounding wells based on a) 3D spatial distance and b) their directional difference. The spatial distance between two wells is calculated using the Euclidean distance formula between their midpoints in 3D space. The midpoints are determined by averaging the start and end coordinates of the lateral section of each well. The formula for 3D Euclidean distance between two points, $P_1(x_1, y_1, z_1)$ and $P_{2(x_2,y_2,z_2)}$, is:

$$d_{\text{spatial}} = \sqrt{(x_2 - x_1)^2 + (y_2 - y_1)^2 + (z_2 - z_1)^2} \tag{7.3}$$

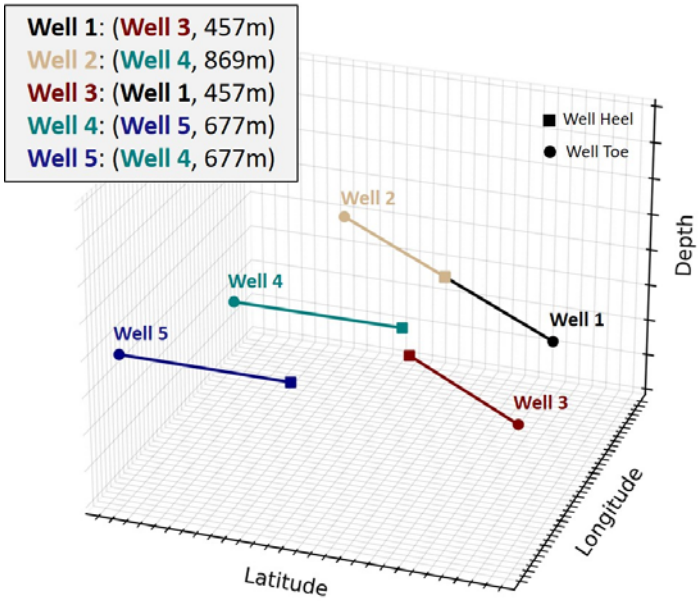

Fig. 7.7 – Effective distance estimation between MFHWs

where x, y and z refer to longitude, latitude and elevation, respectively. Next, the directional difference between two wells is calculated as the angle between their direction vectors. The direction vectors are determined based on the cardinal direction of each well. The formula for the angle θ between vectors $\mathbf{v_1}$ and $\mathbf{v}_2$ is:

$$\cos(\theta) = \frac{\mathbf{v}_1 . \mathbf{v}_2}{|\mathbf{v}_1||\mathbf{v}_2|} \tag{7.4}$$

then, d_e is estimated as

$$d_e = d_{spatial} + \theta \tag{7.5}$$

Fig. 7.7 illustrates an application of the effective distance (d_e) metric among MFHWs in a 3D space. It's evident from the figure that while Well 1 and Well 2 share the same surface location, Well 3 is identified as the closest to Well 1. This observation aligns with the expectations in the MFHW domain, where communication between Well 1 and Well 3 is anticipated if their fracture networks intersect. Similarly, Well 4 is closest to Well 2, and Well 5 is closest to Well 4, not Well 3. This example highlights the integration of both 3D spatial and directional distances in computing the effective distance between MFHWs.

7.2.7 ANN-Based Proxy Model Development

In this section, we consolidate all the extracted, estimated, and interpolated petrophysical properties along with completion-design parameters to serve as input features for a neural network aimed at

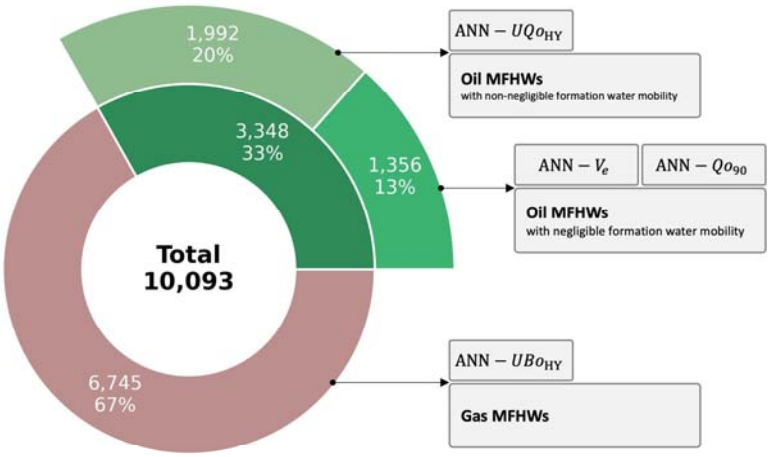

Fig. 7.8 – Montney MFHWs statistics and the associated developed proxies

predicting well productivity. As previously mentioned, our dataset includes data from over 14,299 oil and gas wells completed in the Montney formation. The well log data from these wells were utilized to develop high-resolution 3D maps of petrophysical properties and RQI. Out of these wells, nearly 10,093 are MFHWs with available completion design data. A subset of 3,348 are oil MFHWs, and among them, 1,356 oil wells exhibit negligible formation water mobility, and 1,992 oil have non-negligible formation water mobility. These statistics are illustrated in **Fig. 7.8**.

In this research, we aim to develop four different neural networks to correlate reservoir characteristics and completion-design parameters with: initial effective fracture volume (V_e), cumulative oil production at 90% of ultimate recovery (Qo_{90}), ultimate cumulative oil production assuming a hyperbolic decline of q_o in a semi-log plot relationship with Qo, and Ultimate Barrel of Oil Equivalent (UBo_e) also assuming a hyperbolic decline. The developed proxies are termed as: 1) ANN-V_e, trained on the 1,359 oil MFHWs with negligible formation water mobility; 2) ANN- Qo_{90}, trained on the same oil MFHWs as in the previous development; 3) ANN-UQo_{HY}, trained on the 1,992 oil MFHWs with non-negligible formation water mobility; and 4) ANN-UBo_e , trained on the 6,745 gas MFHWs.

7.2.7.1 ANN Modeling

In this study, the application of ANN is explored for correlating well productivity with completion design and reservoir characteristics. The ANN, inspired by the biological neurons of the human brain, is known for its effectiveness in classifying and recognizing complex patterns in data [23]. The ANN model comprises three main components: the network architecture, the training algorithm, and the activation function [24]. It is structured with a minimum of three layers: input, hidden, and output

layers. These layers are interconnected through weights, and the adjustment of these weights is critical for the model's performance [25].

The training of the ANN model is initiated using a backpropagation of errors algorithm. The data is processed from the input layer through to the hidden layer(s), and then to the output layer. At the output layer, a comparison is made between the estimated and actual data. The difference between the estimated and actual data triggers an update in the weights and biases across each layer. This training process continues iteratively across the entire dataset until the error reduces to a predefined limit (or until the maximum iterations number is met), ensuring the model's performance meets the desired criteria [26].

For optimizing the hyperparameters of the ANN model, a self-adaptive differential evolution (SaDE) method is employed [130]. This optimization seeks to find the best configuration of hyperparameters including the number of layers, neurons, and the type of activation functions to ensure high predictive accuracy while avoiding overfitting. In addition, a cross-validation framework is utilized to partition the dataset into training, validation, and testing subsets. This ensures a robust training and an unbiased evaluation of the model's performance. Through this approach, the ANN model is trained and validated for correlating reservoir characteristics and completion design parameters to well productivity, providing a reliable tool for optimizing completion designs in unconventional reservoirs.

7.2.7.2 ANN interpretation using SHAP

For practical application, beyond the statistical validation of machine learning models, it's crucial to have a physics-based interpretation to comprehend the underlying physics driving the predictions. Understanding why a particular well exhibits a certain level of productivity, or why its productivity is lower or higher compared to others, is vital for making informed decisions. In addressing these demands, we utilize SHapley Additive exPlanations (SHAP) method to interpret our ANN-based proxies. SHAP provides a robust method for interpreting model predictions by allocating each feature an importance value for a particular prediction [131]. It quantifies the contribution of each feature to the prediction for a specific data point in relation to the average prediction of the dataset. This method not only highlights the significance of each feature but also provides insights into complex relationships between features and the target variable, enabling a clearer understanding of the well productivity predictions from both a machine learning and physics-based standpoint.

7.3 Sweet-Spot Identification Results and Discussion

Here we present the high-resolution petrophysical maps constructed based on the log data of more than fourteen thousand wells completed in the upper, middle, and lower Montney formations. Then, we show how could these maps are combined to develop a reservoir quality index (RQI) that represent the reservoir quality of the Montney formation.

7.3.1 3D Maps of Montney Petrophysical Properties

Fig. 7.9 resents the developed 3D maps of the upper, middle, and lower Montney formation, highlighting different petrophysical properties, specifically; ϕ, GR, ρ_b, p_i, S_{hc}, and h_{net}. These high-resolution maps are segmented by the upper, middle, and lower Montney formation. At every geographic map point defined by its longitude and latitude, three sets of data could be extracted: 1) the elevation at that point; 2) the thickness of the upper, middle, and lower Montney formation; and 3) the values of ϕ, GR, ρ_b, p_i, S_{hc}, and h_{net} for each sub-formation.

These maps are developed for three primary reasons: 1) to interpolate missing petrophysical properties of the studied wells; 2) to aid in predicting reservoir permeability on a formation-wide scale utilizing these petrophysical properties; and 3) to be combined together to formulate an RQI, which can identify the reservoir quality at each location within the Montney formation. A prominent observation is found in Cluster 3, situated at the center of the Montney formation, which holds the highest initial reservoir pressure and hydrocarbon saturation levels, explaining why a majority of the Montney MFHWs are located in this region. In fact, over 75% of the Montney MFHWs are completed in this area. On the other hand, only 20% of Montney wells are located in areas with higher porosity and lower gamma ray, indicating a preference by Montney operators for initial reservoir conditions over others. Another point of interest is the distinct variation in formation characteristics, as these maps do not overlap. A section of the reservoir with high ϕ does not necessarily have high S_{hc}, h_{net} or and p_i. This highlights the importance of applying multivariate analysis to integrate these characteristics into a single term as RQI, and to investigate its correlation with well productivity.

7.3.1.1 3D Map of Montney Fracability

Fig. 7.10a presents a 3D map of the estimated brittleness index, serving as an indicator of formation permeability for the upper, middle, and lower segments of Montney. As previously explained, B_i is derived from sonic log data, utilizing the transient times of shear and compression waves. The illustration reveals a notably higher fracture fracability in Cluster 3, while Cluster 1 exhibits the least fracability potential. This observation may further explain why over 75% of Montney MFHWs are completed in Cluster 3. Another observation is that within each sub-formation, deeper zones generally

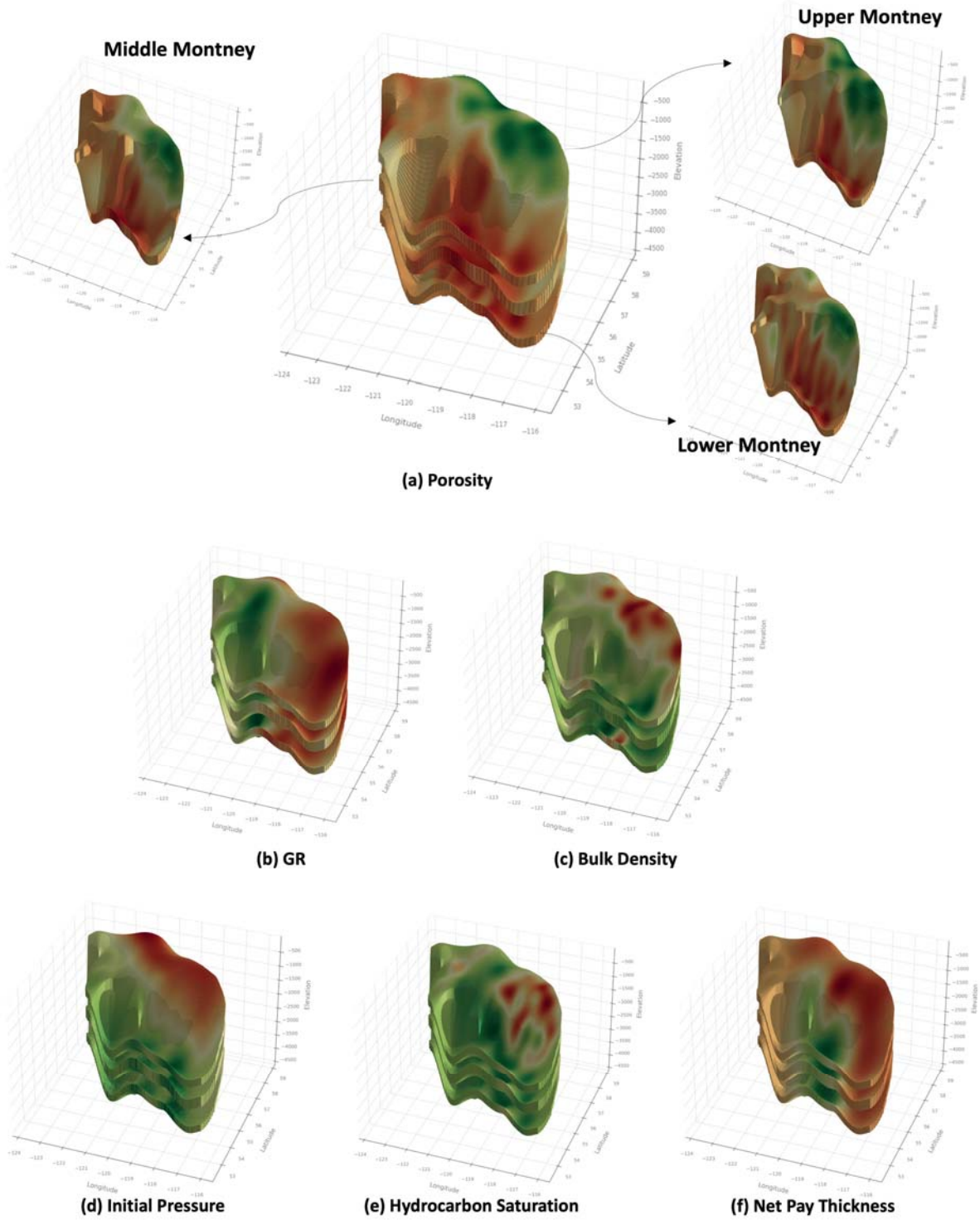

Fig. 7.9 – 3D petrophysical maps of upper, middle and lower Montney formation. **(a)** porosity, **(b)** gamma ray, **(c)** bulk density, **(d)** initial reservoir pressure, **(e)** hydrocarbon saturation and **(f)** net-pay thickness

exhibit higher B_i values. This may be attributable to the likelihood that deeper zones experience greater overburden stresses, potentially leading to a plastic-brittle strain [132], thereby increasing B_i.

Fig. 7.10b displays the distribution of B_i for the upper, middle, and lower segments of the Montney formation. It indicates that there is no significant variation in B_i across the sub-formations. However, the middle Montney exhibits the broadest range of B_i, potentially reflecting a greater heterogeneity in geomechanical properties. Despite the narrow range of B_i, the upper Montney presents the most outliers. These outliers may be attributable to the higher number of wells completed in the upper Montney compared to the other sub-formations.

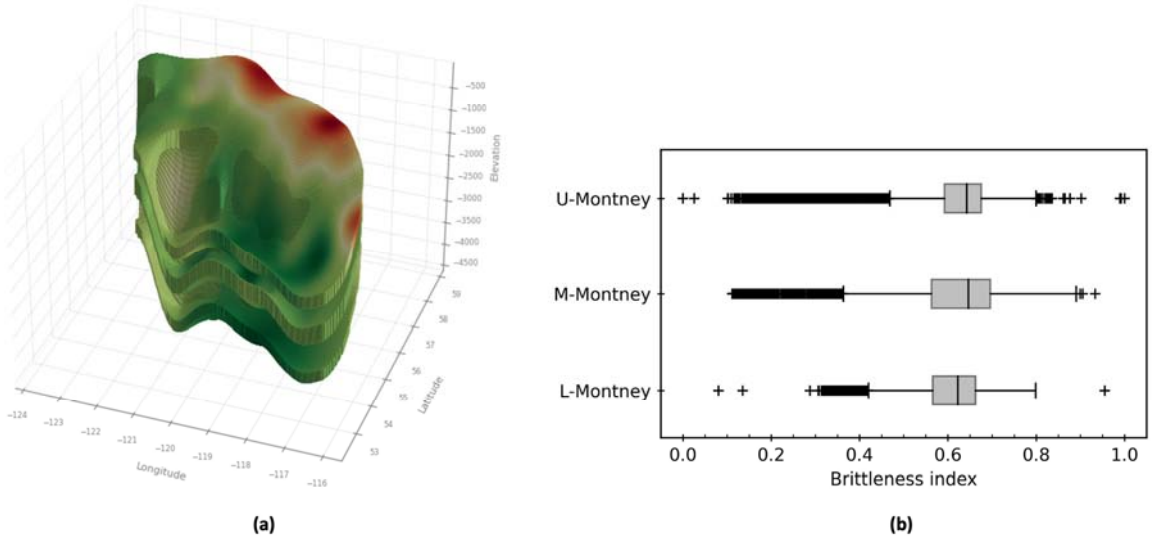

Fig. 7.10 – Brittleness index as **(a)** 3D map and **(b)** distribution for upper, middle and lower Montney formation

7.3.2 Permeability Prediction from well log data

The optimized SVM-K model exhibits a specific architecture characterized by the utilization of a Radial Basis Function (RBF) kernel. The model's training performance, determined by R^2, over 1000 iterations is shown in **Fig. 7.11**a. SVM-K's regularization parameter is established at 2.149, ensuring a balance between margin maximization and error minimization. The width of the ϵ-insensitive zone, which determines the allowable error range without incurring any penalty, is established at 0.193. Furthermore, the model's RBF coefficient (γ), which plays a pivotal role in shaping the decision boundary, is optimized to a value of 0.986. Here is the mathematical representation of SVM-K:

$$k = \exp\left[\sum_{i=1}^{N} \alpha_i e^{(-0.986\,\|x_n - S_i\|^2)} - 0.005\right] \tag{7.6}$$

where;

$\|x - S_i\|^2$ is the squared Euclidean distance between the input x and each support vector s_i. The sum is over all the support vectors ($i = 1\ to\ N$), where (N=50) is the total number of support vectors.

s_i is the support vector $\begin{bmatrix} s_{\phi_i} \\ s_{GR_i} \\ s_{\rho_{b_i}} \\ s_{r_{R_i}} \end{bmatrix}$ as shown in **Table D.1**

α_i is the dual coefficient of each support vector and listed in **Table D.1**

x_n is the normalized input vector $\begin{bmatrix} \phi_n \\ GR_n \\ \rho_{b_n} \\ r_{R_n} \end{bmatrix}$

where;

$$\phi_n = \frac{\phi - 0.122}{0.046}$$

$$GR_n = \frac{GR - 84.573}{37.315}$$

$$\rho_{b\,n} = \frac{\rho_b - 2{,}374.02}{174.106}$$

$$r_{R_n} = \frac{r_R - 0.296}{0.249}$$

where, r_R is the logarithmic of the ratio between deep and short resistivities [$\log(R_d/R_s)$].

Fig. 7.11b presents a crossplot, correlating the predicted k_m generated by the SVM-K model with the core permeability across both the training and testing datasets. The figure highlights the strong predictive capability of the SVM-K model, as evidenced by impressive R^2 values of 0.97 and 0.95, along with AAPE of 7.1% and 9.7% for the training and testing datasets respectively. Considering the simplistic yet potent nature of the SVM-K model, these metrics signify satisfactory predictive

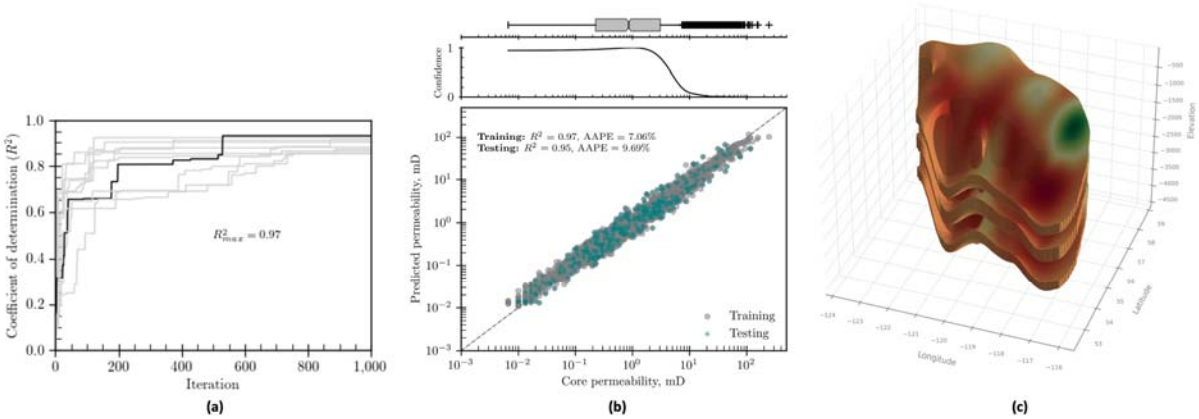

Fig. 7.11 – (a) SVM-K improvement during the optimization process. **(b)** crossplot between predicted permeability from SVM-K and core permeability. **(c)** 3D permeability map for upper, middle and lower Montney predicted by SVM-K model

performance. In addition, the figure further reveals that the model's prediction confidence is predominantly higher for k_m values less than 1mD. This heightened confidence can be attributed to the fact that over three-quarters of the wells utilized to construct this model exhibit k_m values under 1mD. Therefore, in regions of Montney with relatively higher permeability, the SVM-K model's predictions are anticipated to exhibit higher uncertainty.

Fig. 7.11c presents the developed 3D map of permeability for the upper, middle, and lower Montney, achieved by employing the available GR, porosity, bulk density, and resistivity log data to predict missing k_m values for wells lacking core data, followed by interpolation to construct this map. Now, for each well (or for each location) in Montney, we can estimate its formation permeability using the five logs; porosity, bulk density, GR, shallow and deep resistivities. This also explains why nearly 20% of the Montney wells are completed in this Cluster 1 region, even though it has relatively low p_i and S_{hc}. It's probable that the operators in this region prioritized formation permeability when selecting the sweet spots to complete their wells.

7.3.3 Reservoir Quality Index to Identify Sweet Spots

The developed maps of ϕ, p_i, S_{hc}, h_{net}, B_i and k are combined to formulate the RQI, a singular index that encapsulates the reservoir quality at each location in the Montney formation as shown in **Fig. 7.12**. is the variation in RQI across different clusters; Cluster 2 (located on the north-east side) exhibits the lowest RQI, followed by Cluster 1, and then Cluster 3. Explaining why the majority of MFHWs are completed in Cluster 3.

When outliers are excluded, a majority of RQIs, about 90%, fall between 0.25 and 0.85, and this distribution remains fairly consistent across the upper, middle, and lower Montney. However, the

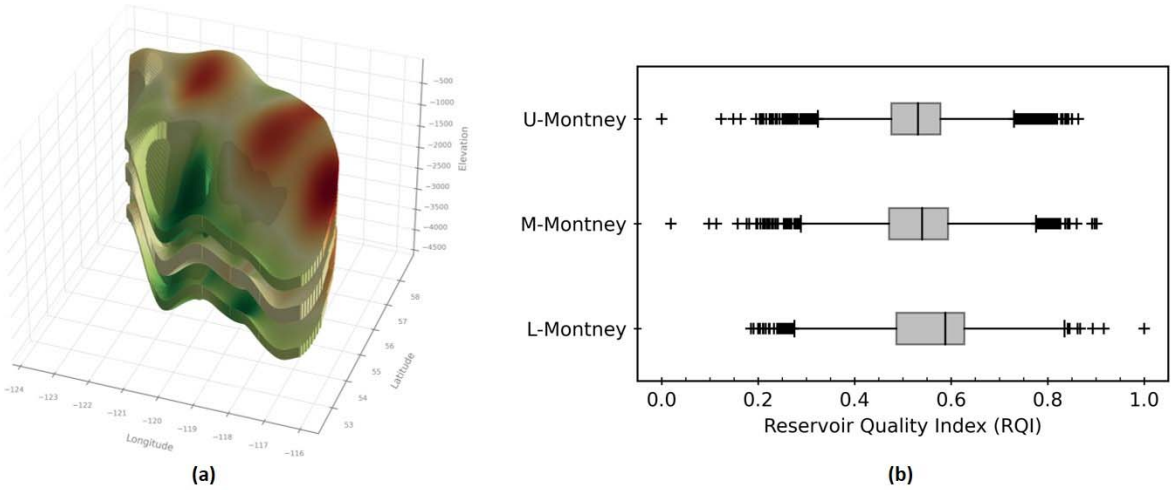

Fig. 7.12 – Reservoir quality index (RQI) as **(a)** 3D map and **(b)** distribution for upper, middle and lower Montney formation

Upper Montney displays more homogeneity as the interquartile range (25th to 75th percentile) of RQIs is narrowly confined between 0.48 to 0.58. In contrast, the Middle and Lower Montney exhibit a broader range by 23% and 48% respectively, indicating a higher level of heterogeneity. This methodology offers operators a straightforward approach to identify the sweet spots based on the petrophysical properties, enhancing the efficiency in well completions across the formation.

7.4 Proxy Modelling Results and Discussion

This section presents the key results obtained from training different neural networks on different datasets to predict the performance indicators: V_e, Qo_{90}, UQo_{HY} and UB_{HY} of Montney oil and gas MFHWs as functions of reservoir characteristics, geomechanical properties and completion-design parameters. For each indicator, a neural network is trained, cross-validated and tested. Subsequent sections will elaborate on the mathematical representation and the physics-based interpretation of each developed neural network.

7.4.1 Proxy Model for Initial Effective Fracture Volume

Utilizing SaDE for hyperparameter optimization resulted in an effectively trained ANN with a distinct architecture: two hidden layers with 64 and 32 neurons respectively. A dropout ratio of 0.2 was adopted to mitigate overfitting, while both hidden layers utilized a Rectified Linear Unit (ReLU) activation function to introduce non-linearity. The training process leveraged Adaptive Moment Estimation [133] as a stochastic optimization method across 1000 epochs, with Mean Squared Error (MSE) serving as the loss function, which facilitated a robust and effective learning mechanism. Here is the mathematical representation of the trained ANN-V_e and the associated weights and coefficients:

$$V_e = e^{11.988\, V_{e_n}} \tag{7.7}$$

where V_{e_n} is the normalized V_e and is estimated as

$$V_{e_n} = \sum_{k=1}^{32} w_{3_k}.\, a_{2_k} + 0.703 \tag{7.8}$$

where the sum is over the 32 neurons in the second hidden layer. w_{3_k} is the weight connecting the k-th neuron in the second hidden layer to the output neuron, V_{e_n}, and listed in **Table D.2**. a_{2_k} is the activation of neuron k in the second hidden layer and is estimated as

$$a_{2_k} = \mathrm{ReLU}\left(\sum_{j=1}^{64} w_{2_{k,j}} a_{1_j} + b_{2_k}\right) \tag{7.9}$$

where ReLU is the rectified linear unit activation function. The sum is over the 64 neurons in the first hidden layer. $w_{2_{k,j}}$ is the weight connecting the j-th neuron in the first hidden layer to the k-th neuron in the second hidden layer. b_{2_k} is the bias of the k-th neuron in the second hidden layer. The values of $w_{2_{k,j}}$ and b_{2_k} are listed in **Table D.2**. a_{1_j} is the activation of neuron j in the first hidden layer and is estimated as

$$a_{1_j} = \text{ReLU}\left(\sum_{i=1}^{155} w_{1_{j,i}} x_{n_i} + b_{1_j}\right) \tag{7.10}$$

where the sum is over the 155 vectorized input features. $w_{1_{j,i}}$ is the weight connecting the i-th input neuron to the j-th neuron in the first hidden layer. b_{1_j} is the bias of the j-th neuron in the first hidden layer. The values of $w_{1_{j,i}}$ and b_{1_j} are listed in **Table D.3**. x_{n_i} is the normalized input parameter, x_i estimated as

$$x_{n_i} = \frac{x_i - \mu_i}{\sigma_i} \tag{7.11}$$

where μ_i and σ_i are the mean and standard deviation of the input features as listed in **Table D.4**.

The crossplot illustrated in **Fig. 7.13**a reveals the correlation between the predicted and targeted normalized V_e across both training and testing datasets. The figure exhibits a strong match between the predicted and targeted values for both datasets, as evidenced by R^2 values of 0.96 and 0.93 for training and testing, respectively, alongside the average absolute percentage error (AAPE) of 2.5 and 2.7% for training and testing, respectively. Furthermore, the figure highlights an elevated confidence in V_e prediction around intermediate values, attributable to the higher sample density in this region. This implies a diminished uncertainty in predicting V_e within the range of 5,000 to 15,000 m^3, compared to other data points, establishing this range as the advisable domain for implementing the proposed ANN-V_e proxy.

Fig. 7.13b showcases the marginal contribution of each input parameter (as reflected by SHAP values) to the predicted V_e, visualized through a BeesWarm plot. Displayed are the top eleven features with the highest contribution/impact on V_e. Here, V_{inj}, d_s, N_s, q_{inj}, TVD, L_l, C_s represent the completion design of a MFHW, while B_i, ϕ_m, and k_m represent the matrix properties of the formation in which the well is completed. Several observations emerge from this figure:

1) Predominantly, the completion design parameters exhibit a more substantial impact on V_e compared to the formation characteristics.
2) Among formation parameters, formation fracability, represented by B_i, is the most crucial determinant of V_e. A higher degree of formation brittleness generally corresponds to a larger

V_e. However, intermediate values could yield either large or small V_e contingent on the completion design practice.

3) The volume of fluid injected per stage, the number of stages, and the spacing between stages are pivotal factors in determining V_e. A larger fluid injection volume per stage typically results in a larger V_e, but a smaller V_{inj} does not necessarily translate to a significantly smaller V_e, denoting a non-linear relationship. Increased fracture spacing notably constrains V_e, likely because larger d_s might result in isolated fracture stages, thus reducing the effective stimulated volume. However, reducing the fracture spacing doesn't necessarily yield a larger V_e as depicted by the limited impact of lower d_s on V_e. This may be attributed to the counter effect of stress shadowing that occurs with tight fracture spacing, limiting fracture propagation and consequently resulting in restricted V_e. Notably, increasing N_s significantly contributes to a larger V_e but nonlinearly, as demonstrated by the asymmetry in the figure, indicating that N_s predominantly has a positive impact on V_e.
4) Both injection rate and pressure, as well as lateral length and the number of clusters per stage, positively influence V_e, although q_{inj} has a more significant impact. TVD exhibits a negative correlation with V_e, suggesting that higher TVD typically represent higher overburden stresses and greater resistance to fracture propagation. Lastly, formations with higher porosity and permeability emerge as better candidates for achieving a larger V_e.

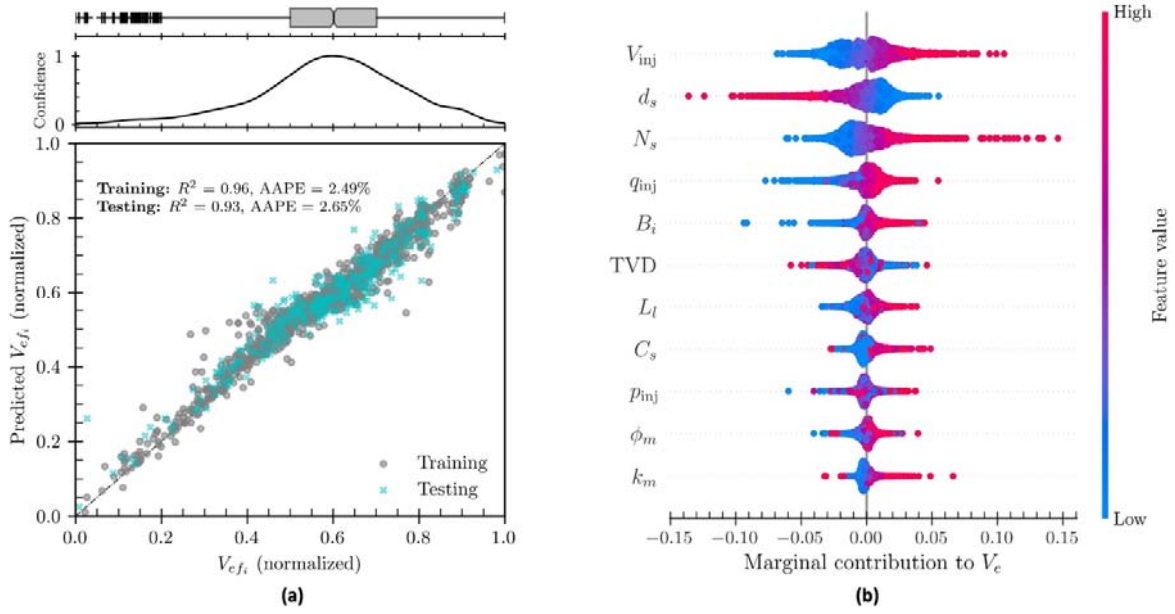

Fig. 7.13 – ANN-V_e model performance as (a) crossplot between ANN-predicted V_e and the targeted V_e for both training and testing datasets. (b) Beeswarm plot of the marginal contribution of top 11 features to the predicted V_e.

7.4.2 Proxy Model for Oil Recovery Performance

Here we introduce two proxy models to predict ultimate oil recovery as functions of reservoir characteristics and completion design. The first model, ANN-Qo_{90}, is an ANN-based model applicable for cases where the formation water mobility is negligible. This model is developed to predict the cumulative oil production when approaching 90% of the ultimate load recovery. The second model, ANN-UQo_{HY}, is another ANN-based model that is applicable when the formation water mobility is significant, rendering both WORM and COPM inapplicable for describing the recovery performance. As highlighted earlier, this model assumes that q_o follows a hyperbolic decline in a semi-log relationship between q_o and Q_o.

7.4.2.1 ANN-Based Qo_{90} Model

The trained ANN-Qo_{90} by utilizing SaDE for hyperparameter optimization yields a neural network with the following architecture: two hidden layers with 64 and 16 neurons, respectively. A 0.2 dropout ratio is applied for both the hidden layers to minimize overfitting. Both hidden layers used a hyperbolic tangent (Tanh) activation function to introduce non-linearity to the neural network. We utilized the adaptive moment estimation as a stochastic optimization method over 1000 epochs with 32 batch size. Again, MSE is utilized as the loss function while learning. Here is the mathematical representation of the developed ANN-Qo_{90}:

$$Qo_{90} = e^{11.013\ Qo_{90_n}} \tag{7.12}$$

where Qo_{90_n} is the normalized Qo_{90} and is estimated as

$$Qo_{90_n} = \sum_{k=1}^{16} w_{3_k}.\, h_{2_k} + 0.805 \tag{7.13}$$

where the sum is over the 16 neurons in the second hidden layer. w_{3_k} is the weight connecting the k-th neuron in the second hidden layer to the output neuron, Qo_{90_n}, and listed in **Table D.5**. h is the activation of neuron k in the second hidden layer and is estimated as

$$h_{2_k} = \frac{e^{2\left(\sum_{j=1}^{64} w_{2_{k,j}} h_{1_j} + b_{2_k}\right)} - 1}{e^{2\left(\sum_{j=1}^{64} w_{2_{k,j}} h_{1_j} + b_{2_k}\right)} + 1} \tag{7.14}$$

where the sum is over the 64 neurons in the first hidden layer. $w_{2_{k,j}}$ is the weight connecting the j-th neuron in the first hidden layer to the k-th neuron in the second hidden layer. b_{2_k} is the bias of the k-th neuron in the second hidden layer. The values of $w_{2_{k,j}}$ and b_{2_k} are listed in **Table D.5**. h_{1_j} is the activation of neuron j in the first hidden layer and is estimated as

$$h_{1_j} = \frac{e^{2\left(\sum_{i=1}^{155} w_{1_{j,i}} x_{n_i} + b_{1_j}\right)} - 1}{e^{2\left(\sum_{i=1}^{155} w_{1_{j,i}} x_{n_i} + b_{1_j}\right)} + 1} \tag{7.15}$$

where the sum is over the 155 vectorized input features. $w_{1_{j,i}}$ is the weight connecting the i-th input neuron to the j-th neuron in the first hidden layer. b_{1_j} is the bias of the j-th neuron in the first hidden layer. The values of $w_{1_{j,i}}$ and b_{1_j} are listed in **Table D.6**. x_{n_i} is the normalized input parameter, x_i estimated as

$$x_{n_i} = \frac{x_i - \mu_i}{\sigma_i} \tag{7.16}$$

where μ_i and σ_i are the mean and standard deviation of the input features as listed in **Table D.4**.

Fig. 7.14a shows a crossplot between the predicted Qo_{90} obtained using the aforementioned ANN-based model and the target Qo_{90}. The correlation is strongly evidenced by R^2 values of 0.98 and 0.93 on the training and testing datasets, respectively. The AAPE for the training and testing datasets is calculated at 0.75% and 3.68%, respectively. Furthermore, the figure illustrates an increased level of confidence towards the higher Qo_{90} values. This is because Qo_{90} is estimated by the WORM model using early production data, assuming a matrix-dominated regime. Wells with higher oil productivity indicate greater reservoir energy and earlier matrix contribution, reducing Qo_{90} estimation uncertainty. Therefore, the ANN- Qo_{90} model is less uncertain for higher energy reservoirs. i.e., those

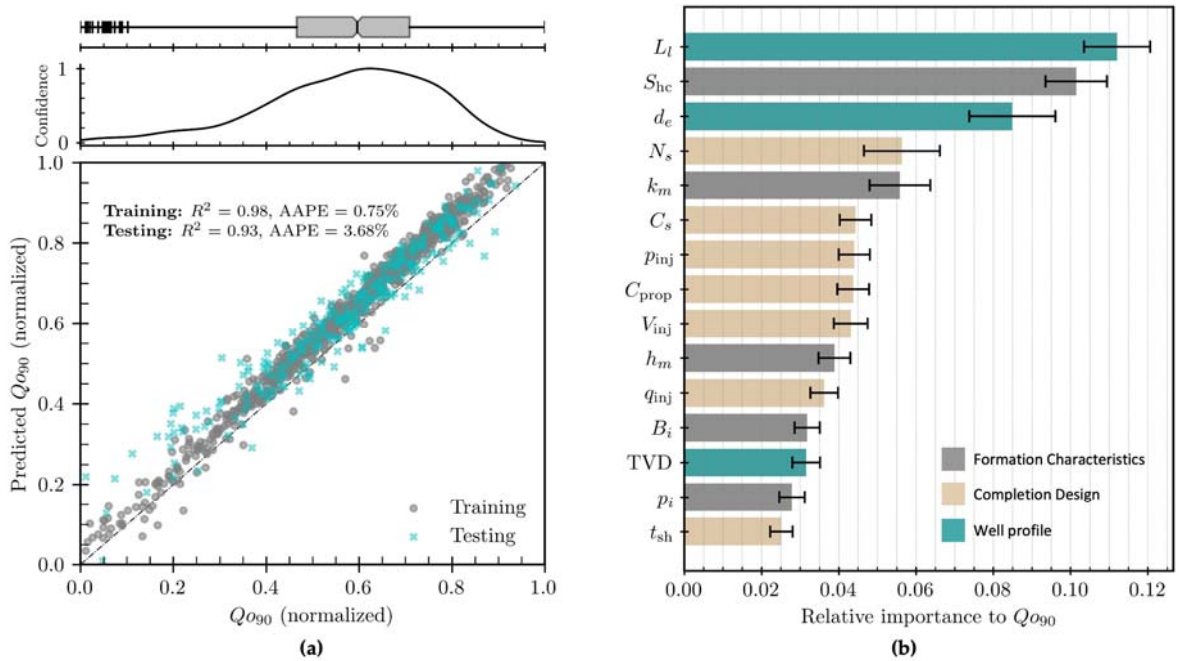

Fig. 7.14 – ANN-Qo_{90} performance as **(a)** crossplot between ANN-predicted and targeted Qo_{90} for both training and testing datasets. **(b)** Relative importance of different input features to the predicted Qo_{90}

with earlier matrix contribution. Additionally, ANN- Qo_{90} predictions are generally biased-high, possibly because the WORM model's Qo_{90} estimates are relatively underestimated and may not be precisely captured by the input petrophysical properties and completion design features.

Fig. 7.14b highlights the relative importance of formation characteristics, completion design, and well profile on the oil recovery performance, specifically in terms of Qo_{90}. The figure lists the top fifteen parameters that significantly contribute to predicting Qo_{90}. Several observations can be made from this analysis:

1. Generally, the completion design and well profile have a more pronounced impact on determining the oil recovery performance of MFHWs. Among the fifteen key parameters governing Qo_{90}, ten are unrelated to reservoir characteristics.
2. The lateral length of the well, its effective distance from nearby wells, and the hydrocarbon saturation are the main parameters that determine oil recovery.
3. Among the reservoir characteristics, hydrocarbon saturation and formation permeability are the most influential in determining oil recovery.
4. Regarding the completion design, N_s, C_s, p_{inj}, C_{prop}, and V_{inj} are identified as the most significant parameters affecting oil recovery.
5. The shut-in period also ranks among the top fifteen parameters controlling oil recovery.

These insights offer a clearer understanding, supporting more informed decision-making for optimizing the oil recovery performance of MFHWs. However, this relative importance does not elucidate how each parameter contributes to Qo_{90}.

Therefore, **Fig. 7.15** illustrates the marginal contribution of these design and formation parameters on oil recovery performance. **Fig. 7.15**a shows the marginal contribution of reservoir characteristics to

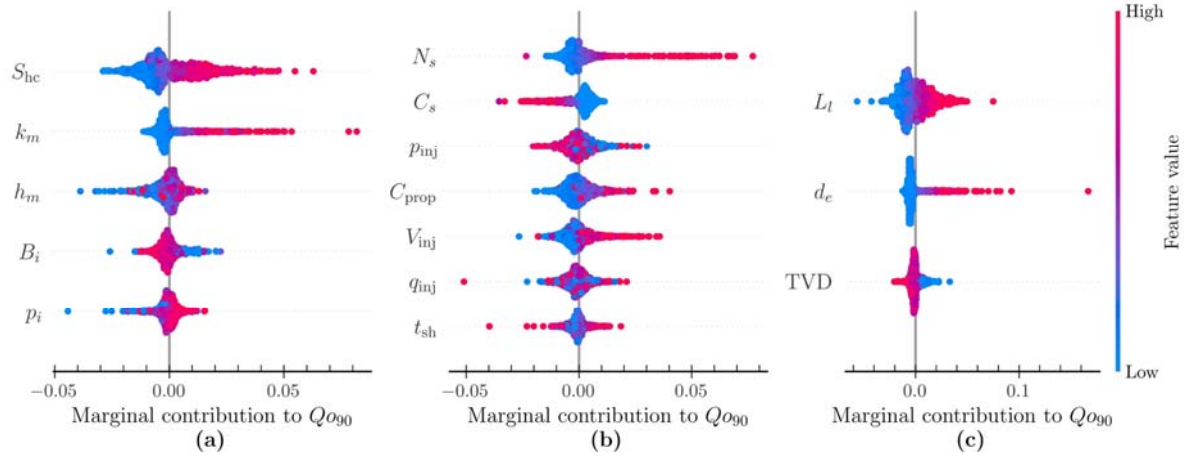

Fig. 7.15 – Marginal contribution of **(a)** formation characteristics, **(b)** completion design and **(c)** well profile to the predicted Qo_{90}

Qo_{90}. Higher S_{hc} and k_m significantly increase Qo_{90}. However, lower k_m does not necessarily lead to much lower oil recovery. The asymmetric contribution of h_m indicates that a lower formation thickness tends to limit the oil recovery, while a considerably higher formation thickness doesn't contribute much to enhancing it. Similarly, lower reservoir energy (p_i) may significantly reduce Qo_{90}, but a very high p_i does not necessary lead to a relative-equivalent increase in oil recovery.

Fig. 7.15b illustrates the relative impact of the completion design parameter on oil recovery. Among these, N_s exhibits the highest positive impact on Qo_{90}, indicating that an increase in the number of stages is expected to result in higher Qo_{90} values. Interestingly, the number of clusters per stage correlates negatively with Qo_{90}. This could be due to an increase in C_s potentially leading to a more complex fracture network, which was demonstrated to positively impact V_e (as previously explained in **Fig. 7.13**). However, it might also contribute to significant water blockage, especially in water-wet formations, resulting in higher capillarity and a relatively lower relative permeability for oil, leading to lower Qo_{90}. Similarly, a higher p_{inj} might be detrimental to Qo_{90}, as it could push more water into the formation interface instead of assisting in fracture propagation. Conversely, C_{prop} and V_{inj} are observed to have a positive impact on Qo_{90}. A higher proppant concentration can reduce effective fracture volume loss post-production, thereby maintaining larger fracture porosity [134] leading to higher Qo_{90}. Both q_{inj} and t_{sh} do not exhibit a clear correlation with Qo_{90} and will be explored individually in the subsequent section.

Fig. 7.15c shows the marginal contribution of well profile on Qo_{90}. Both the well's lateral length and its minimum effective distance to nearby wells significantly affect oil recovery. Generally, larger L_l results in more contact area with the formation, which in turn leads to increased oil recovery.

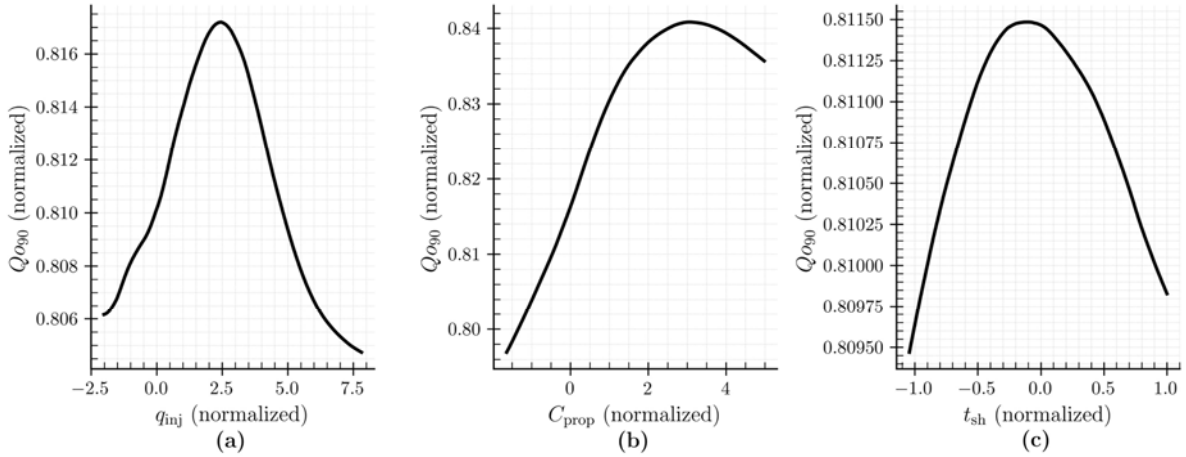

Fig. 7.16 – Individual dependence of the predicted Qo_{90} on (a) average injection rate (q_{inj}) of fracturing fluid, (b) proppant concentration (C_{prop}) and (c) shut-in time (t_{sh})

Similarly, a larger d_e translates to reduced well interference, thereby promoting higher oil recovery. Finally, TVD exhibits the same negative impact on Qo_{90} as it did for V_e. Deeper wells tend to encounter higher overburden stresses and increased resistance to fracture propagation, resulting in less stimulated volume and, consequently, lower Qo_{90}.

The marginal contribution analysis previously discussed did not address the effects of q_{inj} and t_{sh}. Therefore, **Fig. 7.16** presents the individual dependence of Qo_{90} on these parameters, along with C_{prop}. **Fig. 7.16**a illustrates the variation in Qo_{90} with changes in q_{inj}. The figure reveals that increasing q_{inj} initially enhances Qo_{90} up to a certain point, after which further increases in q_{inj} adversely affect oil recovery. This is likely because a very high injection rate could lead to increased water imbibition and elevated water blockage, thereby reducing oil relative permeability and limiting Qo_{90}. Similarly, an increase in C_{prop} initially boosts oil recovery by minimizing fracture volume loss. However, an exceedingly high C_{prop} might result in denser proppant packing within fractures, thereby reducing fracture porosity and connectivity. The shut-in time exhibits a similar trend. An increase in t_{sh} enhances oil recovery, possibly due to factors like skin removal, water blockage removal, and/or counter current imbibition. Some studies also suggest that shut-in might aid in propagating the fracture tip, thereby increasing the stimulated volume. However, a significantly longer t_{sh} might be detrimental as it could lead to increased water trapping, which reduces oil relative permeability and ultimately lowers Qo_{90}. These observations are intriguing as they demonstrate how the proposed model could be leveraged to optimize the completion design, aiming to maximize oil recovery in MFHWs.

7.4.2.2 ANN-Based UQo_{HY} Model

For the oil MFHWs that show significant formation water mobility (i.e., WORM and COPM become not applicable), we develop another proxy named ANN-UQo_{HY} to predict their oil recovery performance. The trained neural network with hyperparameter optimization leads to the following architecture: two hidden layers with 64 and 16 neurons respectively. A dropout ration of 0.2 was applied to the two hidden layers to avoid overfitting. ReLU activation function is applied to the two hidden layers as well. MSE is utilized as the loss function across 1000 epochs with 32 batch size. Here is the mathematical representation of the developed ANN-UQo_{HY}.

$$UQo_{\text{HY}} = e^{12.750\ UQo_{\text{HY}_\text{n}}} \tag{7.17}$$

where UQo_{HY_n} is the normalized UQo_{HY} and is estimated as

$$UQo_{\text{HY}_\text{n}} = \sum_{k=1}^{16} w_{3_k}.\max\left[0, \sum_{j=1}^{64} w_{2_{k,j}}.\max\left(0, \sum_{i=1}^{155} w_{1_{j,i}}.X_i + b_{1_j}\right) + b_{2_k}\right] + 0.806 \tag{7.18}$$

where;

w_{3_k} is the weight connecting the k-th neuron in the second hidden layer to the output neuron, $UQo_{\mathrm{HY_n}}$.

$w_{2_{k,j}}$ is the weight connecting the j-th neuron in the first hidden layer to the k-th neuron in the second hidden layer.

b_{2_k} is the bias of the k-th neuron in the second hidden layer.

$w_{1_{j,i}}$ is the weight connecting the i-th input neuron to the j-th neuron in the first hidden layer.

b_{1_j} is the bias of the j-th neuron in the first hidden layer.

x_{n_i} is the normalized input parameter, x_i estimated as

$$x_{n_i} = \frac{x_i - \mu_i}{\sigma_i} \tag{7.19}$$

where μ_i and σ_i are the mean and standard deviation of the input features. The values of w_{3_k} $w_{2_{k,j}}$ and b_{2_k} are listed in **Table D.7**, while the values of $w_{1_{j,i}}$ and b_{1_j} are listed in **Table D.8**, and the values of μ_i and σ_i are listed in **Table D.9**.

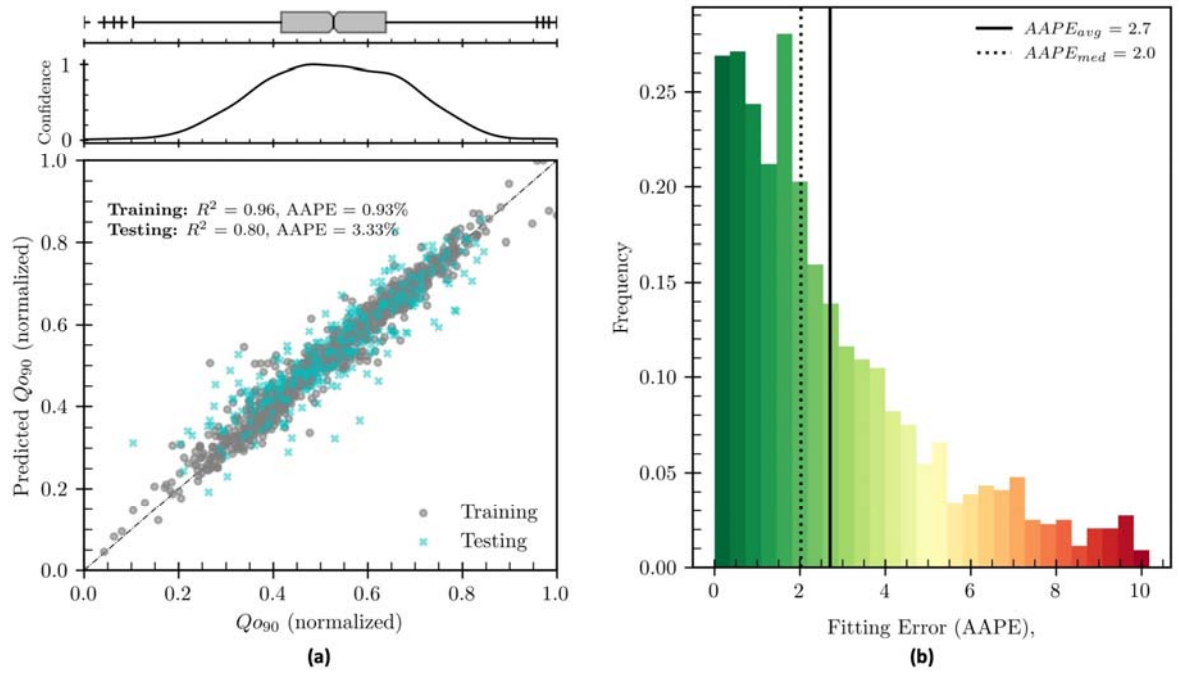

Fig. 7.17 – Prediction performance of ANN-UQo_{HY} in terms of **(a)** crossplot between predicted and target UQo_{HY} and **(b)** Average absolute percentage error (AAPE) distribution on all the dataset

Fig. 7.17a presents a crossplot between the predicted and targeted Qo_{HY}. The figure exhibits a good fit, as evidenced by R^2 values of 0.96 and 0.80 for the training and testing data respectively. It's notable that a discrepancy exists between the fitting performance on the training and testing data. This discrepancy may arise from the uncertainty inherent in estimating Qo_{HY}, as it presupposes that q_o adheres to a hyperbolic decline trend in a semi-log plot relationship with Qo. However, the AAPE distribution across the entire dataset, depicted in **Fig. 7.17**b, highlights the general good fit of the developed ANN-UQo_{HY} model. The figure reveals that the distribution is right-skewed, indicating that for most wells, the model accurately predicts Qo_{HY} using the input parameters. Nevertheless, the relatively higher error, compared to the previous models, stems from the uncertainty associated with the hyperbolic decline assumption. Therefore, in regions where mature MFHWs exhibit a hyperbolic decline, this model could be deployed on new wells to forecast their ultimate oil recovery based on reservoir characteristics and completion design, albeit with moderate accuracy.

7.4.3 Proxy Model for Ultimate BOE Recovery

Here we present the ANN-based model that predicts the ultimate BOE production for gas MFHWs. The trained ANN with optimized hyperparameter is found to have two hidden layers that consist of 64 and 32 neurons respectively. A 0.2 dropout ratio is applied only to the first hidden layer with no dropout for the second layer. A logistic (Sigmoid) activation function is applied for both hidden layers to introduce nonlinearity to the neural network. MSE is utilized as a loss function over 1000 epochs at a batch size of 64. Here is the mathematical representation of the developed ANN-UBO_e:

$$UBO_e = e^{14.445\, UBO_{e_n}} \tag{7.20}$$

where UBO_{e_n} is the normalized UBO_e and is estimated as

$$UBO_{e_n} = \sum_{k=1}^{32} w_{3_k}.h_{2_k} + 0.043 \tag{7.21}$$

where w_{3_k} is the weight connecting the k-th neuron in the second hidden layer to the output neuron, UBO_{e_n} , and listed in **Table D.10**. h_{2_k} is the activation of neuron k in the second hidden layer and is estimated as

$$h_{2_k} = \frac{1}{1 + e^{-\left(\sum_{j=1}^{64} w_{2_{k,j}} h_{1_j} + b_{2_k}\right)}} \tag{7.22}$$

where $w_{2_{k,j}}$ is the weight connecting the j-th neuron in the first hidden layer to the k-th neuron in the second hidden layer. b_{2_k} is the bias of the k-th neuron in the second hidden layer. The values of $w_{2_{k,j}}$ and b_{2_k} are listed in **Table D.10**. h_{1_j} is the activation of neuron j in the first hidden layer and is estimated as

$$h_{1_j} = \frac{1}{1 + e^{-\left(\sum_{i=1}^{155} w_{1_{j,i}} x_{n_i} + b_{1_j}\right)}} \tag{7.23}$$

where $w_{1_{j,i}}$ is the weight connecting the i-th input neuron to the j-th neuron in the first hidden layer. b_{1_j} is the bias of the j-th neuron in the first hidden layer. The values of $w_{1_{j,i}}$ and b_{1_j} are listed in **Table D.11**. x_{n_i} is the normalized input parameter, x_i estimated as

$$x_{n_i} = \frac{x_i - \mu_i}{\sigma_i} \tag{7.24}$$

where μ_i and σ_i are the mean and standard deviation of the input features as listed in **Table D.12**.

This model demonstrates a good fitting performance as shown in the crossplot in **Fig. 7.18**a, with an R^2 value of 0.94 and 0.90 for the training and testing datasets respectively. Additionally, both datasets exhibit an AAPE of less than 2.5%. The model provides more confidence in predicting intermediate UBO_e values due to the relatively higher data points in this region. Thus, lower uncertainty is anticipated when predicting an UBO_e between 150 to 350 kstb. **Fig. 7.18**b illustrates the relative importance of key formation characteristics, completion design, and well profile input parameters on the predicted UBO_e. Several observations can be made:

1. Similar to oil recovery, the completion design and well profile play a significant role in determining the gas recovery performance of gas MFHWs. Of the sixteen key parameters governing UBO_e, eleven are unrelated to reservoir characteristics.
2. The lateral length and number of stages emerge as key determinants of gas productivity performance. Unlike oil MFHWs, hydrocarbon saturation holds relatively low significance in determining the gas productivity of MFHWS.
3. Regarding reservoir characteristics, formation thickness and brittleness are identified as key parameters in controlling gas recovery. k_m, S_{hc}, and p_i are ranked lower in significance.
4. Unlike oil MFHWs, fracture spacing proves to be an important parameter in gas MFHWs productivity.
5. In contrast to oil MFHWs, proppant concentration has minimal impact on the gas MFHWs recovery performance, possibly due to the lesser sensitivity of gas recovery to fracture volume loss compared to oil reservoirs.

As previously mentioned, this relative importance plot doesn't illustrate the exact effect of each input parameter on well productivity. Therefore, **Fig. 7.18**c displays the marginal contribution of the key input parameters to predict UBO_e. This figure showcases how each input parameter contributes to predicting UBO_e for a well that displays 3% more UBO_e compared to the average value among the studied wells. The figure indicates that C_s, d_e, and B_i negatively impact the predicted gas recovery and drive UBO_e for this particular well below the average UBO_e. On the other hand, L_l, N_s, h_m, TVD,

q_{inj}, and k_m exhibit a positive impact on gas recovery, not only compensating for the negative impact of C_s, d_e, and B_i, but also enhancing the overall gas recovery of this well by 3%. Another observation is that the driving parameters here are not the formation characteristics. L_l, N_s, and C_s dominate in controlling how a gas MFHW could perform compared to the average. Also, the main formation characteristic that controls gas recovery here is the formation thickness, which was shown previously to have limited impact on the productivity of oil MFHWs.

7.5 Summary

This chapter presents a series of ANN-based proxy models designed to correlate the oil and gas productivities of over 10,000 Montney MFHWs with reservoir characteristics and completion-design

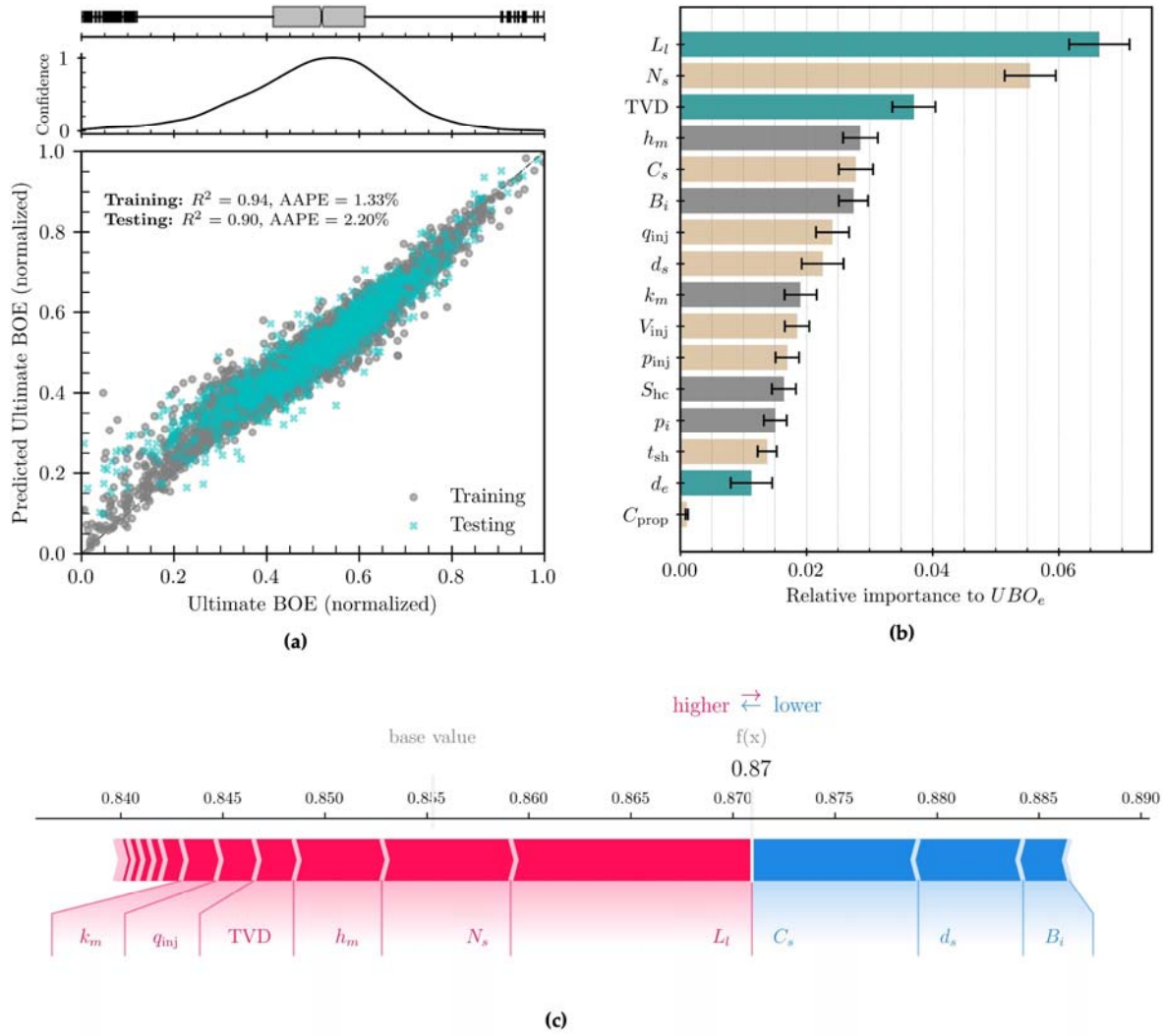

Fig. 7.18 – ANN-UBO_e prediction performance in terms of **(a)** crossplot between predicted and targeted UBO_e, **(b)** relative importance of each input parameter to the predicted UBO_e and **(c)** marginal contribution of each input parameter to UBO_e

parameters. Utilizing diverse datasets that reflect reservoir characteristics and completion practices, these proxies are trained to predict several key productivity metrics including initial effective fracture volume, cumulative oil production at 90% ultimate load recovery, ultimate oil production following a hyperbolic decline trend, and the ultimate barrel of oil equivalent (BOE) for gas MFHWs.

To lay the foundation for this analysis, a comprehensive dataset is compiled, including the petrophysical properties extracted from available well log data. These extracted data are then interpolated using a 3D kriging technique to generate high-resolution 3D maps of porosity, GR, bulk density, initial reservoir pressure, hydrocarbon saturation, and net-pay thickness across the Montney formation. Subsequently, a Support Vector Machine model is deployed to predict reservoir permeability utilizing well log data, specifically porosity, GR, bulk density, shallow and deep resistivities. This model facilitates the interpolation of data for Montney wells missing well log data, thus enabling the generation of an additional 3D permeability map across the upper, middle, and lower Montney formation.

Further, this chapter outlines a workflow to estimate formation fracability from sonic log data and introduces a brittleness index, which is then interpolated across the Montney formation. This brittleness index, along with other petrophysical properties, contributes to the formulation of a Reservoir Quality Index (RQI), serving as a unified measure of reservoir quality. Following this, a methodology to evaluate the efficiency of fracture stage positioning is introduced, showcasing a practical application of the developed RQI. Additionally, a new approach to estimate the effective distances between MFHWs, considering both 3D spatial and directional distances, is introduced. This newly derived parameter is incorporated as an input feature to train the proposed neural networks, enriching the model's ability to accurately correlate well productivity with reservoir and completion parameters. The results suggest the following:

1. Over 75% of Montney MFHWs, are completed in zones exhibiting higher initial reservoir pressure and hydrocarbon saturation. Conversely, around 20% are located in areas with elevated porosity and permeability, coupled with lower gamma ray readings, indicating an operator preference towards initial reservoir conditions.
2. The introduced SVM-K model demonstrates robust predictive ability in estimating reservoir permeability from well log data, as reflected by R^2 values of 0.97 and 0.95 along with AAPE of 7.1 and 9.7% for the training and testing datasets respectively. A mathematical formulation of SVM-K is provided to enhance the model's applicability across varied contexts. Notably, the model's prediction confidence is markedly higher for permeability values below 1 mD, implying potential higher uncertainty in SVM-K predictions within Montney regions possessing relatively higher permeability.

3. RQI analysis reveals a better homogeneity in the upper Montney as opposed to the middle and lower segments. Furthermore, the RQI mapping provides operators with a direct approach to pinpoint sweet spots for future developmental endeavors within the Montney formation.
4. The formulated ANN-based proxy aimed at predicting initial effective fracture volume (V_e) showcases good predictive capabilities, as highlighted by R^2 values of 0.96 and 0.93 on the training and testing datasets respectively. The model exhibits reduced uncertainty particularly within V_e range of 5,000 to 15,000 m^3.
5. Overall, completion design parameters demonstrate a more significant effect compared to formation characteristics. Among formation parameters, formation fracability emerges as a vital determinant of V_e. A higher brittleness index typically correlates with a larger V_e. Critical factors such as fluid volume injected per stage, number of stages, and stage spacing are essential in determining V_e. The model also highlights that increased fracture spacing notably restricts V_e. Additional parameters like injection rate and pressure, lateral length, and number of clusters per stage exhibit a positive correlation with V_e, although q_{inj} holds a more substantial impact. TVD displays a negative correlation with V_e, suggesting that higher TVD generally represents elevated overburden stresses and heightened resistance to fracture propagation. Lastly, formations with higher porosity and permeability emerge as favorable candidates for achieving a larger V_e.
6. Similarly, completion design and well profile significantly impact the oil recovery performance of MFHWs. Among reservoir characteristics, hydrocarbon saturation and formation permeability are pivotal in determining oil recovery. For the completion design, N_s, C_s, p_{inj}, C_{prop}, and V_{inj} are identified as significant parameters affecting oil recovery. The shut-in period also ranks within the top fifteen parameters controlling oil recovery, and a marginal contribution of each input parameter towards predicted oil recovery is proposed.
7. Similar to oil recovery, completion design and well profile significantly influence the gas recovery performance of gas MFHWs. Among the sixteen key parameters governing UBO_e, eleven are unrelated to reservoir characteristics. The lateral length and number of stages are identified as crucial determinants of gas productivity performance.
8. Unlike oil MFHWs, hydrocarbon saturation holds relatively low significance in determining the gas productivity of MFHWs. In terms of reservoir characteristics, formation thickness and brittleness are key parameters in controlling gas recovery. Unlike oil MFHWs, fracture spacing proves to be a significant parameter in gas MFHWs productivity. In contrast to oil MFHWs, proppant concentration has minimal impact on gas MFHWs recovery performance, possibly due to the lesser sensitivity of gas recovery to fracture volume loss compared to oil reservoirs.

7.6 Nomenclature

TVD	True Vertical Depth, m
L_l	Lateral Length, m
$\mathrm{lat_{bh}}$	Bottomhole Latitude, deg.
$\mathrm{lon_{bh}}$	Bottomhole Latitude, deg.
d_e	Minimum Effective Distance
V_{inj}	Average Fluid Pumped per Stage, m^3
Q_f	Foam quality, %
V_{acid}	Injected acid volume, m^3
C_{prop}	Proppant concentration, kg/m^3
N_s	Number of stages
L_s	Stage length, m
d_s	Average fracture spacing, m
C_s	Number of intervals/clusters per stage
t_{sh}	Shut-in time, days
p_{inj}	Average injection pressure per stage, MPa
q_{inj}	Average injection rate per stage, m^3/min
ϕ_m	Matrix porosity, fraction
γ_m	Matrix gamma ray, API
ρ_b	Matrix bulk density, kg/m^3
PE	Photoelectric absorption factor, b/e
k_m	Matrix permeability, md
B_i	Brittleness index
h_f	Formation thickness, m
S_w	Water saturation, fraction
p_i	Initial reservoir pressure, psi
h_{net}	Netpay thickness, m
V_e	Initial effective fracture volume, m^3
Qo_{90}	Cumulative oil production at 90% load recovery, bbl
UQo_{HY}	Ultimate cumulative oil production (from hyperbolic decline analysis), bbl
UB_{HY}	Ultimate barrel of oil equivalent (from hyperbolic decline analysis), bbl
MFHW	Multifracture horizontal well
SaDE	Self-adaptive differential evolution
ReLU	Rectified linear unit
MSE	Mean squared error
AAPE	Average absolute percentage error
μ	Mean
σ	Standard deviation
ANN	Artificial neural netowrk
SHAP	Shapely Additive explanation
RQI	Reservoir quality index

Chapter 8.
Evaluating Geothermal Energy Production from Suspended Oil and Gas wells

8.1 Introduction

Augustine, Tester [135] showed that the average cost to drill a geothermal well with a depth of 5,000 m is 5 million dollars. For enhanced geothermal system (EGS) power plants, drilling costs could account for 42%-95% of the total project cost [136, 137]. Does retrofitting suspended oil and gas wells can help advancing geothermal energy extraction and use across the world? Using suspended oil and gas wells for geothermal applications was initially proposed for converting conventional vertical wells to borehole heat exchangers (BHEs) where water is injected through the annulus between casing and tubing, and the heated water is produced from the tubing [138].

Sliwa, Rosen [139] investigated the possibility of converting the abandoned oil and gas wells near urban areas in the Carpathians in Poland for geothermal energy extraction. They proposed converting the abandoned wells to BHEs by equipping the wellbore with a heat carrier circulation system integrated with heat pumps on the surface to provide heat to the nearby residential areas.

Caulk and Tomac [140] investigated the feasibility of EGS and deep BHE installation in abandoned oil and gas wells in Santa Clara, Monterey and Santa Barbara counties in California. They found that wells' BHT ranges from 40 to 70°C, with some wells reaching up to 90°C. These temperatures are suitable for direct-use low-temperature EGS such as district or greenhouse heating. However, they concluded that deep coaxial BHE is a feasible low-cost and low-risk alternative to EGS due to the uncertainties associated with hydraulic fracturing of these wells that are completed in loosely to moderately consolidated sedimentary rocks of various stress regimes. They concluded that BHE with a diameter of 180 mm for wells deeper than 1,250 m could yield production temperature above 40°C and flowrate ranging from 1.0 to 4.4 l/s.

Macenic and Kurevija [141] studied geothermal energy extraction of an abandoned deep well located in the Drava subbasin in the Croatian part of the Pannonian Basin via closed circulation. They forecasted the available geothermal energy and changes in fluid temperature for 20 years of operation for two cases 1) with a constant base heat load throughout the year and 2) with a variable heat load depending on the environment temperature. The results showed that the maximum potential heat

extraction in a variable system (Case-2) is 1,750 MWh per year. The maximum theoretical stable heat extraction for possible industrial direct heating could be 400 KW for the entire 20 years, with fluid temperature reaching a steady state at 50°C.

Nian and Cheng [142] performed economic and energy analysis to assess the thermo-economic performance of geothermal energy production from an abandoned oil well with a depth of 3,000 m. The results showed that the well could keep a building with an area of 10,000 m^2 at around 26°C with a water flowrate of 20 m^3/h, and the maximum heating area could reach up to 11,000 m^2.

One of the main constraints for EGS is creating sufficient exposure to the high-temperature reservoir to allow for high production rates without reducing reservoir life by rapid cooling. Ideally, this could be achieved by 1) having a horizontal well system as it has a larger contact area compared to a vertical well [143]; and b) increasing the stimulated reservoir volume and heat exchange area by inducing fractures along the horizontal wellbore [144]. Recently, Gong, Guo [145] proposed a 3D thermal-hydraulic numerical model to describe heat and mass transfer and evaluate the effects of multiple hydraulic fractures on the performance of geothermal energy extraction. The results showed that EGS with multi-fractured horizontal wells (MFHWs) has a higher cumulative thermal production and a better heat extraction performance than the conventional vertical EGS. Based on their numerical model, MFHW-EGS performs optimally with seven fracture stages, fracture length of 300 m, and fracture conductivity of 350 $\mu m^2.cm$. However, due to the high directional drilling cost, these techniques are not widely used for geothermal exploitation, limiting the commercial development of EGS [146].

There are 65,535 suspended oil and gas wells completed in WCSB with reported BHT in the geoSCOUT database with more than a thousand suspended MFHWs. These wells have been suspended due to their uneconomic flowrate, but they might have the potential to produce heat. Geothermal energy can be extracted from suspended oil and gas wells by employing either BHE installation [142, 147-152] or EGS [153, 154]. In BHE, a working fluid is circulated through the wellbore. In EGS, a working fluid is pumped through an injection well into an induced fracture network, where it is heated by the formation rocks before being reproduced from a production well.

The general theme of the previously mentioned studies is that they are limited to few numbers of wells in a specific area/county and focus on formation properties and completion data as the main attributes defining the potential of geothermal power extraction from hydrocarbon wells. In this research, a national large-scale study is introduced to analyze all the suspended oil and gas wells completed in WCSB and have reported BHT in geoSCOUT database. A comprehensive framework is developed to combine the big datasets of formation properties, well completion, well logs, operating

conditions as well as the power grids and residential areas (including number of population and building in each area) all over Canada. Another dataset representing the daily average surface temperature nearby well location is extracted from Environment Canada [2] and integrated in this study to calculate heat loss at wellhead and in surface pipelines.

Another challenge associated with the previous studies on retrofitting suspended oil and gas wells into geothermal energy production is interpreting the uncertain BHT data reported for hydrocarbon wells. Generally, BHT is a data point at the end of well completion, but it is usually not known whether or not the wellbore is in equilibrium when BHT is measured [155]. **Fig. E.1** shows the histogram of the reported BHT for more than 400,000 oil and gas wells completed in WCSB. The figure shows that there are thousands of wells with reported BHT above 150°C, and that there are 109 wells with BHT above 200°C. According to Huang, Gosnold [156] and Allan Gray, Majorowicz [157], these high BHT values are uncertain to be utilized to evaluate the geothermal potential of these wells.

Therefore, the first objective of this study is to verify the reported BHT data of the suspended oil and gas wells utilizing the available valid temperature logs. Second, the verified BHT data is used along with other well data to evaluate the geothermal potential of the suspended wells utilizing a supervised fuzzy clustering approach. Then, the geothermal power and production temperature are estimated for each well, where higher power and temperatures support power generation utilizing EGS and lower values support direct hot water use utilizing BHEs [158].

8.2 Methodology

In this paper, the geothermal potential of 65,535 suspended oil and gas wells completed in WCSB is evaluated, indexed, and ranked to identify the possible candidate wells for retrofitting. The successful candidates should satisfy the following conditions: 1) There must be either a power plant or direct heat demand nearby. Unlike hydrocarbon, heat is not easily transportable to long distances as it requires costly insulated flowlines. 2) The reservoir heat resource must be high enough in terms of the bottomhole temperature and flowrate to match the demand. The flowrate depends on formation petrophysical properties but can be enhanced by induced fractures. Other factors affecting the flowrate are the well depth and diameter. For a well to successfully produce heat on a commercial scale, its depth has to be less than 4,500 m [155]. In this paper, successful candidate wells with vertical-large wellbore ($d_w \geq 177$ mm as proposed by Hu, Banks [159]) are considered for BHE utilization. While successful MFHWs candidates are considered for EGS; and 3) well integrity must be good enough to prevent water leakage. To evaluate the geothermal potential of each suspended well, the following attributes are considered: bottomhole temperature (BHT), temperature gradient (TG), true vertical depth (TVD), wellbore diameter (d_w), completion year (y_c), the distance to the nearest power

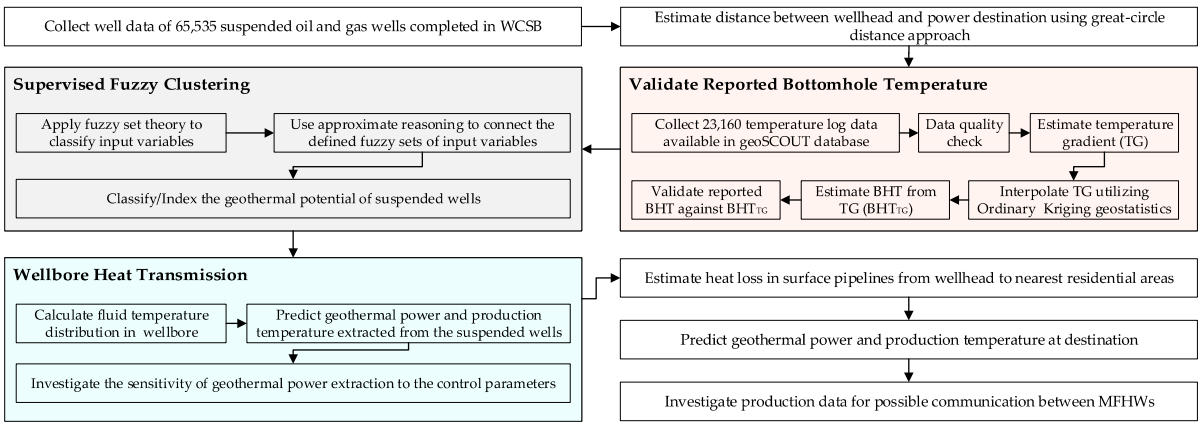

Fig. 8.1 – Methodology workflow for indexing geothermal potential of the suspended oil and gas wells completed in WCSB

plant ($D_{W\text{-}PP}$), electrical grid ($D_{W\text{-}EL}$) and residential area ($D_{W\text{-}RA}$). For the suspended MFHWs, the number of fracture stages (N_s) and lateral length (L_l) are added to the well data in evaluating its geothermal potential.

Well data of 65,535 suspended oil and gas wells completed in WCSB are exported from geoSCOUT database to analyze their geothermal potential. The overall workflow approached in this study is demonstrated in **Fig. 8.1**. The well data considered in this paper are BHT, TVD, d_w and y_c. **Fig. E.2** shows the histogram of these data and their distribution. BHT data has the highest uncertainty among these data as it is only reported as a single value at the end of well completion. To validate BHT data, the following tasks are conducted:

a) Collected 23,160 temperature logs available in geoSCOUT for the oil and gas wells completed in WCSB.

b) Performed a data quality check to filter out the invalid and duplicated temperature logs. The temperature logs with less than 1,000 datapoints, non-reported units, or decreasing trend with depth were considered as invalid. 4,126 temperature logs resulted from this step.

c) Estimated the temperature gradient (TG) of these 4,126 wells by fitting a linear model to the measured temperature data at the bottom 500 m of each well, then estimated both the slope and corresponding fitting performance of this model in terms of average absolute percentage error (AAPE) and coefficient of determination (R^2). This fitting performance is utilized to determine the uncertainty in the estimated TG.

d) Utilized the Ordinary Kriging geostatistical technique, developed by Wackernagel [160], to interpolate TG at the suspended wells with unavailable or invalid temperature logs.

a) Estimated bottomhole temperature from TG (BHT_{TG}) as per Eq. (8.1) where T_s represents surface temperature. According to Environment Canada [2], the daily average T_s in western Canada varies between -22 to 23 throughout the year as shown in **Fig. E.3**. These values are used along with the fitting error resulted from estimating TG to determine the confidence level when comparing the reported BHT against BHT_{TG}.

$$BHT_{TG} = \frac{TG}{100} \times TVD \times T_s \tag{8.1}$$

Then, the distance between the surface location of each suspended well to the nearest power plant ($D_{W\text{-}PP}$), electrical grid ($D_{W\text{-}EL}$) and the center of the nearby residential area ($D_{W\text{-}RA}$) is estimated using the great-circle distance approach:

$$D_{\mathrm{W-x}} = r\Delta\sigma \tag{8.2}$$

$$\Delta\sigma = 2\arcsin\sqrt{\sin^2\left(\frac{\Delta\phi}{2}\right) + \cos\phi_w \cos\phi_x \sin^2\left(\frac{\Delta\lambda}{2}\right)} \tag{8.3}$$

Here, $D_{W\text{-}x}$ is the distance between well's surface location and the nearest x-destination, where x represents power plant, electrical grid or residential area, r is the Earth radius (6,378.137 km) and $\Delta\sigma$ is the central angle between the well location and x-destination and is estimated in this study using the Haversine formula [161]:

$$\Delta\phi = |\phi_x - \phi_w|$$

$$\Delta\lambda = |\lambda_x - \lambda_w|$$

Here, λ_w, ϕ_w and λ_x, ϕ_x are the geographical surface longitude and latitude in radians of well and x-destination, respectively. **Fig. E.2c** shows that there are 629 suspended wells that are less than 5 km away from the nearest power plant and that more than 7,000 suspended wells are more than 100 km away from the nearest power plant.

Finally, a supervised fuzzy clustering (SFC) algorithm is developed as a multivariate analysis tool to classify the geothermal potential (GP) of each suspended well utilizing the estimated $D_{W\text{-}x}$ and TG along with the verified BHT, TVD, d_w and y_c. Here, GP combines 1) the formation properties in terms of BHT and TG; 2) the well completion in terms of TVD, d_w and y_c ; and 3) the accessibility to the nearest x-destination in terms of $D_{W\text{-}PP}$, $D_{W\text{-}EL}$ and $D_{W\text{-}RA}$ to represent the favorability index of the candidate well. Therefore, a well with "Good" GP is relatively newer and closer to an existing x-destination, has a relatively higher BHT and TG, shallower depth and larger wellbore, while a well

with "Poor" GP is the opposite. SFC is setup for two geothermal applications: a) direct use of geothermal power for heating purposes at the nearest residential areas; and b) geothermal electricity production and transportation to the nearest power plant or electrical grid. In the first application, $D_{W\text{-}x}$ is represented by $D_{W\text{-}RA}$, and in the second one $D_{W\text{-}x}$ is represented by $D_{W\text{-}PP}$ or $D_{W\text{-}EL}$, whatever is the shortest.

8.2.1 Fuzzy Set Theory for Input-Variables Classification

Here, a supersized fuzzy classification technique for a physics-based data analysis is used. **Fig. 8.2** shows how we apply the fuzzy set theory to classify the input variables (BHT, TG, TVD, $D_{W\text{-}x}$, d_w, and y_c) into three different fuzzy sets (categories). For BHT, three fuzzy sets are defined as Low, Medium and High. The fuzzy sets Low and High are defined by sigmoidal membership function represented by

$$f(x: a, c) = \frac{1}{1 + e^{-a(x-c)}} \tag{8.4}$$

and the fuzzy set Medium is defined by generalized bell membership function represented by

$$f(x: a, b, c) = \frac{1}{1 + \left|\frac{x-c}{a}\right|^{2b}} \tag{8.5}$$

Here, a defines the width of the membership function, b defines the shape of the curve on either side of the central plateau and c defines the center of the membership function. In the case of BHT, the fuzzy sets are defined in a way that BHT above 100°C is classified as High, and BHT below 35°C is classified as Low. For intermediate value, it is classified as $M_A(x) = m$, meaning that the membership of value x in fuzzy set A is m, where $0 \leq m \leq 1$. The reason for defining these parameters in BHT

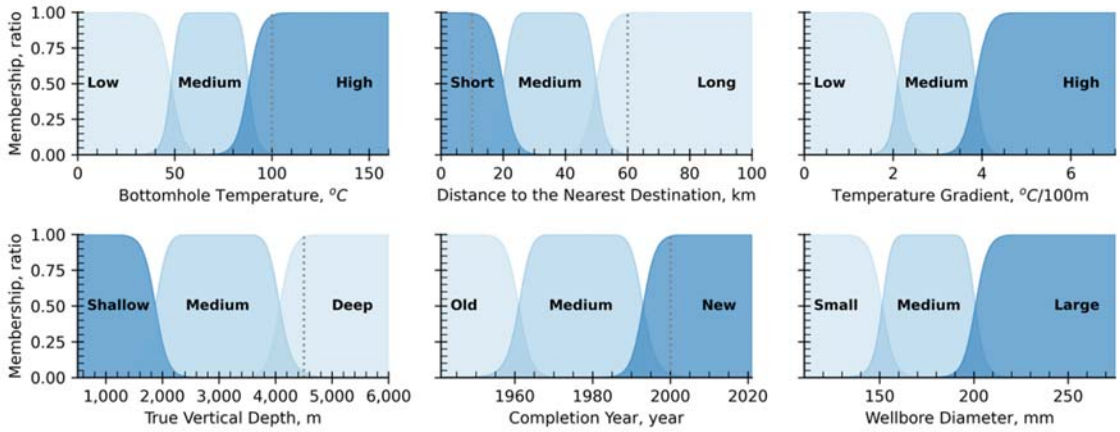

Fig. 8.2 – Fuzzy sets generated for each well parameter to define the distribution of each class

fuzzy classification is that wells with High BHT (above 100°C) can be considered as potential candidates for geothermal extraction depending on the other well data, and wells with Medium BHT (35°C – 100°C) might be potential candidates for a direct heat use depending on the distance from residential areas [140]. For defining the fuzzy sets of $D_{W\text{-}x}$, Short $D_{W\text{-}x}$ refers to the distance less than 10km away from the nearest x-destination while Long $D_{W\text{-}x}$ refers to the distance more than 60 km away. $d_w \geq 177$ mm is considered for large wellbore suitable for BHE utilization as proposed by Hu, Banks [159]. For a well to successfully produce power and heat on a commercial scale, well's TVD shall be less than 4,500 m [155]. Therefore, fuzzy set "Deep" of TVD is defined to consider wells with TVD above 4,500 m as deep wells. Ingraffea, Wells [162] analyzed more than 41,000 oil and gas wells completed after the year 2000. Less than 1.9% of the studied wells demonstrate a loss of structural integrity. Therefore, for the completion year (well's age), wells completed after the year 2000 are considered as new wells as shown in **Fig. 8.2**.

8.2.2 Approximate Reasoning for Geothermal Potential Classification

In SFC, approximate reasoning (fuzzy if-then rule) is used to connect the defined fuzzy sets of BHT, TVD, TG, $D_{W\text{-}PP}$, d_w and y_c to GP of each well. This connection in fuzzy rules is done using linguistic variables (poor, good, shallow, deep, low, high, etc.) and operators (and, or). Fuzzy if-then rules for a c-class in a classification problem with n attributes can be written as:

$$R_j: \text{If } x_1 \text{ is } A_{j1} \text{ and } \dots \text{ and } x_n \text{ is } A_{jn} \text{ then Class } C_j, \quad j = 1,2,\dots,N \tag{8.6}$$

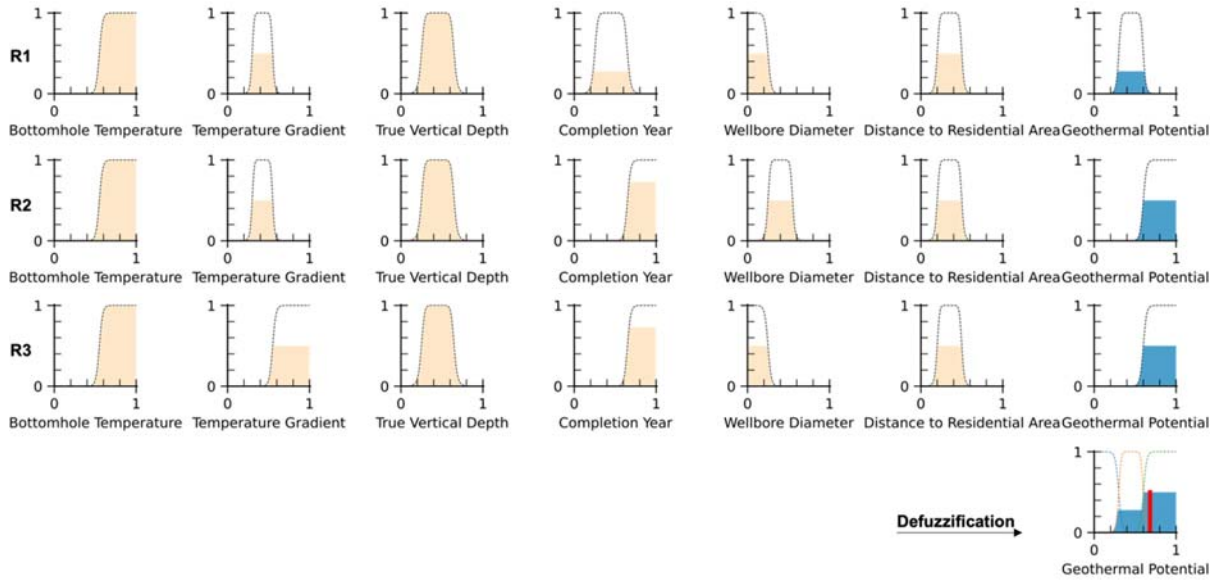

Fig. 8.3 – Example of fired fuzzy rules based on input well data

where **x**= (BHT, TG, TVD, y_c, d_w, $D_{W\text{-}PP}$), A_{ji} is an antecedent linguistic value such as Low and High ($i = 1,2,\dots,n$), C_j is an output GP class (i.e., Poor, Average or Good GP), and N is the number of fuzzy

if-then rules. **Fig. 8.3** shows an example of the three activation rules when classifying a well with High BHT, Medium-to-High TG, Medium TVD, Medium-to-New y_c, Small-to-Medium d_w and Medium $D_{W\text{-}PP}$. So, Eq. (8.6) becomes

$$\text{Rule } R_1: If\ x_1 \text{ is } A_{11} \text{ and } x_2 \text{ is } A_{21} \text{ and } x_3 \text{ is } A_{31} \text{ and } x_4 \text{ is } A_{41} \text{ and } x_5 \text{ is } A_{51} \text{ and } x_6 \text{ is } A_{61} \text{ then Class } C_1,$$

where $(x_1, x_2, x_3, x_4, x_5, x_6)$ = (BHT, TG, TVD, y_c, d_w, $D_{W\text{-}PP}$), (A_{11}, A_{21}, A_{31}, A_{41}, A_{51}, A_{61}) = (High, Medium, Medium, Medium, Low, Low), and C_1 = Average GP. In R_2, the same membership functions in R_1 are activated except for y_c and d_w where New and Medium membership functions are activated respectively. Therefore, GP class becomes Good. R_3 is similar to R_2 except that TG and d_w become High and Low respectively, and the GP class is still High. Then, the output fuzzy sets of the activated fuzzy rules (R_1, R_2 and R_3) are combined together to be defuzzified as shown in the right-bottom corner of **Fig. 8.3** to obtain one value representing the GP of the given well. There are several defuzzification techniques, but the one we applied in this study is the centroid method [61].

8.2.3 Wellbore Heat Transmission

As mentioned earlier, a coaxial BHE (double-pipe BHE) is employed to extract geothermal power from suspended wells as a direct use application of geothermal energy. The existing production casing of the suspended well acts as the outside pipe of BHE. Another smaller thermally insulated pipe is to be installed concentrically to the casing and is used as the inner-producing channel of BHE to produce the continuously injected working fluid from the annulus space [163]. In this study, water is used as

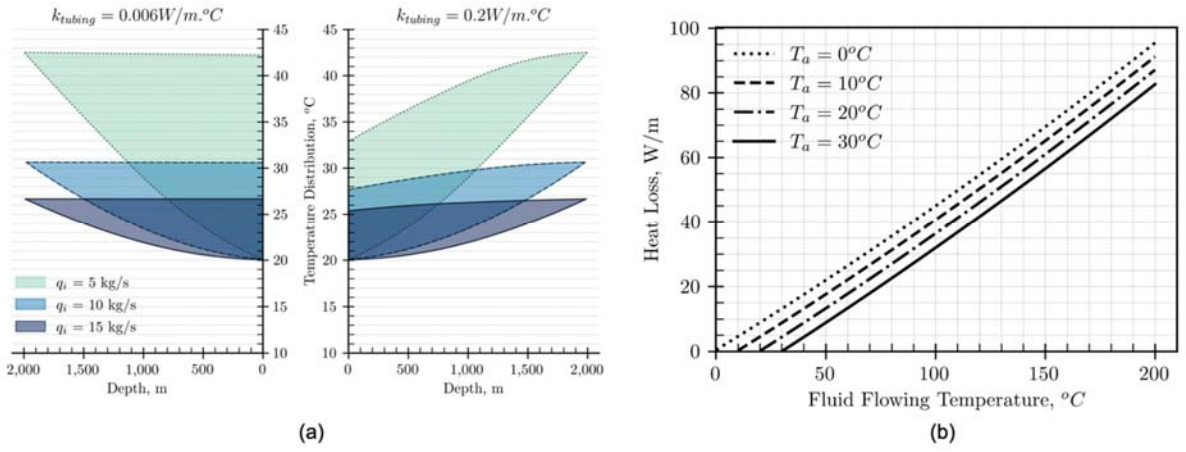

Fig. 8.4 – (a) Effect of BHE's tubing insulation on geothermal heat loss. **(b)** Heat loss in surface insulated pipe based on flowing fluid temperature and ambient temperature

the working fluid for geothermal power extraction because of its high specific heat and thermal stability [164].

The analytical model developed by Ramey [165] is utilized to estimate the temperature distribution of the working fluid in wellbore. Ramey's equation is widely used to describe fluid temperature distribution in a wellbore as a function of well depth, geothermal gradient and injection time, assuming single-phase flow inside wellbore [148, 165-168]:

$$T_{z,t} = az + T_s - aA + (T_{inj} - T_s + aA)e^{\frac{z}{A}} \tag{8.7}$$

here, $T_{z,t}$ is the fluid temperature in wellbore as function of depth (z, m) and injection time (t, days); T_{inj} is the injection temperature, °C; T_s is the average surface temperature in °C for each province [169] and listed in **Table E.1**; a is the geothermal gradient, °C/m; and A is defined as:

$$A = \frac{W c_w f(t)}{2\pi k_r} \tag{8.8}$$

where W is mass flow rate, kg/s; c_w is specific heat of water, J/(kg.K); k_r is thermal conductivity of formation rock in W/(m.K); and $f(t)$ is a dimensionless transient heat-conduction time function for the target formation, defined as

$$f(t) = -\ln\left(\frac{r_w}{2\sqrt{\alpha_r t}}\right) - 0.29 \tag{8.9}$$

here, r_w is wellbore radius, m; and α_r is the thermal diffusivity of the formation rock, m²/s, defined as $k_r/(\rho_r c_r)$ where ρ_r is formation rock density in kg/m³ measured from well-log data for each suspended well and its distribution is demonstrated in **Fig. E.4** for the studied wells; c_r and k_r are the specific heat in J/(kg.K) and thermal conductivity in W/(m.K) of formation rock, respectively. c_r is a linear function of the temperature (T) over a wide temperature interval and can be estimated by $c_r(T_i) + \beta(T - T_i)$ where T_i is the initial temperature, °C; $c_r(T_i)$ is specific heat at initial temperature; and β is a coefficient, J/(kg.°C²) [170-172]. For the studied wells completed in WCSB, Eq. (8.10) derived by Somerton [172] at $T_i = 21^oC$ can be used to estimate c_r of formation rock as a function of formation temperature:

$$c_r(T) = 824.8 + 0.9343(T - 21) \tag{8.10}$$

k_r is also a temperature-dependent property of formation rock and could be estimated by Eq. (8.11) developed statistically by Haenel, Stegena [173], and verified experimentally by Vosteen and Schellschmidt [174]:

$$k_r(T) = \frac{770}{B(350 + T)} + 0.7 \tag{8.11}$$

here B is thermal conductivity coefficient of formation rock and is generally estimated as 0.929 for WCSB [175, 176].

At TVD, Eq. (8.7) can be used to estimate the bottomhole temperature of circulating fluid (BHT_F) at time t from the start of injection. To estimate the production temperature at wellhead, heat loss in the BHE's inner tubing shall be considered. Toth and Bobok [177] demonstrated that the quality of the heat insulation of BHE's inner tubing significantly affects the heat loss in BHE. **Fig. 8.4a** shows that when a 4.5" steel pipe tubing with poly-propylene heat insulation with heat conductivity (k_{tubing}) of 0.2 W/m.°C is installed in a wellbore at depth of 2,000 m and casing size of 7", the heat loss becomes -23, -10 and -5% at injection mass flowrate (q_i) of 5, 10 and 15 kg/s, respectively. However, heat loss becomes neglected when a vacuum-insulated tubing (VIT) with an extremely low heat conductivity (k_{tubing}=0.006 W/m.°C) is installed. In this study, we assume that BHE is applied to suspended wells with inner VIT considering the relatively low overhead expenses of utilizing a suspended well with its casing pipe. Therefore, heat loss in BHE's inner tubing is ignored. Finally, the geothermal well power (P) in Watt is estimated by Eq. (8.12) as a function of q_i, c_w, T_i and BHT_F:

$$P = q_i c_w (\mathrm{BHT_F} - T_i) \tag{8.12}$$

8.2.3.1 Production Temperature and Geothermal Power Sensitivity to Injection Mass Flowrate and Injection Period

Fig. 8.5shows the effect of injection mass flowrate (from 0.1 to 5 kg/s) and injection time (from 1 to 25 years) on production temperature and geothermal power extracted from a suspended well with BHT of 150°C. Generally, increasing injection rate decreases production temperature and increases geothermal power. However, increasing the injection rate to 5 kg/s results in a 600% increase in the geothermal power and a 300% decrease in the production temperature suggesting two different trends as observed by Hu, Banks [159]. In addition, in the first five years of the injection period, the production temperature and geothermal power decrease by 7.7% and 10.25%, respectively. However, in the last five years, the production temperature and geothermal power decrease by 0.76% and 1.05%,

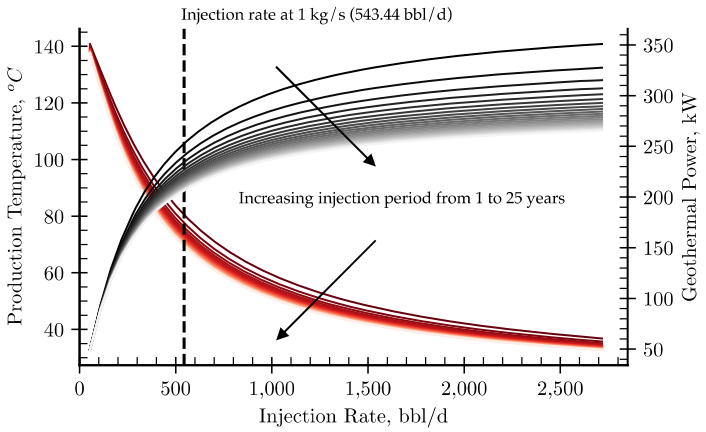

Fig. 8.5 – Effect of injection rate and period on production temperature and geothermal power

respectively, demonstrating a quick drop of the geothermal power and production temperature at the initial running time compared to late time. Therefore, the long-term (25 years) performance of the geothermal power extraction from suspended wells are evaluated and predicted in this study. Considering the direct-use application of geothermal power to heat buildings in the nearest residential areas, the injection rate of 1 kg/s is selected to maintain adequate levels of production temperature and geothermal power.

8.2.4 Heat Loss in Surface Insulated Pipeline

In this study, the geothermal power delivered to the nearest residential areas is estimated. Therefore, heat loss in surface pipelines from wellhead to the center of nearest residential area is considered. According to Frank P. Incropera [178], heat loss from an insulated surface pipeline is a function of pipe's inside- and outside-diameter, operating and ambient temperature, wind speed, insulation type and properties in terms of surface emissivity, thickness and outside diameter. The specifications of the pipeline and insulation are listed in **Table E.1**. Operating fluid temperature is BHT_F, and the ambient temperature (T_a) depends on the wellhead location and residential area. Average T_a for each province is collected from Canada [2] and listed in **Table E.1**. **Fig. 8.4b** demonstrates the heat loss in surface pipeline per meter (with the given specifications) as a function of BHT_F and T_a. For example, if BHT_F is 40°C and T_a is 10°C, the heat loss per each meter of the pipeline is estimated at 13.2 W/m.

8.3 Results and Discussion

8.3.1 Bottomhole Temperature Validation Using Temperature Gradient

Fig. 8.6 shows the contour map of the estimated TG using the validated temperature logs of 4,126 hydrocarbon wells completed in WCSB. The northern area between Alberta and British Columbia has the highest TG between 4 to 5.5°C/100m. Therefore, BHT at 1,500 m shall be around 60 to 80°C, which matches the BHT data reported by CanGEA [179] as shown in **Fig. 8.7a**. Accordingly, a 100°C BHT might be obtained in this area at 1,850 ≤ depth ≤ 2,500 m which is verified by the temperature reported at 2,500 m as shown in **Fig. 8.7a**. This noticeable high TG makes this region in Alberta have the highest favourability index for geothermal extraction as shown in **Fig. 8.7b** and reported by CanGEA [179].

The primary purpose of calculating TG in this study is to validate the BHT data reported for the 65,535 suspended oil and gas wells completed in WCSB. As mentioned earlier, the estimated TGs of the 4,126 wells are geostatistically interpolated to estimate TG for the remaining wells with unavailable or invalid temperature logs. **Fig. 8.8a** shows the cross-plot of estimated bottomhole temperature using Eq. (8.1) and the ones reported in geoSCOUT (single measurement at the end of the completion) for

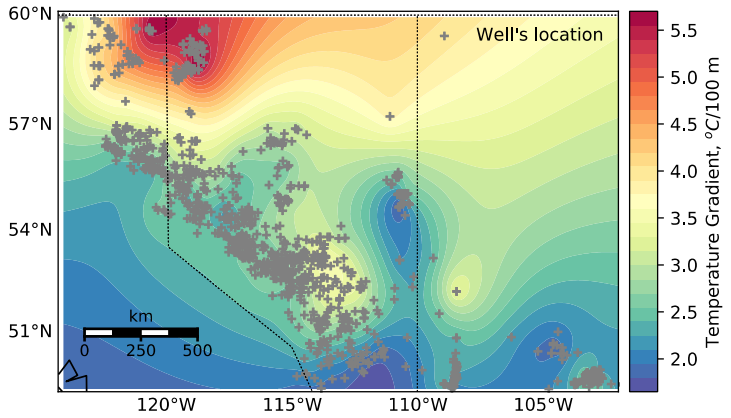

Fig. 8.6 – Contour map of temperature gradient estimated from validated 4,126 oil and gas wells completed in WCSB

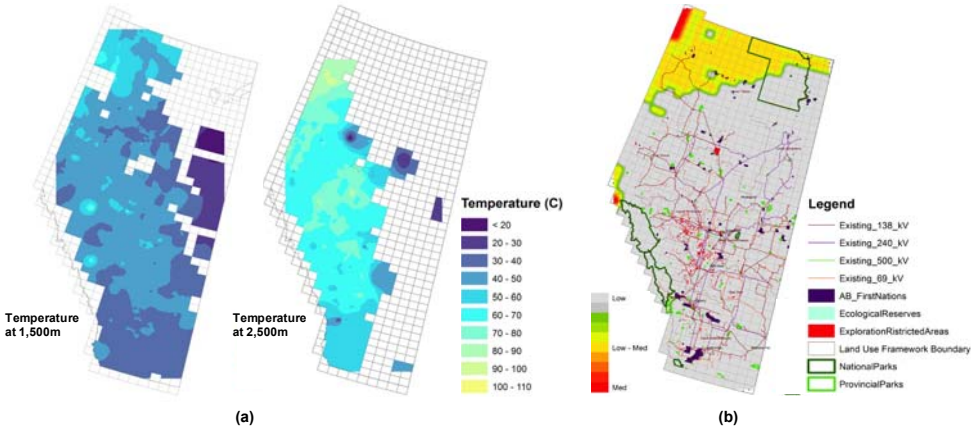

Fig. 8.7 – **(a)** Bottomhole temperature reported at depths between 1,500 and 2,500m in Alberta. (b) Favourability index of geothermal energy extraction in Alberta. Modified from [179].

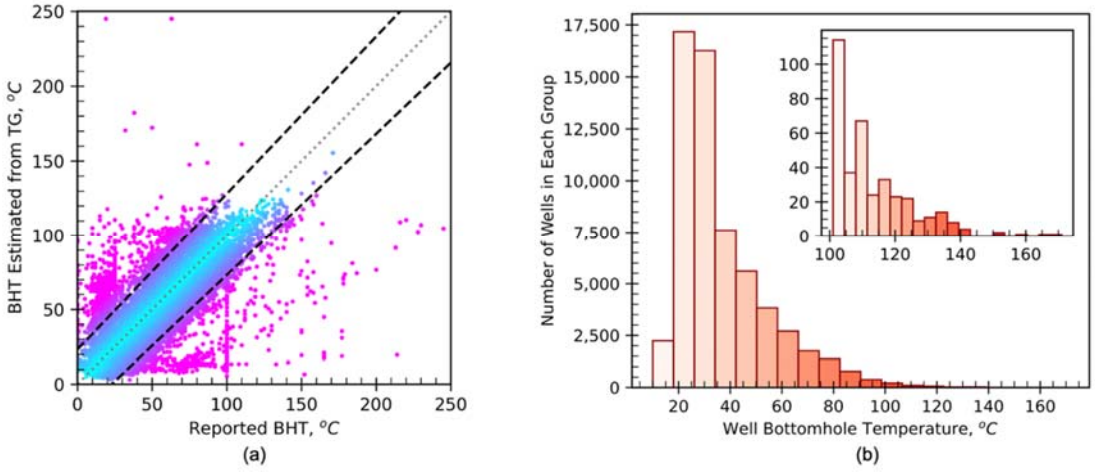

Fig. 8.8 – **(a)** Cross-plot of bottomhole temperature estimated from temperature gradient and the ones reported in geoSCOUT for the 65,535 suspended oil and gas wells in WCSB. Top and bottom black dashed-lines represent the uncertainties in both reported surface temperature from Environment Canada [2] and estimated temperature gradient (fitting error) **(b)** Histogram of the valid bottomhole temperature reported for the suspended wells

the 65,535 wells. The top- and bottom-dashed lines represent the uncertainties in both the surface temperature and estimated temperature gradient from the temperature-log data. 10,784 (17%) wells are shown to have invalid BHT measurements and are filtered out, while the remaining 54,751 wells show BHT measurements that are within the expected range based on their estimated TG. **Fig. 8.8b** shows the updated histogram of the validated BHT data reported for the 54,751 suspended wells and that 412 wells are with reported BHT above 100°C. The maximum reported BHT, in this case, is 161.8°C.

The 412 wells with BHT ≥ 100°C are located in the areas with average to high TG as shown in **Fig. 8.9**. However, the northwest region of Alberta does not show any suspended wells with BHT above 100°C. This region has only six suspended wells with a maximum TVD and BHT of 2,008 m and 80°C, respectively. There are more than 1,250 suspended wells in regions with TG ≥ 4.5°C/100m but with depth ≤ 1,500 m as shown in **Fig. 8.9b**. Therefore, one possible way to utilize these regions for geothermal energy extraction is to deepen the existing suspended wells to reach hotter formations. Another observation is that there are 137 suspended wells located at the highest TG regions, in the northeast of British Columbia, with no nearby power plant. These wells have median and average BHT of 115°C and 121°C, respectively. Among these wells, there are 25 suspended MFHWs with median BHT and N_s of 129°C and 14, respectively. Utilizing these wells for geothermal energy extraction may need extending the nearest power grid.

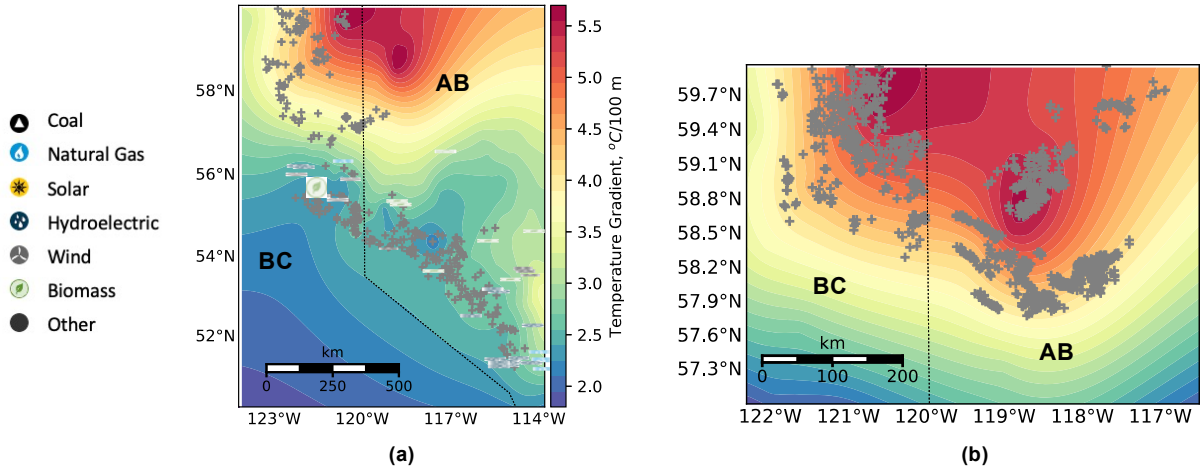

Fig. 8.9 – (a) The suspended wells with BHT above 100°C and nearby power plants. **(b)** Suspended wells with depth less than 1,500m in regions with temperature gradient above 4.5°C/100m

8.3.2 Supervised Fuzzy Clustering Results

Based on the BHT validation results, 54,751 suspended wells are found to have valid BHT data. Wells with incomplete set of input parameters or those more than 50 km away from nearby residential areas

are excluded. The remaining 50,192 suspended wells are considered for geothermal potential evaluation. **Fig. 8.10b** shows the classification of these wells based on the geothermal potential index resulted from the SFC algorithm assuming the relative weights of the input variable as shown in **Fig. 8.10a**. There are 10,724 (21.37%), 38,636 (76.97%), and 832 (1.66%) wells ranked with poor, average and good geothermal potential, respectively. 84% of the wells classified with "Good" GP are suspended gas wells suggesting that suspended gas wells have a relatively high potential for retrofitting. Two-thirds of those wells (65.75%) are completed in the Horn River Formation. The wells with poor, average and good geothermal potential have an average BHT of 36.5, 46.3 and 68.55°C, respectively, as shown in **Fig. 8.11**. The figure shows that "Good" wells are relatively newer wells, closer to residential areas, have higher TG and larger d_w compared to the "Poor" and "Average" wells. The 832 wells classified to have "Good" GP have an average $D_{W\text{-}RA}$, y_c, TG, TVD and d_w of 4,550 m, 2000, 2.9°C/100 m, 2,200 m and 163 mm, respectively. Among these wells, there are more than 300 wells

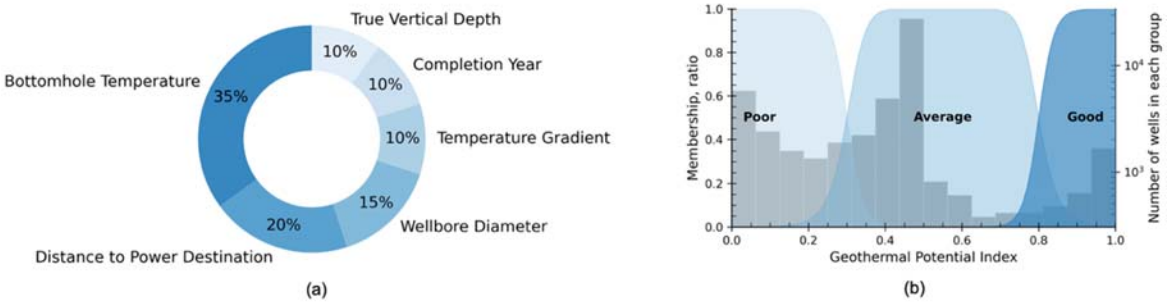

Fig. 8.10 – (a) Relative weights of input variables to the supervised fuzzy clustering (SFC) algorithm. **(b)** Geothermal potential results from SFC

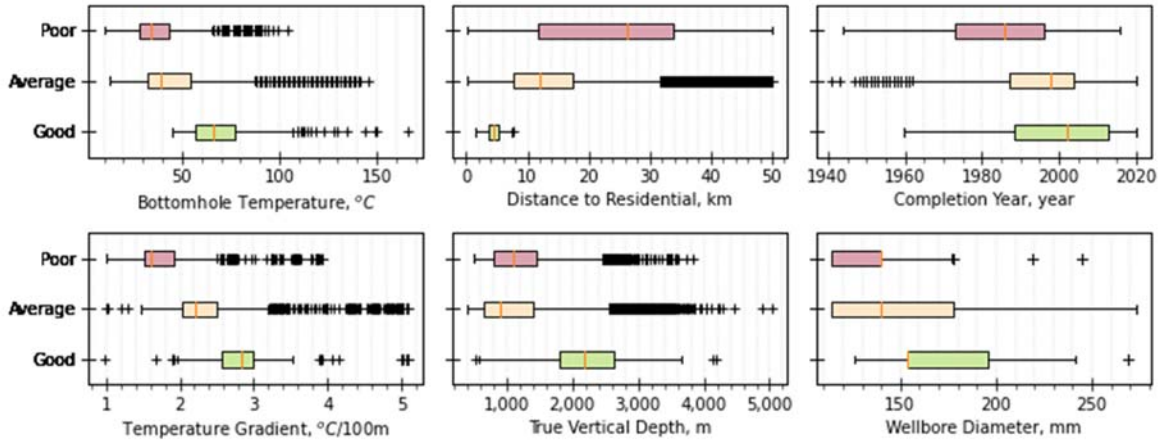

Fig. 8.11 – Statistics of studied parameters in each group. Generally, wells classified with good geothermal potential show higher bottomhole temperature and temperature gradient, shorter distance to nearby power plant, newer completion date and larger wellbore diameter.

with $d_w \geq 177.8$ mm which makes them the best candidates for coaxial BHEs retrofitting, although they do not have insulated casing. Hu, Banks [159] showed that BHE's performance is marginally affected by a thermally insulated casing.

8.3.3 Geothermal Power and Production Temperature from Suspended Wells

Fig. 8.12 shows contour maps of the suspended wells' geothermal power and bottomhole flowing temperature at water injection rate and temperature of 1kg/s (543.44 bbl/day) and 20°C, respectively. Some suspended wells show the potential of producing more than 270 KW of geothermal power with $BHT_F \geq 70^oC$ with coaxial BHEs installation over one year. **Fig. 8.12b** shows the location of 30 wells with $BHT \geq 100^oC$ and $BHT_F \leq 75^oC$.

Fig. 8.13 shows the statistics of generated geothermal power at the wellhead of suspended wells classified with Poor, Average and Good geothermal potential. Good wells could generate an average 75 KW of geothermal power. Among these wells, there are 36 wells that could generate more than 200 KW of geothermal power individually. Average production temperature from Good suspended wells can still reach to more than 46°C with an average geothermal power of 59 KW after 25 years. **Fig. 8.13b** demonstrates the estimated geothermal power at the nearest residential area considering the heat loss in surface pipelines with the specifications and operational parameters listed in **Table E.1**. Good wells could deliver an average 34 KW of geothermal power to the nearest residential areas, and there are 13 wells that could generate more than 100 KW of geothermal power. On average, more than 50% of the geothermal power is lost in surface pipelines (assuming Calcium Silicate insulation type) while transferring to the residential areas from the suspended wells with an average heat loss of 16 W/m.

Fig. 8.14a shows the sensitivity of geothermal power generated from suspended wells to formation bulk density (ρ_b). Formation rocks with higher ρ_b demonstrate a higher potential to generate geothermal power. This is mainly due to the relatively higher thermal conductivity generally exhibited by dense rocks [180]. The studied suspended wells are completed in formation rocks with ρ_b that varies between 1,413 to 3,259 kg/cm^3 as shown in **Fig. E.4**. In this domain, ignoring ρ_b could lead to more than 7.8% relative error in the estimated geothermal power extracted from suspended wells.

Fig. 8.14b demonstrates a comparison of the geothermal power generated from suspended wells considering constant and transient thermodynamic properties during the injection period of 25 years. At the first year, the difference in estimated geothermal power between the two cases is 2.6%. At the end of the injection period, this difference is magnified to 6.8%. Therefore, temperature dependence

of rock thermal properties shall be considered in evaluating long-term performance of geothermal power extraction from suspended wells.

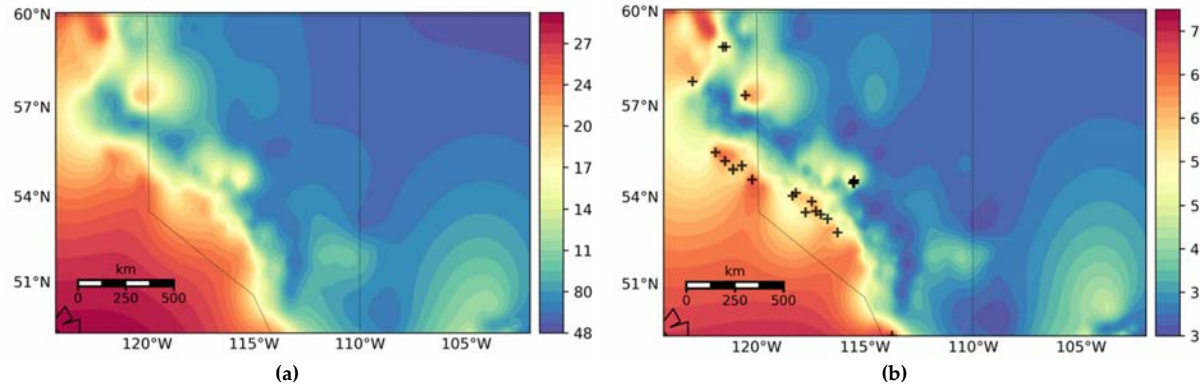

Fig. 8.12 – **(a)** Downhole geothermal power and **(b)** production temperature at water injection rate of 1kg/s (543.44 bbl/day)

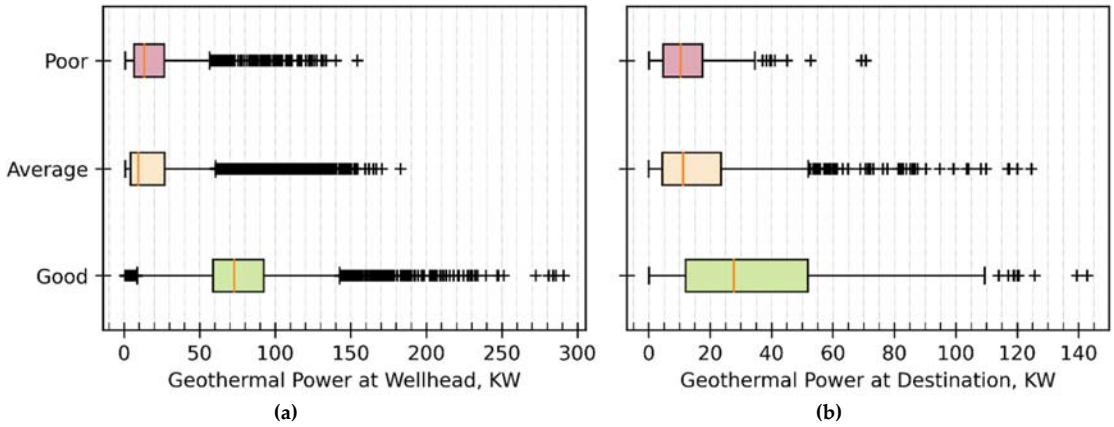

Fig. 8.13 – Geothermal power generated at **(a)** wellhead and **(b)** nearest residential area

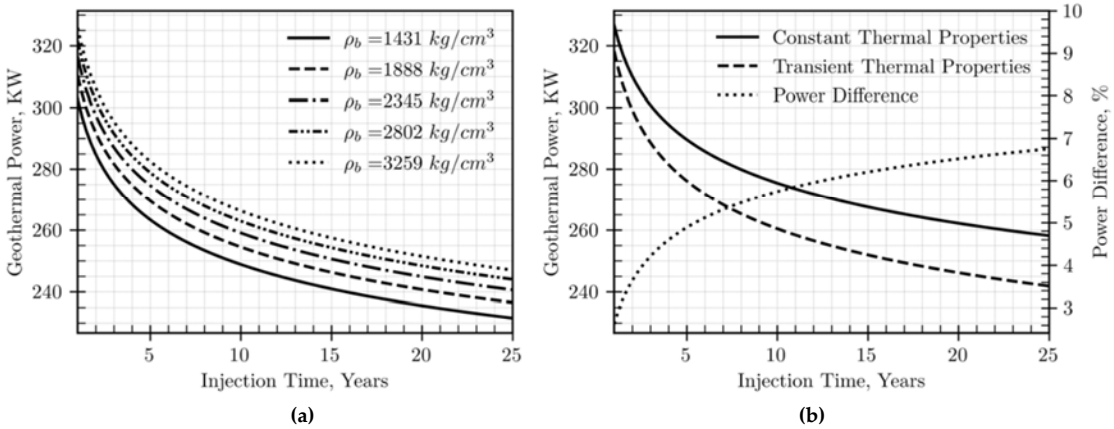

Fig. 8.14 – Effect of **(a)** rock bulk density and **(b)** constant vs transient temperature-depenent properties on estimating potential geothermal power from suspened wells

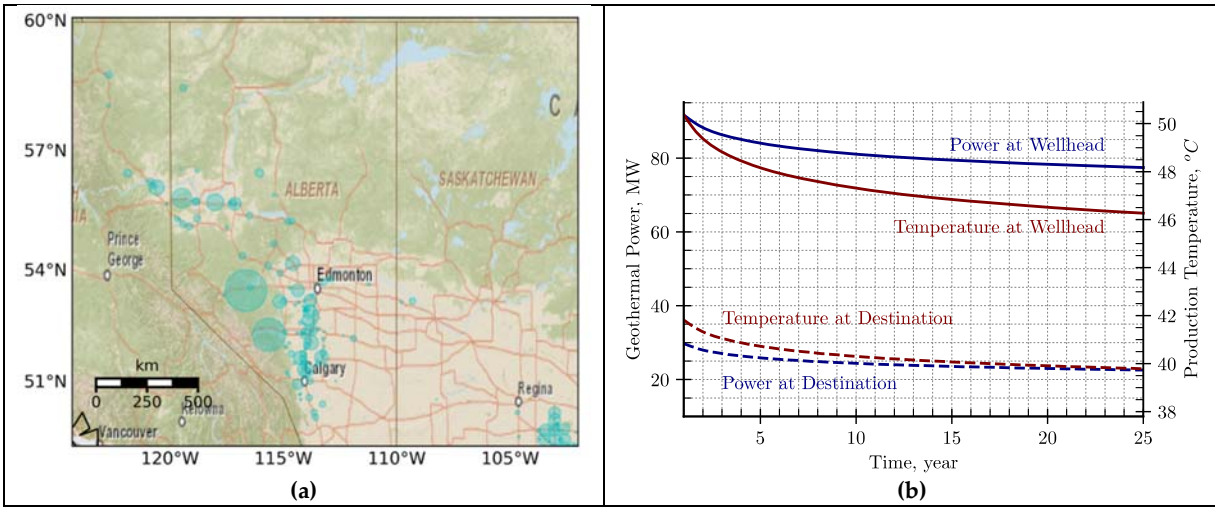

Fig. 8.15 – Potential residential areas to be served by the geothermal power extracted from nearby suspended wells with "Good" geothermal potential

Fig. 8.15 demonstrates the 163 residential areas in Saskatchewan, Alberta and British Columbia that could be served with the geothermal power generated from the nearest 832 suspended wells classified with "Good" geothermal potential. These wells could deliver up to 29.83 MW of geothermal power to directly heat more than 2,700 private dwellings with a total number of populations of 6,506 in those nearby residential areas [181]. In 14 residential areas, the extracted geothermal power could serve more than 25% of the power needed for heating while in 6 residential areas the geothermal power could cover more than 50% of the heating power needed. **Fig. 8.15b** shows the total geothermal power and average production temperature at wellhead and delivered to the nearest residential areas over the operation time of coaxial BHEs in the suspended wells classified with "Good" geothermal potential. The total geothermal power and average production temperature delivered at destination are estimated at 29.83 MW and 41.82°C, respectively, in the first year and dropped to 22.54 MW and 39.78°C, respectively, after 25 years.

8.3.4 Suspended MFHWs with Good Potential for EGS

Among the studied wells, there are 42 suspended MFHWs classified with "Good" geothermal potential. These wells have BHT $\geq 100^{o}C$ and are less than 500 m away from the nearest power grid [min($D_{W\text{-}PP}$, $D_{W\text{-}EL}$)], and are relatively newer wells ($y_c \geq 2009$). Average TVD, TG, d_w, lateral length (L_l) and number of stages (N_s) are 2,827 m, 3.3°C/100m, 141 mm, 1,704 m, and 15 stages, respectively.

Fig. 8.17 shows the normalized completion properties of the 10 MFHWs wells with the highest geothermal potential among the "Good" wells. Min-max scaling method is used to normalize (scale) the range of each completion parameter in [0, 1]. So, for each variable, the normalized value (x_n) is estimated as $(x - x_{min})/(x_{max} - x_{min})$, where x is the original value, and x_{min} and x_{max} are the

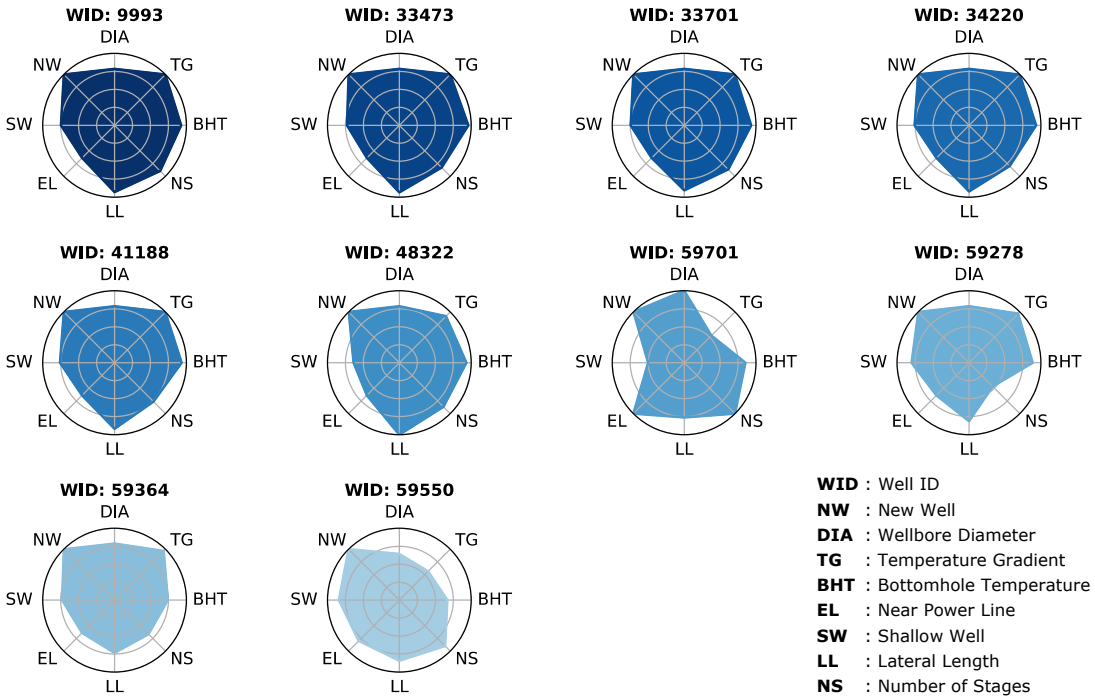

Fig. 8.16 – Normalized completion properties of the 10 suspended MFHWs with the highest geothermal potential

minimum and maximum values of x, respectively. Well-9993 is shown to have the highest geothermal potential among the suspended MFHWs. This well has 27 fracture stages, BHT of 139°C, TVD of 2,492 m and 467 m distance from the nearest power grid and was completed in 2012 with lateral length of 2,456 m.

Fig. 8.16 shows four pairs of MFHWs with high potential of retrofitting into EGS. **Fig. 8.16a** shows Well-56432 which was completed in 2016 with 27 fracture stages, then suspended in 2018. It has BHT of 100°C and 300 m lateral distance from another suspended MFHW (Well-703685) that has 28 fracture stages. Both wells have the same TVD of 2,206 with TG of 4.26°C/100m. Therefore, this well pair can be considered as a potential candidate for EGS where one well is used as an injection well and the second to produce heated water (or other working fluid). **Fig. 8.16c** shows another candidate for EGS. Well-54938 was completed in 2012 with 9 fracture stages, and lateral and vertical distances of 773 m and 84 m, respectively, from Well-686038 which has 13 fracture stages. Both wells were suspended in 2018 and 2017, respectively. The monthly production data shows a 60% increase of the water production rate of well-686038 during the month when well-54938 was being hydraulically fractured. This suggests a communication between the fracture networks of the two wells. **Fig. 8.16d** shows another potential well pair for EGS. Although the lateral and vertical distance between the two wells is 1,750 m and 66 m respectively, there was a 27% increase in the water production rate of Well-61970

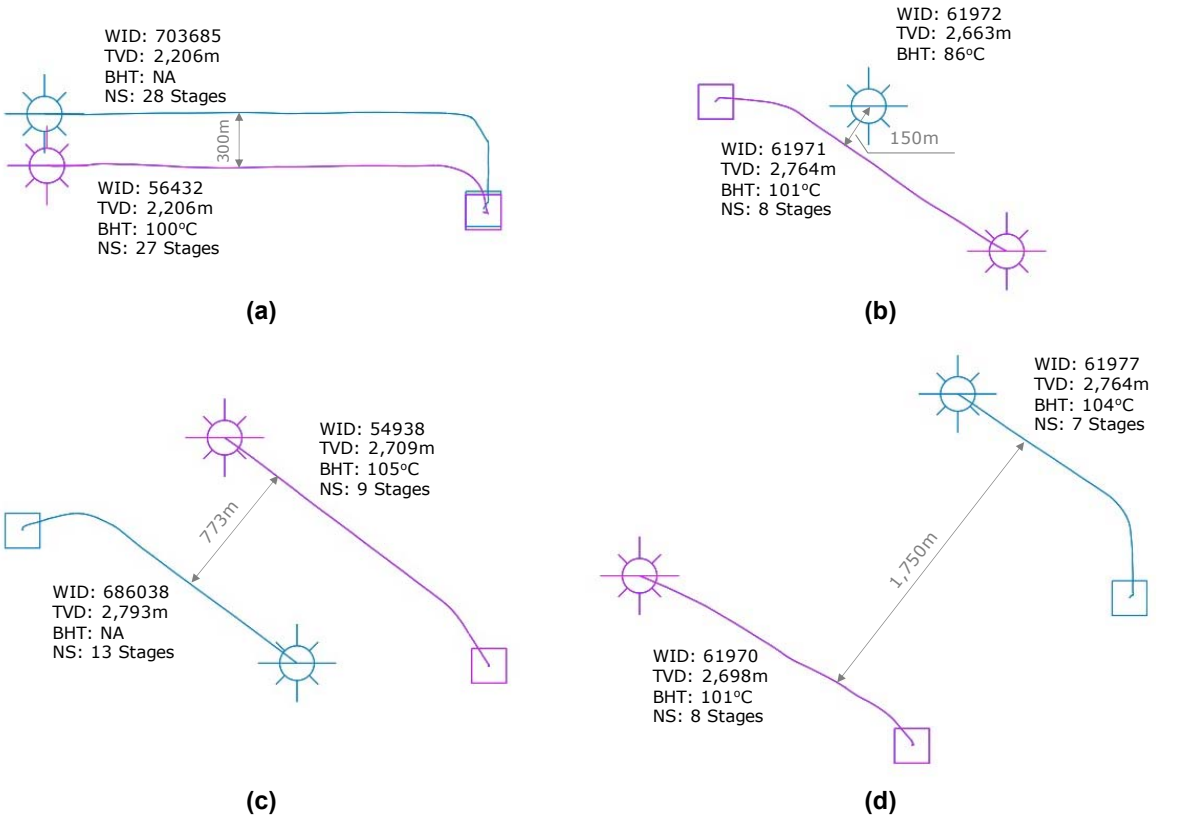

Fig. 8.17 – Examples of suspended MFHWs with the distance to the neighbour suspended well, showing the potential of retrofitting these well pairs into enhanced geothermal systems

when Well-61977 was being fractured suggesting a communication between the wells' fracture networks. The two wells have BHT of 101°C and 104°C respectively. **Fig. 8.16b** shows MFHW-61971 which was completed in 2008 with 8 fracture stages, and lateral and vertical distances of 150 m and 101 m, respectively, from the vertical Well-61972. The vertical well produced 100% more water rate when Well-61971was being fractured.

8.4 Summary

In this study, the bottomhole temperature data reported for 65,535 suspended oil and gas wells completed in the Western Canadian Basin Sedimentary (WCSB) was verified utilizing the 4,126 validated temperature logs by developing a contour map of the temperature gradient distribution. Then, the distance between each suspended well to the nearest power grid and residential area was estimated using the great-circle distance technique. This parameter is then combined along with the verified bottomhole temperature, temperature gradient, true vertical depth, wellbore diameter and well's completion year to determine the geothermal potential index of the wells using a supervised fuzzy clustering (SFC) method. Unlike pure statistical classification techniques, adding supervision to

SFC algorithm allows physics-based indexing of the potential geothermal power of suspended oil and gas wells. SFC allows to define the relative impact of formation and completion properties, and geographic location in determining the geothermal power potential of a suspended hydrocarbon well. The study led to the following conclusions:

1. A bottom hole temperature of at least 85°C at depth 3,000 m or less with wellbore diameter of at least 7" are required to deliver 130 KW of geothermal power at production temperature of 50°C to a residential area 1 km away from wellhead assuming injection fluid temperature and ambient temperature of 20 and 10°C, respectively, and surface pipeline with 3" diameter and Calcium Silicate insulation. On average, more than 50% of the geothermal power is lost while transferring to the
2. residential areas near to the suspended wells with an average heat loss of 16 W/m. Average production temperature from Good suspended wells can still reach to more than 46°C with average geothermal power of 59 KW after 25 years.
3. More than 800 (1.7%) suspended wells are classified with "Good" geothermal potential that could deliver up to 29.83 MW of geothermal power to directly heat more than 2,700 private dwellings in the nearest 163 residential areas. In 14 residential areas, the extracted geothermal power could serve more than 25% of the power needed for heating while in 6 residential areas the geothermal power could cover more than 50% of the heating power needed. After 25 years, the geothermal power of those wells is estimated to drop by 23% assuming an injection flowrate of 1 kg/s. 84% of those wells are suspended gas wells suggesting that suspended gas wells have a relatively high potential for retrofitting. Almost 66% of those wells are completed in the Horn River Formation.
4. The geothermal power extraction's performance can be controlled by varying the injection temperature and injection flowrate. However, injection flowrate has the highest impact; a 10% increase in the injection flowrate led to 3.5% increase in the produced geothermal power and 4.4% drop in the production temperature while 10% increase in the injection temperature led to only 0.6% increase in the production temperature.
5. The studied suspended wells are completed in formation rocks with bulk density (ρ_b) varies between 1,413 to 3,259 kg/cm^3. In this domain, ignoring ρ_b could lead to more than 7% relative error in the estimated geothermal power extracted from the suspended wells.

6. Assuming constant thermal properties of the formation rock led to 6.76% relative error in the estimated geothermal power over the temperature-independent case during an injection period of 25 years. Therefore, temperature dependence of rock thermal properties shall be considered in evaluating long-term performance of geothermal power extraction from suspended wells.
7. 3.7% of the studied suspended wells are MFHWs where 63% of them have valid reported BHT data. Less than 3% of those wells are ranked with "Good" geothermal potential and there are four pairs of suspended MFHWs that are suitable for enhanced geothermal system (EGS) as the production data of each well pair showed inter-connectivity of their fractured networks.
8. 2.6% of the suspended wells are located in regions with a temperature gradient $\geq 4.5^{o}C/100m$ but with a limited potential for geothermal energy extraction either because they are not deep enough ($< 1{,}500$ m) to reach hot formations, or far from nearby power grids and residential areas. Extending the existing nearby power grids and/or deepening those wells could enhance their geothermal potential.

Chapter 9.
Conclusions and Recommendations

This thesis introduces a comprehensive workflow to i) identify optimal sweet spots based on petrophysical properties, while proposing a new unified term to define the reservoir quality, and ii) analyze, evaluate and optimize the completion design of MFHWs, considering both reservoir characteristics and geomechanical properties.

9.1 Conclusions

The key conclusions drawn from this thesis are outlined as follows:

1. The fracture volume loss during flowback and post-flowback can be modelled by a power function of the fracture characteristic rate (FCR) and that the proppant concentration is a key parameter that controls FCR and dimishes fracture closure during flowback.
2. Generally, the functional dependence of well productivity on completion-design varies depending on reservoir quality. In low-quality reservoirs, the effect of completion-design on productivity is less pronounced and the productivity follows reservoir quality. However, in high-quality reservoirs, the effect of completion-design becomes more significant, and the productivity can be reduced due to inefficient completion-design. Moreover, the productivity can be maximized by less intense completion-design in low-quality reservoirs. However, in high-quality reservoirs, intense completion significantly improves the productivity.
3. In several studied black-oil wells, independent flow regimes (stratified flow) of water and oil are observed during early production time, indicating their production under different drive mechanisms. Water is produced from an apparently closed tank comprising induced fractures and the surrounding stimulated matrix, and oil is produced independently at a significantly lower rate due to oil influx from matrix into fractures. In these wells, oil breakthrough shows insignificant effect on water flow regime, as the dominant drive mechanism of water production is the fracture closure, and oil tends to flow independently through its own network.
4. Effective fracture volume, as determined through the WORM, showcases a positive correlation with the estimated volume of microseismic events.
5. The application of a completion design to achieve a similar effective fracture volume on child wells does not necessarily lead to similar oil productivity compared to parent wells. It also depends on the quality of the reservoir at which the parent/child wells are completed.

6. A majority of the studied parent and child wells yield over 50% of the estimated ultimate load recovery within the initial three months of production.
7. Over 75% of Montney MFHWs, are completed in zones exhibiting higher initial reservoir pressure and hydrocarbon saturation. Conversely, around 20% are completed in areas with elevated porosity and permeability, coupled with lower gamma ray readings, indicating an operator preference towards initial reservoir conditions.
8. RQI analysis reveals a better homogeneity in the upper Montney as opposed to the middle and lower segments. Furthermore, the RQI mapping provides operators with a direct approach to pinpoint sweet spots for future developmental endeavors within the Montney formation.
9. Completion design parameters generally exhibit a greater influence compared to formation characteristics. Among formation parameters, formation fracability emerges as a vital determinant of V_e. A higher brittleness index typically correlates with a larger V_e. Critical factors such as fluid volume injected per stage, number of stages, and stage spacing are essential in determining V_e. The model also highlights that increased fracture spacing notably restricts V_e. Additional parameters like injection rate and pressure, lateral length, and number of clusters per stage exhibit a positive correlation with V_e, although q_{inj} holds a more substantial impact. TVD displays a negative correlation with V_e, suggesting that higher TVD generally represents elevated overburden stresses and heightened resistance to fracture propagation. Lastly, formations with higher porosity and permeability emerge as favorable candidates for achieving a larger V_e.
10. Similarly, completion design and well profile significantly impact the oil recovery performance of MFHWs. Among reservoir characteristics, hydrocarbon saturation and formation permeability are pivotal in determining oil recovery. For the completion design, N_s, C_s, p_{inj}, C_{prop}, and V_{inj} are identified as significant parameters affecting oil recovery. The shut-in period also ranks within the top fifteen parameters controlling oil recovery, and a marginal contribution of each input parameter towards predicted oil recovery is proposed.
11. Similar to oil recovery, completion design and well profile significantly influence the recovery performance of gas MFHWs. The lateral length and number of stages are identified as crucial determinants of gas productivity performance. However, unlike oil MFHWs, hydrocarbon saturation holds relatively low significance in determining the gas productivity of MFHWs. In terms of reservoir characteristics, formation thickness and brittleness are key parameters in controlling gas recovery. Unlike oil MFHWs, fracture spacing proves to be a significant parameter in gas MFHWs productivity. In contrast to oil MFHWs, proppant concentration has minimal impact on gas MFHWs recovery performance, possibly due to the lesser sensitivity of gas recovery to fracture volume loss compared to oil reservoirs.
12. A supplementary analysis exploring the geothermal potential of suspended MFHWs completed in WCSB demonstrates that a) a coaxial borehole heat exchanger with 7" diameter installed in a

suspended well with BHT ≥ 85°C at depth ≤ 3,000m can deliver up to 130KW of geothermal power at production temperature of 50°C to a residential area 1km away; 2) 50% of the heating power needed in some residential areas can be gained by retrofitting suspended wells; and c) suspended gas wells have a relatively high potential for repurposing.

9.2 Contributions

We propose a hybrid workflow that integrates analytical methods and machine learning techniques. This innovative approach introduces several new concepts and methodologies, such as:

1. A ML-based model for recognizing, flagging and digitizing flowback data from general pressure-test reports available in the public databases.
2. An iterative method to estimate dynamic effective fracture volume, porosity, and compressibility as functions of pressure and time, aiming to measure the fracture volume loss during flowback and post-flowback.
3. A characteristic fracture closure rate (FCR) to describe the rate at which effective fracture volume reduces during flowback.
4. Supervised fuzzy clustering (SFC) algorithm to rank reservoir quality and completion intensity and analyze their impacts on wells' productivity.
5. A water-oil-ratio model (WORM) that uses a combined analytical and data-driven approach to explain the observed log-linear relationship between WOR and load recovery, analogous to the log-linear relationship between the water/oil relative-permeability ratio and water saturation.
6. A neural network that integrates WORM parameters with key petrophysical properties to analyze the impact of fracture and formation properties on WOR performance, predict WOR as a function of load recovery, forecast ultimate load recovery, and estimate effective fracture volume and initial water saturation in fracture.
7. A cumulative oil production model (COPM) which is a data-driven model to predict oil production as a function of load recovery during the matrix-dominated flow regime.
8. A Support Vector Machine model to predict reservoir permeability using well log data, specifically porosity, GR, bulk density, shallow and deep resistivities.
9. High-resolution 3D maps of porosity, GR, bulk density, initial reservoir pressure, hydrocarbon saturation, net-pay thickness, and formation permeability across the Montney formation.
10. A workflow to estimate formation fracability from sonic log data, introducing a brittleness index, then interpolated across the Montney formation.
11. A Reservoir Quality Index (RQI), serving as a unified measure of reservoir quality based on petrophysical properties.

12. A methodology to evaluate the efficiency of fracture stage positioning as a practical application of the developed RQI.
13. A new approach to estimate the effective distances between MFHWs, considering both 3D spatial and directional distances.
14. A series of ANN-based proxy models designed to correlate the oil and gas productivities of over 10,000 Montney MFHWs with reservoir characteristics and completion-design parameters, utilizing diverse datasets reflecting reservoir characteristics and completion practices to predict key productivity metrics.

9.3 Limitations and Recommendations

Several simplifying assumptions were made in this study such as:

- One potential limitation of WORM and COPM is that they are based on the assumptions of negligible water influx from matrix into fractures and that water production is mainly from fractures with no observed interference between different wells, assuming that the stimulated fracture volume acts as a closed-tank model for water production. These assumptions may not hold true in all cases. Therefore, future research could investigate the impact of mobile formation water on the WOR profile and the applicability of these models to other reservoir types or under different conditions.
- Moreover, the direct applicability of WORM and COPM to shale gas wells might be constrained due to the fundamental differences in the fluid phase behavior and transport mechanisms. However, the underlying conceptual framework could potentially be modified to evaluate Gas-Water Ratio (GWR) performance versus load recovery. Therefore, exploring the applicability of these models in other reservoir types and under different conditions could provide valuable insights.
- WORM is trained on 4,000 Monte Carlo simulation scenarios, assuming that these cases cover a comprehensive range of all probable WOR profiles versus load recovery in tight oil reservoirs. This assumption, however, may not hold. Given the availability of substantial real-field data—consisting of hundreds of wells with high-resolution production data (at least on a daily basis)—are available, the proposed workflow could effectively be applied to real-field datasets and generate tailored ANN models and customized statistical analyses tailored to each production field, potentially augmenting their productivity prediction capabilities.
- The machine learning models proposed herein have been trained on the datasets explored within this thesis. It is critical to validate these findings through domain expertise and supplementary data to ascertain that they are not just artifacts of this particular dataset utilized in this thesis. This

extended validation is essential to confirm that the models are reliable and can be generalized to provide accurate insights and interpretation.

References

[1] CSUR, 2017, Understanding Tight Oil, http://www.csur.com/sites/default/files/Understanding_TightOil_FINAL.pdf.

[2] Environment Canada. *Canadian Climate Normals 1981–2010 Station Data*. Climate Normals & Averages 2021 2021-06-15]; Available from: https://climate.weather.gc.ca/climate_normals/results_1981_2010_e.html?stnID=2205&lang=e&StationName=Calgary&SearchType=Contains&stnNameSubmit=go&dCode=1&dispBack=1.

[3] Ruud Weijermars and Jihoon Wang, 2021, Stress Reversals near Hydraulically Fractured Wells Explained with Linear Superposition Method (LSM), Energies, **14**(11), https://www.mdpi.com/1996-1073/14/11/3256.

[4] EPA, 2016, Hydraulic Fracturing for Oil and Gas: Impacts from the Hydraulic Fracturing Water Cycle on Drinking Water Resources in the United States, www.epa.gov/hfstudy.

[5] D.E. Edwards, et al., *Triassic Strata of the Western Canada Sedimentary Basin. Geological Atlas of Western Canada (Chapter 16)*. 1994, Calgary: Canadian Society of Petroleum Geologists/Alberta Research Council.

[6] Tamer Moussa, et al., Year, "Coupled Versus Stratified Flow of Water and Hydrocarbon During Flowback and Post-flowback Processes," SPE Annual Technical Conference and Exhibition, D031S033R004 Paper No. pp.

[7] M. Honarpour and S.M. Mahmood, 1988, Relative-Permeability Measurements: An Overview, Journal of Petroleum Technology, **40**(08), https://doi.org/10.2118/18565-PA.

[8] R. Aguilera, 1999, Recovery Factors And Reserves In Naturally Fractured Reservoirs, Journal of Canadian Petroleum Technology, **38**(07).

[9] Obinna Ezulike, et al., 2016, Flowback Fracture Closure: A Key Factor for Estimating Effective Pore Volume, SPE Reservoir Evaluation & Engineering, **19**(04), https://doi.org/10.2118/175143-PA.

[10] Yingkun Fu, et al., 2018, Evaluating Fracture Volume Loss During Flowback and Its Relationship to Choke Size: Fastback Versus Slowback SPE/AAPG/SEG Unconventional Resources Technology Conference, https://doi.org/10.15530/URTEC-2018-2903105.

[11] Stephen A. Holditch, 2003, The Increasing Role of Unconventional Reservoirs in the Future of the Oil and Gas Business, Journal of Petroleum Technology, **55**(11), https://doi.org/10.2118/1103-0034-JPT.

[12] Zhenzhen Dong, et al., *Chapter 2 - World Recoverable Unconventional Gas Resources Assessment*. 2016, Gulf Professional Publishing: Boston. p. 53-70.

[13] *Risks, Rewards and Regulation of Unconventional Gas: A Global Perspective*, ed. R.Q. Grafton, I.G. Cronshaw, and M.C. Moore. 2016, Cambridge: Cambridge University Press.

[14] S. Lacy, W. Ding, and S. D. Joshi, Year, "Horizontal Well Applications and Parameters for Economic Success," SPE Latin America Petroleum Engineering Conference, SPE-23676-MS Paper No. pp.

[15] M.. Ostadhassan, et al., Year, "Stability Analysis of Multilateral High Density Pad Wells in the Three Forks Formation," SPE Western Regional Meeting, SPE-174040-MS Paper No. pp.

[16] C.. Cipolla, et al., Year, "New Algorithms and Integrated Workflow for Tight Gas and Shale Completions," SPE Annual Technical Conference and Exhibition, SPE-146872-MS Paper No. pp.

[17] Y.. Cheng, 2012, Impacts of the Number of Perforation Clusters and Cluster Spacing on Production Performance of Horizontal Shale-Gas Wells, SPE Reservoir Evaluation & Engineering, **15**(01), https://doi.org/10.2118/138843-PA.

[18] Qiumei Zhou, et al., 2016, Evaluating Fracture-Fluid Flowback in Marcellus Using Data-Mining Technologies, SPE Production & Operations, **31**(02), https://doi.org/10.2118/173364-PA.

[19] Terry Engelder, Lawrence M. Cathles, and L. Taras Bryndzia, 2014, The fate of residual treatment water in gas shale, **7**, https://www.sciencedirect.com/science/article/pii/S2213397614000202.

[20] Ashkan Zolfaghari Sharak, et al., Year, "Understanding the Origin of Flowback Salts: A Laboratory and Field Study," SPE/CSUR Unconventional Resources Conference – Canada, D011S002R005 Paper No. pp.

[21] Ahmad Salman, Basak Kurtoglu, and Hossein Kazemi, Year, "Analysis of Chemical Tracer Flowback in Unconventional Reservoirs," SPE/CSUR Unconventional Resources Conference – Canada, D011S002R004 Paper No. pp.

[22] Chunlou Li, et al., Year, "Characterization of Hydraulic Fracture Geometry in Shale Gas Reservoirs Using Early Production Data," International Petroleum Technology Conference, IPTC-16896-MS Paper No. pp.

[23] A. Graves, et al., 2009, A Novel Connectionist System for Unconstrained Handwriting Recognition, IEEE Transactions on Pattern Analysis and Machine Intelligence, **31**(5).

[24] R. Lippmann, 1987, An introduction to computing with neural nets, IEEE ASSP Magazine, **4**(2).

[25] Geoffrey E. Hinton, Simon Osindero, and Yee-Whye Teh, 2006, A Fast Learning Algorithm for Deep Belief Nets, Neural Computation, **18**(7), https://doi.org/10.1162/neco.2006.18.7.1527.

[26] Shan Sung Liew, Mohamed Khalil-Hani, and Rabia Bakhteri, 2016, An optimized second order stochastic learning algorithm for neural network training, **186**, https://www.sciencedirect.com/science/article/pii/S0925231215020494.

[27] Canada Energy Regulator. *Natural Gas Pipeline Transportation System*. Facilities we regulate 2021 [cited 2021 08-10]; Available from: https://www.cer-rec.gc.ca/en/data-analysis/facilities-we-regulate/canadas-pipeline-system/2021/natural-gas-pipeline-transportation-system.html.

[28] Lisa Johnson, *New blue hydrogen energy complex in Edmonton announced with $1.3 billion investment*, in *Edmonton Journal*. 2021.

[29] Clean Energy Canada. *Media brief: Hydrogen as part of Canada's energy transition*. 2020 June 2021]; Available from: https://cleanenergycanada.org/hydrogen-as-part-of-canadas-energy-transition/.

[30] Government of Canada. *Crude oil facts*. Energy Facts 2020 June 2021]; Available from: https://www.nrcan.gc.ca/science-data/data-analysis/energy-data-analysis/energy-facts/crude-oil-facts/20064.

[31] US Enviromental Protection Agency, 2011, Draft Plan to Study the Potential Impacts of Hydraulic Fracturing on Drinking Water Resources, https://www.epa.gov/hfstudy/draft-plan-study-potential-impacts-hydraulic-fracturing-drinking-water-resources-february-15.

[32] Dilhan Ilk, et al., 2010, A Comprehensive Workflow for Early Analysis and Interpretation of Flowback Data from Wells in Tight Gas/Shale Reservoir Systems SPE Annual Technical Conference and Exhibition.

[33] Majid Abbasi, Hassan Dehghanpour, and Robert Vincent Hawkes, 2012, Flowback Analysis for Fracture Characterization SPE Canadian Unconventional Resources Conference.

[34] Obinna Daniel Ezulike and Hassan Dehghanpour, 2014, Modelling flowback as a transient two-phase depletion process, Journal of Natural Gas Science and Engineering, **19**, http://www.sciencedirect.com/science/article/pii/S1875510014001115.

[35] Ahmad Alkouh, Steven McKetta, and Robert A. Wattenbarger, 2014, Estimation of Effective-Fracture Volume Using Water-Flowback and Production Data for Shale-Gas Wells, Journal of Canadian Petroleum Technology, **53**(05).

[36] Yingkun Fu, et al., 2017, Estimating Effective Fracture Pore Volume From Flowback Data and Evaluating Its Relationship to Design Parameters of Multistage-Fracture Completion, SPE Production & Operations, **32**(04).

[37] Fengyuan Zhang and Hamid Emami-Meybodi, 2018, Flowback Fracture Closure of Multifractured Horizontal Wells in Shale Gas Reservoirs SPE/AAPG Eastern Regional Meeting, https://doi.org/10.2118/191817-18ERM-MS.

[38] Fengyuan Zhang and Hamid Emami-Meybodi, 2020, Flowback fracture closure of multi-fractured horizontal wells in shale gas reservoirs, Journal of Petroleum Science and Engineering, **186**, http://www.sciencedirect.com/science/article/pii/S0920410519311325.

[39] Arash Dahi-Taleghani and Jon E. Olson, 2011, Numerical Modeling of Multistranded-Hydraulic-Fracture Propagation: Accounting for the Interaction Between Induced and Natural Fractures, SPE Journal, **16**(03), https://doi.org/10.2118/124884-PA.

[40] Nikita Kazakov and Jennifer Lynne Miskimins, 2011, Application of Multivariate Statistical Analysis to Slickwater Fracturing Parameters in Unconventional Reservoir Systems SPE Hydraulic Fracturing Technology Conference, https://doi.org/10.2118/140478-MS.

[41] Lucas W. Bazan, et al., 2013, Key Parameters Affecting Successful Hydraulic Fracture Design and Optimized Production in Unconventional Wells SPE Eastern Regional Meeting, https://doi.org/10.2118/165702-MS.

[42] Qiumei Zhou, John Yilin Wang, and Yitian Xiao, 2020, Identification and illustration of relationships between produced gas and water in marcellus under different spatial and temporal domains through data-driven analytics - Nonparametric model, Journal of Petroleum Science and Engineering, **184**, http://www.sciencedirect.com/science/article/pii/S0920410519308551.

[43] Botao Lin, et al., 2020, Prediction of flowback ratio and production in Sichuan shale gas reservoirs and their relationships with stimulated reservoir volume, Journal of Petroleum Science and Engineering, **184**, http://www.sciencedirect.com/science/article/pii/S0920410519309507.

[44] Shahab Mohaghegh, *Extending the Utility of Decline Curve Analysis*. 2017. p. 127-152.

[45] John Lee and Robert A. Wattenbarger, *Gas reservoir engineering*. SPE Textbook Series. 1996, Richardson, TX: Society of Petroleum Engineers.

[46] Fekete. *Fracture Closure Pressure*. Pre-Closure Analysis 2020; Available from: http://www.fekete.com/san/theoryandequations/welltesttheoryequations/fracture_closure_pressure.htm.

[47] Kenneth G. Nolte, 1979, Determination Of Fracture Parameters From Fracturing Pressure Decline SPE Annual Technical Conference and Exhibition.

[48] G. Tabachnick Barbara and S. Fidell Linda, *Using Multivariate Statistics*. 2007, Boston: Pearson; 6 edition.

[49] Roger Mundry and Charles L Nunn, 2009, Stepwise Model Fitting and Statistical Inference: Turning Noise into Signal Pollution, The American Naturalist, **173**(1).

[50] R. R. Hocking, 1976, A Biometrics Invited Paper. The Analysis and Selection of Variables in Linear Regression, Biometrics, **32**(1), http://www.jstor.org/stable/2529336.

[51] Gareth James, et al., *An Introduction to Statistical Learning*. Springer Texts in Statistics. 2013, New York: Springer-Verlag New York.

[52] Antoine Bertoncello, et al., 2014, Imbibition and Water Blockage In Unconventional Reservoirs: Well-Management Implications During Flowback and Early Production, SPE Reservoir Evaluation & Engineering, **17**(04), https://doi.org/10.2118/167698-PA.

[53] T. Nguyen, R. G. Gosine, and P. Warrian, 2020, A Systematic Review of Big Data Analytics for Oil and Gas Industry 4.0, IEEE Access, **8**.

[54] Daria Khvostichenko and Sergey Makarychev-Mikhailov, 2018, Oilfield Data Analytics: Linking Fracturing Chemistry and Well Productivity SPE/AAPG/SEG Unconventional Resources Technology Conference, https://doi.org/10.15530/URTEC-2018-2903086.

[55] Olubiyi Olaoye and Nancy Zakhour, 2018, Utilizing a Data Analytics Workflow to Optimize Completion Practices While Leveraging Public Data: A Permian Basin Case Study SPE Annual Technical Conference and Exhibition, https://doi.org/10.2118/191416-MS.

[56] Shahab D. Mohaghegh, 2019, Shale Descriptive Analytics; Which Parameters are Controlling Production in Shale SPE Annual Technical Conference and Exhibition, https://doi.org/10.2118/196226-MS.

[57] Tamer Moussa, et al., 2020, The use of flowback data for estimating dynamic fracture volume and its correlation to completion-design parameters: Eagle Ford cases, Journal of Petroleum Science and Engineering, http://www.sciencedirect.com/science/article/pii/S0920410520306525.

[58] Mustafa A. Al-Alwani, et al., 2019, Descriptive Data Analytics to Investigate Stimulation and Completion Trends in the United States: How Proppant and Water Utilization have Changed over Time? SPE Liquids-Rich Basins Conference - North America, https://doi.org/10.2118/197084-MS.

[59] Mustafa A. Al-Alwani, et al., 2019, Descriptive Data Analytics for the Stimulation, Completion Activities, and Wells' Productivity in the Marcellus Shale Play SPE/AAPG/SEG Asia Pacific Unconventional Resources Technology Conference, https://doi.org/10.15530/AP-URTEC-2019-198290.

[60] Kamaluddeen Danyaro, Jafreezal Jaafar, and M. s Liew, 2010, Comparability between fuzzy sets and crisp sets: A Semantic Web approach, International Conference on Education and Educational Technologies - Proceedings.

[61] Werner Van Leekwijck and Etienne E. Kerre, 1999, Defuzzification: criteria and classification, Fuzzy Sets and Systems, **108**(2), http://www.sciencedirect.com/science/article/pii/S0165011497003370.

[62] S. Ashraf and P. C. Shill, Year, "Linguistic Fuzzy Modeling for High Dimensional Regression Problem Using Multi-Objective Genetic Algorithm," 2018 International Conference on Computer, Communication, Chemical, Material and Electronic Engineering (IC4ME2), 8-9 Feb. 2018, Paper No. pp. 1-4.

[63] Shahab D. Mohaghegh, *Shale Analytics*. 2017: Springer International Publishing.

[64] Bo Song, Michael John Economides, and Christine A. Ehlig-Economides, 2011, Design of Multiple Transverse Fracture Horizontal Wells in Shale Gas Reservoirs SPE Hydraulic Fracturing Technology Conference, https://doi.org/10.2118/140555-MS.

[65] Pin Jia, et al., 2018, A novel method for interpreting water data during flowback and early-time production of multi-fractured horizontal wells in shale reservoirs, International Journal of Coal Geology, **200**, http://www.sciencedirect.com/science/article/pii/S0166516218306918.

[66] Sabbir Hossain, Obinna D. Ezulike, and Hassan Dehghanpour, 2020, Post-flowback production data suggest oil drainage from a limited stimulated reservoir volume: An Eagle Ford shale-oil case, International Journal of Coal Geology, **224**, http://www.sciencedirect.com/science/article/pii/S0166516219310766.

[67] Christopher R. Clarkson, Bin Yuan, and Zhenzihao Zhang, 2020, A New Straight-Line Analysis Method for Estimating Fracture/Reservoir Properties Using Dynamic Fluid-in-Place Calculations, SPE Reservoir Evaluation & Engineering, **23**(02), https://doi.org/10.2118/195930-PA.

[68] Fengyuan Zhang and Hamid Emami-Meybodi, 2020, Multiphase flowback rate-transient analysis of shale gas reservoirs, International Journal of Coal Geology, **217**, http://www.sciencedirect.com/science/article/pii/S0166516219304586.

[69] James L. Bush and Donald P. Helander, 1968, Empirical Prediction of Recovery Rate in Waterflooding Depleted Sands, Journal of Petroleum Technology, **20**(09), https://doi.org/10.2118/2109-PA.

[70] A. K. Ambastha and K. H. Wong, 1998, Decline Curve Analysis For Canadian Oil Reservoirs Under Waterflood Conditions, Journal of Canadian Petroleum Technology, **37**(01), https://doi.org/10.2118/98-01-04.

[71] Zhengming Yang, 2009, A New Diagnostic Analysis Method for Waterflood Performance, SPE Reservoir Evaluation & Engineering, **12**(02), https://doi.org/10.2118/113856-PA.

[72] R. Steven Jones, Jr., Brian Pownall, and Jarrid Franke, 2014, Estimating Reservoir Pressure From Early Flowback Data Unconventional Resources Technology Conference.

[73] W. R. Purcell, 1949, Capillary Pressures - Their Measurement Using Mercury and the Calculation of Permeability Therefrom, Journal of Petroleum Technology, **1**(02), https://doi.org/10.2118/949039-G.

[74] Iraj Ershaghi and Osazuwa Omorigie, 1978, A Method for Extrapolation of Cut vs Recovery Curves, Journal of Petroleum Technology, **30**(02), https://doi.org/10.2118/6977-PA.

[75] Iraj Ershaghi and Doddy Abdassah, 1984, A Prediction Technique for Immiscible Processes Using Field Performance Data (includes associated papers 13392, 13793, 15146 and 19506), Journal of Petroleum Technology, **36**(04), https://doi.org/10.2118/10068-PA.

[76] M.. Heidari Sureshjani and C. R. Clarkson, 2015, An Analytical Model for Analyzing and Forecasting Production From Multifractured Horizontal Wells With Complex Branched-Fracture Geometry, SPE Reservoir Evaluation & Engineering, **18**(03), https://doi.org/10.2118/176025-PA.

[77] Hamidreza Hamdi, Hamid Behmanesh, and Christopher R. Clarkson, 2020, A Semianalytical Approach for Analysis of Wells Exhibiting Multiphase Transient Linear Flow: Application to Field Data, SPE Journal, **25**(06), https://doi.org/10.2118/196164-PA.

[78] V.V. Bondar and T.A. Blasingame, 2002, Analysis and Interpretation of Water-Oil-Ratio Performance SPE Annual Technical Conference and Exhibition.

[79] S.J. Lijek, Year, "Simple Performance Plots Used in Rate-Time Determination and Waterflood Analysis," SPE Annual Technical Conference and Exhibition, SPE-19847-MS Paper No. pp.

[80] Y. C. Yortsos, et al., 1999, Analysis and Interpretation of Water/Oil Ratio in Waterfloods, SPE Journal, **4**(04), https://doi.org/10.2118/59477-PA.

[81] Anish Singh Chaudhary, Christine Ehlig-Economides, and Robert Wattenbarger, Year, "Shale Oil Production Performance from a Stimulated Reservoir Volume," SPE Annual Technical Conference and Exhibition, SPE-147596-MS Paper No. pp.

[82] Guowen Lei and Nan Cheng, Year, "Liquid-Rich Shale Versus Conventional Depletion Performance," SPE/EAGE European Unconventional Resources Conference and Exhibition, D021S021R003 Paper No. pp.

[83] M. S. Shahamat and C. R. Clarkson, 2018, Multiwell, Multiphase Flowing Material Balance, SPE Reservoir Evaluation & Engineering, **21**(02), https://doi.org/10.2118/185052-PA.

[84] R. Steven Jones , Jr., 2016, Producing-Gas/Oil-Ratio Behavior of Multifractured Horizontal Wells in Tight Oil Reservoirs, SPE Reservoir Evaluation & Engineering, **20**(03), https://doi.org/10.2118/184397-PA.

[85] Christopher R. Clarkson and Jesse Williams-Kovacs, 2013, Modeling Two-Phase Flowback of Multifractured Horizontal Wells Completed in Shale, SPE Journal, **18**(04).

[86] D. Zeinabady, et al., 2023, Fault Identification for the Purposes of Evaluating the Risk of Induced Seismicity: A Novel Application of the Flowback DFIT, SPE Reservoir Evaluation & Engineering, https://doi.org/10.2118/211100-PA.

[87] David Hosmer, Stanley Lemeshow, and Rodney Sturdivant, *Applied Logistic Regression*. Third Edition ed. 2013, New York: Wiley.

[88] W. K. Hastings, 1970, Monte Carlo Sampling Methods Using Markov Chains and Their Applications, Biometrika, **57**.

[89] Igor Livshin, *Neural Network Prediction Outside the Training Range*, in *Artificial Neural Networks with Java: Tools for Building Neural Network Applications*, I. Livshin, Editor. 2019, Apress: Berkeley, CA. p. 109-163.

[90] M. J. D. Powell, *A Hybrid Method for Nonlinear Equations*, in *Numerical Methods for Nonlinear Algebraic Equations*, P. Rabinowitz, Editor. 1970, Gordon and Breach.

[91] D. O. Ezulike, et al., 2016, Flowback Fracture Closure: A Key Factor for Estimating Effective Pore Volume, SPE Reservoir Evaluation & Engineering, **19**(04), https://doi.org/10.2118/175143-PA.

[92] J. S. Cramer, 2004, The early origins of the logit model, Studies in History and Philosophy of Science Part C: Studies in History and Philosophy of Biological and Biomedical Sciences, **35**(4).

[93] Robert A. Wattenbarger, et al., Year, "Production Analysis of Linear Flow Into Fractured Tight Gas Wells," SPE Rocky Mountain Regional/Low-Permeability Reservoirs Symposium, SPE-39931-MS Paper No. pp.

[94] D.H. Stright, Jr. and J.I. Gordon, Year, "Decline Curve Analysis in Fractured Low Permeability Gas Wells in the Piceance Basin," SPE/DOE Low Permeability Gas Reservoirs Symposium, SPE-11640-MS Paper No. pp.

[95] J.D. Tannich, 1975, Liquid Removal From Hydraulically Fractured Gas Wells, Journal of Petroleum Technology, **27**(11), https://doi.org/10.2118/5113-PA.

[96] Rick Gdanski and Harold Walters, Year, "Impact of Fracture Conductivity and Matrix Relative Permeability on Load Recovery," SPE Annual Technical Conference and Exhibition, SPE-133057-MS Paper No. pp.

[97] John Yilin* Wang, Stephen A. Holditch, and Duane A. McVay, 2010, Modeling Fracture-Fluid Cleanup in Tight-Gas Wells, SPE Journal, **15**(03), https://doi.org/10.2118/119624-PA.

[98] Mingyuan Wang and Juliana Y. Leung, 2015, Numerical investigation of fluid-loss mechanisms during hydraulic fracturing flow-back operations in tight reservoirs, Journal of Petroleum Science and Engineering, **133**, https://www.sciencedirect.com/science/article/pii/S0920410515002041.

[99] B. Zanganeh, et al., 2015, The role of hydraulic fracture geometry and conductivity profile, unpropped zone conductivity and fracturing fluid flowback on production performance of shale oil wells, Journal of Unconventional Oil and Gas Resources, **9**, https://www.sciencedirect.com/science/article/pii/S221339761400055X.

[100] Yingkun Fu and Hassan Dehghanpour, 2020, How far can hydraulic fractures go? A comparative analysis of water flowback, tracer, and microseismic data from the Horn River Basin, Marine and Petroleum Geology, **115**, https://www.sciencedirect.com/science/article/pii/S0264817220300428.

[101] R. Yalavarthi, et al., Year, "Impact of Completion Design on Unconventional Horizontal Well Performance," SPE/AAPG/SEG Unconventional Resources Technology Conference, URTEC-1558757-MS Paper No. pp.

[102] A Agrawal, Y Wei, and S.A. A Holditch, 2012, A Technical and Economic Study of Completion Techniques in Five Emerging US Gas Shales: A Woodford Shale Example, SPE Drilling & Completion, **27**(01), https://doi.org/10.2118/135396-PA.

[103] M.A. Shebl, C. Nyaaba, and R. Yalavarthi, Year, "Role of Detailed Reservoir Characterization and Lateral Placement on Well Performance in the Marcellus Shale Gas Reservoir," International Petroleum Technology Conference, IPTC-16718-MS Paper No. pp.

[104] Ikenna Okeahialam, et al., 2016, Completion Optimization Under Constraints: An Eagle Ford Shale Case Study, SPE Production & Operations, **32**(02), https://doi.org/10.2118/174057-PA.

[105] A. Boulis, R. Jayakumar, and R. Rai, Year, "A New Approach for Well Spacing Optimisation and Its Application to Various Shale Gas Resources," International Petroleum Technology Conference, IPTC-17150-MS Paper No. pp.

[106] Foluke O. Ajisafe, et al., Year, "Impact of Well Spacing and Interference on Production Performance in Unconventional Reservoirs, Permian Basin," SPE/AAPG/SEG Unconventional Resources Technology Conference, URTEC-2690466-MS Paper No. pp.

[107] Richard Cao, et al., Year, "Well Interference and Optimum Well Spacing for Wolfcamp Development at Permian Basin," SPE/AAPG/SEG Unconventional Resources Technology Conference, URTEC-2691962-MS Paper No. pp.

[108] Tamer Moussa, Hassan Dehghanpour, and Melanie Popp, Year, "Reservoir Quality Versus Completion Intensity: An Application of Supervised Fuzzy Clustering on Western Canadian Well Data," SPE Hydraulic Fracturing Technology Conference and Exhibition, D011S001R005 Paper No. pp.

[109] Ripudaman Manchanda, et al., Year, "Parent-Child Fracture Interference: Explanation and Mitigation of Child Well Underperformance," SPE Hydraulic Fracturing Technology Conference and Exhibition, D021S005R005 Paper No. pp.

[110] David C. Johnson, et al., Year, "Offset Fracture Events Made Simple: An Operator's Collaborative Approach to Observe Parent Child Interactions, Measure Frac Hit Severity and Test Mitigation Strategies," SPE Hydraulic Fracturing Technology Conference and Exhibition, D021S005R006 Paper No. pp.

[111] S. Esmaili, et al., Year, "Understanding the Interaction between Parent and Child Using Analytical and Numerical Approaches in Permian Basin – An Operator Perspective," SPE/AAPG/SEG Unconventional Resources Technology Conference, D011S009R001 Paper No. pp.

[112] Cyrille Defeu, et al., Year, "Successful Mitigation of Negative Parent-Child Wells Interaction Using Far-Field Diversion in the Delaware Basin," SPE Annual Technical Conference and Exhibition, D031S038R008 Paper No. pp.

[113] R. Steven Jones, Jr., Brian Pownall, and Jarrid Franke, Year, "Estimating Reservoir Pressure From Early Flowback Data," SPE/AAPG/SEG Unconventional Resources Technology Conference, URTEC-1934785-MS Paper No. pp.

[114] Eric Holderby, et al., 2015, Case Study: Completion-Design Optimization for Barnett Oil-Producing Area, SPE Drilling & Completion, **31**(01), https://doi.org/10.2118/170750-PA.

[115] Ron Dusterhoft, et al., Year, "New Processes and Tools for Design and Execution to Optimize Hydraulic Fracturing Treatments in Shale Reservoirs," SPE Hydraulic Fracturing Technology Conference, SPE-168583-MS Paper No. pp.

[116] M. Y. Soliman, Loyd East, and Jody Augustine, Year, "Fracturing Design Aimed at Enhancing Fracture Complexity," SPE EUROPEC/EAGE Annual Conference and Exhibition, SPE-130043-MS Paper No. pp.

[117] Omkar Jaripatke, et al., Year, "Completion Optimization of an Unconventional Shale Play: Implementation of a Successful Completion Design Optimization Plan and the Results," SPE Annual Technical Conference and Exhibition, SPE-170764-MS Paper No. pp.

[118] K. Furui, et al., 2007, Optimization of Horizontal Well-Completion Design With Cased/Perforated or Slotted Liner Completions, SPE Production & Operations, **22**(02), https://doi.org/10.2118/90579-PA.

[119] Hongjie Xiong, et al., 2020, Optimizing Fracturing Design and Well Spacing with Complex-Fracture and Reservoir Simulations: A Permian Basin Case Study, SPE Production & Operations, **35**(04), https://doi.org/10.2118/194367-PA.

[120] Shuhua Wang and Shengnan Chen, Year, "Evaluation and Prediction of Hydraulic Fractured Well Performance in Montney Formations Using a Data-Driven Approach," SPE Western Regional Meeting, SPE-180416-MS Paper No. pp.

[121] Braden Bowie, Year, "Machine Learning Applied to Optimize Duvernay Well Performance," SPE Canada Unconventional Resources Conference, D021S008R003 Paper No. pp.

[122] S. D. Mohaghegh, R.. Gaskari, and M.. Maysami, Year, "Shale Analytics: Making Production and Operational Decisions Based on Facts: A Case Study in Marcellus Shale," SPE Hydraulic Fracturing Technology Conference and Exhibition, D031S007R004 Paper No. pp.

[123] Saurabh Tandon, Year, "Integrating Machine Learning in Identifying Sweet Spots in Unconventional Formations," SPE Western Regional Meeting, D021S004R007 Paper No. pp.

[124] Junghun Leem, et al., Year, "Data Analytics and Machine Learning Predictive Modeling for Unconventional Reservoir Performance Utilizing Geoengineering and Completion Data: Sweet Spot Identification and Completion Design Optimization," ADIPEC, D021S062R002 Paper No. pp.

[125] Frank Nielsen, *Hierarchical Clustering*. 2016. p. 195-211.

[126] Tamer Moussa, et al., 2018, Development of New Permeability Formulation From Well Log Data Using Artificial Intelligence Approaches, Journal of Energy Resources Technology, **140**(7), https://doi.org/10.1115/1.4039270.

[127] R.M. Holt E. Fjær, P. Horsrud, A.M. Raaen, R. Risnes, *Petroleum Related Rock Mechanics 2nd Edition*. Vol. 53. 2008.

[128] William Vincent Grieser and James M. Bray, Year, "Identification of Production Potential in Unconventional Reservoirs," Production and Operations Symposium, SPE-106623-MS Paper No. pp.

[129] L. A. Zadeh, 1965, Fuzzy sets, Information and Control, **8**(3), https://www.sciencedirect.com/science/article/pii/S001999586590241X.

[130] Tamer M. Moussa and Abeeb A. Awotunde, 2018, Self-adaptive differential evolution with a novel adaptation technique and its application to optimize ES-SAGD recovery process, Computers & Chemical Engineering, **118**, https://doi.org/10.1016/j.compchemeng.2018.07.018.

[131] Scott Lundberg and Su-In Lee, *A Unified Approach to Interpreting Model Predictions*. 2017.

[132] Wei GuoQi, et al., 2023, Coupled relationships between overburden stress and ultra-deep sandstone brittle deformation properties based on in situ CT scanning, **173**, https://www.sciencedirect.com/science/article/pii/S0191814123001220.

[133] Diederik Kingma and Jimmy Ba, 2014, Adam: A Method for Stochastic Optimization.

[134] Tamer Moussa, et al., 2020, The use of flowback data for estimating dynamic fracture volume and its correlation with completion-design parameters: Eagle Ford cases, Journal of Petroleum Science and Engineering, **195**, https://www.sciencedirect.com/science/article/pii/S0920410520306525.

[135] C. Augustine, J. Tester, and B. Anderson, Year, "A COMPARISON OF GEOTHERMAL WITH OIL AND GAS WELL DRILLING COSTS," Paper No. pp.

[136] J. W. Tester, et al., 1994, Prospects for universal geothermal energy from heat mining, Science & Global Security, **5**(1), https://doi.org/10.1080/08929889408426418.

[137] Shyi-Min Lu, 2018, A global review of enhanced geothermal system (EGS), Renewable and Sustainable Energy Reviews, **81**, https://www.sciencedirect.com/science/article/pii/S1364032117310341.

[138] Adelina P. Davis and Efstathios E. Michaelides, 2009, Geothermal power production from abandoned oil wells, Energy, **34**(7), https://www.sciencedirect.com/science/article/pii/S0360544209000607.

[139] Tomasz Sliwa, Marc A. Rosen, and Zbigniew Jezuit, 2014, Use of Oil Boreholes in the Carpathians in Geoenergetic Systems: Historical and Conceptual Review, Research Journal of Environmental Sciences, **8**(5).

[140] Robert A. Caulk and Ingrid Tomac, 2017, Reuse of abandoned oil and gas wells for geothermal energy production, Renewable Energy, **112**, https://www.sciencedirect.com/science/article/pii/S0960148117304275.

[141] Marija Macenic and Tomislav Kurevija, 2018, Revitalization of abandoned oil and gas wells for a geothermal heat exploitation by means of closed circulation: Case study of the deep dry well Pcelic-1, Interpretation, **6**(1), https://library.seg.org/doi/abs/10.1190/INT-2017-0079.1

[142] Yong-Le Nian and Wen-Long Cheng, 2018, Evaluation of geothermal heating from abandoned oil wells, Energy, **142**, https://www.sciencedirect.com/science/article/pii/S0360544217317590.

[143] Pranay Asai, et al., 2018, Performance evaluation of enhanced geothermal system (EGS): Surrogate models, sensitivity study and ranking key parameters, Renewable Energy, **122**, https://www.sciencedirect.com/science/article/pii/S0960148118301083.

[144] Yu-Chao Zeng, Zheng Su, and Neng-You Wu, 2013, Numerical simulation of heat production potential from hot dry rock by water circulating through two horizontal wells at Desert Peak geothermal field, Energy, **56**, https://www.sciencedirect.com/science/article/pii/S0360544213003708.

[145] Facheng Gong, et al., 2020, Evaluation of geothermal energy extraction in Enhanced Geothermal System (EGS) with multiple fracturing horizontal wells (MFHW), Renewable Energy, **151**, https://www.sciencedirect.com/science/article/pii/S0960148119318282.

[146] P. Olasolo, et al., 2016, Economic analysis of Enhanced Geothermal Systems (EGS). A review of software packages for estimating and simulating costs, Applied Thermal Engineering, **104**, https://www.sciencedirect.com/science/article/pii/S135943111630730X.

[147] Xianbiao Bu, Weibin Ma, and Huashan Li, 2012, Geothermal energy production utilizing abandoned oil and gas wells, Renewable Energy, **41**, https://www.sciencedirect.com/science/article/pii/S096014811100574X.

[148] N. M. Wight and N. S. Bennett, 2015, Geothermal energy from abandoned oil and gas wells using water in combination with a closed wellbore, Applied Thermal Engineering, **89**, https://www.sciencedirect.com/science/article/pii/S1359431115005840.

[149] Kai Wang, et al., 2018, A comprehensive review of geothermal energy extraction and utilization in oilfields, Journal of Petroleum Science and Engineering, **168**, https://www.sciencedirect.com/science/article/pii/S0920410518304042.

[150] J. D. Templeton, et al., 2014, Abandoned petroleum wells as sustainable sources of geothermal energy, Energy, **70**, https://www.sciencedirect.com/science/article/pii/S0360544214004198.

[151] D. Sui, et al., 2018, Review and investigations on geothermal energy extraction from abandoned petroleum wells, J. Petrol. Explor. Prod Technol., **89**(5).

[152] Younes Noorollahi, Salman Taghipoor, and Behrang Sajadi, 2017, Geothermal sea water desalination system (GSWDS) using abandoned oil/gas wells, Geothermics, **67**, https://www.sciencedirect.com/science/article/pii/S0375650516301705.

[153] Wen-Long Cheng, et al., 2016, Enhancing geothermal power generation from abandoned oil wells with thermal reservoirs, Energy, **109**, https://www.sciencedirect.com/science/article/pii/S0360544216305618.

[154] Ruud Weijermars, et al., 2018, Redeveloping depleted hydrocarbon wells in an enhanced geothermal system (EGS) for a university campus: Progress report of a real-asset-based feasibility study, Energy Strategy Reviews, **21**, https://www.sciencedirect.com/science/article/pii/S2211467X18300488.

[155] Katherine K. Huang, et al., 2021, Geothermal Assessment of Target Formations Using Recorded Temperature Measurements for the Alberta No. 1 Geothermal Project, Applied Sciences, **11**(2), https://www.mdpi.com/2076-3417/11/2/608.

[156] K. Huang, et al., Year, "Using Oil and Gas Data to Assess Geothermal Resources Within the Western Canadian Sedimentary Basin in Alberta," GRC Transactions, Virtual Conference, 19–23 October 2020, Paper No. pp.

[157] D Allan Gray, Jacek Majorowicz, and Martyn Unsworth, 2012, Investigation of the geothermal state of sedimentary basins using oil industry thermal data: case study from Northern Alberta exhibiting the need to systematically remove biased data, Journal of Geophysics and Engineering, **9**(5), https://doi.org/10.1088/1742-2132/9/5/534.

[158] Mengying Li and Noam Lior, 2014, Comparative Analysis of Power Plant Options for Enhanced Geothermal Systems (EGS), Energies, **7**(12), https://www.mdpi.com/1996-1073/7/12/8427.

[159] Xincheng Hu, et al., 2020, Numerical modeling of a coaxial borehole heat exchanger to exploit geothermal energy from abandoned petroleum wells in Hinton, Alberta, Renewable Energy, **148**, https://www.sciencedirect.com/science/article/pii/S0960148119314855.

[160] Hans Wackernagel, *Ordinary Kriging*, in *Multivariate Geostatistics: An Introduction with Applications*. 1995, Springer Berlin Heidelberg: Berlin, Heidelberg. p. 74-81.

[161] R W Sinnott, 1984, Virtues of the haversine, Sky and Telescope, **68**(2).

[162] Anthony R. Ingraffea, et al., 2014, Assessment and risk analysis of casing and cement impairment in oil and gas wells in Pennsylvania, 2000–2012, Proceedings of the National Academy of Sciences, **111**(30), https://www.pnas.org/doi/abs/10.1073/pnas.1323422111

[163] Gopi Nalla, et al., 2005, Parametric sensitivity study of operating and design variables in wellbore heat exchangers, Geothermics, **34**(3), https://www.sciencedirect.com/science/article/pii/S0375650505000350.

[164] Guodong Cui, et al., 2017, Geothermal exploitation from hot dry rocks via recycling heat transmission fluid in a horizontal well, Energy, **128**, https://www.sciencedirect.com/science/article/pii/S0360544217305923.

[165] H.J. Ramey, Jr., 1962, Wellbore Heat Transmission, Journal of Petroleum Technology, **14**(04), https://doi.org/10.2118/96-PA.

[166] Abdurrahman Satman and Omer Inanc Tureyen, 2016, Geothermal wellbore heat transmission: Stabilization times for "static" and "transient" wellbore temperature profiles, Geothermics, **64**, https://www.sciencedirect.com/science/article/pii/S0375650516300797.

[167] I Kolo, R Sousa, and T Zhang, Year, "Heat transmission in a geothermal wellbore: modelling and application," Proceedings of the 19th Australasian Fluid Mechanics Conference, Melbourne, Australia, Paper No. pp.

[168] J. Hagoort, 2004, Ramey's Wellbore heat transmission revisited, SPE Journal, **9**(4), https://www.scopus.com/inward/record.uri?eid=2-s2.0-13244277596&doi=10.2118%2f87305-PA&partnerID=40&md5=a2d9cd38377980ed974f34dcf3598882.

[169] Environment Canada, *Past Weather and Climate*. 2022, Government of Canada.

[170] Lev Eppelbaum, Izzy Kutasov, and Arkady Pilchin, *Thermal Properties of Rocks and Density of Fluids*, in *Applied Geothermics*. 2014, Springer Berlin Heidelberg: Berlin, Heidelberg. p. 99-149.

[171] D. W. Waples and J. S. Waples, 2004, A review and evaluation of specific heat capacities of rocks, minerals, and subsurface fluids. Part 1: Minerals and nonporous rocks, Natural Resources Research, **13**(2), https://www.scopus.com/inward/record.uri?eid=2-s2.0-29244483855&doi=10.1023%2fB%3aNARR.0000032647.41046.e7&partnerID=40&md5=8054b61ce9b3bb4ae8c1e40db084c94d.

[172] Wilbur H Somerton, *Thermal properties and temperature-related behavior of rock/fluid systems*. 1992: Elsevier.

[173] Ralph Haenel, Lajos Stegena, and Ladislaus Rybach, *Handbook of terrestrial heat-flow density determination: with guidelines and recommendations of the International Heat Flow Commission*. Vol. 4. 2012: Springer Science & Business Media.

[174] Hans-Dieter Vosteen and Rüdiger Schellschmidt, 2003, Influence of temperature on thermal conductivity, thermal capacity and thermal diffusivity for different types of rock, Physics and Chemistry of the Earth, Parts A/B/C, **28**(9), https://www.sciencedirect.com/science/article/pii/S147470650300069X.

[175] Jacek Majorowicz and Stephen E. Grasby, 2010, High Potential Regions for Enhanced Geothermal Systems in Canada, Natural Resources Research, **19**(3), https://doi.org/10.1007/s11053-010-9119-8.

[176] J. Majorowicz, et al., 2013, Geothermal energy as a source of heat for oil sands processing in Northern Alberta, Canada, Heavyoil and Oil-Sand Petroleum Systems in Alberta and Beyond [AAPG Studies in Geology No. 64], https://www.scopus.com/inward/record.uri?eid=2-s2.0-84883687382&partnerID=40&md5=5ec10e4a53a319033f6f5f0d0897d96a.

[177] Aniko Toth and Elemer Bobok, *Chapter 13 - Borehole Heat Exchangers*, in *Flow and Heat Transfer in Geothermal Systems*, A. Toth and E. Bobok, Editors. 2017, Elsevier: Oxford. p. 287-298.

[178] David P. DeWitt Frank P. Incropera, Theodore L. Bergman, Adrienne S. Lavine, *Fundamentals of Heat and Mass Transfer*. 6th ed. 2006: Wiley. 1024.

[179] CanGEA, *CANADIAN NATIONAL GEOTHERMAL DATABASE AND TERRITORIAL RESOURCE ESTIMATE MAPS: ALBERTA* 2010.

[180] Małgorzata Labus and Krzysztof Labus, 2018, Thermal conductivity and diffusivity of fine-grained sedimentary rocks, **132**(3), https://doi.org/10.1007/s10973-018-7090-5.

[181] Statistics Canada, 2017, Population and Dwelling Count Highlight Tables. 2016 Census.

[182] Li Fan, et al., 2011, An Integrated Approach for Understanding Oil and Gas Reserves Potential in Eagle Ford Shale Formation Canadian Unconventional Resources Conference, https://doi.org/10.2118/148751-MS.

[183] Harrison Morton Wadsworth, Year, "Handbook of Statistical Methods for Engineers and Scientists," Paper No. pp.

[184] J.R. Taylor, *An Introduction to Error Analysis: The Study of Uncertainties in Physical Measurements*. 1997: University Science Books.

Appendices

A. Dynamic Effective Fractur Volume

A.1 Fracture Porosity Estimation

Algorithm of fracture porosity estimation as function of ($\mathbf{p}_{\mathrm{wf}}$, V_{ef_i} , M_{prop} , ρ_{prop})

1: $V_{ef_i} \leftarrow$ estimate initial effective fracture volume from HD model

2: $V_{ef} = V_{ef_i} \leftarrow$ dynamic fracture volume

3: **for** $j = 1, \ldots$ number of p_{wf} values in $\mathbf{p}_{\mathrm{wf}}$ **do**

4: $V_{\mathrm{prop}_j} = M_{\mathrm{prop}} / \rho_{\mathrm{prop}}$

5: $\phi_{f_j} = V_{ef} \Big/ \left(V_{ef} + V_{\mathrm{prop}_j} \right)$

6: $\eta_j = \left(1 - \phi_{f_j} \right) \times 100$

7: $C_{f_j} \leftarrow$ estimate using $\left(\eta_j , p_{n_j} = p_{\mathrm{closure}} - p_{wf_j} \right)$

8: $V_{ef_{\mathrm{loss}j}} = C_{f_j} \left(p_i - p_{wf_j} \right)$

9: $V_{ef} = \left(1 - V_{ef_{\mathrm{loss}_i}} \right) V_{ef_i} \leftarrow$ update effective fracture volume

10: // If the mass of produced proppant ($M_{\mathrm{prop}_{\mathrm{prod}}}$) is significant

11: $M_{\mathrm{prop}} = M_{\mathrm{prop}} - M_{\mathrm{prop}_{\mathrm{prod}}}$

12: **return** ϕ_f , C_f , V_{ef}

A.2 Finding Optimum Coefficients in MLR

Sum of squared errors between predicted values using multiple linear regression (MLR) and actual values can be expressed as:

$$\mathrm{Err}\left(\mathbf{w} \right) = \sum_{i=1}^{n} \left(f\left(\mathbf{x}_i \right) - y_i \right)^2$$

where y_i is the actual target, $f\left(\mathbf{x}_i \right) = \sum_{j=0}^{d} w_j x_{ij}$, d is the dimension of the problem (number of CDPs). $x_{i0} = 0$ to give the flexibility of solution not to pass through the origin coordinates. Substituting $f\left(\mathbf{x}_i \right)$ in the previous equation gives

$$\mathrm{Err}\left(\mathbf{w} \right) = \sum_{i=1}^{n} \left(\sum_{j=0}^{d} w_j x_{ij} - y_i \right)^2$$

To find a stationary point, the gradient $\nabla \mathrm{Err}(\mathbf{x})$ is calculated and equated to zero. The objective, $\mathrm{Err}(\mathbf{w})$, is convex with respect to $\mathbf{w}$. Therefore, any stationary point is a global minimum. Hence, the objective is to find $\mathbf{w}$ for which $\nabla \mathrm{Err}(\mathbf{x}) = 0$. Now, set the partial derivatives to 0 and solve the equations for each weight, w_j:

$$\frac{\partial \mathrm{Err}}{\partial w_0} = 2\sum_{i=1}^{n}\left(\sum_{j=0}^{d} w_j x_{ij} - y_i\right) x_{i0} = 0$$
$$\frac{\partial \mathrm{Err}}{\partial w_1} = 2\sum_{i=1}^{n}\left(\sum_{j=0}^{d} w_j x_{ij} - y_i\right) x_{i1} = 0$$
$$\vdots$$
$$\frac{\partial \mathrm{Err}}{\partial w_d} = 2\sum_{i=1}^{n}\left(\sum_{j=0}^{d} w_j x_{ij} - y_i\right) x_{id} = 0$$

This results in a system of $d+1$ linear equations with $d+1$ unknowns $\mathbf{w} = (w_0, w_1, w_2, \ldots, w_d)$. To find the solution of this system of equations, it should be written in matrix notation as

$$\nabla \mathrm{Err}(\mathbf{w}) = 2\mathbf{X}^{\mathrm{T}}\mathbf{X}\mathbf{w} - 2\mathbf{X}^{\mathrm{T}} y$$

Equating this equation to zero, and solving for $\mathbf{w}$, results in optimum weights (maximum likelihood) $\mathbf{w}_{\mathrm{ML}}$ as:

$$\mathbf{w}_{\mathrm{Ml}} = \mathbf{X}(\mathbf{X}^{\mathrm{T}}\mathbf{X})^{-1}\mathbf{X}^{\mathrm{T}} y$$

This equation is then used to find the optimum coefficients that best correlate CDPs to initial effective fracture volume and characteristic closure rate.

A.3 Error Metrics

Average absolute percentage error (AAPE) estimation: The average absolute percentage error AAPE is the measure of the relative deviation from the experimental data and is defined as:

$$\mathrm{AAPE} = \frac{1}{n}\sum_{i=1}^{n}\left|E_i\right|$$

where n is the number of data points and E_i is the relative deviation of a predicted value from a real value;

$$E_i = \left(\frac{y_{\mathrm{real}} - y_{\mathrm{predict}}}{y_{\mathrm{real}}}\right) \times 100$$

Correlation coefficient (CC) estimation: Correlation confident (CC) represents the degree of success in reducing the standard deviation by regression analysis, defined as:

$$CC = \left[1 - \frac{\sum_{i=1}^{n} \left(y_{real} - y_{predict} \right)_i^2}{\sum_{i=1}^{n} \left(y_{real} - \bar{y} \right)} \right]^{1/2}$$

where $\bar{y}$ is the mean value of vector y_{real} and is calculated as:

$$\bar{y} = \frac{1}{n} \sum_{i=1}^{n} \left(y_{real} \right)_i$$

B. Production rates and pressure plots

B.1 Locations of target wells

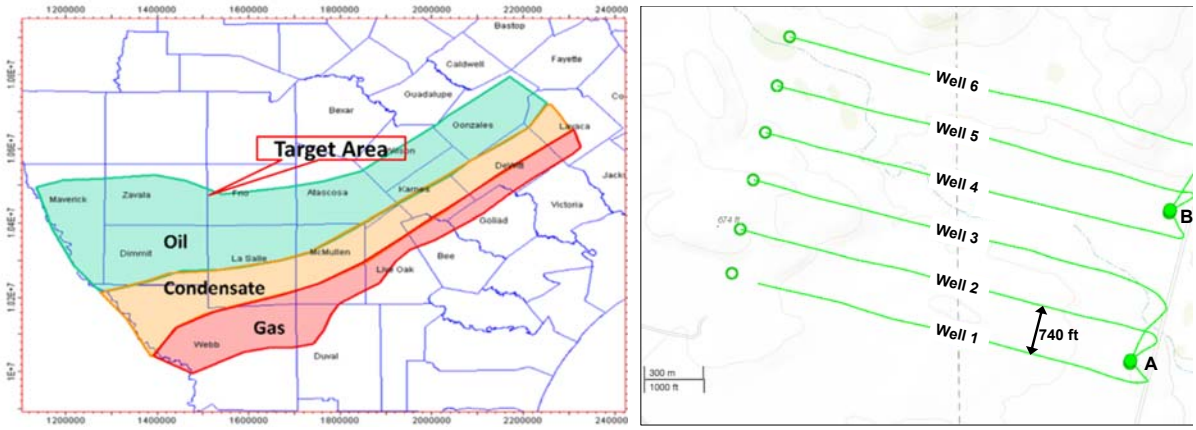

(a) **(b)**

Fig. B.1 – Locations of target wells in **(a)** maturation map of Eagleford formation [modified from [182] and **(b)** a layout of target wells in two pads. Approximate lateral spacing is 740 ft.

B.2 Semilog Plots of Water/Oil/Gas Rates

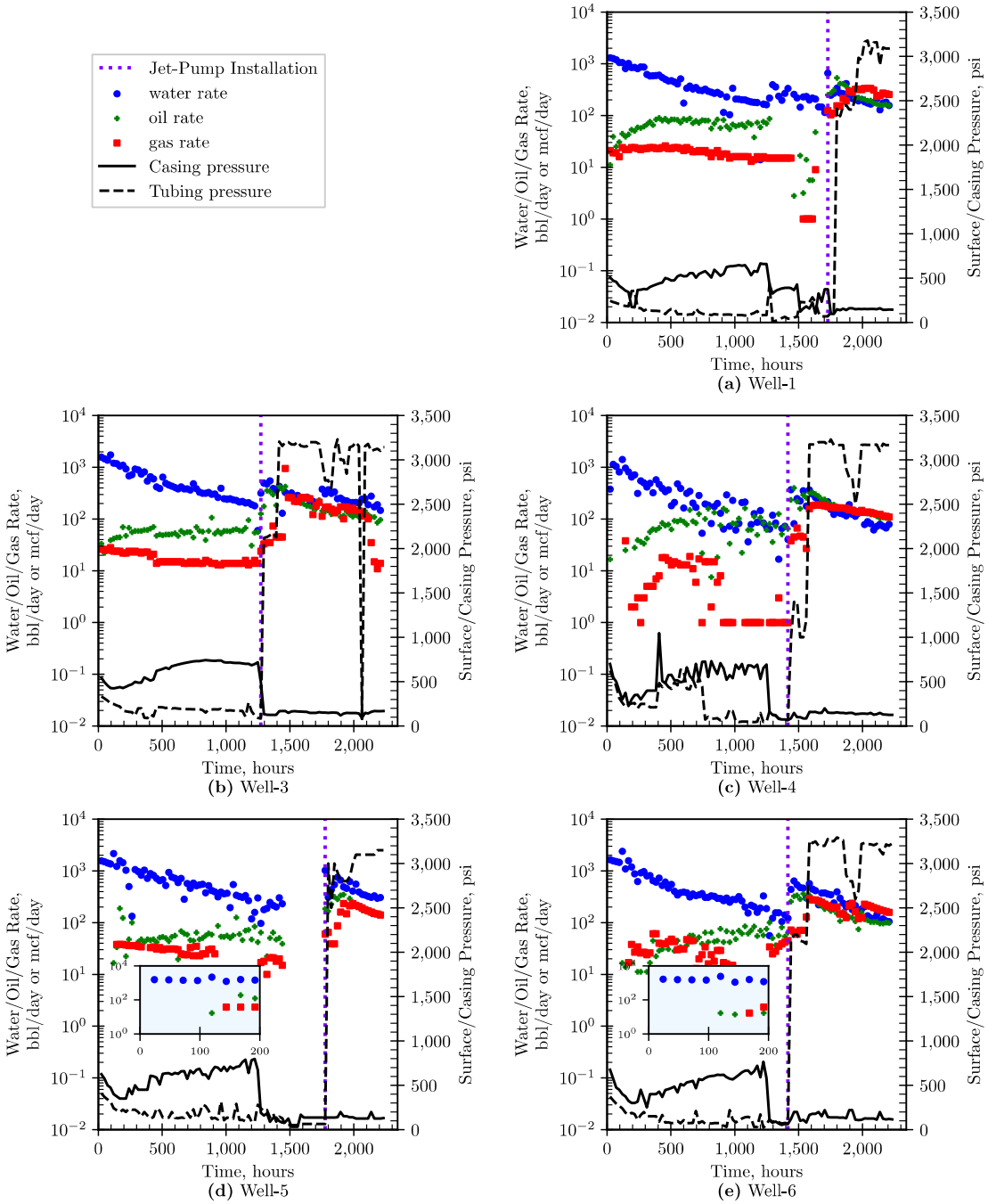

Fig. B.2 – Semi-log plots of water/oil/gas rates and tubing/casing pressures for remaining 5 wells. Sudden increase in rates and tubing pressure is due jet-pump installation after about 1,500 hours. Insets zoom the early 200 hours water/oil/gas rates for wells 5 and 6.

B.3 Water and Oil RNP Plots

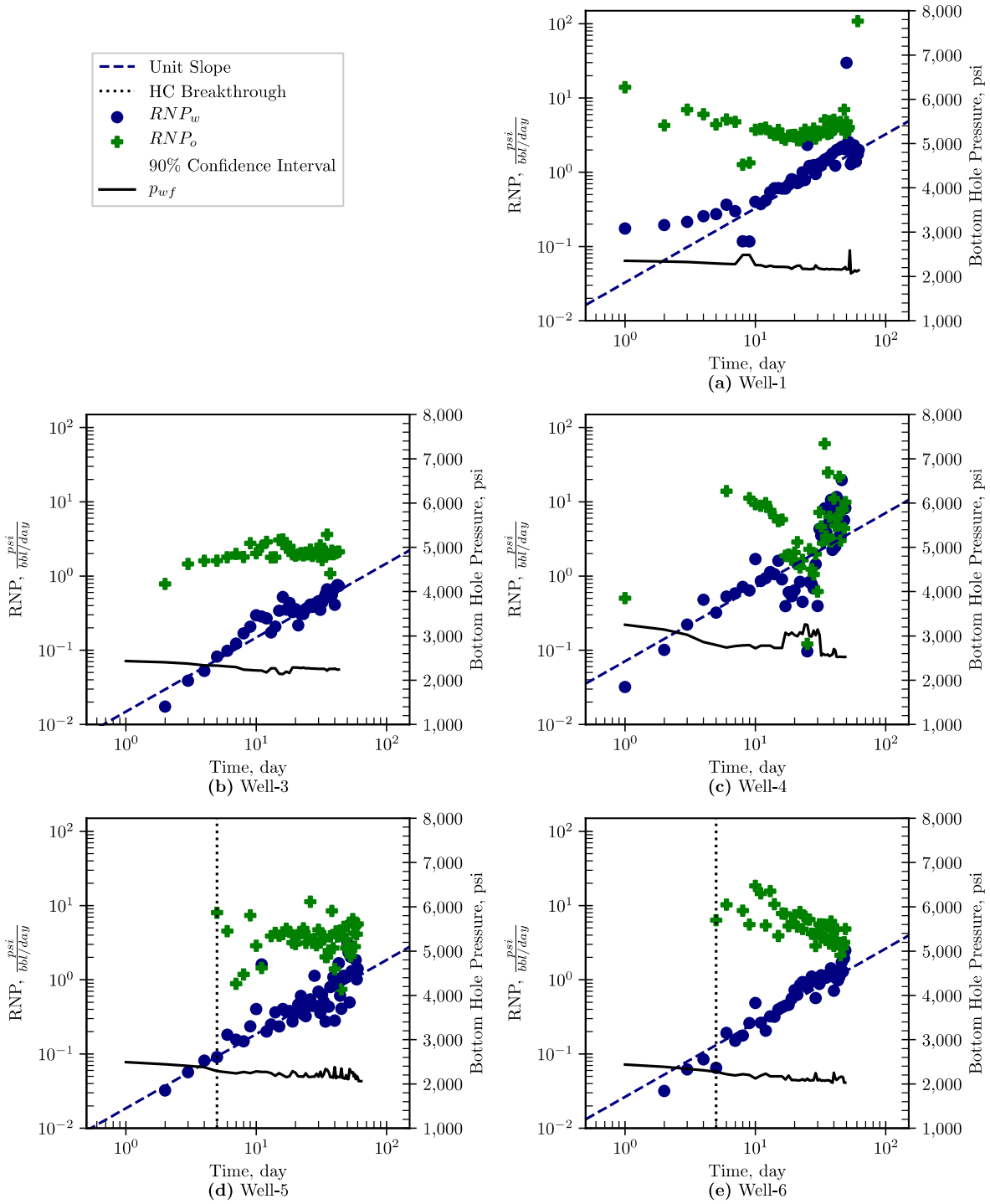

Fig. B.3 – Log-log plot of water/oil rate-normalized pressure (RNP) before jet-pump installation for the remaining five wells. The five wells show unit slope for water RNP while they don't for oil RNP. Secondary axis of estimated bottom hole pressure during the same period.

B.4 Driving indices profiles

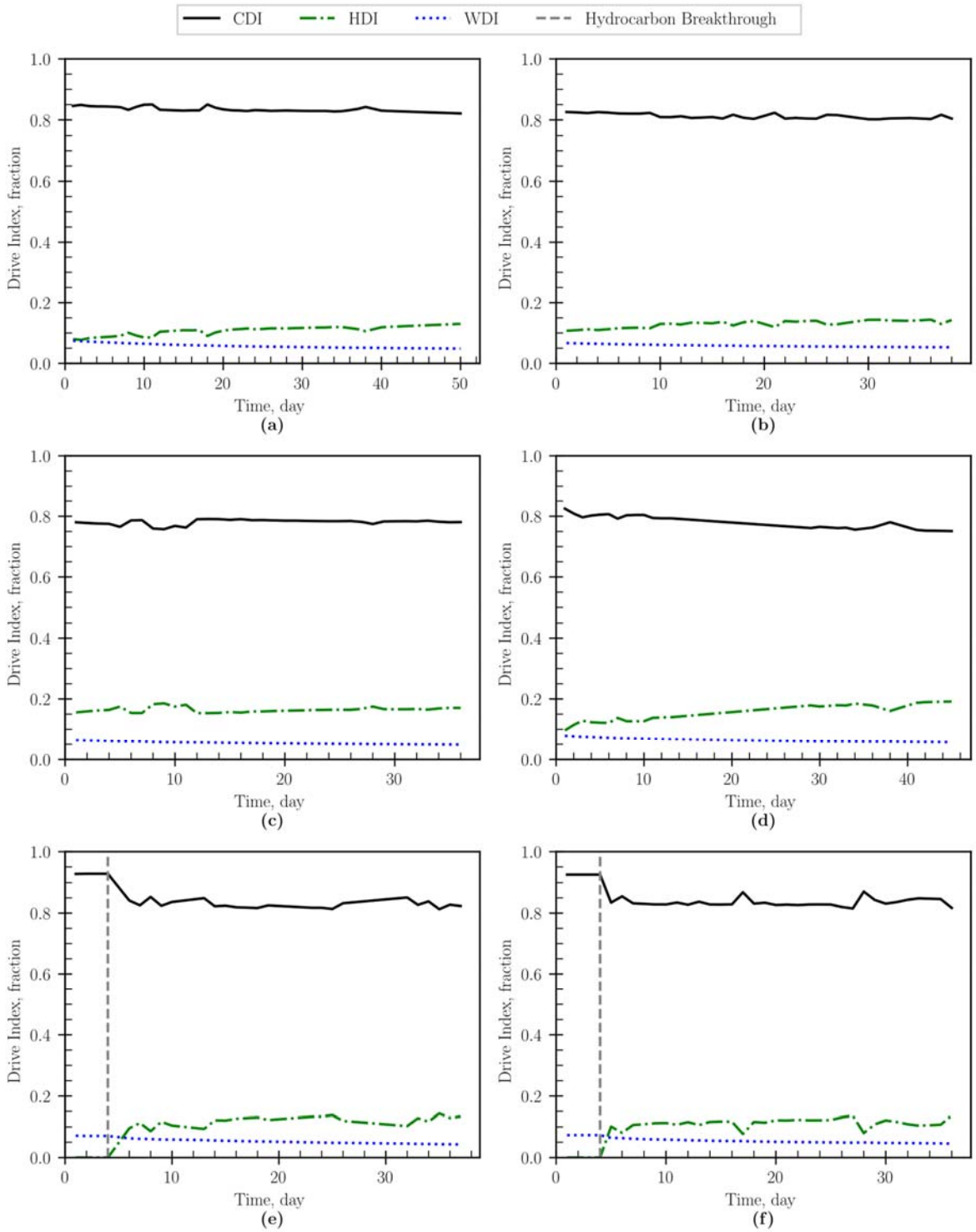

Fig. B.4 – Driving indices profiles during early production time before jet-pump installation for (a) Well-1, (b) Well-2, (c) Well-3, (d) Well-4, (e) Well-5 and (d) Well-6. Wells-5 and 6 show that HDI becomes in act after hydrocarbon breakthrough.

B.5 HD Profiles Before and After Jet Pump Installation

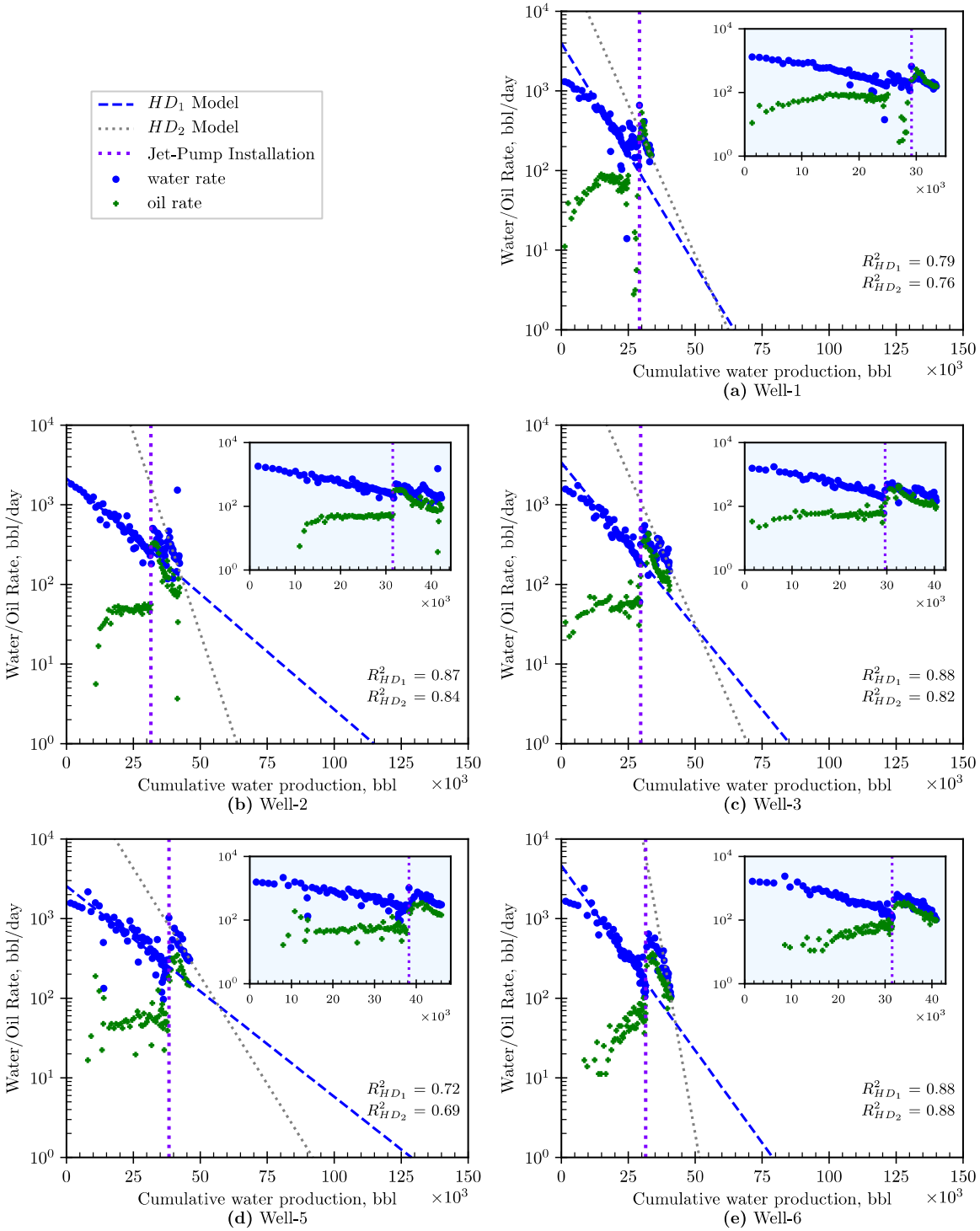

Fig. B.5 – Semi-log plots of water/oil rates versus cumulative water production volume for the remaining five wells. Sudden increase in rates and tubing pressure is due jet-pump installation. Water production data are fitted by straight lines (HD-Model) before and after pump installation. Insets zoom the early water/oil rates.

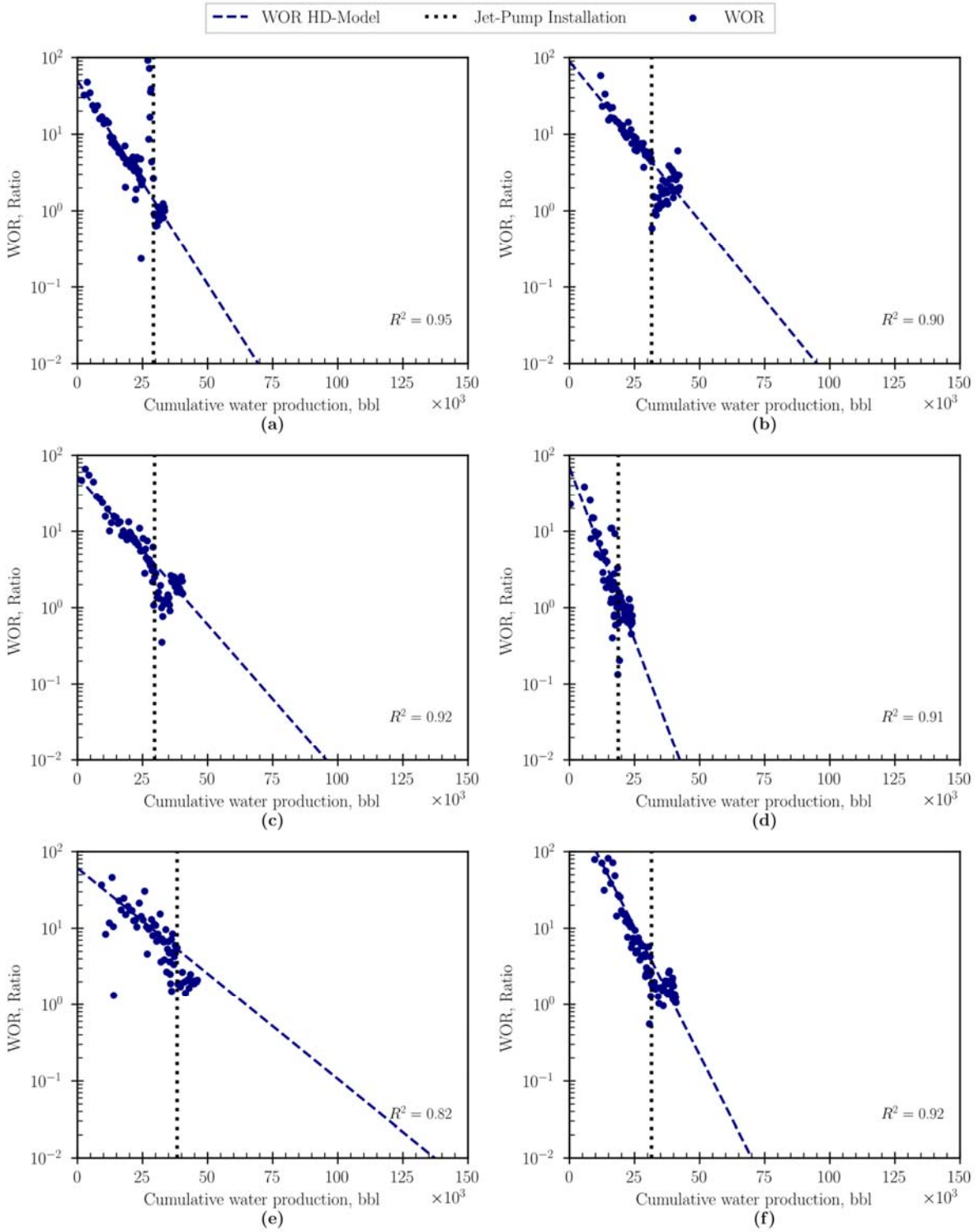

Fig. B.6 – Semi-log plots of water-oil ratio versus cumulative water production generally shows a harmonic-decline trend in (a) Well-1, (b) Well-2, (c) Well-3, (d) Well-4, (e) Well-5 and (d) Well-6.

C. WOR Modelling

C.1 Numerical Simulation

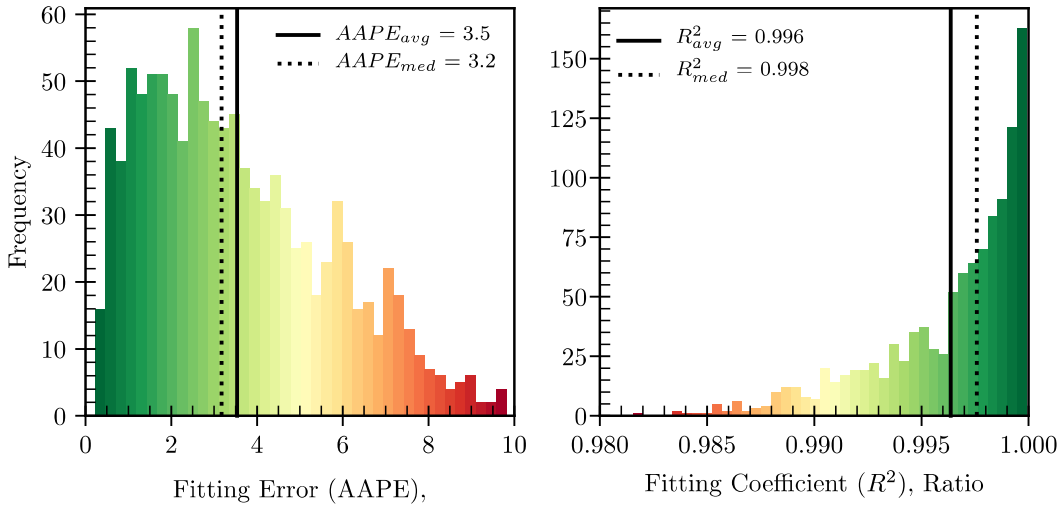

Fig. C.1 – WOR model fitting performance on simulation WOR data

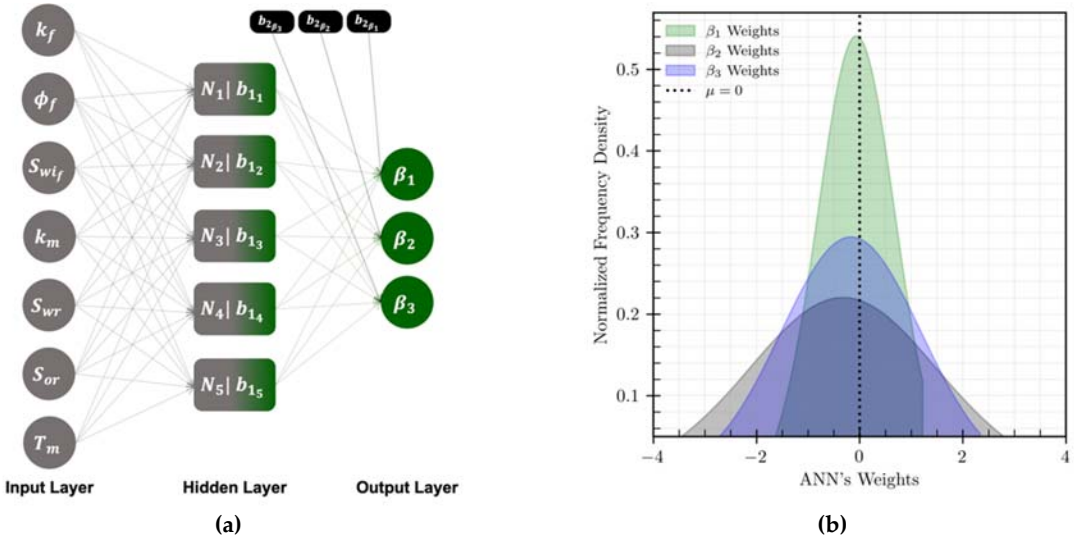

(a) **(b)**

Fig. C.2 – **(a)** ANN structure to predict WOR-model's control parameters. **(b)** ANN weights distribution

C.2 ANN Empirical Correlations (white box)

The extracted empirical correlation from the developed ANN shows that the parameter β_2 could be estimated as:

$$\beta_2 = 1.157\beta_{2_n} + 0.408 \tag{58}$$

where β_{2_n} is normalized β_2 and represented as:

$$\beta_{2_n} = \sum_{i=1} w_{2_i} \frac{1}{1 + e^{-y_i}} + 0.35 \tag{14}$$

where w_{2i} are the weights connecting the N neurons ($N = 5$) in the hidden layer to the output layer as shown in **Table C.1**. y_i is the linear transformation of input variables defined as:

$$y_i = \sum_{i=1} w_{1_{i,j}} x_{n_j} + b_{1_i} \tag{15}$$

where b_{1_i} is the bias in each neuron (h_i) in the hidden layer, $w_{1_{i,j}}$is the weight of the jth input variable in each neuron (h_i), M is the number of input variables ($M = 7$). The trained values of b_{1_i} and $w_{1_{i,j}}$ are listed in **Table C.1**, x_{nj} is the jth normalized input variable (x_j), calculated as:

$$x_{n_j} = \frac{x_j - x_{j_{\min}}}{x_{j_{\max}} - x_{j_{\min}}} \tag{16}$$

where $x_{j_{\min}}$ and $x_{j_{\max}}$ are the minimum and maximum values of the input variables considered in this study as listed in **Table 5.2**. Similarly, the control parameter β_3 is estimated by Eqs. (62) to (20), and the extracted weights and biases are listed in **Table C.2**.

$$\beta_3 = 0.501\beta_{3_n} + 0.038 \tag{62}$$

$$\beta_{3_n} = \sum_{i=1} w_{2_i} \frac{1}{1 + e^{-y_i}} - 0.019 \tag{89}$$

$$y_i = \sum_{i=1} w_{1_{i,j}} x_{n_j} + b_{1_i} \tag{90}$$

$$x_{n_j} = \frac{x_j - x_{j_{\min}}}{x_{j_{\max}} - x_{j_{\min}}} \tag{20}$$

C.3 Estimating WORM parameters: statistical approach

Here, the early-time flowback WOR versus load recovery is fitted by WORM through tuning the control parameter β_1. Then, the control parameter β_2 is estimated as a function of β_1 as:

$$\beta_2 = -1.1\beta_1 + 1.4 \tag{66}$$

This is the regression equation developed by applying a linear regression analysis between β_2 and β_1 as shown in **Fig. C.3a**. Both the 95% confidence and prediction intervals (CI and PI, respectively) are illustrated on the scatter plot. CI and PI are estimated as $\hat{a} \pm te_s$, where $\hat{a}$ is the predicted a value where $a \in \beta_2$, t is the t-multiplier (=2.16 for 95% CI and PI) and e_s is the standard error of the fit, estimated as $\sqrt{e_m}\left[1/n + \left(b-\bar{b}\right)^2/\sum\left(b_i-\bar{b}\right)^2\right]$ and $\sqrt{e_m}\left[1 + 1/n + \left(b-\bar{b}\right)^2/\sum\left(b_i-\bar{b}\right)^2\right]$ for CI and PI, respectively. n is the number of observations (4,000 runs), $b \in \beta_1$, e_m is the mean square error and $\bar{b} = \sum b_i\,/n$. The figure shows that more than 97% of the observed β_2 values are covered by the 95% PI, demonstrating a well-specified regression model [183]. Then, we estimate the average absolute percentage error (AAPE), which measures the fitting error between the observed b and predicted $\hat{b}$. AAPE is estimated as $1/n\ \sum_{i=1}^{n}\left|\left(\hat{b_i}-b_i\right)/b_i\right| \times 100$. Therefore, the β_2 value estimated from Eq. (58), as function of β_1, has an uncertainty of ± 7.2%. **Fig. C.3b** shows 3D crossplot between β_1, β_2 and β_3. The inset figures demonstrate the 2D crossplot of each pair. In this paper, we apply multiple linear regression (MLR) approach to predict β_3 as function of β_1 and β_2, illustrated as:

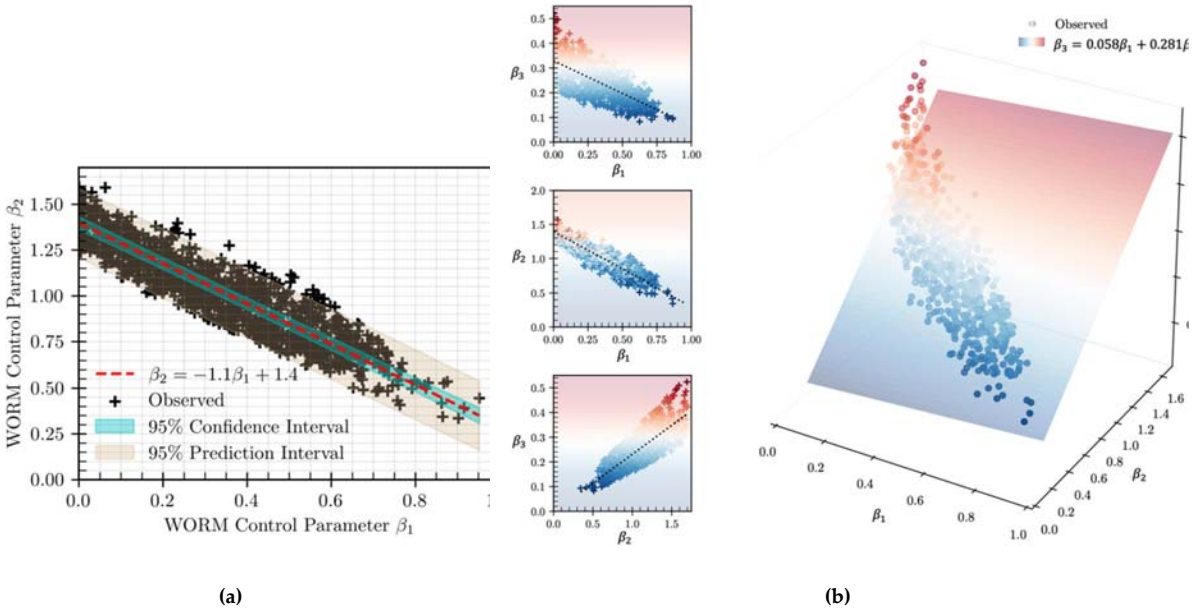

(a) **(b)**

Fig. C.3 – (a) 2D-Crossplot of the WORM control parameters β_2 and β_1. **(b)** 3D-Crossplot of the WORM control parameters β_1, β_2 and β_3, and their regression models.

$$\beta_3 = 0.058\beta_1 + 0.281\beta_2 - 0.072 \tag{67}$$

The coefficients of this correlation demonstrates the relatively higher dependency of β_3 on β_2 compared to β_1. In other words, the ultimate recovery in terms of WOR is more related to the intermediate recovery performance compared to the early recovery. Both the 95% CI and PI are calculated for the MLR model presented in Eq.(67). The results show that more than 96% of the observed β_3 values are within the 95% PI, demonstrating a well-specified MLR model. In addition, the AAPE of β_3 in this case is estimated at ± 14.8%. In other words, the value of β_3 and the corresponding ultimate load recovery estimated from this proposed statistical approach has an uncertainty of ± 14.8%. The main reason behind this high uncertainty is the embedded assumption of MLR that β_3 is linearly correlated to β_1 and β_3. In a future study, different nonlinear models will be tested. In the proposed statistical approach, the WOR control parameter β_1 is estimated by fitting the early-time flowback data by utilizing the WORM represented by Eq (5.9). Then, β_2 is estimated as a function of β_1 by using Eq. (66). Finally, β_3 is estimated by Eq. (67) as a function of both β_1 and β_2.

C.4 Uncertainty analysis for WORM parameter estimation

To integrate the fitting error of β_1 into the β_2 correlation presented in Eq. (66), we assume that the uncertainty in estimating β_1 by utilizing the curve-fitting approach (e_1) is independent from the statistical uncertainty in estimating β_2 ($e_{2,s}$) from Eq. (66). According to Taylor [184], the overall uncertainty in β_2 (e_2) is estimated as:

$$e_2 = \sqrt{e_1^2 + e_{2,s}^2} \tag{94}$$

Similarly, we assume that the statistical uncertainty in estimating β_3 ($e_{3,s}$) from MLR is independent from uncertainties in estimating both β_1 (from curve fitting) and β_2 from Eq. (66). Therefore, the overall uncertainty in β_3 (e_3) is estimated as:

$$e_3 = \sqrt{e_1^2 + e_2^2 + e_{3,s}^2} \tag{95}$$

Table C.1 - Weights and Biases of the ANN model of the control parameter β_2

i	$w_{1_{i,1}}$	$w_{1_{i,2}}$	$w_{1_{i,3}}$	$w_{1_{i,4}}$	$w_{1_{i,5}}$	$w_{1_{i,6}}$	$w_{1_{i,7}}$	B_{1_i}	w_{2_i}
1	-0.78	0.48	1.45	0.12	-0.24	0.31	-2.36	-0.62	0.81
2	0.69	1.81	-0.40	-0.21	1.28	0.99	-2.31	0.33	-0.36
3	0.23	-0.95	-7.12	-0.12	-1.05	-0.89	0.43	0.87	-0.51
4	-0.26	-5.62	1.19	-0.52	2.73	3.04	-3.85	-1.84	0.22
5	0.27	-1.47	-0.69	-0.17	0.32	-0.38	-2.21	1.54	0.69

Table C.2 - Weights and Biases of the ANN model of the control parameter β_3

i	$w_{1_{i,1}}$	$w_{1_{i,2}}$	$w_{1_{i,3}}$	$w_{1_{i,4}}$	$w_{1_{i,5}}$	$w_{1_{i,6}}$	$w_{1_{i,7}}$	B_{1_i}	w_{2_i}
1	-1.02	-2.89	2.15	-0.63	0.66	0.40	-2.89	-1.18	0.70
2	0.84	-0.45	2.33	0.86	-1.08	-0.76	0.72	1.44	0.67
3	-0.42	-0.31	1.29	-0.93	0.18	-4.43	-0.88	-0.19	-0.32
4	0.29	1.62	-1.79	0.48	-1.51	-1.13	0.56	0.95	-0.57
5	-1.27	1.20	0.91	-1.10	1.54	0.82	-0.74	-2.25	0.43

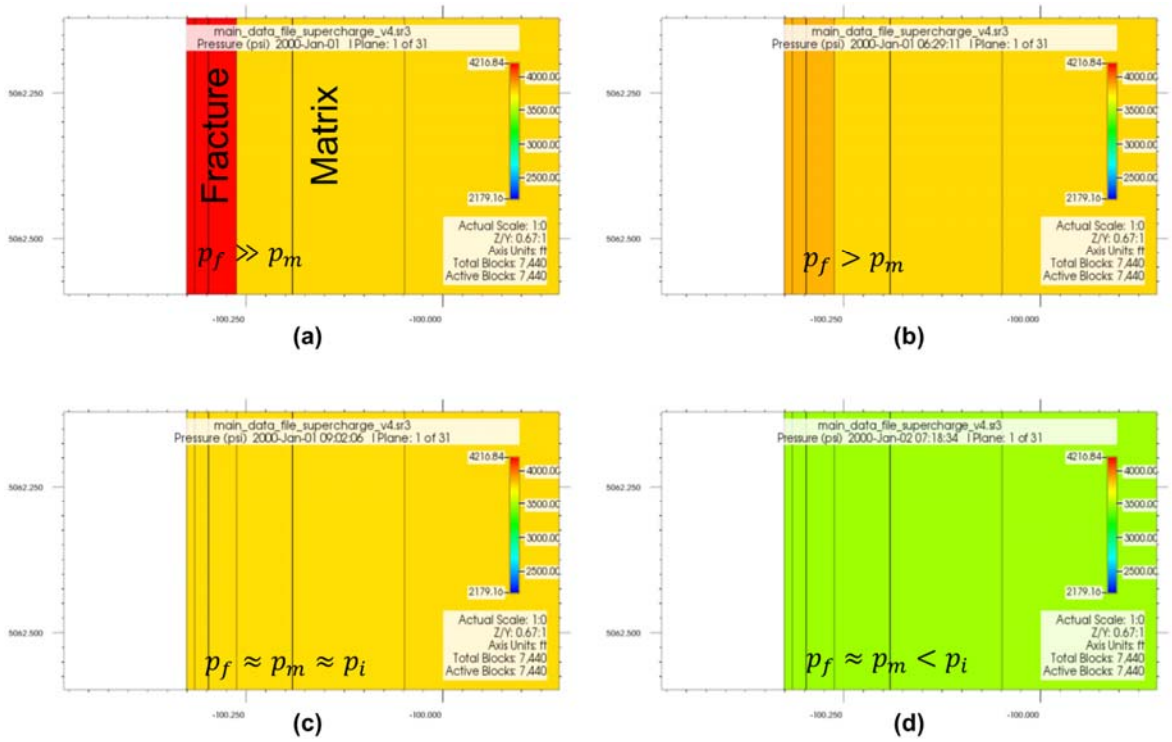

Fig. C.4 – Fracture and matrix pressures changes at different timestamps representing different stages of pressure supercharge until it is ended.

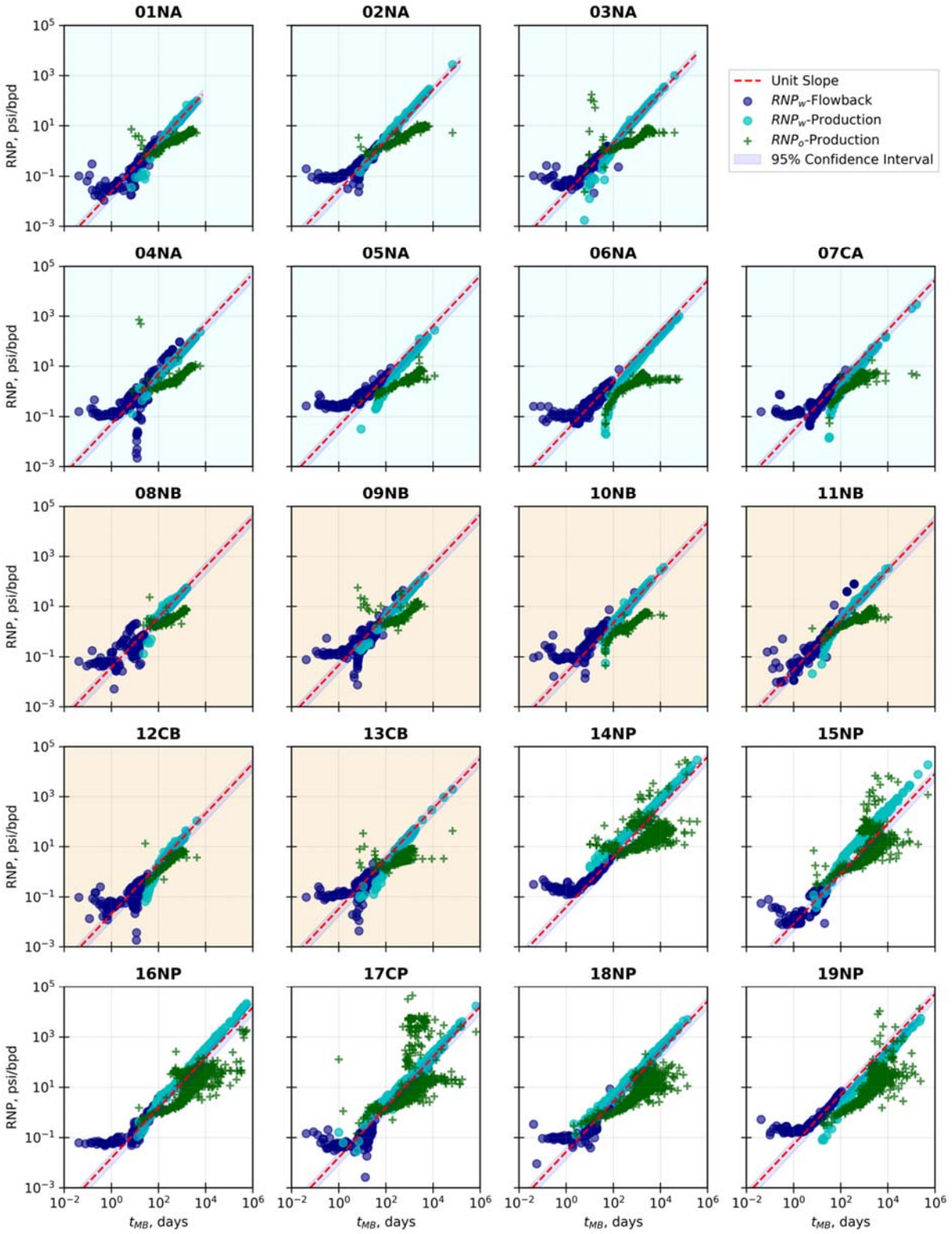

Fig. C.5 – Flowback and post-flowback RNP plots

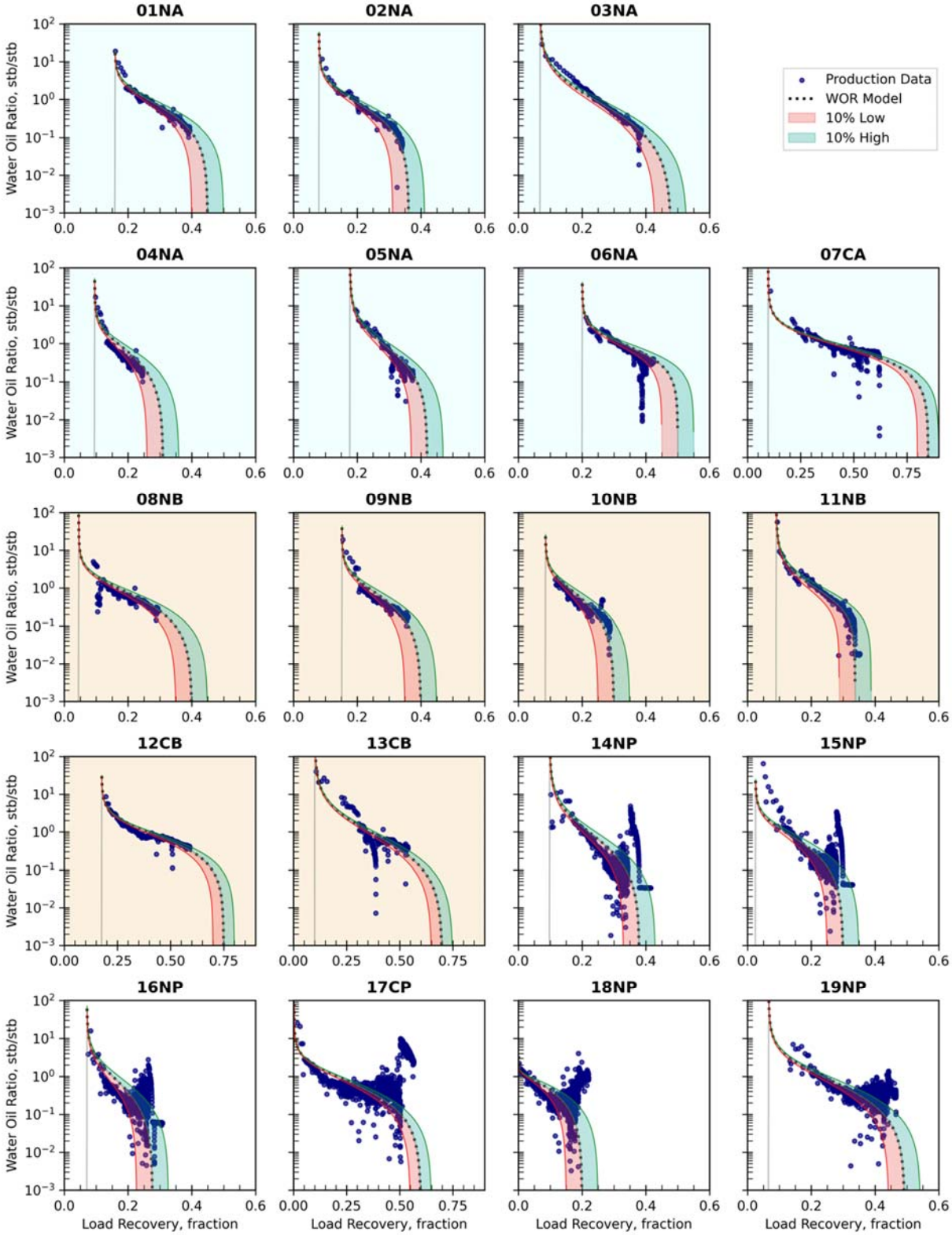

Fig. C.6 – Production WOR modelling and ultimate load recovery prediction

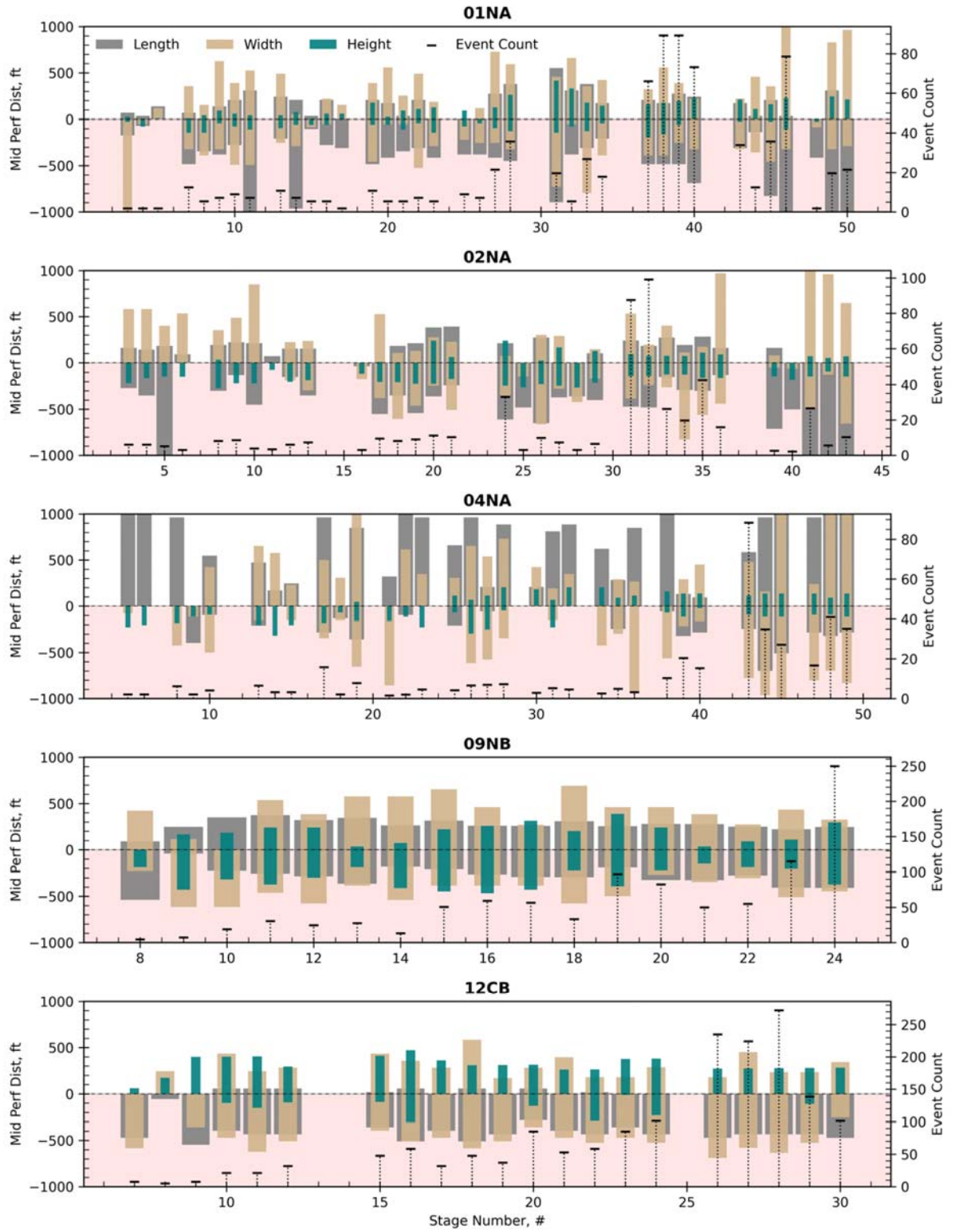

Fig. C.7 – Microseismic event dimensions parallel, perpendicular and vertical to each well by stage

C.5 Design of Experiment for Petrophysical Properties Selection

We conducted a sensitivity analysis to assess the influence of ten different petrophysical properties on the observed simulated WOR trend during load recovery as shown in **Fig. C.8**. Initially, we carefully selected these ten properties to represent fracture, formation, and fluid characteristics. The chosen properties are Swi_f, ϕ_f, k_f, k_m, ϕ_m, Sw_r, So_r, p_i, $\mu_{w/o}$, and T_m. Subsequently, we examined the sensitivity of the simulated WOR trend to these parameters during the load recovery, as demonstrated in the figure.

Swi_f generally exhibits a significant impact on the early-time WOR performance, wherein higher values of Swi_f result in delayed oil breakthrough and consequently higher WOR during the initial flowback period. A similar effect is observed with ϕ_f. Conversely, higher ϕ_f typically lead to enhanced ultimate load recovery due to the increased fracture pore space, which improves load recovery and restricts water trapping. Similarly, k_f exerts a similar influence at late times, with higher k_f values corresponding to improved load recovery. However, k_m exhibits the opposite effect. Increased k_m typically facilitate faster oil influx from the matrix into the fracture, resulting in accelerated oil breakthrough and lower WOR during the early flowback period. Nonetheless, higher k_m lead to reduced ultimate load recovery due to the enhanced support of oil influx into the fracture, resulting in lower water relative permeability and subsequently reduced load recovery.

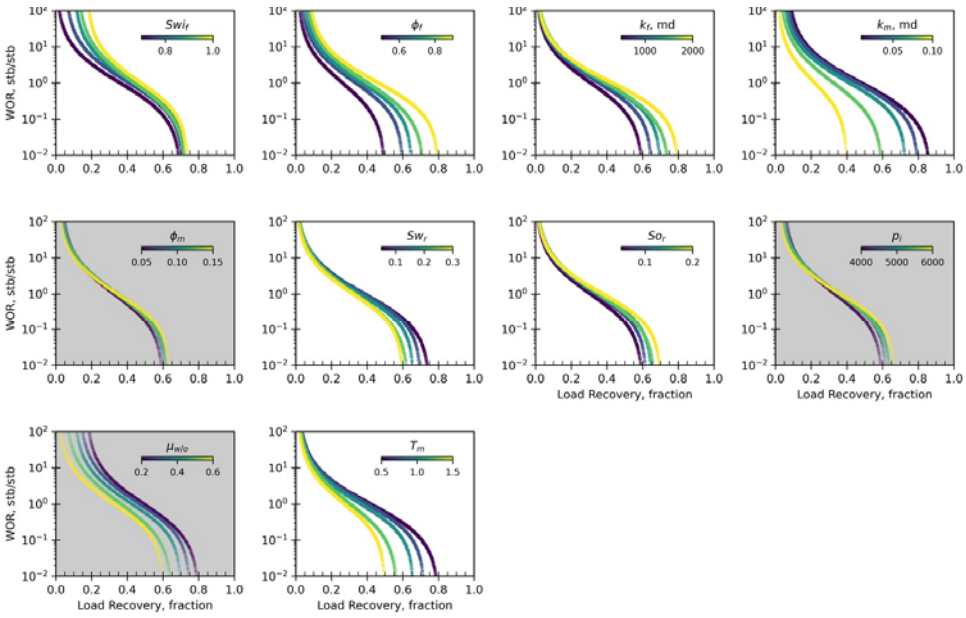

Fig. C.8 – Simulated WOR trend sensitivity to different petrophysical properties

While larger ϕ_m indicates a larger volume of oil in the matrix (assuming immobile formation water) and slightly faster oil breakthrough, its impact on the WOR performance is negligible and can be disregarded. Similarly, higher p_i indicate more energy and may result in slightly faster oil breakthrough, but their influence on the WOR trend is minimal. Sw_r, So_r and T_m have noticeable effects on the WOR performance as the ultimate load recovery is approached. Higher Sw_r generally indicate a larger amount of unrecoverable water, leading to reduced load recovery. Conversely, higher So_r values imply lower oil recovery and consequently higher WOR at late times. Additionally, higher T_m indicate reduced damage between the matrix and fracture, facilitating increased oil influx from the matrix to the fracture (assuming immobile formation water) and resulting in lower ultimate load recovery.

Finally, the effect of $\mu_{w/o}$ on the WOR performance is monotonic. A relatively higher oil viscosity (i.e. less $\mu_{w/o}$) typically reduces oil mobility and causes the complete WOR curve to shift monotonically towards the right. Furthermore, considering the well's lifetime, $\mu_{w/o}$ is usually assumed constant; hence, $\mu_{w/o}$ is not considered in this study. Consequently, we concluded that Swi_f, ϕ_f, k_f, k_m, Sw_r, So_r and T_m are the key parameters to be considered during the development of WORM.

C.6 WORM Sensitivity to capillary pressure in the matrix

Here, we conduct a study on the impact of capillary pressure on the WOR profile. To showcase this, we have developed five cases with varying capillary pressure profiles and used IMEX to demonstrate the sensitivity of the WOR profile to capillary pressure in the matrix as shown in **Fig. C.9**. We have observed that as capillary pressure increases, oil breakthrough occurs earlier, and the single-phase water flowback period shortens. This is due to the increased influx of oil from the matrix into the fracture, which results in significantly lower WOR at the same stage of load recovery, thereby supporting oil production. However, higher capillary pressure may lead to lower ultimate load recovery, as the WOR curve shifts to the left, resulting in a lower ultimate load recovery. Our developed WORM has been able to fit the simulation data by adjusting the coefficients; β_1, β_2 and β_3, which are linked to petrophysical properties (ϕ_f, k_f, S_{wi_f}, k_m, S_{wr} and S_{or}).

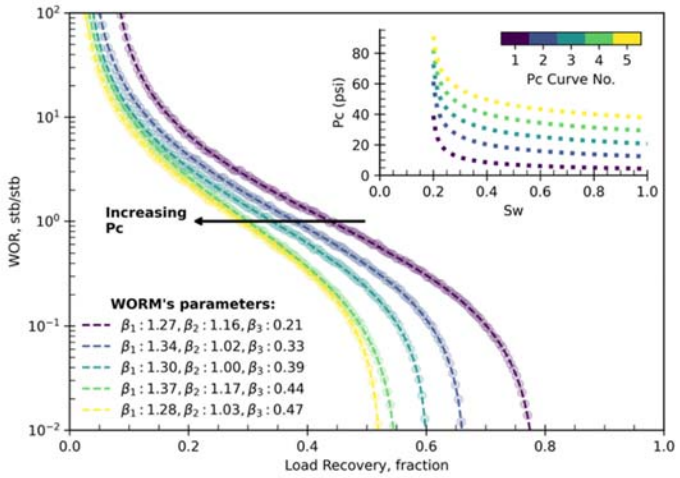

Fig. C.9 – Effect of capillary pressure on WOR profile. Inset figures shows different capillary pressure profiles

C.7 WORM application on Montney oil MFHWs

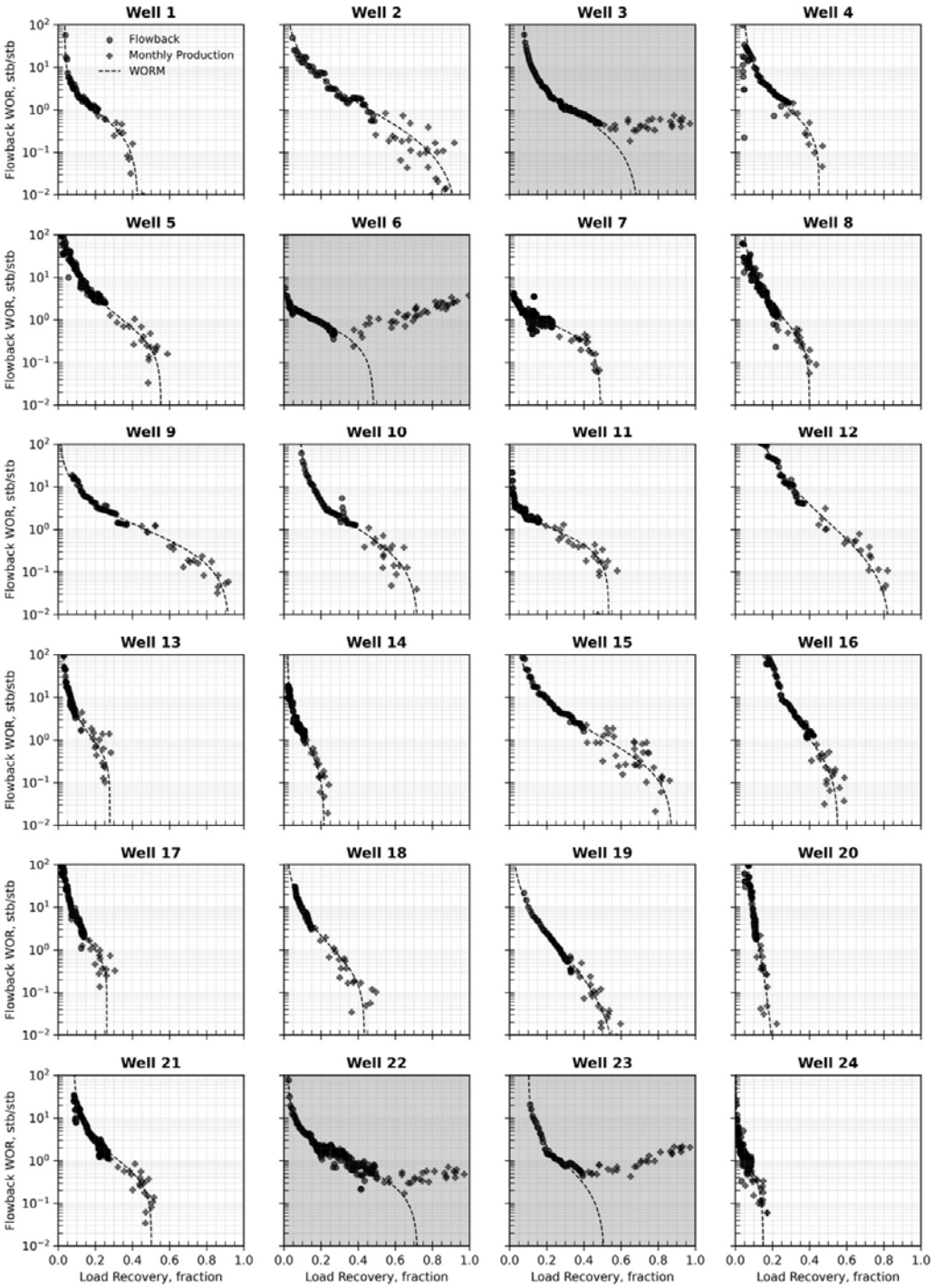

Fig. C.10 – WORM application to the monthly production data of 24 oil MFHWs completed in the Montney formation. Wells 3, 6, 22 and 23 demonstrate a potential of mobile formation water or/and nearby well interference

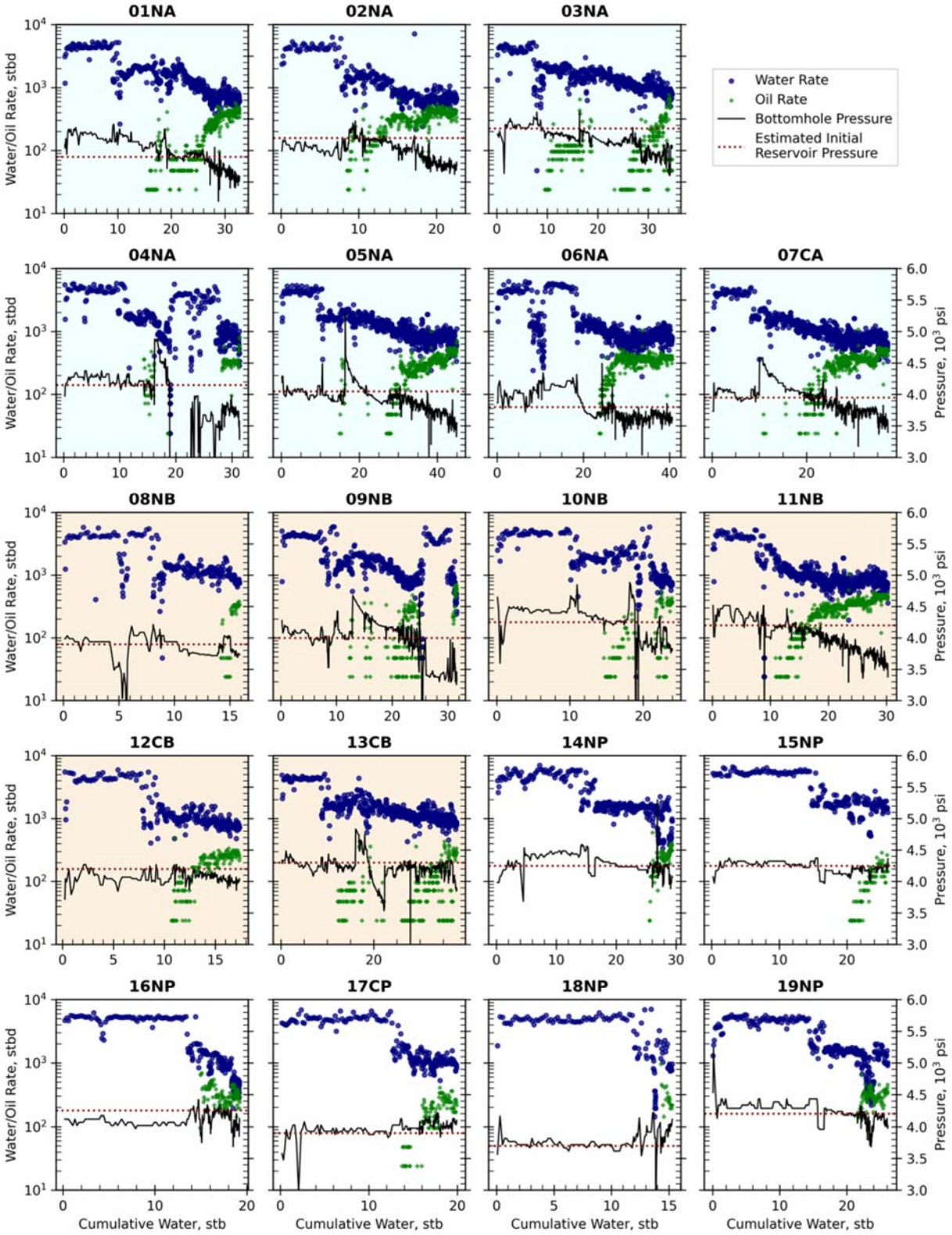

Fig. C.11 – Using early flowback data to estimate average reservoir pressure

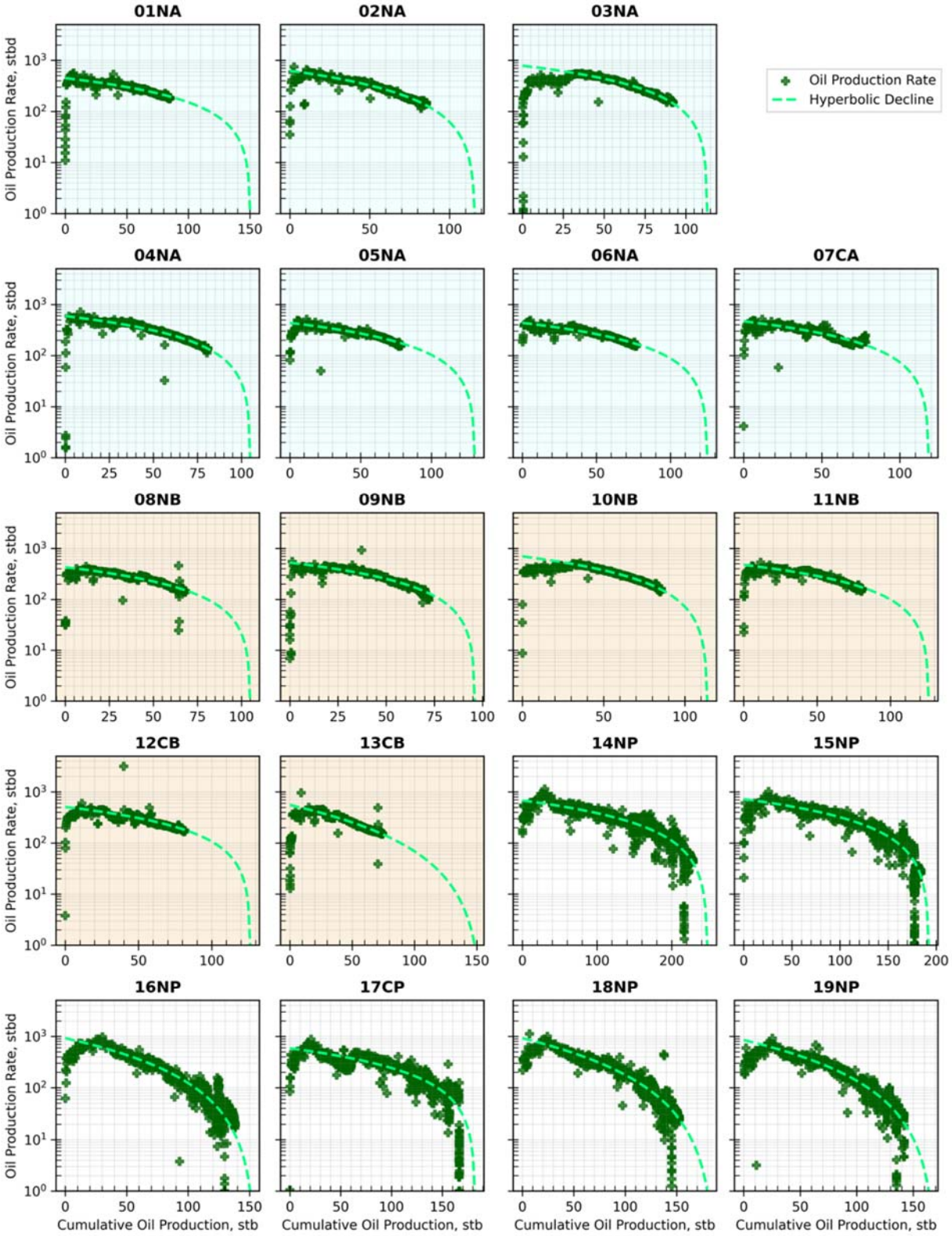

Fig. C.12 – Cumulative oil production prediction using hyperbolic decline model

D. Trained Models Weights and Coefficients

Table D.1 - SVM-K's support vectors and dual coefficients

i	s_ϕ	s_{ρ_b}	s_{GR}	s_{r_R}	α
1	1.38	-0.77	1.11	0.28	0.63
2	-0.03	0.52	-2.54	0.65	0.69
3	-0.80	0.45	0.73	-0.67	-0.70
4	0.52	0.16	-1.77	-0.74	1.89
5	-0.80	0.70	0.88	-0.33	2.15
6	0.71	-0.66	0.68	-1.13	1.36
7	-1.50	1.03	-0.94	-1.09	-1.14
8	-1.75	-8.58	-0.49	0.56	-0.58
9	-0.36	0.34	0.14	-0.12	0.30
10	-0.31	0.02	-1.28	-1.13	-0.45
11	-0.24	0.24	-0.44	-0.50	-0.14
12	0.41	-0.20	1.31	1.78	0.04
13	1.55	-1.02	-1.30	-0.09	1.22
14	0.92	-0.52	2.10	-0.87	0.58
15	-1.77	1.35	0.30	-0.20	-0.66
16	-1.62	0.96	1.27	0.79	-1.12
17	-1.19	0.74	-1.91	-0.90	-0.78
18	2.78	-1.42	0.06	-0.42	0.25
19	0.20	0.34	-2.33	1.67	0.98
20	-0.31	0.27	-0.63	-0.06	-0.19
21	-1.59	0.85	-1.18	2.21	-1.22
22	-0.43	0.27	-1.02	2.85	-1.20
23	-0.55	0.52	-0.31	0.76	-0.68
24	0.92	-0.48	1.16	-1.07	-0.22
25	-0.47	0.20	0.16	-1.21	-0.11
26	0.24	-0.12	0.63	3.06	0.25
27	-0.54	0.52	0.48	-0.87	1.27
28	-1.24	0.67	0.18	1.98	-1.48
29	2.39	-1.31	-0.39	0.38	0.87
30	0.81	-0.12	-0.44	-0.11	0.65
31	0.94	-0.09	-2.32	-1.03	0.73
32	-0.38	0.27	-0.02	3.73	-0.04
33	-0.82	0.45	-0.95	-1.05	0.08
34	1.81	-0.95	-0.27	-0.51	-0.62
35	0.94	-0.48	0.07	0.49	-0.12
36	0.85	-0.41	0.64	-0.65	-0.68
37	-1.13	0.60	-0.94	2.19	1.00
38	1.06	-0.16	2.29	1.19	1.29
39	-0.73	0.42	0.89	-0.38	-0.78
40	-0.80	0.63	0.04	0.36	-0.05
41	0.74	0.06	-2.35	-0.54	-0.26
42	0.39	-0.34	-1.38	-1.17	-1.43
43	2.20	-1.31	-0.79	-0.96	0.99
44	1.59	-0.84	0.11	1.14	0.80
45	2.32	-1.20	0.02	-0.91	0.98
46	-1.34	0.74	-1.25	1.55	-0.86
47	1.96	-1.06	-0.21	1.17	0.09
48	-0.78	0.49	0.59	-0.67	-2.15
49	0.38	0.13	-0.55	-0.16	0.02
50	-0.66	0.42	1.24	-0.18	-1.45

Table D.2 - ANN-V_e's weights and coefficients for the second hidden layer

k	1	2	3	4	5	6	7	8	9	10	11	12	13	14	15	16	17	18	19	20	21	22	23	24	25	26	27	28	29	30	31	32
1	0.2	-1.4	0.1	0.1	0.4	-0.7	0	0.2	-0.9	-0.5	-0.3	-0.6	0.2	-0.1	-0.5	0	-0.9	-0.1	0.1	-0.7	0	-0.1	0.1	0.1	0	-0.4	-0.9	-0.8	-0.6	-0.1	-0.7	-0.2
2	0	0	-0.2	-1.2	-0.1	0	-0.7	0.2	0.3	0.1	0	0	-0.5	-0.1	0.1	-1	0.1	0.1	0.2	0	0	0.1	0.1	0.3	0.2	0.3	0.1	0.1	0.1	0.1	0	0.1
3	-1	-1.1	0	0	0.3	-0.8	0.1	0	0	-0.1	0.1	-0.4	0	-0.1	-0.3	-0.1	-0.2	-0.2	0	-0.6	0	-0.3	0	0	0	-0.8	-0.1	-0.1	-0.7	0	-0.8	-0.3
4	0	0	0	-0.3	0.2	0	-0.8	-1.3	0.2	-0.3	-0.6	0	-0.8	-0.5	0	-0.2	0	0.1	-0.9	0	-0.3	0	-0.9	-1.5	0.1	-0.1	0	0.1	0	-0.6	0	0
5	0	0	-0.6	-0.2	0.1	0	0.1	-0.1	-1.3	0	-0.4	0	-0.8	0.1	0	-0.5	0	0.1	-1	0	-0.3	0.1	0	-0.3	-0.8	0.1	0	0	0	-0.1	0.1	0
6	-0.8	-1.4	0	0	-0.1	-0.7	0	0.1	0	-0.3	0.1	0.1	-0.1	-0.3	0.2	0	-0.4	0.1	0	-1	0.1	-0.4	0.1	0	0.1	-0.1	-0.3	0.1	-0.5	0.1	-0.3	0
7	0	0	-0.1	0.1	0	0	-0.5	0.1	-0.1	0	-0.8	0	-0.2	-0.1	0	-0.3	0.1	0	0	0	0.1	0	0.1	-0.9	-0.8	0.1	0	0	0	-0.9	0	0
8	0	0	-0.1	-0.5	-0.2	0.1	-0.2	0.1	0	0.1	-0.5	0.1	-0.7	-0.1	0	-0.5	0.1	0.1	0	0	-1.1	0	-0.1	-0.5	-1.1	-0.5	0	0.1	0.1	-0.7	0.1	0
9	0	0	-0.1	-0.4	-0.4	0	-0.1	-0.2	-0.5	0.2	-0.7	0.1	-0.4	-0.3	0.1	0	0	0.1	-0.3	0.1	-1	0.1	-0.9	-0.4	-0.3	-0.1	0	0.1	0	0	0.1	0.1
10	0	0	-1.3	-0.1	-0.1	-0.3	-0.8	-0.4	-0.6	-0.4	-0.8	0	-1	-0.4	0	-0.5	0.1	0.1	-1.1	0.1	-0.2	0	-0.3	0.1	0	0	0	0	0	0	0.1	0
11	0	0	0.1	-0.2	0	0	-0.3	-0.6	-0.1	-0.8	0.1	0.1	0	0	-0.1	-0.7	0	0	0	0	-0.6	0	-0.6	0	0.2	0	-0.1	0	0	-0.9	0	0
12	0	0	0	-0.4	-0.1	0	-0.8	0.1	-0.1	0	0	0	0.2	-0.1	0	-0.3	0	0.1	0	0	0	0	0.1	-0.7	-0.7	0.1	0	0	0	0	0	0
13	0	0	-0.1	0.1	0	-0.6	-0.8	0	0	0.1	-0.9	0	0	0.1	0.2	-0.2	0	-0.9	0	0	0.1	-1.1	0.1	0.1	-0.3	0.1	-0.7	-1.1	-1.1	-0.5	-0.2	0
14	0.1	-1.5	-0.5	0.1	0.3	0	0.1	0.1	0.3	0.2	0.1	0	0.1	0.3	0	0	0	0	0.1	-0.1	0.1	0.1	0.1	0.1	-0.2	-0.9	-1.3	0.1	-1.4	0	0.1	0.1
15	-0.1	-0.1	-0.8	-0.3	-0.8	-0.1	0.1	-1.3	-0.3	-0.2	-0.4	0	0.1	0.2	0	-0.5	0	-0.1	-0.8	0	-0.9	0	-0.1	0.1	-0.3	0	-0.1	0	0.1	-0.8	-0.1	0
16	-1.3	-1.1	0	0	0.1	-1	0	-0.1	0	-0.2	-0.1	0	0	0.1	0	0	0	-0.8	0	-1	0	-1.2	0	0	0.1	0.1	0	0	0	0	-0.5	0
17	0	0	-0.8	0.1	0.1	0	-0.1	-0.3	0	0	-0.3	0	0	-0.1	0	-1	0	-0.1	0	0	0	0	0	0	0	0	0	0	0.1	-0.4	-0.1	-0.1
18	0	0	0	-0.7	0	0	-0.1	-0.5	0.1	-0.5	-0.7	0	-1.4	-0.2	0	-0.5	0.1	0	0.1	0	0.1	0	-0.4	0	-0.9	0	0	0	0.1	-0.8	0	0
19	0	0	-0.1	0	-0.4	-0.6	0.1	0	-0.1	-0.4	-0.7	0.1	-1.2	0.2	0.1	-0.7	0	0.1	0	0	-0.6	0	-0.1	-0.1	-0.7	0.1	0	0	0.1	0.1	0.1	0.1
20	0.1	0.1	-0.7	-0.4	-0.5	0.1	-0.6	-0.7	-0.3	0	0.1	0.1	0.2	-0.4	0.1	0.1	0.1	0.1	0	0.1	-0.6	0.1	-0.3	0	-0.3	0.1	0	0.1	0.1	0	0	0.3
21	0.1	0	-0.1	-0.9	0	0	-1.1	0.1	0.1	0.1	0	0.1	-0.4	-0.2	0	0	0.1	0	0.1	0	-0.5	0	-0.8	0.1	-0.5	0.1	0	0	0	-0.1	-0.1	0.1
22	0	0	-0.5	-0.4	-0.2	0	-0.2	-0.8	-0.7	0	-0.5	0	0	0.2	0.1	0.1	0	0	-0.8	0	-0.7	0	-0.3	-0.7	-0.2	0.1	0	0	0.1	0	-0.1	0
23	0	0	0	-0.1	-0.5	0	-0.5	-0.1	-0.5	-0.8	0.1	0	-1.2	-0.2	0	-0.5	0.1	0	0.1	0	0.1	0	-0.1	-0.7	-0.3	0	0	0	0	-0.6	0.1	0.1
24	-0.3	0	-0.2	-0.8	-0.2	-0.1	0.3	-1	-0.5	-0.2	-0.9	0.3	0	0	0.5	-0.6	0.5	0.4	-1	0	-0.7	-0.2	-0.1	-0.2	0.3	-0.1	-0.1	0.3	-0.1	-0.5	0.4	0
25	-0.6	-0.9	0.1	0	0.2	-0.8	0	0.1	0.1	0.1	0.1	-0.4	0	-0.6	-0.4	-0.1	-0.6	-0.3	0	-0.9	0	-0.8	0	0	0	-0.7	-0.4	-0.5	-0.9	0	-0.3	-0.7
26	0.2	0	-0.5	-0.1	-0.9	-0.2	0.1	-0.9	-0.6	-1	0.2	0.1	0.2	0.4	0.3	0.1	0.1	0.1	0	0.1	-0.9	0.1	-0.8	0	0	0.2	0	0	0	0	0.1	0
27	-0.3	-0.8	-0.1	0	0	-1.3	-0.1	0	0	0	0	0	0.1	0	0	-0.3	0	0	0	-0.7	0	-1.1	0	0	0.1	0	-0.7	0	-0.1	0	-0.6	0
28	-0.1	0	-1.4	0	0.3	-0.3	0	0.1	0.2	0.2	-0.2	-0.1	-0.1	-0.5	-0.4	-0.1	-0.7	-0.2	0	-0.1	0.2	-0.1	0.3	0.1	-0.1	-0.2	0	-0.2	-0.9	-0.9	0.1	-0.3
29	-0.1	-0.1	0	-1.4	0.1	-0.6	-0.1	0	-0.7	-0.5	0	0	-0.1	0.1	0	0	0	0	0.1	0	0	0	0	-0.1	0	0	-0.4	0	-0.6	0	0	0
30	0	0.1	-0.4	-0.2	-0.4	0	0	-0.1	-0.1	0.1	-0.7	0.2	-0.2	0.3	0.4	0	0	0.2	-0.1	0.1	0	0.2	-1.2	-0.7	-0.6	0.6	0	0.3	0	-1.1	0.2	0.4
31	0	0	0.1	0.1	0	0	-0.6	-1.1	-0.8	-0.6	0	0.2	0.1	0.2	0.1	-0.3	0.2	-0.1	-0.9	0	-1.1	-0.2	0	-0.4	-0.3	0	0	0.1	-0.1	-0.4	0.1	0.1
32	-0.8	-1.1	-0.2	-0.2	-0.3	-0.6	-0.3	-0.4	0	-0.4	-0.2	0	0.1	-0.2	-0.3	-0.3	0.1	0	0	-1	-0.1	-0.4	-0.6	-0.2	-0.7	0.1	0.1	0	-0.7	-0.4	-0.7	0.2
33	-0.8	0	0.1	0	0	-0.1	0	0	0.1	0	-0.7	-0.6	0.1	-0.2	-0.6	-0.5	-0.9	-0.5	0.1	0.1	0	-0.9	0	0	0.1	-0.7	-0.6	-0.8	-0.7	-0.6	0.1	-1
34	0	-1.5	0.1	0.1	0.1	0.1	-0.3	0.1	-0.2	-0.1	-0.1	-1.6	0.1	-0.3	-0.3	0	-0.1	0	0	-0.7	0	-1.1	0	0.1	-0.1	-0.7	-1.4	-1.1	0	0	-0.5	0
35	-0.4	-0.1	-1	-0.3	0.3	-1	0.2	-0.5	0	0.2	-1	-0.2	-0.9	0	-0.1	0	-0.2	0.1	-0.4	-0.5	-0.7	-1.1	-0.1	0.1	0.1	-0.1	-1	0	0	-0.5	-0.3	0
36	-1.2	-1.1	-0.1	0	0	-0.6	0.1	0.1	0.1	-0.7	0.1	-0.3	0	-0.5	-0.2	0	-0.5	-0.3	0.1	-1	0.1	-0.2	0	0.1	0	-0.9	-0.1	-0.3	-0.6	0	-0.3	-0.9
37	-0.1	0.1	0	-0.5	0	-0.1	-0.4	-1.1	-0.4	0.1	-0.4	0	0	-0.1	0.1	-0.6	-0.1	0.1	0	0	-1.2	0	-0.4	0.1	-0.9	0	-0.1	0	0	0	-0.1	0
38	0	0	-0.8	-0.1	-0.1	0	0	0	-0.1	0	-0.7	0	-0.1	-0.4	0	0.1	0	0	0	0	0	0	0.1	-1.1	-0.2	0	0	0	0	-1.1	0	0
39	-1.3	-1.2	0	-0.1	0.1	-0.1	0.1	0.1	0	-0.2	0.1	0	-0.2	-0.3	-0.1	0.1	0	-0.1	0	-0.2	0	-1	-0.2	-0.3	0	-0.1	-1.1	0	-1.1	-0.7	-1.3	0
40	0.1	-0.1	-0.5	0	-0.1	0.1	-0.5	0.1	-0.6	-0.2	-0.1	0.1	-0.1	-0.1	0	0.1	0.1	0	0	0.1	-0.3	0	-0.3	-0.9	-0.2	0	-0.1	0	0	-0.2	0.2	0.1
41	-1.1	-1.2	0.2	-0.1	0.3	-0.7	-0.1	0.3	-0.1	0	-0.3	0.1	0.2	-0.3	0	0.1	-0.2	-0.1	0.3	0	-1.1	-0.4	0.2	-0.3	0.1	-0.2	-0.2	-0.2	-0.9	-0.5	-0.3	0
42	-1.3	-0.6	0.1	-0.1	0.1	-0.6	0.3	0	0.2	0	0.1	0.1	0	-0.2	-0.3	-0.6	-1.5	-1.6	0.1	-1	0	0.1	0	0	0	0.1	-0.8	-1.2	-0.8	0	-0.9	0
43	0	0	-0.7	-0.6	-0.1	0	-0.4	-0.8	0	0.1	-1	0	-0.1	-0.1	0.1	0.1	0	0	-0.9	0	-0.6	0	0	0	0	0	0	0	0	-0.3	-0.1	0.1
44	0	0	-0.1	-0.2	-0.1	-0.1	-0.2	-0.2	-0.1	-0.1	-0.2	-0.1	0.1	-0.2	0	-0.5	-0.1	0.1	-0.1	0	-0.8	0.1	0.1	-0.9	0.1	0	0	0	0	-0.9	0	0.1
45	-0.7	-0.7	0.1	0	0.2	-0.8	-0.4	0	-0.1	0.1	0	-1.1	0.1	0	-0.6	0.1	-0.9	-0.8	0.3	-1.1	0.1	-0.5	0.1	0	0	-0.1	-0.7	-0.7	-0.3	0.1	-0.5	-1
46	0	0.1	-0.7	-0.2	0.1	0	0.2	-0.6	-0.1	-0.8	0	0.1	-0.1	0	0	0	0	0	0.1	0	-0.9	-0.1	-0.7	0.1	-0.6	0	0.1	-0.1	0	-0.4	0	0.1
47	-0.8	-0.5	0	0	0.1	-0.7	0.1	0	0.1	-0.2	0	-0.3	0	-0.3	-1.4	0.1	-0.4	-0.4	0	-0.4	0	-0.9	0	0	0	-0.3	-1.2	-0.4	-0.2	0	-0.6	-0.4
48	0	0	-0.8	0.1	-0.1	-0.1	-0.1	-1	-0.6	-0.5	-0.5	0.2	0	-0.3	0.1	-0.4	0.1	0.1	-0.7	0	-0.8	0	0.1	0.1	-0.8	0	0	0.1	-0.2	-0.5	0.1	0.1
49	0	0.1	-0.9	-0.8	-0.9	0	0.1	0	0	-0.9	0.1	0	-0.5	0.4	0.3	-0.1	0	0.3	-0.4	0.3	0	0	-1.1	-0.2	0.2	0.2	0.2	0.2	0	-0.3	0.2	0.1
50	0	0	-0.1	0.1	0	0	-0.7	-0.1	-0.6	-0.8	-0.3	0	0.1	-0.2	0.1	-0.7	0	0	-1	0	0	0	-0.1	-0.2	-0.6	0	0	0.1	0	0	0	0
51	0.2	-1.3	0	0	0.1	-0.9	0	0	-0.1	-0.5	-0.1	-0.9	0.1	-0.5	0	0	-1.2	0	0	0.2	0	-1	-0.2	0	0	-0.7	-0.9	0	-0.5	0	0.1	0
52	0	0	0.1	0	-0.7	0.1	0	-0.9	0	-0.9	-0.2	0	-0.8	0.1	0.1	0	0	0	0	0	0	0.1	-0.8	0	0.1	0.1	0	0	-0.7	-0.8	0	0.1
53	0	0.1	-0.9	0.4	0.2	-0.1	0.2	0	0.2	-0.4	0.1	0.1	0.3	-0.1	0.3	0.2	0	-0.1	-1.4	0	0	0.1	0.1	0.1	0.2	0.5	0.1	0	0	-0.5	-0.1	0.2
54	0	0	0.1	-0.5	0.1	0	-0.1	0.1	-0.1	0	0.1	0	-0.6	-0.1	0	-0.2	0	0	0.1	0	0.1	0	-1.5	-0.6	-0.4	0.1	0	-0.1	0	0.1	0	0
55	-0.4	-0.9	0.1	-0.1	0.1	-0.7	0	0.1	0.1	0.2	0.1	-0.1	0	-0.2	-1	0	-0.1	0	0.1	-0.5	0	-0.4	0	0	0.1	-0.3	-1	0	-0.4	0	0.3	-0.1
56	-0.2	-0.2	-1.3	0.1	0.1	-0.4	0	0	-0.1	0.1	0	0	0.1	-1	-0.3	-0.1	0	-0.2	0	-0.2	0	-0.8	0.1	0	0.1	-0.1	-0.3	-0.2	-0.2	0	0	-0.4
57	0	0	-0.7	0.1	-1	0	-0.6	-0.3	-0.5	-1.1	-0.2	0.1	0.1	-0.1	0.2	-0.2	0.2	0.1	-0.3	0.1	-1	-0.1	-0.2	-0.5	-0.1	0.1	-0.1	0.1	0	-0.8	0.2	0
58	-0.1	0.1	0	0.1	0	-0.9	0	0	0	-0.2	-0.1	0	0.2	-0.1	-0.1	0	-0.1	-0.1	0.1	0	0	-1.4	0	0	-0.4	-0.5	-0.1	0	-0.9	0	0	-0.2
59	0	0.1	-0.8	0	-0.9	-0.1	-0.7	-1	-0.6	-0.5	0.1	0	0	0	0	-0.4	0	0.1	-0.8	0	-0.9	0.1	-1	0	0.1	0.1	0	0.1	0	-0.7	-0.2	0
60	-1.2	-1.1	0	0	0.1	-0.9	-0.5	0	-0.3	0.1	0.2	-1	0	0.2	-0.2	0.2	0	-0.1	0.1	-1.3	0	0.2	0	0	0.1	-0.1	0.1	0.1	-0.1	0	-0.1	-0.2
61	0	0	-0.7	0.2	0	-0.1	0.1	0	-0.2	-0.8	-0.4	0.1	-0.8	0.1	0.1	-0.7	0	0	-0.9	0	-0.6	0	0.1	0	0.2	0	0	0	0	-0.2	0.1	0
62	0	0	-0.8	-0.8	-0.1	0	0.1	-0.1	-0.8	0	-0.9	0	-1	0.1	0	-0.6	0	0	-0.5	0	0.1	0	-0.1	-0.2	-0.6	0.1	0	0	0	-0.1	-0.1	0
63	-0.2	0	0	0.1	0.1	-0.6	0.1	0	0	0	0	-1.2	-0.1	-0.6	-0.3	-0.3	-0.9	-0.3	0	-0.4	0	0	0	0	0	0	-0.2	-1.1	-0.3	0	-1.4	-0.5
64	-1.4	-1.3	0	0.1	0	-0.8	0	0	0	-0.2	0.1	-1.5	0.2	-0.6	-1	0.1	-1.1	-0.6	0.1	-1.8	0	0.2	0	0.1	0	-0.7	-0.8	-1.2	0.3	0	0.1	-1.2
b2	0.1	0.1	0	0.1	0.1	0.1	0	0.1	0.1	0	0	0.1	0	-0.2	0.1	0	0.1	0.1	0.1	0.1	0.1	0.1	0.1	0.1	0.1	0	0.1	0.1	0.1	0.1	0.1	0.1
W3	0.1	0.1	-0.2	-0.1	-0.1	0.2	-0.2	-0.1	-0.2	-0.3	-0.2	0	-0.1	0.3	0	-0.3	0	0	-0.1	0.1	-0.2	0.1	-0.1	-0.1	-0.2	0.1	0.1	0	0.1	-0.3	0.1	0

Table D.3 - ANN-V_e's weights and coefficients for the first hidden layer

i	1	2	3	4	5	6	7	8	9	10	11	12	13	14	15	16	17	18	19	20	21	22	23	24	25	26	27	28	29	30	31	32
1	0	-0.2	0.1	-0.1	-0.3	0	-0.1	-0.1	0	0.2	-0.2	-0.2	-0.2	0	-0.2	0.2	-0.3	0.1	0.2	-0.1	-0.1	0.4	0.3	0.1	0.2	-0.2	0	-0.2	0.2	-0.2	0	0.2
2	-0.4	0.1	-0.2	-0.1	0	0.1	0.1	0.1	0	-0.4	0	0.1	0.2	0.2	0	-0.1	0	0.2	0	-0.1	0	0	0.1	-0.1	-0.1	0	-0.1	0	-0.2	0	0.1	0.1
3	0.1	-0.1	0.1	0	-0.2	0.1	0	-0.3	-0.2	-0.2	0.2	-0.1	-0.2	-0.2	-0.3	0.3	0.2	0.2	0	-0.1	-0.2	0	0.1	0	0.1	-0.5	-0.1	-0.1	0.3	-0.6	0.1	0.2
4	-0.1	-0.2	0.4	0	-0.2	0	-0.2	-0.1	0	0.1	-0.1	-0.1	0.1	-0.2	-0.1	-0.2	0	-0.2	0	-0.4	-0.4	-0.1	-0.2	-0.2	0	-0.4	0.1	0	0	-0.2	-0.3	-0.1
5	-0.2	-0.1	0	-0.2	0	-0.2	0.1	-0.1	-0.2	-0.1	0.2	0.1	0.2	-0.1	-0.6	0.1	0	0.1	0	0	-0.1	-0.1	0.2	-0.1	-0.1	0	0.1	0.2	-0.1	0	0	-0.2
6	0	0.1	0.1	0	0	-0.1	-0.2	0.1	0.1	0.1	0.2	0	-0.1	0	0	0.1	-0.2	-0.1	-0.2	0.2	0.2	0.2	-0.2	0.1	0	0.1	-0.1	0.3	-0.2	0.4	0.1	-0.1
7	0	0	-0.2	0	0.3	0	0	0	0.3	0	-0.2	0.1	0.1	0	0.2	-0.5	0.2	0.1	0	-0.2	0.1	0.1	0	-0.1	-0.1	0.1	0.2	0	-0.1	-0.1	0.1	-0.1
8	0.2	0	0	0.1	0	0.1	-0.2	-0.2	-0.1	0.1	0	-0.1	0	-0.1	-0.1	0	0	0	0.2	0	-0.1	-0.1	0.2	0.1	0.1	-0.1	-0.1	0	0.1	-0.1	0.1	-0.1
9	0.2	0.1	0.1	0	-0.1	-0.2	0	0.2	-0.1	-0.2	0	0.2	0.1	0.1	0.1	0.1	0.1	0.2	0.3	0	-0.3	-0.1	0.1	-0.1	0	0.1	0	-0.1	-0.1	0	-0.2	-0.2
10	-0.1	-0.1	0.1	-0.1	0	0.1	0.2	0	-0.1	-0.1	0.1	-0.1	0	-0.1	0.1	0	-0.1	0	-0.1	-0.1	0.1	0.1	-0.1	0.1	-0.2	0.1	0.1	-0.1	-0.1	0	0	0
11	0	0	-0.1	0.2	0	0.3	0.1	-0.2	-0.2	0.2	0.1	0	-0.1	0	0	-0.1	-0.2	-0.2	-0.1	-0.1	0.1	0.1	0	-0.4	-0.1	-0.1	0	-0.2	0	0.1	0.1	0
12	-0.1	0	0.1	0	0.2	0	-0.2	0.3	0.1	0.1	0.3	0.2	0	-0.9	0.3	0.1	0.3	0	-0.5	0	0	-0.1	0	-0.1	0.1	-0.5	0.4	-0.4	-0.7	0	0	-0.3
13	-0.1	0	0.1	0.1	0.1	-0.1	-0.2	-0.1	0	0.1	-0.4	0	-0.3	-0.3	0	-0.2	-0.3	0	0	0	-0.1	-0.1	0.1	-0.2	-0.4	0	-0.1	0	-0.1	0	0	0.3
14	0	-0.3	0.2	0	-0.3	-0.2	0	0.1	0	-0.1	0.1	0	-0.1	-0.1	0	-0.2	-0.1	0	0.1	0.1	-0.1	-0.1	-0.1	0.2	0	0.3	0.1	-0.2	0	0	-0.1	0.4
15	-0.1	-0.3	0.2	-0.2	-0.2	0.1	0	-0.2	-0.1	-0.1	-0.1	0	0	-0.3	-0.1	0.2	-0.2	-0.3	-0.1	-0.1	-0.1	-0.1	-0.3	-0.1	0.2	-0.2	0.1	0.2	-0.1	-0.1	-0.1	-0.1
16	0.2	0.2	-0.1	0	-0.1	0	0	0	0.2	0.2	-0.2	0	0.3	-0.1	0	0	0.3	-0.1	-0.1	0	0.1	-0.1	0.2	0	-0.3	-0.1	-0.1	0	0.3	0.1	-0.4	0.2
17	-0.2	0.1	0	0.1	0.1	0.2	-0.2	-0.2	-0.1	0.1	-0.1	-0.1	-0.1	0	-0.1	0	0	-0.1	0.2	-0.1	0.1	-0.1	0.1	-0.2	0	0	-0.2	-0.1	0	0	0.2	-0.2
18	-0.1	0	0	-0.2	0.2	0.3	0.2	0.4	-0.1	0.1	0.2	-0.2	0	-0.1	-0.2	0.3	-0.2	0.2	0	-0.4	-0.1	0.1	0.2	0.2	0.1	-0.2	0	-0.2	0.2	0	-0.3	0.5
19	0	-0.1	0.1	0.1	0.1	0.1	0.1	0	-0.1	0	0.3	0	-0.1	0	0	-0.2	-0.1	-0.1	0.1	0.1	0.2	0.1	0.1	0.1	-0.2	0	-0.1	-0.1	0.1	0.1	0.2	0.1
20	0.1	0.1	0.1	0.1	0.1	0	0.2	0.1	0.1	0.2	-0.3	0.1	0	0	0.3	-0.1	0	0.1	0	-0.1	-0.1	0	0.2	0	0.2	-0.1	0.2	0.1	-0.3	0.1	0.1	0.2
21	-0.2	-0.1	0.2	0	0	0.1	0.1	-0.1	-0.2	-0.1	0.1	-0.1	-0.2	0	-0.1	0.1	0.2	-0.1	0	0	-0.1	0	-0.2	0.2	0.1	0	0.1	0.2	0.1	0	-0.1	-0.1
22	0.3	0.2	0.5	0	0	0.2	0	-0.1	0.2	0.1	0.2	-0.1	0	0.2	0	-0.2	0	0	0	-0.1	-0.1	0.1	0.1	0.3	0.3	-0.1	-0.1	0	0.1	0.1	0.2	0
23	0	0	0.1	0.1	-0.1	-0.2	0.2	0.1	0.1	0.1	-0.1	0	0.4	0.1	0.2	-0.2	-0.1	-0.2	0.2	-0.4	-0.2	-0.2	-0.1	0.2	-0.1	0	-0.1	0.3	0	0.1	-0.2	-0.3
24	-0.2	0	0	0.1	0.1	-0.2	0.2	0	0	0	0.3	0.1	0.2	-0.2	-0.2	-0.6	0	0.1	0.1	0.1	-0.1	0.1	0.1	0	0.1	-0.1	0.2	-0.2	0.1	-0.2	0.1	0.1
25	0.2	0.2	-0.2	0.1	0.1	-0.1	0.1	0.1	-0.2	0.2	-0.1	0.1	-0.1	-0.2	0	0	-0.1	0.2	0.1	0	0	-0.2	0.4	0.3	0.1	-0.1	0.1	0.1	0.1	-0.2	0.3	0.1
26	-0.1	-0.1	0.1	-0.2	-0.1	-0.1	-0.1	-0.2	0.1	0	0.1	-0.3	0	-0.5	-0.1	0.1	0	-0.1	-0.2	-0.2	-0.2	0.3	0.1	0	0	0.2	-0.1	0	0	0.1	0.2	0
27	0	0	-0.2	0.3	0	-0.1	-0.4	-0.3	0	0	0.1	-0.1	0.1	0	-0.2	-0.1	-0.1	0.1	-0.1	0	0.1	0.2	0.2	0.2	-0.2	-0.3	-0.2	-0.1	0.1	-0.1	0	-0.1
28	-0.1	0	0.1	0.4	0.3	-0.1	-0.1	-0.2	0.3	0	0.1	0.3	0	0	0.3	-0.1	0.2	0.1	0	0.2	0.2	0.1	-0.1	-0.2	0	-0.1	0	0.1	-0.1	0	-0.2	-0.2
29	0	-0.2	0.1	0.1	0	0.1	-0.1	-0.1	0.1	0	0.2	-0.1	-0.1	-0.1	-0.1	0.1	0	0.2	0	0.1	0.2	0	0	0	0	-0.1	-0.1	-0.1	-0.3	-0.3	0	0
30	-0.5	0	0.1	0	0.1	-0.4	-0.2	-0.2	0	-0.3	0.2	0.1	-0.1	-0.1	-0.3	-0.2	0.1	-0.1	-0.7	0	-0.1	0.1	0	-1.1	-0.2	-0.2	0.2	-0.5	0	-0.1	0.2	-0.2
31	0	0	-0.2	-0.3	0.3	0	0.2	-0.2	0.4	-0.1	-0.3	-0.1	-0.3	-0.5	-0.4	-0.4	0.3	-0.5	-0.3	0.1	-0.2	-0.3	-0.2	0	0	0.1	-0.4	-0.6	0.1	0.1	0	-0.1
32	0	-0.1	-0.5	0.1	0.1	-0.2	-0.2	0.1	0.1	0.1	-0.1	0.2	-0.5	0	0.2	-0.1	-0.1	0.3	0	0	0	-0.1	0.1	-0.1	0.3	-0.1	-0.6	0.1	0.1	0.1	-0.1	-0.1
33	-0.2	-0.1	-0.2	0	-0.2	-0.1	0	-0.1	-0.2	0	0	0	-0.1	-0.1	0.1	-0.1	-0.1	0	-0.2	0	0.1	0	-0.1	-0.3	-0.1	0	0.1	0.1	-0.2	0	0	-0.1
34	0	-0.8	-0.2	-0.5	0	-0.5	-0.3	0.1	0	0.1	-0.3	-0.6	-0.4	-0.3	-0.1	0.2	0	0	0	-0.2	0	0	0.1	-0.4	-0.1	-0.7	-0.2	0.1	-0.4	0.1	-0.3	-0.1
35	-0.4	0.1	0	-0.1	-0.2	-0.1	0.2	0	-0.4	-0.1	-0.2	0.1	0.2	0.2	0	0.1	0.1	0	0	0.1	0.2	0.2	-0.2	0	0	0.1	-0.2	-0.1	-0.1	-0.1	0	-0.2
36	-0.1	0	-0.1	-0.2	-0.2	0.3	-0.2	-0.1	-0.2	-0.1	0	0	0	0.2	-0.1	-0.2	-0.1	0	0.1	-0.3	-0.1	0.1	-0.1	0	-0.3	0	0	-0.1	0.1	0	-0.1	-0.2
37	0.2	0.1	-0.3	0.1	-0.4	0.1	-0.2	0.1	0.1	-0.2	0.1	-0.1	-0.2	0.1	-0.2	-0.2	-0.4	0.2	0	-0.2	0	0	0.1	0	-0.1	-0.3	-0.5	-0.4	0.2	0	-0.1	-0.1
38	-0.2	-0.3	0	-0.2	-0.2	0	-0.1	-0.2	0	-0.1	0	-0.2	-0.2	-0.3	-0.3	-0.3	-0.2	0.1	-0.3	0	-0.1	-0.2	0	-0.3	0	-0.2	-0.1	-0.1	-0.1	-0.1	-0.3	-0.3
39	-0.4	0	0.4	0.4	0.1	0	0.1	0	-0.1	-0.4	-0.3	0	-0.3	0	0.1	-0.2	0.1	-0.2	-0.3	-0.4	-0.3	0.1	-0.3	0.2	0.2	-0.2	0.3	-0.2	0.2	-0.1	0.1	0.4
40	-0.5	-0.1	-0.3	-0.1	-0.1	-0.1	0.2	-0.9	0.1	-0.3	0.1	-0.4	-0.1	-0.2	-0.2	-0.5	-0.2	-0.8	0.2	-0.2	0.1	0.4	-0.7	-0.3	-0.5	-0.8	0	0.1	-0.4	0.1	0	0
41	-0.6	-0.7	-0.5	-0.6	-0.9	-0.4	0.3	-0.1	-1	-0.7	-0.3	-0.3	-0.5	-0.3	-0.1	-0.2	-0.2	0	-0.3	-0.3	-0.2	-0.4	-0.7	-0.3	-0.4	-0.2	-0.6	-0.2	0.3	-0.5	-0.4	-0.1
42	0.2	-0.5	0.2	-0.2	0.2	0.2	-0.1	-0.2	-0.2	-0.7	0.1	0	0.1	-0.1	-0.1	-0.2	0	0.1	-0.5	0	-0.1	-0.3	-0.1	-0.3	0	0.1	0	-0.1	0	-0.7	0.2	-0.3
43	-0.2	-0.1	-0.2	-0.2	-0.2	0	-0.1	0	-0.1	-0.4	-0.2	0	0	-0.1	-0.1	0.1	0.1	-0.3	0.2	-0.2	-0.1	-0.1	-0.2	-0.1	-0.3	-0.2	-0.1	0.3	-0.3	-0.1	0	-0.4
44	-0.6	-0.3	-0.2	0	-0.1	-0.2	0	0	0.1	0.3	-0.1	0	-0.4	0	-0.1	0	-0.3	0	-0.1	-0.1	-0.2	0.3	0.1	0.1	0	0	-0.2	-0.1	0.1	-0.1	-0.3	0
45	-0.2	0	-0.2	-0.1	0	-0.3	-0.2	0.1	0	-0.1	0	-0.1	-0.2	-0.2	0.1	0.1	-0.1	-0.1	0	-0.2	0	0.1	-0.1	-0.3	-0.2	-0.2	-0.1	-0.6	-0.1	0	-0.3	0.1
46	0.1	-0.3	0.5	-0.1	-0.2	0.9	-0.3	-0.1	0	0	-0.1	-0.1	0	-0.1	0	-1.1	-0.3	0.1	-0.6	-0.2	0.6	0	-1.2	-0.1	-0.1	0.3	-0.3	0.1	0.9	-0.1	-0.1	-0.1
47	-0.3	-0.1	-0.1	-0.7	-0.1	0	0.3	0.3	-0.1	-0.1	-0.1	-0.1	-0.2	0	-0.3	-0.2	0.1	0.2	-0.1	-0.3	-0.8	-0.6	0.1	0	-0.2	0	-0.1	-1	0.2	-0.1	-0.2	-0.3
48	-0.2	-0.1	0.2	-0.1	0.3	0.4	-0.3	0	0	0	-0.2	-0.4	-0.5	0.6	0.8	0.1	-0.5	-0.4	-0.2	0	-0.2	0	0.2	-0.1	-0.2	0.1	-0.1	-0.3	0.4	0.1	-0.1	0.1
49	0	0	-0.1	0	0.1	0	-0.1	-0.1	-0.1	0	-0.1	-0.1	0	-0.2	-0.2	0.1	0.1	-0.1	0.1	-0.1	0.1	-0.1	-0.1	0.1	-0.2	0.1	0.1	0.1	-0.2	0.1	-0.1	0
50	-0.2	-0.3	-0.3	0	0.1	0.1	0.5	-0.1	-0.5	0.4	0.1	0.1	0.4	0	0.5	-0.2	0	-0.2	0	0	0.3	0.4	0.1	0.3	-0.1	0	0.1	-0.2	0	0	-0.1	-0.1
51	-0.1	-0.1	-0.1	-0.1	0.1	0	-0.1	0	0	0.1	0.1	0.1	0.1	0.1	0.1	0	-0.1	0.1	0	0	0	-0.1	0.1	0.1	0.1	0.1	-0.2	0	0.1	0	0	0
52	-0.6	0	-0.5	-0.3	0.3	-0.2	-0.5	-0.4	-0.2	-0.2	-0.8	-0.2	0.4	0	0	-0.2	0	-0.1	-0.5	0.4	-0.3	0.5	0.5	0	0	-0.5	-0.7	-0.2	0.2	-0.4	0.5	0
53	-0.2	0.1	0	0.1	-0.1	-0.3	0.1	-0.2	-0.1	0	0	0.3	0.1	-0.2	-0.1	-0.3	0	0	-0.1	0.2	-0.1	-0.1	0	0	-0.2	0	0.1	0.1	0.1	-0.2	0	-0.3
54	0.2	-0.2	0	0.1	-0.2	-0.1	0.1	0.1	-0.1	0.1	-0.3	0	0	-0.2	0	0.1	0	-0.1	-0.3	0	-0.5	0	0.1	-0.2	-0.1	-0.2	0.7	0.3	-0.1	0	0	0.1
55	-0.1	-0.1	-0.2	0.1	0	-0.1	-0.1	0	-0.2	0.1	0	-0.1	0.1	0.1	0.1	0.1	0.1	0.1	0	-0.1	0	0.1	0	0.1	-0.1	0	0.1	-0.1	0.1	0.1	-0.1	0
56	-0.5	-0.4	-0.6	-0.1	-0.3	-0.4	0.1	-0.3	0.3	-0.1	0	-0.1	0	0.2	0.1	0	-0.3	-0.1	0	-0.5	-0.3	0.1	-0.3	-0.8	0.7	0	0.1	-0.4	0.1	0.1	-0.5	-0.2
57	-0.6	0	-0.3	-0.1	-0.4	0.5	-0.3	0.1	0	-0.1	-0.5	0	0.1	-0.2	0.2	-0.3	0.1	0.3	0.2	-0.2	0.4	-0.4	0.1	-0.4	0.3	-0.2	-0.2	-0.1	0.4	-0.1	0	-0.1
58	0	-0.7	0.4	-0.7	0.1	0.4	0.2	-0.1	-0.4	0	0.1	0.2	-0.1	-0.4	0	-0.4	-0.6	0.4	-0.4	0.1	-0.4	0.4	0.1	-0.4	0	-0.4	0	0.2	0	0	-0.2	0
59	-0.1	0.1	-0.1	0.1	-0.4	0.1	0	-0.2	0	-0.1	-0.6	-0.3	-0.4	0.1	-0.1	0	-0.2	0	0.3	-0.6	-0.3	-0.4	0.1	-0.2	0.2	0.2	0.3	-0.2	-0.3	0.1	-0.2	0
60	0.5	-0.1	-0.1	0.2	-0.1	0.1	-0.1	-0.4	0.3	0.1	-0.1	-0.2	0.2	0.1	0	0	-0.1	0.1	-0.5	-0.1	-0.1	-0.5	0.1	-0.1	0.1	0.1	0.2	0.1	-0.1	0.1	-0.2	-0.2
61	-0.2	0.1	0.1	0.4	-0.2	0.2	0	-0.2	-0.6	0.1	-0.3	0	0.3	0.2	0.2	0.1	0.1	0.1	0.3	0.2	0.3	-0.1	0	0	-0.2	0.1	0.3	-0.6	-0.1	0	-0.1	-0.2
62	0.2	0.1	0.1	0.1	0.4	0.5	-0.2	0.2	0.1	0.2	-0.3	0	0	-0.6	0.3	0.1	-0.2	0.3	-0.4	0.1	0	-0.1	0.1	-0.3	-0.4	0.1	-0.4	0.1	-0.2	-0.6	0	-0.3
63	-0.1	0	0.9	-0.1	-0.1	-0.3	-0.1	0.1	0	-0.3	-0.3	0	0	0.2	-0.1	0	-0.1	0.3	-0.2	0.1	0.5	-0.1	0	0	0	0	-0.1	0.1	-0.1	0	-0.1	0
64	-0.1	-0.2	-0.1	0	0.2	-0.1	0.1	-0.1	0.1	-0.2	0.1	0	0.1	-0.1	-0.4	0	0.1	0	-0.2	0.4	0.1	-0.2	0.1	-0.1	0.1	-0.2	-0.2	-0.1	0	0	0	0
65	-0.2	-0.1	-0.3	0	0.1	0	0	0	0	-0.1	-0.3	-0.3	-0.3	-0.1	0	-0.1	-0.3	-0.8	0.2	-0.3	-0.1	0.5	-0.5	0	-0.2	-0.3	-0.1	-0.2	-0.1	0.1	-0.1	-0.2
66	-0.1	-0.2	-0.1	-0.1	0	0.1	0	0.1	-0.1	-0.1	-0.1	0	0.1	-0.2	0	-0.4	-0.1	-0.2	-0.2	0	-0.1	-0.1	-0.2	-0.1	0	-0.1	-0.1	0	-0.1	0.1	0.1	0.1
67	-0.1	0.1	-0.1	0	-0.2	-0.3	0	-0.4	-0.1	-0.1	0.1	-0.4	0	0.1	-0.1	-0.1	0.5	0.2	-0.2	-0.2	-0.2	0.1	0.4	0	0	0.1	0	-0.1	-0.1	-0.5	0.1	-0.1
68	-0.1	0.1	-0.1	0.1	0.1	-0.1	0.1	0.1	0.1	-0.1	-0.2	-0.1	0.1	0	0.1	-0.1	0.1	-0.1	0	0	-0.1	-0.1	0.1	0	-0.1	0	0.1	0.1	0	-0.1	0	-0.1
69	-0.4	-0.1	0	-0.1	0	0.1	-0.2	0	-0.3	-0.4	-0.3	-0.5	0.4	0.2	0.1	0	0.1	-0.4	-0.2	-0.2	-0.2	-0.2	-0.5	-0.1	-0.3	0.1	-0.4	0	0.6	0	-0.1	0.1
70	0.1	-0.6	0.3	0.4	-0.2	0.2	-0.2	0.2	-0.7	0.1	-0.5	0.7	0.2	-0.4	0.6	0.3	0.4	-0.5	-0.6	-0.1	-0.6	-0.2	0.1	-0.8	0.2	-0.1	-0.3	0	-0.1	0.2	-0.1	-0.7
71	0.1	-0.4	0	-0.1	0.1	-0.1	-0.1	-0.1	0	0.3	0	0.2	0.1	0	-0.1	0.5	-0.1	0.3	0.1	-0.2	-0.1	0.2	0.5	0	0.1	-0.2	-0.4	-0.1	-0.1	0.1	0.4	-0.1
72	0.1	0.1	0.1	0.1	0.1	0.1	-0.1	-0.1	-0.1	0	0.1	0.1	-0.1	-0.1	0.2	-0.2	0.2	0.1	0.1	-0.1	0.1	0.1	0.1	0	0.1	-0.1	0.1	0.2	0	0	0.1	0

i	1	2	3	4	5	6	7	8	9	10	11	12	13	14	15	16	17	18	19	20	21	22	23	24	25	26	27	28	29	30	31	32
73	0	0	-0.1	-0.2	-0.1	0.1	-0.1	0	0.1	0	-0.1	-0.2	0	0.1	0.1	0.1	0.1	0	-0.1	0.2	-0.1	-0.1	0.1	-0.1	0.1	-0.1	0.1	0.2	0.1	0	0	-0.1
74	0.1	-0.1	0.1	0	0.1	0.1	-0.1	0.1	0	0	0	0.2	0	0.1	-0.2	-0.1	0.1	0.2	-0.1	0	0.1	0	0	0.1	-0.1	-0.1	-0.1	-0.1	0	0	0.1	-0.1
75	0	0	0	-0.1	0.1	0	0.1	-0.1	0.1	-0.1	-0.2	0	-0.2	0	0.2	0.1	0	-0.1	0	0.1	-0.1	0	-0.1	0.1	-0.1	0.1	0.1	0.2	0	-0.1	0.1	0.1
76	0.1	-0.1	0	-0.1	0	0.2	-0.1	0.1	-0.1	-0.2	-0.2	0.2	0.1	-0.2	-0.1	0.1	-0.1	0	-0.1	0.1	0	-0.1	-0.2	0	0	0	0.4	0.1	0	0	-0.2	0
77	-0.2	0	-0.1	0	0	-0.3	-0.1	0.1	-0.1	0.4	-0.1	-0.1	0.1	-0.1	-0.2	-0.4	0.1	-0.1	-0.1	-0.1	0.3	-0.1	-0.3	0.1	0	0	-0.1	0	0.1	0	-0.1	0.1
78	-0.1	-0.3	0	-0.6	-0.2	-0.2	-0.2	-0.2	-0.4	0	-0.7	-0.3	-0.4	-0.5	0.1	0.1	0.2	-0.4	-0.5	0	0	-0.4	-0.8	0.2	-1	-0.3	-0.1	0.4	-0.2	-0.3	-0.4	0
79	0.3	0	0.1	-0.1	-0.1	-0.1	-0.1	-0.1	-0.2	-0.1	-0.7	0	0	-0.2	0	0.1	0	0.2	0.1	-0.5	-0.1	0	-0.3	-0.1	0	0.1	0.5	0	-0.2	-0.2	-0.5	0.1
80	-0.1	-0.1	-0.1	-0.1	0.1	0	-0.2	0.2	-0.1	-0.2	-0.1	-0.1	-0.3	-0.1	-0.1	0	-0.1	-0.2	0	-0.5	0.1	-0.1	-0.2	0.1	0.8	0.1	-0.3	0.2	-0.1	0.1	-0.1	-0.2
81	-0.1	0	0	-0.4	0.1	0	-0.4	0.2	0	0.1	-0.3	0	0	-0.7	-0.1	0.1	0.2	0.3	0.1	-0.3	-0.4	-0.2	0.2	-0.5	0	-0.4	-0.2	0	-0.1	0.1	-0.3	-0.2
82	0.4	-0.2	0	0	0	-0.3	0.4	0.1	-0.1	-0.1	-0.1	-0.1	0	-0.1	0	-0.3	-0.1	-0.1	-0.2	-0.1	0.1	0	0	0	-0.1	0.1	-0.2	0.2	-0.2	-0.1	-0.2	-0.1
83	-0.4	0.1	-0.1	0	0.1	-0.1	-0.2	0.1	0.1	0.3	0.1	0.4	-0.4	-0.2	0	-0.2	0.1	0.6	0.8	0.3	-0.2	0.1	0	-1.3	-0.7	-0.3	0	-0.3	0.4	0	-0.1	-0.1
84	-0.5	0	-0.1	0	0.2	0.1	-0.2	-0.6	-0.1	0	-0.3	0	0.1	0	-0.3	0.1	-0.3	0	0	-0.2	0.2	0.1	-0.1	-0.6	-0.2	0.1	-0.2	0.1	0.1	-0.3	0.1	-0.1
85	-0.1	0	0.1	-0.8	-0.1	-0.8	0	-0.1	-0.6	-0.6	-0.1	0	-0.1	0.2	-0.2	-0.2	0	-0.4	0.1	0.2	0.4	0.3	-0.6	0.2	-1.2	0.3	0.6	-0.4	0.1	0.2	-0.1	0
86	-0.3	-0.1	0.3	0.1	0	-0.4	0.4	-0.1	-0.1	-0.4	0.6	0.1	0.1	-0.2	0	-0.1	0.1	0.4	0.1	0.1	0	-0.1	0.5	-0.1	0	0.2	-0.2	-0.1	0.1	-0.1	0.5	0.1
87	0	0	0.2	0	0.1	-0.2	0	0.1	0	-0.2	0	-0.1	0	0	0	0	0.1	0.1	0	-0.1	0.1	0	0	-0.1	0	-0.1	-0.3	0	-0.1	-0.1	-0.1	-0.1
88	0.1	0	0.5	-0.2	-0.1	0.2	-0.1	0.1	-0.3	-0.3	-0.1	-0.3	0.8	-0.1	0.1	0.2	-0.3	-0.3	0.3	-0.3	-0.1	-0.4	-0.4	-0.2	0.1	0.1	-0.1	0	-0.5	0.1	-0.2	-0.1
89	-0.2	-0.4	-0.3	-0.4	0	0	0.2	-0.2	-0.1	-0.3	0.4	0.2	-1.1	0.4	0.1	-0.1	-0.1	0.3	0.6	0.3	-0.1	-0.2	0.2	0.4	-0.4	-0.2	-0.3	-0.3	0.3	-0.5	0	-0.8
90	0.1	0	0.1	0	-0.2	0.1	0.1	0	-0.1	-0.1	0	0.1	0.1	-0.1	0	-0.1	-0.3	0.1	0.1	-0.1	-0.1	0	0	-0.1	-0.2	-0.2	0	0.1	0	-0.1	0	0
91	0	-0.1	0	0.2	0	0.1	0	0	0.1	0.1	0	0	-0.2	0.1	-0.1	0.2	0	0.2	0.1	0	-0.1	0	-0.1	0	0.1	-0.1	0.2	0	0.1	0	0.1	0
92	0	-0.3	-0.3	-0.3	-0.2	-0.1	-0.2	-0.1	-0.2	-0.3	0.2	-0.1	0.1	0	-0.1	0.1	0.1	-0.6	-0.2	0	0	-0.1	-0.4	0.1	-0.1	0.1	-0.2	-0.3	-0.1	0	0.1	0
93	0	0.1	-0.1	0.1	-0.1	-0.1	0.1	0	0.1	0	-0.1	0.1	0.2	-0.1	-0.1	0	0	0	0	0.2	0.1	0	0	0	-0.2	-0.2	0.1	0.1	0.1	0.1	-0.2	0
94	-0.1	-0.1	0	-0.1	-0.1	-0.1	0	0.1	0	0	-0.1	-0.1	0	0.1	0	-0.1	-0.5	-0.1	0.1	-0.3	0.1	-0.2	-0.1	-0.2	0.3	0	0	-0.1	-0.1	0.2	0.1	0.1
95	0	-0.1	0	-0.1	0	0	0.1	0.1	-0.1	0.1	-0.2	0.1	0.1	0.1	-0.2	0	0	0	0.1	0	0	-0.1	-0.2	0.1	0.1	0.1	-0.2	0.1	0.2	0	0	0.2
96	-0.1	0	-0.1	0	-0.1	0	-0.1	-0.1	-0.1	0.1	0	-0.1	-0.2	-0.1	0.1	0.3	-0.1	-0.1	0	-0.1	0	0	0	-0.1	0.4	-0.1	0.6	0	0	-0.1	-0.1	0.1
97	0	-0.4	0.1	-0.2	0.2	0.3	0.1	0	-0.2	0	-0.6	0	0.2	0.3	-0.4	0.3	0.6	-0.5	0.1	0.2	0.6	-0.1	0.3	-0.2	0.2	0	-0.5	0.2	-0.1	-0.4	-0.3	-0.1
98	0.1	0.1	0	0	-0.1	0	0.2	0	0.1	0	0.1	-0.2	0.1	0	-0.1	-0.1	0.2	-0.1	-0.1	0.1	0.1	0	-0.1	-0.2	0	-0.1	0	0.1	-0.1	0	0.1	0.1
99	-0.2	-0.1	-0.1	-0.2	0	-0.2	0	0	0.1	0.1	0	-0.1	-0.1	0	0.2	-0.1	-0.1	0	-0.1	0.1	0.1	-0.1	-0.1	0	0	0	0	0	0	-0.1	-0.1	0.1
100	0	-0.2	0.1	-0.1	-0.1	0.1	0.1	-0.1	-0.3	-0.1	-0.2	-0.6	0	0	-0.1	0.1	0	-0.1	-0.2	-0.1	-0.2	-0.2	-0.2	0	0.1	0	-0.1	0	-0.2	0.1	-0.1	0.1
101	-0.3	0.2	-0.2	0.2	-0.1	-0.6	-0.2	-0.1	0	-0.6	-0.5	-0.1	-0.2	0	0.2	0.2	0	-0.2	-0.1	0.2	0.1	0	-0.3	0.5	0	0.1	0.2	0.1	0.2	-0.2	-0.2	0.1
102	0.1	0.1	0	-0.1	0	0.1	0	0.1	-0.1	-0.1	0	0.2	0.1	-0.1	0.1	-0.6	-0.1	-0.1	-0.1	0.3	-0.1	0	0.1	-0.1	-0.3	-0.1	0	-0.5	0	-0.1	0.1	-0.1
103	-0.1	-0.1	0	-0.1	0.1	-0.1	-0.1	0.2	-0.1	0	-0.1	-0.1	0.1	-0.1	0.1	-0.1	0	0	0	0	0.1	0.1	0	0	-0.1	0.1	0.1	0.1	0	0.1	-0.1	-0.2
104	0	0	-0.1	0.1	0.1	0.2	0.1	0	0.2	0	0.1	-0.1	-0.1	-0.1	0.1	0.4	-0.1	-0.1	0.1	0.2	0	0.1	-0.2	0.1	-0.1	0.2	0.5	0	-0.2	-0.1	-0.1	0
105	-0.2	0	-0.1	-0.4	-0.1	-0.2	-0.1	-0.3	0.1	-0.2	0.2	-0.3	0.1	0.2	0.1	-0.4	0.2	0.3	0.3	-0.5	0.1	0.2	0.2	0.1	0	-0.1	-0.9	0	-0.1	-0.4	-0.1	0.1
106	0.5	-0.2	0.1	0.2	-0.5	0.2	-0.2	0.2	-0.7	0.2	0.5	0.1	-0.2	0.4	-0.2	-0.2	-0.5	-0.4	0	0.4	-0.1	-0.1	0.2	-0.1	-0.1	-0.4	0.3	0.4	0.1	0.4	0.1	0.1
107	-0.1	-0.1	0	0.1	-0.1	0	0	0.2	0.1	0	0.1	0.1	0.1	0.1	0.1	0	0	0.2	0	0	0.1	0.1	-0.2	0	-0.1	0	0.1	0.1	-0.1	0.1	0	0.1
108	0	0.1	0.1	0.2	0.5	0.1	-0.2	-0.1	-0.2	-0.1	-0.2	0.1	0.1	-0.1	-0.1	0.3	-0.1	-0.1	0	0.6	0.6	0.1	-0.1	-0.1	-0.1	0	-0.1	0	0.4	0	-0.1	0
109	-0.2	0.1	-0.1	0	0	-0.1	-0.1	-0.1	-0.2	0.1	0.1	0.2	0	-0.1	0	0	-0.1	0	0.1	0.2	0.1	0	0	-0.1	0	-0.1	0.2	0.1	0.1	0	-0.1	-0.1
110	-0.2	0.5	-0.1	0.2	0.4	0.1	0.1	-0.1	-0.2	0.1	-0.1	0.1	-0.1	0	0.1	0	-0.1	0.4	-0.1	0	0	0	0.5	0.1	0	0.4	0	-0.2	0	0.1	0	-0.2
111	-0.4	-0.2	0	-0.2	-0.4	-0.4	-0.3	0	-0.4	0.2	0.1	0.3	-0.4	-0.2	-0.3	-0.6	0.1	0	-0.6	-0.1	-0.1	-0.6	-0.1	-0.4	-0.1	-0.3	-0.3	-0.1	0.1	0	0.3	0.2
112	-0.1	-0.3	0.2	-0.6	-0.5	-0.4	-0.2	0	-0.3	0.2	-0.1	-0.1	-0.6	-0.2	-0.2	0.2	-0.3	0.1	0.2	0.1	-0.3	-0.3	-0.9	0.5	-0.2	-0.1	-0.9	-0.2	0.4	0	-0.1	-0.4
113	-0.1	-0.1	0.1	-0.1	-0.2	-0.1	-0.1	0	-0.1	0.1	-0.1	-0.1	-0.1	0.1	0	0	-0.2	0	0.1	0	-0.1	0.1	0.1	0.1	0.1	0.1	0.1	0.2	0.1	-0.1	0.1	-0.1
114	-0.2	0.2	-0.1	0.1	-0.1	0	0	-0.1	-0.3	0	-0.2	0	0.2	0	0.1	0	0.1	-0.1	0.1	0.1	0.1	-0.1	-0.1	-0.1	-0.5	-0.1	-0.1	-0.1	0	0.1	-0.2	0
115	-0.1	0	0.4	0	0.1	-0.1	0	0.1	-0.2	-0.1	-0.1	-0.3	-0.4	0.1	0	0.1	-0.1	0.2	0.1	-0.5	-0.1	0	0.2	0	-0.1	-0.1	0	0.1	0	0.1	-0.1	0
116	-0.1	-0.1	0.3	-0.5	0.1	-0.1	-0.5	-0.1	-0.2	-0.1	0.1	-0.5	-0.5	0.3	-0.1	0	0.3	-0.3	0	-0.7	-0.2	-0.2	-0.1	0	-0.1	0.1	-0.1	-0.4	-0.2	-0.1	0	-0.2
117	-0.1	-0.2	-0.2	0.1	0.1	-0.1	0	-0.1	0	-0.1	0.1	0.1	-0.1	0.1	0	0.1	0.1	0.1	0	-0.1	0.1	-0.2	-0.2	0.1	-0.1	0.1	-0.1	0	0.1	0.1	0.1	0.1
118	-0.1	0	0.8	0.1	0	0.7	-0.1	-0.1	-0.1	-0.2	-0.7	-0.1	0	0.1	-0.1	0.8	-0.4	-0.2	0	-0.2	-0.4	-0.2	0.1	-0.4	-0.1	0	-0.4	-0.1	-0.2	0	0	0
119	-0.2	-0.1	0.1	0.1	0	-0.1	-0.1	0	0.1	0	-0.1	-0.1	0.5	0.1	0	0.1	-0.3	-0.1	-0.1	-0.2	-0.1	0	-0.1	0	0.4	0	0.3	0.2	0.1	-0.2	-0.1	0
120	0.1	-0.3	-0.5	0	-0.3	-0.2	0.1	-0.3	-0.3	-0.4	0.3	-0.1	0	0.2	-0.4	0	-0.1	-0.2	-0.5	-0.1	0.1	0.2	-0.8	-0.5	-0.2	-0.7	0.1	-0.9	0.1	0	0.1	-0.3
121	0.1	-0.1	0.1	-0.3	0	0	0.1	0.1	0.1	0	0.3	-0.1	0.1	-0.2	-0.1	0.1	-0.1	0	0	-0.3	0.2	0.1	0.1	-0.1	0.1	0.1	-0.3	-0.2	-0.2	-0.2	0.2	-0.1
122	0.1	-0.1	-0.1	0.1	-0.8	0	-0.8	0.1	-0.1	0.4	-0.2	0.1	0	0	0	0.1	-0.4	0.2	-0.1	0.2	-0.7	-0.3	-0.1	0.3	-0.1	0.2	-0.1	-0.5	-0.3	0	-0.1	0
123	-0.1	-0.1	0.1	-0.1	0.4	0.4	0.1	-0.5	-0.1	-0.6	0.4	0.4	0	-0.2	0.1	0.1	0	-0.4	-0.3	-0.3	0.1	-0.1	0.1	-0.2	0.2	0	-0.1	-0.2	-0.3	-0.1	-0.2	0.4
124	0.3	0.1	-0.3	-0.2	0	0.1	-0.1	-0.1	-0.4	-0.2	-0.4	0.1	0	-0.1	-0.1	0.4	-0.3	-0.2	-0.4	-0.2	0	0	-0.2	-0.2	0.3	0.2	0.5	-0.1	0	0.1	-0.1	0
125	-0.3	-0.2	-0.4	0.8	0	0.3	-0.2	-0.1	-0.1	0.6	-0.1	0	-0.2	-0.1	-0.1	0.1	0	0.3	0.1	-0.4	-0.5	-0.1	0.6	0.1	-0.3	0.1	0.4	0	-0.2	0	-0.1	-0.1
126	-0.1	-0.1	-0.1	0	-0.1	-0.2	0.2	0	0	0.5	0.1	0.1	0	-0.3	-0.1	0	-0.2	-0.1	-0.1	0.4	0	0	0	-0.1	-0.3	-0.1	0	0.1	0.1	0	0	0.1
127	-0.2	0	-0.3	0	-0.1	-0.3	-0.3	0.2	0.2	0	-0.2	0.1	0.1	-0.1	0.3	-0.1	0	0.1	-0.1	-0.1	-0.1	0.1	-0.1	0.1	-0.2	-0.2	0	-0.1	0	0.2	0.3	-0.3
128	0.1	-0.3	0	0	0	0	0.5	-0.2	0.1	0	0	-0.1	0	-0.2	-0.3	-0.4	-0.3	-0.3	0.4	-0.2	-0.1	0	0.1	-0.1	-0.2	-0.1	-0.2	0.1	0.4	0	0	0
129	-0.4	0.1	0.1	0.1	-0.3	-0.1	0.2	0.3	0	0	0.2	0.2	0	-0.2	-0.2	0	0	-0.4	-0.3	0	0.2	0	0.1	0.2	0.1	0.1	-0.2	0.1	-0.2	-0.3	0	0.1
130	0	-0.1	-0.1	0.1	-0.2	-0.1	-0.1	-0.2	0	0	0.1	0.2	0	-0.1	-0.1	-0.2	0.1	-0.1	0	0.1	-0.1	-0.1	0	0.1	0.1	0.1	-0.1	0.2	0.3	-0.2	0.1	0
131	-0.1	0.1	-0.1	-0.1	0.1	0.4	0.2	0	0.1	0	0	0.2	0	0.2	0	0	-0.2	0.3	0.2	0.1	0	0.1	-0.1	-0.4	0.2	0	0.1	0.1	-0.1	0	-0.3	0.1
132	-0.7	-0.3	-0.2	-0.7	-0.6	-0.1	-0.2	-0.2	-0.3	-0.7	0.2	-0.6	-0.5	-0.2	-0.2	-0.1	-0.1	0	0.2	0.9	0.1	0.2	-0.6	-0.2	0.1	0.9	-0.2	0.7	0.5	-0.8	-0.1	-0.2
133	-0.4	-0.1	-0.5	0.2	0	-0.9	-0.1	0.1	0.3	-0.1	-0.4	0	0.2	0.1	-0.2	-0.2	0.1	0.2	-0.3	-0.2	0.2	0	-0.2	-0.2	-0.1	0	0.6	0.7	0.3	0.1	-0.2	-0.1
134	-0.4	-0.1	-0.2	-0.1	0	-0.3	0.4	0.1	0	-0.5	0.2	0.3	-0.3	0.1	0	0.6	0.4	0.5	-0.1	-0.3	-0.1	-0.4	0.2	0.1	-0.1	0.2	0.5	-0.4	0.2	0	0.2	-0.1
135	-0.1	0.1	0	-0.1	0	0	0.1	0	-0.1	-0.1	0	0.1	0	0	0.1	-0.2	0	-0.1	0	0	0.1	0.2	0	0	0.1	-0.1	-0.1	-0.1	0	0.1	0.1	0.1
136	0	0.1	0	0.1	-0.2	0.1	0	0.2	-0.1	0	-0.1	-0.1	0	-0.1	-0.2	-0.1	-0.1	0.1	0	0	0.1	0	0.1	0.1	-0.1	0.1	0.1	0.1	-0.1	0.1	-0.1	0
137	0.6	-0.1	-0.2	-0.1	-0.2	-0.5	-0.4	-0.1	0.1	-0.3	-0.1	0	-0.4	-0.1	-0.1	-0.4	0.4	-0.4	0	0.4	-0.5	-0.1	-0.2	-0.4	-0.3	-0.3	0.1	-0.1	0.2	-0.1	0.2	-0.1
138	-0.1	-0.1	0	0.1	0	0	0.1	0	0.1	0	-0.1	0	-0.2	-0.2	0.1	0.1	-0.1	0	-0.1	0.1	0.1	-0.2	0.2	0	-0.1	0.1	0.1	0	0	-0.1	-0.1	0.1
139	0	-0.1	0.4	0	-0.1	-0.3	-0.4	-0.1	-0.2	-0.3	-0.3	-0.3	0.4	0	-0.1	0.5	-0.1	-0.6	-0.5	0	-0.3	-0.5	-0.9	0	0.4	0	0.7	0.3	-0.2	0	-0.2	-0.3
140	-0.1	-0.1	-0.1	-0.1	0	0	0	-0.1	-0.1	0	0.1	0.1	0.1	-0.1	0.1	0	0	-0.1	0.1	0	0	-0.1	-0.1	-0.1	0.1	0.1	0	0	-0.2	0.1	0.1	0.1
141	-0.2	-0.2	0	-0.1	-0.1	-0.1	0.1	-0.1	-0.1	0.4	-0.4	0	-0.4	0	-0.1	0.4	0	0.1	0	-0.1	0.1	-0.5	0.2	-0.1	-0.2	0.2	-0.2	-0.1	0.6	-0.1	-0.2	0.1
142	0	-0.2	-0.1	0	0	0	0.2	0	0	0	-0.1	-0.1	-0.1	0	-0.1	-0.2	0	-0.1	0.3	-0.1	0	0	-0.1	0.1	0	0.2	-0.4	-0.3	0.1	0.1	-0.1	-0.1
143	0.3	-0.6	-0.3	-0.2	0.4	-0.2	0.2	0.2	0	-0.1	0.2	-0.1	0.2	-0.1	0.2	0.4	-0.2	-0.2	-0.6	0.4	0.2	-0.4	-0.1	0	0	-0.2	0.4	-0.5	-0.4	0	-0.7	0.5
144	0.2	-0.1	0.1	-0.3	-0.3	-0.3	0.1	-0.3	-0.4	-0.2	-0.2	0	-0.7	-0.2	-0.2	0.6	-0.1	0	0.1	-0.2	-0.2	0	0.1	-0.1	-0.5	-0.1	-0.1	-0.1	0.4	-0.3	-0.3	0.1
145	0	0	0	-0.1	0	0.2	0	0	0	0	0.1	0	-0.1	-0.1	-0.1	-0.4	-0.3	0	-0.1	-0.1	0	-0.1	0.1	-0.3	-0.1	0.1	-0.1	0.1	-0.1	0.1	-0.4	0.1
146	-0.1	-0.5	0	-0.1	-0.4	0	0.2	-0.4	-0.3	0	0	0.2	-0.3	-0.3	-0.5	-0.2	-0.2	0	0	-0.1	0.1	-0.3	-0.1	-0.5	-0.1	0.4	0	-0.7	0.3	0.3	-0.6	-0.2

i	1	2	3	4	5	6	7	8	9	10	11	12	13	14	15	16	17	18	19	20	21	22	23	24	25	26	27	28	29	30	31	32
147	-0.4	-0.1	-0.3	0	0.2	-0.4	0.1	-0.3	0.1	-0.1	0.1	-0.2	-0.3	0	-0.1	-0.1	-0.1	0	0.1	-0.2	0	-0.2	0	0.1	-0.2	-0.1	-0.1	-0.1	-0.2	-0.3	-0.4	-0.3
148	0	0.1	0.1	-0.1	0	0	-0.3	0.1	-0.3	0	-0.1	0	-0.1	-0.3	0	0	0.1	-0.2	-0.1	-0.2	0	-0.3	-0.2	-0.3	-0.1	-0.1	-0.1	-0.2	0	0	0.1	0
149	-0.2	0.1	0	-0.7	-0.3	-0.1	-0.3	0	-0.1	-0.2	0.3	-0.1	-0.5	-0.3	-0.5	-0.3	-0.4	0	-0.7	0.1	-0.1	0.3	-0.1	0	-0.1	-0.4	0.1	-0.3	0.2	0.2	0.4	0.4
150	0	0.1	0	-0.1	0.1	-0.2	0.1	0.1	-0.1	-0.1	0	0.1	-0.4	0.1	-0.1	-0.1	-0.2	-0.3	-0.1	-0.4	0.1	-0.1	-0.1	-0.1	0	-0.1	-0.6	0.1	-0.1	0	-0.3	-0.1
151	0	-0.1	0.1	-0.1	0.1	0.1	-0.1	0.1	0	0.1	-0.1	0.2	-0.5	-0.4	0	-0.6	-0.2	0.1	-0.1	-0.4	0	0	0.1	0	0	-0.2	0	-0.4	0	-0.2	0	0.1
152	-0.1	0.1	0.1	-0.1	0.1	-0.1	-0.5	0.1	0.5	0	0.2	0.1	-0.1	0	0.1	-0.5	-0.2	0.4	-0.1	-0.2	0.1	0	0	0.1	0	-0.1	-0.2	-0.1	0.2	-0.1	0.2	-0.1
153	-0.1	-0.1	0	-0.1	0.2	0.1	0.1	0.1	0.1	0	0.1	-0.1	-0.1	-0.1	0.1	-0.1	-0.1	0	-0.1	0.2	0.1	0.1	-0.1	0.1	-0.1	0.1	0.1	-0.1	-0.1	-0.1	0.1	0.1
154	-0.1	0.1	0	0	0.1	-0.1	0.2	0.4	0.1	0.6	-0.1	0.1	-0.2	-0.1	-0.2	-0.1	0.1	0.2	0	-0.1	-0.2	0.2	0.5	0.1	-0.1	-0.1	-0.2	-0.1	0.5	-0.1	0	0.2
155	0.1	0	0.1	0	0	0	0.1	-0.2	0.1	-0.1	-0.2	-0.2	0	0.1	0.1	0.2	0	-0.2	0	0	-0.1	0.2	-0.1	-0.2	-0.2	0.1	0.2	0	0.3	0.1	0.1	-0.1
B1	-0.2	-0.2	-0.1	-0.2	-0.1	-0.2	-0.1	-0.1	-0.2	-0.1	-0.2	-0.1	-0.2	-0.2	-0.1	-0.1	-0.1	-0.1	-0.2	-0.2	-0.1	-0.1	-0.1	-0.2	-0.2	-0.1	-0.2	-0.2	-0.1	-0.3	-0.1	-0.2

Table D.3 continued…

i	33	34	35	36	37	38	39	40	41	42	43	44	45	46	47	48	49	50	51	52	53	54	55	56	57	58	59	60	61	62	63	64
1	0	0.1	0	0	0.2	0.1	-0.1	0.2	0	-0.1	0	-0.4	-0.1	-0.2	0.1	-0.2	-0.5	0.1	0	-0.1	-0.4	-0.1	0	0.3	-0.1	-0.1	-0.3	0.2	0.1	0.2	0.1	-0.2
2	0.2	0.2	0	-0.2	0.2	0.2	-0.2	0.1	-0.1	0.1	-0.2	-0.1	0.1	0	-0.1	-0.1	0	0.2	0.1	-0.2	0	-0.2	0.1	0	0	-0.3	0.2	-0.1	0.2	-0.1	0.1	-0.1
3	0.2	0.2	-0.3	0	0.3	-0.2	0.1	-0.1	0.2	-0.1	-0.2	0.1	0.1	-0.3	0.1	0	-0.2	0	0.2	0	0.1	0.1	0	0	-0.1	0.2	-0.1	-0.2	0	-0.2	0.2	-0.2
4	0	0	0	0	-0.2	-0.4	0.1	0	-0.1	0	0	-0.4	-0.3	0	-0.4	0	0	-0.3	0	0	0	-0.1	-0.1	0.1	0.1	-0.2	0	-0.2	-0.2	-0.1	-0.1	0.3
5	-0.1	-0.1	0	-0.2	0	0.1	0.1	0	0	0	0	0.1	0	0.1	0	-0.4	-0.4	0.1	0.1	0.1	-0.2	0	0.2	0	0	0	0.2	-0.2	0	-0.1	-0.1	0
6	0.3	0	0	-0.1	-0.1	0	-0.3	0	0	0.1	0.1	0	-0.1	0.2	-0.2	0.2	-0.1	0	-0.1	-0.2	-0.2	0	0	-0.1	0	-0.1	-0.1	0	-0.2	0.2	-0.1	0.1
7	0.1	-0.4	0.2	-0.3	0.1	0.2	0	0.2	-0.3	0	0.5	-0.1	0	0	-0.4	-0.1	0	0.1	-0.2	0.1	0	0	0	-0.2	0.4	-0.3	0.2	-0.3	0.1	-0.1	-0.2	0
8	-0.2	0.1	-0.1	0.1	0	-0.1	0.1	0	-0.1	0	-0.1	-0.1	0	0	-0.1	-0.1	0	-0.1	-0.1	0.1	0	0.1	0	0.1	-0.2	-0.1	0	0	0.1	0.2	-0.2	0
9	-0.1	-0.1	0.2	0.2	0.1	-0.1	0	-0.1	-0.1	-0.1	-0.2	0.1	0.1	0	0.2	0	0.1	0	0	0.2	-0.1	0.1	-0.2	0	-0.2	-0.1	-0.2	0.2	0.3	0	0.1	0
10	-0.1	-0.1	0	0	0	0	-0.2	0	0.1	0	0	0	0.1	-0.1	0.1	-0.2	0	-0.2	0.2	-0.1	0	-0.1	0.1	-0.2	0.1	0	-0.2	-0.1	0	-0.1	0.2	-0.1
11	0	0	-0.1	0.1	0	-0.1	0	-0.2	0	-0.1	0.1	-0.3	-0.1	0.2	0.2	-0.2	-0.1	0	0	-0.2	0	0	0.1	0.1	0.1	-0.1	0.1	0	-0.2	-0.1	0.1	-0.2
12	-0.3	0	-0.8	0.1	0	-0.1	0.1	0	-0.3	-0.9	-0.4	0.4	-0.5	0.1	0.1	0	0	0.1	0.1	0.1	-0.2	-0.7	-0.5	-0.2	0	0.1	-0.4	0.1	0.1	-0.1	-0.2	-0.2
13	-0.2	-0.2	0	-0.3	0	0.1	-0.1	0.1	0	0	0.1	0	-0.2	-0.3	0	0	-0.1	0.2	0	0	-0.1	0.1	-0.4	-0.2	0.2	0	0	-0.4	0	0.1	-0.4	-0.4
14	0	0.1	-0.2	-0.1	0.3	0	0.1	-0.1	0.1	-0.1	-0.1	0	0	-0.2	0.1	0.1	0.1	-0.1	0	0	0	-0.2	0	-0.1	0.1	0	0	0.1	-0.3	0.1	0.1	-0.1
15	0	0	0	0.1	-0.3	-0.2	0.1	0.2	-0.2	-0.4	-0.4	0.1	0.2	0	0	-0.3	-0.1	0	-0.1	-0.3	0.2	0.2	0.1	-0.3	-0.2	0.2	-0.1	-0.2	0.2	0	0	0.1
16	-0.1	-0.2	0.2	0	0	0.1	0.1	0	0.1	0.4	-0.1	0.1	-0.2	-0.1	0.1	0.1	0	0	-0.1	-0.1	0.1	0.1	0.1	0.1	0.1	-0.1	0.1	-0.3	-0.1	0.1	-0.2	0
17	-0.1	0.1	0.1	0.1	-0.1	-0.1	0	0	-0.1	-0.1	0.2	-0.3	-0.3	0.1	0	-0.2	0	0	0.1	-0.1	-0.1	-0.1	0.2	0	0	-0.1	0	0	0	-0.3	-0.2	0.2
18	-0.2	0.2	0.1	-0.1	-0.1	0.2	-0.2	0.2	0	-0.1	0	-0.1	-0.1	-0.1	-0.2	0.2	0.1	0	0.1	0.3	0.1	0.3	0	0	0	0.3	0.1	0.2	0.1	0.2	0	0
19	-0.1	-0.2	0.3	0.2	0	0	0	0	0.2	0	-0.1	0	0.1	0.2	-0.1	-0.2	-0.2	0.1	0.1	0.3	-0.1	0	-0.2	-0.1	0	0	0.3	0.1	0	0	0	-0.1
20	-0.1	-0.1	0	-0.1	0.1	0.3	-0.1	0	-0.1	0	-0.1	-0.1	0.1	-0.3	0	0.1	0.3	0.2	0.2	-0.3	-0.2	0	0	0	-0.1	0	0.2	0.1	-0.1	0.2	0	0.1
21	0.1	-0.1	0.2	0	0.1	0	0.1	0.2	-0.1	-0.1	0	0.1	0	0.1	0	0.1	-0.1	0	-0.1	-0.3	0.2	0.1	0.1	0.2	0	0.1	0.1	-0.1	0.3	-0.1	-0.1	-0.2
22	-0.1	-0.1	0.1	0	0.1	0	-0.1	-0.1	0.2	-0.1	0	0	0.2	0.1	0	-0.1	0	-0.1	0.1	-0.1	-0.1	0.5	-0.2	0.3	0.2	0	0.2	0	0	0.2	-0.2	0.2
23	-0.1	-0.4	0	0.1	-0.1	0	0.1	0	-0.3	-0.1	-0.1	-0.2	-0.1	0.2	0	-0.1	0.2	-0.3	0.1	-0.1	0.1	-0.1	0	0.1	-0.1	-0.1	0	-0.2	0.2	0.1	-0.2	0.2
24	0.2	-0.3	-0.1	-0.1	0.1	-0.2	0.1	0.1	0	0.1	-0.1	0.2	0.1	0.2	0.1	0.2	-0.3	0.1	0.2	0	0.2	0	0.1	-0.3	-0.1	-0.2	0	0	0.2	0.2	0	-0.3
25	0.2	-0.2	-0.2	0.1	0.3	-0.1	0.3	0	-0.3	-0.1	-0.2	0.1	0.3	-0.4	0	0.3	0.1	0.2	0	-0.1	0.3	-0.1	0.3	0.2	-0.2	0.1	0.1	-0.2	0.1	0.1	-0.1	-0.1
26	-0.2	-0.1	-0.2	0.1	-0.2	0	0.3	0.1	0.1	-0.1	0.2	-0.1	-0.3	0.1	-0.4	0	0	-0.2	0.2	-0.2	-0.2	0	0.1	0.1	0.2	0.1	0.1	-0.2	-0.2	0.3	-0.3	0.2
27	-0.1	0.1	0	0.2	0	-0.1	-0.2	0	-0.3	-0.1	-0.1	0	-0.5	-0.3	0	-0.1	-0.5	-0.1	-0.2	0.1	0.1	0.1	0.2	0.3	0.1	0	-0.1	-0.1	-0.2	0.1	-0.2	-0.1
28	0	0	-0.1	0	-0.1	-0.1	0.2	0	0.2	0	-0.1	-0.1	0.2	0	0	0	0.3	0.1	-0.1	0	0	0	0	0	0	0.1	-0.1	-0.1	0	0	0	0.2
29	-0.4	-0.1	0.1	0.1	0.1	0.1	0	0.1	-0.4	0.1	-0.2	0.1	-0.1	-0.2	0	0.1	0.1	0	0.1	0.1	-0.1	-0.1	0.1	-0.1	0	0	-0.4	-0.1	-0.3	0.1	0.2	0.2
30	0	-0.3	-0.4	-0.5	-0.1	0.4	0.1	0.1	0.1	-0.1	-0.3	-0.2	0.1	0.2	0	0.1	-0.2	0.3	-0.3	0	0	0	-0.3	-0.3	0	-0.1	-0.1	-0.1	0.2	0.1	0	0.1
31	-0.1	0	0	-0.1	-0.4	0.1	-0.7	0.2	-0.1	0.1	0.4	-0.4	0	0.1	-0.3	-0.3	0	-0.1	-0.2	0.2	-0.2	-0.1	-0.1	0.1	0	-0.1	-0.2	-0.1	0	0	0	0.1
32	-0.5	-0.8	-0.2	-0.2	0.2	0	0.2	0.5	0	0.2	-0.2	0.2	-0.1	0	-0.5	-0.2	-0.1	0.2	0.1	0.2	-0.3	-0.1	-0.2	0.1	0.3	0	0	-0.5	0.1	0.2	-0.5	0.6
33	-0.3	0.1	-0.2	0.1	0.1	0	0.1	0.1	-0.1	0	-0.4	-0.1	-0.2	-0.1	-0.4	-0.2	-0.2	0	-0.1	-0.1	0	-0.1	0	-0.2	0	-0.1	-0.2	-0.2	-0.1	-0.2	-0.1	-0.2
34	-0.4	-0.3	-0.1	-0.1	0.3	-0.3	-0.6	-0.2	-0.8	-0.3	0.3	-0.2	0.1	-0.2	0	-0.1	0.1	-0.3	0.1	0	-0.2	0	-0.2	-0.1	0.1	0	-0.1	-0.3	0.2	0	-0.3	-0.5
35	0.1	0.1	-0.1	-0.6	-0.2	-0.2	0.1	-0.2	-0.1	-1	-0.2	-0.1	-0.2	0	0	0	-0.1	-0.3	0.1	0.1	-0.4	0.1	0.1	0	0	-0.1	0.1	0.2	-0.3	0	-0.2	0
36	0.3	-0.3	0	0	0	-0.1	-0.1	0	0.4	-0.3	0	0	0	0	0	0	-0.1	-0.1	0	-0.2	0.1	-0.1	-0.1	-0.1	-0.1	-0.1	-0.1	-0.2	0	-0.1	0.1	-0.2
37	0.1	-0.3	0	-0.1	0	0.1	-0.2	-0.5	0	-0.1	0	-0.1	0.1	-0.4	0.2	0.1	-0.3	0.1	-1.1	-0.3	0.2	0	0	-0.8	0	0.1	-0.3	-0.4	-0.2	0	-0.2	-0.8
38	-0.3	-0.3	0	-0.1	-0.1	-0.1	-0.3	0	-0.2	-0.2	-0.1	-0.1	-0.2	-0.2	-0.3	-0.2	-0.3	0	-0.2	-0.2	-0.1	-0.1	-0.3	-0.2	-0.1	-0.1	-0.3	-0.1	-0.2	0	-0.1	-0.1
39	-0.5	-0.2	0	0.1	0.2	0.4	0.2	0.2	-0.1	-0.4	-0.2	-0.1	0	0	-0.2	-0.4	-0.3	-0.3	0	-0.7	-0.1	-0.2	-0.3	-0.3	-0.2	-0.3	-0.1	0	-0.3	-0.2	-0.2	0.3
40	-0.1	0.1	0	-0.4	-0.6	-0.2	-0.1	-0.3	-0.4	0.9	-1.1	0.3	-0.2	0.4	-0.5	-0.3	0.1	0.1	-0.4	-0.7	-0.1	-0.1	-0.2	0.4	-0.2	-0.2	0.1	0.1	0	0.3	0.1	0.2
41	-0.2	-0.3	0.1	-0.3	-0.3	-0.2	-0.4	0.2	-0.3	0	-0.1	-0.4	-0.2	-0.2	-0.2	-0.1	0	0	-0.1	0.2	-0.4	-0.5	-0.8	-0.4	-0.4	-0.1	-0.5	-0.2	-0.2	0	0	-0.6
42	0.2	-0.2	-0.2	0.1	0.3	0	-0.2	-0.4	-0.6	-0.1	0	0.4	0.1	0.1	-0.3	0.3	0.1	0.2	-0.2	-0.3	-0.3	-0.1	-0.3	-0.1	-0.1	-0.3	-0.1	-0.1	0	-0.3	0	-0.5
43	-0.4	-0.1	-0.4	0	-0.2	-0.4	0	-0.1	0.1	-0.3	0	-0.2	-0.3	0.1	0	-0.1	-0.6	-0.3	0	-0.2	0	-0.3	-0.1	-0.3	0	0.1	0.1	-0.3	-0.1	-0.2	0	0
44	0.1	-0.2	-0.1	-0.3	0	0.1	-0.1	-0.1	0	0.1	0	0	-0.1	-0.1	0	-0.1	0	-0.3	-0.2	0	0	0.1	-0.1	0.1	0.1	-0.1	-0.2	-0.1	0	0.2	-0.1	-0.2
45	0.1	-0.1	0	-0.2	0	-0.1	-0.4	0.2	-0.2	-0.1	0.1	-0.2	-0.2	-0.1	0	-0.4	-0.2	0.1	-0.1	-0.2	-0.5	0	-0.1	0	-0.2	-0.2	-0.3	0	-0.2	-0.2	-0.1	-0.5
46	-0.4	0.1	-0.1	0	-0.2	-0.8	0.1	0.2	0	-0.2	-0.1	-0.1	0.4	0	0.2	0	-0.2	-0.1	0.2	0.1	0	-0.4	-0.1	-0.2	-0.3	-0.1	-0.8	-0.1	0	-0.1	-0.1	-0.3
47	-0.2	-0.1	0	-0.2	0.2	-0.1	0	-0.4	-0.3	-0.3	0.5	0.3	-0.3	-0.7	0.2	-0.8	-0.1	-0.1	-0.6	0.1	0.4	-0.3	-0.2	0.3	0	-0.1	0.4	0.1	0.3	-0.3	0	0
48	-0.5	-0.2	-0.1	-0.2	0.2	0.1	-0.1	-0.1	0	0.2	0.5	-0.3	0	-0.6	0.5	0	-0.3	0.1	-0.1	0	-0.3	-0.3	0.1	0	-0.1	0.5	0	-0.1	-0.1	-0.1	-0.2	0
49	0.1	-0.1	0	0	0.1	0.1	-0.1	0.1	-0.1	0.1	0.1	0	0	-0.1	0	0.1	0	0.1	0	0	0	0	0.1	0	-0.1	0.1	-0.1	-0.1	0	-0.1	0	-0.1
50	-0.1	0	0	0.1	-0.1	-0.2	-0.2	-0.2	0	-0.1	0	0	0	0.4	0.3	0.1	0	0.2	-0.2	0.4	0	0	-0.2	0	0.3	-0.1	-0.2	-0.3	-0.1	0.5	-0.1	-0.6
51	0	-0.1	-0.2	0.1	-0.1	0.1	0.1	0.1	0.1	0	0.1	0.1	0	0.1	-0.1	0.1	-0.1	0.2	-0.1	0	0	0	0.1	-0.1	0.1	0.1	0	-0.1	0.1	0	-0.1	0.1
52	-0.1	-0.7	0.3	-0.2	0.2	0.3	-0.4	-0.1	-0.2	-0.1	0.1	0.1	-0.4	-0.3	0	0	-0.3	-0.3	0.2	-0.4	-0.1	0.3	0.5	-0.4	0.6	0.3	0.5	0.1	0.2	-0.2	0.2	-0.6
53	-0.2	-0.1	-0.3	-0.3	-0.2	0.1	-0.1	-0.2	0	0.1	0	0	0.1	-0.1	-0.2	0.2	0	0	-0.2	0	-0.4	0	-0.2	-0.2	-0.2	0	0	0	0.1	-0.2	-0.2	0.1
54	0	-0.1	0.1	-0.1	-0.5	0.1	0.1	0.1	0.1	-0.1	0.2	0.1	-0.2	0.1	0	-0.1	-0.1	-0.1	0.3	-0.1	-0.2	0.4	-0.1	0.1	-0.1	0.8	-0.1	-0.1	-0.1	-0.5	0	0
55	-0.1	0.1	0.1	0	0	0	-0.1	0.1	0	0	0.2	0	0.1	0.1	0.1	0	0	0	0.1	0	0.1	-0.1	0.2	0	0	0.1	0	-0.1	0	-0.1	0	0
56	0	0.1	0.2	0.3	0.2	-0.1	0	0.1	-0.1	0	-0.2	-0.4	0.2	0.1	-0.3	-0.3	-0.1	0.2	0	0	0.1	-0.4	-0.1	0	-0.6	-0.3	-0.7	0.1	-0.1	0	0	0
57	0.5	-0.1	-0.4	-0.1	0.3	-0.3	-0.6	-0.1	0.1	0.1	-0.2	-0.2	-0.2	-0.3	-0.2	-0.1	-0.3	-0.3	0.1	0	-0.5	-0.4	-0.8	-0.4	-0.1	-0.1	0	-0.1	0.3	0.2	-0.2	-0.2
58	0.4	-0.2	-0.4	0.3	0	0	0.1	0.2	-0.2	-0.1	0	0.5	-0.2	0.3	-0.2	0.4	-0.2	0.4	0	-0.5	0	0.1	-0.2	-0.2	-0.2	-0.1	-0.2	0.2	0.4	0.8	0.3	0

i	33	34	35	36	37	38	39	40	41	42	43	44	45	46	47	48	49	50	51	52	53	54	55	56	57	58	59	60	61	62	63	64
59	-0.2	-0.1	0	0.2	-0.3	0.1	0.1	-0.9	0.2	-0.2	0	-0.6	-0.2	-0.1	0	0	-0.6	0	-0.2	-0.3	-0.8	-0.1	0.1	-0.1	0	-0.4	0.1	-0.1	0.2	-0.3	-0.1	-0.3
60	-0.2	0.2	-0.4	0	0.1	-0.1	0	0.3	-0.7	-0.3	-0.2	0.3	-0.1	0	-0.2	-0.4	-0.2	0.3	0.5	-0.3	0.2	0.3	0.1	0.4	0	-0.1	-0.4	0.3	0.2	0.1	0	0.1
61	0.1	0.4	-0.4	-0.3	0.4	0	-0.5	-0.7	0.2	0.2	0.1	0.1	0	-0.2	0.2	0	-0.5	0	-0.1	-0.5	0.3	0.3	0.1	-0.5	-0.9	0	-0.6	-0.2	0.3	0.1	0.4	-0.3
62	-0.3	0.2	0	0.1	0	-0.4	-0.5	-0.1	-0.8	0.1	-0.2	-0.4	-0.5	-0.4	0.5	0.2	-0.4	0.2	-0.2	0.4	-0.7	-0.3	0	0.3	-0.3	0.4	-0.1	0.4	0.1	0.3	-0.4	0
63	0	-0.4	0	0.1	0.4	0	0	-0.1	0	0.2	0.2	0	0.4	0.1	-0.4	0	-0.1	0.1	-0.2	-0.2	0.2	0.1	-0.1	-0.4	0.1	0	0	0	0.1	-0.3	-0.1	0.4
64	-0.1	-0.4	0.1	-0.1	-0.2	-0.1	0.3	-0.2	-0.1	-0.1	0.1	-0.1	-0.2	0.1	-0.3	-0.1	-0.1	0.2	-0.1	0	0.1	-0.1	0	-0.3	0	0.5	0	-0.1	-0.1	-0.2	-0.1	0
65	-0.3	0.2	-0.1	0.1	-0.3	-0.3	-0.1	-0.2	-0.2	-0.9	0	-0.4	0	-0.1	0	-0.2	-0.3	-0.2	0	-0.6	0	0	0.2	-0.2	-0.1	-0.2	0.3	-0.1	0.2	-0.2	-0.5	-0.3
66	0.1	0.1	0	0	0	-0.1	-0.2	0.1	0	-0.2	0	-0.2	0.1	-0.1	-0.1	0	0	-0.1	-0.4	0	0.1	0.3	-0.1	-0.1	-0.1	-0.1	0.1	-0.1	0.1	0.1	-0.6	0.1
67	0.1	-0.4	0.1	0.1	0.2	0.3	0.2	0.1	-0.2	-0.1	-0.1	0.1	0	0	0.1	-0.3	-0.1	-0.3	-0.1	-0.3	0.1	-0.1	0	0	0	-0.3	0.1	0.2	-0.3	0.1	-0.1	-0.1
68	0.1	0	-0.1	0	-0.2	0.1	-0.1	-0.1	0.1	0	0.1	0.1	0	-0.1	0.1	0	0.1	-0.1	0	0	0.1	0.1	0.1	-0.1	0	0	0.2	0	-0.1	0	0.1	-0.1
69	0	-0.3	0	0.5	-0.3	0.1	-0.5	-0.7	0	0.2	0.1	-0.1	0.5	0	1	0.2	-0.2	-0.8	0.3	-0.3	0	0.5	0.7	0.3	0	0.4	-0.1	-0.1	-0.1	-0.4	0.4	-0.3
70	-0.3	0.1	-0.1	0.3	-0.1	0.2	-0.1	-0.2	-0.2	-0.5	0.2	-0.2	0.2	0.2	-0.4	0.2	-0.1	-0.5	-0.1	-0.2	-0.1	-0.2	0.3	-0.4	-0.1	0.1	0.4	-0.5	-0.2	-0.1	-0.6	0.5
71	-0.1	-0.3	0	0	1	0.1	0.2	0.4	-0.1	-0.3	0.1	-0.1	-0.2	0.1	-0.4	0.1	-0.1	0.4	-0.1	0.3	0.1	0.1	0.2	-0.2	-0.1	0.2	0.1	0	-0.1	0.2	-0.5	-0.1
72	0	-0.1	0	0	-0.1	0.1	-0.2	0.1	0.2	0	0.1	0.1	-0.2	0	0.1	0	-0.1	0.1	0.1	-0.1	-0.1	0.1	-0.1	0	0.1	0.1	-0.1	0	-0.2	-0.1	0.1	0
73	0.1	0.1	-0.1	0.1	0.1	0.2	0	0	-0.1	-0.1	-0.1	0	0.1	-0.1	-0.1	0.1	0	0.1	0	-0.1	0	0	0.1	-0.1	0.1	0.2	-0.1	-0.1	0	-0.1	0	0.1
74	0	0.1	0.1	0.1	0	-0.1	-0.1	-0.2	-0.1	0.1	0.1	0	0	0.2	0	-0.1	0.1	0	-0.2	0.2	0.1	0	0.1	0.2	0	0	-0.1	-0.1	-0.1	0.1	0.2	-0.1
75	0.1	0	0	-0.1	0.1	0.2	-0.1	0	-0.1	-0.1	0.1	0.1	-0.2	0.1	0.1	-0.1	0	0	0	0	-0.1	-0.1	0	-0.1	0	-0.1	-0.2	-0.1	0	-0.1	-0.1	-0.1
76	0	0.5	0	0.4	-0.2	0.1	0.2	-0.1	-0.1	-0.1	-0.1	-0.1	-0.1	-0.1	-0.1	-0.1	0.1	0.2	-0.1	-0.1	-0.1	-0.2	0.1	0	-0.6	0	-0.2	0.1	-0.1	0	0	0
77	0	-0.3	0.1	-0.2	-0.2	0.1	0	0	0.2	-0.2	-0.1	-0.1	0.4	0	0.1	0.2	0.2	-0.2	-0.1	0.1	0.1	-0.1	-0.3	0	-0.1	-0.1	-0.1	0	0.1	0	0.3	-0.1
78	0.4	-0.4	0.3	0	-0.6	0	0.3	0	-0.2	-0.2	-0.3	0	0.3	-0.1	0	-0.4	0	0.3	-0.2	0.4	-0.1	-0.1	-0.4	-0.7	-0.1	0.1	-0.1	-0.3	0.1	-0.2	-0.9	0.2
79	-0.1	0.2	0.2	0.5	-0.1	-0.2	0	-0.1	0.2	0	-0.1	0.2	0.1	-0.2	0.1	0	-0.1	-0.2	0.1	-0.9	0	-0.2	0	0.2	-0.1	0.1	-0.5	0.4	0.1	-0.1	0.2	-0.3
80	0	-0.2	-0.1	0	-0.1	0	0.2	-0.1	0.1	0.4	-0.4	-0.3	0.1	0	0.7	0.2	-0.2	0	0	-0.2	-0.1	-0.2	0.1	0.6	-0.3	-0.1	0.1	-0.2	0	-0.1	0.1	0.1
81	-0.8	-0.8	-0.7	-0.5	-0.2	0	0.2	-0.5	0.3	0.4	-0.2	0	-0.3	-0.1	-0.1	-0.4	-0.1	0.4	0	0.2	0.2	0	0.4	-0.2	0.4	0.1	0.3	-0.3	-0.2	-0.5	-0.4	0.1
82	0.1	-0.2	-0.1	0	-0.4	-0.1	-0.1	-0.1	0	-0.1	-0.2	0.1	-0.1	-0.3	0.1	0.1	-0.1	-0.1	-0.1	-0.4	0	0.1	0	0.2	0.1	-0.2	-0.1	0.2	-0.5	0.5	0.2	0.2
83	0.1	-0.4	0.1	-0.2	0	0	-0.1	0.3	-0.1	-0.2	-0.2	-0.1	-0.4	0.1	-0.2	0.1	0	0.1	-0.1	-0.2	-0.2	-0.1	-0.3	-1	-0.1	0.2	-0.1	-0.4	0.1	0	0.2	-0.5
84	-0.1	0.4	-0.2	-0.9	0.2	-0.3	-0.2	0.5	-0.2	-0.1	-0.1	-0.2	-0.2	0	-0.7	-0.1	-0.4	0.1	-0.7	-0.3	0	-0.1	-0.6	-0.5	0.4	0.1	-0.1	0.1	0.1	-0.1	-0.1	0.1
85	0.6	0	-0.3	-0.9	-0.2	0.4	-0.5	0.1	0	-0.5	0	0.2	0.4	-0.3	-0.3	0.1	0.3	0.2	-0.3	-0.2	0	0.2	-0.3	-0.4	-0.2	-0.1	-0.5	0	-0.1	0.3	-0.8	-0.4
86	0	-0.6	0.1	-0.1	0.5	0.3	0	0.1	-0.1	-0.3	-0.1	0.2	-0.2	0.1	-0.6	-0.1	-0.2	0.2	-0.1	0.1	0	0	-0.1	-0.2	-0.1	0	-0.1	-0.5	0.1	0.6	-0.3	0.1
87	-0.1	-0.1	0	-0.1	-0.2	-0.2	0.1	-0.2	0	0.1	0	0	-0.1	0.2	0.2	0	0.1	0	-0.1	-0.3	0.1	-0.1	-0.1	0	0	0.2	0	-0.1	-0.1	0.1	0	0.1
88	0.3	-0.3	-0.1	-0.1	-0.1	0	0.4	0.2	0.3	-0.1	0.1	-0.1	0.2	-0.5	-0.2	-0.2	-0.1	-0.2	0.5	-0.2	-0.2	0	-0.2	0.6	0.3	0.2	0	-0.3	0.3	-0.5	0.1	0.2
89	-1	-0.2	0.6	0.2	0.2	0	-0.2	-0.4	0	0	0	0.5	-0.3	0.1	0.5	-0.1	0	0.7	-0.2	0.1	-0.1	0	-0.3	0.5	-0.3	-0.3	-0.2	0.1	-0.2	-0.2	-0.1	0
90	0.1	0.1	0.1	0	-0.1	0	-0.2	0	0	0.1	-0.2	0	0	-0.1	0.2	0	0	-0.2	0	0	0.1	0	-0.2	0.4	-0.1	0.1	0	-0.1	0	-0.1	-0.1	-0.1
91	0.1	0.2	-0.1	0.1	-0.1	-0.1	0.1	0.1	0.1	-0.1	0	0	0	-0.1	0.1	0	-0.1	0	0	0	0	0.1	0	0.1	0.1	0.1	-0.2	0	0.1	-0.1	-0.1	-0.1
92	0.2	0	-0.1	0.1	0	-0.3	0	0.1	0.1	0.1	-0.1	0.1	0.1	-0.1	0	0.1	0	-0.1	0	-0.2	-0.1	-0.3	0.2	0	-0.8	-0.2	0	-0.2	-0.4	-0.7	0.2	-0.1
93	-0.1	0	0	-0.1	0.1	-0.2	-0.2	0.1	0.2	0.1	0	-0.1	-0.1	0	0.1	-0.1	-0.2	-0.2	-0.1	-0.1	0	0	0	0	0.1	-0.2	0.1	0	0.1	0	0.1	-0.1
94	0	0	0.1	0.1	-0.1	-0.1	-0.1	0	0	0	0	-0.4	0.1	0	0.3	-0.1	-0.1	0	0.1	0.1	-0.1	0.1	0	0.2	0.1	-0.1	-0.1	-0.1	0	-0.1	-0.1	-0.1
95	-0.1	0	0	0	0.1	0.1	-0.1	0.1	-0.1	0	-0.1	-0.1	0.1	0	0.1	0.2	0.1	0.1	0.1	0.1	-0.1	-0.1	0	-0.1	0.2	-0.1	-0.1	0.1	0.2	0	-0.1	-0.1
96	0.3	0	-0.2	-0.1	-0.1	0	-0.2	-0.1	-0.1	-0.1	0	-0.3	0	-0.1	0.1	-0.1	-0.1	0.3	0	0	-0.1	0	-0.3	0.1	-0.2	-0.1	0	-0.3	0.1	-0.1	-0.1	-0.2
97	0	-0.8	-0.2	-0.4	-0.4	0.2	-0.1	-0.3	-0.2	0	-0.1	-0.3	0	-0.1	-0.2	-0.6	0	0.1	-0.5	-0.1	0	-0.2	-0.3	0	-0.2	0.2	0.1	-0.4	-0.3	0.1	-0.4	-0.3
98	-0.1	0.1	0	0.1	-0.1	0.1	0.1	0	0	0	0	0.1	-0.1	-0.1	-0.1	0	-0.1	-0.2	-0.1	0.1	0	0	0.1	-0.1	-0.1	0.1	-0.1	0.1	0.1	0	0.1	0
99	0	-0.2	-0.1	-0.1	-0.1	-0.1	0.2	0.1	-0.1	-0.1	0.1	0	0.1	-0.1	0.1	-0.1	0.1	0.1	0.1	0.2	0	-0.1	0	0	-0.1	-0.1	-0.1	0.1	0.2	-0.1	-0.1	0.1
100	0.1	0.4	0	0	-0.1	-0.2	-0.2	-0.3	0	0	-0.6	-0.5	0.2	0.1	0.7	0	-0.1	0	-0.2	-0.1	-0.2	0.1	0.2	-0.1	0.1	0.1	-0.3	0	-0.1	0.2	-0.2	0.2
101	-0.1	-0.2	-0.1	-0.1	-0.1	-0.1	0.2	0.3	-0.1	-0.4	0.6	0.1	-0.6	-0.1	0	-0.1	0.1	0	0	-0.2	0.2	-0.1	-0.2	-0.2	-0.1	0	0.2	0.2	-0.3	-0.3	-0.6	0.2
102	-0.1	0.2	0.2	-0.2	0.2	0.1	0	0	0.1	0.1	0.2	-0.4	0	-0.1	-0.1	0	-0.1	0	0	-0.1	-0.1	-0.1	-0.2	0	0	-0.1	0.1	0.1	-0.1	0	0	0
103	0.1	-0.1	-0.1	0.1	-0.1	-0.1	-0.2	0	0.1	-0.1	0	0	0	0	0.1	-0.1	-0.1	0	0.1	0.1	0.1	-0.1	0	0	0	0.1	0	-0.1	0.1	0	0.2	-0.1
104	0.1	-0.1	0.1	-0.1	0.8	0	0.1	0.2	0.1	-0.4	-0.2	0	-0.2	0	0	0.1	0.1	0.2	-0.2	0	0.1	0	-0.1	0	0	-0.2	0	0.1	0.2	0.1	-0.3	-0.1
105	-0.1	0	-0.5	-0.2	0.3	0	0.2	-0.8	0.1	-0.2	0.1	0.1	-0.4	-0.3	0	0.4	-0.2	-0.1	0.4	-0.1	-0.4	-0.4	-0.1	-0.1	-0.3	0.3	0.3	-0.6	0.2	0.2	-0.4	-0.3
106	0.2	0	-1.1	0	0.1	-0.2	0	-0.1	0.3	-0.4	-0.4	-0.2	0	0.5	0	0	-0.1	-0.1	-0.4	0.3	0.2	-0.2	-0.2	0.2	-0.6	0.1	-0.2	0.1	0.2	0.5	0	-0.1
107	0	-0.1	0	-0.1	0	0.1	-0.1	-0.1	0	-0.2	-0.2	0.1	0.1	-0.1	0.1	0.1	0.1	0	0	-0.1	0.1	-0.1	0	-0.1	0.1	0	0.1	0	0	-0.1	0.1	0.1
108	0	-0.1	0.1	0.1	-0.2	-0.1	0.3	-0.1	-0.3	0	-0.4	-0.1	-0.1	0.5	-0.1	0	0	0.2	0.1	0.5	0	-0.1	-0.1	0.8	-0.2	0	-0.2	-0.2	-0.1	0.1	-0.2	0
109	0	0.1	-0.1	-0.2	0.1	0.1	-0.1	0	0.1	0	0.1	-0.1	-0.1	-0.1	0.1	0	-0.1	0.1	0.1	-0.1	0	-0.1	0.1	0	0	-0.1	0	0	0.1	-0.1	-0.1	0.1
110	-0.2	-0.1	-0.1	-0.1	-0.1	0.3	-0.1	0.1	-0.1	0.1	0	0.2	0	0	0	0.2	0.2	0.5	-0.1	-0.1	0	0.2	0.1	-0.1	0.3	-0.1	0	-0.1	0.6	0.3	0	-0.2
111	-0.4	0	0	0.1	-0.2	-0.1	-0.2	-0.2	-0.3	0.1	-0.4	0.4	0.4	-0.2	0	-0.2	0.3	0.2	0	0.2	-0.6	-0.4	-0.2	-0.6	0.3	0.1	0.1	-0.4	0.2	0	-0.1	-0.3
112	0.1	0.2	-0.1	0	-0.2	-0.2	0.1	0.7	-0.4	-0.6	0	0.3	0	-0.5	-0.1	-0.1	0.4	0.1	0	0	0.1	-0.2	-0.2	0.6	-0.3	0.3	-0.1	0	0.2	-0.6	-0.1	-0.2
113	-0.1	0	0.1	-0.1	-0.2	-0.1	0.1	0	0.1	-0.2	0.1	0.1	0	-0.1	0	0	0.1	0	0.1	-0.1	0.1	0	0	-0.1	-0.1	-0.1	0	0	0	0	0	0.2
114	-0.1	0	0.1	0	0	0.3	-0.2	-0.1	0.1	-0.1	-0.2	-0.1	0	0	0.3	0.1	-0.1	0	-0.1	-0.1	-0.2	0	-0.2	0	0.2	0.1	-0.2	-0.1	-0.1	0.1	0.1	0.1
115	0.5	0	0.1	0.1	0	0	0	0.1	0.1	-0.1	0	0	-0.1	0	0.1	0	0	-0.2	0	0	0	0.1	0	-0.3	-0.2	0.1	-0.1	-0.2	0.1	-0.1	0.1	0.4
116	-0.2	0.2	-0.2	0.1	-0.4	-0.2	-0.2	-0.6	0	-0.6	0.3	-0.4	-0.3	-0.1	0.1	0.3	0	0.2	0.3	-0.1	-0.3	0.4	-0.1	-0.2	0	0.3	-0.6	0.2	-0.4	-0.6	-0.2	-0.1
117	0.1	-0.1	0.1	0	-0.1	-0.1	-0.2	0	0.1	0	-0.1	0.1	0	0.1	-0.1	0.1	0	0	0	0.1	0.1	0	-0.1	0	-0.1	-0.1	0	0.2	-0.1	-0.1	-0.1	0
118	0	0.3	0.1	-0.1	-0.2	-0.1	-0.1	-0.4	-0.1	-0.5	-0.1	0	0.5	0	0.3	0.2	0	-0.3	-0.1	-0.2	0.2	0	-0.2	-0.3	-0.1	0.4	-0.1	-0.2	0	-0.5	0.3	-0.1
119	0.2	0	0.2	-0.1	-0.1	-0.1	0.1	-0.1	-0.1	0.8	-0.2	-0.2	0	0.1	0.1	0.1	-0.2	-0.1	0.1	-0.1	0	0.1	-0.1	-0.1	-0.1	0	0	0	-0.1	0.1	0.1	-0.2
120	-0.2	-0.5	0.1	0.6	0.2	-0.3	-0.1	0.2	0.5	-0.4	-0.3	-0.2	-1	-0.1	0.1	-0.6	-0.2	0.3	-0.3	0	0.2	0	0	0	-0.1	0.3	-0.5	0	0.2	0.4	0	-0.6
121	-0.1	0	-0.1	-0.1	0.1	0.2	-0.1	-0.2	-0.1	-0.1	0	0.1	0.1	-0.1	0.1	-0.1	0	-0.1	0	0	0	-0.5	-0.1	0.1	0	-0.2	0.1	-0.1	-0.1	0	0	0
122	0	0	-0.1	0	0	-0.1	0.2	0.3	0.1	0.1	-0.3	-0.1	-0.1	0	-0.1	-0.3	0	-0.1	-0.4	-0.1	-0.3	-0.1	-0.1	0.2	-0.1	0.1	-0.1	0	0.1	-0.3	-0.1	-0.1
123	-0.1	0	-0.1	0	0.3	0	-0.4	0.3	0.1	0.2	0.6	-0.1	0.2	0.1	-0.1	-0.1	0	0	-0.5	-0.1	-0.3	-0.1	-0.8	-0.1	0.2	-0.2	0.3	0.1	0.2	-0.2	0.3	0.2
124	0.5	0.3	-0.1	-0.2	0	0	0.3	-0.2	-0.1	0	-0.1	-0.1	0.4	0	0.1	-0.1	0.1	-0.1	-0.5	-0.3	0.1	0	0.3	0	-0.1	-0.1	0.1	0.1	-0.1	-0.5	0.1	-0.5
125	0.1	0.3	0.1	-0.1	-0.3	-0.1	-0.4	-0.1	-0.1	0	0	-0.3	0.1	0.1	-0.1	-0.1	0	0	-0.2	0.2	0.3	0	-0.1	-0.1	0	-0.1	0.1	0.1	-0.1	-0.1	-0.1	-0.2
126	0.3	-0.6	-0.2	0	0.5	-0.1	-0.1	-0.2	0	-0.1	0.7	-0.1	-0.1	0.1	-0.4	0	-0.1	0.2	-0.1	0.2	0.1	0.2	0.1	-0.1	-0.1	0	0	-0.5	0	0	0	-0.1
127	-0.3	0	0.1	0.1	-0.4	0.1	-0.2	-0.5	-0.5	0	0.1	0	0	-0.2	-0.1	0.1	0.1	-0.2	0.1	-0.1	0	0.1	-0.1	0	-0.2	0	-0.2	-0.2	0.1	0	0.2	-0.2
128	-0.1	-0.1	0	-0.2	-0.2	-0.1	-0.1	-0.1	0	-0.3	-0.5	0	0	0.3	0.2	-0.1	-0.1	-0.2	-0.6	-0.3	-0.1	0	0.1	-0.2	-0.2	0	-0.1	-0.6	0.1	-0.1	0.1	0.1
129	0.2	-0.2	0.4	0.1	-0.1	-0.3	0.5	0.1	-0.1	-0.1	0	0.5	0.2	0	0	-0.1	-0.1	-0.2	-0.6	0.3	-0.3	-0.1	0.2	-0.1	0	-0.4	-0.3	0.2	-0.3	-0.1	0.3	-0.3
130	0.2	0	0.1	0.1	0.1	-0.2	0.1	-0.3	0	0	0.3	0.2	0.1	0.3	-0.1	0	-0.1	0.2	0.1	-0.1	0	0.2	-0.1	-0.1	-0.1	0.1	0.1	0	-0.1	0.1	0.1	0
131	0	-0.3	0	-0.1	0.5	0	-0.2	0.1	0	0	-0.2	-0.1	0.2	0.2	0.1	-0.1	-0.1	0	0.1	0	-0.2	-0.1	-0.4	0	-0.1	-0.2	-0.1	0.2	0	0.4	0.3	0.1
132	0.4	0.2	-0.3	-0.3	0.1	0.2	-0.5	0	-0.2	-0.3	0.4	0.1	-0.1	0.2	-0.2	-0.2	0	0.1	0	0.1	-0.3	0	0	-0.5	-0.4	0	-0.8	0.1	-0.4	0.2	-0.3	-0.1

i	33	34	35	36	37	38	39	40	41	42	43	44	45	46	47	48	49	50	51	52	53	54	55	56	57	58	59	60	61	62	63	64
133	-0.1	0	-0.1	-0.2	-0.3	0.2	-0.3	-0.2	0	0	0.4	-0.4	0	0	0	0	-0.1	0	0.8	0.1	-0.1	-0.2	0.5	0	0	-0.3	0	-0.1	-0.4	0.1	-0.1	0.1
134	0.3	0.2	-0.1	0.1	0.2	0	-0.2	0	0	0.1	0.2	-0.2	-1	-0.3	0.1	0.1	-0.2	-0.1	0	0.2	0.3	-0.1	0.2	0	0.5	0.1	-0.1	0.4	-0.1	-0.4	0.5	-0.4
135	-0.1	0	0	-0.1	0.1	-0.1	0.1	-0.1	0	0	-0.1	0	0	0.2	0	0	0.1	0.1	0	0.1	0	0.1	0.1	-0.1	0.1	-0.1	0	0.2	-0.1	0	-0.2	-0.1
136	0	-0.1	0	0	-0.1	0.1	0.1	-0.1	0	-0.2	-0.2	0	-0.2	0	0	0.1	-0.1	0	-0.1	0.1	0.1	0	0	0.1	0.1	-0.2	-0.2	0.1	-0.1	0	0	0.1
137	-1	-0.1	0.8	0.1	0.2	-0.1	0.2	0	-0.1	0.1	0.2	0.4	-0.1	0	0.1	-0.1	-0.1	0.1	0.1	0	-0.3	-0.2	-0.4	0	-0.5	-1.2	-0.7	0	-0.5	-0.2	-0.4	-0.1
138	0.1	0	-0.1	0	0	0.1	0	0	-0.1	-0.1	0.2	-0.1	-0.1	-0.1	0	0.1	0.1	0	0.1	-0.1	0.1	0	0.1	-0.1	0.1	0.1	-0.1	0.2	-0.2	0.1	0	-0.1
139	0.1	0.4	0.3	0	-0.7	-0.3	-0.4	-0.2	-0.2	0.8	0.3	0	0	0.2	0.7	-0.4	0.1	-0.4	0.7	0	-0.1	-0.2	0.9	0.3	-0.6	0.4	-0.3	0.4	-0.5	-0.8	0.2	-0.1
140	-0.1	0	-0.1	-0.1	-0.1	0	-0.1	0	0.1	0	0.1	0.2	-0.1	0	0	0	0	0	0	0.1	0	-0.1	0	-0.2	0.2	0	-0.1	0	-0.1	0.1	0.1	0
141	0.1	-0.8	-0.1	0.3	0.3	0	0	-0.3	-0.1	-0.7	-0.2	-0.1	-0.1	-0.2	0.1	-0.2	-0.1	0	0	0	0.1	-0.2	-0.1	-0.5	-0.2	0.1	0	-0.5	-0.1	0.1	-0.3	-0.1
142	0	0.1	-0.7	0	-0.2	0.1	-0.2	-0.2	-0.1	-0.2	-0.2	0	0	0.1	-0.5	-0.1	-0.3	0	0.1	-0.3	-0.1	0.4	-0.7	0	-0.3	-0.4	0.2	0	0	-0.3	0.2	0.3
143	-0.1	0	-0.3	0	0	0.2	0	0.2	-0.5	0.4	-0.3	0.1	0.3	0	0	0.5	-0.1	-0.3	0.1	0.3	0.1	0.4	-0.4	0	0.1	0.1	-0.1	0.1	-0.5	0.4	0.2	0.1
144	0	0	-0.2	0	0.4	-0.1	-0.5	0	-0.2	0.4	0.1	-0.4	-0.2	-0.5	-0.2	0.4	-0.3	-0.1	0.1	0.7	0.3	0.1	-0.3	0	-0.3	0.1	0.3	0.2	-0.1	0	0.1	-0.3
145	-0.1	-0.3	0	-0.2	-0.1	-0.2	0	0.1	-0.1	-0.1	-0.2	-0.1	0.1	0.1	0.3	0	0.1	0.2	0.2	0.1	0.2	-0.1	0	0	-0.1	0.2	-0.1	0.1	0	-0.2	0.4	0.2
146	0	0	-0.1	-0.4	0	-0.3	-0.1	0.1	-0.1	0.3	0.1	-0.2	-0.2	-0.2	-0.1	-0.2	-0.3	-0.1	0.4	0.2	-0.5	0	-0.4	0.1	0.1	0.5	0.2	0	-0.3	0	-0.1	-0.1
147	0	0	-0.1	-0.1	-0.2	0	0.2	-0.3	-0.2	0	-0.2	0	-0.3	-0.1	-0.2	-0.2	0.1	-0.1	0.1	-0.1	0	0	0.1	0	-0.3	0.1	0	0	0	0	-0.3	-0.2
148	0	-0.2	-0.1	-0.2	0.1	-0.1	-0.1	-0.1	-0.2	-0.9	-0.2	-0.3	-0.2	-0.2	-0.1	-0.2	-0.1	0	-0.5	0	-0.5	-0.2	-0.2	0	-0.1	-0.1	0.1	-0.2	-0.3	-0.2	-0.1	-0.3
149	-0.4	-0.6	-0.4	-0.5	0.2	-0.1	-0.5	-0.1	-0.3	-0.2	0	0.2	0	0.3	0.1	0.5	-0.1	0.4	-0.3	-0.3	-0.1	0.3	-0.5	-0.1	0.3	-0.2	-1	-0.1	-0.2	0.2	0.5	0.4
150	0.4	0.3	0	-0.1	0	-0.2	0.1	-0.2	0.2	-0.8	-0.1	0	-0.1	-0.1	-0.2	-0.3	0.1	-0.2	0.4	0	0	0	0	0.1	0.1	-0.3	0	-0.3	-0.1	0	-0.2	-0.1
151	-0.1	0.2	-0.1	0	-0.2	0.1	0.1	-0.1	0.1	-0.1	-0.2	-0.4	0	0.1	-0.1	0	-0.1	-0.2	0	0.1	0	0.1	-0.2	0.2	0.1	-0.3	-0.1	-0.1	0.1	-0.1	0	0.1
152	0	-0.2	-0.3	0.1	-0.1	-0.1	-0.4	-0.5	0.1	-0.5	0	-0.4	-0.2	0	-0.4	0.7	0.1	0.3	0.4	0	0.1	-0.4	0	0	0.4	-0.1	0.1	-0.1	0	0	-0.2	-0.1
153	0.1	0	0	-0.1	0.1	-0.1	0.1	-0.1	0	0.1	0	0.1	0.1	0	0	-0.1	0	0.1	-0.1	0.1	0.1	0	0.1	0	-0.1	-0.1	0.1	0	-0.1	0	0	-0.2
154	-0.1	0	0	-0.1	0	-0.2	-0.2	0	0	-0.1	-0.1	0.1	-0.1	-0.2	-0.1	0.1	0.1	-0.1	0.1	-0.5	0	0	-0.4	0.1	0.3	-0.1	0	-0.1	-0.1	0	0	0.2
155	0	0.1	0	0	-0.1	-0.1	0	-0.1	-0.3	0	0.1	0	-0.1	0.2	0	-0.1	0	0.1	0.1	-0.2	0	0	-0.3	0	0.1	0.1	0	-0.1	0.2	-0.2	-0.2	0.1
B1	-0.2	-0.2	-0.2	-0.2	-0.1	0	-0.2	-0.2	-0.2	-0.2	-0.1	-0.1	-0.2	-0.1	-0.2	-0.2	-0.2	-0.1	-0.2	-0.1	-0.2	-0.1	-0.2	-0.1	-0.1	-0.2	-0.1	-0.2	-0.1	-0.2	-0.1	-0.2

Table D.4 - Normalization coefficients of the ANN-V_e's and ANN-Qo_{90} input parameters

Parameter	μ	σ
TVD	2,313.60	451.19
l_l	2,244.27	618.53
lat_{bh}	55.79	0.85
lon_{bh}	-120.27	1.38
d_e	0.36	0.88
V_{inj}	614.59	382.4
Q_f	3.09	12.4
V_{acid}	55.87	78.84
P_c	229.25	1,276.26
N_s	30.68	18.08
l_s	54.85	39.72
d_s	83.64	38.61
C_s	3.04	2.71
t_{sh}	27.52	20.28
p_{inj}	54.08	11.36
q_{inj}	8.39	2.55
ϕ_m	0.08	0.01
GR	110.82	14.2
ρ_b	2.62	0.02
PE	3.52	0.25
k_m	4.19	8.77
B_i	1.93	0.18
h_f	161.61	56.23
S_w	0.22	0.08
p_i	3,756.20	653.65
h_{net}	12.07	12.49

Table D.5 - ANN-Qo_{90} 's weights and coefficients for the second hidden layer

k	1	2	3	4	5	6	7	8	9	10	11	12	13	14	15	16
1	0.3	0.1	0	-0.5	0.3	-0.3	-0.9	0.1	0	-0.6	0.3	-0.8	-0.4	-0.4	0.5	-0.4
2	-0.5	0.4	0.2	0.4	-0.7	-0.3	-0.1	0.1	-0.2	-0.2	-0.4	0.2	-0.1	-0.2	0	-0.3
3	0.3	-0.4	-0.1	0.5	0.2	0.5	0.3	-0.7	0	0.3	-1.5	0.9	0.2	0.4	0.2	0
4	-0.1	0.2	-0.1	0.6	-0.2	0.5	-0.1	-0.4	-0.1	0.5	-0.5	0.7	0.1	-0.1	-0.3	0.8
5	-0.1	0.1	0.4	-0.3	-0.2	0.3	0.9	0.3	-0.2	0.6	-0.2	0.3	0.5	0.1	0.3	0.3
6	-1.1	-0.1	0.6	0	-0.6	0.4	0	-0.1	0.2	0.2	-0.2	0.1	0.1	0	-0.1	0.1
7	0	-0.1	0.1	-1.6	0.2	-0.1	0.1	0.8	0	-0.1	1.6	-0.7	0	-0.2	0.1	-0.5
8	0	0.6	0.1	0.3	0.1	-0.5	0.2	-0.4	-0.2	-0.3	0.2	-0.4	0.4	0.2	0.3	-0.5
9	-0.4	0.2	0.2	-0.5	-0.2	-1.2	-0.5	1.3	0	-0.3	1.2	-0.6	-0.4	-1.5	-0.4	-0.6
10	-0.5	-0.4	0.1	-0.1	-1	-0.1	-0.2	-0.4	-0.1	-0.5	0.1	-0.1	-0.4	0.3	-0.3	0.2
11	-0.5	0	0.5	-0.7	-0.5	-0.7	-1.1	0.5	0	-0.4	0.6	-1.4	-0.3	-0.5	-0.7	0
12	0.2	0	0.3	-0.2	0.1	-0.1	-1	1.3	0	-0.2	0.3	-0.4	-0.8	-0.9	0.1	0.3
13	-0.3	0.1	0.6	0.2	-1.2	0.8	-0.2	-0.4	0	-0.4	-0.3	0.7	0.3	-0.1	0.1	-0.1
14	-0.7	-0.1	-0.1	-0.2	-0.9	0.1	0.1	0.1	0	0.2	-0.2	-0.4	0.5	-0.3	-0.4	0.4
15	0	0.1	0.2	0	0.3	-1.2	-0.1	0.8	-0.1	-0.8	1.2	-1.1	-0.1	-0.5	-0.1	-0.9
16	0	0.1	0	0.2	0.1	0.3	2.5	-0.9	0	0.3	-0.3	0.3	0.6	1.5	0.2	0
17	-0.2	0.2	-0.3	0.7	0.1	0.1	0.9	-0.2	0	-0.6	-0.6	0.5	0.1	0.7	-0.3	-0.6
18	0.4	0.3	-0.1	-1.4	-0.6	-0.1	0.2	0.8	0.1	0.3	1.7	-0.2	0.7	0	-0.1	0.4
19	0.1	-0.2	1	-0.6	-0.4	-0.3	-1	0.4	-0.1	0	0	-0.7	0.4	-1	-0.1	0.6
20	0.1	0.2	0.9	-0.4	-0.4	-0.2	0.1	0.3	0	0.6	0.1	-0.5	0.2	-0.1	0	0.4
21	0	0.5	0.2	0.6	0.4	0.2	-0.2	-0.2	-0.2	-0.4	-0.3	0.3	-0.2	0.1	0.1	-0.6
22	-0.5	0.1	0.6	-0.4	-1	-0.1	-0.2	0.3	-0.2	-0.3	0.2	-0.7	0.3	-0.4	0.1	-0.2
23	0.1	0.1	-0.5	-0.6	-0.2	0.2	-0.8	0.4	0	0	0.4	-0.3	-1	-0.5	-0.2	0.1
24	0	-0.6	-0.2	0.4	0	0.4	0.4	-0.8	0.1	0.1	-0.3	0.5	-0.5	0.5	0.5	0.2
25	-0.1	0.1	0.3	1.4	0	0.5	0.6	-0.3	-0.1	0.1	-0.4	0.5	0.2	-0.3	-0.1	0.1
26	0.2	0	-1.9	0.1	0.9	0	0.3	0	-0.2	-0.8	0.3	0.2	-0.2	0.1	0	-0.2
27	0.2	-0.1	0.1	-0.6	-0.5	-0.8	0	0.5	-0.1	-2.1	0.2	-0.7	-0.1	-0.2	0.2	-1.8
28	0	0	0.1	-0.1	0.1	0.3	1.7	-1.4	0	0.2	-0.2	0.3	0.6	2	0	0.2
29	0.1	-0.2	0.4	0.3	0	-0.6	-0.1	-0.1	0.1	-0.7	0.4	-0.6	0.2	-0.2	0.6	-0.5
30	-0.7	0.3	-0.8	0	-0.2	1.3	-0.5	0.1	-0.1	0.1	0.4	0.9	0.2	0.4	0.4	0.1
31	-0.2	0.1	-0.5	-0.2	0.4	0	-0.7	-0.1	-0.1	0.4	-0.6	-0.3	-1.3	-0.3	-0.1	0.9
32	0.7	-0.1	0.9	-0.2	0	-0.3	0	0.3	0.1	0.7	-0.1	0.1	-0.3	-0.4	-0.1	0.6
33	-1	-0.1	0.5	0.9	-0.8	-0.3	-0.1	-0.1	-0.1	-0.4	-0.4	-0.1	0.3	0.1	0.1	-0.2
34	-0.1	0	0.3	1.3	-0.1	-0.1	0.2	-0.8	-0.1	0.2	-2.3	0.2	0.1	0.2	-0.1	0.2
35	0	0	0.4	0.3	-0.2	0.5	-0.1	-0.1	0	1.7	-0.7	0.4	0.2	0.3	0.1	1.4
36	0.1	0.1	0.4	0.2	-0.2	0	0.6	-0.3	-0.1	0	-0.3	-0.2	1.4	0.1	0	0.1
37	-0.5	0	0.2	0.3	-0.7	0.7	0.2	-0.3	0	0.4	-0.2	0.4	0	0.4	-0.2	0.6
38	0.2	-0.4	0	-0.1	0.7	0.5	0	-0.4	0	-0.2	-0.5	0.2	-0.7	0.5	0.7	0
39	0	-0.6	-0.1	0.7	0.7	0.2	-0.1	0.1	0	0.1	-0.1	0.7	-0.7	-0.3	-0.1	0.5
40	0	-0.3	-0.3	-0.3	-0.2	-0.3	-0.5	0.3	0.2	-1.5	0.4	-0.5	-0.2	-0.2	0.2	-1
41	-0.2	0.2	0.4	0	0	-0.2	-0.1	0.1	-0.2	0.1	0.1	-0.4	0	0	-0.5	0.4
42	-0.3	-0.2	0.5	-0.8	-0.1	-1.1	-0.1	1	0.2	-0.2	0.1	-2	0.4	-0.6	0	-0.1
43	0.2	0.2	0	0.9	-0.2	0.5	0	-0.6	-0.2	0.7	-0.4	0.6	-0.3	0.2	-0.3	0.3
44	0	-0.1	-0.6	-1	0.1	0.3	-0.1	0.2	0.2	-0.3	0.3	-0.4	-0.8	0.4	-0.4	0.2
45	-0.6	0.1	-0.1	0.3	0	-0.1	-0.3	-0.7	0	0.4	0	0.4	-1.2	-0.4	0.3	-0.2
46	-0.3	-0.3	0.4	-0.8	0	-0.9	0.2	0	0.2	0.2	0.7	-0.7	1.1	-0.1	0.6	0.4
47	1.7	0	0.2	0	1	-0.2	-0.1	-0.3	0	-0.2	-0.2	-0.1	0.1	0.1	0.4	-0.4
48	0.4	0.1	-0.5	-0.1	-0.3	-0.2	0.8	-0.2	0.2	0.3	0.1	0.1	0	0.7	1	-0.5
49	-0.4	0	0.3	0.1	-1	0.4	-0.2	0	0	-0.3	-0.2	0.5	0.1	-0.1	-0.3	0.2
50	0	0.1	0	0.7	-0.4	0.1	0.2	-0.8	-0.1	-0.1	-0.8	0.6	0.4	0.6	0.2	0
51	-0.5	0.3	0.4	0.3	-0.3	-0.6	0	0.2	-0.2	-0.1	-0.3	-0.4	0.2	-0.2	-0.3	-0.2
52	0.8	0.1	0	-0.1	0.7	0.8	-0.4	-0.3	0	0.2	-0.5	0.4	0.1	0.3	-0.6	1.2
53	0	-0.1	-0.5	0.3	0.3	0	0.2	0	0	1.5	-0.9	0.3	0	0.5	0.3	1.3
54	-0.7	0	0.6	0.1	0.7	0.2	0	0.5	0	-0.5	-0.6	0.1	0.1	-0.6	-0.5	0.4
55	0.3	0.1	0	-0.2	0.1	0.1	0.6	-0.2	0	0.1	-1	-0.5	1.4	0.6	-0.1	0.2
56	-0.5	0.3	-0.2	0.2	-0.3	0.5	0.2	-0.3	-0.2	0.5	-0.1	0.5	0.2	0.2	0.1	0.5
57	0.4	-0.2	0	0.2	0.2	0	0.3	-0.1	0.2	0	-0.2	-0.1	0.3	0.7	1.1	-0.4
58	0.2	0.1	0	-0.5	0.3	-1.2	-0.2	0.5	0.1	-0.2	0.6	-0.6	-0.2	-0.6	0.3	-0.3
59	0.4	0.1	-0.1	0	0.3	1.3	0.8	-0.7	0	0.2	0.5	0.7	0.8	0.5	0.1	0.5
60	0.4	0.2	-0.9	-0.3	1	-0.7	0.5	-0.1	0	-0.2	0.2	-0.5	0.2	0.4	-0.6	-0.1
61	0.3	-0.4	0.3	-0.3	-0.5	-0.5	0	-0.2	0.2	-0.4	-0.6	0.2	-0.7	0.2	0.2	-0.2
62	0	-0.3	0.4	-0.3	-0.5	0.4	0.1	-0.6	0	-0.6	0.8	-0.1	-0.3	0.4	-1	-0.6
63	0.3	0.2	0.9	-0.6	-0.1	-1.3	-0.6	0.4	-0.2	0.3	0	-1.1	-0.1	-0.4	-0.2	0.1
64	-0.3	0.1	-0.3	0.3	0.2	0.4	0.3	0	-0.2	0.3	0	0.4	-0.3	-0.1	-1.2	0.6
b2	0.2	0	0.1	0.1	-0.5	0.5	0.6	-0.7	0.4	0.4	-0.6	0.6	0.1	0.3	0.1	0.2
W3	0.3	0.1	0	-0.5	0.3	-0.3	-0.9	0.1	0	-0.6	0.3	-0.8	-0.4	-0.4	0.5	-0.4

Table D.6 - ANN-Qo_{90}'s weights and coefficients for the first hidden layer

i	1	2	3	4	5	6	7	8	9	10	11	12	13	14	15	16	17	18	19	20	21	22	23	24	25	26	27	28	29	30	31	32
1	-0.1	0.1	-0.1	-0.2	-0.1	0	0	0.5	0.2	0	0	0.1	0.2	0	0.3	0.1	0	-0.2	0.2	0.4	0	0.3	-0.4	-0.1	0	-0.3	0.3	-0.1	0.4	-0.2	-0.2	-0.1
2	0.4	0.3	-0.5	-0.3	-0.3	0	-0.1	0.1	-0.5	0.4	0.5	0	0.5	0.2	-0.5	0	0.1	-0.3	0.1	-0.2	0.6	0	0.2	-0.1	0	0	0.1	0.1	-0.5	0.2	0.1	0.4
3	-0.3	-0.4	0.6	0.3	0.2	-0.2	-0.2	-0.2	-0.1	-0.4	-0.5	-0.3	-0.6	-0.3	-0.1	0.5	0.5	-0.1	-0.5	-0.5	-0.1	-0.5	0.1	0	0.2	0.4	-0.2	0.2	-0.3	0	0.1	-0.3
4	0.3	0.1	-0.5	-0.3	-0.3	0.1	0.2	-0.1	0.2	-0.1	0.3	0.2	0.1	0.1	0.1	-0.4	-0.1	0.2	0.2	0.1	-0.1	0.2	0.2	-0.4	-0.2	0	0.3	-0.4	0.1	0.1	0.2	0.3
5	0.5	0.2	-0.3	-1	0.1	-0.2	0.6	0.1	0	0.1	0	0.2	-0.3	-0.5	0	-0.1	-0.3	-0.1	0.1	0	0.3	0	-0.1	0.8	-0.1	0	0.3	-0.1	0.3	0.1	-0.1	0.5
6	-0.5	-0.1	0.3	0.3	0.1	-0.1	-0.4	-0.1	-0.5	-0.1	-0.3	-0.2	0.3	-0.2	-0.4	0.2	0	0	-0.1	0	-0.2	-0.7	-0.2	0	0.3	-0.2	-0.5	0.3	-0.1	0.1	-0.1	-0.5
7	-0.1	0.3	-0.2	0.3	-0.1	0.1	0.1	-0.2	0.2	0.1	0.1	0.2	0.1	0.3	0.2	-0.1	-0.1	-0.1	0.4	0.3	-0.4	0.3	0	0.6	0.1	-0.3	0	-0.3	0	0.1	0	-0.1
8	0.3	-0.1	0.1	0.1	0	-0.2	0.4	0.1	0.2	0	0.1	0.1	-0.2	0.1	0.1	-0.1	0	0	-0.1	0.4	-0.4	0.1	0.1	-0.4	-0.2	0.1	0.1	-0.2	0.1	-0.2	-0.1	0.3
9	0	0.2	-0.4	-0.2	-0.4	-0.2	0.1	0.2	0.1	0	0.1	0	0.3	0	0.1	-0.1	0.1	0.2	0.1	-0.2	0.5	-0.2	0.2	-0.2	-0.2	0	0.2	0	0.1	0	0	0
10	0.4	0.1	0.3	-0.4	0.1	0.2	-0.1	-0.1	0	-0.1	0	0.2	0	-0.2	0.1	-0.1	-0.1	-0.3	0.1	0	0	0.1	-0.1	0.1	-0.2	-0.1	0.3	0	-0.1	-0.1	-0.1	0.4
11	0.1	-0.1	-0.2	0.3	0.3	0.4	-0.1	-0.1	0.4	0.2	0.4	0.6	-0.1	-0.1	0	-0.3	0.1	0.1	0.3	0.5	0	0.3	0.1	0	0	-0.2	-0.2	-0.2	0.1	-0.3	0.1	0.1
12	-0.3	-0.1	0	0.3	0.5	0	0.1	-0.5	0.1	0.1	0.2	0.2	0	0.2	-0.2	-0.2	-0.1	0.1	0.5	0.1	-0.3	0	0.4	-0.2	-0.2	-0.1	-0.1	-0.4	-0.5	-0.1	0.2	-0.3
13	0	0.3	0.4	0.4	0	0.3	-0.4	-0.5	0.1	-0.1	-0.1	-0.1	0.4	0.4	-0.1	0	0.2	-0.1	0.2	0	0.2	0.3	-0.1	0	0.1	-0.1	-0.4	-0.2	0	0	0	0
14	0	-0.3	0.1	-0.2	0.1	-0.1	0	-0.1	-0.2	-0.4	0.2	-0.2	-0.4	0	-0.1	0.3	0.1	-0.1	-0.1	0.1	0.2	0.2	-0.2	0.4	0	-0.1	0	0.1	-0.3	-0.1	-0.2	0
15	0.1	0.2	0	0.1	0.1	-0.2	-0.6	-0.2	-0.4	-0.1	0.1	0	0.2	-0.2	-0.2	-0.2	-0.2	-0.8	-0.1	-0.2	0.5	-0.3	0.1	0.6	0.3	0.1	-0.2	-0.1	0.1	0.1	0	0.1
16	-0.4	-0.2	0	0.3	0	0.3	-0.1	0.2	0	-0.3	0.1	-0.1	-0.5	-0.1	-0.2	0.2	0.3	-0.1	-0.1	0	-0.1	0	0.1	0.4	0.1	0.3	-0.1	0.1	-0.2	-0.2	0	-0.4
17	0.7	-0.3	0.4	-0.4	0.2	0.3	0.3	0	0.4	0.1	0.1	0.1	0.5	0	0.1	-0.1	0	-0.2	0	0.5	0.1	0.5	-0.3	-0.1	0.4	-0.6	0.3	-0.2	-0.1	-0.1	-0.3	0.7
18	0	-0.5	0.3	-0.1	0.1	0	-0.1	0	-0.2	-0.1	-0.3	-0.3	0.2	0	0	0.2	0	-0.2	-0.1	-0.4	0.1	0	-0.4	0.2	0.4	0.1	0.3	0	0.2	0.1	-0.2	0
19	0	0.3	0.2	0	-0.3	0	0.1	-0.2	0.2	0.1	0	0.4	-0.3	0.1	0.1	-0.4	-0.1	-0.2	0.1	0	0.2	0	0.3	-0.9	-0.1	0	0	-0.5	0.1	-0.1	0.3	0
20	-0.3	0.3	0	0.1	0	-0.1	0	0	-0.2	-0.1	0.1	-0.1	0	-0.1	-0.1	-0.1	-0.2	-0.1	0	0	0.1	0.2	0.1	0.6	0	0.1	-0.2	-0.1	-0.1	0.2	0.1	-0.3
21	0	0.4	-0.6	0	-0.7	-0.1	0.3	-0.1	0.6	0.3	0.5	0.2	0	0.2	0.4	-0.6	-0.5	0.3	0.1	-0.1	0.1	0.2	0.5	-1	-0.4	0	0.5	-0.6	0.1	0.1	-0.1	0
22	-0.2	-0.2	0.3	0	-0.1	-0.5	-0.1	0	-0.4	0.2	-0.5	-0.1	0.1	-0.3	-0.2	0.1	0.3	0	-0.5	-0.1	0.2	-0.8	0.2	-0.2	-0.2	0.5	-0.3	0.2	-0.7	0.4	0.1	-0.2
23	0.1	0	0.1	0.5	-0.2	0.3	-0.3	0.3	0	-0.3	0.2	-0.2	0.3	0.3	-0.1	-0.1	0.3	-0.2	0	-0.1	0.1	0.4	0	0.2	0.2	0.1	-0.1	0.1	0	0.4	-0.1	0.1
24	0.7	-0.2	0.3	-1.9	0	-0.1	-0.1	-0.1	-0.1	0.6	-0.1	0.7	0.5	0	-0.1	0.1	0.4	-0.1	-0.1	-0.4	-0.1	0.1	-0.3	0.4	0.1	0.1	0.4	0.2	-0.2	0.2	0.1	0.7
25	0	-0.1	0	0.2	0.1	-0.1	-0.1	-0.3	0.1	-0.1	-0.1	-0.1	0	-0.2	-0.1	-0.1	-0.1	-0.2	-0.3	-0.1	0.1	-0.3	-0.1	0.2	-0.3	0.3	-0.1	0.1	-0.3	0.4	0.3	0
26	-0.1	0	-0.1	0.5	-0.2	0.3	-0.2	-0.3	0	0.3	0.4	0.3	-0.2	0	0.1	-0.3	-0.3	0	0.1	0.1	-0.8	0	0.5	0.2	-0.1	-0.3	-0.2	-0.2	0	-0.4	0.7	-0.1
27	0.7	0.1	0.6	0.4	-0.7	-0.1	-0.4	-0.2	0.2	0	-0.4	0.3	-0.2	-0.1	0.3	-0.3	0.5	-0.4	-0.3	-0.1	0.2	-0.3	-0.1	0.1	0	0.1	0.2	-0.2	0.2	-0.1	0.2	0.7
28	0.2	0.5	0.4	-0.5	0	-0.2	0	0.3	-0.4	0	-0.4	0	0.3	-0.2	-0.1	0.2	0.2	-0.1	-0.2	0.1	-0.1	0.5	-0.3	0.6	0.2	-0.1	0	0.3	0.3	0	-0.4	0.2
29	-0.8	0	-0.1	0.8	-0.1	-0.2	0.4	0.2	0.3	0.4	0	-0.3	-0.3	0	0.3	-0.1	0	0.5	-0.3	0.2	0	-0.2	0.1	-0.6	-0.2	0.2	0.1	-0.1	-0.3	-0.2	-0.2	-0.8
30	0.7	0.4	-0.1	-0.6	0.3	-0.2	-0.2	-0.1	0.1	-0.4	0.1	0.3	0	-0.2	0	0.1	-0.2	-0.1	0.1	0.1	0.4	-0.1	-0.2	-0.4	0.2	-0.1	-0.1	0	-0.2	-0.3	0.4	0.7
31	-0.3	0.5	0.1	0.6	0.6	0.9	0.1	0	0.2	0.1	0.2	0.6	0.8	0.3	0	-0.2	0.1	0.2	0.2	0.5	0.2	0.8	0.4	-0.1	-0.3	-0.5	-0.2	-0.5	0.2	0.2	0.2	-0.3
32	0.3	0	1	-0.4	0.8	0.5	0.1	-0.4	-0.7	0.4	-0.7	0	0.2	0.1	-0.4	0.5	0.2	-0.3	-0.6	-0.7	0.2	-0.3	-0.4	0.6	-0.3	0.1	-0.1	0.7	-1.2	-0.1	-0.5	0.3
33	-0.3	0.1	0.1	0.2	1.5	-0.4	0.4	-0.2	0.3	-0.5	-0.1	-0.1	-0.7	0.1	-0.3	0.2	-0.6	0.5	-0.2	0.4	0	-0.8	0.3	-0.1	-0.2	0.1	-0.1	0	-0.1	0.5	-0.5	-0.3
34	0.3	0.3	-0.4	-0.1	-0.4	0.5	0	0.9	-0.1	0.4	0.4	0.2	0.6	0.5	0.1	-0.2	-1	-0.2	0.5	0.8	-0.6	1.1	0	-0.1	-0.2	-0.8	-0.1	-0.2	-0.1	-0.2	0	0.3
35	0.1	0.3	-0.3	-0.6	-0.5	-0.1	0.3	0.1	0.2	0	-0.5	-0.8	0.4	0.1	0	0.2	0.9	0.3	-0.9	-0.1	-0.5	-0.3	0.3	0.5	0.5	0.6	-0.3	0.5	0.7	0.2	0.2	0.1
36	0.2	-0.1	0.6	-0.1	-0.6	-0.7	-0.2	-0.2	-0.2	-0.1	-1.2	-0.3	-0.4	-0.3	0	0.5	0.5	0.2	-0.4	-0.8	-0.7	-0.4	0.2	0.3	0.4	0.9	0.7	0.4	0	-0.1	-0.2	0.2
37	-2.4	-0.8	0.8	0.7	-0.5	-0.1	-0.8	-0.3	-0.4	0.4	-0.3	-0.8	-0.1	0.3	-0.1	0.1	0.3	-0.2	0.1	-0.3	0.3	-0.1	-0.6	-0.1	0.4	0.1	0	0.3	-0.4	-0.1	-0.1	-2.4
38	-0.2	0.2	0.1	0	-0.1	0.2	-0.2	0	0	0.1	0	-0.1	0.3	0.2	-0.2	0	-0.1	-0.2	0.1	-0.1	0.1	-0.1	-0.1	0.2	0	0.1	0	0.1	-0.2	0	0	-0.2
39	-0.6	0.2	0.5	-0.1	1	0.8	-0.6	0	-0.3	0.3	-0.3	0.2	0.4	0.3	-0.7	0.2	-0.2	0.3	0.6	0.3	0	0.1	-0.1	0.4	0.6	-0.7	-0.8	0.3	0.2	-0.6	0.4	-0.6
40	-0.3	0.1	0	0.4	0.6	-0.1	-0.1	0.5	-0.2	0	-0.5	-0.2	-0.1	0	-0.2	0.4	-0.1	0	0.1	0.6	0.4	0.3	-0.1	-0.1	0.6	-0.1	0.1	0.5	-0.5	0.6	0.2	-0.3
41	-0.1	0.2	0	0.4	0.2	0.4	-0.1	0.2	-0.2	0.1	0	0	0.3	0.3	-0.1	-0.2	0	0	0	-0.2	0.1	0.1	0.1	0.2	-0.2	0.1	-0.4	0	0	0.4	0	-0.1
42	0.1	-0.4	-0.1	0.2	-0.5	-0.2	-0.4	-0.5	0.4	-0.4	0.3	0.4	0.1	0.3	-0.1	-0.4	0.9	-0.6	0.7	0.4	0.2	-0.1	-0.1	0	-0.4	0.1	-0.1	-0.2	-0.1	-0.5	-0.4	0.1
43	-0.1	-0.1	0.1	-0.2	0.2	-0.2	-0.1	-0.1	-0.1	0	-0.2	-0.2	0.1	0	0	0.7	0	-0.1	0	0.1	-0.3	-0.1	-0.5	0.1	0.4	-0.2	0	0.4	0.1	-0.1	-0.4	-0.1
44	0.7	0.4	1.3	1.8	-0.1	-0.2	-1.8	0	1	0.5	0.3	0.3	-0.5	0.3	-1	-0.4	-0.2	0.2	0	0.2	0.5	0.2	0.6	-0.2	-0.2	0.5	-0.3	-0.6	-0.3	0	0.7	0.7
45	-0.2	0.2	0.2	0.1	0.2	0.6	-0.3	0.1	0	0.4	0.2	-0.1	0.2	0.2	0	0	0.1	-0.1	0	0	0.2	0.4	0	-0.1	0.1	-0.1	0	0.2	-0.2	0.1	0	-0.2
46	0.1	0	-0.1	0.1	0	0	0	0.1	-0.1	-0.1	-0.2	0.2	0	0	0.1	-0.1	0	0	0	0	-0.2	0.1	-0.1	0	0.1	0	0.1	0.2	-0.1	0.1	0.1	0.1
47	0.1	-1.2	1.2	-0.1	1.2	-0.2	0.1	0.4	-0.1	-0.6	-0.6	-0.5	0.1	0	0.1	0.1	-0.2	-0.5	1.1	0.4	0.6	-0.5	-0.9	-0.1	0.7	-0.2	-0.3	-0.1	0.5	0	0	0.1
48	-0.3	0.4	0	-0.8	0.3	0	-0.2	0.5	-0.5	0	-0.3	-0.5	0.2	-0.1	-0.3	0.3	0.3	-0.2	-0.2	-0.3	-0.1	-0.1	-0.3	-0.2	0.4	0	-0.3	0.3	-0.3	0.3	-0.2	-0.3
49	0.1	-0.3	-0.3	-0.1	-0.3	-0.3	0.2	0.1	0.3	-0.5	0.5	0.1	-0.2	0	0.3	-0.3	-0.1	0.5	0.5	0.2	0.2	0.2	-0.1	-0.8	-0.5	-0.3	0.3	-0.3	0.1	0.2	-0.4	0.1
50	0.1	0.1	0	0.1	0	-0.1	0	0.1	-0.1	0	-0.1	0.1	0	0	-0.1	0.1	0.1	-0.1	0.1	0.1	-0.1	0	0	0	-0.1	0.1	0.1	0	-0.1	-0.1	0.1	0.1
51	0	-0.1	-0.1	-0.1	0	0	0	-0.2	0.1	0.1	0.1	-0.2	-0.1	0.1	-0.1	0	0.1	0.1	-0.1	0.1	0	0.1	0.1	0.1	0.2	0	0.1	0	0.1	0.1	0	0
52	-0.1	0.1	0.2	0.5	0.6	-0.1	0.2	0.1	0.3	-0.4	-0.2	0.5	-0.8	-0.1	-0.1	-0.4	-0.8	-0.1	0.5	0.2	0	-0.2	-0.3	0	0.4	0.1	-0.9	-0.4	-0.7	0.4	0.7	-0.1
53	0.1	-0.1	0.4	0.6	-0.1	-0.3	-0.8	-0.3	-0.1	-0.2	-0.4	0.4	-0.3	-0.2	-0.5	-0.1	0.2	0.1	-0.2	-0.3	0	-0.1	0.3	-0.1	-0.4	0.2	-0.5	-0.2	0.2	0.3	0.5	0.1
54	0	0.1	0.1	0	0	0.1	0.1	0.1	0.1	0	0.1	0.1	0.1	-0.2	0.1	0	0.1	-0.1	0.1	0	0	0.1	0.1	0.1	0.2	0.1	-0.2	-0.1	-0.1	-0.1	-0.2	0
55	-0.1	-0.1	-0.1	0.1	0	0.1	-0.1	-0.1	0	0	0.1	-0.1	0.1	-0.2	0.1	-0.1	-0.1	-0.1	-0.1	-0.1	0	0	0	0	-0.1	0.1	-0.1	0.1	-0.1	0.2	0	-0.1
56	0.3	0.1	-0.6	0.1	-0.3	-0.4	0.2	-0.3	0.3	0	0.7	0.2	0.7	0.1	0.2	-0.7	-0.7	0.1	0.5	0.8	-0.4	-0.3	0.6	0.4	0.1	0	0.6	-0.6	0.1	-0.3	-0.2	0.3
57	0.6	0.1	-0.8	-0.3	0.4	0.1	0	0	0.2	0.3	0.3	0.4	0.1	-0.5	-0.1	-0.8	-0.2	-0.7	0.3	0.1	0.8	-0.2	0.3	-0.6	-0.2	0	0.1	-0.4	0.2	0.5	0.6	0.6
58	0	0.2	-0.2	0	0.1	0.3	-0.1	0.1	0.2	0.3	0	-0.2	0.3	0.1	0	0	0	-0.1	0.1	0.1	0	0.2	0	-0.3	0	0	-0.2	-0.1	-0.3	0.3	0	0
59	-0.5	0	0.3	-0.2	0.4	0	-0.5	0.4	-1	-0.3	0	0	-0.2	0.2	-0.3	0	-1.4	-0.4	-0.7	0.1	-0.6	-0.2	-0.2	0.6	-0.3	0	-0.3	0.2	-0.7	-0.2	0.6	-0.5
60	-2.4	0.2	-0.1	1.4	0.3	1.5	-0.7	-0.4	-0.7	-0.2	-0.3	-0.1	-0.5	1.3	-0.2	1.2	0.6	0.7	-0.8	-0.4	-0.4	0.9	-0.8	0	0.1	0.7	-1	0.8	-0.4	0.3	-0.9	-2.4
61	0.4	-0.1	-0.9	1.4	0.4	0.2	-0.6	0.3	-0.4	0	-0.4	-0.3	0	0.1	0.2	0.4	0.2	0.9	-0.4	0.3	0.2	-0.6	0.5	-0.1	0.9	0.1	0.3	0.4	0.3	0.2	0.2	0.4
62	-0.8	-0.5	0.1	0.4	-0.6	-0.2	-0.3	-0.2	-0.7	-0.2	0.2	0.8	-0.2	0.8	-0.9	-0.7	-0.3	-0.7	0	-0.6	-0.2	-0.4	1.7	2.9	-1.1	0.7	-1.2	-0.8	0.3	0.3	1.3	-0.8
63	-0.2	-0.1	0.3	0.8	-0.8	1	0.5	-0.9	-1	0.6	-0.4	0.2	-0.2	0	-1.1	0.6	-1.1	-1.1	-0.3	0.1	0.3	-0.7	0.1	1.2	0.3	0.1	-1.2	0.5	-1.6	0	0.7	-0.2
64	-1	0.6	-0.2	0	0.5	1.6	0	-0.3	0.2	0.7	0.3	0.1	-0.2	1.1	-0.8	0.1	-0.2	0.1	-0.2	0.1	-0.8	1.2	-1.6	-1.3	-0.5	0.3	-0.7	0.2	-0.8	0.4	0.5	-1
65	-0.9	0.2	1.2	0.3	0.7	-0.1	-0.1	0.4	-0.3	-0.3	-0.1	-1.8	-0.1	-0.2	-0.1	0.2	0.3	0	-0.2	-1.3	-0.1	-0.6	-0.3	0.4	-0.3	1	-0.1	0.3	-0.2	0.2	0	-0.9
66	0.1	0.1	0.1	-0.1	-0.1	0	0.1	-0.1	-0.1	0	0.1	-0.1	0.1	-0.1	-0.1	0.1	0.1	0.1	0.1	0.1	-0.1	0	0.1	0	0.2	0.1	0	0	-0.1	0.1	0	0.1
67	-0.1	0.2	0.1	0.1	0	0	0	-0.1	0.1	0	-0.1	0	0	0.1	0.1	0	-0.1	-0.1	-0.1	0	0	0	-0.1	0.1	-0.1	-0.1	0	-0.1	0.1	0	0.1	-0.1
68	0.1	0.1	-0.1	0.1	-0.1	-0.1	-0.1	-0.2	0	-0.2	0.1	0.2	-0.1	0	0.1	-0.2	0	-0.1	-0.1	0	0	-0.1	0.1	-0.1	0.1	0	-0.1	-0.1	0	-0.1	-0.1	0.1
69	-0.6	-0.7	-0.4	-0.4	-0.4	0.9	0.1	0.3	-0.1	0.1	0.2	0.9	0.9	-0.4	-0.2	-0.9	-1.1	0.5	0.9	0.4	-0.2	0.3	-0.8	0	0.8	-0.7	-0.5	-0.9	0.2	-0.8	-0.4	-0.6
70	0.1	0.7	-0.4	-0.4	0.5	0.7	0.1	0.3	0.6	0.4	0.1	-0.4	0.9	0.8	0.1	-0.4	-0.5	0.2	0.2	0.6	0	0.8	-0.5	0	-0.5	-0.8	0.2	0.3	0.7	0.6	-0.6	0.1
71	-0.7	-0.5	-0.5	0	2	-0.7	0.4	-0.6	-0.2	-0.2	0.5	1.1	-1.1	-0.1	0.3	0.1	-0.7	0.2	-0.2	0	-0.1	-0.1	0.4	0.3	-0.6	0.1	-1.2	0.3	0.1	-0.3	0.4	-0.7

i	1	2	3	4	5	6	7	8	9	10	11	12	13	14	15	16	17	18	19	20	21	22	23	24	25	26	27	28	29	30	31	32
72	0.8	-0.3	-0.1	-0.7	-0.5	-0.7	0.5	0.1	0.6	-0.2	0.2	0.5	-0.5	-0.6	0.7	-0.6	-0.3	0.1	0	-0.1	-0.2	-0.3	0.4	-0.1	-0.7	0.5	0.4	-0.8	0.7	-0.3	0.2	0.8
73	0	0.2	-0.2	-0.1	0.2	0.1	0.1	-0.1	0	-0.1	0	0.1	0	0.1	0	-0.1	0	0.2	0.1	-0.1	0	-0.1	-0.1	0	0	-0.1	0	0.1	0	-0.1	0	0
74	0.1	0	-0.1	-0.1	-0.1	0	0.1	0.1	0	-0.1	0	-0.1	0	0	-0.1	-0.1	0.1	0.1	-0.1	-0.1	0.1	-0.1	0	0	-0.1	0.1	0	-0.1	0	0.1	0.1	0.1
75	0.1	-0.1	-0.1	0.1	0	0	-0.1	-0.1	-0.1	0	0	-0.1	0	0	0	0.1	-0.1	0	0	0.1	0.1	-0.1	0.2	0	-0.1	0	-0.1	-0.1	-0.1	0.1	0.1	0.1
76	-1.2	-0.5	0.5	1.1	-1.3	-0.2	0.8	-0.3	-0.8	-0.5	-0.4	0	0.4	-0.7	-0.6	0.1	0.4	-0.4	0.1	-0.4	-0.2	0.3	-0.2	0.5	0.4	0.3	-0.5	0.9	-0.6	-1.9	0.4	-1.2
77	1.1	-0.5	0.2	-0.7	-0.5	-0.6	0.2	-0.2	0.2	-0.4	0.3	0.5	-0.4	-0.8	0.6	-0.3	-0.6	0	0.4	-0.3	-0.3	-0.5	0.4	0.2	-0.3	0	0.1	-0.7	0.7	-0.7	0.7	1.1
78	-0.8	1.4	-0.2	0.5	0.4	0.5	-0.8	1.5	0.2	0.4	0.5	-0.2	0.1	0.2	-0.1	-0.2	-0.1	-1.1	0.5	0.3	1.2	0	-1.2	-0.6	0.1	-0.3	0.3	0	-0.1	0	0.3	-0.8
79	0.4	-0.4	0.6	-0.1	-0.3	0.3	-0.6	-0.6	-0.5	0.5	-0.2	0.1	0.6	0.5	-0.3	0	0	-0.1	0.4	-0.4	-0.4	-0.1	0.6	0.7	0	-0.6	-0.5	-0.5	0.1	-0.4	0.3	0.4
80	0.2	-0.9	0.6	-0.4	-0.7	-0.9	0.3	-1	-0.3	-0.6	-0.6	0.3	-0.9	-0.7	-0.1	-0.1	0.3	-0.2	-0.3	-0.9	-0.5	-1	0.7	0.4	-0.8	0.7	-0.2	-0.1	-0.1	0.1	0.6	0.2
81	-2.2	-0.8	-0.5	-0.9	-0.3	-0.4	0.2	-0.4	-0.2	-0.4	0.1	0.4	-0.6	0.4	0	-0.2	0.4	0.4	0.2	-0.5	0.2	0.1	0.8	0.4	-0.4	0.6	0.3	0.1	-1.2	-0.2	0.1	-2.2
82	0.1	0	-0.1	0.1	-0.1	0.1	-0.1	0.2	-0.1	0	0.1	0.1	0.1	0	-0.1	0	-0.1	-0.1	-0.1	-0.1	0.1	0.1	-0.1	-0.2	-0.1	0.2	-0.1	0.1	0.1	0	0.1	0.1
83	-0.6	0.8	-0.5	0.9	0.7	1.2	-0.6	0.3	-0.1	0.6	0.2	-0.3	0.3	0.8	-0.5	0.8	0.1	0.1	0.4	0.4	0.5	0.7	-0.1	-0.9	0.8	-0.8	-1	0.4	-0.6	0.8	0.4	-0.6
84	0	-0.2	0.2	0.7	0.1	0.1	-1.6	-0.3	-1	-0.1	-0.5	-0.1	0.1	-0.5	-0.3	0.7	0.4	0.2	-0.1	0.1	-0.1	-0.2	-0.4	-0.3	0.8	-0.3	0.3	0.5	0.7	-0.1	-0.3	0
85	0.1	-0.7	0	-0.4	-0.2	0.9	0.4	-1	0	0.6	0.2	0.1	1.1	1.3	-0.2	-0.2	0	-0.5	-0.3	0.1	-0.9	-0.1	0.3	0.4	0.2	-0.2	0	-0.5	0.5	0.4	-0.3	0.1
86	-1.3	-0.3	-1	0.7	1.6	0.3	-0.9	-0.1	0.1	-1.6	-0.3	0.4	-0.2	-1	0.3	0.9	-0.7	0.1	-0.1	0.5	-0.3	-0.6	0.1	-0.8	0.4	-0.3	-0.7	-0.1	-0.8	0.3	-0.5	-1.3
87	0.2	-0.1	-0.3	-0.2	-0.1	0.1	0.4	-0.1	0.4	0.3	0.2	0.7	0.1	-0.1	0.2	-0.5	0.1	0.4	0	-0.1	0	0.1	0.5	0.4	-0.6	0.7	0.2	-0.4	0.5	0.1	-0.2	0.2
88	0.2	0.2	-0.1	0.1	-0.8	-0.4	0	0.4	0.2	0.2	0.3	-0.6	-0.2	-0.1	0.1	0.3	0.4	-0.3	-0.2	-0.4	0.4	0	-0.8	-0.4	-0.1	0.3	0.5	0.5	0.3	0.1	-0.2	0.2
89	0.3	0.5	-0.4	-0.1	1.1	0.3	0.6	0.2	-0.1	0	0.1	-0.3	0.2	-0.5	0.2	0	-0.2	1.1	-0.4	0.3	0.7	0.6	0.5	0	-0.7	0.1	-0.1	-0.1	0	0.2	0	0.3
90	-0.1	0.1	0	-0.1	0	0	0.1	-0.1	0	0.2	-0.1	-0.1	-0.1	0.2	0.1	0	0.1	-0.1	-0.1	-0.1	0.1	-0.1	0	0.1	-0.1	0	-0.1	0.1	0.1	0.1	-0.2	-0.1
91	-0.1	-0.5	0.3	-0.6	-0.9	0.2	0.2	-0.6	0.2	0.4	-0.6	-0.5	0.2	0.1	0	-0.4	0.6	0.2	-0.2	-0.7	-0.1	-0.5	0.3	0.4	-0.4	0.3	1.3	0.1	0.1	-0.4	-1.6	-0.1
92	0.5	0.7	0.5	0.4	0.9	-0.1	-0.4	-0.1	-0.1	-0.2	-0.6	-0.5	0	-0.3	-0.6	0.6	0.6	0.7	-0.2	-0.4	0.5	0.1	0.8	0.2	0.2	0.2	0	0.2	-1	1.1	-0.3	0.5
93	-0.2	0.1	0.1	0.5	0.2	0	0	0	0.4	0.1	0.3	-0.1	0.1	0.1	-0.1	0.2	0.1	0.3	0.2	0.3	-0.3	0.1	0.2	-0.2	0	-0.2	0.2	-0.1	0	-0.2	0	-0.2
94	0.1	-0.1	-0.1	0	0	-0.1	-0.1	0.2	0	0.1	0	-0.2	0.1	0	-0.1	0	0.1	0.1	0.1	0	0	-0.1	-0.1	0	-0.1	0.1	0	0.1	-0.1	-0.2	0.2	0.1
95	0.1	0.1	0	0.1	-0.2	0	-0.1	-0.2	0	0	-0.2	-0.1	-0.1	0.2	-0.1	0	0.1	-0.1	0.1	-0.1	0	0.1	0.1	0	-0.1	0.1	0.1	0	0	0.1	0.1	0.1
96	0.5	-0.4	0	0.1	-0.8	-0.2	-0.4	-1	0.3	0.3	0.3	0.8	0.2	0.2	0	-0.7	0.2	0	0.7	-0.3	-0.4	0	0.6	-0.1	-0.5	0.2	0.5	-0.8	0.1	-1	0.4	0.5
97	-0.6	0.4	-0.5	-0.2	0.1	0.5	-0.1	0.7	-0.3	-0.1	0.5	0.4	0.3	-0.4	0.3	0.3	0.5	-0.3	0.3	0.7	1.1	0.4	-0.3	-0.9	0.8	-0.1	0	0.2	0	-0.1	0	-0.6
98	0.1	0	0	0.1	0.1	0.1	0	-0.2	0.1	0.2	0.1	0	-0.1	0.1	0.1	0.1	-0.1	0	0	0	-0.1	-0.1	0	0	-0.1	-0.1	0	-0.1	0	0.1	0.1	0.1
99	0	0.1	-0.1	0.1	0.1	0.1	-0.1	0.1	0.2	-0.2	0	0.1	-0.1	0	0.1	0	-0.1	0	-0.1	0.1	-0.1	0.1	0	0.1	0.1	-0.1	-0.1	0.1	0	-0.1	0.1	0
100	-0.1	-0.1	0	0	-0.2	-0.2	0.1	0	0.2	0	0.4	0.1	-0.1	0.2	0.2	-0.4	-0.1	-0.2	0.5	-0.1	0	0.1	0.1	-0.5	0	0	0.1	-0.1	-0.3	-0.3	0.1	-0.1
101	0.1	-0.1	-0.1	0	0.1	0	-0.2	0	-0.1	0.1	0	-0.2	0.1	0	0.1	-0.1	0	0.1	0.1	0.1	0	0	0.1	-0.1	0	0	0.1	-0.1	0.1	-0.1	0	0.1
102	0.1	0.2	0.1	-0.1	-0.2	0	-0.1	0.1	-0.1	0	0.1	0	-0.1	0	0.1	0.2	-0.1	-0.1	0	0	0	0	-0.1	0.1	0	0	-0.1	0.1	0	0.1	0.1	0.1
103	0	0	-0.2	-0.1	0.1	0	0	0.1	-0.1	0.1	0	0.1	0	0.1	-0.1	0.1	-0.1	-0.1	-0.1	0.1	0.2	-0.1	-0.2	0.2	0.1	-0.1	0.1	0.1	0.2	0	0	0
104	0	0	0	-0.1	-0.1	-0.1	0.1	-0.1	0	-0.1	0.1	-0.1	0.1	0	0.2	0.1	0.1	0	0.1	0.1	0.2	-0.1	0	0	0.1	0	0	-0.1	-0.1	0.2	0	0
105	-0.5	0.4	-1	0.2	0.6	-0.4	0.6	0.2	0.9	-0.2	0.8	-0.6	-0.2	0.3	0.6	0.2	-0.3	1.1	-0.5	0.4	-1.5	0.4	0.5	-0.4	-0.6	0.1	1.2	0.5	-0.1	-0.4	0.2	-0.5
106	0	0	0.1	0.1	0	0.1	0.2	0	-0.1	0.1	0	-0.2	0.1	0.1	0.1	0.1	0.1	0	-0.1	0	0	0	0	0	0.1	0.1	0.1	0	-0.1	0.2	0.1	0
107	0.1	0	0.1	0.1	0	-0.1	-0.1	0.1	0	-0.1	0	-0.1	-0.1	0	-0.1	0	-0.1	-0.1	0.1	0.1	0	0	-0.2	-0.1	0.1	-0.2	-0.1	0	0.1	0.1	0	0.1
108	-0.4	0	-0.2	-0.4	-0.1	0.1	0.1	-0.1	-0.4	0.8	0	0.3	0	0.3	-0.6	-0.3	-0.1	-0.1	0.3	-0.1	-0.1	-0.2	0.2	0.6	0.2	-0.2	-0.1	-0.1	0.1	0	0	-0.4
109	-0.2	-0.1	0	0	0.2	0.1	0.2	-0.2	0.1	-0.1	0.1	-0.1	0	0.1	0.1	0.1	0.1	-0.1	-0.1	0	0	0.1	-0.1	0	0	0.1	0	0	0	0.1	0.1	-0.2
110	0	0.1	0.3	0.1	-0.3	-0.2	0	0.1	-0.3	0.2	-0.5	-0.1	0.1	-0.2	-0.2	0.2	-0.2	-0.5	-0.5	-0.6	0.4	-0.5	-0.1	0.5	-0.3	0.4	-0.3	0.1	0.1	0	0.3	0
111	-0.8	0	-0.4	0.5	-0.2	-0.6	-0.4	0	-0.4	-0.6	0	-1	0.3	1.1	-0.5	-0.2	0.1	0.4	-0.3	-0.4	0.4	-0.3	0.6	-0.9	-0.6	0.5	-0.5	-0.1	-1.2	0.7	1.1	-0.8
112	-0.2	-0.1	0.1	0	0.1	0.1	0.1	-0.1	0	0.2	0	-0.1	0.1	-0.1	0.1	-0.1	0.1	-0.2	-0.1	0.1	0.2	0.1	0	0	-0.1	0	0.1	0.1	0.1	-0.1	0	-0.2
113	0.1	0.1	0.1	0	0	-0.1	0	0.1	-0.1	0.1	0.1	-0.1	0	0.1	-0.1	0	-0.1	-0.1	-0.1	-0.1	-0.1	-0.1	-0.1	0	0.1	0.1	0	0	0	0	-0.1	0.1
114	-0.2	0.2	0	-0.2	-0.1	-0.2	-0.1	0	0.1	0.1	0.1	0	0.2	0	0	-0.1	0.1	0	0	0	-0.1	0	0.1	0	0.1	0	-0.1	-0.1	-0.1	-0.1	0	-0.2
115	0.3	0.1	0.3	0.4	1	-1.1	-0.6	0.2	-0.2	-0.7	-1	0	-0.6	-0.4	-0.2	0.4	0.1	-0.1	-0.1	-0.3	0	-0.5	-0.5	-0.3	0.2	1.1	-0.8	0.3	-0.2	0.5	0.5	0.3
116	1.4	-1.5	0	-1.6	-1	0	-0.2	-0.9	-0.4	-0.1	-0.1	1	0.5	-0.3	-0.7	-0.3	-0.1	-0.1	0.1	-0.6	-0.9	-0.1	0.3	1.4	-0.3	-1.5	-0.9	-0.2	0.3	-0.7	0.9	1.4
117	0	0.7	0	0.8	0.6	0	-1.1	0.2	-0.5	0.6	-0.9	-0.3	0.9	-0.3	0.2	0.9	1.5	-1.4	-1.2	-1.2	-1	-0.6	-0.1	-0.6	1.2	1.4	0.4	-0.2	-1.1	0.9	0	0
118	0	0.4	0.3	0.2	-0.8	-0.1	0	-0.2	-0.2	0.2	0	-0.1	0.3	0	-0.2	-0.5	-0.1	-0.7	-0.2	-0.7	-0.1	-0.3	0.3	0.2	-0.6	0.3	0.3	-0.5	-0.1	0.2	0.4	0
119	-0.7	0.5	-0.2	1.4	0.1	0.6	-0.6	0.9	-0.6	0.4	0.2	-0.6	0.2	0.9	-0.6	0.6	0.2	-0.2	-0.2	0.6	0.4	0.3	-0.3	-0.1	0.3	0	-0.6	0.7	-0.5	0.7	0.2	-0.7
120	0.4	0.5	0.1	-0.5	-1	0.3	-0.6	0.5	-0.8	0.1	0.4	0	0.5	-0.4	0.9	0	0.1	-0.9	0.6	0.6	1.3	0.7	-0.5	0.5	-0.4	-0.4	1.1	-0.1	1.3	-0.7	0	0.4
121	-1.2	0.2	0.4	0.8	0.1	0.6	-0.8	0.4	-0.8	-0.2	-0.6	-0.8	0.7	0.2	-0.9	0.8	0.7	-0.5	-0.6	-0.3	0.5	-0.4	-0.9	0.4	1	-0.1	-0.7	0.9	-0.6	0.6	-0.2	-1.2
122	-0.6	-0.4	0.3	0.5	0.3	0.1	-0.2	-0.5	-0.7	-0.1	-0.4	-0.2	0	0.6	-0.8	0.4	0.3	-0.6	-0.4	0.2	-0.2	-0.4	0	0.7	0.4	-0.1	-0.6	0.4	-0.2	0	0.3	-0.6
123	0	0.7	0.5	-0.6	1.4	0.1	0.7	0.6	-0.3	0.2	-0.5	-0.5	0.5	0.7	-0.1	0.6	0.3	1	0.3	0.2	0.6	0.4	0.1	0.2	0.5	-0.1	-0.3	0.5	-0.6	0.6	-0.1	0
124	-0.1	-0.4	-0.2	-0.4	-0.2	-0.7	0.6	-0.4	0.3	0	0.2	0	-1.3	-0.6	0.3	-0.2	0	0.2	-0.2	-0.5	0.4	-0.6	0.6	-0.5	-0.3	0.8	0	0.7	-0.4	-0.1	0.7	-0.1
125	0.1	0.1	-0.1	-0.1	0.1	0	0	0.1	0.2	-0.1	-0.1	-0.1	0	-0.1	0	0	0.1	0.1	0	0	-0.1	0	0	-0.1	0	0.1	0.1	-0.1	0	0	0	0.1
126	-0.9	0.4	0.3	-0.2	1.1	0.1	0.2	0.5	-0.2	-0.2	-0.7	-1.4	-0.3	0.1	-1.4	1.5	0.4	-0.8	0	0	0.4	-0.2	-0.7	-0.6	1.4	0.3	-1.6	1	-1.7	0.7	0.1	-0.9
127	-1.3	0.3	0.2	-0.7	0.3	0.3	-0.3	0	-0.2	0.4	-0.1	-0.5	-0.3	0.6	-0.6	0.5	-0.1	0.3	0.1	0.3	-0.6	-0.3	-0.3	0.5	0.4	0.2	-0.8	0.4	0	-0.4	0	-1.3
128	0.1	0.5	-0.3	-0.6	0.3	-0.2	0.2	0.9	0	0	0.2	0.5	0.1	0	0.3	-0.3	0.4	-0.3	0	0.4	0.3	0.2	-0.7	-0.3	0.9	-0.4	-0.1	0	-0.1	-0.2	-0.5	0.1
129	0.3	-0.3	0.8	1.2	0.9	-0.5	0.3	-0.3	0.3	-1	0.3	0	-0.4	-0.4	0.3	0.5	-2.1	-0.6	-0.7	-0.3	-0.7	0.4	0.3	0	2	0.1	-1	0.1	-0.6	0.5	0.3	0.3
130	0	-0.3	0.2	0.1	0.5	0.5	0	-0.3	-0.1	0	-0.2	0.3	0.3	-0.1	0	0.1	-0.6	-0.4	-0.5	0.2	0	-0.1	-0.2	0.4	0.1	-0.8	-0.4	0	0.4	0	0.3	0
131	0	-0.1	-0.1	0	-0.1	0.2	0	0	0	0	-0.1	0.1	-0.2	0	-0.1	0.1	0.1	-0.1	0.1	0.1	0.1	0	-0.1	-0.1	-0.1	0.1	-0.1	-0.1	0.1	-0.1	-0.1	0
132	0.9	0	-0.3	-0.3	-1.1	-1	0.1	-1.2	-0.4	-0.7	0.2	1.1	1.1	-1	-0.4	-1	-0.8	0.9	1	0.6	-1.3	0.9	-1.3	0.2	-0.4	-0.9	0.4	-1	0.5	-1.3	-0.6	0.9
133	0.4	-0.1	0.4	0.1	-0.1	0.4	-0.2	-0.5	0.2	0.2	-0.1	0.4	0.3	-0.1	0	-0.3	-0.2	0	-0.1	-0.4	-0.1	0.1	0.4	0.3	0	-0.2	0	-0.5	0.4	0.1	-0.1	0.4
134	1	0.2	-0.2	-1.4	0.6	0.3	0.8	1	1.2	-0.2	1.8	-0.4	0.3	1.3	0.6	0	-0.3	0.2	0.6	0.1	-1.2	1	-1.3	-0.5	-0.1	-0.5	1.3	0.1	0.6	0.1	-0.4	1
135	-1.5	0.2	0.3	0.2	0.3	0.1	-1.5	-0.1	-0.1	0.3	-0.9	-1.1	-0.9	0.3	-0.8	0.3	0.4	0.2	-0.1	-0.4	0.1	-0.1	0.2	-1	0.9	0.4	-1.2	0.6	-2	0.4	1.1	-1.5
136	0	-0.1	0	0	0.1	-0.1	-0.1	-0.1	-0.1	0.1	0	-0.2	-0.1	0.1	0.1	0.1	-0.1	-0.2	-0.1	0.1	0.1	0	0.2	0	0.2	-0.2	0.1	0	0.1	0	0.1	0
137	0.4	0.5	-0.1	0.2	0	0.4	0	-0.1	-0.2	0.6	0.1	0.1	0.4	0	-0.1	0.1	0.1	-0.3	0	0.7	0.8	0.6	0	0.1	0.3	-0.4	0	-0.1	-0.2	-0.1	-0.1	0.4
138	-0.4	-0.6	-0.1	0.6	0	0	0.2	-0.2	-0.4	-0.1	-0.7	0	-0.2	-0.6	0.1	0	0.3	0	-0.8	-0.2	0.4	-0.8	0.1	0.3	0	0.4	-0.2	0	0.2	-0.1	-0.1	-0.4
139	-1.1	-1	-0.4	0.8	0.5	-0.5	1.1	-0.4	0.9	-0.7	0.2	-0.6	-1.8	0.3	0.7	-0.5	-0.3	0.5	0.3	-0.9	-1.1	-0.7	0.4	-0.5	-1.1	0	0.2	-0.5	-0.5	-0.8	0.3	-1.1
140	-0.1	0.2	0	0.1	0.1	0	-0.1	-0.1	-0.1	0.1	0	0.1	0.1	0	0	0	0	0.1	0.1	0	-0.1	-0.2	-0.1	-0.1	0.2	0	-0.1	0.1	0.1	0	0.1	-0.1
141	-0.4	0.1	0.2	0.9	-0.2	0.4	-0.1	0.8	-0.5	0.2	-1.1	-0.7	0.9	-0.5	-0.1	0.4	-0.5	-0.1	-1.4	-0.7	1.3	-0.1	0	0.4	0.2	0.8	0.1	0.4	-0.2	1.5	-0.7	-0.4
142	1.4	0	0.9	-0.7	0.1	-0.4	0.2	0.3	0.2	-0.2	0	0.6	0.2	-0.4	0	-0.7	-0.5	0	1	0.6	0.3	-0.1	0	-0.3	-0.6	-0.2	0.2	-0.3	0.4	-0.4	0.1	1.4
143	-1.3	-0.6	1	-0.4	-0.3	0.2	-1.9	0.2	0.6	-0.8	-0.9	0	0	0.9	-0.4	-0.2	-1.5	0.5	0	-0.2	-0.5	-0.2	-0.2	-1.3	-0.2	0.3	-0.8	-0.1	-0.1	-0.9	-0.4	-1.3
144	-0.1	0.1	-0.3	0	0.7	0.5	-0.3	0.8	-0.8	0.5	0	-0.1	0.4	-0.4	-0.1	0.1	0.3	0.4	-0.2	0.2	0.8	0.4	-0.9	-0.8	1	0.7	-0.3	0	-0.4	0.7	-0.5	-0.1

i	1	2	3	4	5	6	7	8	9	10	11	12	13	14	15	16	17	18	19	20	21	22	23	24	25	26	27	28	29	30	31	32
145	-0.1	0.9	-0.4	0.2	0	0.4	0.1	0.6	0.2	0.2	0.3	0.3	0.4	0.2	0.2	-0.5	-0.2	0.8	0.2	0.6	-0.3	0.2	0	-0.4	0.2	-0.3	-0.5	-0.6	-0.5	0.2	0.3	-0.1
146	-0.3	-0.4	0.1	0.3	-0.1	-0.2	0	0.4	0	-0.1	0	-0.2	-0.5	-0.4	0.2	0.3	0.3	-0.3	0	-0.2	0.2	-0.3	0	-0.2	0.2	0.2	-0.3	0.1	0	0.2	0.1	-0.3
147	-0.2	-0.2	0.2	0.5	0.2	0.2	0	-0.2	-0.1	0.3	0.1	-0.3	0.1	-0.1	-0.1	0.2	0.1	0.3	0	0	-0.2	0	0	0	-0.1	-0.4	-0.3	0.2	-0.1	-0.1	-0.1	-0.2
148	-0.2	0.5	0	-0.5	0.1	0	-0.3	0	-0.1	-0.1	-0.2	-0.2	0.4	0	-0.1	0	0	-0.3	-0.3	0	0.3	0.4	-0.1	0.2	0	-0.1	0	0	-0.2	-0.1	-0.1	-0.2
149	0.3	-0.1	-0.5	0	-0.4	0.4	0.2	0.4	0.3	0.3	0.6	0	0	0.1	0.3	-0.2	-0.5	0.3	0	0.1	0.3	0.1	0.4	0	0.1	0	-0.8	-0.5	0.6	-0.5	0.2	0.3
150	0.4	0.3	-0.4	0.3	0.2	-0.2	-0.3	0.6	-0.5	-0.4	-0.1	0.2	-0.2	0.7	-0.5	0.4	0.4	0.2	0.2	0.1	0.5	0.1	0.4	0	1.1	1	0.1	0.1	-0.3	0.7	0.1	0.4
151	0.2	-0.4	-0.4	-0.1	-0.5	-0.2	0.3	-0.3	0.5	-0.5	0.4	0.3	-0.3	-0.2	0.5	-0.6	-0.1	0.4	0.2	0.1	-0.3	0	0.5	-0.4	-0.4	-0.3	0.4	-0.3	0.3	-0.2	0.1	0.2
152	0.1	-0.6	0.4	0	-0.3	-0.1	0.3	-0.2	-0.2	-0.4	-0.1	0	0.1	-0.4	-0.3	0.4	-0.3	-0.1	-0.2	-0.3	0	-0.4	-0.2	0.2	-0.4	-0.2	0	-0.1	0.3	0	0.1	0.1
153	0	0.1	-0.1	0.1	-0.1	0.1	-0.1	0.1	-0.1	0.1	-0.1	0.1	0	-0.1	0	-0.1	0.1	0	0.1	0.1	-0.1	-0.1	0	-0.1	0.2	0	0	0	0	0.1	-0.1	0
154	0	0.1	0.1	0.1	0	0	0	-0.1	0.1	-0.1	-0.1	0.1	0.1	-0.1	0.1	-0.1	-0.1	0.1	0	-0.1	0	0.1	-0.1	-0.1	0.1	0	0	0.1	0.1	0	-0.1	0
155	0	0.1	0.1	-0.2	0	-0.1	-0.1	-0.2	-0.1	0	0.1	0.1	0	-0.1	-0.1	0	0	0	-0.1	0	0.1	-0.1	0	0.1	0	0.2	0	0	0.2	0.2	-0.1	0
B1	-0.1	0.1	0.1	0.1	0.1	0.1	-0.2	0	-0.1	0.1	0	-0.1	0.2	0.1	-0.1	0.1	0	0	0.1	0.1	0	0.1	-0.1	0	0.1	-0.1	-0.1	0.1	-0.1	0	0	-0.1

Table D.6 continued…

i	33	34	35	36	37	38	39	40	41	42	43	44	45	46	47	48	49	50	51	52	53	54	55	56	57	58	59	60	61	62	63	64
1	0.2	0.4	0.1	0.1	0.1	0	0.3	-0.6	0.2	0	0.3	-0.4	0	-0.2	0.4	0.1	0.2	0.1	0.1	0.2	-0.3	-0.1	-0.1	0.2	-0.2	0.2	0.2	0	0	0.2	0	0.3
2	-0.1	0.3	0.4	0.2	-0.1	0.3	-0.1	-0.3	0.4	-0.2	-0.1	0.2	-0.3	0.1	-0.1	-0.1	0	0.2	0.2	-0.2	0.4	0.1	0.3	0.1	0.4	-0.5	-0.5	0	-0.1	0	0.4	-0.1
3	-0.2	-0.6	0.5	0.1	0.2	-0.2	0.2	0.2	-0.7	-0.2	-0.4	0.5	0	0	0	0.3	0.4	-0.5	0.1	-0.1	0.2	0.4	-0.2	0.2	0.2	0	0	0.2	0.5	-0.4	-0.4	-0.3
4	0.1	-0.1	-0.1	-0.3	-0.1	-0.1	0	0	0.3	0.3	0.1	-0.2	-0.2	0.1	0	-0.3	-0.2	0.2	-0.1	0.2	-0.1	0	-0.1	-0.2	-0.1	-0.1	0.1	-0.2	-0.1	-0.3	-0.1	0.1
5	-0.3	-0.3	-0.3	-0.3	0	-1.1	0.1	0.1	0	0.3	0	0.2	0.1	-0.1	0	0.3	0	-0.3	-0.2	-1	-0.1	-0.2	-0.1	-0.2	0.1	0.5	1.2	0	-0.1	-0.1	-0.1	0.2
6	0.2	-0.1	0.2	0.4	-0.2	0.1	0	-0.1	-0.1	0.1	-0.3	0.3	-0.1	0	-0.1	0.2	-0.1	-0.1	0.3	-0.4	0.1	0.5	0.1	0	0.2	0.4	-0.2	0.5	-0.1	-0.1	-0.2	-0.3
7	0.2	0.1	0	0.2	0	0.2	0.1	0.6	-0.4	0.2	0.1	0	-0.3	-0.1	-0.1	-0.2	-0.2	0.3	0	-0.3	-0.2	0.2	0	-0.2	-0.5	-0.2	-0.4	-0.2	-0.1	0	0	0.6
8	0	-0.1	0	-0.3	0.1	-0.2	-0.3	-0.4	-0.2	0	0.3	-0.1	0.3	-0.1	-0.1	0	-0.1	-0.2	-0.1	0.7	-0.1	0	-0.1	-0.1	-0.2	0.2	0.3	-0.1	0.2	0	0	0.3
9	-0.1	0	0	0	-0.2	-0.2	0.1	-0.4	0.1	-0.2	0	0.1	0	0	-0.1	0.1	0.3	-0.1	0.1	0.1	-0.1	-0.3	-0.3	-0.1	0	-0.1	0.3	-0.3	0	0	0.3	0.3
10	0	-0.1	0	-0.3	-0.1	-0.1	0.5	-0.4	-0.2	-0.2	0	0	0	-0.1	0.2	0.2	0.2	0	-0.1	-0.1	0.1	-0.1	-0.1	0	-0.1	0.2	0.2	-0.2	0	0.3	-0.1	-0.1
11	0.4	0	-0.2	0	0.1	0.1	-0.1	0.2	-0.1	0	0.3	-0.3	-0.2	-0.2	-0.1	-0.1	-0.6	0.1	-0.2	-0.1	0.4	-0.4	0.2	0	0	-0.5	0.1	0	0.1	0.2	0.1	0.1
12	0.6	-0.3	0.1	0.8	-0.1	-0.1	0	0.3	-1.1	0.1	0	0.1	0	-0.1	0	0.1	-0.2	0.2	-0.1	-0.4	0.7	0.3	0.2	-0.1	0.7	0	0	0	-0.1	0	-0.2	0.2
13	-0.3	0.6	0.1	0.3	0.2	0.2	-0.1	-0.2	0	0.2	-0.2	0.2	0.3	-0.2	-0.1	-0.2	-0.5	0.4	0.5	0.3	0.5	0.3	0.4	0	0.1	0.3	-0.3	0	-0.1	-0.1	0	0.1
14	-0.3	-0.4	0.4	-0.1	0.3	-0.1	0.1	0.1	0.1	0	0.2	-0.2	0.3	-0.1	0.2	0.2	0	-0.4	0.1	0.1	0.1	0	-0.1	0.2	-0.6	0.3	0.1	-0.1	0.1	-0.2	0	0.2
15	-0.2	0.1	0.5	-0.2	-0.1	0.3	0.3	1	0.2	0	-0.4	-0.2	-0.1	0.2	-0.8	0.1	-0.1	0.1	0	-0.3	0.4	0.2	0.3	-0.3	0.3	0.1	-0.7	0	0	0.1	0	-0.4
16	0.2	-0.3	0.1	0.2	-0.2	0.4	0.1	0	-0.6	0.2	0	0	0.4	-0.1	-0.2	0	-0.1	-0.3	-0.2	0.2	0.1	0.3	0	0.1	-0.3	-0.5	-0.2	0	0.3	-0.3	0.1	0
17	0.2	0.2	0.2	-0.2	0.5	-0.2	-0.2	0	-0.1	-0.3	0.3	-0.6	-0.7	-0.1	0	0	0	-0.1	-0.4	0.7	-0.3	-0.8	0.1	0.1	-0.7	0	0.2	0.1	-0.3	0.1	0	0
18	0.1	0.7	0.5	0.1	0.4	0.1	0.2	0.2	0	-0.6	-0.1	0	-0.6	-0.1	0.3	0	0.6	0	0.1	-0.2	-0.5	-0.1	-0.2	0.1	-0.4	0.8	-0.1	0	-0.3	-0.1	-0.3	-0.2
19	0.2	-0.2	0	-0.3	-0.3	0.4	-0.2	0	0	0.1	0	0.3	-0.1	0.3	-0.4	-0.2	-0.7	-0.1	-0.2	0.2	-0.1	0	0.4	-0.2	-0.5	-0.5	-0.4	-0.5	0	0.3	0.1	0
20	0.1	0.1	0	0.2	0	-0.1	0	0.4	-0.1	0.3	0	0.2	-0.2	0.3	-0.4	0	0	-0.1	0	0.2	0	0	0.1	-0.2	0.2	0.1	-0.1	0	-0.2	-0.1	-0.2	0.2
21	-0.4	0.2	-0.8	-0.5	0	0.6	0	-0.2	0.8	0	0.3	-0.8	0.4	-0.1	0.1	-0.3	-0.2	0.1	-0.6	0.1	-0.1	-0.8	0.1	-0.2	1.2	-0.2	-0.7	-0.1	0	-0.2	0.4	-0.5
22	-0.3	-0.2	-0.2	0.1	-0.3	0.1	0.2	0.1	-0.2	-0.2	-0.4	0.5	0.5	0.2	-0.5	0	0.3	-0.1	0.1	-0.9	0.3	0.1	-0.2	0.1	0.1	-0.1	-0.6	0.4	0	-0.1	0.1	-0.4
23	-0.4	0.2	0.3	-0.1	-0.1	0.2	-0.2	0	-0.1	0.4	0	0.3	0	0	-0.1	-0.3	0	0.2	0.4	0.2	0.1	0.2	0.1	0	-0.2	-0.4	-0.4	0	0.2	-0.5	-0.2	0.2
24	-0.4	0.4	0.2	-0.4	0	-0.1	0	-0.1	1.9	-1.7	0	-1.1	0.1	-0.1	-0.2	0	0	0.4	0.2	-0.4	0	-0.1	0	0.1	-0.3	0.1	-0.2	0.2	0	0.1	0.3	-0.2
25	-0.3	0.2	-0.2	-0.2	-0.2	-0.3	0.3	-0.1	0.2	0	-0.1	-0.1	0	0.2	-0.3	0	-0.1	-0.1	-0.1	-0.3	0	0.1	0.1	0	0.2	0	0.3	0.1	0.3	0.1	-0.3	-0.2
26	0.3	0.1	0.3	0.3	-0.7	0.3	0.3	0.4	-0.3	0.4	0.2	0.6	0.5	0.3	0.2	-0.2	-0.2	-0.1	-0.2	0.1	0.1	0.1	-0.1	-0.2	-0.1	-0.2	-0.1	-0.4	-0.3	0.2	0.2	0.6
27	-0.2	0.2	0.5	-0.3	-0.1	-0.3	0.8	0.4	0	0	0.3	0.3	0.7	0.1	-0.5	0.2	-0.3	-0.5	0.2	-0.2	0	-0.2	0.1	0.2	-0.3	0.1	0.3	-0.6	0.3	0.4	-0.1	0.2
28	0	0	0.3	0	0.2	-0.4	0.1	-0.4	0.2	0	-0.1	0.1	0.1	-0.3	0	0.3	0	0.2	0.2	-0.1	0.2	0.1	0.1	0.1	0.2	0.7	0	0	-0.4	0.2	-0.2	-0.2
29	0.4	-0.8	-0.4	-0.3	-0.1	0	-1.1	-0.3	0.1	0.4	0	0	0.1	-0.3	-0.3	-0.1	0	0.2	-0.4	0.1	0	-0.1	-0.1	-0.3	0.2	-0.5	0.3	-0.1	0.1	0	0.6	0.1
30	0.1	-0.1	0.5	-0.1	0	-0.4	0.3	0.3	-0.2	0	0.1	0	0	-0.2	-0.1	0.3	0.1	-0.3	-0.2	0.8	0.5	0.2	0.2	0.2	0.1	-0.1	0.5	0.2	0	0	-0.2	0
31	0.4	0.4	-0.4	0.3	-0.3	0.2	0.5	-0.2	-0.2	-0.3	0	0.8	0.3	0.4	0.3	-0.6	-0.1	0.6	-0.5	0.4	-0.6	0	0.1	-0.7	-0.3	0.2	-0.3	-0.2	-1.1	0	0	0
32	-0.2	0.4	0.1	-0.1	-0.7	0	0.8	0.2	-0.4	-0.4	-0.4	0.3	-0.4	0.1	-0.2	0.1	0.3	-0.2	0.5	-0.4	-0.4	0	-0.3	0.1	1	0.2	0.5	0.2	-0.4	1.5	0.4	-0.6
33	0.2	-0.6	-0.2	0.5	1.9	0.4	-0.1	-0.7	-0.3	-0.1	0	-0.1	-0.7	-0.6	-0.1	0	0.2	-0.4	-0.4	-0.2	-0.1	0	0	0.3	0.8	0.7	0	0.1	0.2	-0.9	-0.5	-0.2
34	0.4	0.6	-0.1	0.5	0.4	0.3	-1.2	-0.6	-0.1	0.8	0.3	-0.4	-0.2	0.2	0.7	-0.3	0	0.6	0.3	0.4	0	0	-0.1	0.1	0.3	-0.2	0.3	-0.5	-0.2	-0.1	0	0.4
35	-0.4	-0.2	-0.2	-0.3	-0.6	-0.2	-0.2	0.2	0.3	0	-0.8	0.1	-0.2	0.2	-0.8	-0.7	-0.5	-0.1	1.1	0.3	-0.2	0	0.1	-0.1	0.2	-0.3	-0.3	0.1	0.6	-0.2	0.4	-0.2
36	0	-0.4	-0.1	-0.2	-0.5	0.1	-0.2	-0.5	0.6	-0.3	-0.9	-0.4	-0.2	-0.1	-0.3	0.8	0.2	-0.1	0.5	-0.5	0.2	0.1	-0.5	0	-0.7	0.2	-0.6	0.3	0.6	0.2	-0.2	-0.7
37	-0.3	0.5	0.5	-0.2	0.1	0.5	0.1	0.4	0.3	-0.5	-0.4	-0.6	0.1	0	0	0.1	-0.3	0.8	0.9	-0.7	0.2	0	0.1	0	-1	-0.2	-1.5	0	0.1	0.5	0.5	0.3
38	-0.1	0.2	0.3	0.1	0.1	0.1	-0.1	0	0.1	-0.2	-0.1	0.1	0.1	-0.1	0	-0.2	-0.2	0.1	0.1	0	0	0	0	0.2	0	-0.2	-0.3	0.1	0	-0.1	0	0
39	0.8	0.2	0.3	1.2	0.5	0.9	-0.6	0.1	-0.1	-0.4	0.1	-0.2	-0.6	0	0.4	-0.6	0.1	0.2	0	0.3	0.4	0.1	0.2	0.2	0.3	0.3	-0.7	0.4	-0.7	-0.1	0.1	0.3
40	0.1	-0.2	0.2	0.2	0.4	0.3	-0.1	-0.1	-0.2	0.4	-0.1	0.1	-0.3	-0.1	-0.1	-0.4	0	-0.2	0.5	0.3	0.4	0.2	0.3	0.3	0.3	-0.2	-0.1	0.2	-0.3	-0.1	-0.5	0.3
41	0.2	0	-0.1	0.1	0.1	0.5	-0.1	0.1	-0.2	-0.5	-0.2	0.2	-0.1	0.1	0.1	-0.3	0.1	0.3	0	-0.3	-0.2	0.1	0.2	-0.1	0.4	-0.1	-0.1	0	-0.3	0.1	-0.2	-0.1
42	0	-0.4	-0.5	0.3	0.4	0.4	0.4	0.8	0.8	-0.4	0.5	-0.5	-0.4	-0.3	-0.1	0	-0.9	-0.3	0.2	-0.5	0.5	0.2	0.4	-0.6	0.4	-0.1	-0.6	-0.2	0.5	-0.1	-0.2	0.7
43	0	0.1	0.6	0.1	0.3	0	-0.1	0	-0.2	0.1	-0.1	-0.2	-0.3	-0.3	0.2	0.2	0.2	0.2	0.3	0.1	0.2	-0.2	0	0.4	-0.4	0.2	-0.1	0.4	0	-0.1	0	-0.1
44	-0.1	0.4	1.2	0.3	-0.7	0	0	0.1	0.4	0	-0.4	1.7	0.8	0.8	-1	-0.5	-0.6	0.6	0.2	0.1	0	-0.1	-0.1	-0.6	0	-0.4	0	-0.5	-0.3	0.6	0.2	-0.1
45	0	0.4	0.1	-0.2	0.3	0.5	0	-0.1	0	0	0.1	0.1	0.3	0	-0.1	-0.3	-0.1	0.3	0.1	0.2	0.1	0.1	0.1	-0.2	0	-0.3	-0.3	-0.2	-0.1	0	0.4	0.2
46	0.1	-0.1	0.1	0	-0.1	-0.1	-0.1	-0.2	-0.1	0.1	0	-0.2	-0.1	0.1	-0.1	-0.1	0	0	0	0.2	0.1	0.1	0.1	-0.1	0	0.1	-0.1	0.1	0	0.1	0	0
47	0.1	-0.2	0.5	0.6	0.9	-0.2	0.1	0.7	0.2	-0.2	0.1	0.4	-0.8	0.2	1	0.3	0.3	-0.2	0.6	-0.2	-0.1	0.3	0.5	0.4	0.6	0.7	0.3	0.3	-0.2	-0.8	-0.6	-0.9
48	0.1	0.2	0.2	0.4	-0.1	0	0.1	-0.2	-0.1	-0.7	-0.3	0	-0.4	0.2	0.1	-0.1	0.2	0	0.2	-0.1	0.3	0.3	0.3	0.4	0.6	0.2	-0.5	0.2	-0.2	-0.3	-0.5	-0.1
49	-0.2	-0.1	-0.4	-0.3	-0.1	-0.2	0	-0.2	0.2	-0.1	0.5	0	0.2	-0.3	0.3	0.1	0.1	-0.1	-0.2	-0.1	-0.2	-0.4	0.2	0.2	-0.3	0.1	-0.1	-0.3	-0.2	0	-0.2	0.4
50	0.1	-0.1	-0.1	0.1	0	-0.2	0.1	0.1	-0.1	0	0.2	0	-0.1	0	0.1	0	0.1	0.1	0.1	0.2	0.1	0.1	0.1	-0.1	-0.1	-0.2	0	0.1	-0.1	-0.1	-0.1	0.1
51	0	0	0.1	-0.1	-0.1	0.1	-0.1	0	-0.1	0.1	0.1	0	-0.1	0.1	0.1	0.1	-0.1	0	0	0	0.1	0	-0.1	-0.1	-0.1	-0.1	-0.1	-0.1	0.2	0	0.2	0
52	0.2	0.5	0.4	1.1	0.2	0.1	0.6	0.7	-0.4	-0.3	0.2	-0.7	-0.5	-0.3	0.8	-0.2	-0.6	-0.5	-0.3	0.1	0.2	1.1	0.8	0.1	0.4	-0.1	0.2	0.1	-0.4	-0.6	-0.8	0.3
53	-0.3	-0.7	0.2	0.4	-0.2	0	0.4	-0.2	-0.6	-0.4	-0.3	0.1	0.2	0.1	-0.5	0.1	0.1	-0.3	-0.3	-0.1	0.2	0.6	-0.4	-0.1	-0.4	0.4	-0.1	0	0	0.5	-0.2	-0.5
54	0.1	-0.2	0.1	0.1	0.1	0	-0.1	0	0	0	0.1	-0.1	0.1	-0.1	0.1	0.1	-0.1	0	0.2	-0.1	0.1	0	-0.1	0.1	0.1	0	0.1	-0.1	-0.1	0	0.1	0

i	33	34	35	36	37	38	39	40	41	42	43	44	45	46	47	48	49	50	51	52	53	54	55	56	57	58	59	60	61	62	63	64
55	0.1	0	-0.1	0.2	-0.1	0	0	0.1	0.1	0	0	0	-0.2	0.1	0.1	0.1	0.1	-0.1	-0.1	0	0	0.1	0	0	0.1	0.1	0.1	0	0.1	0.1	0	0
56	0.2	0.1	-0.5	-0.4	-0.3	-0.2	-0.1	-0.1	0.3	0.4	0.4	-0.1	0.4	-0.2	-0.1	0.1	-0.3	0.7	-0.2	0.4	-0.1	-0.6	0.1	-0.2	-0.3	-0.2	0.6	-0.4	-0.2	-0.1	0.6	0
57	0.2	0.1	-0.3	-0.2	-0.1	-0.4	0.1	0.4	0.2	0	-0.4	1	-0.3	0.7	-0.6	0.1	-0.5	0.1	-0.1	0.1	0.3	0.1	0.1	-0.8	0.3	-0.4	0.4	-0.5	-0.3	0	0.1	0.3
58	-0.2	-0.1	-0.1	-0.2	0	0.1	-0.5	-0.1	-0.1	0.3	-0.3	0.2	0	0.1	0	0	0.1	0.1	0.3	0.2	0.2	-0.2	0.2	0.2	0.1	0	-0.1	0	0.3	-0.2	0.1	0.2
59	0.5	0.2	0	0.8	1	-0.3	-0.2	-0.2	0.8	0.1	-0.4	3.4	0.1	-0.1	0.8	0.2	0.5	0	-0.3	0.4	1.2	-0.2	-0.1	1.2	1.2	0	0.2	0.4	-0.1	-0.4	-0.5	0.9
60	-0.5	0.5	-0.8	0.4	0.7	1.8	0.3	-0.2	0.6	-0.4	0.4	-0.7	0.5	0.3	0.5	-1.4	-0.5	-0.6	0	-0.9	-1	0.3	0.2	0.7	-0.2	0	-1.5	1.6	0.4	-0.7	-0.5	-1.2
61	-0.8	0.4	0.1	0.1	0.8	0.6	-0.8	-0.6	-0.8	0.2	0.2	-0.1	0.1	0.3	0.2	-0.1	0.5	0.5	-0.4	-0.7	-0.7	1.2	0.2	0	1.2	0.6	-0.9	0.1	-0.2	-0.2	-0.2	0.5
62	-0.6	0.3	-1.9	1.2	-0.7	1	0.5	-0.5	0.8	-0.3	0	2.9	1.3	0.9	0	-1	0.1	0.5	-0.1	-1.9	-0.7	1	-0.1	-1	-0.4	0	-0.3	-0.9	0.6	0	-0.6	-0.5
63	1.1	0	1.2	1.4	-0.4	0.6	0.4	-0.6	-1.3	0	-0.3	0	0.4	-0.4	-0.3	-0.4	-0.9	-0.3	-0.6	1.4	1.4	0.5	0.6	0.1	0.2	1.3	-0.3	0.5	0.3	-0.4	1	-0.4
64	-0.1	0.8	2.6	1.2	2	0.2	0.1	0.3	0.6	0.2	-0.6	-0.1	-0.7	-0.1	0.3	-0.5	0	0.2	-0.1	1.3	0.3	1.1	1.6	0.4	0.6	0	-0.6	0.1	0.3	-0.4	-0.2	0.7
65	0	-0.1	0	0.1	0	0.6	0.6	0.8	0	-1.3	-0.7	0.5	-0.4	0.5	0.4	-0.5	0.3	-0.2	0.2	-0.3	0.2	0.7	-0.3	-0.2	0.7	-0.2	-0.3	-0.1	0.4	0.3	-0.6	-0.3
66	-0.1	0	-0.1	-0.1	0.1	0.1	0.1	-0.1	0.1	-0.1	0.1	0.1	-0.1	-0.1	0	0.1	-0.1	0	-0.1	0	-0.1	0	0.1	0.2	-0.1	0.1	0	0	0.1	0.1	0.2	0.2
67	0	0	0.1	-0.1	0.1	0.1	0	-0.1	0	0.1	0	0.1	0.1	-0.2	0.1	-0.1	0.1	0	-0.1	0.1	0	0.1	-0.1	0	0	-0.1	-0.2	-0.1	0.1	0.1	0.1	0
68	0	0	0	0	-0.1	0.1	0	-0.1	-0.1	0.1	-0.1	-0.1	0	-0.1	-0.1	0	0	0.1	0.2	-0.2	0.1	-0.1	0.1	0.2	0.1	-0.1	0.1	0.1	-0.1	0	-0.1	0
69	0.7	1	0.8	0.8	0.6	-0.6	0.6	0.2	0.2	-1.5	-0.2	0.7	-0.5	-0.2	0	1	-0.1	0.7	-0.1	-0.6	0.3	0.6	-1.1	-0.7	0.1	0.4	0.5	0.2	-0.7	0.8	0	0.4
70	-0.3	0.9	-0.2	0	0.9	-0.1	-0.4	-1.5	0.5	-0.1	0.6	-0.1	-0.7	-0.2	1	-0.4	0.5	0.7	0.9	0.9	-0.7	0.1	0.3	0	-0.3	0.1	0.5	0.3	-0.9	0.2	-0.1	0.5
71	0	-1.3	-0.6	0.5	-1.3	-0.4	-0.2	-0.3	0.2	-0.9	0.2	0.4	0.1	-0.5	0.2	0.1	0	-1.1	-0.7	-0.1	0.2	1.1	-0.1	0	0.2	-0.2	0.3	0.4	0.5	0	0	0
72	-0.3	-0.5	-0.8	-0.7	-0.6	-0.7	0.4	-0.4	0.7	-0.4	0.4	-0.3	0.2	-0.4	0.5	0.5	0.2	-0.7	-0.6	-0.3	-0.3	-0.2	-0.2	-0.1	-0.5	0.4	0.6	-0.3	0.5	0.2	-0.4	0.2
73	0.1	0.1	-0.1	0	0.1	0.1	0.2	-0.2	0.2	-0.1	-0.1	0	-0.1	0.1	0.2	0	-0.2	0	0.1	-0.1	0.1	0	0.1	0	0.1	0.2	0	0	0	0.1	0	-0.1
74	0	-0.1	0	0.1	0.1	-0.1	0	0.1	-0.1	-0.2	-0.1	-0.1	-0.1	0.1	0.1	0.2	-0.1	0	0.1	-0.1	0	-0.1	0	-0.2	0.2	0.1	-0.1	-0.1	-0.1	0.1	-0.1	0.1
75	0	0.1	0.1	-0.1	-0.2	-0.1	-0.1	-0.1	0	0.1	-0.1	0	-0.1	0.1	-0.1	0.1	0.1	0.1	0	0.1	-0.2	0	-0.1	0.1	0.1	0.1	0	0	0	0.1	-0.1	-0.2
76	0.4	-0.4	-0.7	0.8	0.7	0.7	0.7	-0.1	-0.5	-0.7	0.1	0.1	0.9	-0.2	0.8	0.6	-0.4	-0.2	-0.4	-0.8	0.4	0.5	0	-0.2	0.7	0.6	-0.2	0.2	-0.3	0.7	-0.1	-0.9
77	0	-0.4	-0.5	-0.6	-0.4	-0.5	0.7	0.5	0.8	-0.5	0.8	-0.4	0.1	-0.1	0.9	0.5	0.2	-0.8	-0.4	-0.6	-0.5	0	-0.2	0.1	-0.7	0.2	0.6	-0.4	0.2	0.3	-0.5	0
78	0.1	1	1.2	-0.1	1.1	-0.3	-0.2	0.1	-0.4	0.6	0.1	0.2	0	0.4	-0.1	-0.3	0	-0.3	0.1	1.1	-0.1	0.6	0.6	0.1	0.4	-0.1	0.4	-1.2	-0.2	0.4	-0.3	0.5
79	-0.3	-0.7	0.5	0.4	-0.5	0.3	-1	0.9	0.4	-0.6	-0.1	-0.2	0.6	0.4	-0.5	-0.5	-0.4	0.8	-0.1	-0.3	-0.4	0.4	-0.2	-0.3	0	-0.6	0.3	-0.8	-0.1	1	-0.2	0
80	-0.5	-1.1	-0.5	-0.4	-0.8	-0.5	0.6	0.4	0.5	-0.9	-0.4	-0.6	0.5	-0.1	-0.2	0.4	0.4	-0.7	-0.6	-0.7	-0.1	0.5	-0.6	-0.2	0.1	0.5	0.4	0.1	0.6	-0.3	-0.9	-0.7
81	0.2	-1	-0.3	-0.2	-1	0.8	-0.9	0.1	-0.3	-0.4	-0.2	0.7	0.2	-0.5	-1.5	0.3	-0.8	0.4	-0.1	-0.3	0.2	0	-0.5	0.3	-0.2	-0.7	-0.9	0.1	0.6	0.1	0.1	-1.1
82	0	-0.2	0.1	0.1	0.1	0.1	0	-0.1	0	-0.1	0.1	-0.1	0.1	0.1	0	-0.1	0	0.1	-0.1	0	-0.1	-0.2	0.1	0.1	0.1	0	0.2	0.1	0.1	0.1	-0.1	-0.1
83	0.4	0.6	0.7	1.1	0.7	1	-0.6	0	-1.1	0.8	-0.3	0.8	-0.5	0.6	0	-0.9	-0.6	0.2	0.4	0.7	0.5	0.6	0.9	-0.2	0.7	-0.6	-0.9	0.4	-0.6	-0.6	0.1	0.9
84	0.2	0	1.3	0.3	1.1	0.5	0.4	-0.2	-0.4	-0.2	0	-0.7	-0.6	-0.1	-0.2	0.6	0.5	0	1.5	-1.1	0.2	0.1	-0.1	0.6	0.6	0.4	-0.9	0.4	0	0.1	-0.4	0.1
85	-0.6	2.2	0.1	1.2	-0.6	-0.7	0.2	-0.5	0.5	-0.2	0	-0.1	-0.1	0.2	0.4	-0.9	0.5	1.7	1	-0.2	-0.9	0	-0.6	-0.6	0.7	0.3	0.3	-0.3	-0.6	0.1	-0.3	-0.4
86	0.5	-0.1	-0.2	2	1.7	0.2	-1	0	-1.9	-1	-0.2	0.9	0.7	0.4	1.7	0.2	1.1	0.1	0.3	-0.6	0	0.3	-0.2	-0.5	0.3	1.5	0.2	-0.4	-0.2	0.1	-1.4	0.2
87	-0.2	-0.3	-0.4	-0.6	-0.4	0.2	0.5	0.1	0.2	0	0.4	-0.2	0.3	-0.3	0.1	0.2	-0.3	0.3	-0.4	-0.1	0	-0.2	0.3	-0.4	-0.4	0	0	0.3	-0.2	0.6	-0.2	-0.5
88	-0.4	0	0	-0.6	-0.4	-0.3	0	-0.3	0.1	0.6	0.1	0.1	-0.3	-0.1	-0.3	0.1	0.1	-0.1	0.2	-0.2	-0.3	-0.2	-0.1	-0.1	-0.7	0.2	0	-0.2	0.4	-0.1	0	0
89	0.3	0.2	-0.6	-0.2	1.5	0	0.5	-0.4	-0.1	0.8	0.2	-0.2	1	0.2	0.5	0	0.5	0.2	-0.2	1.1	0.4	0.2	0.1	0	0	0.2	0.3	0	0.2	-0.5	0.3	-0.1
90	0	0	-0.1	0.1	-0.2	-0.1	-0.1	0.2	0.1	0	0.1	0.1	0	-0.1	-0.1	0	0	-0.2	0.2	0	-0.1	0	0.1	0	0.2	0.1	-0.1	-0.1	-0.1	-0.1	0.1	-0.1
91	-0.5	0.1	0	-1.3	-0.5	-0.3	0.5	0.3	0.7	-0.8	0.2	-0.1	0.5	-0.5	0.2	0	0.5	0.5	-0.1	-0.3	-0.4	-0.8	-0.7	-0.2	-0.1	0.3	-0.1	0.5	-0.3	0.5	0.6	-1.1
92	-0.3	-0.5	0.5	-0.1	0.4	0	-0.2	-0.6	-0.7	0.2	-0.8	1	-0.2	-0.3	-1.2	-0.1	0.6	-0.4	-0.3	1.2	-0.3	0.6	0.1	-0.6	1.2	0.6	-1	0	-0.2	-0.4	-0.4	0.1
93	0	0.2	0.2	-0.1	-0.1	0.3	-0.1	-0.4	-0.1	-0.1	0.2	-0.4	0.1	-0.1	0	0	0.2	0	-0.2	0	-0.2	0.1	-0.2	0	-0.1	-0.2	-0.2	-0.1	0.3	0.3	0.2	0.3
94	0	-0.1	-0.2	0	0	0.1	0	0	0.1	-0.1	0	0	-0.1	0	0	-0.1	0.1	0	0	-0.1	-0.1	0.1	-0.1	-0.1	0.1	-0.1	-0.1	-0.1	0.1	0	-0.1	-0.1
95	0	-0.1	0.1	0.1	-0.2	-0.1	-0.1	-0.1	0	0	0	0	-0.1	-0.1	0.1	-0.1	-0.1	0.1	-0.1	0	0.2	0.1	0	0.1	0.1	-0.2	0.1	-0.1	-0.1	0	0.2	0
96	0.2	-0.5	-0.1	-0.2	-0.3	-0.1	-0.2	-0.1	0.3	-0.4	0.2	-1	0.3	0.2	-0.2	0.7	-0.6	0.1	-0.1	-1.3	0.2	0.2	-0.1	-0.3	-1	0	-0.1	-0.6	-0.3	0.5	-0.3	0.5
97	0.4	-0.7	0.6	-0.4	0.6	-0.3	0	-0.5	0	0.8	-0.2	-0.2	-0.6	-0.7	-0.5	0.4	-1.2	-0.1	0.7	0.5	0.4	-0.1	1.1	0.7	0	-0.8	1.3	0.1	0.6	-0.3	0.6	0.8
98	0	0.2	0	0.1	0.1	-0.1	0.1	0	0.2	0.1	0.1	0.1	0	-0.1	-0.1	-0.1	0	-0.1	0	0	0	0	0.1	0.2	-0.2	0.1	0	0.1	-0.1	0	-0.1	0.2
99	0	0.1	-0.1	-0.1	0	-0.1	0	0.1	-0.1	-0.2	0.1	-0.1	-0.1	-0.1	-0.1	-0.1	0	0	0.1	0	0.1	0	0	0.1	0	-0.1	0	0	0.2	0	0	0.1
100	0.3	-0.1	-0.2	-0.4	-0.1	0	-0.3	0.2	0.1	0.2	0.1	-0.1	-0.1	-0.5	0	-0.3	-0.3	0.1	-0.2	-0.1	0.2	-0.3	0.2	0.3	-0.2	-0.6	0.2	-0.1	0.2	-0.2	0.2	0.2
101	-0.1	0.1	0	0.1	0.1	0	0	-0.1	0	0.1	-0.1	0.1	0.2	-0.2	0.2	0	-0.1	-0.2	-0.1	0.1	-0.1	0.1	-0.1	0.1	0	0	0.1	0	-0.2	0	0	-0.1
102	0.1	0	0	-0.1	-0.1	-0.1	0	0.1	0	0	0	-0.2	0.2	0.1	0.1	0.1	0	0	0.2	-0.1	0	0	0.1	0.1	-0.1	0	-0.1	-0.2	0	0	-0.1	-0.1
103	0.1	0	0	0	-0.1	0.1	0.1	0.1	0	0.2	0	0.1	0	0.1	0	-0.1	0.1	0.1	0.1	0	-0.1	0	-0.1	-0.1	0	-0.2	-0.1	0	-0.1	-0.1	0	0.1
104	-0.1	0.1	-0.1	0	0	0.2	0.1	0.2	0.1	0	0.2	0	0	-0.1	0.1	0.2	0.1	0.1	0	0.1	-0.1	-0.1	0.1	0	0	0.1	0	-0.1	-0.1	0.1	0	-0.1
105	-0.3	-0.1	-0.7	0	0	0	-1	-1.2	0	0.7	1	-0.6	1	-0.2	0.6	0.2	0.9	0	0	0.9	-0.2	-0.9	-0.8	0.7	0.2	-0.1	0.9	-1.2	1.3	-0.1	-0.3	0.8
106	0.1	-0.1	-0.1	0	-0.1	-0.1	-0.1	0	0.1	-0.1	0.1	-0.1	0.1	0.1	0	0.2	0	0.2	0.1	-0.1	0.1	0.1	-0.1	0.1	0	-0.1	0.1	-0.1	0.1	0	-0.1	0.1
107	0	0	-0.2	0	0.2	0	0	-0.1	0.1	0.1	0.1	0	0.1	-0.1	0.1	-0.1	0.1	-0.1	-0.1	0	0.1	-0.1	-0.1	-0.1	-0.1	-0.1	0	0.1	-0.1	0.1	-0.1	0
108	0	0.2	0.6	0.2	0	0.1	0	0.9	0.2	-0.1	0	-0.1	-0.4	-0.3	0.1	-0.1	-0.3	0	0.1	0.2	0.3	0.5	0.6	0.3	0.4	0.1	-0.2	0.6	-0.2	-0.2	-0.3	0.1
109	0.1	-0.2	-0.1	-0.1	0.1	-0.1	-0.1	-0.1	-0.1	-0.2	0	0.1	0.1	0	0	-0.1	0	-0.1	-0.1	-0.1	0	-0.2	0	0.1	0	0.1	0	0	0.1	0.1	0.1	-0.1
110	-0.2	0	-0.2	0	-0.2	-0.1	0.2	0.5	0.2	-0.2	-0.4	0	0.1	0.4	-0.4	0.1	0.2	0.1	0.4	-0.5	-0.1	0.3	-0.3	-0.4	0.2	-0.4	-0.2	0.1	-0.1	0.3	-0.5	-0.7
111	-0.6	0.6	-0.7	-0.2	0.3	0.1	-0.5	-1.2	0.1	0.4	-1	0.4	-0.2	-0.6	-1.4	-0.1	-0.2	0	0.5	0.3	0.9	0.8	-0.2	0.1	0.3	0.8	-0.7	0.1	0.6	-1	-0.1	-0.3
112	0	-0.1	-0.1	0	-0.2	-0.1	0	-0.1	-0.1	0.1	0.2	-0.1	0.1	-0.1	-0.1	0	0	-0.1	-0.1	-0.1	-0.2	-0.1	0.1	0.2	-0.1	0	0.1	-0.1	0.1	-0.1	0	0.1
113	-0.1	0	0	0.1	0.1	0	0.2	0.2	0.2	-0.1	-0.1	-0.1	0.1	0	0.1	-0.1	0.1	-0.1	-0.2	-0.1	0.1	0.1	0	-0.1	-0.2	0	0.1	-0.1	0	-0.1	-0.2	-0.1
114	-0.1	0.1	0	-0.1	0.1	-0.1	-0.1	-0.1	-0.1	-0.1	0	0	0	0	-0.1	0.2	0	0	0	-0.1	-0.1	0.1	0.1	-0.1	0	-0.1	0	0.1	0.1	-0.1	0.1	-0.2
115	-0.5	-0.6	0.7	0.9	0.6	-0.7	0	0.3	-1.3	-0.2	-0.5	0.1	0.6	-0.1	-0.1	0.4	0.1	-1	0.5	-0.3	0.6	1.2	-0.1	0.2	-0.1	0.4	0.5	0.5	0.3	-0.4	-0.9	0
116	0.8	0.1	0.2	1.7	-0.7	0.3	0	0.3	1.5	-1.6	-0.3	1	-0.2	0.3	-0.5	0.4	0.1	-0.3	0.1	-0.5	0.2	0.4	-0.7	-0.2	0.5	0.3	0.1	-0.2	-1	0.5	0	0.4
117	-1.1	1.1	0.4	-1.1	-0.7	0.5	-0.2	0.7	0.4	-0.2	-1.9	1.7	-0.3	0.8	-2.3	-0.5	-0.8	0.4	0.7	-0.3	-0.5	-1	0.5	-0.9	1.7	-1.3	-1.4	0	-0.5	-0.4	0.6	-1.1
118	-0.3	0.4	0	-0.2	-0.5	0	0.6	0	0.8	-0.5	-0.3	0	0.4	0.4	-0.5	-0.1	-0.2	0.2	0.4	-0.5	-0.3	0.1	0.1	-0.1	-0.5	0.2	-0.4	-0.5	0.2	0.6	0	-0.1
119	0	0.6	0.4	0.3	0.4	0.5	-0.8	-0.7	-0.3	0.8	-0.4	0.8	-0.3	0.7	-0.3	-0.9	-0.3	0.2	0.6	0.8	0.3	0.4	0.1	0.4	0.5	-0.8	-0.8	0.4	0.1	-0.9	0.7	0.3
120	0	0.6	0.8	-0.4	-0.4	-0.2	0.2	-0.6	1.1	0	1.3	1.3	-0.5	0.6	0.4	0.7	0.7	0.2	0.3	1.5	-0.8	-0.9	0	0.4	-0.7	0.7	0.5	-0.6	-0.6	0.7	0	0.5
121	-0.1	0.7	0.6	0.4	0.2	0.6	0.1	0.3	-0.2	0	-0.8	0.5	-0.6	0.2	-0.7	-0.4	0.1	0.5	1	-0.2	0.5	0.7	0.3	0.6	0.4	-0.1	-1.2	0.6	-0.5	-0.4	-0.2	-0.8
122	0.1	0.1	0.1	0.4	0.2	0.7	-0.2	0.3	-0.4	-0.1	-0.4	0.6	-0.1	0.1	-0.3	-0.7	-0.2	0.1	0.2	-0.2	0.3	0.1	-0.1	0.4	0.3	-0.2	-0.6	0.5	-0.4	-0.3	-0.1	-0.6
123	-0.6	0	-0.2	1.2	0.5	0.5	-0.1	-0.9	-0.9	0.3	0.1	0	-0.1	0	0.3	-0.6	0	0.5	0.4	0.2	-0.4	0	0	0.7	1.2	-0.5	-0.7	0.2	-0.4	0.2	-0.1	0
124	0.3	-0.6	-0.5	-1	-0.7	-0.3	0.2	0.4	0.2	-0.1	-0.4	0.1	0.3	-0.1	0	-0.1	-0.7	-1.1	-0.8	0	0.3	-0.1	0.2	-0.2	-0.1	-0.4	0.1	0.2	1	-0.5	0.7	0.2
125	0.1	-0.1	0.1	0.1	0.1	0	0.1	-0.1	0.1	-0.1	0.1	-0.2	-0.1	-0.1	0	0	-0.1	-0.1	0.1	0.1	0.1	0.1	-0.1	-0.2	0.1	0.1	0.1	-0.1	0	0	-0.1	0.2
126	-0.2	0.2	1.5	-0.3	1.2	-0.2	0.2	1.1	-1.1	0	-0.9	0.8	-0.2	0.1	-0.2	-0.5	-0.4	-0.5	1.7	-0.3	0.2	1	0.6	1	0.5	0.2	0	1.2	0.1	-0.7	-0.4	-0.2
127	0.2	0.4	0.5	0.3	0.2	1.5	0.5	0.4	0	-0.1	0.4	0.7	0.5	-0.2	0.7	-1	0	0.7	-0.3	-0.3	-0.1	0.7	0.1	0.2	-0.4	0.3	-2	-0.3	0	0.6	0.4	-0.3

i	33	34	35	36	37	38	39	40	41	42	43	44	45	46	47	48	49	50	51	52	53	54	55	56	57	58	59	60	61	62	63	64
128	0.1	0.5	0	-0.1	1.8	0	-1.5	0.6	1	0.5	0	-0.1	-0.7	-0.1	-0.3	0.1	0	-0.1	-0.2	0.5	0	-0.3	0.3	0.4	-0.2	0.1	-0.4	-0.5	-0.1	-1.5	0.1	0
129	0.5	-0.4	0.6	0.5	-0.2	-0.5	0.2	1.7	-1.6	-0.7	-0.7	-0.3	0.6	0.4	0.1	0.4	0.3	-0.3	1.9	0.2	0.3	-0.3	-0.1	-0.5	0.3	0.6	0.6	0.9	0.3	-1.2	-0.8	-0.6
130	0.9	0.1	0.4	1.1	-0.1	0.4	0	0.2	-0.3	-0.1	0.1	-0.7	0.6	0.2	0.3	0	-0.5	0.2	0	-0.3	0.1	0.4	0.2	-0.4	-0.6	0.2	0	-0.1	-0.7	0.2	0	0.4
131	0.1	0.1	-0.1	0	0.1	0.2	0	0.1	-0.1	0	0.1	0	-0.1	0.1	0	0	0.1	-0.1	0	0.2	-0.1	-0.2	0.1	0	0.1	0.1	-0.1	-0.1	-0.1	0.1	0	0.1
132	1.4	0.3	-0.8	0.9	0.6	-0.8	0.3	-0.1	0.6	-0.7	0.4	-0.5	1.4	-0.2	-0.2	1	0.1	0.7	-0.7	-1	1.4	-0.9	-1.5	-0.3	-0.1	0.6	0.9	0.2	-0.6	0.6	0.9	0.4
133	-0.3	0.1	0.1	0.5	-0.7	-0.1	0.2	0.2	-0.2	-0.7	0	0.2	-0.1	0.4	0.3	0	0.1	0.2	-0.4	-0.6	-0.4	0.1	-0.3	-0.6	0.3	0.4	0.1	0	-0.8	0.1	-0.3	-0.6
134	-0.6	1	1.3	-0.5	1.3	-0.2	-1	-0.8	-0.3	0.6	0.9	-1.3	-0.3	-0.1	1	-0.9	-0.3	0.2	0	0.1	-0.5	-0.6	0.8	0.6	0.5	-1.3	0.5	-0.3	-0.1	-1	-0.3	-0.2
135	0.2	-0.3	1.5	1.2	0.6	0.7	-0.3	0.4	-0.9	0.3	-1	0.9	-0.2	-0.3	-0.2	-0.2	-0.1	0.1	1.2	-0.2	0.8	0.7	0.3	0.1	1.1	-0.1	-1.7	1	0.2	-0.5	-0.2	0
136	-0.1	-0.1	-0.1	0	0.1	-0.2	0	0	-0.1	0.1	0	0	0.2	-0.1	0	0.1	-0.1	0.1	0.1	-0.1	0.1	-0.1	-0.1	0.1	0	-0.2	-0.1	0	0	-0.1	0	-0.1
137	0.3	0.3	0.1	0.1	0	0.2	-0.2	-0.3	-0.1	0.5	-0.1	-0.2	0.2	0.2	-0.4	-0.3	-0.3	0.7	-0.2	1.8	-0.1	-0.1	0.4	0	-0.3	-0.2	-0.1	0.2	-0.4	0.1	0.6	0.3
138	0.4	-0.4	-0.1	0.1	-0.5	0.4	0.6	0.5	-0.2	-0.3	-0.6	0	0	0.3	-0.6	0.5	0	-0.4	0	-0.1	0.2	-0.2	0	-0.3	-0.2	0.6	-0.3	0.3	0.4	-0.1	0.2	-0.6
139	-0.6	0	-1.3	-0.3	-0.7	0.9	-0.6	0.1	-0.6	-0.3	0.7	-0.8	-0.4	0.1	0.6	-0.7	1.1	0.8	-0.8	-0.4	-0.8	-0.2	-0.8	-0.6	-0.3	-0.4	-1.1	-1	1	0.5	-0.2	0.2
140	-0.1	-0.1	0.1	0.1	0.1	-0.1	0.1	-0.2	-0.1	0.1	0	-0.1	0	0.1	0.1	0	-0.1	-0.1	-0.1	0	0.1	-0.1	0.1	0.1	-0.1	-0.1	0.2	-0.1	0.1	0	-0.1	-0.1
141	-1.2	0.5	-0.3	-0.7	-0.3	0.3	0.2	0	0	-0.3	-1.3	0.8	0	0.2	-1.3	-0.2	0.4	0.5	0.6	0.3	0.1	-0.1	0	-0.2	0.8	0.4	-0.5	0.9	-0.2	-0.4	1	-1.1
142	0.5	-0.4	0.2	-0.2	0.4	-1.1	0	-0.1	0.2	-0.3	0.3	-0.2	-0.7	-0.3	0.4	0.6	-0.5	-0.3	-0.7	0.9	0.7	0	0	0.2	-1.1	-0.1	1.2	0.1	-0.2	0.8	0.1	0.6
143	1.2	-0.7	-0.8	1.3	-0.1	1.5	-0.6	0.5	-1.3	-0.3	0.2	-1	1	-0.6	0.3	-1.2	0	-0.3	0.3	-0.6	0.9	-0.9	-0.4	0.1	-0.2	-1.4	-0.3	1.3	0.5	-0.5	0.3	0.5
144	0.2	0.9	0.6	0.2	0.9	-0.6	-0.4	-0.3	0.4	0.3	-0.8	0.5	-0.7	-0.2	-0.3	0.2	-0.2	0.3	0.2	0.7	0.6	0.7	0.3	-0.1	0.3	-0.5	-0.7	0.8	0.1	-0.5	0.7	0.1
145	0.6	-0.2	-0.2	0.5	0.5	0.3	-0.6	0.2	-0.8	0.9	-0.2	0	-0.4	0	0	-1	-0.6	0.7	-0.1	0.6	-0.1	0	1	0.2	-0.2	-0.9	-0.2	-0.1	-0.2	-0.9	-0.1	0.2
146	0	-0.1	0	0	-0.2	0.1	-0.2	0.4	-0.3	0.1	-0.1	0.5	-0.1	0.2	-0.2	0.3	0.1	-0.5	-0.2	0.2	0.3	0	0	0	0.4	0.2	-0.4	0.3	0.2	-0.5	-0.1	-0.1
147	0.2	-0.3	0.1	0.5	0.5	0.4	0.2	-0.3	-0.3	0.1	0	0.1	0.1	-0.1	0	0.1	-0.2	0	0	-0.2	0	0.2	0	0	0	0.1	-0.5	0	-0.1	0	0.4	0.3
148	-0.2	0.3	0.2	0.3	-0.2	-0.3	-0.1	0	0.2	-0.4	-0.2	0	0.1	0.1	0.1	-0.1	0.3	0.5	0.3	0.1	-0.1	0.2	0	-0.2	-0.1	0	0.2	-0.2	-0.1	0.3	-0.2	-0.5
149	0.3	0.6	-0.2	-0.5	-0.5	-0.4	-0.1	-0.5	0.8	0.6	0.2	-0.2	0	0.1	-0.2	0	-0.2	0.1	-0.4	0.2	-0.2	-0.2	-0.2	-0.4	-0.8	0	0.1	-0.3	0.1	0	0.3	0.4
150	0	-0.3	0.1	-0.8	-0.5	0.3	-1.1	1.1	0	-0.4	-0.2	-0.2	-0.4	-0.8	-0.2	-0.3	-0.2	0.2	0.2	-0.1	0.5	0.5	0.5	0.6	0.3	-0.3	-0.7	0.9	0.6	-1.9	-0.3	-0.3
151	-0.1	-0.5	-0.5	-0.1	-0.2	-0.1	-0.1	-0.1	0.3	0	0.3	-0.4	0.2	-0.1	0.3	0.4	0.5	-0.3	-0.6	0.2	-0.1	-0.3	-0.2	0.2	-0.4	-0.1	0	-0.1	0.4	-0.1	0	0.3
152	-0.1	0.1	-0.3	-0.2	-0.4	-0.6	0.4	-0.2	0	-0.5	0	-0.4	-0.1	0.3	0.6	0.2	0.3	-0.3	0.2	-0.3	-0.4	0.2	-0.2	-0.1	-0.2	0.5	0.2	-0.2	-0.2	0.2	-0.3	-0.1
153	-0.1	0	0.1	-0.1	0.1	-0.1	-0.1	-0.2	0	-0.1	0.1	-0.2	0	-0.1	0.2	0	0	0	0	-0.1	0	0	0.1	0	0	0	0	0.1	-0.1	0	0	0
154	0	0	-0.1	0.1	-0.2	0.2	-0.1	0.2	-0.1	-0.1	0.1	-0.1	-0.2	0.2	0.1	-0.1	-0.1	-0.1	-0.1	-0.2	0.1	-0.1	0.2	0	0.1	0	-0.1	0	0	0	-0.2	0.1
155	0	0	0	0	0.2	-0.1	0	-0.1	0	0.1	0	0	0.1	0.1	0	-0.1	0	-0.1	0.1	0.2	0.1	-0.2	-0.1	0.1	0.2	0.1	0.1	0.1	0	0	0	0
B1	0	0.2	0.2	0.2	0	0.2	0	-0.1	-0.1	-0.1	-0.1	0	0	0	0	-0.1	-0.1	0.3	0.2	0.1	0.1	0.1	0	0	-0.1	0	-0.3	0	-0.1	0.1	0	0

Table D.7 - ANN-UQo_{HY}'s weights and coefficients for the second hidden layer

k	1	2	3	4	5	6	7	8	9	10	11	12	13	14	15	16
1	0.1	-0.1	-0.4	0	0	-0.4	-0.2	-0.1	-0.4	0	-0.4	-0.3	0	-0.4	-0.1	-0.1
2	-0.4	0	-0.4	0.1	0	-0.3	0	0.1	-0.1	-0.3	-0.2	-0.3	0.1	-0.2	0	0.3
3	0.1	0.1	0.2	0	-0.1	0.1	-0.7	0.3	0.1	0.1	0.1	0.2	-0.1	0	0.2	-0.5
4	0.1	0.1	0	0	-0.5	0	0	-0.2	0	0.1	0.1	0.1	0	0	-0.5	-0.2
5	0	0.2	0	-0.6	-0.7	0	0.2	-0.4	0	0	-0.1	-0.1	0.3	0	-0.3	-0.1
6	0.2	0.1	0.1	0.2	0.1	0.2	0	0	-1.1	0.1	-0.9	0	0	-1.1	0	-0.2
7	0	-0.2	0.1	-0.8	-0.7	0	-0.4	-0.1	0	0	0	0	-0.3	0	-0.4	-0.2
8	-0.5	-0.6	0.2	0.1	-0.1	0	-0.1	-0.3	0.1	0.2	0.2	0.1	-0.2	0.1	-0.1	0.1
9	0	0	0	-0.7	-0.5	0	-0.1	-0.5	0	0.1	0.1	0.1	0	0	-0.6	0.1
10	-0.8	-0.4	0	0.1	-0.4	0	0.1	-0.4	0	0	0	0	-0.1	0.1	-0.6	-0.3
11	-0.1	-0.6	0.1	0	-0.3	0	-0.3	-0.3	0	0.1	0.2	0.2	-0.2	0.1	-0.2	-0.4
12	-0.4	-0.2	-0.3	0.2	0.2	-0.8	0	-0.5	-0.2	-0.9	-0.5	-0.8	0.3	0	-0.1	-0.1
13	0	-0.6	0	-1.2	0.2	0.1	0.1	-0.7	0	0	0	0.1	-0.4	0	-0.4	0
14	0	0	-0.9	0	0	-1.1	0	0	-0.8	-1.4	0	0	0	-0.5	0	0
15	-0.3	-0.2	0	-0.4	-0.1	0.1	-0.5	-0.2	0	0	0	0.1	-0.5	0	-0.2	-0.2
16	0.1	0.1	0	0	0.1	-0.4	0.1	-0.1	0	0.1	0.1	0	0.1	-0.1	0.1	-0.3
17	0	-0.6	0.1	-0.2	-0.4	0	-0.4	-0.3	0.1	0	0	0.1	-0.2	0	-0.4	-0.3
18	0	-0.3	0.1	-0.5	-0.3	0	-0.5	-0.2	0	0	0.1	0.1	-0.6	0	0	0
19	0	0.1	0.1	-0.4	-0.2	0	-0.3	-0.2	0	0.1	0.1	0.1	-0.6	0	-0.3	0.2
20	-0.4	0.1	0	0	0	-0.1	0	0	-0.5	-0.6	-0.6	-0.7	0.1	0.1	0	0.2
21	-0.1	0	0.1	-0.5	-0.7	0	-0.4	0	0	0.1	0.2	0	-0.5	0.1	0.1	-0.2
22	0	-0.4	-0.1	-0.3	-0.3	0	-0.4	-0.2	0	0.1	0.1	0	-0.6	0	-0.2	-0.1
23	-1.1	-0.1	-0.1	0	0.1	-1.5	0.1	-0.6	0.1	0	0.1	-0.2	0	0.1	-0.1	0.1
24	-0.8	-0.2	-0.1	0.1	0.1	-0.3	0.2	-0.3	-0.3	-0.3	-0.3	-0.3	0.2	-0.1	0	-0.1
25	-0.8	0	0	0	0	0	0.1	0.1	0	-0.8	-0.7	-0.9	0.1	0	-0.1	-0.1
26	0	-0.7	0.1	-0.4	-0.5	-0.7	-0.7	-0.2	0	0.1	0.1	0.3	-0.9	-0.6	-0.2	0
27	0	0	0	0	0	0	-0.3	0	-0.7	0	0	0	0	-1.1	-0.2	-0.5
28	-0.7	-0.2	0	0	-0.5	0	-0.2	-0.1	0	0	0.1	0	-0.1	0	0	-0.3
29	-0.5	0	0	0	0	0	-0.5	0	0.1	0	0	0	0	0	0	0.1
30	0.1	0	-0.7	0	0	-0.8	0	0	-0.6	-0.7	-0.3	-0.3	0.1	-0.2	0.1	0
31	0	-0.5	0	0	-0.2	0.1	-0.4	-0.6	0.1	0	0	0.1	-0.1	0	-0.2	-0.2
32	0.1	-0.3	0.1	-0.3	-0.4	0	-0.4	-0.2	0.1	0.1	0.1	0.1	-0.2	0.1	-0.3	-0.2
33	-0.7	0	-0.2	0	0	-0.2	0	-0.2	-0.3	-0.3	-0.1	-0.1	0	-0.6	0	-0.5
34	-0.1	-0.4	0	-0.2	-0.1	0.1	-0.3	-0.1	0.1	0	0.1	0	-0.3	0.3	-0.2	-0.4
35	-0.1	0.1	0.3	0.1	0	0.1	0	0.3	0.1	0.1	0.3	0.4	-0.1	0.1	0.1	0
36	-0.2	0.1	-0.5	0.2	0.1	-0.5	0	0	-0.6	-0.5	-0.4	-0.3	0	-0.6	0.1	0
37	-0.1	-0.3	0.1	-0.2	-0.3	0	-0.3	-0.2	0	0	0	0	-0.3	0.1	-0.2	0.1

k	1	2	3	4	5	6	7	8	9	10	11	12	13	14	15	16
38	-0.3	0	-0.7	0.1	0.1	-0.3	0	-0.1	-0.4	-0.6	-0.5	-0.7	0.2	-0.5	0	-0.1
39	-1.1	-0.3	0	0	0	0	-0.3	-0.2	0	0	0	0	-0.1	0	-0.3	-0.1
40	-0.4	0.1	-0.5	0	0	-0.4	-0.2	0.1	-0.5	-0.3	-0.2	-0.4	0.1	-0.5	-0.5	-0.2
41	0	-0.6	0.1	0.2	0.1	0.2	-0.5	-0.4	0.1	0.1	0.1	0.1	0	0	-0.5	-0.3
42	-0.6	0.1	-0.2	0.1	0.1	-0.2	0.2	0.1	-0.1	0	0	-0.1	0.1	-0.5	0.2	-0.1
43	-0.5	0	-0.1	0	0	-0.5	0	0	-0.6	-0.8	-0.9	0	0	-0.9	0	-0.2
44	-0.8	0	-0.3	0	0	-0.8	-0.1	0	-0.2	-0.9	-0.1	-0.4	0.1	-0.2	0	0.1
45	0.1	-0.4	0.2	0.2	-0.3	0.2	-0.3	-0.4	0.1	0.1	0.2	0.1	-0.2	0.2	-0.9	-0.2
46	0	0	0	-0.1	-0.9	-0.1	-0.8	-0.5	0	0	0	0.1	-0.1	0	-0.5	-0.2
47	0	-0.4	0.2	0	-0.1	0	-0.2	0	0.1	0.1	0.1	0.3	-0.2	0.2	-0.2	-0.1
48	-0.6	0	-0.5	0.1	0.1	-0.5	0	-0.2	-0.5	-0.4	-0.3	-0.2	0.1	-0.8	0	0.1
49	0	0	0	-0.3	0	0	-0.2	-0.4	0.1	0	0	0	-0.6	0	-0.5	-0.3
50	0.1	-0.5	0.2	-0.2	-0.3	0.1	-0.6	-0.1	0.1	0.1	0.1	0.1	-0.9	0	-0.2	-0.2
51	0.1	-0.3	0	-0.7	-0.6	0	0.2	-0.2	0	0	0.1	0.1	0.1	0	-0.3	0.1
52	-1	-0.5	-1.4	0.1	0.1	-1.3	0.1	0.1	-0.4	-1.1	-0.4	-0.3	0.1	-0.5	-0.3	-0.1
53	0.1	-0.4	0	-0.5	-0.3	-0.1	-0.4	-0.5	-0.1	0	0	0.1	0	0	-0.3	-0.5
54	0.1	-0.3	0	-0.1	-0.1	0	-0.2	-0.3	0	0	0	0	0	0	-0.2	-0.3
55	0.1	-0.1	0	-0.1	-0.6	0	-0.1	0	-0.2	-0.6	0	0	-0.3	0.1	-0.1	0.1
56	0	-0.1	0.1	-0.7	-0.4	0	-0.6	-0.2	0.1	0	0.1	0.2	-0.2	0.2	-0.5	0.1
57	0	-0.3	0.2	0.1	-0.6	0.1	-0.6	-0.3	0.1	0.1	0.1	0.1	-0.8	0.1	-0.4	-0.1
58	-0.1	0.1	-0.3	0.1	0.1	-0.5	0.1	-0.4	-0.4	-0.5	-0.4	-0.3	0.1	-0.3	0.1	0
59	0.1	-0.4	0.4	-0.7	-0.4	0.1	-0.6	-0.3	0.2	0.1	0	0.2	-0.8	0.2	-0.2	0.1
60	0	0	0.1	-0.5	-0.5	0	-0.6	-0.1	0	0	0.1	0.1	-0.2	0	-0.1	0
61	-0.3	0	-0.1	0	0	-0.3	0	0	-0.4	-0.4	-0.2	-0.2	0	-0.4	0	0
62	0	-0.3	0.1	-0.7	-0.6	0	0	-0.4	0	0.1	0.1	0.1	-0.1	0	-0.4	-0.2
63	0.1	-0.4	0.5	-0.7	-0.4	0.4	-0.2	-0.3	0.1	0.3	0.2	0.4	-0.4	0.5	-0.3	-0.2
64	-0.7	-0.1	-0.4	0.1	0.1	-0.2	0	0.1	-0.2	-0.2	-0.3	-0.3	0.1	-0.3	0.1	-0.2
b2	0	0.1	0.1	0.1	0.1	0.1	0.1	0	0.1	0.1	0.1	0.1	0.1	0.1	0.1	-0.1
W3	0.2	-0.1	0	-0.1	-0.1	0.1	-0.1	-0.2	0	0.1	0	0	-0.1	0	-0.1	-0.1

Table D.8 - ANN- UQo_{HY}'s weights and coefficients for the first hidden layer

i	1	2	3	4	5	6	7	8	9	10	11	12	13	14	15	16	17	18	19	20	21	22	23	24	25	26	27	28	29	30	31	32
1	-0.1	-0.1	0.2	0	-0.1	0	-0.2	0	0	0.1	0.1	-0.1	-0.1	-0.2	-0.1	-0.3	-0.1	-0.3	0	0	0.2	-0.2	-0.2	0.2	0.2	-0.2	-0.4	0.1	0.1	-0.1	0	0
2	-0.1	0.3	0	0	0	-0.2	0.2	-0.1	0.2	-0.1	0.2	0.1	0.1	-0.3	0.2	-0.2	0.4	0.2	0.1	0	0	0.3	-0.1	-0.2	-0.2	-0.1	0.2	0.1	-0.1	-0.3	0.2	0
3	-0.2	0.1	0	-0.1	0.1	-0.1	0	0	0.2	-0.2	0.1	0.1	0.2	0	-0.3	0	-0.3	-0.1	-0.2	-0.1	0	0	0.2	0.2	0	-0.1	0.2	-0.4	0	0.1	-0.1	-0.1
4	0.2	0.2	0.1	-0.1	-0.1	-0.1	0.3	-0.1	0	0.2	0	-0.1	0.1	-0.2	0	0.1	-0.1	0.1	-0.1	0	0	0.1	0	-0.1	0	0	-0.1	0.3	0.1	0.1	0.2	0.2
5	-0.5	0.1	-0.3	-0.2	-0.2	-0.1	0.1	-0.1	0	-0.1	-0.1	0.1	0	0	0.1	0.2	-0.2	-0.1	0	0.2	-0.1	0.2	-0.1	0.1	0.1	-0.2	0	-0.1	0	0.3	-0.1	0
6	0.2	-0.1	-0.1	0	0	0	0	-0.1	-0.1	0	0.1	0.2	0.1	0	0.1	-0.1	0.1	0.1	0	0.1	0.1	0	0	0.1	0.1	0.1	-0.1	0	0.1	0	0	0.1
7	-0.2	0.2	0.1	0	0	-0.1	0.1	0.1	-0.1	0.1	-0.1	-0.2	0.1	0	0	0.2	-0.1	0	0	0	-0.2	0.2	-0.1	0	-0.1	0	0	-0.1	-0.3	0	0.1	0
8	-0.2	-0.1	-0.1	0.1	-0.2	-0.2	-0.1	0.1	-0.2	0.1	-0.1	-0.1	-0.1	0.1	0.1	0	-0.1	0	0	0.2	-0.1	-0.1	0.1	-0.1	0.1	-0.3	0	-0.1	0	0	-0.1	0
9	0	0.3	0	0.1	0.2	0	0	0.2	-0.1	0.1	-0.1	-0.2	0	0	0.1	-0.1	-0.1	0.2	-0.1	-0.1	0.1	0	-0.1	-0.1	-0.3	-0.2	-0.1	0.1	-0.2	-0.2	-0.1	-0.1
10	-0.1	-0.1	-0.1	0	0	0	-0.1	-0.1	-0.2	0.2	0.1	-0.1	-0.2	0	-0.1	0	0	-0.1	0.2	0.1	0	0	0.1	0.1	-0.1	0.1	-0.3	0.2	0	0	0	0.1
11	-0.1	0	0.1	-0.1	-0.1	-0.3	0	-0.1	0.1	0	0.1	-0.2	0.1	0	-0.1	0.2	0.2	0	0.1	0	0	0.1	0.1	0.1	-0.1	-0.1	-0.1	0	0	0	0.2	0.1
12	0.3	0.1	0	0.2	-0.1	0.1	0.2	0.2	0.3	0.1	0	0.2	0.3	0.1	-0.2	0.2	-0.1	-0.3	0	0.1	0.2	0.1	0.1	-0.2	0.1	0.1	0	0	-0.2	0	0.1	-0.2
13	-0.1	-0.2	-0.2	0.2	0	0	-0.1	0.1	0.2	0.2	-0.2	0	-0.1	-0.5	-0.2	0	-0.1	-0.3	0	-0.2	0	-0.1	-0.1	-0.3	0.1	-0.1	-0.2	0.2	0.2	0	0	-0.2
14	0	-0.1	-0.2	0.2	0	-0.1	-0.2	0	-0.2	-0.1	0	0.1	-0.4	0.1	0	-0.1	-0.1	0.3	-0.1	0.1	-0.1	0	0	-0.1	0	-0.1	0	0.1	0.1	0.1	-0.3	0
15	0.1	-0.2	0.1	-0.1	-0.2	0.1	-0.3	-0.1	-0.5	-0.1	0.1	0	0	0	-0.2	-0.1	0.2	-0.1	0.2	-0.3	-0.1	0	-0.3	0	0.1	0	-0.2	0.1	0.1	0	0	0
16	0	0.1	0	0	0.1	0.1	0.1	0	-0.1	0	-0.1	0.1	0.1	0.1	-0.1	-0.1	0	-0.1	0.1	-0.1	0	-0.2	0.1	-0.1	0.1	0.3	0.2	0	0.1	0.1	0.1	0
17	0	0.1	0	-0.1	-0.1	-0.1	0.2	0	0	0.3	0.1	0.2	0.1	-0.1	-0.2	-0.1	-0.1	0	0.1	0.2	0.1	0.1	-0.1	0.1	-0.5	-0.4	0.1	-0.1	-0.2	-0.4	0.1	0
18	-0.2	-0.2	-0.1	0.1	0	0	0.2	-0.3	0	0.1	-0.4	-0.2	-0.2	0	0	-0.2	-0.1	-0.1	0.1	-0.1	0.1	0.1	-0.2	0.1	0.3	-0.2	0.1	0	0.4	0.2	0	-0.3
19	0.2	0.1	-0.3	0.2	-0.2	-0.2	-0.1	0	0	0.2	0.1	0	0	0.2	0.1	0	-0.3	0	-0.2	0.1	-0.1	0	0.2	-0.2	-0.1	0.1	-0.1	0	0	-0.1	0	-0.1
20	0.1	0.1	-0.2	0.2	0.3	0	-0.2	-0.3	0	0.1	0.1	0.1	0	-0.2	0	0	0	-0.3	0.1	0.1	-0.2	0.1	-0.1	0.2	-0.2	0.1	-0.2	-0.1	0.1	0	0.2	-0.3
21	0.1	0.2	0	0.1	0	0	0	-0.2	-0.2	-0.3	0.1	-0.1	0	-0.1	0	0.2	0.3	-0.2	0.3	0	0	-0.4	0.1	0	-0.4	0.3	-0.2	0.2	0	0.1	0.2	0.1
22	-0.1	0	-0.2	0	0.4	-0.1	0.2	-0.2	-0.1	0	0.2	0.3	0.2	0.1	0.2	0.2	0	0.3	0	0.1	0.1	-0.2	0.8	-0.1	-0.1	0.3	0.1	0.1	-0.1	0.2	0	0.2
23	0.2	0.1	0.1	-0.1	-0.2	0	0.1	0.1	0.1	0.1	0	-0.3	0	-0.3	0.1	0.1	-0.1	0.2	-0.2	-0.1	0.1	-0.1	0	0.3	-0.2	0.2	-0.1	0	0	-0.2	-0.1	0
24	-0.1	0.2	-0.2	0	-0.2	-0.4	-0.2	0.1	-0.1	-0.5	0.1	-0.4	-0.5	-0.6	0.1	0	0	-0.2	0	0.1	-0.2	-0.1	-0.4	-0.1	0	-0.6	-0.3	0.2	0	-0.1	-0.3	-0.1
25	0.1	0.1	-0.2	0	0.1	0.1	0.2	0	-0.2	-0.2	0.2	-0.2	0.1	-0.2	0.2	-0.1	-0.1	0.2	-0.1	0	0.1	0.1	0.2	0.1	-0.1	0	0	0.1	0.1	0	0	-0.2
26	0.2	0	0.2	-0.1	-0.1	-0.2	-0.1	0.1	-0.2	0.1	-0.1	-0.3	-0.3	0	0.1	0.1	0	-0.1	-0.1	0.2	-0.3	-0.1	-0.3	-0.3	0.1	0	-0.1	0	0	-0.4	-0.1	0.2
27	0.1	0.2	-0.1	-0.2	0.1	-0.3	-0.2	0.1	-0.3	0	0.2	-0.5	0.1	0.2	-0.2	0.1	-0.1	-0.1	0.1	0.1	0	-0.1	0.1	0.1	-0.2	0.1	0.2	-0.2	-0.2	-0.1	0	0
28	0.2	-0.1	-0.2	0.1	0	0.2	0.2	-0.1	0.1	0.1	0.1	0.2	0.1	0.1	0.2	0.1	0	-0.2	0	0.2	-0.1	0.2	0.1	0	0.2	-0.1	-0.1	0.1	0.1	0	-0.1	0
29	0.1	0.1	0	0	-0.2	-0.1	0	0	-0.1	0.1	0.1	0	0.1	-0.2	0	0.1	-0.1	0	-0.1	0.2	0.1	0	0	0	-0.2	0.1	-0.3	0.1	0	0.1	0.2	0
30	-0.1	-0.1	0.1	-0.1	-0.4	0.2	-0.2	-0.1	0	-0.6	0.2	0.2	0.1	0.2	-0.2	-0.3	-0.1	-0.2	-0.7	0	-0.2	-0.1	0.1	0	0	-0.2	0	-0.1	0.1	0	-0.2	-0.1
31	0.2	-0.9	-0.1	0.2	0.1	-0.5	-0.2	-0.2	-0.3	0.1	0.2	0	0	0	0.2	0.2	-0.1	-0.2	-0.5	0	0.3	0	-0.2	-0.3	-0.3	0.2	-0.2	-0.1	0	-0.1	0.2	-0.1
32	0.2	0	-0.2	0	0	-0.2	-0.1	0.3	0.1	0.2	-0.5	0	-0.2	-0.1	0	-0.2	0.1	-0.1	-0.4	-0.3	-0.3	0.1	-0.2	-0.1	0	-0.3	0	-0.1	0	-0.2	0.3	-0.3
33	0	0.3	-0.2	0	0.2	-0.4	0.2	-0.2	0.1	-0.4	-0.7	-0.1	0.1	-0.4	-0.1	0	0.2	0.1	-0.4	0	0.2	0.1	0.2	0	-0.4	-0.2	0	0	-0.3	-0.1	0	-0.2
34	-0.2	0.3	-0.6	0.2	0.1	-0.4	-0.1	0	-0.1	0.2	0	-0.4	-0.1	0	-0.1	-0.3	-0.3	-0.2	0.3	-0.1	0.2	-0.5	-0.4	-0.4	0	-0.1	0.1	-0.2	-0.4	-0.2	-0.3	-0.3
35	0.1	-0.1	-0.6	-0.3	-0.4	-0.1	-0.1	0.2	-0.2	-0.1	-0.1	-0.6	0	0	-0.2	-0.3	0.2	0.1	-0.3	-0.4	-0.3	-0.2	0	0.1	-0.4	-0.2	-0.3	-0.3	-0.3	-0.3	0.1	0
36	0.2	0.2	-0.3	0.1	0.3	-0.1	-0.1	-0.1	-0.8	-0.2	-0.5	0	-0.7	-0.1	0	-0.2	0	-0.1	0.4	-0.2	-0.4	-0.2	0	0.3	-0.2	-0.3	-0.2	-0.2	-0.1	-0.2	0	0.1
37	-0.1	-0.2	0.1	-0.6	-0.2	0.1	0.2	-0.4	0	0.1	-0.2	-0.1	-0.2	0	0	0.1	0	-0.1	0	0.1	-0.1	0	0	-0.2	0.1	-0.2	0	0.2	0	0	-0.3	0.1

i	1	2	3	4	5	6	7	8	9	10	11	12	13	14	15	16	17	18	19	20	21	22	23	24	25	26	27	28	29	30	31	32
38	-0.1	-0.1	-0.1	-0.2	-0.2	0	-0.1	-0.1	-0.2	0	-0.2	-0.2	-0.2	-0.1	-0.2	-0.2	-0.2	0	0	-0.2	-0.1	-0.1	-0.1	-0.1	-0.1	-0.2	0	-0.1	0	-0.1	-0.1	0
39	-0.2	-0.3	0.1	0	0	0	0	0	0.1	0	-0.1	0	-0.2	0	-0.4	-0.1	0	0	-0.2	-0.2	-0.1	0.3	0	-0.2	0.1	0	-0.1	-0.3	0	0	0	-0.1
40	-0.5	0	-0.1	0	0.1	-0.4	0	0	0.1	-0.2	0	0	0.3	-0.1	-0.1	-0.1	0	-0.3	0	-0.1	0.1	0.2	-0.1	-0.1	0	-0.1	0.1	-0.1	-0.3	0.1	0	-0.2
41	-0.3	-0.4	-0.4	0.1	-0.5	-0.2	-0.2	-0.6	0.3	0.2	-0.2	-0.1	-0.3	0	0.1	0	-0.2	-0.2	0.2	-0.1	0.1	-0.1	-0.1	-0.1	0	-0.3	-0.2	-0.4	-0.2	-0.1	-0.4	-0.1
42	0.3	-0.2	-0.2	-0.5	-0.1	0.1	-0.2	0.1	-0.6	0	-0.2	-0.2	-0.2	0.2	0.2	0	-0.1	-0.1	-0.1	0	-0.3	0.4	-0.2	0.2	-0.2	-0.1	-0.2	0	0.3	-0.1	-0.1	-0.2
43	-0.2	-0.1	0	0	0	-0.2	-0.1	-0.1	-0.2	-0.3	0	-0.1	0.1	-0.3	-0.3	-0.2	0.1	-0.2	-0.1	-0.1	-0.2	-0.1	-0.3	-0.1	-0.2	-0.2	-0.2	0.1	0	-0.1	0.1	-0.2
44	0.1	0	-0.5	0.1	0.2	0	-0.1	0	-0.2	-0.4	0	-0.5	-0.2	-0.1	0	-0.1	-0.2	0	0	-0.4	0.1	0	-0.1	-0.5	0.1	-0.2	0.2	-0.1	-0.3	-0.1	-0.2	0
45	-0.1	0	-0.1	0.2	-0.1	-0.1	-0.1	0	0.2	-0.1	0.1	-0.2	0.1	-0.1	-0.2	-0.1	0.1	-0.3	0	-0.3	-0.1	-0.1	0	-0.2	-0.3	-0.1	-0.1	-0.2	-0.2	-0.1	0	0
46	-0.1	0	0	0	0.1	0.1	0	0.1	0.1	-0.1	0.1	0	-0.1	0.1	0.1	0	-0.1	0.1	-0.2	0.1	0	0	0	0	-0.2	-0.1	0.1	0.1	0.1	-0.1	0.2	0
47	0.5	0	-0.2	0.1	0	-0.1	-0.5	-0.1	-0.9	0.2	0.1	-0.1	-0.3	0.2	-0.3	-0.3	0.4	-0.1	-0.1	-0.2	-0.1	-0.2	0	-0.1	0	-0.3	0.1	-0.1	0	-0.2	-0.3	-0.6
48	-0.2	-0.2	-0.1	0.3	-0.4	-0.1	0	0.3	0	0	-0.1	0.5	0.2	0.1	-0.1	-0.1	0	0.2	-0.3	0.1	-0.1	0.1	-0.1	0.1	-0.1	-0.2	0.1	0.1	0	0.2	0.2	-0.1
49	0.1	0	0.2	0	-0.1	0	0.1	0	-0.1	-0.1	0.1	0.1	0	0.1	-0.1	0.1	0	0.1	0.1	0	0.1	0.1	0.2	0	0.1	-0.1	0	0	0.1	0.1	0	-0.1
50	-0.2	-0.1	-0.1	0	-0.1	-0.1	0.2	-0.1	-0.1	0.1	-0.1	-0.1	0.1	-0.2	-0.1	0	0.1	0.1	-0.1	-0.1	-0.1	0	0.1	-0.1	-0.1	0.1	0.2	-0.1	0.2	-0.1	0	-0.1
51	0.1	0.1	0.1	0	0	0	0.1	-0.1	-0.1	0	0.2	0	-0.1	0	0.1	0	0.1	-0.2	0	0	-0.1	0.1	0.1	0	0	0.1	0	0	-0.2	0.1	-0.2	0.2
52	0	-0.1	-0.1	-0.4	-0.2	-0.4	-0.1	-0.3	0	-0.5	0	-0.2	-0.2	0.1	-0.3	-0.1	-0.1	-0.4	-0.2	-0.1	-0.2	-0.1	-0.2	-0.1	-0.2	-0.1	0.6	-0.4	0	-0.3	-0.2	0
53	-0.2	-0.2	0	-0.1	0.3	-0.2	0.1	-0.3	0.1	-0.1	0	-0.4	-0.1	0.2	0.1	0.1	-0.2	-0.2	-0.2	-0.3	0.2	0.2	-0.3	-0.3	-0.3	-0.2	-0.1	0.1	-0.2	-0.4	0	0.1
54	0.1	0.1	0.1	-0.1	0.1	-0.1	0	-0.2	-0.1	-0.1	0.1	0.1	-0.2	-0.1	0.1	0.1	0	-0.1	-0.2	0	-0.1	0	0	0	0	0	0.1	-0.2	-0.1	0	0.1	-0.1
55	0	-0.2	0.1	0.2	0.1	0.1	0	-0.1	0	0.1	0	-0.1	-0.1	-0.1	0.2	0	0	-0.1	0	-0.1	-0.1	-0.1	0.1	0.1	-0.1	0	0	-0.2	-0.2	0	0.2	0
56	0	-0.2	-0.1	-0.2	-0.3	0	-0.5	-0.1	-0.5	-0.1	0	0.1	-0.2	-0.4	-0.1	-0.1	0	0.1	0.1	0.3	-0.4	-0.1	-0.1	-0.1	0	0.1	0.1	0	-0.1	-0.1	-0.1	-0.1
57	0.3	-0.2	-0.2	0.2	-0.3	-0.4	-0.4	-0.1	-0.2	0.1	-0.4	-0.1	-0.1	0.2	-0.3	-0.2	-0.1	0.1	0	-0.1	0	-0.5	-0.1	0.1	0.2	0.3	-0.1	-0.1	-0.3	-0.1	0	-0.2
58	-0.1	0	-0.1	0.5	0.2	-0.1	0.3	0	0.2	0.2	-0.1	0	0.4	0	0.1	-0.1	0.6	0.1	0	0.1	0	0	0.1	0	0.1	0.1	-0.2	0.4	-0.1	-0.1	0.1	0.2
59	-0.3	0.2	0.1	0.2	0.3	0	-0.1	-0.5	0.1	-0.1	0	-0.1	0.2	0	-0.3	-0.2	-0.1	-0.5	0.6	-0.1	-0.1	-0.2	-0.2	0.7	-0.3	-0.3	0	0.4	0.1	-0.4	0	-0.1
60	0	0	-0.3	-0.8	-0.3	0	-0.2	0.2	-0.2	-0.2	-0.1	-0.2	-0.1	-0.3	-0.1	-0.1	-0.4	0.3	-0.2	-0.3	0.2	0.2	-0.1	-0.1	-0.1	-0.1	0	0.1	0.6	-0.2	0.1	0.2
61	-0.1	-0.5	0.3	0.1	0.1	-0.3	-0.1	-0.2	-0.8	-0.1	0	-0.1	-0.3	-0.1	0.1	-0.2	0.3	0	0	-0.1	-0.1	-0.4	0	0.3	-0.2	-0.1	0	0	-0.1	0.1	-0.2	0
62	-0.1	0.2	0	0.5	0.3	0.2	0.3	0.1	-0.3	0.5	0.2	0.1	0.6	-0.2	0.2	-0.1	0.5	0	0.4	0.3	0.1	0.1	0.1	-0.3	0	0	0	0.3	0.2	0	-0.1	-0.1
63	-0.1	0.3	-0.1	0	-0.1	0.1	0	-0.3	0.3	-0.3	-0.3	0.2	-0.3	0.1	0.3	-0.1	0.1	0	-0.1	-0.2	-0.5	0.5	-0.2	-0.2	-0.3	0.1	-0.1	-0.3	0.1	-0.1	-0.5	-0.3
64	-0.2	-0.2	-0.1	-0.2	-0.1	0	0.1	0.3	-0.7	-0.4	-0.3	0.2	0.2	-0.1	-0.2	-0.1	-0.1	0	0.3	0	0	0.2	-0.1	-0.1	0.3	0.1	0.1	-0.2	-0.4	-0.1	0.1	-0.2
65	0	-0.2	-0.1	0.1	-0.2	-0.1	0	-0.3	0.1	0.2	-0.2	0.2	-0.2	-0.2	-0.4	0.1	-0.4	0	-0.1	0.1	-0.2	-0.6	0.1	-0.1	-0.3	0	0	-0.2	-0.5	-0.2	0	-0.2
66	0	0.1	0	-0.1	0.2	0.1	0.1	0.1	0	-0.1	-0.1	-0.1	0.1	-0.1	-0.1	-0.1	-0.1	0	-0.1	-0.1	0.2	0	0.2	0	-0.1	0	0.1	-0.1	-0.1	-0.1	-0.1	-0.1
67	-0.1	-0.1	0.1	0.1	0.1	0.1	0	-0.2	-0.1	0.1	-0.1	0	0	0	0	0	0	0	0.1	0.1	0.2	0.1	0.1	-0.1	-0.1	-0.1	0.1	0.1	-0.1	0	0	0
68	0.2	-0.1	0.1	0	-0.1	0.1	0	-0.2	0	0	0.1	-0.1	-0.2	0.1	-0.1	-0.1	0	-0.2	0	0	0.1	0.1	0	0	0.2	-0.1	0	0	0	-0.1	0.1	0
69	0	0.7	-0.1	0.1	-0.1	0	-0.1	0	-0.2	-0.1	-0.3	-0.2	-0.5	-0.1	-0.1	0.1	-0.3	0	-0.1	0.1	0	-0.4	0.1	-0.1	-0.1	-0.1	-0.1	0	0.1	-0.4	-0.1	-0.1
70	-0.5	-0.2	0.4	0.1	-0.1	-0.1	-0.1	-0.2	-0.7	-0.1	-0.5	0.1	-0.1	-0.6	0.7	0.1	-0.3	0	-0.1	-0.3	0.2	-0.3	0.1	-0.4	-0.1	-0.2	0.3	0.1	-0.1	0.4	0.1	-0.2
71	-0.1	-0.3	-0.5	-0.2	-0.2	-0.3	-0.4	0.5	-0.2	-0.3	0	0	0.2	-0.2	0	-0.1	0	0.4	-0.2	0.1	-0.1	0.1	0	-0.4	-0.1	0	-0.3	0	-0.2	0	0.1	-0.1
72	0.2	-0.2	0.1	-0.1	-0.1	0	-0.1	-0.1	-0.1	0.1	-0.1	0.1	0	-0.3	0.1	0.1	0	0	0	0.1	-0.1	0.1	0	0	-0.2	0	-0.1	0.2	-0.2	0.1	-0.2	-0.2
73	-0.1	0	0.1	0.1	0	0.1	-0.1	-0.1	-0.2	-0.1	0	0.1	0.1	0.1	0	-0.1	0	0	0	0	0.1	0	0.1	0	0	-0.1	0.1	0.1	0	0.1	-0.1	0.2
74	0.1	0.1	0	-0.1	0.1	0.1	-0.1	0	0.1	0	0.1	-0.1	0.2	-0.1	-0.1	0.1	0	0.1	-0.2	0.2	0	0.1	0.1	-0.2	-0.1	-0.1	-0.1	-0.1	0.1	-0.1	-0.1	0.1
75	0.2	0.1	-0.1	0.1	0	0	-0.2	0	0.1	-0.2	0.1	-0.2	-0.2	-0.1	0.1	0.1	0.1	0	-0.1	-0.1	0.1	0.1	0	-0.1	0.1	0.1	0	0.1	0.1	0.1	0.2	0.2
76	0.1	0.1	-0.3	0	0	0.1	-0.2	-0.1	0	0.1	-0.2	0	0	0	-0.1	0	0.3	0	-0.1	0.2	0.1	0	-0.3	-0.2	0.1	-0.1	0	0	-0.1	-0.1	0	-0.2
77	-0.2	0.1	0	-0.6	-0.2	0.3	-0.4	-0.1	-0.4	-0.4	0	-0.1	-0.4	0	0	0.5	-0.1	0.1	-0.2	0.2	-0.5	0	-0.1	-0.2	0.3	0	0	-0.4	0	0.5	-0.4	-0.1
78	-0.3	-0.4	-0.1	0	0	-0.2	-0.8	0.1	0.5	0.1	-0.1	0	0	-0.4	-0.2	-0.2	0.2	-0.5	-0.3	0.4	-0.2	0.2	-0.1	0	0.2	-0.2	0.1	-0.2	0.3	0	0.1	-0.3
79	-0.5	-0.2	0	-0.1	-0.1	0.4	-0.1	-0.2	0	-0.1	-0.2	0.3	-0.5	0.6	-0.1	0	-0.2	-0.4	0	-0.2	-0.3	-0.2	-0.1	-0.1	-0.5	-0.1	0.2	0.1	0	0.1	-0.3	-0.7
80	0	0.2	0	0.1	0.4	0	0.2	-0.2	0.1	0.1	-0.1	-0.1	-0.5	-0.1	0	0	0	-0.1	-0.2	0.1	-0.1	-0.2	-0.1	0.1	-0.2	-0.2	-0.2	0	-0.1	-0.2	0.2	0.1
81	-0.1	0.3	-0.5	-0.1	0.2	0.1	0	0	0	0.2	0.2	-0.2	-0.3	0.8	-0.1	0	0.5	0.3	-0.1	-0.1	0	-0.1	-0.1	-0.2	-0.4	-0.4	-0.1	-0.1	0.1	-0.3	0	-0.2
82	0.2	0.2	0.1	0.1	-0.2	-0.1	0.2	0.1	-0.1	0	0	-0.2	0	-0.1	-0.1	0.1	0	0.1	0.1	0	-0.2	-0.1	-0.1	0.1	0.1	0.2	0.1	-0.1	0	0	0	0.1
83	0.1	-0.1	0.1	-0.1	0.1	-0.5	-0.1	-0.1	0	-0.1	0.1	0.1	0.6	-0.1	0	0.1	0.6	-0.1	0	-0.1	-0.1	-0.1	-0.2	0.1	-0.3	0.6	0.2	-0.1	-0.1	-0.4	0.5	0
84	0.1	-0.7	-0.4	0.1	-0.7	0	-0.2	0.3	0.2	0.1	-0.2	0	0	0.1	0.1	-0.5	0	-0.3	0	-0.2	-0.1	-0.1	-0.2	0.2	0.1	-0.2	0.2	-0.1	0	-0.1	0.1	0.1
85	-0.3	-0.1	-0.7	-0.2	0.1	0	-0.5	-0.1	-0.1	0.1	0.1	-0.5	-0.6	-0.5	-0.3	-0.1	0	0.3	-0.1	0.1	0	-0.1	-0.4	-0.3	0	-0.5	0.3	0.2	0	-0.7	-0.2	0.5
86	0.2	0.1	0.2	0.2	-0.1	0.4	-0.1	0.1	0.1	-0.1	-0.1	-0.2	-0.1	-0.1	-0.1	0.1	0.2	0.2	-0.2	-0.1	-0.1	0	0.1	0.3	-0.3	0.1	-0.1	0	0.3	0.4	-0.2	0
87	0	0.1	-0.1	0.1	-0.1	-0.2	-0.1	-0.1	0	0.1	0	-0.1	0.6	0	-0.1	0.1	0.5	0.3	-0.1	0	0.1	-0.1	0.4	-0.3	0.1	-0.1	0.1	0.1	-0.1	0	0.2	0
88	0.3	0.1	0	0.3	-0.2	0.3	-0.3	-0.3	-0.1	0.1	-0.3	0.2	0	0.3	0	-0.2	0.1	-0.1	-0.2	-0.2	-0.1	-0.2	0.1	0	0.1	0	-0.2	0	-0.1	0.3	0	0.1
89	-0.2	0.1	-0.2	0.2	0	0	0.1	-0.7	-0.4	0.5	0	0.1	-0.3	-0.4	0.2	0.3	-0.2	-0.3	0.3	0.2	0	0.4	-0.1	-0.1	0.2	0.1	0.1	0.1	0.4	0.3	-0.1	-0.1
90	-0.1	-0.1	0.1	0.1	-0.1	0	0	0.1	-0.1	-0.1	-0.1	0.1	-0.1	0	-0.1	0	-0.1	0	0.1	-0.1	-0.1	0	-0.1	0.2	0.1	-0.2	0.1	0.1	0	-0.2	-0.1	0
91	0.2	-0.2	-0.1	-0.4	0.1	0.3	-0.1	-0.1	-0.3	-0.1	-0.4	0.4	-0.7	-0.1	0.1	0	-0.3	-0.3	-0.1	0.2	-0.1	-0.7	0	0.1	-0.2	0	-0.2	0	-0.1	-0.3	-0.3	-0.1
92	0.1	0.5	0	-0.2	0.1	0.4	0.3	-0.2	-0.2	-0.1	-0.3	0.3	-0.5	0	-0.2	-0.2	0.2	-0.1	0	0	0	0	-0.4	-0.1	-0.1	0	0	-0.2	-0.2	-0.1	0	0
93	-0.1	0	0.1	-0.1	0.1	0	0	-0.1	-0.2	0.2	0	-0.2	-0.1	0.2	0	0	0.1	-0.2	0	-0.1	0.1	-0.3	-0.3	-0.2	-0.1	0	0.1	0	-0.1	0.1	0.2	0.1
94	0	0.1	-0.1	-0.1	0.1	0	0	-0.1	0	0	0	-0.1	-0.1	0.1	0.1	0	0.1	0.1	0.1	-0.1	-0.1	0	0	-0.1	0	0.1	0.1	-0.2	0	0.1	0.1	-0.2
95	-0.1	0	0.2	0.1	-0.2	0	0	0	-0.1	0	0.1	0.1	0	-0.1	-0.1	-0.1	0	0	0.1	0.2	-0.1	-0.1	0	-0.1	-0.2	0	0	0.1	0	0	0	-0.1
96	0.1	0.1	-0.1	0.3	-0.2	-0.2	-0.2	-0.2	-0.1	-0.1	-0.1	-0.3	0.1	-0.1	0.1	-0.1	-0.1	-0.3	-0.1	0.1	0	-0.1	0.1	0.1	0.4	-0.1	0	-0.1	0.4	0	0	-0.3
97	-0.1	-0.2	-0.3	0.1	-0.1	0.1	-0.4	0.4	0	-0.1	0	-0.2	-0.2	-0.2	-0.5	0.1	0	0.2	-0.1	-0.1	-0.4	-0.3	0	-0.3	0	-0.1	0.1	-0.5	0.1	-0.2	0	-0.4
98	0	-0.2	0.1	0	0.1	0	0	0.1	-0.1	0.1	-0.1	0	0.1	0.1	0.1	0	0.1	0.1	0.1	0.1	-0.1	0	0	-0.1	-0.1	0.1	0	0	-0.1	0.1	0.1	0
99	0	0	-0.2	-0.1	-0.1	-0.1	-0.2	0.1	0	0	-0.2	0.1	-0.1	0.1	0	0	-0.1	-0.1	0.1	0.2	-0.1	0	-0.1	0	0.1	0.1	0	-0.1	0.1	0.1	-0.2	-0.1
100	-0.1	-0.1	0	-0.1	0	0.1	0.1	0	0.2	0	0.1	0.1	0.1	0.1	-0.1	0	0.1	0	-0.1	0.1	0.1	0	-0.3	-0.1	0.1	0	0.2	0	0.1	-0.3	-0.1	-0.1
101	-0.1	0	0	-0.1	0.1	0.1	0.2	0.1	-0.1	0.1	0.1	0.1	0	-0.1	0.1	0	-0.1	0	0	0	0	0.1	0.1	0.1	0	0.1	-0.1	0	-0.1	-0.2	-0.1	0
102	-0.1	-0.1	-0.1	0	0.1	-0.2	0.2	-0.1	-0.2	0.1	0	0	0.1	0.1	0	-0.1	0.2	-0.1	-0.1	0.1	-0.1	-0.1	0.2	0.1	0	-0.1	0.1	0	0	0	0.1	0.1
103	-0.1	0.2	0.2	0	0.1	-0.1	-0.1	0	0.1	0.1	0	-0.2	0.1	0.1	-0.1	0	-0.1	0.1	0.1	0	0	0	0	-0.1	-0.1	-0.2	-0.1	-0.1	0.1	0.1	0.2	0
104	0	0	-0.1	0	-0.1	-0.1	0.1	0.1	0	0	0.1	0.1	0	-0.2	-0.1	0	-0.1	-0.1	-0.1	-0.1	0.1	0	0.1	0.1	-0.1	0	0	0	0	0.1	0.1	-0.1
105	0	0	-0.2	0	-0.2	-0.3	-0.6	-0.4	-0.3	-0.3	0	-0.2	-0.4	-0.1	-0.1	-0.1	0.6	-0.5	0	0.1	-0.3	0.1	0.1	-0.2	0.1	-0.1	0	0	-0.3	0	-0.7	0.2
106	0	-0.1	-0.1	0.2	-0.2	-0.1	-0.1	0.1	0.1	-0.1	0.1	0.1	0.1	-0.1	0	0.1	-0.1	0	-0.1	0	-0.1	0	0.1	-0.1	-0.1	0.1	0	-0.1	0	0.1	0	0.1
107	-0.1	-0.1	0	-0.1	0	-0.1	0	-0.1	0	-0.1	0	0	0	-0.1	0.1	-0.1	0.1	0.1	0.1	0	0	-0.1	0.1	0.1	0	0	0	0.1	-0.1	-0.1	0.1	0.1
108	0.1	0	0.2	-0.3	0.1	0	0.1	-0.2	0	0	0	0	0	-0.1	-0.1	0	0.3	0	0.1	0	0.1	0.1	0.1	0.1	-0.1	0.1	-0.2	0.1	-0.2	0	-0.1	-0.3
109	0.1	0.1	-0.1	-0.1	0	-0.1	0	0	0.4	0.3	-0.1	0.1	-0.1	-0.1	-0.1	0	0.2	0.1	0.1	0.1	-0.1	0	0	-0.1	-0.2	-0.1	-0.3	-0.1	0.1	0.1	0	0
110	0	0	0.1	-0.3	-0.3	-0.1	0	0	-0.4	0	0.1	0.2	-0.1	-0.1	0.1	-0.1	-0.7	0.1	-0.2	-0.1	0.1	0	0.2	0.4	0.1	-0.1	-0.1	-0.2	-0.6	0.1	-0.2	-0.1

i	1	2	3	4	5	6	7	8	9	10	11	12	13	14	15	16	17	18	19	20	21	22	23	24	25	26	27	28	29	30	31	32
111	0.1	-0.2	-0.2	0.2	-0.2	0.1	0.6	-0.1	-0.9	0.2	0	0.1	-0.2	-0.1	0.1	0.2	0.1	0.1	0	0.1	0.1	0	-0.1	0.1	-0.4	-0.2	-0.1	0	0	0.2	0	0.1
112	-0.1	-0.2	0	0.1	0.2	0.1	0.1	-0.2	-0.1	0.1	0	0.1	-0.1	-0.1	-0.1	-0.1	0	0	0	-0.1	0.1	-0.2	0.1	-0.1	-0.1	0.1	0.2	-0.1	0.1	0.2	-0.1	-0.1
113	0.1	-0.1	-0.1	0.1	-0.2	-0.1	-0.1	0	0.1	-0.1	0	0	0.2	0.1	-0.2	0	0	-0.1	-0.1	0	-0.2	-0.2	-0.1	0.2	0.1	-0.1	0.1	0.1	-0.1	0.1	0.1	0.2
114	0.1	-0.1	0	0.1	-0.1	-0.2	0.1	0	0.1	-0.1	-0.1	0	0.1	-0.1	0.1	-0.1	0	0.2	0.2	0	0.1	0	-0.1	0	0.1	0	0	0.1	0	0.1	0.1	-0.1
115	0.2	-0.1	0	0.1	-0.2	-0.3	0.6	-0.2	0.1	0	0	-0.4	-0.1	0.2	-0.1	-0.1	-0.3	-0.1	0	0	-0.2	-0.2	-0.1	0.1	0	-0.2	0.1	0.3	-0.1	-0.1	-0.1	-0.3
116	-0.2	-0.5	-0.2	-0.1	0	-0.3	0	0	0.1	0	-0.1	-0.3	0	-0.1	0.5	-0.1	0.3	0.1	-0.1	-0.2	-0.4	0.1	0.2	0.1	-0.1	0	-0.4	0	-0.2	-0.1	0.3	-0.7
117	0	-0.1	0.1	0.4	0.4	0	0.1	0.4	0.1	-0.1	0	0.1	0.2	-0.3	0.2	-0.2	0.3	0.1	0.7	0.2	-0.1	0	0	0	-0.4	-0.1	-0.1	0.2	0.1	0	0.3	0.7
118	0	-0.2	0.1	-0.1	-0.1	0.1	-0.1	0	-0.1	-0.3	0	0	0.1	0.1	0.1	0	-0.1	0	0	0.1	0	-0.1	-0.1	0	0	0	0	-0.2	-0.1	0	-0.1	-0.1
119	-0.4	0.1	-0.1	-0.1	-0.1	-0.2	-0.1	0	-0.1	0.1	0.1	-0.2	-0.1	-0.1	-0.1	-0.2	0.1	0	-0.1	0	-0.1	0	-0.1	0	-0.1	-0.1	-0.1	-0.2	0	-0.3	0	-0.3
120	0.6	0.2	-0.1	-0.2	0.2	0	0	-0.4	-0.3	-0.2	-0.2	0.1	-0.1	0.2	-0.2	0	-0.4	0.3	0.2	-0.3	-0.2	-0.6	0	-0.6	-0.7	-0.1	-0.3	0	0.5	-0.3	0.1	-0.3
121	0.1	0	0.2	-0.1	-0.1	0.1	-0.2	-0.1	-0.2	0	0.1	-0.1	0.1	-0.2	0	0	-0.1	-0.1	-0.2	0.1	0.1	0.1	-0.1	-0.2	-0.2	0	0.1	0.1	0	-0.1	-0.2	-0.1
122	-0.1	0	0	0	0	0.2	0.1	-0.1	-0.2	-0.3	-0.2	0	-0.4	0	0.1	-0.1	0.1	0.1	0.1	-0.3	-0.4	-0.3	-0.1	-0.2	-0.1	-0.2	-0.1	-0.2	0.1	-0.1	-0.2	0
123	0	-0.2	-0.5	0.2	0.1	-0.2	-0.2	0.2	0.1	0.2	0.4	0	-0.3	-0.3	0.1	-0.2	-0.1	-0.1	-0.8	-0.1	0.4	0.2	-0.1	0.3	0.1	-0.1	-0.1	0.2	-0.1	0.3	0.1	0
124	0.1	0.4	-0.4	0.4	0.2	-0.3	0.4	0	0.3	-0.1	-0.1	-0.4	-0.2	0	-0.1	-0.1	-0.5	-0.1	0	0.1	-0.4	-0.1	0.1	-0.1	-0.1	0	0	0.4	-0.3	-0.1	0	-0.5
125	0.2	0.1	0.1	0.1	0.1	-0.2	0.2	0	-0.1	0	-0.1	0	-0.1	0.1	0.1	0.1	-0.1	-0.1	0.1	0.1	0.1	-0.1	0.1	0.1	-0.2	0.1	0	0.1	0.1	-0.1	0	-0.1
126	0	0	-0.2	-0.2	-0.1	-0.3	0	-0.1	-0.1	0.2	-0.1	-0.1	0	0.2	0	0	0	-0.1	0	-0.1	-0.1	-0.1	0	-0.2	0.1	0	0.2	0.1	0	0	0.1	-0.4
127	0.1	0.3	-0.1	0.2	-0.1	0.2	-0.4	-0.4	0	-0.2	0.4	0	0.3	0	-0.3	0.2	0.1	0	-0.1	0.2	0.1	-0.2	0	-0.2	0.1	0.1	0.2	0	0	0.3	-0.1	-0.2
128	0.1	0	-0.1	0.1	-0.1	0.1	0.1	0	-0.3	-0.2	0.2	0.4	-0.1	-0.2	0	-0.1	-0.6	-0.2	0.1	-0.1	0	0.2	0	-0.1	-0.2	0.1	0.2	0.1	0.1	-0.2	-0.1	0.3
129	-0.6	-0.3	0.1	-0.2	-0.3	-0.1	-0.1	0	0.1	0.3	0.2	-0.5	0.2	0.2	-0.1	-0.3	-0.2	-0.4	0.2	-0.5	0	0.3	0.3	-0.2	-0.3	0.1	0.4	-0.1	0.3	-0.4	0.2	-0.4
130	-0.1	0.1	-0.5	0.2	0	-0.1	-0.2	-0.1	-0.6	-0.1	-0.3	0	-0.3	0.2	0.1	-0.1	-0.1	-0.1	0	0	-0.1	-0.2	-1	0.1	-0.2	-0.2	0	0.4	0.1	-0.1	-0.1	-0.1
131	0.1	0	0.1	-0.1	0.1	0.1	-0.1	-0.2	-0.1	0	0.1	-0.2	0	0.2	-0.1	0.1	-0.2	0	0	0.1	0	0.1	-0.1	0.1	-0.1	0.1	0	-0.1	0	-0.1	0	-0.1
132	-0.1	-0.1	0	-0.1	-0.1	-0.1	0	0.1	-0.1	0	0.1	-0.1	0	-0.1	0	0	0.2	0.1	-0.1	-0.1	-0.1	0	-0.1	-0.1	-0.1	0.2	0.1	0.1	-0.1	0.1	0	0
133	-0.1	-0.1	-0.5	0.1	0	0.1	0	-0.1	-0.1	0.1	0	0.1	-0.1	-0.8	-0.1	-0.1	-0.5	0.2	-0.1	0.1	0	-0.1	-0.4	-0.1	-0.2	0.2	-0.1	-0.1	0.1	0	0	0
134	-0.5	0.1	-0.2	-0.5	0	-0.3	-0.3	-0.3	-0.5	-0.6	0	0.4	-0.1	0.4	-0.3	0.2	0.1	0.5	-0.3	0.1	-0.3	-0.2	0	0.1	0.1	0.1	-0.1	-0.5	-0.3	0	-0.2	0.1
135	-0.2	-0.1	0.2	-0.3	0	-0.8	0	0.2	0	0	-0.4	-0.1	0.1	-0.1	-0.1	0.1	-0.3	-0.2	-0.1	0	0	0.4	0.2	-0.1	-0.2	0.2	0	0	-0.2	-0.3	0.3	-0.3
136	-0.1	0.1	0.1	0.1	0.2	-0.2	-0.1	-0.1	-0.1	-0.1	-0.1	0	-0.1	0.1	0	0.1	-0.1	-0.2	0	0	0.1	0.1	-0.1	0	-0.1	0	0	-0.1	0.1	-0.1	0.1	0
137	-0.1	-0.4	0	0.1	0.3	0.1	0.4	-0.1	0.4	0.2	0.7	0.1	0.3	0.2	0.2	-0.3	0	-0.4	0.2	-0.4	-0.1	0.2	0.5	-0.4	-0.1	-0.4	-0.2	0	0	-0.2	-0.3	0.3
138	0.1	-0.2	0.4	0.1	0	-0.1	0	-0.1	0.5	0	-0.2	-0.1	0.3	-0.1	0.1	-0.1	0.4	0	-0.1	0.1	0.1	0.7	0.1	-0.1	-0.1	-0.1	-0.4	0.1	-0.1	0	0.6	0
139	0	0.3	-0.2	0	-0.1	0.3	0	-0.1	-0.2	-0.1	-0.1	-0.1	-0.1	-0.6	0.1	-0.1	-0.5	0.1	-0.1	-0.1	0	0	-0.2	0.2	-0.1	0.4	0	-0.1	-0.2	0.1	-0.2	-0.1
140	-0.2	-0.1	0	-0.2	-0.1	-0.1	-0.1	0	0	-0.1	0.1	-0.1	0	0.1	-0.1	0	-0.1	0.1	-0.1	0.1	-0.2	-0.2	0	-0.1	0	0.1	-0.1	0	0	-0.1	0.1	-0.1
141	0.1	0.1	-0.6	-0.1	0.1	0.2	-0.1	-0.3	-0.1	-0.1	0.3	-0.3	0	-0.5	-0.1	-0.2	0.3	0.1	-0.2	0.2	0	-0.1	-0.2	0.3	0	0.4	0.1	0	0	0.1	-0.1	-0.4
142	-0.2	-0.1	-0.4	-0.6	0	0	0.2	0.1	0.1	-0.2	-0.2	-0.2	0.2	0.1	0.1	-0.2	-0.5	0.2	0	0.3	0	-0.2	-0.5	0.4	0.1	0	-0.6	-0.1	-0.2	-0.1	0.4	0.3
143	0.3	0.1	-0.2	-0.1	-0.3	-0.2	-0.1	-0.2	0.3	0	-0.1	-0.4	-0.2	0.3	-0.2	-0.1	-0.4	-0.3	-0.2	-0.3	-0.2	-0.4	-0.2	0.3	-0.1	0	-0.3	-0.2	-0.3	-0.5	-0.4	-0.5
144	-0.2	-0.3	-0.2	0	-0.1	0.1	0.2	0.3	0.7	-0.2	0.6	-0.1	0.9	-0.2	-0.2	0.5	-0.3	0	0	-0.1	-0.1	0.2	0	-0.1	-0.1	-0.1	0.6	-0.1	0	-0.1	-0.2	0.1
145	-0.4	-0.1	0.4	0	-0.1	0.1	0	-0.1	-0.1	-0.2	0.3	-0.1	0	-0.4	0	0	0.3	0.2	0	0	-0.1	0.8	-0.1	0.1	-0.2	-0.3	0.2	-0.1	-0.1	-0.4	-0.1	0.3
146	0	0.2	0	0	0.2	0.1	-0.1	-0.2	0	-0.1	-0.2	-0.2	-0.1	0	-0.1	0	0	-0.1	-0.3	-0.3	-0.4	0.1	-0.1	-0.2	-0.2	0.2	0	-0.2	-0.2	-0.1	0	-0.2
147	0	-0.1	-0.1	-0.1	-0.1	-0.2	-0.3	0	-0.3	0	0	-0.1	-0.1	-0.1	-0.2	-0.1	-0.2	-0.1	-0.2	0	-0.1	-0.1	-0.2	0	0	-0.2	-0.3	0	0	-0.2	-0.2	0
148	-0.1	0	-0.1	-0.2	-0.2	-0.2	0	-0.3	0	-0.2	-0.5	-0.3	-0.1	-0.3	-0.4	-0.1	0.1	0	-0.2	0.1	0	0.1	-0.2	-0.2	-0.5	-0.2	0	0	-0.2	-0.4	0.1	-0.2
149	-0.4	-0.1	-0.2	-0.2	-0.3	0	-0.2	0	0	-0.3	-0.2	-0.3	-0.2	0.5	0.3	0.3	0	-0.5	0	-0.3	-0.4	0	-0.2	0.1	0	0	0	-0.4	0.2	0.2	-0.1	-0.2
150	-0.2	-0.3	-0.5	-0.4	-0.2	-0.1	0	-0.2	-0.1	0.2	-0.5	0.2	0	-0.4	0.1	-0.2	0.1	0.3	0.3	-0.2	0.1	-0.1	-0.1	0.1	-0.1	-0.3	0.1	-0.4	0.2	-0.3	0	-0.3
151	-0.1	0.2	0.1	0.5	-0.3	-0.1	-0.1	-0.5	-0.1	0	0	-0.1	-0.2	0.1	-0.2	-0.1	-0.5	-0.6	0	0	0	0	0.5	-0.1	0	0	0.1	0.1	0.4	-0.2	-0.2	0.3
152	-0.2	-0.1	-0.1	0.1	-0.2	-0.1	0.2	-0.2	0	-0.1	-0.1	0	0.1	0	0.1	-0.1	0	0.1	0	0	0.1	0.4	0.1	-0.1	0.1	0	0.1	0	0.1	0.1	-0.2	0.1
153	0	0	0.1	0	-0.2	-0.1	0.1	0	-0.2	0.2	0.1	0	-0.1	-0.1	-0.1	-0.2	0.1	-0.1	-0.2	0.1	0.1	-0.1	0.1	0.1	0.2	0.1	0	-0.1	-0.1	-0.1	0.1	-0.1
154	0	-0.1	0.1	0	-0.1	0.1	0.1	0	0.1	-0.1	0.1	0.1	-0.1	-0.2	-0.1	-0.2	0.1	0	-0.1	-0.1	0.1	0.1	-0.1	-0.1	0.2	-0.1	0	-0.1	-0.1	0	0	0
155	0	0	0.1	0.1	0.1	0.1	-0.2	-0.1	0.1	0	0.1	0	0.1	0.1	-0.1	-0.2	-0.1	-0.1	-0.1	0.1	0	-0.1	-0.1	0	0.1	0.1	0.1	-0.1	-0.1	-0.1	0.2	0.1
B1	-0.1	-0.2	-0.2	-0.1	-0.2	-0.2	-0.1	-0.1	-0.1	-0.1	-0.1	-0.1	-0.1	-0.2	-0.1	-0.2	-0.1	-0.2	-0.1	-0.2	-0.2	-0.1	-0.2	-0.2	-0.2	-0.2	-0.1	-0.1	-0.1	-0.2	-0.1	-0.1

Table D.8 continued…

i	33	34	35	36	37	38	39	40	41	42	43	44	45	46	47	48	49	50	51	52	53	54	55	56	57	58	59	60	61	62	63	64
1	0.1	-0.1	-0.1	0	-0.1	0.2	0	0	-0.1	0.1	0.1	0	-0.4	0.1	-0.2	-0.1	-0.2	-0.2	-0.1	0.1	-0.1	-0.2	-0.2	-0.1	-0.2	0.1	-0.4	0.3	-0.1	0	-0.1	0.2
2	-0.1	-0.1	0.2	-0.4	0.2	-0.4	-0.1	-0.1	0	-0.2	-0.1	-0.2	0.1	-0.1	0.2	-0.3	0.1	0.1	0	-0.1	0	0	-0.1	-0.1	0.1	0.1	0	0.1	-0.1	0.1	0	0
3	0	-0.2	0.1	0	-0.1	0	-0.3	0	0.2	0.1	-0.2	-0.3	0	-0.2	-0.2	0.3	0	0.2	0	0	0	-0.2	0	0	0	0.1	-0.2	0.1	0.1	-0.1	0.1	0
4	0	0	0	0.1	0.1	0.2	-0.1	0.1	-0.2	0.1	0	0.1	0.2	0	0.1	0.1	-0.1	0.2	0.3	0	0.2	0.1	0	-0.1	0.2	0.1	0	-0.2	0.2	-0.2	-0.1	0.1
5	0.1	-0.2	-0.4	0.1	0.1	0	-0.1	-0.5	0	-0.3	-0.2	0.1	0	-0.1	0	-0.3	-0.2	0	0	0.2	0	-0.1	-0.2	-0.3	-0.1	0.1	0	0.1	-0.1	-0.1	-0.2	0
6	-0.1	0.2	-0.1	0	-0.1	0	0	0.1	0	0.1	0.1	0.1	0	0	0.1	0.1	-0.1	0	-0.1	-0.1	0.1	0.1	0	-0.2	0.1	-0.2	0.1	0	-0.1	-0.2	0	0.1
7	0	-0.2	0	0.1	-0.1	0.1	-0.1	-0.1	-0.1	0.2	-0.2	-0.2	0.5	0.1	0.1	0	0	0	0.1	0.1	0.1	0.1	0	0.2	-0.2	-0.2	0.2	-0.2	0.2	0.1	0	-0.1
8	0.1	-0.1	0	0.1	0.1	0.1	-0.1	-0.2	0.1	0.1	0	0	0	-0.1	0.2	0	-0.1	0	0.1	-0.1	0	-0.2	-0.1	0	-0.2	-0.1	-0.3	0	0	0.1	-0.1	-0.2
9	-0.1	-0.1	-0.1	-0.1	-0.1	-0.3	0.2	0.2	0	0	0.2	0	0.1	0.1	0	0.2	-0.1	0.2	0	0	-0.1	0	-0.1	0	0	0	-0.1	0	0.2	-0.1	0.1	-0.3
10	0.1	0	0	0	0.2	0	0	0.1	-0.3	-0.1	0	0	-0.1	0	-0.1	0.2	0.1	0.1	-0.1	-0.1	0.2	0.1	-0.3	0	0	0.1	-0.1	-0.1	-0.1	-0.2	-0.2	-0.1
11	0	-0.3	0.2	0	0.1	0.2	-0.1	0	0.1	0.1	-0.1	0	-0.2	-0.2	0	-0.2	0.1	0	0.1	-0.1	0.1	0.1	0.1	-0.1	0.3	-0.1	-0.1	0	0.1	0.3	0	0.1
12	-0.2	-0.1	0	0.2	0	0.3	0.1	0.1	0.1	0.1	0	-0.1	0.2	-0.1	0	0.2	0.2	-0.1	-0.1	0.1	-0.3	0	0.4	0.2	0	0	0.3	0.2	0.1	0	0.3	-0.2
13	0	0	0	-0.1	0.2	-0.3	0	-0.1	0	-0.1	-0.2	-0.4	-0.2	-0.2	0	0.1	0.1	0.1	0.1	-0.1	0.2	0	-0.1	0.1	0	-0.3	0.1	0	0	0.2	0.1	0.2
14	0.1	0	0.2	-0.1	0.2	0.1	-0.2	-0.1	0	-0.1	0	-0.1	-0.1	0.1	-0.1	0.1	-0.1	0.2	0.1	-0.1	-0.1	-0.2	0.1	0.1	-0.1	0	-0.1	0.1	0.1	0	-0.2	0.1
15	0.1	0.1	0	-0.1	0	-0.3	-0.3	-0.2	-0.2	0.1	-0.3	0	-0.2	0.1	0.2	0	-0.2	-0.2	0	-0.2	0.1	0.2	-0.1	-0.1	0.2	0.1	0.1	-0.1	0	0.1	0.1	0.1
16	0	0	-0.1	-0.1	0.1	0	0.1	0.1	0	0	0.1	0	-0.2	0	-0.2	0.1	0	-0.2	-0.1	0	0.1	-0.2	0.1	0.1	-0.1	0	-0.3	0.1	0	0	0	0
17	-0.1	-0.6	-0.2	0.1	0	-0.1	0.1	0	0.1	-0.3	0	0.2	0	-0.3	-0.3	-0.1	0	-0.1	-0.2	-0.4	0.3	0.1	-0.4	0.2	-0.2	-0.1	-0.2	-0.2	0	-0.2	0.1	-0.1
18	0.1	0.5	-0.1	0.1	0.3	0.2	0	0	-0.7	-0.4	-0.1	0.1	0.1	-0.2	-0.1	-0.3	0	-0.2	0	-0.1	-0.4	-0.1	-0.3	0.2	0.1	0.2	0	-0.2	0.2	-0.3	-0.2	-0.1
19	-0.1	-0.1	-0.1	0.2	-0.2	0.3	0.2	-0.2	0.3	0	-0.1	0	-0.2	0	0.1	0.1	0.3	0.4	0	-0.1	0	0	0.1	-0.2	0.2	0.1	-0.3	0.1	-0.1	-0.4	-0.4	0.3
20	0	0	-0.2	-0.1	0	0	0.1	-0.1	-0.3	-0.1	-0.2	0	-0.1	0.2	0.2	0	-0.1	0	-0.2	0.3	0	0.1	0.2	-0.2	0.1	-0.4	0.1	-0.2	-0.1	-0.3	-0.2	-0.1
21	0	0	-0.3	0.4	-0.1	0.4	0.4	0.2	-0.1	-0.2	-0.4	-0.1	0.1	0.2	0.1	0	-0.2	0	-0.2	0.6	-0.2	0	0	-0.2	0	0	-0.1	0	0.2	0	-0.1	0

i	33	34	35	36	37	38	39	40	41	42	43	44	45	46	47	48	49	50	51	52	53	54	55	56	57	58	59	60	61	62	63	64
22	0.4	0	0	-0.1	-0.2	0.1	0.5	0.1	0	0	0.1	-0.2	0	0.3	0.1	0.2	0.1	0.1	0.4	0	0.1	0	0	0.1	0.1	-0.2	0.1	0.2	-0.1	0	-0.2	0.1
23	0.2	0	0.2	-0.1	0	0.1	-0.1	-0.2	0	0.1	0	0.2	0	0.2	-0.1	-0.1	0.2	0.1	0	-0.2	0.2	0.1	0	0.1	-0.1	-0.2	0	0.1	0.1	0.1	0.3	0.1
24	0.3	0	-0.1	0	0	0	-0.2	0	-0.4	-0.2	0.3	0.2	-0.1	-0.6	0.1	-0.1	-0.1	0.1	-0.4	-0.1	-0.5	-0.4	-0.3	0.2	-0.1	0	-0.2	-0.2	-0.1	-0.2	-0.3	0.2
25	0.1	0	0.2	0.1	-0.1	-0.1	0.1	0.1	0.1	0	0.1	0	-0.1	0.2	-0.1	0.2	-0.1	0.2	0.2	0.2	0	0	0.1	-0.2	0.1	-0.2	0	0.1	-0.2	-0.2	-0.1	-0.3
26	-0.2	-0.1	-0.1	-0.6	0	-0.3	-0.1	-0.2	-0.1	-0.2	0.5	0.4	0.1	-0.2	0.2	0	0.1	0	0.2	-0.3	0.3	0.2	0	0.1	-0.2	0.1	0.1	-0.3	0	0.1	-0.3	0.1
27	0.1	0	0.2	0.1	-0.2	0.2	0.2	-0.1	-0.1	0.1	0.1	0	-0.2	0.1	0	-0.2	0	-0.4	-0.1	-0.1	-0.1	-0.3	0	-0.1	-0.1	0.2	0.1	0	0.2	0	-0.4	0.2
28	0	0	0.2	-0.1	0.2	-0.2	-0.1	0.3	-0.2	-0.2	0	0.1	0.2	-0.1	-0.1	-0.1	-0.3	-0.3	0.1	0.1	0.1	0	0	0.1	0.1	0.1	0.2	0	0.1	-0.1	-0.1	0
29	-0.1	0.1	-0.1	0.1	-0.1	-0.1	0.2	-0.1	-0.1	0.1	0	-0.1	-0.2	0	0.1	-0.3	0	0	0	0.1	-0.2	0.1	0.1	0	0.2	0.1	0	-0.2	-0.2	-0.1	0	-0.4
30	0	-0.1	0	-0.3	-0.1	-0.4	0	-0.3	0	-0.1	0	-0.1	0	0	-0.1	0	0.1	0.2	0.1	-0.5	-0.5	-0.4	-0.4	-0.3	-0.1	0	0.2	0.2	-0.3	0.1	0	0
31	-0.2	0.2	-0.4	0.2	0	0	-0.3	0	-0.1	-0.2	-0.2	-0.1	-0.1	0.1	0.2	0.4	-0.1	0.1	-0.4	-0.4	0	0.3	0.2	-0.1	0	0	-0.3	0	-0.5	-0.2	-0.3	-0.2
32	0.6	-0.1	-0.2	0	-0.2	0	0.3	-0.2	-0.2	0.2	-0.2	0.4	-0.1	-0.4	-0.3	-0.4	0.2	-0.2	-0.1	-0.2	-0.3	-0.3	-0.3	-0.4	-0.1	0	-0.3	-0.1	0.1	-0.6	-0.3	-0.1
33	0.1	0	-0.4	-0.1	-0.1	0	-0.1	0	0	0.1	0.1	-0.3	-0.2	0.1	-0.3	-0.5	-0.1	-0.1	0.2	0.2	0	-0.3	0	-0.1	-0.2	-0.2	0.2	0	-0.2	-0.3	-0.3	-0.3
34	0.2	-0.2	0.1	0	-0.2	0.1	-0.1	-0.3	0	-0.2	0	0.1	-0.3	0	0.1	-0.4	0.3	-0.1	0	0.1	0.1	-0.1	0.1	0.3	-0.2	0.1	-0.2	-0.2	0	-0.2	-0.1	-0.2
35	0.3	-0.4	-0.1	-0.3	-0.1	0.1	0.1	-0.1	0.1	-0.2	0.1	0.1	-0.4	0.1	-0.4	0.1	-0.3	-0.3	-0.3	0	-0.1	0.1	0	0	-0.1	-0.2	-0.3	-0.1	0.1	-0.1	0.3	0
36	0.2	0	-0.1	0.5	0	0.1	-0.3	0.2	-0.4	-0.3	-0.2	0.3	0.4	-0.3	0.6	0.1	-0.3	-0.1	0	-0.2	-0.4	0.1	-0.3	-0.3	0.8	0.1	-0.6	-0.2	0	-0.2	-0.4	0
37	-0.1	-0.2	0.1	-0.4	0.1	-0.2	-0.1	0.1	-0.1	0.1	0	-0.3	-0.2	-0.1	-1	-0.3	-0.1	-0.5	0	-0.1	0.2	0.2	-0.4	0.1	-0.3	-0.1	-0.2	-0.2	0	0	0	0.1
38	-0.2	-0.3	-0.1	-0.3	0	-0.3	-0.2	-0.1	-0.2	-0.1	-0.1	-0.2	-0.1	-0.1	-0.3	-0.2	-0.2	-0.2	0	-0.1	0	-0.1	-0.3	-0.2	0	-0.2	-0.2	0	-0.1	0	-0.3	-0.2
39	0.1	-0.1	0.1	0.2	0	-0.1	0.1	-0.3	0	0	0.3	-0.1	-0.1	-0.3	-0.1	-0.1	0	0	-0.3	-0.1	0	-0.2	0.1	0	0	-0.2	0	-0.3	-0.2	0.1	-0.1	-0.2
40	-0.1	-0.2	0.3	0.2	0	0.1	-0.1	0	-0.3	0.1	0.2	0.2	-0.2	-0.2	0.1	-0.1	-0.1	-0.1	-0.4	0	0.2	0.2	0.1	-0.1	-0.1	0.1	0	0	0.6	0	0.2	0.1
41	-0.2	0.1	0	0	-0.1	0.1	0.1	0.1	-0.3	0	-0.3	-0.3	-0.1	-0.1	0	0	-0.2	0	-0.1	0.1	-0.1	-0.2	-0.2	-0.1	-0.2	-0.3	-0.5	0	-0.3	-0.1	-0.2	0
42	0.2	-0.1	-0.1	0.1	-0.3	0.4	-0.2	-0.4	-0.5	-0.1	0.3	0	-0.3	0.1	0.1	0	-0.2	-0.3	-0.2	-0.1	0	0.4	0	-0.1	0.1	0.4	0.1	-0.2	-0.1	0	-0.2	-0.4
43	-0.2	-0.1	-0.3	-0.1	-0.3	-0.1	0	-0.3	-0.1	-0.5	-0.2	0	0.1	0	-0.2	-0.2	0	-0.4	-0.1	-0.2	0	0	-0.3	-0.2	-0.1	-0.2	-0.2	-0.2	0	-0.1	-0.3	-0.1
44	0.3	0	0	-0.2	-0.2	-0.1	0	-0.4	0	-0.1	-0.1	-0.1	-0.7	-0.5	-0.1	-0.1	-0.2	-0.1	-0.1	-0.4	-0.2	-0.2	0.1	0	0	-0.3	-0.1	-0.1	0	-0.5	-0.1	0.1
45	0	-0.2	0	-0.2	0	-0.4	-0.2	-0.1	0	-0.2	-0.2	-0.2	-0.1	-0.2	-0.1	-0.2	-0.1	0	-0.3	-0.2	-0.1	-0.1	-0.2	0	-0.2	-0.2	-0.2	0	0	0	-0.1	-0.2
46	0.2	0	-0.1	-0.1	0	-0.1	-0.1	0.1	0.1	0	0.1	-0.1	-0.1	0.1	0	-0.1	-0.1	0	0.1	0	0.1	-0.1	-0.1	0	-0.1	0.1	-0.1	0.2	0.1	0.1	-0.1	0
47	-0.4	0	-0.1	0.1	-0.2	0.1	0.2	-0.3	-0.2	-0.1	0	-0.1	-0.3	-0.2	-0.3	0.2	-0.3	-0.2	-0.5	-0.2	0.1	-0.4	-0.2	-0.4	0	-0.4	0	-0.1	-0.2	-0.6	-0.2	-0.3
48	0.3	0	-0.1	0	-0.1	0.2	0.2	0.2	-0.2	0.1	0	-0.1	-0.1	0.2	-0.1	-0.1	-0.2	-0.2	-0.1	-0.1	-0.1	0.2	0.1	-0.4	0.1	0.1	-0.2	-0.1	-0.1	-0.1	-0.3	0.1
49	0.2	0.2	0.1	0.1	-0.1	0.1	-0.2	0	0.1	0	0	0.1	0.2	0.1	-0.1	0	0.1	-0.1	-0.1	0.2	0.1	0	0	0.1	0	0	-0.2	0.1	0.1	0.1	0	0
50	0	0.1	-0.1	0.1	0.1	0.1	0	-0.1	-0.1	-0.1	0.1	0.1	0.1	0	0.2	0.1	0.1	0.1	-0.1	-0.1	0	-0.2	-0.1	0	0.1	0	0	-0.1	-0.1	-0.1	0.2	0.1
51	0	0.1	0.1	0.1	0.1	-0.1	-0.1	-0.1	0.2	0	0.1	-0.1	-0.1	0.1	0.1	0.1	0.1	-0.1	0.2	0.1	0	0	0.1	0	-0.1	0	0	-0.1	-0.1	0	0.1	0.1
52	0	0.1	0	-0.1	-0.2	-0.2	0	-0.1	-0.2	-0.3	0.1	-0.3	-0.4	0	-0.1	-0.5	-0.2	0.1	0.1	0.3	0.2	-0.3	-0.1	-0.1	0	-0.3	-0.1	0.1	-0.2	0	-0.1	-0.2
53	-0.2	-0.1	-0.2	-0.5	-0.2	0	-0.2	-0.1	0	-0.1	0	0.1	-0.1	-0.1	-0.6	0.2	0	-0.1	-0.1	-0.1	-0.1	0.1	-0.3	-0.2	-0.3	0	0	0.1	0.1	-0.1	-0.2	-0.2
54	0	-0.2	-0.1	0	0.2	-0.1	0	0.1	-0.1	0	0.2	-0.1	-0.1	0.1	0.1	0.1	0.1	0.1	0	-0.1	0.1	0.1	0.1	0.1	0	-0.1	0.1	-0.2	-0.1	-0.1	-0.1	0.1
55	-0.1	-0.2	0.1	0.1	0.1	-0.1	0.1	-0.1	0.1	0	0.1	-0.1	-0.1	0	-0.1	0	-0.1	0	-0.1	0	0	0	-0.2	0	0	-0.1	-0.1	-0.2	-0.1	-0.1	0.2	-0.1
56	0	0	-0.2	0	0.1	-0.1	-0.1	-0.3	0.2	-0.4	0	-0.1	-0.2	0	0.1	-0.2	-0.2	-0.1	0	-0.2	-0.1	0.1	-0.4	-0.2	0.1	0	-0.1	-0.2	-0.2	-0.2	-0.4	-0.2
57	-0.3	0.2	0.2	0	0.1	-0.2	0.1	-0.2	-0.4	-0.1	-0.2	-0.2	-0.2	-0.2	-0.1	0.2	-0.3	-0.3	-0.2	-0.4	-0.3	0.8	0	-0.4	0.5	0.5	-0.2	0.1	0.5	0.6	-0.1	0.3
58	0	0	0.1	0.1	-0.1	-0.1	0	0.1	-0.1	-0.2	0.1	-0.1	0.1	0.3	0.1	0	0	0	0.4	-0.1	0.2	0.1	-0.1	0.1	0.1	-0.2	0	0.2	0	0	-0.1	-0.1
59	-0.2	0	0.1	0	0.1	-0.1	0.1	0.3	-0.1	0	-0.1	-0.5	0.1	-0.1	0	-0.1	-0.1	0.2	0.1	0	0.3	-0.2	0	-1	-0.4	-0.2	-0.1	0	-0.2	-0.2	0.1	-0.2
60	-0.1	-0.1	0	0.1	0.1	0.2	0.1	-0.4	0	-0.1	-0.2	-0.4	0	0.2	-0.1	-0.3	-0.3	-0.4	-0.1	-0.1	-0.4	0	-0.2	-0.1	-0.1	0.1	0	0	-0.3	-0.2	0	-0.4
61	0.1	-0.4	-0.4	-0.5	0.1	-0.3	0	-0.6	-0.4	0.1	-0.2	0.1	0	0.1	-0.5	0.1	-0.3	-0.3	-0.2	-0.2	-0.5	0	-0.2	0.2	-0.6	-0.1	-0.1	0.1	-0.2	0.1	-0.2	-0.1
62	-0.6	0.1	-0.1	0.2	0.2	0.3	0.1	0.3	-0.1	-0.1	0.1	0	0	0.2	0.1	0	0	-0.2	0.2	0	-0.4	0.3	-0.1	-0.3	0.1	0.3	0	0.6	-0.1	-0.1	-0.1	-0.2
63	0.3	0.1	0	-0.1	0	0.1	-0.2	0.2	-0.5	0	-0.1	0	0.4	0	0	0.6	-0.3	-0.3	0	-0.1	-0.5	-0.2	0.1	0	-0.2	-0.3	0.1	-0.2	0	-0.2	0	0.1
64	0.5	0	-0.1	-0.4	-0.4	-0.4	0.1	-0.2	0.2	0	0	-0.6	0.1	0	-0.1	-0.1	0.3	0.1	-0.1	-0.1	0	0.3	0	0.2	-0.1	-0.1	-0.1	0.4	0.1	0.3	0.2	0
65	0	0.1	0.1	0.2	-0.1	-0.1	0	0.2	0.2	-0.4	0.1	0.1	-0.1	0.1	0	0	-0.1	-0.2	-0.2	0.1	0.3	-0.2	-0.4	0.1	-0.3	-0.2	0	-0.2	0	0.2	-0.2	0.1
66	-0.1	-0.2	0.1	-0.1	-0.1	-0.1	0.1	-0.1	0.1	0	-0.2	-0.1	0	0	-0.1	0.1	0	-0.1	0	0.2	0.1	0.1	-0.2	-0.2	-0.1	0.1	-0.1	-0.1	-0.1	0.1	0	-0.1
67	0.1	-0.2	0.1	0	0.1	-0.1	-0.1	-0.1	-0.1	0.1	0.1	0	0	0	0.1	-0.1	-0.1	-0.1	-0.1	0.1	0.2	0.1	0.1	0.1	0	-0.2	-0.1	0	-0.1	0.1	-0.1	-0.1
68	0.1	0	-0.1	0.1	0.1	0.1	-0.1	0.1	0	-0.1	0.1	0	-0.1	-0.2	-0.1	0.2	0	-0.1	0	0	0.1	0	0.1	-0.1	-0.1	0	-0.1	-0.1	-0.2	0.1	-0.2	0.1
69	0	0.1	-0.1	-0.1	-0.1	0	-0.1	-0.1	-0.2	-0.1	-0.1	0.4	0.1	0	0.1	-0.1	0	0	-0.2	-0.2	-0.1	-0.2	0	-0.1	-0.1	0.4	-0.1	0	-0.1	-0.2	0	0
70	-0.2	-0.2	-0.2	0.1	0.4	0	0.2	-0.1	-0.3	-0.1	0.1	-0.2	-0.1	0.4	-0.1	-0.1	0	-0.1	-0.3	0.1	0.4	0	0	0.2	-0.2	-0.5	-0.1	0.4	0.3	-0.1	0	0
71	0.1	0.4	-0.1	-0.2	-0.2	-0.2	-0.1	-0.3	-0.1	-0.2	-0.3	-0.7	0.1	0.4	-0.1	-0.1	-0.1	0	0.2	-0.1	0.1	0.1	-0.1	0	0.3	-0.1	-0.1	0	0.1	0	-0.1	0
72	0.2	0	-0.1	0.1	0	0	0	0	-0.3	0	0.1	0	0.1	-0.4	-0.1	0	0.1	-0.2	-0.2	-0.1	-0.2	-0.1	-0.2	-0.2	0.1	-0.2	-0.1	0.1	-0.1	-0.5	0	0
73	0.1	-0.1	-0.2	-0.1	-0.1	0.2	-0.1	0	-0.1	-0.1	-0.1	-0.1	0	0	0	0	-0.1	0	0	0.1	-0.2	0	-0.1	0.1	-0.1	-0.1	-0.2	-0.2	0.1	-0.1	0	0
74	0.1	-0.1	-0.2	-0.1	0.1	-0.1	0.1	0.1	-0.1	0	0.1	0	-0.2	0	0.1	0.1	0.1	-0.1	-0.1	0	0	0	0	0	-0.1	-0.2	0	-0.1	0	0.2	0.2	-0.1
75	0.1	0	0	0	0	0.1	-0.1	0	0.1	0.1	-0.1	-0.1	0	-0.1	-0.1	0.2	0.1	0	0.1	-0.2	0	0.1	0.1	-0.1	-0.1	-0.1	0	0.1	-0.1	0.1	0.2	0.2
76	-0.1	-0.1	0.1	0	-0.2	0	0.2	-0.1	-0.1	-0.1	0.1	-0.1	-0.1	-0.1	0.1	0	0.2	0.1	-0.1	-0.1	0.1	0	-0.1	0.1	0.2	-0.1	0	0	0	0.5	0	-0.1
77	-0.1	0	-0.1	0.4	-0.1	0.1	-0.4	-0.1	-0.1	0	0.1	-0.1	0	0.2	0	-0.1	-0.1	-0.1	0.1	0.5	-0.3	-0.2	0	-0.2	0.1	0.3	0	-0.1	0.1	-0.1	0	-0.2
78	-0.1	-0.2	0.2	-0.1	-0.3	-0.2	-0.1	-0.1	0.1	0	-0.3	0	-0.3	0.3	-0.6	-0.2	-0.3	-0.1	0.3	-0.2	0	0	0	-0.2	-0.2	-0.1	0.1	0.1	-0.3	0.1	0	-0.1
79	-0.2	-0.3	-0.1	0	0	-0.1	-0.6	-0.3	0	0	-0.5	-0.2	0	-0.5	0	0.3	-0.4	-0.1	-0.3	0	-0.4	-0.4	-0.2	0.4	-0.4	0.5	-0.1	-0.1	0.6	0.2	-0.6	-0.1
80	0.2	0	0.1	0	-0.2	0	-0.1	0.2	-0.3	0.4	-0.1	0.1	0.1	-0.3	-0.1	0.1	0.1	-0.1	-0.1	-0.1	-0.5	-0.2	0	-0.1	0.1	-0.2	-0.1	-0.1	-0.1	0	-0.1	0.1
81	0	0	-0.3	0.4	0.2	0.2	-0.6	0	-0.1	0	-0.1	-0.3	0.1	-0.3	0	-0.1	-0.4	-0.3	0	-0.3	0	0.2	-0.1	-0.4	-0.1	-0.2	0	0	0.4	0.1	-0.1	0.1
82	-0.1	-0.1	0	0	-0.2	-0.1	0	0.1	-0.1	0.1	0.1	0	-0.1	0.1	0.1	0.2	-0.1	0	-0.1	0.1	0.2	0.1	0	-0.1	0	-0.1	0	0	-0.1	0.1	-0.1	-0.1
83	-0.3	-0.1	0.1	-0.1	0.3	0	-0.1	-0.1	0	-0.1	0.1	0.1	0.1	0.5	-0.1	0	-0.1	-0.1	0.4	0	0.2	0	-0.1	-0.1	0.4	0	0	-0.1	-0.1	0.7	0.4	0.1
84	-0.3	-0.2	0	0.2	0.3	-0.6	0	0.2	0.1	0.1	-0.1	0.1	-0.1	-0.1	-0.5	0.1	0.3	0.1	0.2	-0.4	-0.1	-0.3	-0.2	-0.6	-0.1	-0.1	0.1	-0.1	0.1	0.4	-0.4	-0.1
85	-0.8	-0.2	0.1	0.4	0.1	0.3	-0.3	0.3	-0.2	-0.1	0.2	-0.4	-0.2	0	0.1	-0.2	-0.3	0.1	0.2	0.1	0.2	0.2	-0.1	-0.2	-0.3	0.1	-0.1	0	-0.2	0.2	-0.1	0.2
86	-0.2	-0.1	-0.1	0	0.1	0	-0.1	0.1	0	0.1	-0.2	0.1	-0.1	0	0.1	-0.5	-0.2	0	0	0.3	0	-0.2	0	-0.2	0.1	0	0	0.1	-0.2	0.1	-0.1	-0.1
87	-0.2	0.2	0.1	0	0.2	-0.1	0.1	0	-0.4	-0.1	0.1	0	-0.1	-0.1	0.1	-0.7	-0.1	0.1	-0.1	0.1	0	0.1	0	0	-0.1	0.1	-0.1	-0.1	0	-0.2	0.2	-0.1
88	0.3	0	0.2	0.2	0	-0.1	0.1	-0.2	0.1	-0.1	0.1	0.2	-0.2	-0.2	0.4	-0.1	0.1	0.2	-0.2	0.1	-0.1	0.1	0.3	-0.2	0.2	0.2	-0.5	-0.2	0	-0.2	0.1	-0.1
89	0	0.3	-0.3	0	-0.7	-0.3	0.7	-0.4	-0.1	0.2	0	-0.5	-0.1	-0.2	0	0.1	0.3	0.1	0	0.1	-0.2	0	0	-0.1	0.3	0.1	-0.5	-0.1	-0.2	-0.5	-0.3	-0.4
90	0	0.1	0	-0.1	0.1	0	-0.1	0	0	-0.1	-0.1	0	0	-0.1	-0.1	-0.2	0.1	-0.1	-0.1	0	0.1	0.1	0	0.1	0	0	0.1	0.1	0.1	0.1	0.2	-0.1
91	0.2	0.3	-0.5	0.2	-0.1	0.1	0.3	0	-0.1	0	0	0	-0.2	-0.3	-0.2	-0.1	0	-0.4	-0.4	0.1	0	-0.2	0	0	-0.5	0.3	-0.6	0	0	0.3	-0.1	-0.1
92	-0.2	-0.1	-0.3	-0.1	-0.1	0	0.1	-0.1	-0.5	0	-0.4	-0.1	0.1	0	-0.1	0	0	-0.3	-0.3	0	0.2	0.1	0	-0.1	-0.2	-0.1	-0.2	-0.1	0.1	0	0.2	0
93	-0.1	0	-0.3	-0.2	0.1	0	0.2	0	-0.3	0.1	0.1	-0.2	-0.1	-0.2	-0.1	-0.1	-0.4	0	-0.4	0	-0.2	-0.3	0	0.1	-0.2	-0.1	0.1	0.1	0	-0.1	0	-0.2
94	0	0	-0.1	0	0.1	0.2	0.1	0	0	-0.1	0	0	-0.1	0.1	0.1	0	0.1	0.1	0	0	0	-0.1	0	-0.1	0.1	0.2	0.1	0.1	0.1	0	-0.1	0
95	0.1	-0.1	-0.1	-0.1	-0.1	0	0.1	0.2	0	0.2	0	0.1	-0.1	-0.2	0.2	-0.1	-0.1	0	0	-0.2	0.1	-0.1	0	0.1	0	-0.1	0.1	0	0	-0.2	0	-0.1

i	33	34	35	36	37	38	39	40	41	42	43	44	45	46	47	48	49	50	51	52	53	54	55	56	57	58	59	60	61	62	63	64
96	0.3	0	0	-0.1	0	-0.1	-0.1	0.2	0	-0.1	0.2	0.3	0	0.1	-0.2	-0.1	0	0.1	0.2	0.1	-0.3	-0.1	0	0	0.1	-0.1	0	0.1	-0.1	-0.2	0.1	-0.2
97	-0.2	0.3	0.2	-0.1	-0.1	-0.1	0	0.4	0.2	-0.2	0	-0.3	-0.1	0.3	-0.5	0.2	0.2	0	0	-0.2	0.2	0	0.1	-0.1	-0.2	-0.1	0.1	0	-0.1	0.1	0.1	0.1
98	0.1	-0.1	0.1	-0.1	-0.1	0	0.1	0.1	0.1	-0.1	0.1	0	-0.1	-0.1	0	0.1	0	0	-0.1	0.1	0	0.1	-0.1	0	0.1	0.1	0.1	0	0	0.1	0.1	-0.1
99	0.1	-0.1	-0.2	0	-0.1	-0.1	0	0.1	0	0	-0.1	0	0	0.1	0.1	0	0.1	0.1	-0.1	0	0	-0.2	0	0.1	0	-0.1	-0.1	0.1	-0.1	0.1	0	0.2
100	0.3	-0.1	-0.1	-0.3	0	0.2	0.1	0.2	0.2	-0.2	0	0.1	-0.1	-0.1	0.1	-0.1	0.2	0	0	-0.7	0	0	-0.1	-0.1	0	-0.1	0.1	0.1	-0.2	-0.1	-0.2	-0.1
101	-0.1	-0.1	0	0	0.1	0.1	0	-0.1	0	0.1	-0.1	-0.1	0	0.1	0.1	0.1	-0.1	-0.1	0	-0.1	-0.1	-0.1	0	0	-0.1	-0.1	0.1	0.1	-0.1	0.1	0.1	-0.1
102	0.2	0.1	0.1	0.1	-0.1	0	0	-0.1	-0.1	0	-0.1	0	0.1	-0.1	-0.2	0.1	-0.2	0	-0.1	-0.1	-0.1	-0.1	-0.1	0.1	0	0	-0.1	-0.1	-0.1	-0.1	0.1	0
103	0.1	0	0	0	-0.1	-0.1	0.1	0.1	-0.1	0	0.1	-0.1	0	0	-0.1	0.1	0.1	0	0	0	0	-0.1	0.2	0	0	0.1	-0.1	0.1	0.1	0	0	0.1
104	0.1	-0.1	0	0	0.1	-0.1	-0.1	0.1	-0.1	-0.1	0	0	0	0	0	0	0	0.1	-0.1	0	-0.1	0.1	0.1	0	-0.1	-0.1	0	-0.1	0.1	0	0	0
105	-0.4	0	0	0.2	-0.1	0.4	-0.6	-0.1	0	-0.1	-0.1	-0.1	-0.1	0.1	-0.1	-0.3	-0.2	0.1	0	0	0.2	-0.4	0.2	-0.4	-0.3	-0.2	0	0.2	0	0.1	-0.1	-0.2
106	0	0	0	-0.1	-0.1	0	-0.1	0	0	0.1	0.1	0.1	-0.1	0.1	0	0.1	0.1	0	0	0.2	0	-0.1	0	0.1	-0.1	0	-0.1	0.1	0.1	0.1	0.2	0
107	0.2	-0.1	-0.1	-0.1	-0.1	-0.1	0.1	-0.1	-0.1	0.1	-0.1	-0.1	0	0.1	-0.1	0	0	0	0.1	-0.1	0	0	0	-0.1	0.1	-0.1	0	-0.1	0	-0.1	0.2	0
108	0	0	0.1	-0.2	-0.1	0.1	-0.1	-0.3	-0.2	0	0.1	-0.2	-0.3	0.4	0	0.5	0.2	0	0.1	-0.5	-0.2	-0.2	0	0	-0.1	0.2	0.1	-0.1	-0.5	-0.3	0	-0.2
109	-0.1	0.1	0	-0.1	0.2	0	0.2	-0.1	0	0	0	-0.2	0.3	0	0	0	0.4	0	0.1	0.1	0.1	0.2	-0.1	0	0.1	0.2	0.1	0.1	0	0.2	0	-0.2
110	-0.1	0	-0.1	-0.1	-0.6	-0.1	-0.4	0.3	0.1	0	0	0.2	-0.3	0.1	-0.1	0	-0.2	-0.1	-0.2	0.2	-0.3	-0.1	0.1	0	0	0.1	0	0	0.3	-0.6	-0.1	-0.1
111	0	0.1	0.1	0	0	-0.2	0.4	-0.1	-0.1	0	-0.3	-0.1	0	-0.1	0	-0.2	0	-0.2	0.2	0	-0.2	0.2	0.1	-0.1	-0.3	-0.2	-0.5	0.5	-0.1	-0.1	-0.1	-0.1
112	-0.1	0	0.1	0	0	0	0	0.1	0.1	0.2	0.2	-0.1	-0.1	0.1	-0.1	0.1	-0.2	0.1	0.1	0.1	-0.1	0.1	0.1	0.1	0	0	0	-0.1	0.1	-0.2	0	0.1
113	-0.1	0.1	0.1	-0.1	0.1	0	0.1	-0.1	-0.2	-0.2	0	-0.1	0.1	0	0.1	-0.1	0	0	0	-0.1	0.1	0.2	0	-0.2	-0.1	-0.1	-0.1	0	0.1	-0.1	-0.1	-0.1
114	0.1	0	0.2	-0.1	0.1	0	0.1	-0.1	0	0.1	0.2	0.1	0.1	-0.1	0.2	-0.1	0.1	0.2	-0.2	0.1	-0.1	0.2	0.1	0	-0.1	-0.1	0	0.1	0.1	0.1	0	0.1
115	-0.1	0.2	0.3	-0.1	-0.2	0.1	0	0.4	-0.3	0	-0.2	0.3	0	-0.2	0	0	0.1	-0.1	0.2	-0.1	-0.2	0.2	-0.1	0.2	-0.1	0.1	-0.1	-0.1	0.4	0	0	0.3
116	-0.4	-0.1	0	0.1	0.3	-0.1	-0.2	-0.5	-0.3	0.2	0.2	-0.2	0	0.5	-0.4	-0.1	0.1	-0.2	0.1	0.1	0	0.1	-0.2	-0.5	0	-0.1	0.1	-0.2	0.1	-0.1	-0.5	-0.1
117	-0.2	0.3	0	0.1	0.8	-0.1	-0.1	-0.1	-0.1	0	-0.2	0	0.2	0	0.3	-0.1	0.7	-0.1	-0.1	-0.2	-0.2	0.8	-0.1	0.4	-0.1	0	-0.1	0.1	-0.3	0.8	-0.1	-0.1
118	0.3	0.1	0	-0.1	-0.2	0	0.1	0.4	-0.1	-0.1	-0.2	-0.1	0	-0.2	0	-0.1	-0.2	0	0.1	0.2	-0.1	0.1	0.2	0	-0.1	-0.1	0.1	-0.2	-0.2	-0.1	-0.1	0
119	-0.2	0	-0.1	-0.1	-0.1	0	0	-0.1	-0.2	0	0	-0.1	0	0.2	0	-0.3	0.1	-0.1	-0.2	-0.1	-0.5	-0.2	0	-0.1	-0.2	-0.1	0	0.1	-0.2	0.3	-0.1	0.1
120	0.4	0	0.1	-0.1	-0.2	-0.2	0	-0.2	-0.2	-0.4	0.3	0.2	-0.2	-0.4	-0.2	-0.2	-0.1	-0.2	-0.1	-0.1	-0.4	-0.2	-0.2	0	0	-0.4	-0.3	0.1	0.1	-0.4	-0.1	-0.2
121	0.2	0	0.1	-0.1	0	-0.2	0	0.1	0.2	0	0.2	0.1	-0.1	0	0.1	0	0	-0.1	0.1	-0.1	-0.1	0.2	0	0.1	0	-0.2	-0.1	0	0	0.1	-0.2	-0.1
122	0	0	-0.1	0.1	0	0.1	-0.3	-0.1	0.2	0.1	0.1	0	-0.1	0	-0.1	0.1	-0.3	0.1	-0.1	-0.1	-0.2	0	-0.1	0.2	-0.1	0	-0.1	0	0	0	-0.1	0.1
123	-0.5	-0.1	0.1	-0.1	-0.2	0	0.1	-0.1	0	0	-0.1	-0.3	-0.3	0	-0.2	0	0.2	0.3	0	-0.1	0	-0.8	-0.2	0	-0.3	-0.1	-0.4	-0.2	0.2	0	-0.2	-0.2
124	0.1	-0.1	-0.1	-0.2	0	0.1	0.2	-0.3	0	-0.1	-0.2	0.1	-0.1	0.3	-0.3	0.1	0.5	-0.2	0	0	-0.1	-0.4	-0.2	0	-0.3	-0.1	0	0.3	0.1	-0.3	-0.1	0
125	0.1	-0.1	0.1	0.1	0	-0.1	-0.1	-0.2	0.1	-0.2	0.1	0.1	0.1	0	-0.1	-0.1	0	0.1	0	0	0	-0.1	0.1	0.1	0.1	-0.1	0.1	0.1	0	0.1	-0.1	0
126	-0.1	0	-0.1	-0.1	-0.1	-0.1	-0.1	0.4	-0.1	0	0	-0.6	0	0	-0.1	0.3	0	-0.1	-0.3	0.1	0.2	-0.4	-0.1	0.1	0.3	0.1	-0.1	0.1	0	-0.3	-0.2	0.2
127	0.1	-0.1	0.1	0	0.1	0	-0.2	0.1	0.2	0	0.2	-0.5	-0.1	0.2	-0.2	0	-0.6	-0.2	0	0.2	-0.1	-0.2	-0.1	-0.6	-0.3	0.1	0	0.3	-0.2	0.1	0.3	0
128	-0.1	-0.4	-0.1	-0.1	-0.1	-0.1	0.3	-0.4	0.2	0	0.3	-0.2	0.4	0.3	0.2	-0.4	-0.3	-0.1	-0.2	-0.1	0.1	0.2	-0.2	0.1	0.2	-0.1	-0.2	-0.1	-0.2	-0.2	-0.2	-0.2
129	-0.3	0.3	-0.3	0	-0.2	0.3	0.3	-0.1	0	-0.1	-0.2	0.4	-0.3	-0.7	-0.5	0.7	-0.1	-0.6	-0.3	-0.7	0.2	-0.1	0.1	0.3	0	-0.6	0.1	0	-0.4	-0.1	0	-0.2
130	0	-0.1	-0.1	-0.1	0	-0.2	-0.1	-0.1	-0.4	-0.2	0.2	0	0.2	-0.2	-0.1	-0.1	-0.2	0.1	-0.2	0.1	0.1	-0.5	0.2	0	0	0.1	-0.2	-0.2	0.4	-0.7	-0.2	0
131	0	0	0.1	0	-0.1	0.2	0.1	0	-0.1	-0.1	0.1	-0.1	0	0.1	0.1	0.1	-0.1	-0.1	0	0.1	0	0	0.1	0	0.1	-0.1	0.1	0.1	0.1	-0.1	0	0.1
132	0.1	0.2	0	-0.2	0.1	0.1	-0.1	-0.2	-0.3	0	-0.3	0.2	0	-0.1	0.1	0.3	0	-0.2	-0.3	0	0.3	0	0.1	0	0.1	0	-0.1	-0.2	0.1	-0.1	0	0
133	-0.2	0	0.1	0	0.1	-0.1	0	-0.1	-0.1	0	0.1	-0.1	0	0	-0.1	0.1	0	0.1	0	0	-0.3	-0.2	-0.2	0	0.1	-0.3	0.1	0	0.1	-0.3	-0.2	0.1
134	0.2	-0.3	-0.2	0.2	-0.6	0	-0.2	-0.1	-0.1	0	-0.4	0.2	0.2	-0.1	-0.6	-0.3	-0.3	0.1	0	0.2	-0.3	-0.4	-0.1	0.2	-0.1	0.1	-0.1	-0.4	0	-0.2	-0.1	-0.1
135	0.2	-0.2	-0.3	-0.2	-0.1	0.1	-0.1	-0.1	0.2	-0.2	-0.4	0	0.1	-0.6	-0.1	0	0	-0.2	-0.2	-0.3	-0.1	-0.1	-0.4	-0.3	0.4	0	-0.2	-0.2	0.2	-0.7	0.2	0.1
136	-0.1	0	-0.1	0	-0.1	0.1	0.1	0.1	0	0.1	0.1	0	0	0	-0.1	-0.1	0	-0.1	0	0	-0.1	0.1	-0.1	0	0.1	0.1	-0.1	0.1	0	-0.1	-0.1	0
137	-0.3	0.2	-0.1	0.1	0.4	-0.1	0.5	-0.2	0	0	-0.3	0	-0.1	-0.3	0	0	0.3	-0.1	-0.2	-0.4	0.1	0	-0.2	0.4	-0.3	-0.1	0	0.4	-0.1	0.1	-0.1	-0.4
138	0	-0.2	0.1	-0.1	0	-0.2	0	0	0.4	0	-0.1	-0.1	-0.1	0.6	0.1	0	0.3	0	0.7	0.1	-0.1	0.4	0.1	0	-0.1	-0.1	0.3	0.1	0	0.3	0	0.1
139	0.2	-0.2	-0.2	0	-0.1	0.4	0	-0.1	0.2	0	0.2	0.9	-0.3	-0.4	-0.1	-0.1	-0.4	0.1	-0.2	-0.1	0	0.4	0.1	-0.2	0.6	-0.5	-0.1	-0.2	-0.5	-0.2	-0.1	-0.1
140	0	-0.1	-0.1	0	0	0	0.1	0.2	0	0	-0.1	0	0	-0.1	0	0.1	-0.2	-0.1	-0.1	0.2	-0.1	0	-0.1	0.1	0.1	0	-0.2	0.2	0.1	-0.1	0	-0.1
141	0.6	-0.2	0.4	-0.2	0	0	-0.3	0.3	0.3	-0.3	0.3	-0.4	0	0.3	-0.1	-0.2	0.2	0	-0.2	0.3	-0.5	-0.2	0.3	0.1	0.2	-0.1	-0.5	0.4	0.1	0.1	-0.2	0.2
142	0.2	-0.3	0.3	-0.2	-0.2	0	-0.2	0	-0.3	-0.2	0.2	0	0	0.1	-0.1	0	-0.1	-0.1	0.1	-0.4	-0.5	0.2	0	0.4	0.4	0.1	0.4	-0.5	-0.2	-0.1	-0.4	0.2
143	-0.3	0.1	0.1	0.1	-0.5	-0.2	0	0.3	-0.3	0	0.1	0	0	-0.1	-0.4	-0.1	0.1	-0.1	-0.3	-0.3	0	-0.2	0	0.5	-0.1	-0.1	-0.4	-0.1	0.3	-0.3	0	-0.2
144	-0.2	0.1	0	-0.1	0.4	0	0.2	-0.2	0.2	0.1	-0.1	-0.2	0.3	0.3	-0.1	0.1	0.3	0	0.7	-0.3	0.4	-0.1	-0.2	0	0	-0.1	0	0.1	-0.1	1.1	0.1	0
145	0	0.4	-0.3	-0.2	0.1	-0.1	-0.1	-0.1	-0.3	0.1	0	0.5	-0.1	-0.1	0.1	-0.1	-0.2	0	0.1	0	-0.1	0.2	-0.2	0	-0.1	-0.1	0	-0.1	-0.1	0	-0.1	0.1
146	0	-0.2	0	-0.2	0	0	0	0	0.1	-0.3	-0.1	0	-0.1	-0.2	-0.1	-0.2	0	0.2	-0.1	0.1	0.1	0.2	-0.1	-0.3	0.3	0.2	-0.2	-0.6	0.2	0	0.1	-0.2
147	0	-0.1	-0.2	-0.1	-0.2	-0.3	0.1	0.1	0	-0.1	-0.3	0	-0.2	-0.1	0.2	0	0	0.1	-0.2	0	0	-0.1	0	-0.1	-0.2	-0.1	-0.1	-0.2	-0.2	-0.1	-0.2	-0.1
148	0.1	0.2	0	-0.3	-0.1	0	-0.1	-0.7	-0.3	-0.2	0.1	-0.3	-0.2	0	-0.1	-0.3	0	-0.3	-0.1	-0.3	-0.2	0	0	-0.1	0.1	-0.3	-0.4	0	-0.4	-0.1	-0.2	0.1
149	-0.3	-0.5	0	-0.3	-0.1	-0.3	-0.6	0.1	0	0.3	0	0.4	0.3	-0.1	-0.1	-0.1	0.1	0	0	-0.1	-0.1	0	-0.4	-0.1	-0.3	-0.1	0.1	0	0.2	0.1	-0.3	0
150	-0.4	0.2	0	-0.1	-0.2	-0.1	-0.1	-0.3	0.1	-0.2	-0.3	-0.3	-0.4	0.1	-0.3	0.1	0	-0.3	0	-0.6	0	0	-0.2	0	0	-0.1	-0.2	-0.1	-0.2	0.2	-0.1	-0.2
151	-0.2	0	0.1	0.1	0	0.1	-0.1	0.1	0	-0.1	0.3	-0.1	-0.2	-0.2	-0.1	-0.1	0	0.2	-0.1	0	0.2	-0.2	-0.1	-0.1	0.3	0.1	0	0.3	0	-0.2	-0.3	0
152	0	0.1	0	0	0	-0.1	-0.1	0	0	0	-0.3	0	-0.1	0.1	-0.1	0	0	0	-0.2	0	-0.1	0.1	-0.1	0	0	-0.1	-0.1	0.1	-0.1	0	-0.1	-0.1
153	0	-0.1	0	0.1	-0.1	0	-0.1	0.1	-0.1	0.1	0	0.2	-0.1	-0.1	-0.1	0	-0.1	0.1	0.1	0.2	-0.1	-0.1	0.1	0	-0.1	-0.1	-0.1	0	0	0.1	-0.1	0.1
154	0	0.1	-0.1	-0.1	0.1	0	-0.1	-0.1	0.1	0	0.2	0.1	0	0.1	0.1	-0.1	0.1	0.1	0.1	0	0.1	0.1	-0.1	0.1	0	0.1	0	0	0	0.1	-0.1	0.1
155	-0.1	0.1	-0.1	-0.1	0.1	0.1	0	0.1	-0.1	-0.1	0.1	0	0.1	0.1	-0.2	-0.1	0.1	-0.1	0	-0.1	0	-0.1	0.1	-0.1	0	0.1	-0.1	0	0.1	-0.1	-0.1	-0.1
B1	-0.1	-0.2	-0.2	-0.1	-0.1	-0.2	-0.1	-0.2	-0.1	-0.2	-0.2	-0.1	-0.1	-0.1	-0.2	-0.1	-0.1	-0.2	-0.1	-0.2	-0.1	-0.2	-0.2	-0.1	-0.2	-0.2	-0.1	-0.1	-0.2	-0.1	-0.2	-0.2

Table D.9 – Normalization coefficients of the ANN-UQo_{HY}'s input parameters

Parameter	μ	σ
TVD	1983.01	433.34
l_l	2051.17	679.21
$\mathrm{lat}_{\mathrm{bh}}$	55.21	0.58
$\mathrm{lon}_{\mathrm{bh}}$	-118.41	1.21

Parameter	μ	σ
d_e	0.55	1.00
V_{inj}	0.48	0.50
Q_f	284.62	301.52
V_{acid}	0.18	0.38
P_c	0.44	0.50
N_s	8.79	20.11
l_s	33.81	58.68
d_s	271.14	179.77
C_s	34.60	31.71
t_{sh}	35.94	41.36
p_{inj}	74.99	40.61
q_{inj}	1.85	1.80
ϕ_m	16.48	17.25
GR	37.92	15.33
ρ_b	6.13	3.71
PE	0.10	0.03
k_m	98.94	14.15
B_i	2.62	0.04
h_f	3.08	0.24
S_w	9.17	20.14
p_i	1.84	0.24
h_{net}	114.67	51.36

Table D.10 - ANN-UBO_e's weights and coefficients of the second hidden layer

k	1	2	3	4	5	6	7	8	9	10	11	12	13	14	15	16	17	18	19	20	21	22	23	24	25	26	27	28	29	30	31	32
1	-0.1	-0.2	-0.3	0	-0.1	-0.3	0	-0.2	0	0	0	0	-0.4	0	-0.2	0.1	-0.9	-0.4	-0.3	0.3	-0.4	0.6	-0.2	-0.5	-0.2	-0.9	-0.3	-0.5	0.8	-0.7	1.5	0.5
2	-0.2	-0.2	-0.6	-0.4	-0.3	-0.5	-0.1	0.3	0.3	-0.1	0.1	0	-0.2	-0.4	0.1	-0.2	0	-0.1	-0.2	-0.1	-0.2	0.3	-0.3	-0.5	-0.3	-0.6	0.2	0	-0.2	-0.1	1.4	-0.7
3	-0.5	-0.4	0.2	-1.2	-1.2	0.1	-0.3	-0.1	0.4	-0.2	-0.2	0.4	-0.6	-0.3	-0.1	0	0.2	0.1	-0.1	0.1	0.3	-0.1	0.3	-0.3	-1.5	-0.2	-0.4	0	-0.4	-1	-0.2	0.2
4	-0.2	-0.1	-0.2	-0.9	-0.3	1.2	-0.2	0.2	-0.1	0.1	0.1	-0.1	-0.9	-0.2	-0.3	-0.2	-0.8	0	0.2	0.2	0.4	0	-0.4	0.2	-0.2	-0.8	0.2	-0.2	0.2	-1.8	-0.4	-1.1
5	-0.3	-0.7	-0.3	-0.3	-1.2	0.3	-0.7	-0.1	0.5	0.1	0.1	0.4	0.4	-0.3	-0.2	-0.1	-0.2	-0.1	-0.2	0.1	-0.8	-0.3	-0.4	-0.1	-0.2	-0.5	-0.2	-0.2	-0.5	-0.7	0.1	-1.6
6	-0.6	-0.5	-0.5	-0.1	-1.1	-0.5	0	0.2	0.2	0	0.2	0.9	-0.5	0	-0.2	-0.3	-0.2	-0.6	0.2	-0.1	-0.2	0.3	-1.1	0.3	-0.5	-0.6	-0.1	-0.6	0.2	0.1	0.9	0.1
7	0.1	0.3	-1	-0.4	-0.3	-0.2	-0.8	0.1	0.2	0.2	0.1	1	-1.3	-0.1	0.1	0.3	-1.3	-0.2	-0.8	0.1	-0.2	0	-0.3	-0.3	-0.3	-0.4	0.1	0.2	0.4	0.2	0.7	-0.5
8	-0.3	0.4	0.1	-1.5	-0.7	0.3	-0.5	0.2	0.4	-0.1	0.3	0.5	-1	-0.2	0.2	0	0	0.3	0.4	0.5	0.1	-0.4	-0.1	-0.3	0.2	0	0.2	-0.2	-0.1	0.2	0	-1.3
9	-0.5	0.2	-0.3	-0.4	-0.2	-0.1	0.1	0	0.3	-0.5	0	-0.3	-0.8	0.1	0	0.1	-0.2	-0.6	-0.2	-0.2	-0.2	0.3	0	0	-0.2	-0.3	0.2	0	0	-0.8	0.2	-0.2
10	0	-0.3	-0.6	-0.3	-0.3	0.3	-0.4	0.3	0.1	0.3	0.1	0.2	-0.6	-0.5	-0.4	0.2	-0.5	-0.5	0	0.1	-0.1	-0.3	0.1	-0.3	-0.4	-1	-0.1	0	1.1	0	0	-0.5
11	-0.4	0.1	-0.7	-1.1	-1.4	0	-0.8	0.2	0.6	0.1	0.2	0.6	0.6	0.2	0.1	-0.1	0.1	-1.3	-0.2	-0.3	-0.5	-0.3	-0.3	0.5	0	-0.4	0.3	0.1	-0.3	-0.7	-0.2	-0.1
12	-0.8	0	-0.5	-0.1	-0.6	-0.3	0	-0.2	0.2	0.2	0.1	0.3	-0.5	0.3	0.1	0.1	-1.1	-0.3	-1.3	-0.2	-0.1	0.6	-0.3	-0.2	-0.1	-0.7	-0.1	-0.8	0.4	-0.3	1.2	-0.5
13	-0.1	0.6	-0.3	0.3	0.5	-0.1	0.7	0.8	-0.2	0	-0.1	0	-0.3	-0.1	-0.1	0.1	-0.5	-0.1	-0.8	0.8	0	0.3	-0.2	0.5	-0.4	0.1	-0.3	0.1	0.1	-1.1	1.1	-0.2
14	-0.1	-0.2	-0.3	-0.6	-0.6	-0.4	-0.1	0.4	-0.1	-0.2	0.2	0.5	-0.6	-0.5	-0.4	-0.2	-0.4	-0.2	-0.3	-0.1	-0.4	0.6	-0.5	-0.2	-0.4	-0.4	0.1	-0.3	-0.1	-0.1	1.6	-0.6
15	-0.3	-0.9	-0.2	-0.2	-1.4	-0.2	-0.8	0.2	1	-0.2	0.1	0.3	-0.2	-0.2	-0.2	0	-0.6	0.1	-0.1	0.1	0.3	0	-0.7	0.2	-1	-0.5	0.2	0.1	0.3	-0.2	0.5	0.1
16	-0.2	-0.7	-0.3	-0.9	-0.7	0.2	-0.7	-0.2	0	-0.4	0.2	0.5	-0.2	-0.6	0.2	0	-1.2	-0.8	-0.1	0	-0.2	-0.3	-0.1	-0.3	0.5	-0.1	0.8	0.2	1	0.4	-0.9	0.1
17	-0.4	-0.1	-0.1	-1.2	-0.7	0.4	-0.1	-0.1	0.1	-0.5	-0.3	0.4	-1.2	-0.5	-0.1	-0.1	-0.1	-0.2	-0.8	0	-0.4	0.3	-0.2	-0.1	0.1	-0.5	0	-0.2	0.5	0	0	-0.2
18	-0.3	0.1	0.3	-0.8	-0.2	0.7	-1	0.3	0.2	-0.4	0	0.3	-1.1	-0.4	0.3	0.3	-0.6	0.1	0.2	0.4	-0.7	0.2	-0.1	0.1	-0.5	-0.5	-0.1	-0.3	0.1	-0.3	0.4	-0.3
19	0	-0.6	-0.6	-0.4	-0.2	-0.4	-1.1	-0.2	-0.2	-0.3	-0.1	1.5	0.3	0.1	-0.1	0.4	-0.1	-1.3	0.2	0.1	0.1	-0.4	-0.8	-0.5	0.1	-0.3	0.1	-0.5	0.3	-0.2	1.3	-0.3
20	-0.3	-0.5	-0.5	-0.7	-0.4	-0.3	0.1	0.4	0.4	-0.3	0.1	0.2	-0.2	0.2	-0.1	-0.2	-0.4	-0.1	-0.1	-0.1	-0.1	0.3	-0.1	0	-0.2	-0.7	0	-0.2	0.1	-0.7	1.1	-0.1
21	-0.2	-0.5	-0.2	-2.2	-0.4	0.3	-0.6	0.1	0.3	-0.2	-0.1	0.3	-0.3	-0.5	-0.2	-0.1	-0.4	-0.5	0	0.2	-0.4	-0.3	-0.5	0.1	-0.3	-0.6	0.2	0.2	0.3	-0.2	0.2	-0.7
22	-0.3	-0.1	0	0	-0.2	-0.1	-0.3	0.1	0.1	-0.3	-0.2	0.1	-0.6	-0.2	-0.3	-0.2	-0.8	-0.5	0.2	0	-0.1	0.2	-0.1	0	-0.2	-0.7	-0.1	-0.4	0.2	-0.6	1	0.1
23	-0.3	-0.4	-0.5	-0.1	0.1	-0.2	0	1	0	0.2	0	-0.1	-0.7	0.2	-0.3	0.1	0.4	-0.3	0.2	0	-0.3	0.1	-0.3	-0.6	0.1	-1	0.1	-0.4	0.2	-0.2	1.3	0.1
24	-0.3	0.1	-0.6	0.1	-1.2	-0.3	0.2	0	0.2	0	0.3	0.5	-1.1	-0.1	0.1	-0.1	-0.7	0.3	0.5	0.2	0.4	0.1	0.3	0.3	-0.7	-0.2	-0.2	-0.2	0.7	-0.9	1.6	0.1
25	-0.3	-0.2	-0.3	-0.1	-0.4	0.4	-0.3	0.1	0.2	0.3	0.1	0.2	-0.8	-0.4	-0.4	0	-0.1	0.1	0	0.2	-0.3	-0.2	-0.6	0	0.1	-0.5	0	-0.1	0.3	-0.8	0.2	-0.7
26	-0.1	-0.7	-0.1	-1	-0.5	0	0.7	-0.4	-0.2	0	0.2	-0.2	-0.4	-0.9	0.2	0.3	-1.2	-0.7	0	0.3	-0.6	0.3	-0.2	0.2	0	0	0.2	0	0	-0.5	-0.1	-0.3
27	-0.5	-0.5	-0.6	-0.4	-0.3	-0.4	-0.9	-0.3	0.6	-0.2	-0.1	0.3	0	-0.4	-0.2	-0.1	-0.4	-0.3	-0.1	0.3	-0.3	0.1	-0.3	-0.4	0.2	-0.2	-0.2	0	0	-0.1	1.6	-0.4
28	0.1	-0.2	-0.8	-0.5	-0.6	0.2	-0.4	0.3	-0.1	-0.2	0.1	0.2	-0.6	-0.3	-0.3	0.3	-1.4	-0.4	-0.3	-0.2	0.2	0	-0.1	-0.1	-0.1	-0.2	0.1	0.3	0.9	0.2	0.3	-0.1
29	-0.1	-0.6	-1	0.1	-0.2	-0.1	0.2	0.1	-0.1	-0.3	0.2	0.8	-0.3	0	-0.2	0	-0.4	0	-0.2	0	-0.1	0.1	-1	-0.5	-0.3	-1.3	-0.2	-0.1	0.6	-0.2	1.3	-0.5
30	-0.5	-0.3	-0.3	-0.8	-0.9	-0.2	-0.5	-0.2	0.5	-0.1	-0.2	0.3	-0.9	-0.2	0	0.3	-0.3	-0.1	-0.3	-0.2	0.4	0.4	-1.6	0	0	-0.2	0.1	0	0.4	-0.3	0.1	-0.5
31	-0.4	0.5	-0.8	-0.1	-0.8	-0.2	-0.6	0.1	-0.2	-0.2	0	-0.1	-0.7	-0.3	-0.1	0.3	-0.1	0.1	0.5	-0.2	-0.4	0.1	-0.4	-0.6	-0.1	-0.5	0.1	-0.1	0.3	0	1.2	-0.6
32	-0.2	0.5	0.2	-0.8	-1.1	0	-0.3	0	0.4	-0.1	-0.1	0.3	-0.1	0.4	0	0.1	-0.2	-0.2	0.3	0.1	-0.2	0.4	-0.9	0.1	-0.2	-0.5	0	-0.5	0.3	-0.7	1.3	-0.5
33	-0.3	0	0.1	-0.7	-0.1	0.4	-0.5	0.4	0.1	-0.1	0	-0.2	-0.7	0	-0.1	0	-0.3	-0.1	0.2	0.2	-0.5	-0.1	-0.6	-0.7	-0.3	-0.3	-0.1	-0.3	0	-0.3	0.4	-0.4
34	-0.2	0.1	-0.8	-1	0	0.1	-0.7	0.1	0.5	0.2	0	0	-0.4	-0.1	0	0.1	-0.5	-0.5	0	0	-0.5	-0.2	-0.8	-0.2	0.2	-0.4	-0.1	0	0.3	-2.5	-0.1	-1.2

k	1	2	3	4	5	6	7	8	9	10	11	12	13	14	15	16	17	18	19	20	21	22	23	24	25	26	27	28	29	30	31	32
35	-0.3	-1	-0.3	-0.1	0.4	0.1	-0.2	0.4	-0.3	-0.4	-0.2	0	-2	0	-0.7	0.2	-0.3	0.2	-0.1	-0.3	-0.5	0.4	-0.4	-0.1	-0.4	-0.4	0.2	-0.2	0.1	-1.4	-0.2	-0.5
36	-0.2	-0.2	-0.6	-0.3	0.4	-0.3	0.4	0.2	-0.1	-0.1	0.1	0.6	-0.3	-0.2	0.1	0.1	0.1	-0.2	-0.4	-0.1	-0.6	0.4	-0.6	-0.7	-0.1	-0.5	0.4	-0.3	0.1	-0.1	1.4	-0.9
37	-0.3	-0.7	-0.4	-1	-0.9	0	-0.3	-0.2	-0.1	0	-0.2	0.3	-0.3	0.1	0	-0.2	-0.2	-0.2	-0.2	0.5	-0.4	-0.2	-0.5	-0.4	-0.2	-0.5	0.2	-0.2	1	0.3	0.1	-0.3
38	-0.5	-0.5	-0.8	-0.2	-1.3	-0.4	-0.2	-0.2	0.2	0	0	0.1	-1.2	0	-0.5	0.2	-0.7	-0.3	-0.4	-0.1	-0.2	0.4	-0.8	0	0.1	0	0.3	0	-0.4	0	2	-1
39	-0.2	-0.5	-0.5	-0.8	-1.6	0.7	0.4	0.4	0.2	-0.2	0	0.7	0.2	-0.4	-0.1	0.1	-0.2	-0.5	0.3	0.2	0.4	0	-0.2	0.2	-0.6	-0.2	-0.3	-0.1	0.7	-1.2	0.4	0.3
40	-0.2	0.2	-0.7	-0.4	-0.8	0.3	0.2	0.2	-0.4	-0.1	0.1	-0.1	-0.3	-0.2	0.2	-0.1	-0.3	-0.7	-0.4	-0.1	0	-0.1	-0.7	-0.4	0.1	-0.2	0.2	0.4	1.7	-0.3	0.9	-0.4
41	-0.4	-0.8	-0.3	-0.4	-0.1	0.5	-0.4	0	0	-0.2	-0.4	-0.1	0.1	0	0.1	0.1	-0.1	-0.2	0.6	0.1	-0.3	-0.5	-0.2	-1.4	-0.2	0.1	-0.1	-0.4	0.2	-0.1	-0.4	-0.8
42	-0.2	-0.3	-0.5	-0.6	-0.5	-0.3	-0.4	-0.1	0.2	0	0.1	0.1	0.7	-0.2	-0.4	-0.2	-0.6	-0.6	-0.4	0.6	-1	0.1	-0.6	-0.3	0.3	-0.4	0.2	-0.3	0.3	-1.7	1.2	-0.5
43	-0.3	-0.5	-0.3	-1.3	-0.3	0.4	0.1	0.2	0	0.2	0	0	-0.8	-0.2	-0.1	0.3	-0.6	-0.4	-0.1	0.2	-0.4	0	-0.4	-0.1	-0.6	0	0.2	0.1	0.9	-0.1	0.2	-0.4
44	-0.2	-0.8	-0.3	-0.3	-0.4	-0.2	-0.1	-0.2	-0.4	-0.2	-0.1	-0.1	-0.1	-0.3	0.4	0	-0.5	0.4	0.5	0.7	0.2	0.4	-0.5	-0.1	-0.1	0	0.4	-0.3	1	-0.3	0.8	-0.7
45	-0.3	0.1	-0.7	-0.9	-0.9	0	-2.1	0	-0.2	-0.1	0.5	-0.1	-0.8	-0.1	0	0.1	-0.6	-1	-0.2	0	-0.6	0.2	-0.6	0	-0.2	-0.6	-0.2	0	0.1	-2.3	0.1	0.2
46	-0.1	0.5	0.1	-1	-0.4	0.3	0.1	0.8	0.2	0.2	-0.1	0.3	-1.1	-0.4	0.4	0.2	-0.5	-0.5	0.2	0.9	-0.2	0.3	-0.3	-0.5	-0.4	-0.3	0.2	0.1	0.1	-0.1	1.9	-1
47	0.1	-0.2	-0.3	-0.5	0	0.3	-0.1	0.6	0.4	-0.1	0	-0.3	0.2	-0.2	0.1	0.2	-0.8	-0.5	0.2	0.4	0.2	0.4	0.2	-0.4	-0.6	-0.3	-0.2	-0.3	0.2	-1.1	0.5	0
48	0.1	0.1	-0.5	-1.3	-1.4	0.7	-0.2	0.4	0.2	-0.2	-0.4	-0.1	0.3	-0.2	0	0	-0.9	0	-0.1	0.4	0	0.5	0.8	-0.1	-0.5	-1	-0.4	0	0	-1.7	0.1	-0.3
49	-0.4	-0.4	-0.6	-0.2	-0.9	0.3	-0.5	0.2	-0.1	0.1	0.2	-0.1	-0.4	-0.3	-0.4	0.3	-0.4	0	-0.2	0.2	-0.6	-0.1	-0.4	-0.4	0.1	-0.4	0.6	0.2	0.2	-0.3	0	-0.3
50	-0.2	-0.2	-0.5	-0.7	-0.6	0.1	0.2	0	0	-0.5	0.3	-0.3	-1	0	0	0.3	-0.3	-0.2	0	-0.2	-0.2	0.4	-0.1	0.2	-0.6	-0.3	-0.1	0.1	0.6	-0.4	0.1	-0.1
51	-0.4	-0.6	-0.7	-0.1	-0.2	-0.1	-0.1	0.4	0.1	-0.3	0	0	-0.9	0	-0.1	0	0	-0.1	-0.2	-0.3	0.3	0.2	-0.2	-0.3	-0.1	-0.6	0	-0.2	0.1	-0.3	1.3	-0.5
52	-0.4	-0.4	-0.2	-1	0.2	0.4	-1	-0.2	0.3	-0.3	-0.1	-0.1	-0.3	-0.5	0.2	0.1	-1	-0.7	-0.1	0.1	0.2	0.4	-0.3	0.2	0	0.1	-0.1	-0.2	0.3	-0.1	0.1	-0.8
53	0.3	-0.6	-0.2	-0.6	0.2	-0.1	-0.4	0.8	0.5	0.2	-0.2	0.3	-1.1	-0.1	0.3	0	-0.4	-0.2	-0.1	0.2	0	0.5	-0.1	-0.9	0	-0.4	-0.3	0	-0.5	0	2.5	1.2
54	-0.1	-0.2	-0.3	-0.6	-1	0.3	-0.3	0.2	0.1	-0.1	0.1	0.1	-0.6	-0.3	-0.3	0	-0.4	-0.2	0.2	0.1	-0.1	-0.2	-0.3	0	-0.2	-0.6	0.1	-0.1	0.4	-0.3	0	-1.4
55	-0.3	0.1	-0.1	-0.8	-0.5	0	-0.2	0.1	0.7	-0.3	0	0	-0.7	-0.1	-0.2	-0.3	0.1	0.8	-0.1	-0.1	-0.6	0.4	-0.1	0.2	-0.1	-0.8	0	-0.5	-0.2	-0.8	-0.2	-0.5
56	0	-0.7	0.4	-0.6	0.2	-0.2	-0.1	0.4	0.3	0.2	0.1	0.6	0.2	-0.4	0.4	0.1	-1	0.1	-0.4	-0.2	-0.5	0.3	-0.5	-0.1	-0.2	0.1	0.4	-0.2	0.4	-1.1	0.1	-0.4
57	-0.2	-0.3	-0.5	-0.3	-0.9	-0.5	-0.4	0.1	0.3	-0.2	0.2	0.1	-0.5	-0.4	0	0	-0.1	0.1	-0.1	0	-0.2	0.4	-0.8	-0.3	-0.4	-0.6	0.2	0	0	0	0.3	-0.2
58	-0.2	-0.4	-0.2	-0.3	-1.2	0.3	-0.4	0.3	0.1	0.2	0	0.1	0	-0.2	-0.2	0	-0.4	-0.4	0.1	0.1	-0.1	-0.4	-0.5	-0.2	0.2	-0.6	0.3	0.1	0.4	-0.3	0	-0.8
59	-0.2	0.2	-0.6	-1.2	0	-0.4	-0.6	0.2	0.1	0.1	0.1	0.3	0.1	0	0.2	-0.2	-0.2	0.1	0.1	0.1	0	-0.6	-0.5	-1.3	-0.7	-0.2	0.3	0.2	0.6	-0.6	0.9	-0.6
60	0	-0.1	-0.3	-0.1	-0.1	0	-0.2	0.6	0	0.3	0.3	1.7	-0.7	0	0	0.1	-0.7	0.1	-0.1	0.1	-0.7	-0.5	-0.2	-0.4	0.3	-0.2	0	0	-0.2	0.2	0.4	0.5
61	-0.2	0	-0.8	-0.2	-1.3	-0.5	-0.4	-0.2	0.8	-0.4	-0.1	0.3	-0.8	-0.5	0	0.2	-0.8	-0.2	-0.1	0	0	0.1	-0.9	-0.6	-0.1	-0.2	0.1	0.2	0.2	-0.2	1.2	-0.1
62	0	0.4	-0.2	-0.7	-0.1	-0.1	-0.2	0.1	-0.2	-0.4	0	0.4	-0.3	-0.3	-0.3	-0.1	-0.3	-0.2	0.3	0	0.1	0.6	-0.2	0	-0.9	-0.3	-0.3	-0.1	0.2	0.1	0.9	-0.4
63	-0.3	-0.3	0.2	-0.1	-1.2	0.4	-0.6	0.3	0.3	-0.1	0.1	-0.4	-1.9	0.2	-0.4	0	-0.3	-0.8	-0.5	0.3	0.3	0.5	-0.4	0.1	-0.6	-0.2	0	-0.4	-0.5	0.1	-0.4	-0.9
64	-0.1	0.2	-0.7	0.1	-0.8	-0.3	0.2	0.2	1.3	-0.1	0.3	-0.3	-0.5	0	-0.5	0.1	-0.6	-0.2	-0.5	-0.2	-1.1	0.3	-0.8	0.4	0.2	-0.3	-0.1	0.1	0.5	0.3	-0.2	-0.3
b2	-0.2	-0.5	-0.1	-0.8	-0.7	0.1	-0.5	0	0.3	-0.1	0.1	0.2	-1	-0.1	-0.2	0	-0.2	-0.5	0	0.1	-0.4	0.2	-0.5	-0.3	-0.3	-0.8	0.1	0	0.3	-0.4	0.4	-0.6
W3	0.3	-0.1	0.2	0.3	-0.3	0.2	-0.1	-0.2	0.2	0.1	0.1	0.2	-0.3	0.2	-0.1	-0.2	0.3	-0.1	0.1	-0.2	-0.2	0.2	0.2	-0.2	-0.1	0.2	0.1	0.1	0.2	-0.3	0.2	-0.2

Table D.11 - ANN-UBO_e's weights and coefficients of the first hidden layer

i	1	2	3	4	5	6	7	8	9	10	11	12	13	14	15	16	17	18	19	20	21	22	23	24	25	26	27	28	29	30	31	32
1	-1.5	-0.9	1.5	2.1	1.2	-1.3	-1.1	0.9	0.1	4.9	0.1	-0.8	0	-2.2	-1.7	-0.9	-0.6	-0.2	0.6	-0.2	-2.4	-0.3	1.2	-0.9	1.3	-0.5	-2.2	0.1	2.2	-0.9	0	0.5
2	-0.1	0.4	0	0.5	1.9	0.9	-0.5	0.6	0.1	0	2.2	0	-1.3	0	-0.2	-0.5	-1.4	-0.8	0.3	1.1	0	0.6	0.3	1	0.2	-1.9	0.5	-0.4	0.4	0.4	-0.5	0.4
3	-0.6	1	0.1	-0.7	0.6	-0.3	0.8	1.3	0.3	-1.2	0.3	0.9	0.2	0.5	-0.1	0.7	0.5	0.7	2.3	-0.3	0.5	-0.2	0.8	-0.8	-1	0.1	1.1	0.3	1.3	1.3	0.4	-0.1
4	-0.3	0.2	-0.5	-0.2	-0.4	-0.9	-0.2	-0.3	-0.6	-0.6	0.2	-0.7	0.1	0.2	-0.6	0.4	0.4	-0.4	-0.8	-0.4	0.5	0.2	-0.6	0.6	1.3	0.2	-1.1	1	-1.3	-0.4	0	-0.1
5	-0.2	-0.2	-0.9	-0.7	-0.6	0	0.8	-0.3	-0.7	0.7	0.2	0.1	0	0	0.8	0.6	-0.5	0.1	-0.2	0	0	-0.4	-0.3	-0.5	-0.9	-2.1	0	0.5	0.1	0.5	-0.3	0.6
6	-0.5	1.3	-0.4	-0.2	-0.6	-0.7	-0.3	-0.3	-1.4	-0.7	0.3	0.4	0.7	0.5	0	-0.9	-1	-0.1	-0.1	0.6	0.7	0.1	0.7	-0.3	2	1.1	0.9	0	-0.1	-0.2	-0.3	-0.8
7	0	-1	0.6	0.5	-0.5	0.4	0.5	0.8	-0.9	1.9	-0.8	-1.2	0.3	-0.4	1.1	0.5	-0.6	0.5	-1.2	0	0.6	-0.4	-0.3	0.2	-0.4	-0.5	0.9	-0.3	0.9	-3	0.3	-0.2
8	0	-0.1	0	0.6	0.3	-0.5	-0.4	0.6	-0.1	0.2	0.1	0.2	-0.3	0.1	0.7	-0.1	-0.6	0.9	-0.2	0.9	0.2	-0.8	0	0.2	-0.1	0.1	0.9	0.4	0.2	0.3	-0.7	0.4
9	1.4	-0.4	-0.1	0.7	-0.2	-0.9	-0.5	-0.9	1.1	0.1	-0.6	0.7	0.4	0	-0.9	0.5	1.5	-0.3	-0.3	-1.1	-0.1	0.1	0.1	0.1	0.9	-1.4	-1.9	-0.5	0	-0.3	0	0.4
10	0.7	0.3	-0.4	-0.2	-0.2	-0.3	0.6	-0.4	-1.2	-0.1	0.1	-0.9	0.3	0.3	0.3	-0.4	-0.2	-0.6	0.1	0	-0.4	-1	0.6	-0.2	-1.6	-0.2	-0.1	-0.7	0.5	-0.4	0.1	-0.4
11	-1.3	-0.4	-0.9	-0.5	0.6	1	0	0.4	0.1	-0.4	0.3	-0.4	-0.6	0.9	0.1	0.3	-1.4	0.1	0.3	0.6	1.2	1.2	-0.2	-0.8	-1.5	1	0.6	1.2	0	0.5	0.3	-0.3
12	-0.6	-0.3	1.1	0.5	0.1	-0.2	0	0.8	0.7	2	-0.1	-2	0	-0.3	0.2	2.1	-0.7	-0.7	-0.3	-0.1	2.5	0	-1.1	0	0.7	-2.2	-0.2	0.3	0	-0.3	-1.1	0.8
13	0.8	0.3	0.1	-0.4	-0.1	-0.8	-0.1	-0.2	0.7	1.5	-0.1	0.6	-1.3	-0.6	1.3	-0.4	-0.4	-1.8	-1	0.4	0.4	2	-0.3	0.7	2.3	-1.4	0.3	0.2	0.1	0.4	-0.2	1.4
14	1.1	-0.3	-0.5	-0.5	0.2	1	0	-0.2	-1.1	0.1	0.2	-0.6	-0.2	0.5	-0.6	-0.1	0.1	-0.7	-0.2	-0.6	-1.4	-0.6	0.2	-0.5	0.1	-0.9	0.4	0.1	-0.2	0.9	-0.8	0.2
15	-1.1	-1	0.1	-0.6	0.6	0.1	0.5	0.3	-0.6	-0.4	-0.1	0.5	0.5	-1.4	-0.2	0.5	-0.6	-0.6	0.8	-0.1	0.2	-1.2	-0.5	-0.1	-0.6	-0.5	0.4	-0.2	-0.1	0.9	-0.2	-0.1
16	0.3	-0.7	0.7	0.2	0.6	1.5	1	1.4	0	0.1	-0.6	0.6	0	-0.6	-0.5	-0.4	0.9	1	0	-0.2	0.4	0.6	-0.1	1	0.3	0.7	-0.7	-1.4	-1	0.7	-1.8	0.8
17	0.6	0	0.8	0.3	-1	-0.2	-0.5	-0.4	0.2	-0.7	1.4	0.1	-0.4	0.2	-1.9	0	-1.9	-0.6	0.5	0.6	0.6	2.1	0.4	0.7	0.2	-0.2	-0.3	0.9	-1	1.2	0.2	-0.2
18	-0.7	-1.3	-0.7	-0.3	0.5	0.2	0.2	-1.1	-0.1	1.1	-0.5	-0.9	-0.2	-0.5	0.2	-0.4	-1.3	-0.1	0	-0.2	-0.6	-0.9	0.6	-0.6	0.4	-0.8	0	0.6	0.5	-0.8	1.4	-0.7
19	0.7	1.2	-0.6	-0.8	1.4	0.3	1.3	-1.1	0.8	-0.3	1.2	-0.8	0.1	0.5	1.8	-0.3	-0.6	-1.3	0.3	1	0.6	-0.7	-0.9	-0.4	-0.6	0.2	-0.3	-0.2	0.5	-0.4	0.5	0.1
20	0.1	-0.5	-0.2	0	-0.4	2.6	-1	-1.6	0.3	0.6	-1.1	0.2	-0.8	-0.5	1.2	0	-0.1	0.1	-0.5	2.7	-1.1	0.6	0.7	1.7	-1.9	-1.2	0.3	-1.1	-0.3	1	0	-1.1
21	0	-0.1	-0.1	-0.3	-0.3	-0.2	-0.5	1.8	-0.3	0	-0.2	0.3	-0.7	0.2	-0.3	-0.5	0.5	0.8	-0.2	0.6	-0.4	0	0.3	0.3	-1.1	0.7	-0.1	1	-0.1	0.6	0	-0.2
22	0.3	-0.7	1.1	1	0.3	0.9	-0.8	0.3	-0.2	-0.7	1.2	-0.8	0.7	-0.8	1.3	0	-1.9	1.1	-0.5	1.3	0.2	-0.3	0	0.1	0.1	1.2	0.8	-1.2	-1.3	1.2	0.8	-1.1
23	1.1	1.6	0.8	-1	-1.1	-0.5	0.1	1.2	-0.4	0.4	-0.3	0.2	0.9	1.1	-0.8	-0.5	0.5	1	0.1	0.8	0.7	0.9	1.2	0.9	0.7	-0.8	0.1	0.8	-0.1	-1.8	0.9	1.3
24	-0.1	0.7	-0.3	-0.9	-0.1	-0.7	0.9	0.8	0.1	-2.7	-0.4	0.7	0.3	0.7	0.4	0.2	1.5	-0.7	0.1	0.6	-0.1	-0.9	1.3	-4.7	-1.6	-1	0	1	-3.2	1.8	0.2	-3.5
25	-1	0.4	0.7	-0.9	-1.7	0.7	-0.9	0.6	0.2	0.4	-0.4	-2	0.2	0.3	0.1	0.3	-0.7	1.1	-0.2	-0.4	3.7	0.5	0.1	1	-0.7	-1	1.5	-0.7	-0.5	-1.3	-0.2	0.1
26	-2.7	0.4	0.5	0.5	-0.1	-1.6	-1.8	0.4	0.2	0.4	-0.4	0.1	-0.5	1.1	0.2	-0.7	-0.7	0.4	-0.4	0.6	-0.1	-1.7	3.2	-1.1	-0.4	0.5	-0.4	-0.3	-0.1	-2.2	1.1	0
27	-0.2	-0.7	0.3	-0.9	0.7	0.2	-2.1	0.3	-0.5	-0.1	0.1	-2.5	-0.3	-0.6	-0.3	-1.5	-0.3	-1.9	-0.1	-0.7	1	0.6	-0.8	0.4	0.5	0.3	-0.1	-2.2	0.1	0.6	-0.9	-0.5
28	1	-0.3	-0.6	-0.5	0	0.4	0.4	0.1	-0.4	1.3	-0.1	-0.2	0.1	0.3	0.9	0.8	0.5	-0.6	-0.2	1.1	-1	1.5	1.1	0.6	0.5	-0.1	0.1	1.2	0.2	0.1	0	-0.2
29	0.5	-0.2	-0.5	0.2	1.1	-0.7	0	0.1	-0.1	2	-0.2	0.3	-0.5	-0.1	1.4	-0.8	-0.2	-1.2	-0.9	0.7	0.2	-0.7	0.6	-0.3	-0.9	0.2	-1	0.3	-1.5	0.3	-0.5	0.2
30	-1.4	-0.5	-1	0.9	-2.9	1.8	0.4	-1	-2.9	-1.7	0.9	1	0.5	0.7	-0.6	-1.3	0.8	-1.2	-0.5	0	0	-5.6	-1.7	-2	0.5	-0.6	-1.5	-1.3	-3.2	3.1	-0.3	-4.4
31	-0.9	-1.3	0.9	-0.7	0.5	-1.4	-1.6	-1.5	0.2	2.3	-0.4	0.9	-0.4	1.1	-2.8	2	0	-0.5	-2.1	-0.2	0.7	-0.1	0.1	-4.6	-1.7	0.3	-1.6	1.4	-0.6	-0.8	-1.2	-2.3
32	-0.1	0	-0.1	-0.1	0	0.1	0	-0.1	0	-0.1	-0.1	0.1	0	0.1	0	-0.2	0	0	-0.1	0	-0.1	0.1	0.1	-0.1	0	0	0	0	0.1	-0.1	0.1	0.1
33	-1.7	0.9	0	-0.8	-1.4	-0.8	-1.3	0.2	0.3	-0.6	-0.8	-1.6	-1.8	-1.4	0.9	-2	-0.3	-1.8	-1	-0.8	0.2	-1.1	0.5	0.6	0.7	-0.9	-1.4	-0.4	-0.7	-2.2	-0.6	0.3
34	0.5	-2.3	-3.5	-2.1	-0.3	-0.6	-0.1	-0.8	1	0.7	-0.1	-0.1	-2	-3.4	-0.5	-1.8	-1.5	2.4	-2.2	-1	-1.5	-0.5	-0.3	-0.8	0.4	-1.6	0.6	0.5	-1.3	1.6	-1.1	-1.8
35	0.1	-0.6	-0.8	-1.2	-0.5	-0.2	0.3	0.2	-0.1	0.1	-1.4	-2.3	-0.3	-0.3	-1	-1.7	-1.4	-0.6	0.4	-0.5	-1.4	0.8	-0.6	-0.1	-1.1	-1.1	0.3	-0.7	0.3	-0.7	-0.2	-0.4

i	1	2	3	4	5	6	7	8	9	10	11	12	13	14	15	16	17	18	19	20	21	22	23	24	25	26	27	28	29	30	31	32
36	-0.4	-0.3	-0.8	0	-0.4	-0.8	-0.1	0.3	-0.3	0.1	0.3	-0.3	0.4	-0.1	-0.5	0.5	0.5	0.1	0	-0.2	-0.4	-1.3	0	-1.1	-1.8	0.3	-1.2	0.1	0	0.3	-0.5	-0.2
37	-0.1	-0.3	-0.7	-0.1	1	-5	-1	-4	-2.1	-3.1	-0.3	0.4	-0.8	0.7	0	0.3	-0.1	0.3	-0.3	0	0.1	0.7	-1.7	-1.9	-4.2	0	0.7	-1.2	0	-2	0.5	-1.2
38	-1.1	-0.7	-0.8	-1.1	-0.9	-1	-0.8	-0.9	-0.9	-0.4	-0.9	-1	-1.3	-0.5	-0.9	-1.1	-0.9	-0.7	-0.9	-0.8	-0.5	-0.8	-1.1	-0.9	-0.5	-1.3	-0.6	-0.8	-0.7	-1	-0.8	-1
39	0.3	-2.5	-3.7	-0.5	-0.8	0.1	-1.1	-0.2	-0.8	0	0.3	0.3	-2.8	-1.7	0.3	0.2	-1.7	1.1	0.2	-0.4	-1.2	-4.4	2	-2.9	-4.8	-0.3	-0.6	-0.7	-2.7	-0.8	-1.5	-2
40	-2.6	0.8	0.5	-1.1	-0.5	-0.7	0.4	1.1	-1.7	-0.3	-1	-2	0.1	-1.3	-0.7	-0.5	-0.7	0.3	0.3	-0.9	0.6	-2.1	-0.7	0.2	0.2	0.4	0.2	-0.7	-1.3	0.1	-0.2	-2
41	-1.1	-2.6	-2	-0.8	-1.8	0.8	1.5	-2.4	-3.1	-2.8	0.9	2.5	-0.8	-0.7	-1.6	-0.2	-2.8	1	-1.4	-2.5	-3.3	0.2	-2.1	1.1	-0.2	-3.4	0.8	3	-2.3	3.7	-0.6	0.2
42	-3.4	-0.3	-2.8	-1.8	0	-3.2	-1.6	-1.4	-0.1	-0.3	-1.2	0.5	-2.1	-1.5	0.2	-4.2	-1.4	-1.2	-2.4	0	-1.7	-3.6	0	-1.5	0.8	-0.9	-2.1	-2.8	-1.9	-2.4	-1.3	-1.3
43	-0.3	-0.1	0.8	-1.3	-0.6	-0.5	-0.7	0.3	0.1	-3.5	-0.5	-1.1	-0.7	0.2	-1.2	-0.2	0.1	-0.8	2.3	-1.2	0.5	-1.4	-0.9	-0.9	-0.7	-0.3	-0.2	-0.5	-0.5	0.5	-0.2	-1.7
44	-0.2	-1.1	-0.1	0	-0.7	-0.6	-1.1	0	-0.9	1.2	-0.2	-2.1	-0.3	-0.6	-0.2	-0.3	-0.4	-0.3	-0.7	-0.2	0.1	1.2	-0.4	-0.7	-1.1	-0.9	-0.5	-0.4	0.4	-1.5	-0.3	-0.1
45	0.5	0.2	-0.7	-1.7	0.4	-0.4	0.3	-0.8	0.5	0.2	-0.8	-0.1	-0.6	1	-0.3	-1.2	-0.5	-0.9	-1.1	-1.2	0.4	0.2	-0.6	-1	-0.9	-0.8	0.1	-0.2	-0.8	0.4	-0.3	-0.3
46	-1.7	0.5	-0.9	-0.2	0.4	1.6	-0.4	0.3	-0.9	-2.5	-0.5	-2.9	0.9	0.2	0.2	1.5	-3.3	-2.2	-1.6	-0.1	1.3	-0.7	1.2	-0.1	0.1	0.1	0.8	0.6	0.3	-1.3	0.2	2.6
47	-2.1	-1.9	-4.2	-0.4	0.3	0.7	-0.4	-0.6	-0.5	-0.1	-2.1	-3.3	0.2	-3.3	-1.6	1.1	1.8	-2.7	0.9	-0.6	0.4	-0.6	-1.3	0.8	0.7	-3.3	0.9	-2.2	0.1	-3.5	-0.1	-1.2
48	-0.3	-2.3	0.1	-3.2	0.7	-0.7	0.7	0	-0.5	1.3	-1.2	0.2	-1.2	-2.5	-0.4	-1.4	-2	0.4	-1.8	-1.6	0.6	-1.5	-2.3	-1.6	-1.6	-2.1	-0.3	-0.3	0.3	-3	-2.2	-2
49	0.1	0	0.2	0	-0.1	0	0.1	0	-0.1	-0.1	0.1	0.1	0	0.1	-0.1	0.1	0	0.1	0.1	0	0.1	0.1	0.2	0	0.1	-0.1	0	0	0.1	0.1	0	-0.1
50	-0.3	1.2	-2.6	-0.8	-2.6	1.1	-0.8	-1.3	-1.4	0.1	0.3	0.5	-0.4	0	-0.5	1	0.5	0	-2.3	0	-2.5	-1.4	-0.9	0	-3.6	0	-0.8	1.3	-2.6	0.4	-2.5	0.9
51	0.1	0.1	0.1	0	0	0	0.1	-0.1	-0.1	0	0.2	0	-0.1	0	0.1	0	0.1	-0.2	0	0	-0.1	0.1	0.1	0	0	0.1	0	0	-0.2	0.1	-0.2	0.2
52	-0.6	-5.5	-0.7	0.1	-0.5	1.6	-1	-0.3	-2	-0.4	0.6	-2.2	-0.2	-3.5	-0.1	-1.6	3.2	0.2	-0.5	-0.3	-0.4	-1.8	-1	-0.2	-0.2	0	-2.7	0.6	-1.1	-0.3	-2.7	-2.4
53	-0.8	0.3	0.4	0.4	-1.6	-1.6	-1.4	-0.8	-1.7	-0.3	0.4	-0.9	-2.6	0.1	-0.1	-0.8	-2.2	-0.5	-0.7	0	-0.7	-0.2	-0.3	-0.5	-0.2	-0.8	-0.7	-0.6	-0.3	-1.1	-0.1	-0.5
54	-2	1.1	-1.2	-0.8	-0.9	-0.5	1.8	0.8	-0.5	-0.8	-0.8	0.1	2.2	0.7	-2.4	0.3	0.6	1.2	1	-1.3	0	-0.9	1	-1.6	-0.9	1.4	-0.1	0.1	0	-0.5	1.2	-0.8
55	0	-0.2	0.1	0.2	0.1	0.1	0	-0.1	0	0.1	0	-0.1	-0.1	-0.1	0.2	0	0	-0.1	0	-0.1	-0.1	-0.1	0.1	0.1	-0.1	0	0	-0.2	-0.2	0	0.2	0
56	-1.1	-3.1	-1.3	-1.7	-1.1	-1.7	-0.9	3.1	-1.3	-2.2	-1	0.4	0.1	-1.2	0.3	0.7	0.4	0.5	0.5	-0.4	-1.4	-1.4	-0.5	-2	-0.6	-4.5	-2	0	-5.3	0.3	-2	-4
57	-0.5	-1.7	-0.7	-1.7	1.1	1.9	-1.3	-1.8	-0.1	-0.6	-0.3	-1.8	2.4	-2.4	-1.5	1.6	-1.2	-1.2	-2.8	-0.3	-0.5	-1.9	-0.8	0.5	0.9	-1.9	1.4	1.2	0.1	1.4	-1.6	-0.3
58	1.5	-0.4	2.5	1.6	1.1	-0.8	0.6	0.9	0.5	0	1	0.1	1.2	-0.5	1.9	-1.4	-0.9	-0.4	2.1	2.2	-1.5	0.8	-1.6	1.9	1.5	-3.9	-1.6	-2.5	2.9	0.2	-1.3	-1
59	1	0.2	0.6	0.9	0.9	-0.2	-0.3	0.2	2.2	-0.7	-1.7	-1.1	-1.3	-1.1	0.1	1.4	-1.6	0.8	0.7	1.2	-1.7	-0.1	2.3	-1.6	1.9	-1	0.1	-1	1	1.2	-1.6	-0.1
60	0.8	-0.2	-0.3	0.8	-0.9	0	-1	-0.4	1.9	-1.5	-0.5	-1.1	-2.1	-1.2	-0.8	2.2	-2.8	-0.7	0.4	-0.1	-0.5	1.5	-0.2	0	-0.4	0.3	0.2	0	-1	0.4	0.3	0.6
61	0.8	-0.1	-2.1	0.9	2.7	0.9	-1	-0.5	-1.4	0.6	-2.6	0	-0.8	-0.3	-0.3	-1.7	-2.4	-0.9	-1.2	-0.5	0.4	-0.4	0.5	-1	1.2	-0.5	0.9	1.8	-1	-1.7	-0.1	1.2
62	-1.3	-0.6	-0.4	0.2	-1.5	1.3	-0.5	-0.1	0.3	-1.4	-1	-1.1	1.2	0.4	-2.9	-0.4	1.5	-0.9	0.2	-1	0	-1.3	1.9	-1.8	-2.1	0.2	-2.3	-0.7	0.2	0.3	0.6	-1.6
63	0.5	0.5	-0.7	0.1	-0.1	-0.1	0.4	-1.5	-0.1	0.5	0.6	-0.4	-0.5	0.5	-0.1	-0.1	-0.5	-0.8	-0.2	0.6	-0.7	0	0.3	1.2	0.1	-0.4	-0.2	0.5	0.6	-0.5	0.4	0.4
64	3.4	2.6	-0.8	1.2	1.5	-0.1	1.5	-2.5	0.7	-0.2	2.6	0.5	-1.3	1.1	2.3	-1.4	-2	-0.6	-1.5	0.8	0.1	1	-0.2	-0.5	0.9	-0.3	3.5	-1	0.5	-0.7	1.3	0.9
65	0.6	-0.2	0.6	0.3	0.6	-2.4	0.7	0.8	-0.2	0.9	0.2	-1.6	-0.6	-0.2	-1.9	1.4	-0.3	-0.5	1.4	-2.9	0.4	-0.4	-0.2	-1.5	0.6	-1	-1.1	-0.1	1.4	-1.8	2.1	0.8
66	-0.8	-0.9	0.3	-0.4	-0.5	-0.1	-0.5	0.3	-0.5	-0.9	-0.2	-0.6	1.3	-0.9	-1	0.2	0.6	0.4	-0.4	-0.7	0.3	-0.4	-0.8	-0.7	-1.1	0.7	-0.2	-0.1	-0.6	0.2	-0.7	-1.1
67	-0.8	-1.9	-1.4	-2.8	-0.3	0.3	0.2	0.8	-0.1	0	-1.6	1.6	3.1	-1.5	0.1	1.3	1.6	0.4	1	-0.3	-0.3	-1.3	1.4	-2	-1.6	-1.3	-1	1.7	-1.4	0.6	-0.3	-2.3
68	0.2	-0.1	0.1	0	-0.1	0.1	0	-0.2	0	0	0.1	-0.1	-0.2	0.1	-0.1	-0.1	0	-0.2	0	0	0.1	0.1	0	0	0.2	-0.1	0	0	0	-0.1	0.1	0
69	-0.1	-0.4	-0.8	-2.5	-1.5	-0.1	-0.2	1.2	0.3	-0.6	0.3	-0.7	-4	-2	0.7	-1.6	-2	0	-1.8	-0.1	0.5	2	-1.9	1.8	-0.7	-2.5	-2.7	0.7	-1.3	-0.6	-0.8	0.2
70	-2.7	-0.3	-0.3	0.3	-2.9	-1.2	-1	-1.5	2.3	-1	-1.2	0.1	-0.9	-0.9	-1.8	1.3	1.3	-2	-0.4	-0.8	-1.6	0.9	-0.6	-0.9	0.9	-1.4	1.7	0.1	-0.6	-1.6	-1.1	-0.4
71	0.1	0.1	-0.1	-0.2	0	0	-0.1	0.1	0.1	0.1	0.2	0	-0.1	-0.1	0	0	-0.1	0.1	-0.2	0.1	-0.1	0.1	-0.1	-0.2	-0.1	0	0	0.1	-0.2	0	0	-0.1
72	0.1	-0.2	0.1	0	0.1	0	-0.1	0	-0.1	0.1	0.1	0.1	0	-0.1	0.1	0.1	0.1	0	-0.1	0.1	-0.1	0.2	-0.1	0	-0.1	0.1	-0.1	0.2	-0.2	0.1	-0.2	-0.1
73	-0.1	0	0.1	0.1	0	0.1	-0.1	-0.1	-0.2	-0.1	0	0.1	0.1	0.1	0	-0.1	0	0	0	0	0.1	0	0.1	0	0	-0.1	0.1	0.1	0	0.1	-0.1	0.2
74	-0.9	-0.9	-1.4	-1.1	-1.8	-0.3	-1.1	-0.3	-1.1	0.2	-0.7	-1.9	2.2	-1.3	-0.7	1.4	0.7	-1.2	-0.7	-0.2	-1.2	-1	-0.1	-0.5	-3	0.3	-1.7	0.1	0	-0.1	-1.3	-0.5
75	0.2	0.1	-0.1	0.1	0	0	-0.2	0	0.1	-0.2	0.1	-0.2	-0.2	-0.1	0.1	0.1	0.1	0	-0.1	-0.1	0.1	0.1	0	-0.1	0.1	0.1	0	0.1	0.1	0.1	0.2	0.2
76	-0.1	1	0.7	-0.7	-0.3	0.7	1	-0.2	-0.2	-0.1	-1.7	-1.1	0.8	0.3	-1.2	-1.5	2.1	-0.8	0.8	-0.4	-0.1	0.9	0.7	-1.7	-0.1	-0.5	-0.2	0.4	-0.6	0.4	-0.8	-0.6
77	-0.2	0.2	0	-0.1	0.1	0	0	0	0.1	0	0	-0.1	-0.1	0	0	0	-0.1	0.1	-0.2	-0.1	-0.2	0	-0.1	-0.2	0.1	0	0	0	0.1	0.2	0.1	-0.1
78	-1.7	1.3	0.2	0.1	1.3	-1.5	-1.7	0.1	-0.8	1.9	1.1	2	-0.5	0.2	-3	0.2	-0.4	-2.2	1.8	1.5	-0.6	-0.2	1.8	0.2	2	-1.4	-0.3	-0.1	-1.7	0.7	1.7	-1.4
79	-1	0.1	-0.7	-1.4	0.2	-0.7	1	-0.1	-1.6	0.1	0.1	-1.1	0.1	-0.9	1.4	0.7	0.4	-0.9	-0.3	1	-0.1	0.8	1	-0.4	-3.2	1.1	-0.2	1.1	-0.3	-0.4	0	-0.3
80	0.9	0.8	0.2	0.7	1.2	0	0.4	-0.9	0.9	-1.4	0.1	0.5	-1.2	0.9	0.8	-1.5	-1.7	-0.7	-0.3	0.3	0.6	0.1	-0.2	0.2	0.7	0	0.9	-0.8	0.1	0.6	0.5	1.3
81	1.1	-0.2	-0.9	1.7	0.3	1.8	-0.2	-0.6	0.8	1.4	-0.3	0.5	-1	0.4	-0.7	-2.2	-1	0	-0.8	1.2	0.5	0.6	0.3	0.6	1.9	-0.6	-1.3	-1.2	1.1	-0.1	-2.9	0.6
82	-1	1.4	1.7	1.3	-0.5	-0.4	-0.6	1.7	1.1	-1.7	-0.9	-1.6	1.7	-0.3	-0.5	1.5	-2.1	0.2	-1.2	0.3	0.6	-1.2	-0.3	1.1	0.5	1.9	-2	-2.2	0.5	-0.6	-0.3	0.5
83	-1	-1.4	-1.3	0.1	0.1	0.1	-0.5	0.6	-0.2	-1.2	-0.4	-0.2	1.8	-1.6	0.2	2.2	2.8	-1.4	1.3	-1	-1	-0.7	-1.2	0.6	-0.9	-1.1	-1	0.3	-0.8	-0.2	0	-1.6
84	-0.9	-1.9	-1.8	-1.3	0.4	0.3	-1.5	0.4	-1.2	-1.7	1	0.2	-1.9	0	-0.2	-1.7	0	0.3	0.3	0.1	-1.5	-0.1	-0.4	0.4	0.3	0.2	-0.7	-2.1	-1	-0.7	0.6	-3.3
85	1.4	-3.5	-0.7	-1.1	-0.8	0.8	-2.4	0.6	1.4	-2.8	-4.1	1.2	-0.9	-1.5	-1.4	-0.2	3.1	0.8	2.6	-2.2	-2.3	-2.5	1	-4.3	0.3	0.7	-1.3	0.6	-2	-1.5	-0.8	-0.4
86	0.4	0.2	0.4	-0.7	0.1	-0.1	0	0.3	0.2	-0.1	-0.2	0.1	-0.1	0.1	0	0.1	0.2	1	0	0.1	0.1	0.1	0.2	0.4	0	-1.2	-0.8	0	0.1	0.1	-0.2	0.1
87	0	0.1	-0.4	-0.5	0	0.1	-0.1	0.1	0.1	0.1	0	0.1	0	0.1	0	-0.3	-0.4	0.5	-0.1	0.1	0	0.1	0.1	0.3	-0.1	-0.7	0.1	0.1	0	0	0.1	0.2
88	-1.6	-1.6	-1.7	-3.7	-1.8	-0.2	-3.3	-0.7	-0.4	-0.4	1.1	1.2	0.1	-3.4	-0.8	-0.9	0.3	-3.4	-0.1	-1.3	-2.8	0.3	-0.5	0.1	-3.6	-3.4	-0.3	0.8	-2.7	1.9	0.3	-0.9
89	1.8	0.8	0.7	-3.1	-1	0.1	0.5	0.3	-1	0.6	-0.4	-1.9	-3.4	-0.9	0.8	-2.5	-0.6	0.1	-0.6	-2.5	0.8	-0.5	0.3	-1.2	0	-2.5	0.8	0.7	0	-0.1	1.8	-2.9
90	0.4	0.6	0.1	2	-0.5	-0.5	-0.3	-0.7	0.2	-0.5	0.5	0.9	-2.5	3.3	0.2	-2.6	-0.4	-1.3	-1.6	-0.4	-1.4	-1.8	-0.9	1.7	-0.9	-4.5	0	1.5	-1.4	1.3	-1.5	0.9
91	0	-0.2	-0.1	-0.1	-0.1	0.1	0.1	-0.1	0.1	-0.1	-0.1	0.1	-0.1	0.1	0.1	0	-0.1	-0.1	-0.1	0.2	0.1	-0.1	0	0.1	-0.1	-0.1	-0.1	0.1	-0.1	0.1	0.1	-0.1
92	0.2	0.6	-0.9	-0.1	0.1	0.2	0.4	-0.1	-0.6	0.3	-0.2	-0.1	-0.4	0.3	-0.3	-0.4	-0.3	-0.3	0.2	-0.1	-0.2	0.1	0.5	0.5	0.1	-0.1	0.3	0.1	0.2	-0.7	0.4	0.6
93	-0.1	0	0.1	-0.1	-0.1	0	0	-0.1	-0.1	0.1	0.1	-0.2	0	0	0	-0.1	0.2	-0.1	0	-0.1	0.2	0	0.1	-0.2	0	0.2	0.1	0	-0.1	0.1	0.1	0.1
94	-0.8	-1.3	-1.1	-1	-0.6	0	-0.3	-0.5	-0.5	0	-1.5	-0.5	0.5	-1.1	-0.6	-0.9	0.6	-0.3	-1.1	-0.7	-0.3	-1.4	-0.2	-0.9	-0.5	0.3	-1.7	0.6	-0.6	-0.2	-1	-1
95	0.3	0.2	0.5	0.2	0	-0.2	-0.1	-0.5	0	0.2	0.4	0.1	-0.2	-0.2	0.3	-0.1	-0.4	0.1	0.1	0.3	-0.1	0.3	0	-0.1	0.1	-0.1	0.1	-0.6	0.2	0.4	0	0.4
96	0	0.1	0	0	-0.1	0.1	-0.2	-0.2	-0.1	-0.1	-0.1	-0.1	0.1	-0.1	0.1	0	-0.1	0	-0.1	0.1	0	0	0.1	0	-0.1	-0.1	-0.1	0.1	0.1	-0.1	0	-0.1
97	1	0.7	-3.2	-2.2	-1.2	-2.8	1.6	-0.5	-0.8	1.7	-1.9	-0.4	-1.4	-0.1	-0.4	-1.3	-2.7	-0.4	-1	-0.5	-2	-4.7	-0.3	-0.7	-3.2	-0.3	0.5	0.4	3.5	-2.7	1.4	0.8
98	0	-0.2	0.1	0	0.1	0	0	0.1	-0.1	0.1	-0.1	0	0.1	0.1	0.1	0	0.1	0.1	0.1	0.1	-0.1	0	0	-0.1	-0.1	0.1	0	0	-0.1	0.1	0.1	0
99	0	0	-0.2	-0.1	-0.1	-0.1	-0.2	0.1	0	0	-0.2	0.1	-0.1	0.1	0	0	-0.1	-0.1	0.1	0.2	-0.1	0	-0.1	0	0.1	0.1	0	-0.1	0.1	0.1	-0.2	-0.1
100	0.3	-2.7	-1.5	0.8	-0.9	-0.1	0.5	-2.7	0.9	0.8	0.7	-0.7	0.2	-2.3	2.4	0.2	-1.7	-0.3	-1.7	1.6	-0.1	-1.7	1.4	2	0.3	1	-1.3	-0.6	0.5	0.7	-1.6	-0.8
101	-0.7	-0.4	0.6	-2.6	1.3	0.7	0.1	-0.5	-0.9	-3.2	-0.2	0.1	0.6	-0.5	-1.7	-0.8	-0.5	-0.9	0	-0.4	0.8	2.9	-1.7	2.3	0	-0.6	0.6	-1	0	-0.5	-1.2	-0.9
102	-0.7	-0.4	-0.1	-0.5	0	0.2	0.1	-1.2	0.1	-0.7	-0.4	1	-0.3	0.9	0.4	-0.4	0	-0.5	0.4	-0.1	-0.7	0.3	-1.1	0.3	0.2	-0.7	0.9	0.3	1.8	0.2	-0.6	0.2
103	-0.1	0.2	0.2	0	0.1	-0.1	-0.1	0	0.1	0.1	0	-0.2	0.1	0.1	-0.1	0	-0.1	0.1	0.1	0	0	0	0	-0.1	-0.1	-0.2	-0.1	-0.1	0.1	0.1	0.2	0
104	1.6	3.6	-1	-0.2	2.6	0	2.4	0.6	1.4	0.3	0.2	-0.1	0.5	1.6	3.3	-1.1	-1.8	-0.5	1.3	1.3	0.1	1.6	-0.6	0.9	0	0.2	3.9	0.2	3.4	2	0.2	0.7
105	-5.9	-0.4	1.4	0	0.1	-0.8	0.5	1.9	-1.3	-0.2	-0.3	-4.9	0.4	0.8	-0.9	1.7	-0.6	0.7	0.6	-0.8	3	-0.8	-0.4	-1.2	-2.9	0.5	-0.8	1.1	0.2	-2.1	-1.2	-2.2
106	-1.6	-1.7	-2.3	-1.5	-1	0.9	0.1	3.1	-0.9	-0.9	-0.8	-0.1	-2	-0.9	2.2	-0.9	-0.1	0.5	-1.2	-3.5	3.2	-1.8	-0.4	-2.4	-2	0.7	0.1	0.7	-2.5	0	-0.8	-0.5
107	-0.1	-0.1	0	-0.1	0	-0.1	0	-0.1	0	-0.1	0	0	0	-0.1	0.1	-0.1	0.1	0.1	0.1	0	0	-0.1	0.1	0.1	0	0	0	0.1	-0.1	-0.1	0.1	0.1
108	0.5	-0.4	0	-0.9	0.2	-0.1	0.2	-0.4	0.3	0.1	-0.2	0.1	-0.2	-0.8	0	0.1	0.1	0	0.7	0.1	-1	0.3	0	0	-0.5	-0.4	0	0	0.2	0	0.2	0.4

i	1	2	3	4	5	6	7	8	9	10	11	12	13	14	15	16	17	18	19	20	21	22	23	24	25	26	27	28	29	30	31	32
109	-0.4	-1.1	0.3	-0.2	-1.1	0.2	-0.7	0.1	-1	-0.3	-0.1	-0.3	0.6	-0.9	0	-0.9	0	0.3	-0.5	-0.3	-0.7	-0.6	-0.1	-0.6	-1	0.3	-1.1	-0.6	-0.6	0.3	-1.1	-1.1
110	0	0	0.1	-0.2	0	-0.1	0.1	0.1	0.1	0.1	0.1	0.2	-0.1	-0.1	0.1	-0.1	0	0.1	-0.1	-0.1	0.1	0	0.2	0.1	0.1	-0.1	-0.2	0.1	0.1	0.1	-0.1	0.1
111	-1.2	0.6	0.4	1.9	0.5	-1.8	0	-0.2	1	-2.4	-1.1	1.3	3.5	-1.1	-0.2	0.6	2	-0.8	-0.3	-3.6	-0.3	-1.1	0.1	-0.1	-1.9	-2.1	1.7	-3.4	-1.9	-5	1.3	0.3
112	0.4	-2	1.1	-0.2	-2	-0.7	0.8	0.9	-1.5	-0.4	1.1	-0.9	1.4	-0.6	-0.6	2	3.2	2.8	0.4	-0.9	0	-0.9	-0.2	-0.9	-0.6	0.3	-0.1	2.1	-0.5	1.1	0.9	-3.2
113	-0.4	0.2	-0.2	-0.9	-0.7	0.3	0.1	-0.4	0	-1.5	-1.3	0.5	0.7	0.9	-0.7	-0.1	0.5	-0.1	0.7	-0.6	-0.2	-0.2	0	-1.2	-0.1	0.6	0.9	0.9	-0.1	0.6	1	-1.2
114	0.2	-1.1	-2.2	-1.8	-2.4	0.4	-0.6	-2.1	-0.9	-2.5	-1.5	1.2	1.5	0.8	-1.4	-1.4	1.4	0.7	-1.2	-1.7	-0.7	-0.8	-0.2	-1.5	-1.1	2.4	-1	1.5	-2.2	1.7	1.4	-2
115	0.9	-0.7	0.2	0.9	0.9	-0.2	-0.3	-0.7	0.3	0.9	1	-0.8	-0.3	-0.4	1.1	-0.1	-0.8	-1.1	-0.9	0.3	-0.1	0	-0.5	1.5	0.9	-1	-0.8	-0.6	-0.2	-0.1	-0.7	1.4
116	-1.6	0.4	-0.6	-1.2	-0.2	-0.7	-0.5	-0.6	1.2	-0.5	-0.1	0.2	-0.8	-2.9	-3.5	1.6	0.8	2.1	-1.4	-2.2	-0.3	-1.4	1.8	-1.2	-2.4	-0.4	-2.4	-0.6	-2.6	-2.9	0	-1.5
117	0	-0.1	0.1	-0.1	0.1	0.1	0.1	-0.1	0	-0.1	0	0.1	0.1	0	0.2	-0.1	0	0.1	0.1	0.2	-0.1	0	0	0	0.1	-0.1	-0.1	0	0	0	0	-0.1
118	1.8	-0.1	-0.7	-1.1	1.2	0	0.3	-1.8	-0.3	-2.5	-1.1	1.2	-0.5	0.7	-0.3	-1.2	2	-0.1	-0.2	-0.4	-0.4	0	-1.1	-1.3	0.6	3.7	0.8	2.2	-0.5	1.9	1.6	0.1
119	0.5	0.2	0.3	-0.5	0.1	-0.5	-0.4	0.3	0.3	0.1	0.2	0.1	-1	0	0.3	-1.1	-0.8	0	0.5	0.1	0.1	0.4	0.1	0.2	0.4	-0.2	0.3	-0.2	0	0	0.3	0
120	0.4	-0.3	-2.2	-0.6	-4.1	-2.5	1.2	0.5	-3.8	-2.7	-2	1.1	-0.8	0.5	-0.2	-0.9	1.2	1	-0.3	-1.2	1	-2.7	-0.1	-1.1	2.3	-1.7	0.2	-0.6	-1.5	-1.9	0.4	-1.8
121	-0.9	-1.2	0	1.1	-0.7	0	-0.1	-0.5	-2.2	-0.4	0.1	0	-0.5	-0.1	0.5	-0.7	0.5	-0.9	-0.4	-0.3	-1	-1.3	1.1	0.7	0.7	-2.2	-0.7	1.1	-0.8	-1.3	-0.9	-1.1
122	2.2	-2.9	-1.7	-2.3	-0.7	-1	0.3	-2.2	-0.6	-0.3	-3	-0.6	-0.8	-1.8	-0.4	-0.4	-0.5	-0.5	-0.7	-2.2	-2.1	-0.7	-1.8	1.7	0.1	-1.6	-1.4	0.3	1.6	-1	-2.7	1.8
123	-0.5	-0.6	0.8	1.5	2.3	-0.3	0.8	-0.2	-0.7	3.4	-0.1	-2.4	1	0.5	-0.2	0.2	-1.1	-1.8	-2.6	-0.7	1.4	-2.3	-2.1	-1.2	-0.3	-1.7	1.3	-2.3	-2	-0.1	-0.3	-1
124	-0.4	-0.3	0.6	0.3	0.6	0.3	0.8	1.2	1.2	-0.4	0.5	0.4	-0.4	-0.3	-1.1	1.3	0.2	1.6	0.1	0.4	0.2	0.2	-1.7	-0.9	0.1	0.6	-0.4	0.8	-0.9	0.6	-1.4	-1.3
125	-2.1	-1.3	-1.2	-0.2	-0.7	0.8	-2.7	0.2	-0.7	-0.4	-1.9	0.5	0.4	-1	-0.9	-0.8	0.6	-0.4	-0.5	-0.5	-0.3	-1.3	-0.5	-1.7	-1.3	1.3	-2.3	0	1.1	-2.6	1	-1.8
126	0.1	0	0.1	0	0	0	0	-0.1	-0.1	0.2	0.1	0.1	0	0.1	0	0	-0.1	0.1	-0.1	-0.1	-0.1	-0.1	-0.1	-0.2	0.1	0	0.2	0	0.1	-0.1	0.1	0
127	0.5	1.6	-5.7	-0.2	-0.2	-3.1	-2.3	-1.3	-1.7	0.1	-1	-1.1	0.8	-0.6	0.7	-2.4	-1.6	-0.4	0.4	-0.2	-3.4	0.6	-0.1	-0.9	-0.7	0.3	-1.1	-4.3	0.8	-0.4	0	0.5
128	-1	-0.6	-0.3	1	0.5	0.3	0.2	0	-1.4	0.7	1.5	-1.6	-1.3	0.1	1.2	0.1	-1.4	-1	-1.4	0.8	1	0.1	-1.5	1.7	1	-0.4	1.3	-0.6	0.5	-0.2	-1.4	1.1
129	0	-3.1	0	0	-0.1	-0.1	-0.7	1.3	-0.8	1.6	-0.9	-0.6	0.5	-2.1	0.2	1.4	-1.1	-2	-1.1	-0.8	-0.4	-0.7	-5.5	-0.6	2.1	0.3	0.8	0.6	-2.3	0.1	-3.4	-1.1
130	-0.1	0	0.1	0.2	-0.1	0	0.1	0.1	-0.1	-0.1	-0.2	0.1	-0.2	0	0.1	0	0.2	-0.1	0.1	0	-0.1	-0.1	-0.1	0.1	-0.2	0	0	0	0.1	-0.1	0.2	0.1
131	-0.6	-0.8	2.1	-0.7	0.2	1.1	-1	-2.8	-1.3	-2.1	1.5	0.4	-0.9	-0.3	0	-1.8	-0.1	-2.2	1.4	-0.3	-1.3	-1.7	-1.6	-2	-3	-1.9	-1.1	0.5	0.4	2.5	1.6	0
132	-0.9	2.6	-2.2	0.9	-1.6	1.5	-2.1	-2.7	-1.8	1.7	2	-0.2	-0.9	0.6	2.1	-1.7	-0.8	-1.7	1.1	3	1.1	1.6	0	2.9	-0.3	-1.1	1.4	-2.8	-0.3	-0.9	-1.2	0.8
133	1.4	0.8	0.7	-0.7	0.2	0	-0.8	0.2	-0.5	-0.8	0.9	0.3	-1.4	-0.6	2	-3.1	-2.5	0.2	0.9	2.2	-1.6	0.3	-0.5	2.2	-1.1	-2.5	1.8	-2.4	-1.1	1	0.4	0.2
134	0.6	0.2	-0.6	-0.7	-0.9	-0.4	0	-0.4	0.5	1	-1.1	-0.1	-0.3	1.9	1.7	-1.5	-2.3	2.5	-1	-0.9	-2.3	0.6	1	-0.7	1.3	-0.5	0.8	-1.4	-0.3	0.4	1.1	-0.7
135	-0.2	-4.2	-1.2	0.4	-2.7	2.3	-1.4	0.4	-2.4	0.2	-2.5	-3.1	-1.2	-2.6	-2.5	-0.2	0	0.8	-0.2	-2.9	-1.5	-2.6	-1.4	1.2	1.5	1.5	-1.8	1.9	-0.3	-1.6	1.1	-0.5
136	-0.1	0.1	0.1	0.1	0.2	-0.2	-0.1	-0.1	-0.1	-0.1	-0.1	0	-0.1	0.1	0	0.1	-0.1	-0.2	0	0	0.1	0.1	-0.1	0	-0.1	0	0	-0.1	0.1	-0.1	0.1	0
137	-3.3	1	0.5	-1.3	1.1	0.5	-0.4	-1.2	1.7	-0.7	2.6	-0.1	-0.6	-0.6	-2.7	-0.8	-1.3	1.6	0	1.9	-1.3	1.9	0.5	-0.1	-0.2	-1.1	0.4	-1.6	-2.8	-0.5	0.2	0.4
138	0.1	-0.1	-0.1	0.1	0	-0.1	0	0	0.1	0	-0.1	0.2	0.1	-0.1	0.1	-0.1	0	0	0.1	0.1	0.1	0	0.1	-0.1	-0.1	0	0.1	0.1	-0.1	0.2	-0.1	0
139	-1.9	-0.5	-0.2	-0.2	0.6	0.9	-1.7	0	-1.6	-1.8	0.7	-0.3	0.6	-0.5	2.1	1	-1.8	-0.9	-0.5	0.5	1.5	-1.2	0.6	-0.2	0.1	-0.6	-1.3	-3.4	0	1.3	-1	-1.3
140	-0.2	-0.1	0	-0.2	-0.1	-0.1	-0.1	0	0	-0.1	0.1	-0.1	0	0.1	-0.1	0	-0.1	0.1	-0.1	0.1	-0.2	-0.2	0	-0.1	0	0.1	-0.1	0	0	-0.1	0.1	-0.1
141	-0.1	0	0	-0.1	0.2	0.2	-0.4	-0.2	0	0.2	0	0.3	-0.9	-0.2	0.3	-1.4	-0.7	0	-0.1	0.3	0	-0.2	0.2	-0.1	0	0.2	-0.2	-0.4	-0.1	0.1	0.3	-0.1
142	-0.7	1.2	1	-0.6	-2	0.3	0.7	-5.5	-0.2	0.3	-1.2	-0.5	-1.8	1.1	-0.3	-0.1	0.4	0.1	-1.9	-0.4	0.2	-0.3	-0.4	-1.1	-0.9	0	-1.2	0.7	-0.5	0.3	-0.6	0.1
143	0.4	-0.5	-1.3	0	1	-0.5	0	-0.7	1.8	0.5	0	-3.2	1.3	0.4	-0.4	1.3	-2	-0.5	-1	0.4	1.3	1.5	2.2	0.2	-0.7	1	-1.6	1.1	1.2	-0.1	-2.4	0.8
144	-1.7	0	-0.2	-1.5	1.1	0.3	-0.8	-2.2	0	-2.5	-0.6	-1.2	-0.1	0.1	0.3	0.8	1.4	-1.8	0.6	-2.5	-0.1	1.5	-2.5	-0.3	-1	-2.6	-1.2	-0.1	0	1	-1	-0.2
145	-0.6	-1.3	0.6	-1	-1.9	1.6	-0.4	-1.5	2	0.5	2.2	-0.8	-0.7	-1	0.1	0.1	1.3	-2.6	-1	-1.4	1.6	-0.1	0	-0.7	-1	-1.3	-0.1	0.8	0.7	-0.2	0.7	0.6
146	-1.5	-0.3	-0.8	-0.2	0	-3.1	0.2	0.5	-0.4	0	-1.3	-1.1	-1.3	-0.1	-0.5	-1.3	1.1	0.7	-0.1	-1.2	0.2	0.8	1	-1.8	1.3	0.6	-0.8	-0.5	-2.9	0.7	1.3	-0.4
147	-0.9	-0.1	-0.2	-1.2	-0.4	-0.8	-0.5	-0.5	-0.5	-0.6	-1.6	-1.2	-2	0.5	-0.8	-1.1	-0.8	0.7	-0.6	-0.5	-0.6	-0.6	-0.9	-0.5	-0.1	-1.6	-0.3	-1.2	-0.2	-0.8	0.4	-0.9
148	-0.7	-1.2	-0.9	-2	-1.7	-1.1	-0.8	-0.7	-0.8	-1.3	0	-0.7	-0.4	-2.7	-0.7	-0.8	-0.5	-1.9	-0.9	-0.6	0.4	0.1	-0.3	-1.4	-1.6	-0.3	-1.3	0.3	-1.3	-1.5	-1.5	-1.2
149	-0.5	0	-2.4	-1.1	0.7	-1.8	-1.7	-1.6	0	-0.7	0.5	2.1	-0.2	-1	1	0.1	-0.1	-0.1	0.3	0.6	-2.4	-2.1	-0.3	-0.8	-1.3	2	1.2	1	-2	2.5	-3.8	0
150	-0.6	-0.9	-1	-0.1	-0.2	-0.1	-0.4	-0.2	-0.8	-0.1	-0.4	-0.6	-0.4	-0.7	-1.3	-1.7	-0.1	-0.4	0.1	-0.9	-0.4	-1	0.1	-0.1	-0.1	-1	-1.1	0	0	-0.4	-0.5	-0.3
151	-0.6	-1.3	-0.9	-0.1	-0.8	-0.1	-0.3	-0.4	-0.5	0	-0.9	-0.5	0.5	-1.1	-0.8	-1	0.2	-0.5	-0.5	-0.5	-0.5	-1.4	-0.2	-0.7	-0.4	0.1	-1.5	0.7	-0.4	-0.2	-0.6	-0.8
152	0.8	-1.1	0.4	-1.5	-2.2	0.3	-1.1	0.3	-1.7	0.4	-0.5	0.8	0	-0.8	-1.3	1.1	3.6	-0.7	0.2	0.7	-0.9	-1.1	-1.3	-1.4	0.9	1.2	-1.9	-2.5	-1.9	-1.1	0.5	-2
153	-0.3	-0.5	-0.7	-0.7	-1	0.1	-0.8	-0.7	-1.1	-2	-0.3	1.3	0.9	-0.7	-1	-0.6	0.7	0.6	-0.9	-0.8	-0.3	-0.3	-0.1	-0.2	-1.1	0.9	-0.2	0.2	-1.5	-0.2	0.1	-0.5
154	-0.5	-0.8	-0.1	-0.2	-0.9	-0.2	-0.5	0.7	-0.3	-0.1	-0.2	0	0.4	-0.7	-0.4	0.2	0.5	0.6	-0.6	-0.3	0.4	-0.4	-0.2	-0.6	-1.2	0.5	-0.7	0.4	-1.8	-0.1	-0.3	-1.4
155	1.2	-1	1.6	2.9	1.1	1.8	-0.5	2	-0.2	0.7	1.9	-0.5	1	4.3	-1.5	3.2	-0.3	0.5	-0.6	-0.1	1.1	-2.7	-1.5	1.8	0.5	0.9	1.7	-1.7	3	0.4	-0.3	0.1
B1	-1.1	-0.8	-1	-1.1	-1	-1.1	-1	-0.9	-0.9	-0.4	-0.8	-0.9	-1.3	-0.7	-0.7	-1.1	-0.9	-0.8	-0.9	-0.8	-0.6	-1	-1	-1	-0.7	-1.3	-0.7	-0.9	-0.9	-1.2	-0.9	-1.1

Table D.11 continued…

i	33	34	35	36	37	38	39	40	41	42	43	44	45	46	47	48	49	50	51	52	53	54	55	56	57	58	59	60	61	62	63	64
1	-0.3	2	1.1	0.1	-0.1	0.3	-0.3	1.8	2.4	-2.5	1.5	-1.7	-1	-0.6	-0.8	-1.2	-0.1	-0.4	0.9	-0.7	-0.1	2.3	-0.3	-1.2	-3.6	2.3	-0.3	0.7	-1.4	-1.7	0	-1.6
2	0.6	1.2	0.2	0.6	-0.5	1.4	0.4	0.5	0	0.1	0	-1.5	-0.5	0.3	-1.4	-0.4	-1.8	0.1	0.2	-0.6	-0.5	0.2	-0.3	1.2	1.3	0.7	0.8	-0.6	0.1	-0.3	-0.8	0.7
3	0.1	0	0	1.4	1.2	0.6	-1	0.5	1.6	-0.3	-1.3	0	-0.2	0.1	-0.6	-0.3	1.4	0.1	0.8	-0.1	0.5	-3.4	0.8	0.9	1.7	-4.3	0.8	0.4	1.7	-0.4	0.1	-0.6
4	0	-0.4	-0.9	0.2	-1.2	-1	-0.1	-0.5	-0.4	0.3	0	-0.2	-0.1	-0.1	0.1	0.1	-0.4	-0.1	-0.4	-0.4	-0.2	0.1	-0.7	0.2	-0.3	1.2	-0.8	-1.8	-0.9	0.3	-0.4	0.1
5	-1.6	-0.7	-0.8	0.6	-0.6	0.7	-1.3	-0.2	-0.9	0.2	-0.1	-0.9	-0.7	0.2	-0.6	-0.6	-1	-0.5	-0.3	0.3	0.5	-1.3	-0.1	-0.3	0.2	-2	-1.3	0.9	0.1	0	-0.2	1.4
6	0.4	0.3	0.2	0.4	-0.4	0	-0.6	-0.5	-0.2	1.3	-0.1	0.3	1.3	-0.2	0	0.2	-0.3	-1.2	0.6	0.5	0.5	0	-0.2	-0.4	0.4	0.6	-0.3	0.7	-0.4	0.3	0.2	0.4
7	0.7	-0.6	-1	-0.7	-0.3	-0.9	-1.1	0.1	-0.4	0	-0.1	0.1	-1.1	0.6	0.6	1.2	-1	-1.2	0.3	-0.7	-0.4	1	-0.1	-0.1	-1	0.7	1.3	-1.1	0.8	0.1	-0.5	-0.4
8	0.2	0	-0.1	0.1	-0.2	-0.3	0	0.4	0.1	-0.5	0.4	-0.5	-0.1	0.1	0.4	0.8	-1	-0.1	-0.1	0.1	0.7	0.4	0.2	0.1	-0.2	0.3	-0.2	0.2	-0.8	-0.6	0.4	0.5
9	-0.2	0.6	-0.1	-0.1	0.5	-1.3	-1	0.7	-0.4	-0.9	-0.4	-0.6	-0.2	0.4	-0.2	-0.1	1.2	-0.1	-0.3	0.3	0.1	-0.1	0.7	0	-1.4	-0.3	-0.5	0	-1.6	0.7	0	-1.8
10	-0.1	0	-0.2	-0.4	0	-0.6	-0.6	-0.8	0.2	0.9	-0.9	0.1	0	-0.3	-0.2	-0.1	0	-0.1	0	-0.6	-0.4	-0.4	-0.4	0	0.2	-1.8	0.1	0.7	1.1	-0.2	-1.3	0.3
11	0.2	-0.8	0.4	0.5	0	1.8	0.3	1.2	0.7	-0.5	-0.5	-1.2	-0.5	-0.6	-0.2	-0.6	1	0.1	-0.4	-0.2	0.5	-1.2	-0.2	-0.2	0.4	-0.2	0.3	0.8	0.7	-0.5	-0.4	0.6
12	0.1	0	-0.2	-0.6	1.6	-0.1	0.6	0.6	0.1	0.5	0.4	-0.3	-0.1	-0.8	-0.2	0.1	-0.2	-0.7	-1.9	-1.6	-1.3	0.9	0.4	1	-1.7	3.7	4.1	0.4	1.3	-0.1	0.1	-0.2
13	0	1.9	0.3	-0.6	-0.3	-0.8	-0.1	0.6	-0.6	0.5	0.5	-1.7	1.7	-0.2	1.5	1.7	0.9	0.8	-0.2	-1.8	-0.5	1.7	1	0.5	-0.6	0.7	0.4	-0.1	0.3	0.3	-0.2	-1
14	0.2	0.1	-0.8	-0.3	0	0.4	-0.5	0.4	-0.2	0.2	0.1	0.4	-0.6	-0.4	-0.1	-0.8	0.1	-0.2	-1.6	-0.6	-0.4	-0.9	-0.9	-1.6	1.2	0.2	0.3	0.5	-0.4	0.5	-1.1	0.3
15	0.6	-0.2	-0.6	0.5	0.8	0.1	0.9	-0.3	0.2	-0.4	-0.7	0	-0.3	-0.5	-0.5	-0.8	-0.3	0.9	0.6	0	-1.2	0.1	-0.4	0.5	-0.7	-0.2	0.7	-0.4	-0.2	-0.5	-1.2	-1.5
16	0.4	0.1	1	-1	1.2	-1.7	0.5	-0.1	0.2	0.3	0.6	1.3	0.2	-0.1	-0.5	0.9	0.2	-0.5	-1.5	-0.9	0.8	0.4	1.5	-0.1	-0.5	0.2	-0.1	-0.3	-0.9	1	0.9	0.4
17	-1	-0.5	0.1	-0.3	-2.5	-0.3	0.5	-0.2	0.3	-0.5	-1.6	0.6	-0.1	-0.2	0.6	0.4	-0.2	0.7	0	-0.2	0.9	0.1	-1.6	0.3	0	0	-0.5	-1	-0.1	-0.1	0.1	-0.9
18	0.1	-0.5	-0.8	-0.6	0	-0.3	0.3	0.1	-0.7	-0.1	1.1	1.2	1	0.6	0.5	0.7	-0.6	0.4	1.5	-0.8	0.9	-0.3	1.4	0.4	-0.4	-1.2	0.8	0.2	0	-0.6	0.8	0.1
19	-1.6	1	-0.2	0.7	-2	1.5	-0.6	-0.3	0.2	0.4	-2.4	0.2	0.9	-2.8	-1.3	0.1	1.1	1.2	-0.2	-0.5	-2.1	-0.6	1.2	2	0.2	0.1	-1	2.2	0.7	-1.1	-1.6	0.6

i	33	34	35	36	37	38	39	40	41	42	43	44	45	46	47	48	49	50	51	52	53	54	55	56	57	58	59	60	61	62	63	64
20	0	-1.3	0.8	-1.1	-0.7	-0.1	0	-0.5	-0.6	0.1	0.7	-0.3	-0.2	-0.3	-0.2	-0.4	-1.4	1.3	0.6	1.1	-0.2	-2.7	1.7	-0.6	1.3	-4.8	0.1	-0.7	-1.1	1.4	0.5	0.3
21	0.7	0.6	-1.1	-0.4	-0.8	0.1	1.2	-0.3	0.5	0.2	1.4	0.3	-0.4	0.5	0.4	0.6	-0.4	-0.6	-0.2	0.2	1.3	-0.3	-0.3	0.1	0.8	-0.4	1.1	1.5	-0.8	1.4	0	0.6
22	0.7	0.5	0.5	-2	0.1	-0.8	-0.1	-1.1	1.3	0.1	-0.9	0.7	0.1	0.8	0.2	0.1	0.1	0.5	0.5	1.7	0.3	0.5	0	-0.7	0.9	-0.3	0	0.4	0.8	-0.2	1.1	0.8
23	0.3	0.4	-0.8	1.1	0.6	0.5	-0.4	0.4	0.5	1.6	-0.4	0	1	0.7	-1.2	-1	-0.3	0	1.1	0.3	-0.5	0.6	-0.2	0.4	0.8	0.5	0.9	-0.4	0.1	0.3	-0.3	0.7
24	0.2	0.2	0.1	-1.6	0.9	-0.1	-0.6	-0.5	0	-1	0	0.2	-0.5	-0.2	0.4	0	0.1	-0.3	0.8	0.9	0.3	-1.5	-2.5	0.8	0.1	-1.1	-4.4	1	0.3	-0.2	0	0.2
25	2.4	-0.9	0.3	-0.7	-0.4	-0.4	2.1	-0.7	-0.3	0.6	0.8	0.8	0.5	1	0.7	1	0.7	0.9	0.2	0	-0.3	0.7	-0.3	0.5	0.9	0.1	2.5	0.6	0.5	1	-0.3	-0.7
26	1.8	0.4	2.1	0.8	-2.1	-2.5	-1	-2.3	0.5	-1.1	-1.2	-1	0.5	0.3	0.9	1.3	-0.6	0.5	1.2	0.6	0.7	-0.2	0.8	0.2	0.8	-0.7	0.4	-1.4	0	0.7	-0.3	0.2
27	1	0.2	-0.1	-0.4	0.7	-0.2	-0.1	-0.4	0.3	0.4	-0.4	0.8	0.2	1.1	-1.1	-1.5	0	-1.7	-0.7	0	1.5	-1.9	-0.3	0	0.8	-1.5	1.3	-0.9	-0.1	0.5	-1.6	0.8
28	-0.2	-0.4	0.3	0	0.4	0.2	0	0.2	-0.1	1.3	0.8	0.3	-0.3	0	1	-0.3	0.9	0	0.5	0.3	-0.2	-0.8	0	0.7	0.5	0.4	0.2	0.6	0	0.3	0.6	0.1
29	0.4	0.8	0.9	-0.3	0.4	-1.3	-0.4	-0.5	-0.3	0.8	0.5	-0.4	-1.9	-0.9	0.4	-0.1	0.5	0	0.6	0.4	-0.1	-0.5	0.7	0.1	-1.2	0.7	0.7	-0.2	-0.5	-0.2	0	0.8
30	1	-0.5	0.7	-1.2	-0.7	-1.9	-2.7	-2	0.3	-0.5	-0.4	0.8	1.7	-2	-3.1	-0.5	-0.5	1	0.1	-2.1	-0.4	-0.1	-1.3	0	2	0.1	-0.8	-0.7	-0.5	-0.3	0.3	-0.7
31	-1.1	-1.6	0.9	-0.7	-1.1	-0.4	-0.2	1.4	-4.2	-2.4	-0.8	-2.5	-1.6	-0.4	-3	-2.8	0.2	-0.4	-1.6	-0.7	-0.6	-1.8	0.3	-0.4	1.3	2.4	-3.7	-0.9	-1.9	-0.4	-2.9	-2.1
32	0.1	0	0.2	0	-0.1	0.1	0.1	0.1	-0.1	0.1	-0.2	0	0.1	-0.1	-0.1	-0.2	0.1	0	0	-0.1	-0.1	-0.1	-0.1	-0.1	-0.1	-0.1	0.2	0.1	-0.1	0.1	-0.1	-0.1
33	-0.5	-1.7	-1.7	0	-0.4	-3.3	-0.5	0.2	-0.1	-0.7	-1	-1.2	-2.8	-0.3	0.4	0	-1.3	1.5	0.1	-0.4	-1.3	0.8	-2.4	-2	-0.4	-0.3	0.1	0.2	0	1	-0.6	1
34	-1.4	-1.7	-0.1	-1.1	-1.5	0.7	-1.9	0.8	0.3	-3.1	0.7	0.2	0	0.8	0	-1.7	1.6	-3	1.8	0.8	-0.2	-1	0.5	-0.6	-3.3	2.3	0.2	-2.2	-0.9	-2.4	1.3	-0.4
35	-0.8	0.6	-0.2	-0.4	0.1	1.1	0	-2.1	-0.2	-1	-0.2	-0.4	-1.1	0.1	0.9	0.5	-2.2	-1.6	-1.7	-1.8	-0.3	-0.4	0	-0.5	-1.6	-0.5	-0.8	-0.2	-0.4	-1.3	-1.6	-1.1
36	-1.5	0.1	-0.4	-0.1	-0.6	-0.9	0.1	-0.4	0.4	-0.6	-0.7	-0.7	-0.4	-1.3	-0.8	-0.3	-0.4	-0.1	0	0.3	-0.4	0	-0.3	-0.1	-0.9	0.2	-1	-0.2	-0.7	-1.5	0	-0.1
37	-0.1	0.9	-2.2	-0.6	-0.3	-0.2	0	-1.6	-4.9	2.5	-0.4	-0.4	1.1	-2	-4.9	-1.5	2.7	-1.8	0.2	0.2	-0.3	-1.3	0.7	0.6	-0.7	-2.8	-0.8	-1.8	-0.4	-1.8	-0.1	-1.5
38	-1	-1.2	-0.8	-0.8	-1.1	-1.2	-1.1	-0.7	-0.9	-0.7	-0.8	-1.1	-0.5	-1.3	-1.1	-0.8	-0.8	-0.5	-0.6	-1	-1.3	-0.4	-1.1	-0.8	-0.5	-0.2	-1.3	-1	-0.9	-0.6	-1	-1
39	-0.8	1.3	0.6	-4.2	1.9	-0.3	-2.2	-0.5	-1.9	-1.1	-1.3	0.2	-2	0.2	-0.2	-2.4	2.7	-1.4	-0.2	-0.8	0.9	-1.3	-2.5	-2.9	0.3	1.6	0.1	2.2	-1.3	-3	-1.9	1.8
40	-0.7	-1.4	-2.1	-0.2	0.6	0.3	0.4	-1.4	0.4	-0.4	-0.4	-0.6	-3	-0.2	-1	-2.6	-0.2	-2.1	-0.6	-0.4	-1.1	0	-1.7	-2.7	-0.6	-0.6	-0.3	0.4	0.4	0.1	-2.3	-1
41	-2.7	-1.3	-5.1	-2.1	-2.3	0.7	-3.2	-1.1	-2.4	-1.6	-4.7	0.1	-1.6	-3.8	-2.4	-6	-2.9	0.2	-2.6	-1.1	-2.3	-2.5	-3.6	-1.7	-1.9	-3.3	-1.9	0.2	-1.1	-0.2	0.1	0.2
42	-1.1	-1.2	-0.1	-1.5	-3.7	-1.3	-2.1	-2.4	-2.5	-0.3	-0.7	0.2	-1.8	0.1	-1.8	-3	-1.9	-0.7	0.1	-1.1	-1.5	-0.6	-1.3	-2.4	-1.5	0.6	-2	0.4	-3.3	-0.6	0	0.1
43	-0.7	-0.9	-0.9	0.9	0.2	-0.2	-1.5	-0.4	0.7	0	-1.4	0.2	0.6	-1.2	-2.2	-0.7	0.9	0.2	-0.2	-0.5	-2.7	-2.1	-0.7	-1.4	1.4	-2	-1.3	-1.3	-0.1	-0.6	-1.9	-1.4
44	0.1	0.4	0.4	-0.9	0.4	-1.2	0.6	0	0	-1	0.3	-1.9	-0.1	-0.1	0.9	0.7	0.1	-1.3	-0.6	-0.5	0.4	0.6	0.1	0.7	-0.9	0.4	0.6	-0.7	0.6	-0.6	-0.5	-0.6
45	-0.3	-0.3	-0.7	0.3	-0.4	-0.6	-1	0.5	-1.5	-0.8	0	-0.3	-1.5	-1	-0.6	-1.2	-0.4	-0.3	0.1	-0.5	-0.5	-0.2	-0.2	0	-0.4	-1	-0.3	-2.3	-0.2	0.4	-0.4	-0.3
46	-1.3	-1.7	-2.1	-0.8	-2.3	0.7	-0.6	-0.9	-0.9	-1.6	0.9	-1.9	-0.3	-1.5	-0.6	3.1	0.9	-1.1	-2.6	-1.2	0.2	1.7	0.3	2	0.5	1.2	0.8	3.3	0.5	0.2	-1.3	0.8
47	0.5	0.3	-0.4	-4	0.7	-2	-0.8	0.7	-1.3	-1.7	0.1	-1.8	0.6	0	-0.1	0.2	2	0.2	-3.1	-0.9	-1.6	0.4	-3.8	-0.7	2.3	1	0.3	2.5	1.4	-1	-0.9	-0.9
48	0	1.2	0.1	-1.7	3.4	2.6	0.9	1.6	-0.7	1	1.8	0.3	-1.2	-2	-1	0.7	-0.4	-0.2	0.4	-1	-4.5	0.6	2.5	0.5	-0.6	0	-0.9	-1	-0.2	0	-0.9	-2.1
49	0.2	0.2	0.1	0.1	-0.1	0.1	-0.2	0	0.1	0	0	0.1	0.2	0.1	-0.1	0	0.1	-0.1	-0.1	0.2	0.1	0	0	0.1	0	0	-0.2	0.1	0.1	0.1	0	0
50	-3.2	-2.4	-2.1	0.9	-3.3	-0.3	-1.5	-2	-2.1	-0.3	-1.8	0.5	-3.1	0.5	0.7	0.8	0.4	-1.6	0.1	0.2	1.8	-1.2	0.5	-0.3	0.4	-0.7	-1.5	0.9	0.1	0.5	1.3	1.2
51	0	0.1	0.1	0.1	0.1	-0.1	-0.1	-0.1	0.2	0	0.1	-0.1	-0.1	0.1	0.1	0.1	0.1	-0.1	0.2	0.1	0	0	0.1	0	-0.1	0	0	-0.1	-0.1	0	0.1	0.1
52	1.2	0.3	0.3	-3.8	-3.7	-4.2	1.9	-2.2	1	-3.2	-1.7	-1.3	0.2	-1.5	-0.4	-1.3	-0.8	0.7	-1.6	0.2	0.2	-1.2	-1.5	-0.9	-4.5	1.2	-1.2	-0.6	-2.8	-2.1	-0.3	-0.5
53	-0.7	-0.8	-0.2	-0.1	-1	-0.1	-0.5	-2.5	-0.1	0	-0.8	-0.8	0.4	0.3	0.3	0.3	-0.4	-0.5	-0.4	-1	-0.8	0.1	-0.3	-0.8	-0.5	0.3	-1.4	-0.8	-1.4	-0.3	-0.8	-0.4
54	-1.3	-1.4	-0.9	1.1	1	1	-0.4	-0.8	0.6	-1.5	-0.4	-0.6	-1.2	1.2	-0.5	-0.4	0.7	-0.5	1	1.7	2.4	-0.5	-0.9	-0.9	0	-0.4	-0.3	2.2	0.8	-0.7	-0.4	-1.2
55	-0.1	-0.2	0.1	0.1	0.1	-0.1	0.1	-0.1	0.1	0	0.1	-0.1	-0.1	0	-0.1	0	-0.1	0	-0.1	0	0	0	-0.2	0	0	-0.1	-0.1	-0.2	-0.1	-0.1	0.2	-0.1
56	-0.9	-1.3	-0.6	-2.5	0.4	-1.6	-1	0.1	1.1	0.1	-2.3	-0.2	-0.2	-2.2	-2.4	-0.9	-2.4	0.3	-0.1	-2.5	-3.7	-2.4	-1.1	-4.7	-1.6	-3.3	0.9	-1.3	-1.7	-2.3	-0.3	-2.2
57	1.5	1.8	-0.3	-0.1	0.7	0.4	-1.7	0.6	-3.3	-1.4	1.6	-1.2	0.7	-1.2	0.1	0.6	1	2.3	-1	-0.2	-0.5	2.4	0.9	-0.5	-1.3	0.6	0.1	-3.7	-2.2	0.1	-1.7	0.3
58	-1.6	-0.1	-1	1.3	1.5	0.4	0.5	0.6	0.7	1.1	0	0.1	-1.9	0.1	2.3	-0.4	-3.6	-0.4	2.4	1.3	-2.6	-0.8	-0.3	-0.6	-0.7	-0.6	-1	-2	-1.3	-2.8	0.6	2.2
59	1.8	0.4	-0.5	-1.2	0.4	1	0.9	-1.1	-3.7	-0.1	1.3	0.1	0.8	-0.2	0.7	1.2	-2.3	-0.7	1.4	1.1	1.1	1	0.8	-2.7	0.6	0.4	-0.7	-3.3	-0.9	0.3	-0.2	-0.5
60	0.2	1.4	0.2	1.4	0.6	0.3	-0.6	-0.6	0.5	-0.6	0.3	-1.8	2	0.1	0.2	-0.4	0.9	-0.3	1.9	1.7	1.1	-0.3	1	1.7	-0.8	0.1	0.9	-3.3	0.1	-0.7	-0.6	-0.3
61	-0.7	-0.9	0.6	-1.5	0.5	1.8	-4.1	-2.9	-3.7	0.5	-1.1	-2.4	-1.3	-0.7	-3.2	-2.6	0.8	-1.3	0.5	0	0.8	0.7	-0.2	1.3	-0.7	0.5	-1.3	-1.9	0.9	-0.4	0.5	-1.7
62	1.7	-0.2	1.1	-0.9	-1.3	-4.5	-0.7	-4.9	-0.2	-1.7	-0.7	0	1	1	-1	-1.9	0.9	1.5	0	-1.7	-2.7	-1.5	-1.2	1.1	1.7	-0.9	-0.2	-0.5	-2.3	-2.2	-0.1	-0.7
63	-0.5	0.5	0.8	1.1	-0.5	0.5	0.3	-0.1	-0.7	0.3	-0.1	-0.2	0.3	0.5	0.2	1.2	-0.2	0.2	-0.8	-0.5	0.7	0.1	0.4	0.8	0.4	-0.1	-0.4	0.6	-0.3	1	0.1	0.1
64	-0.2	2.7	1.3	0.7	-3.7	2	0.4	-1.7	-2.9	-0.7	-0.6	-1.2	-0.7	1.1	1.4	0.9	0.5	-0.2	-0.5	-1.2	0.7	-0.3	-0.1	1.5	0.2	-0.9	-1.7	2.6	2	-0.4	-0.1	2.2
65	1.8	0.8	0.5	1	2.8	0.4	0	0.3	1.6	-0.1	1.9	-0.7	1.4	-0.1	-1.4	0.5	0.3	-0.6	-1.2	-0.9	-1.6	0.7	-1.7	0.7	-1.9	0.3	2.2	0.8	0.4	-0.7	-2.3	-1.4
66	-0.6	-1.6	-0.9	-1.2	-0.5	-0.6	-0.1	-0.8	0	-0.8	-0.4	-0.1	-0.2	-0.5	-1.2	-0.7	-0.3	0	-1	-0.2	-0.9	-0.3	-0.7	-0.6	-0.8	-0.1	-0.3	-0.9	-1	-1	-0.4	-0.3
67	-1.7	-1.1	-0.8	-2.2	1.2	-0.5	-2	-0.4	0.6	-0.9	-0.7	0.8	-1.4	-2.4	-1.8	-1.8	0.8	-2.2	1	2.1	-0.8	-3.6	-0.8	-0.6	-1.3	-1.8	-0.6	1	-0.1	-3.3	-0.8	-1.6
68	0.1	0	-0.1	0.1	0.1	0.1	-0.1	0.1	0	-0.1	0.1	0	-0.1	-0.2	-0.1	0.2	0	-0.1	0	0	0.1	0	0.1	-0.1	-0.1	0	-0.1	-0.1	-0.2	0.1	-0.2	0.1
69	0.7	-1.2	-1.1	-2	-1.5	0.2	0.5	-2.6	0.8	-1.7	-0.2	-1.5	0.4	-1.2	0.6	-0.5	-2.1	-1.6	-1.9	-2.2	0.8	2.3	-0.5	0.8	-1.9	-0.6	0.7	-0.1	-2.4	-1.3	-1.5	-1.1
70	1.4	-1.1	0.8	-0.5	-0.7	1.2	-0.3	-1.9	-0.2	-2.1	2.2	-3.2	1.3	-0.5	-1.6	-4.8	0.5	-0.9	-0.6	2.2	-0.8	0.5	-2.1	-1	-0.1	0.2	-0.6	-3.9	-1.9	0	-0.3	-1.4
71	0.2	0.2	0.1	0.1	-0.2	0	0.1	0	0.1	0	-0.1	-0.2	0.1	0.1	-0.1	-0.1	-0.1	0	0.1	0	0.1	0	0.1	0	0.1	0	0	0.1	0	-0.1	0.1	0
72	0	0.1	0	0.1	0	0	0	0	-0.1	0	0.1	0	0.1	0.1	-0.1	0.1	0.1	-0.2	0.1	-0.1	-0.1	-0.1	0.1	0.1	0.1	-0.2	-0.1	0.1	-0.1	-0.1	0	0
73	0.1	-0.1	-0.2	-0.1	-0.1	0.2	-0.1	0	-0.1	-0.1	-0.1	-0.1	0	0	0	0	-0.1	0	0	0.1	-0.2	0	-0.1	0.1	-0.1	-0.1	-0.2	-0.2	0.1	-0.1	0	0
74	-1.1	-1.2	-1	-0.7	-0.9	-2.1	-0.7	-1.1	-0.1	-1.3	-1.3	-0.5	-1.4	-1.1	-1	-0.9	-2.7	-1	-0.7	0.7	-0.6	-0.1	-0.4	-0.3	-1.4	-1.2	-0.6	-0.3	-2.1	-0.8	-0.5	-1
75	0.1	0	0	0	0	0.1	-0.1	0	0.1	0.1	-0.1	-0.1	0	-0.1	-0.1	0.2	0.1	0	0.1	-0.2	0	0.1	0.1	-0.1	-0.1	-0.1	0	0.1	-0.1	0.1	0.2	0.2
76	-1.9	-1.1	-1.5	0.1	0.5	0.7	-1.4	-0.3	-1.5	-0.1	-0.3	0.1	-1.1	0.3	-0.9	-1	-0.6	-1.7	2.1	0.4	0.1	-0.4	-1.7	-1.4	-0.6	-0.5	-1.1	1.8	0.9	-0.3	0	0
77	-0.1	0	-0.1	0	0.2	0.2	-0.1	0	-0.1	0	0.2	-0.1	0.1	0.2	0	-0.1	-0.1	-0.1	0.1	0.1	-0.2	0	0	0.1	0.1	0.1	0	-0.1	0	-0.1	0	-0.2
78	-1.5	-2	-2.1	1.9	1.3	-2.6	-2.8	0.6	0.1	1.3	2.7	0.2	0.7	1.2	-0.3	-0.5	2.5	0.7	2.5	-1.5	0.2	-2.4	-2.2	-1.5	1.4	1.3	1.5	1.1	0.7	0.2	-1.7	-2.7
79	-2.3	-0.4	-1.1	-0.4	-0.3	-0.2	-0.3	-1.4	-0.7	-0.8	-1.9	0.1	-1.9	-1.9	0	-0.6	-1.7	-1	-0.1	1.3	-0.9	-2	-0.6	1.3	-1.6	-3.3	-0.7	-1.3	0	-2.5	0.5	0.4
80	0.1	0.4	0.4	1	-1.9	1	0.2	-0.1	-0.4	1.3	-0.1	0.2	0.4	0.9	1.1	0.4	0.3	0.2	0.4	-0.5	0.9	0	0.3	0.2	0.4	0	0.1	0.6	1.1	0.3	0	1.1
81	0	0.2	2.7	0.9	-1.2	-1.9	2.4	-0.1	-0.1	-0.5	-0.1	0.4	-0.4	-4.2	-0.3	0	-1.4	0.8	1.1	-1	-1.9	-0.4	-2.3	0.2	0.3	-0.6	-3.3	0.2	-2.1	-0.4	0.1	1.4
82	0.3	2.1	1.1	-1.3	-2.9	-1.2	-0.4	-3	0.4	-1.3	-1.7	-0.6	-1.3	-0.5	-1.6	0.8	0.7	2.2	-1.1	-1.7	-2.9	-0.1	1.4	0.1	-0.3	0.1	-0.4	-1.9	-2.6	0.7	1.8	-0.2
83	0.2	-0.5	-0.1	-0.3	1.6	-0.3	0.1	0.7	0.1	-0.2	1.2	1.4	0.1	-1.7	-1.4	0.1	0.9	1.5	-0.8	0.9	-1.7	0.2	-0.2	-1.1	0	-0.2	0.4	-0.7	-1.2	0.7	-0.6	-0.4
84	0.6	0.1	0.4	-1.2	-0.3	-0.7	-2.9	-1	0.8	0.3	0.6	-0.7	1.3	-4.6	-2.2	-2.4	0.9	0.7	0.5	-1.2	-1	-2.2	-1.3	-1.8	0.3	-2.8	-0.7	-2.4	0.6	-3.5	-1.5	0.4
85	-1.5	-0.3	0.9	-3.2	0.9	0.1	-2.1	0.5	1	0.7	-0.7	1.4	1.5	-0.3	1.3	-1.7	-0.4	0.5	-0.3	1.4	-0.3	1.7	0.6	-1.9	-0.4	3.1	-0.4	-2.1	-1.6	0.9	-0.3	3.6
86	-0.9	0.1	-0.1	0.1	-0.6	-0.1	1.2	0.2	0.6	0.1	0.1	-0.5	0	-0.1	0.6	-0.1	-0.1	0	0.1	-0.1	0.1	0.1	0	0.1	-0.2	1	-0.3	0.1	-0.2	-0.1	-0.2	-0.3
87	-0.2	0.2	0.1	0	0.2	0	-0.1	-0.1	0.1	-0.1	-0.2	0	-0.2	-0.1	0.3	0.1	-0.5	0.2	-0.1	-0.1	0.1	0.1	0	0	-0.3	0.2	-0.3	0	0	-0.4	-0.1	-0.1
88	-0.3	-2.4	-0.4	-1.3	1.7	-2.8	-2.8	1.6	-2.7	-0.2	-1.8	-0.2	-1	-3.4	-2.4	-1.1	-1.6	0.4	0.8	-2.3	-1.2	-1.8	-1.5	-2.6	-0.1	-2.7	1.4	0.5	0.1	-0.3	-1.1	-0.6
89	0.8	-3.3	-0.9	-1	1.1	-1.9	0.7	2.5	-0.2	0.6	-0.1	0.2	-1.3	-0.9	-0.9	-1.8	0.1	0	1.4	-2.1	-3.2	1.4	2.2	-3.9	2	-1.7	0.3	-2.3	3.2	2.3	-1.9	-1.2
90	-0.7	2.1	-0.5	1.1	0.9	-0.7	-0.7	0.6	-4.1	-1.1	-0.6	2	-1.4	0.9	-0.5	-0.5	-1.5	0.3	1	-2.1	1.4	0.6	-2.1	-0.1	0.2	0.4	0.8	-1.7	-0.4	1.4	-0.8	-0.2
91	0	0	0.1	0.2	-0.1	0.1	0	0.1	0.1	0	0.1	0	-0.1	-0.1	0	0	-0.1	-0.1	-0.1	0.1	0.1	0	0	0.1	0	0.1	-0.1	0.1	0	0	-0.1	-0.1
92	0	0	-0.4	0.2	-0.3	0.3	-0.3	-0.1	0	0.4	-0.1	-0.3	0	0.7	-0.1	0	0.1	-1.3	-0.8	-0.2	0.5	0	0.1	0.5	0.4	-0.2	0.4	0.9	0.3	0.4	-0.7	-0.2
93	-0.1	-0.1	0.1	-0.2	0.1	0	0.1	0	-0.1	0.1	0.1	-0.2	-0.1	0	-0.1	-0.1	-0.2	0.1	0	0	-0.1	-0.1	0	0.1	-0.2	-0.1	0.1	0.1	0	-0.1	0	-0.2

i	33	34	35	36	37	38	39	40	41	42	43	44	45	46	47	48	49	50	51	52	53	54	55	56	57	58	59	60	61	62	63	64
94	-0.5	-0.5	-1	-1.5	-1	-0.8	0	-1	-0.4	-0.9	-0.5	0.3	-0.7	-0.8	-0.6	-0.5	-0.5	-0.5	-0.5	0.2	-0.8	-0.4	-0.5	-0.8	-0.2	-0.1	-0.5	0.5	-0.7	-0.6	-0.1	0
95	0.3	0.2	0.1	-0.3	-0.3	-0.1	0.5	0.3	0.6	0.2	0	-0.1	0	-0.6	-0.2	0.1	-0.1	0.4	0.3	-0.6	-1.1	-0.3	0.3	0.3	-0.2	0.3	0.2	-0.4	-0.2	-0.8	-0.1	-0.1
96	0.1	-0.1	0.1	-0.1	0.1	-0.1	-0.1	0.1	0	-0.1	0.1	0.1	0	0	-0.2	0	0.1	0.1	0.2	-0.1	-0.1	-0.1	0	0.2	0	-0.1	0.1	0.1	-0.1	-0.1	0.1	0
97	0.1	1.2	1	0.1	1.7	1.1	-0.2	1.9	-1.1	2.7	1.9	-0.8	-2.7	-1.4	-1.6	0.6	1.6	-0.6	0.6	-1.7	-4.4	-1.1	2.2	1.5	0	-0.6	0.4	-2	1.1	-0.7	-0.8	-1.7
98	0.1	-0.1	0.1	-0.1	-0.1	0	0.1	0.1	0.1	-0.1	0.1	0	-0.1	-0.1	0	0.1	0	0	-0.1	0.1	0	0.1	-0.1	0	0.1	0.1	0.1	0	0	0.1	0.1	-0.1
99	0.1	-0.1	-0.2	0	-0.1	-0.1	0	0.1	0	0	-0.1	0	0	0.1	0.1	0	0.1	0.1	-0.1	0	0	-0.2	0	0.1	0	-0.1	-0.1	0.1	-0.1	0.1	0	0.2
100	1.1	-1.8	-1.4	-2.6	-1.5	-1.4	0.1	-0.5	-0.5	0.1	-1.4	-1.8	0.6	-0.9	1.7	-0.3	-0.9	0.7	0	-0.4	-1.1	-0.8	0	0	0.9	2.1	1.4	-0.5	-1.1	1.5	-2.2	-0.6
101	0.1	-0.2	-1.5	-0.6	1.9	0.6	0.6	-1.7	-1.7	0.4	-1.4	0.7	1.9	0	-1.3	-0.9	-2.4	0.5	-3.1	0.9	-0.6	-2.1	-1	-0.1	0.4	-3.2	1.5	2.1	-0.9	0.3	-1.7	0.3
102	-0.3	-1	-0.5	0	-1.1	0.5	-0.3	0.9	-0.7	-0.2	-1.2	0.5	0.4	-0.4	-0.6	0.4	-0.4	1.3	-1.6	-0.5	-0.8	0.5	1.4	0.5	0.7	0.1	0.3	-0.2	0.2	-0.3	-0.4	0
103	0.1	0	0	0	-0.1	-0.1	0.1	0.1	-0.1	0	0.1	-0.1	0	0	-0.1	0.1	0.1	0	0	0	0	-0.1	0.2	0	0	0.1	-0.1	0.1	0.1	0	0	0.1
104	0.1	1.2	-0.1	3.4	0.2	2.9	-0.3	-0.1	-0.1	1.4	-0.2	1.3	1.2	0.6	0.8	1.7	-0.9	0.2	0.4	0.2	0.8	0.3	1.1	2.4	0.2	-0.1	2.4	1.2	1.9	1.5	0.1	-0.2
105	-1.2	-0.6	0.9	-0.6	0.5	-0.9	1	1.6	-2.2	-4.2	-0.2	-2.9	-1.4	1.7	-1.7	0	-0.8	0.4	-3	-1	-1.9	0.8	1.4	-0.1	-0.8	-1.5	-1	1.2	-0.3	1.3	-2.3	-0.5
106	0.1	-1.1	-1.6	-2.1	0.7	2.4	1	0.3	-2.2	-3.1	1.8	-1.5	0.5	-1.2	-0.6	0.1	1.5	-0.7	1.2	0.9	2.5	-1.6	-3.4	-2.1	-0.7	-1.5	-0.2	0.2	-0.3	-2.2	-1	0.3
107	0.2	-0.1	-0.1	-0.1	-0.1	-0.1	0.1	-0.1	-0.1	0.1	-0.1	-0.1	0	0.1	-0.1	0	0	0	0.1	-0.1	0	0	0	-0.1	0.1	-0.1	0	-0.1	0	-0.1	0.2	0
108	0.2	0.2	-0.1	-0.2	0	0.2	-0.2	0.4	0.6	-0.1	0.2	-0.3	-0.1	-0.2	-0.1	-0.2	-0.4	0.1	0.6	-0.1	-1.1	-0.6	0.1	0.2	-0.8	-0.8	0.1	-0.3	0	-0.8	0.1	-0.2
109	-0.5	-1.2	-1.1	-1.6	-0.4	-0.5	-0.2	-0.5	-0.4	-0.3	-0.6	-0.2	-1.1	-0.4	0.3	-1	-0.7	-1.2	-0.3	0.7	0.1	-0.5	-1.2	-0.7	-1	-0.2	-0.4	0.2	-0.5	-0.6	-0.1	0.1
110	-0.1	0.1	-0.1	-0.1	0	-0.1	-0.1	0	0.2	0	0	0.1	-0.2	0.1	-0.1	0	-0.1	0.1	0	0	0.1	0	0.1	0	0.1	0.1	0.1	0	0.1	-0.1	0	-0.1
111	1.9	0.2	-0.7	-0.6	0.3	1.4	1.5	0.9	0.2	0.6	0.1	0.4	0.6	1.4	-1	-1.6	1.1	-1.2	0.6	0.2	0.6	1.3	-3.5	-1.2	2.2	0.6	-0.2	-0.2	2.2	-1.3	-2.4	-2.9
112	1.6	1.2	-0.2	-2.2	2.2	0.7	0.5	3.2	2.2	-1.2	0.1	0.1	-0.6	-1.9	-2.7	-2.8	1	0.5	0.5	0.1	-1.2	2.1	-1.9	-0.3	-1.4	1.5	-0.6	-1.4	1	-1.4	-1	-0.9
113	-1.6	-1.2	-1.1	0.6	1.1	0.3	-1.1	0	0.3	-0.5	-0.8	1	-0.2	-0.2	-1.8	-1	0.1	-1.4	0.5	1	-0.3	-2	-0.3	-0.6	0.9	-0.9	-0.4	0.3	1.4	-0.7	-0.3	-0.5
114	-3.4	-2.8	-2.9	1.2	-0.9	-0.6	-1.7	-0.7	-1.3	-1.2	-3.3	2.5	-1	0.1	-1.3	-1.5	-1	-0.7	0.8	2.5	1.8	-2.1	-1.5	-1.7	0.8	-1.6	-2.4	-0.7	-0.8	1.5	1.4	2.8
115	0.7	1.5	1	-0.9	-1.3	-0.6	1.1	-0.3	-0.5	0.8	0.2	-0.6	1.1	-0.4	1.2	1.6	-0.3	1.1	-0.7	-0.9	-0.3	1.4	1.1	1	-0.3	1.2	-0.3	-0.9	-0.8	0.8	0.8	0.1
116	0.8	-1.2	0.9	-1.4	-0.3	-1.1	-2.1	0.1	1.3	-2.3	-0.9	-0.1	0.1	0	0.2	0.4	1.7	-0.3	0.4	0.1	-0.7	-1	-0.3	0.1	-1.9	-1.3	2.3	-1.4	-0.8	-1	1.7	2
117	-0.1	0	0	0.1	0	0	-0.1	0	-0.1	0	-0.1	0	-0.1	0	0.1	0.1	0	-0.1	-0.1	0	-0.2	0.1	0	0	-0.1	0.1	-0.1	0	-0.1	0	-0.1	-0.1
118	-1.1	0.8	-1.8	1.7	-1.3	1.3	-0.9	-0.2	1.3	-0.1	-2.1	-0.6	1	0.4	-1.8	-1.1	1.4	-1.7	1	1.4	0.5	-1.9	0.1	0.7	0.1	-0.5	-0.7	-1.1	1.8	-1.6	0.1	-1.1
119	0.2	0.4	0.2	0	-0.4	0.1	0.1	0.1	0.3	0.2	0.2	-0.5	0.4	0.2	0.5	0.2	0.7	-0.1	0.3	-0.5	0.1	0.1	0.1	-0.1	0	0.1	0.2	0.2	0.2	-0.1	0.2	-0.3
120	1.3	-1.6	-1.8	2	-2.2	-3	-1.7	1.1	1.9	-0.3	-0.3	-1.1	1.5	2.2	2.6	4	0.4	-3.2	1.5	1.5	1.2	0.6	0	0.3	-2.7	1.4	-1.7	-2.9	0.7	-2.3	-1.4	0.9
121	-0.9	-0.3	0.6	0.4	-0.3	0.4	-0.6	-1.2	-1.5	-0.2	-0.1	0.6	0	0.6	0.6	0	-0.9	-1.4	0.2	0.1	1	1.6	0.1	-0.8	-0.6	0	-0.3	0.7	0	-0.8	0.1	0.6
122	-1.8	1.1	-2.6	-1.5	0.3	-2.4	-0.3	-0.3	-0.9	0.5	0.2	1.1	-1.7	-2.8	-0.7	-0.8	-2.5	0.8	-1	-0.7	-2.2	0.1	-0.5	-1	0.2	-0.2	1	-2.1	0.3	1.7	-0.5	0.1
123	0	1.6	-1.5	0.9	-1	0.1	-0.4	-0.9	0.9	0.2	0.9	-1.1	3.6	-0.8	2.6	0.9	-0.7	-1.5	-0.3	1.2	0.3	4.3	-0.6	0.4	1.9	0.2	-0.5	-1	-0.3	-0.2	1.3	0.5
124	0.7	-0.1	-0.5	-0.3	0.5	0.8	0	1.2	1.4	0	-0.4	-0.2	0.2	-1.4	-1.5	-1	0.1	0.9	0.9	1.5	-0.7	-0.1	-0.7	0.8	0	0	-0.8	-1.1	-0.5	-0.5	0.3	-0.9
125	-1.5	-2.3	0.5	1.9	2.2	0.1	-1	-1	-0.2	0.3	0.1	-0.6	1.8	0.9	-3.3	-1.9	-1	-1	-0.9	0.5	0.5	-1.1	2	0.9	0.2	-0.8	-1	-0.8	-2.1	0.6	-1.9	-0.8
126	-0.1	0.1	-0.1	0	-0.1	-0.1	-0.1	0.1	0.2	0	0	-0.2	0	0.1	-0.1	0	-0.1	0	-0.1	0.1	0.1	0.1	-0.1	0.1	-0.2	0.1	-0.1	0.1	0	-0.1	0	0.2
127	-3.8	-3.4	-2.9	-2.5	-1.3	-3.1	-0.5	-0.9	-0.5	-0.1	-1.8	-1.2	-1	-0.4	-0.8	-0.6	-0.6	0.2	-0.6	0.5	-1.2	-0.3	-0.5	-1.2	-1	1	-0.3	-0.2	-0.8	-2.7	1.6	-1.1
128	-0.6	1.1	-0.1	0.4	-1.3	1	0.6	0.5	-0.2	-0.9	0.6	-0.5	-1	-1.6	-0.8	0.2	-0.8	0	-1.9	-0.3	-0.5	1.8	1.2	0.7	0.3	0.9	-0.2	0.4	-0.6	0.2	0.2	-0.2
129	1.1	1.1	-0.5	-1.3	-0.3	0	-0.1	-2.5	-0.4	0.7	0.8	1	0.4	-1.4	-0.7	-0.4	-1	0.2	-1.9	-0.2	-3.7	3.2	0.3	-0.5	-1.2	2.8	-0.2	-1.8	-1.5	-0.1	-1.1	-0.6
130	-0.1	-0.1	0.1	-0.1	0	0.1	0	-0.1	0.1	0.1	0.1	0	0.1	-0.1	-0.1	-0.1	-0.1	0.2	0	0.2	0.2	0.1	0.2	0	0	0.1	-0.1	-0.2	0.2	0.1	-0.1	0
131	-0.3	1.5	0.8	-0.1	1.5	-0.8	0.7	0.2	0.5	-1.4	-2.4	-0.6	-0.6	-0.4	-1.2	-2.7	-1.9	0.6	-1.1	-0.1	0.8	-1.8	1.1	-0.6	0.9	-2.2	-0.7	0.9	0.9	0	0.3	-0.4
132	-0.5	-3.1	0.8	0.8	-1.1	-0.5	0.5	-2.5	-0.7	-0.6	-0.2	0.1	1.2	3.4	0.9	-0.4	-0.4	-1.6	-1.2	0	-0.6	0.1	2.7	0.5	1.4	0.7	0.8	1.5	-2	3.2	-0.3	0.5
133	-1.8	0.6	-0.2	0.7	0.5	0.1	-0.3	0.6	-0.9	0.7	-2.2	1.5	1.3	2.9	2.2	-0.7	0.8	0.5	0.5	-3.6	1.1	0.1	0.6	-1.8	1.9	-0.2	-1.1	-2	-0.7	1.9	0.2	0.9
134	-1.4	1.1	0.8	0.6	-0.2	2.6	-1.6	0	-2.7	0.4	0.3	-2.1	-1.9	2.2	2.1	1.3	2.1	-0.3	0.2	-1.4	0.2	0.5	-0.9	-1.3	0.9	0.7	-1.2	2.5	0.3	-0.7	-0.3	1
135	-1.6	-2.8	-3.2	0.6	-1.4	-3.1	0.5	-0.3	-0.6	0.7	-1.1	1.4	-1.5	1.1	1.2	-1	-1.9	0.4	-1.9	1.7	-0.5	-1.7	-0.2	-3.1	-0.1	-1.1	1.6	2.3	0	2.1	-1.7	-1.1
136	-0.1	0	-0.1	0	-0.1	0.1	0.1	0.1	0	0.1	0.1	0	0	0	-0.1	-0.1	0	-0.1	0	0	-0.1	0.1	-0.1	0	0.1	0.1	-0.1	0.1	0	-0.1	-0.1	0
137	1	2	1.7	-0.3	-2.2	0.4	0	0.3	-1.3	-3	0.6	-0.4	-2.7	0.6	-2.6	-1.9	-0.4	0.7	0.5	0.5	2	-0.1	-2	1.1	0.9	1.9	-0.9	1	-0.1	-1.9	0.4	0
138	0	-0.1	0.2	-0.1	0	-0.2	0.2	0	-0.1	0	0	0	-0.1	0	0.1	0	0.1	0	0.2	0	-0.1	0.1	0.1	0	-0.1	-0.1	0.2	0.1	0	-0.1	0	0.1
139	-0.5	-0.8	0.5	0.1	-0.7	-1	-0.5	-1	-1	-0.5	-0.3	0.1	-0.4	0.4	-1.5	-1.6	-0.2	-3.2	-0.5	-1	0.9	-0.3	-0.2	0.5	1	1.2	-0.6	0.5	-1.5	0.8	-1	1.5
140	0	-0.1	-0.1	0	0	0	0.1	0.2	0	0	-0.1	0	0	-0.1	0	0.1	-0.2	-0.1	-0.1	0.2	-0.1	0	-0.1	0.1	0.1	0	-0.2	0.2	0.1	-0.1	0	-0.1
141	0.1	-0.1	0.1	0	0.2	0.1	-0.2	0	0.1	-0.2	-0.1	-0.4	0	0.2	0.5	0	-0.4	0	0.4	0	0.2	-0.1	0	0.3	0	0	-0.1	-1.8	-0.5	0	0.2	0.2
142	-1	-0.8	-1.4	0.5	0.2	0.8	0.1	-1.5	-5.5	-0.5	-0.1	0	-3.1	-0.2	0.5	-0.7	-0.5	-1.6	-1	-0.9	0.4	-0.3	-0.1	-0.6	0.2	-0.5	-0.2	1.2	-0.8	1.2	0.1	-1.7
143	0.3	0.2	1.1	0.6	-0.8	-2.1	-0.8	-1	0.7	-2.6	-1.9	-1	-2.4	-0.3	-0.5	0.1	-1.3	1	-0.3	-1.5	1.9	0.2	2.7	3.1	-1.3	0	-0.1	-1.8	-1.3	0.4	0.9	-0.2
144	-1.6	1.5	0.6	-0.4	2.7	-0.7	-0.6	0.8	1.2	-0.3	-2.3	-0.7	0.3	-2	-1.4	-0.2	1.2	-0.3	-1.7	-2.5	-0.9	-0.7	1	-0.6	-1.2	0.9	-1.8	-0.7	1.3	-1.1	-1.2	-1.6
145	1.5	-0.8	0	-0.1	0.6	-1.6	-2	3	0.8	-1.3	2.1	-1	-0.2	-2.2	-1.8	-0.8	1.7	1.1	0	-1.3	-3.3	1.7	-0.1	-0.2	-0.5	1.3	3.8	0.1	0.4	-1.2	-1.6	-1.5
146	0.1	1.6	-0.8	-0.8	-1.2	0.4	-0.6	1	0.6	-3.2	0.2	-0.5	-0.8	-1.8	-1.5	-2.3	1.2	-0.8	-0.8	0.1	-0.5	-0.2	1.1	0.3	0.4	-0.9	0.6	-1.3	0.2	0.2	-1.1	-1.2
147	-0.5	-0.8	-0.1	-0.5	-0.4	-0.2	0	-1.6	-0.8	-0.1	-0.7	-0.5	-0.6	0.5	0	-1.9	-0.8	0.1	-1.5	-0.1	-0.4	0.4	-1.2	-1.1	0	0.1	-1.4	-0.8	-0.5	-0.2	-0.8	-0.4
148	-1	-0.3	-0.8	-0.9	-0.7	-1.2	-1.5	0.5	-0.2	-1.3	-0.9	-1	-0.7	-2.6	-1.3	0.1	0.2	-0.5	0.5	-1.6	-0.8	-2.3	-0.2	-0.6	-1.4	-1.2	-0.2	0	-1	-2.1	-1	-0.4
149	0.9	-0.9	-1.5	-1	-2.4	-0.8	-1.3	-0.9	-1.3	-1.8	-0.1	0.9	0	-1.3	0.3	0.1	-0.2	-1.3	0	0.6	-2.5	-0.4	-1.2	0	0.5	1	-3.1	-4.8	-1.6	1.8	0.8	-2.7
150	-0.3	-0.2	-0.4	-0.4	-1.4	-1.1	0	-0.7	-0.2	-0.6	-1.1	0.1	-0.7	-0.3	-0.5	-0.3	-1.3	-0.8	0.1	-0.3	-0.8	-0.4	-0.3	-0.2	-0.3	-0.1	-0.3	0.1	-0.6	0.4	-0.4	-0.3
151	-0.5	-0.6	-0.7	-0.9	-1.2	-0.7	-0.3	-0.7	-0.5	-0.8	-0.6	0.1	-0.6	-0.8	-0.6	-0.5	-0.6	-0.6	-0.4	0.1	-0.6	-0.4	-0.6	-0.7	-0.2	-0.1	-0.5	0.6	-0.6	-0.5	-0.1	0.1
152	-1.3	0.7	-0.8	-2.2	1.7	-1.8	-2.6	-2.1	-0.4	-0.6	-2.8	1.6	0.1	-1.2	-2.6	-2.3	-0.6	-2.8	-0.1	0.1	0.4	-2.4	-1.8	-2.2	-0.7	-2.5	0.6	-1	0.1	-0.1	-0.6	0.3
153	-0.7	-1	-1.5	-0.5	-0.4	-0.3	-0.4	-0.5	-0.6	-0.2	-1	1.2	-1	-0.5	-0.4	-0.9	-0.6	-0.4	-0.1	0.9	0.2	-1.6	-1.8	-0.7	0.2	-1.3	-0.5	-0.6	-0.6	0.7	0.4	1.1
154	-0.3	-0.3	-0.2	-1.7	0.3	-0.9	-0.2	-0.4	0.4	-0.3	0.1	0	-0.3	-0.1	-0.8	-0.7	0.4	-0.1	0.1	0	-0.1	0	-0.3	-0.3	-0.3	0.1	-0.5	-0.4	-0.8	-0.3	-0.1	-0.1
155	1.3	-1.2	-0.5	1.3	0.1	-0.6	0.8	-2.7	1.3	1.5	0.8	-1.8	0.5	-1.4	-1.4	1.5	0.2	-0.3	-3.4	1.8	-0.9	-1.3	0.3	-0.6	3.4	0.1	0.5	-1.3	-0.9	2	0.7	1.3
B1	-0.9	-0.9	-0.9	-0.9	-1	-1	-1.1	-0.8	-0.9	-0.9	-1	-1	-0.7	-1.1	-1	-0.9	-0.6	-0.6	-0.8	-1.2	-1.3	-0.5	-1	-1	-0.7	-0.2	-1.2	-0.8	-1.1	-0.8	-1	-0.8

Table D.12 - Normalization coefficients of the ANN-UBO_e's input parameters

Parameter	μ	σ
TVD	2348.74	452.03
l_l	2203.07	645.18
lat_{bh}	55.83	0.87

Parameter	μ	σ
$\mathrm{lon}_{\mathrm{bh}}$	-120.43	1.36
d_e	0.33	0.82
V_{inj}	0.57	0.49
Q_f	663.19	413.24
V_{acid}	0.07	0.26
P_c	0.63	0.48
N_s	3.31	13.03
l_s	60.30	78.53
d_s	407.99	10740.42
C_s	27.83	17.89
t_{sh}	61.61	46.89
p_{inj}	98.08	55.23
q_{inj}	3.13	2.65
ϕ_m	27.80	20.34
GR	54.86	10.44
ρ_b	8.41	2.56
PE	0.08	0.01
k_m	111.87	14.32
B_i	2.62	0.02
h_f	3.56	0.23
S_w	3.87	8.19
p_i	1.94	0.18
h_{net}	164.75	57.04

E. Geothermal Data Statistics

E.1 Pipeline and Insulation Specifications

Table E.1 – Pipeline and insulation specifications for heat loss estimation in surface pipeline

Parameter, unit	value
Surface pipeline inside diameter, mm	77.90
Surface pipeline outside diameter, mm	88.90
Wind Speed, m/s	3.50
Insulation type	Calcium Silicate
Surface emissivity	0.9
Insulation thickness, mm	50
Insulation outside diameter, mm	188.9
$T_{amb}{}^{*}$ – Alberta (Edmonton Station), °C	2.60
T_{amb} – British Columbia (Fort St John Station), °C	2.36
T_{amb} – Saskatchewan (Saskatoon Station), °C	3.13
T_{amb} – Manitoba (Winnipeg Station), °C	4.6

*T_{amb}: yearly average ambient temperature, °C

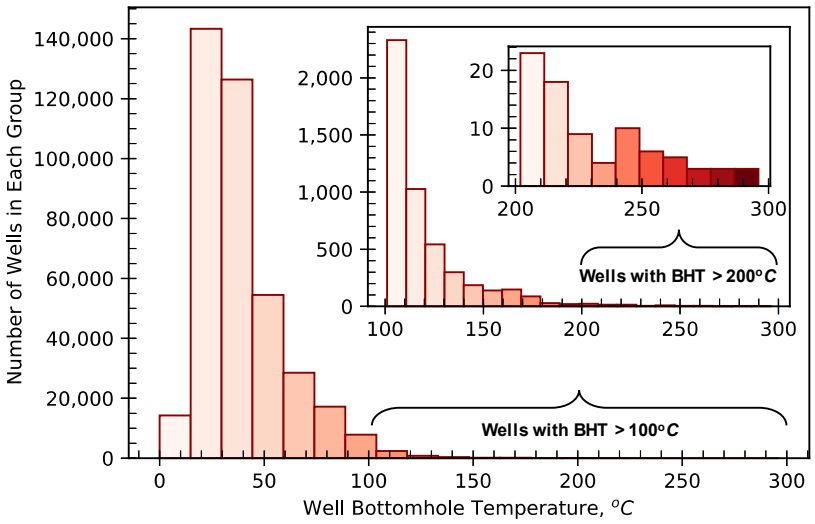

Fig. E.1 – Histogram of oil and gas wells with different bottomhole temperature reported in geoSCOUT database. First inset figure shows histogram of wells with bottomhole temperature above 100°C. Second inset figure shows histogram of wells with bottomhole temperature above 200°C.

E.2 Well Data Distributions

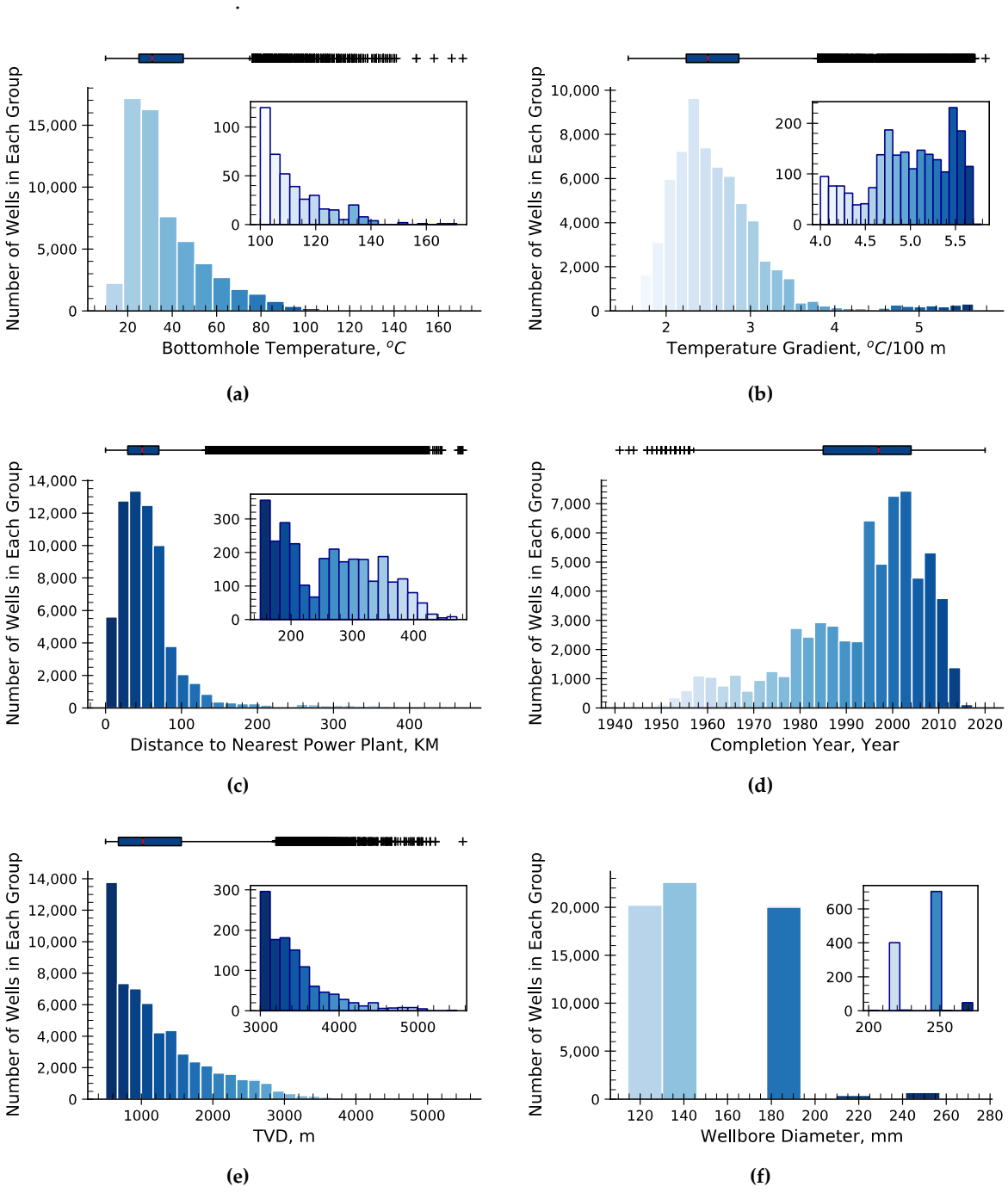

Fig. E.2 – Histograms of the well data of suspended oil and gas wells completed in WCSB showing the distribution of the studied parameters

E.3 General Geothermal Data

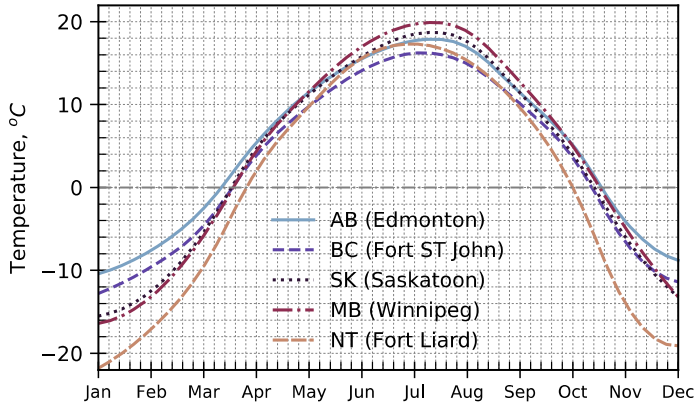

Fig. E.3 – Average surface temperature distribution in western Canada from 1981 to 2010 [2]

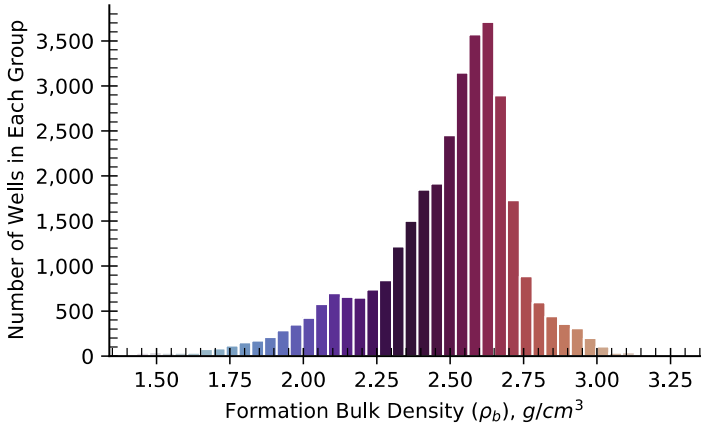

Fig. E.4 – The distribution of formation rock bulk density (estimated from well-log data) for the studied suspended oil and gas wells completed in WCSB

Copyright Permissions

Chapter 2: https://doi.org/10.1016/j.petrol.2020.107584

License number	0920-4105
License date	26-Oct-23
Order number	1410753
Type of Use	Republish in a thesis/dissertation
Thesis title	A Hybrid Analytical and Machine Learning Workflow for Completion Design Optimization in Unconventional Reservoirs
Requested Publication	Journal of petroleum science & engineering
Pages	13
Distribution	Worldwide
Lifetime Unit Quantity	More than 2,000,000
Permission Type	GRANT
Portion	Chapter/article
Requester name	Tamer Moussa

Chapter 3: https://doi.org/10.2118/204194-MS

License number	978-1-61399-748-2
License date	25-Oct-23
Order number	1410349
Type of Use	Republish in a thesis/dissertation
Thesis title	A Hybrid Analytical and Machine Learning Workflow for Completion Design Optimization in Unconventional Reservoirs
Requested Publication	SPE Hydraulic Fracturing Technology Conference and Exhibition
Pages	12
Distribution	Worldwide
Lifetime Unit Quantity	More than 2,000,000
Permission Type	GRANT
Portion	Chapter/article
Requester name	Tamer Moussa

Chapter 4: https://doi.org/10.2118/201464-MS

License number	9781613997239
License date	25-Oct-23
Order number	1410280
Type of Use	Republish in a thesis/dissertation
Thesis title	A Hybrid Analytical and Machine Learning Workflow for Completion Design Optimization in Unconventional Reservoirs
Requested Publication	SPE Annual Technical Conference & Exhibition (20ATCE)
Pages	19
Distribution	Worldwide
Lifetime Unit Quantity	More than 2,000,000
Permission Type	GRANT
Portion	Chapter/article
Requester name	Tamer Moussa

Chapter 5: https://doi.org/10.2118/217443-PA

License number	1086-055X
License date	25-Oct-23
Order number	1410350
Type of Use	Republish in a thesis/dissertation
Thesis title	A Hybrid Analytical and Machine Learning Workflow for Completion Design Optimization in Unconventional Reservoirs
Requested Publication	SPE JOURNAL
Pages	22
Distribution	Worldwide
Lifetime Unit Quantity	More than 2,000,000
Permission Type	GRANT
Portion	Chapter/article
Requester name	Tamer Moussa

Chapter 6: https://doi.org/10.2118/209136-MS

License number	9781613998540
License date	25-Oct-23
Order number	1410279
Type of Use	Republish in a thesis/dissertation
Thesis title	A Hybrid Analytical and Machine Learning Workflow for Completion Design Optimization in Unconventional Reservoirs
Requested Publication	SPE Hydraulic Fracturing Technology Conference and Exhibition
Pages	18
Distribution	Worldwide
Lifetime Unit Quantity	More than 2,000,000
Permission Type	GRANT
Portion	Chapter/article
Requester name	Tamer Moussa

Chapter 8: https://doi.org/10.1016/j.renene.2022.06.090

License number	0960-1481
License date	26-Oct-23
Order number	1410752
Type of Use	Republish in a thesis/dissertation
Thesis title	A Hybrid Analytical and Machine Learning Workflow for Completion Design Optimization in Unconventional Reservoirs
Requested Publication	Renewable energy
Pages	14
Distribution	Worldwide
Lifetime Unit Quantity	More than 2,000,000
Permission Type	GRANT
Portion	Chapter/article
Requester name	Tamer Moussa